ENHANCED INTERFACES AND TRAIN CATEGORIES FOR DYNAMIC COMPATIBILITY ASSESSMENT OF EUROPEAN RAILWAY BRIDGES

Limitations of DER/LIR and improved Spectral Methods

DELIVERABLE INFORMATION	
Work package number:	WP1
Work package title:	Definition of Dynamic Train Categories (DTCs) for ensuring compatibility of the interface between trains and bridges
Deliverable number:	D1.2
Deliverable title:	Limitations of DER/LIR and improved Spectral Methods
Due date of deliverable:	31-12-2025
Actual submission date:	11-05-2025
Responsible partner	UPV
Revision:	
Dissemination level:	

This project has received funding from the Europe's Rail Joint Undertaking under Horizon Europe research and innovation programme under grant agreement No. 101121765 (HORIZON-ER-JU-2022-ExplR-02).

PUBLICATION HISTORY

Version	Date	Description	Responsible
V1	11-05-2025	Initial submission	Pedro Museros / UPV

CONTRIBUTORS TO THE DELIVERABLE

Name	Institution	Role
Pedro Museros	UPV	Deliverable responsible
Carlos A. Riascos	UPV	Contributor
Willan E. Cueva	UPV	Contributor
Juan G. Benito	UPV	Contributor

Firmado por MUSEROS ROMERO PEDRO - ***2720** el día 11/05/2026 con un certificado emitido por AC FNMT Usuarios

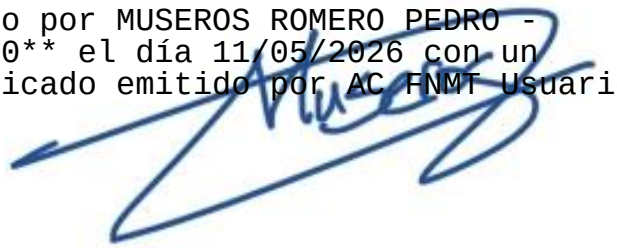

PROJECT CONSORTIUM

Coordinator

Universidade do Porto
UPORTO, Portugal

Beneficiaries

Kungliga Tekniska Hoegskolan
KTH, Sweden

Universidad Politecnica de Madrid
UPM, Spain

Bundesanstalt Fuer Materialforschung Und –Pruefung
BAM, Germany

Deutschen Bahn InfraGO AG
DB, Germany

Acoustique Et Vibrations Logiciels Scientifiques
AVLS, France

Affiliated Partners (to UPM)

Universitat Politecnica de Valencia
UPV, Spain

Universitat Jaume I de Castellon
UJI, Spain

Universidad de Sevilla
UdS, Spain

Administrador de Infraestructuras Ferroviarias
ADIF, Spain

Associated Partner

University Of Huddersfield
HUD, UK

Acknowledgments: This project has received funding from the Europe's Rail Joint Undertaking under Horizon Europe research and innovation programme under grant agreement No. 101121765 (HORIZON-ER-JU-2022-ExplR-02).

TABLE OF CONTENTS

1 Introduction

Within WP1 in the framework of project *InBridge4EU* (henceforth "the Project"), and regarding specifically Tasks 1.3 and 1.4 dedicated to the analysis and update of the Spectral Methods (SM), various relevant aspects were mentioned in the *ERA Technical Note* (ERA, 2022) as, for instance: "The formula for Train Signature was derived from the decomposition of excitation at resonance (DER method), as well as the Residual Influence Line (LIR) method. In the original studies describing the derivation of the method and from its application a number of limitations have been identified. **These limitations potentially preclude the application of Train Signature and the spectral methods to current passenger traffic which has different train architecture characteristics to the characteristics of the first high speed trains.**

An improved Train Signature technique […] could **enable the quick evaluation of the relativity of the load effects of a proposed train versus the load effects produced by existing train(s) which have been previously demonstrated to be compatible with existing bridges.** For the verification of the proposed train/bridge compatibility to be valid (undertaken on the basis that the dynamic load effects from the proposed train are not greater than the dynamic load effects from existing trains), **it is important that the revised Train Signature technique does not:**

- **underestimate the load effects of the proposed train; and**
- **overestimate the load effects of the existing trains that are operating.**

It should be noted that one limitation may apply to one of the above trains but not to the other **depending upon the train architecture characteristics of each train.** This issue has the potential to make invalid the relative comparison of dynamic load effects from proposed and existing trains. **A revised spectral method should have the potential to enable the very quick determination of the maximum dynamic increment of static loading and maximum bridge deck acceleration for either an individual bridge or for use in parametric studies**".

To provide an answer to such need of revised SM, Task 1.3 of the Project aims first to provide an assessment of the limitations of the current SM (methods DER and LIR), and the errors involved. Such assessment is to be carried out by comparison of the results predicted by SM *vs*. those predicted by accurate time-stepping calculations (TSC), in a suitable number of relevant scenarios. In this document, *Duhamel's integral* is used as the reference TSC method.

Subsequently, Task 1.4 of the Project aims at proposing improved SM capable of assessing resonance and impact scenarios with the mentioned goal of allowing a quick determination of the maximum dynamic increment of static loading and maximum bridge deck acceleration for either an individual bridge or for use in parametric studies. The accuracy of the new proposed SM is again to be tested *vs*. the results of TSC.

This document is organised as follows. Of general interest for the document are:

- Section 2: which summarises the objectives of Tasks 1.3 and 1.4 of the Project and gives an outline of the sections of the document dedicated to each objective.
- Section 3: this section presents the basic formulation of current SM (DER and LIR), with a summary of the improvements to those methods provided by committee ERRI D214.
- Section 4: contains a review of the shortcomings of SM reported in technical literature, and proposes a list of key shortcomings (KS) to be investigated in this document, in relation to the objectives described in section 2.

- Section 5: describes the methodology adopted here to investigate the KS, and to test the new proposed SM, as regards: the rolling stock and bridges considered; strategies employed for each KS; and various measures of error levels used in different sections of the document.

Related to Task 1.3:

- Section 6: presents a basic comparison of the performance of LIR and DER methods in simply supported (SS) bridges, for different types of rolling stock.
- Section 7: analyses the KS related to the dynamic response of SS bridges.
- Section 8: analyses the KS related to the dynamic response of bridges not SS, considering cases when more than one mode of vibration is relevant (torsion and multi-span bridges), as well as portal frames.

Related to Task 1.4:

- Section 9 analyses and proposes new SM capable of assessing resonance and impact scenarios in SS bridges. Those SM include an evaluation of the most relevant improvements to DER and LIR proposed by ERRI D214.
- Section 10 presents improved SM for cases when more than one mode is relevant, including torsion, multi-span bridges, and an evaluation of the potential of CQC method in relevant cases.
- Section 11 presents improved SM for beams with both ends rotationally restrained and portal frames.
- Section 12 analyses the frequency domain approach alternative for the derivation of SM.
- Section 13 presents novel results about the performance of longitudinal load distribution factors to be used conveniently with SM.

As a closure to deliverable D1.2:

- Section 14 summarises the dissemination actions undertaken so far in relation to Tasks 1.3 and 1.4, and those planned before the end of the Project.
- Section 15 presents a summary of the main findings discussed in D1.2.
- Section 16 summarises the main conclusions of this research.
- Appendix A describes the basic methodology used in this document to calculate relative error measures from cumulative response envelopes (*exceedance analysis*).
- Appendix B contains an anonymous description of the passenger train (PT) rolling stock considered in this document.
- Appendix C contains an anonymous description of the freight train (FT) rolling stock instead.
- Appendix D contains an anonymous and graphical definition of the trains included in model named PT60 (see section 5.1.9).
- Appendix E is a comprehensive graphical report of the error levels in the computation of vertical acceleration and displacements using LIR and DER, for the train model PT60.

The list of abbreviations in Table 1 is used throughout:

Table 1: List of abbreviations.

Abbreviation	Meaning
PT	Passenger train
FT	Freight train
CB train	Train with conventional bogies (conventional train)
AB train	Train with articulated/Jacobs bogies (articulated train)
SA train	Train with single axles (regular train)
EQD train	"Train" consisting of a series of equidistant loads
ERS beam	Beam with elastically restrained supports
PSC bridge	Prestressed concrete bridge
SS bridge	Simply-supported bridge
STC bridge	Steel/composite bridge
FE / FEM	Finite Elements / Finite Element Method
FIL	Forced influence line
FIL_h	Forced influence line, homogeneous solution
FIL_p	Forced influence line, particular solution
RIL	Residual influence line
TSC	Time-stepping calculation

2 Summary of objectives for Tasks 1.3 and 1.4

This section contains summarised information from the *Description of Action* of project *InBridge4EU* (*Grant Agreement*, Annex 1).

2.1 Objectives of Task 1.3

Title of Task 1.3: Limitations of current spectral (DER/LIR) methods and assessment of errors arising from not fulfilling the conditions for their application

In this task it will be established:

- Under what conditions SM are accurate and reliable for defining the dynamic response of bridges. This includes train parameters (i.e., length of formations), speed, symmetry of formations, and other parameters → See sections 6 and 7.
- The limitations of SM to bridge parameters and typologies (i.e., simply supported deck beams, deck torsion, redundant continuous deck bridges, portal frames) → See section 8.

2.2 Objectives of Task 1.4

Title of Task 1.4: Proposal of improved spectral methods capable of assessing resonance and impact scenarios

This task is aimed at developing improvements of SM for considering:

- The possible critical effect of the train while on the bridge (point 1.4c of ERA Technical Note (ERA 2022)) → See section 9.
- Feasibility of including more than one frequency, and alternative more precise methods for establishing upper bounds of the sums of harmonics → See section 10.
- Spectral Methods applied to the analysis of portal frames and beams with end rotational restraints → See section 11.
- A complementary spectral approach in the frequency domain based on theory of random vibrations → See section 12.
- Spectral Methods combined with reduction factors for longitudinal distribution → See section 13.

The alternative proposals will be checked against dynamic transient analysis methods and tested for a representative set of trains and bridges.

3 Formulation of Spectral Methods (SM) according to committee ERRI D214/RP6

3.1 D.E.R. method

The DER (Decomposition of the Excitation at Resonance) method is an analytical framework developed to evaluate the dynamic response of railway bridges subjected to moving loads. Initially formalized in the ERRI D214 report RP6 (ERRI D214 1999), this method has profoundly influenced the evolution of European standards, particularly EN1991-2. The core idea of the DER method is to express the generalized force, $Q(t)$ -Eq. (1)- as a Fourier series. This decomposition uses the convoy crossing time over the bridge as the fundamental period, T. Each term in the series is modulated by the beam bridge's mode shape function, $\phi(\cdot)$, and amplified by the magnitude of the applied forces, F_i.

Mathematically, this representation allows the input force to be transformed into a series of sines and cosines. The DER method then retains the fundamental harmonic of the Fourier series, and applies this input to the simply-supported (SS) bridge idealized by its first bending mode, thus delivering estimates of the structural acceleration. The focus is on the maximum amplitude of this response, which is determined through three multiplicative terms detailed in Eq. (2).

Specifically, $\phi(\cdot)$ represents the fundamental mode shape function of the beam bridge, t_i denotes the time delay for the entry of the i-th axle onto the bridge, v is the train speed, and L is the bridge span length. Eq. (2) is used to calculate the maximum acceleration at mid-span, a_{max}, where:

1. C_t, an integration factor defined in Eq. (3), where K is the effective stiffness in generalized coordinates and f_0 is the fundamental frequency of the bridge.
2. A(L/λ), the influence line described in Eq. (4), quantifies how each punctual load can contribute to the response for different values of λ.
3. G(λ), the convoy's spectrum, outlined in Eq. (5), captures the effects of the sequence of moving loads.

$$Q(t) = \sum_{i=0}^{N-1} F_i \prod_{L/v}(t - t_i)\phi\big(v(t - t_i)\big) \tag{1}$$

$$a_{max} = C_t \, A\left(\frac{L}{\lambda}\right) G(\lambda) \tag{2}$$

$$C_t = \frac{8\pi L n_0^2}{K} = \frac{4}{m\,\pi} \tag{3}$$

$$A\left(\frac{L}{\lambda}\right) = \left|\frac{\cos\left(\frac{\pi L}{\lambda}\right)}{\left(\frac{2L}{\lambda}\right)^2 - 1}\right| \tag{4}$$

$$G(\lambda) = \max_{(0 \le k \le N-1)} \left\{\frac{1}{\zeta_k}\sqrt{\left(\left(\sum_{i=0}^{k} F_i \sin\left(\frac{2\pi x_i}{\lambda}\right)\right)^2 + \left(\sum_{i=0}^{k} F_i \cos\left(\frac{2\pi x_i}{\lambda}\right)\right)^2\right)}\left(1 - e^{-\frac{\zeta 2\pi x_k}{\lambda}}\right)\right\} \tag{5}$$

For computing the vertical displacement, the output of Eq. (2) has to be complemented by (a) dividing the result by ω^2, and (b) adding the *static displacement at resonance* ($\delta_{st,res}$), as described in point (D) below.

This basic DER formulation is the most popular one, due to its simple implementation as a product of three terms. However, the D214 committee RP6 (Part A) proposed a number of potential improvements to enhance the accuracy of the method. Those improvements are summarised below:

(A) RP6 – Part A – 5.5.1: For the computation of the vertical acceleration, do not consider as subtrains the effect of heavier front power cars, but include them instead in the rest of subtrains. This applies to

vehicles as ICE2 or ETR-Y-500, where the power cars have much heavier axles. However, no guidance was provided as to what should be considered a "much heavier" axle ("*essieux beaucoup plus chargés*"). The relative importance of the first heavy power cars will increase with damping (RP6 mentions 4% as relevant case).

(B) For the computation of the vertical acceleration, take the highest value between Eq. (2) and the impact acceleration ("*chargement rapide*"), which is based on the use of coefficient φ'. The impact acceleration considers all axles, including eventual heavier locomotives.

(C) For the computation of the vertical displacement, it is not mentioned whether the subtrains of heavier front power cars (ICE2, ETR) should also be discarded or not. Discarding them would be an approach consistent with point (A) above.

(D) Moreover, the static displacement component it to be added to the resonant displacement. That displacement is referred to as *static displacement at resonance* ($\delta_{st,\mathrm{res}}$, in what follows) and is due exclusively to the passenger coaches (not including any kind of power car).

(E) Finally, the impact displacement, which is based on the use of coefficient φ', is computed analogously to point (B) above, and the maximum among the values obtained from points (D) and (E) is retained.

3.2 L.I.R. method

The LIR method (Residual Influence Line) is a second simplified approach for estimating accelerations and displacements in SS beams under the passage of trains. Originating from the ERRI D214 report RP6 (ERRI D214 1999), the method calculates the superposition of phase-shifted free vibrations generated by each axle of the train as it leaves the bridge.

This method uses the classical closed-form solution for the temporal response of the SS bridge, Eq. (6). Once the point load leaves the bridge, i.e., at the instant $t = L/v$, where L is the bridge length and v is the velocity of a single point load, the bridge enters free vibration. By estimating the displacement and velocity at this instant, the maximum amplitude of the bridge during the free vibration phase can be evaluated. The result of this approach for practical values of damping ratio ζ is referred to as *Residual Influence Line* (RIL), and is given in Eq. (8). Additionally, m represents the linear mass of the beam. This expression determines the RIL curve which, as it is known, features zones of maxima and minima responses, the latter referred to as cancellations. Moreover, K is the nondimensional speed, which is the ratio between the excitation frequency and the natural frequency ω_0 of the bridge; and ω_d is the damped frequency.

By amplifying the RIL curve with the superposition effect of the load convoy characteristics, or signature (see Eq. 9), the bridge acceleration can be estimated as defined in Eq. (7). The (damped) signature is defined based on each load F_i, along with its respective position d_i, relative to the first load entering the bridge. Furthermore, V and T refer to the velocity of the loads and the natural period of the bridge under study in Eq. (2.2.4).

$$y(t) = \frac{y_{\mathrm{stat}}}{(1-K^2)^2+(2\zeta K)^2}\{(1-K^2)\sin(K\omega t) - 2\zeta K\cos(K\omega t) + \\ + Ke^{-\zeta\omega t}\left[\frac{2\zeta^2+K^2-1}{\sqrt{1-\zeta^2}}\sin\left(\omega\sqrt{1-\zeta^2}\,t\right) + 2\zeta\cos\left(\omega\sqrt{1-\zeta^2}\,t\right)\right]\} \quad (6)$$

$$a_{\max} = \Gamma_{\max}\cdot G \quad (7)$$

$$\Gamma_{\max} = \frac{1}{mL/2}\frac{K}{1-K^2}\sqrt{1 + e^{-2\zeta\pi/K} + 2\,e^{-\zeta\pi/K}\cos\left(\frac{\pi}{K}\right)} \tag{8}$$

$$G = \sqrt{\left(\sum_{i=1}^{k} F_{i\theta_i\cos}(2\pi\delta_i)\right)^2 + \left(\sum_{i=1}^{k} F_{i\theta_i\sin}(2\pi\delta_i)\right)^2}$$

$$\theta_i = e^{-2\pi\delta_i\zeta} \tag{9}$$

$$\delta_i = \frac{d_k - d_i}{\lambda}$$

$$\lambda = VT$$

For computing the dynamic displacement, the factor $\frac{2}{mL}$ in Eq. (8) has to be replaced by $\frac{2L^3}{EI}$. However, that procedure does not consider the forced effect of the loads on the span and unusable results would be obtained.

The simplest strategy is to add the static displacement at resonance $\delta_{st,res}$ (see point (D) in section 3.1) to the dynamic displacement. That one will therefore be considered here as the basic procedure for calculation of displacements in this document, both for DER and LIR.

Report RP6 (Part B) from D214 points out also some problems detected in the simplest version of LIR (Eqs. (7) and (8) combined, *i.e.* product of three terms). The relevant comments in that report, regarding the vertical accelerations, are the following:

(F) Too weak minimum values obtained for $K<1/3$.

(G) Too strong values obtained for train Corail, and $K\approx0.5$. This effect is described as being analogous to point (A) in previous section, when DER method was described. The Corail train is described as having power cars with heavier axles than the passenger coaches.

(H) It is emphasised that the subtrains are an idealization which does not fully corresponds to reality, because when part of the full train (a subtrain) is in the LIR, some axles may be producing forced response (LIF = *ligne d'influence de l'oscillation forcée*, in what follows—forced response influence line). That forced response may either increase or decrease the contribution of the subtrain placed in the LIR.

(I) An improvement proposed by D214 is to obtain an estimate of the forced acceleration by taking into account the homogeneous solution due to the loads that can be simultaneously on the bridge, and to retain that value whenever it's larger than the usual term from the signature of the free vibration. Such strategy requires a reformulation of the signature, because (*i*) the loads to consider in that calculation are just the ones on the bridge, and (*ii*) the (no longer residual) influence line of the homogeneous forced vibration is[1], for low damping:

$R(K) = \frac{K}{1-K^2}$, which can be named as *homogeneous forced influence line* (FIL_h). (10)

[1] An erratum seems to exist in the formula in section 7.1 on page 15 (Part B) of the RP6: $\frac{2K}{1-K^2}\cos\frac{\pi}{2K}$ is correct for zero damping, but for low damping the "franchissement term" is $\frac{K}{1-K^2}\sqrt{1 + e^{-2\zeta\pi/K} + 2\,e^{-\zeta\pi/K}\cos\frac{\pi}{K}}$.

The D214 claims good results for the acceleration with this approach. The reason behind this formulation is that null values of free oscillation will appear near K=1/3, 1/5, etc., as it is well known, but no equivalent cancellations of the homogeneous forced vibration exist since the initial conditions of such homogeneous vibration must always compensate the particular forced solution. Therefore, at the speeds of cancellation, the homogeneous vibration appears initially as an alternative.

Doubts may arise as of what position to consider for the loads on the bridge, because D214 mentions only that they are out of phase with the loads outside the bridge. Therefore, the position of the loads on the bridge should be determined in order to apply the FIL_h, see section 9.1.5.

(J) A second proposed improvement considers an out-of-phase combination of the homogeneous forced solution, with the LIR solution. The D214 claims good results for acceleration, also for K≈0.5. this method is discussed in section 9.1.6.

(K) A third proposed improvement is to obtain also the term due to the forced particular solution and combine with the homogeneous and free vibration with an SRSS strategy. This possibility would be required for achieving acceptable performance in computing the vertical displacements, but is not further explored by D214. Besides, given that the results point (J) above have not been consistently satisfactory, this option is not investigated further.

(L) The last improvement proposed in RP6 (Part B) is to assimilate the particular solution to a free vibration, and then retain the maximum value between that approximation and the bare LIR result. Committee D214 mentions that the method is less rigorous. However, the part of the train acting on the span should be taken into account (forced vibration), which is common to points (I) and (J) above for the acceleration. Therefore, the accuracy of the proposals of points (I) and (J) should be examined first before testing variant (K) for the displacements. Given that those options have not been found sufficiently satisfactory in a wide ensemble of spans and rolling stock, this option is not explored firther.

As can be seen, a number of improvements were also explored by ERRI D214, but were not formulated in full detail and tested extensively. Those ideas were taken as a departure point in Task 1.4 to test refined SM. However, it is clear from these proposed improvements that the simplicity of the three-term formulas will be lost to a greater or lesser degree.

4 Reported and key shortcomings of SM

4.1 Reported shortcomings of SM

Aside from the shortcomings summarised in previous section in this document, it was also described in milestones MS3 and MS4 of this Project that some known or envisaged shortcomings/limitations of SM have been reported in various sources, as described below:

The first source considered is **EN1991-2:2023** (CEN, 2023), where the following limitations are described:

3.1.1. Valid only in SS bridges with beam bending behaviour [*i.e.* it neglects torsion and 3-D behaviour, and bridge types other than SS (for instance, portal frames)].

3.1.2. Only the first (bending) mode of vibration of the bridge is taken into account [*i.e.* torsion or other bending modes are neglected; this affects multi-span continuous bridges, for example].

3.1.3. Not valid for non-resonant conditions where it is not an upper bound.

3.1.4. Not valid for short trains and short subtrains where dynamic excitation does not arise from fully developed resonance.

3.1.5. Not valid for trains where the spacing of axles varies from the normal pattern within the train.

In addition to these five shortcomings, others significantly different are set forth by the **ERA Technical Note** (ERA, 2022), as follows:

3.1.6. Train Signature and DER method do not capture a critical case that occurs whilst a train is on a bridge before the whole length of the train has passed over the bridge, for example the case of a power car or locomotive with different axle spacings to the remainder of the train.

3.1.7. Train Signature and DER method are not suitable for comparing the load effects of trains on short span bridges or for excitation from short wavelengths.

3.1.8. Terms neglected in the derivation of the Train Signature technique and DER method can be more significant than retained terms (e.g. 2^{nd} or 3^{rd} terms in Fourier series derivation).

3.1.9. Train Signature technique and DER method errors increase as the train length deviates from an exact multiple of the repeating vehicle length.

3.1.10. Train Signature technique and DER method were developed primarily from consideration of maximum bridge deck acceleration and the accuracy of the technique for determining displacements should be investigated and improved.

Moreover, the description of **Task 1.3 in the Grant Agreement of the Project** mentions the following issues to be investigated, in addition to the ten shortcomings described above:

3.1.11. It should be established under what conditions SM are accurate and reliable as regards the speed of trains.

3.1.12. Same as previous point, regarding the symmetry of formations.

3.1.13. Limitations to the use of SM in SS deck beams.

3.1.14. Same as previous point, considering also deck torsion [see point 3.1.1 above].

3.1.15. Limitations to the use of SM in continuous bridges [see point 3.1.2 above].

3.1.16. Same as previous point, in portal frames [see point 3.1.1 above].

Finally, it is also to be considered that the recent guideline **Rail Industry Guidance Note GEGN8616** (RSSB, 2024) stipulates the following in its Appendix J:

3.1.17. "*For example, other CEN DIBRST studies have shown that away from resonant speeds the load effect due to the proposed train formation can in fact be greater than the comparator train and/or a dynamic load model whereas Train Signature incorrectly indicates the load effect is less (the formula for Train Signature was derived taking into account dynamic behaviour at resonance). Note: ERRI D214 Report 9 states that Train Signature can be used to compare the relative load effects of trains at resonance and away from resonance. However more recent CEN studies and prEN1991-2:2021 indicate the technique is only suitable for comparing the relative dynamic loading characteristics of trains under resonance conditions*".

Analysis of the reported shortcomings:

- 3.1.1. Stems from the hypotheses of the methods, which neglect behaviours other than bending in SS bridges.

3.1.2. Stems from the hypotheses of the methods, which neglect modes other than the fundamental.

For the fundamental torsion mode, these previous shortcomings can be overcome, given that the differential equation in nondimensional form is identical to the first bending mode, except for a constant (see section 8.1). Then, a question that remains open for task 1.4 is whether the response of the bending mode and torsion mode can be suitably combined when using SM. The same applies for structures where more modes may contribute significantly, as for instance continuous bridges.

Moreover, points 3.1.1 and 3.1.2 above can be considered as a combined, single limitation of SM, which reduces their applicability to SS bridges idealised by solely its fundamental bending mode.

Ongoing and past experimental work from other partners in InB4EU has proved that there is uncertainty regarding the actual damping ratios of higher global modes. Previous studies show that, under forced vibration, the damping ratio of higher modes sometimes exceeds the damping of the fundamental mode; also, in other cases it increases with the amplitude of the applied force (In2Track2, 2021). Given those uncertainties, it is considered here that simplified analysis methods (as the SM) should be based on the fundamental bending and torsion modes only, whose influence on the response is predominant. Since testing higher modes at relevant amplitudes under forced vibration is not generalised so far, such uncertainty persists about how they effectively contribute to the maximum acceleration response of SS bridges, and thus to ballast instability.

Also, for structures where SSI can be of relevance, SM have been developed with success, and the effect of strong damping in the mitigation of higher modes has been emphasised (Zangeneh et al., 2021). Moreover, the influence of higher bending modes on vertical accelerations is markedly reduced by longitudinal load distribution effects, therefore having a lesser participation in the maximum response of bridges—at least in SS configuration (Moliner et al., 2024).

Particularly, some local modes such as plate modes—that may affect the behaviour particularly of floors in metallic bridges—, cannot be considered by the current versions of SM. The development of SM that can tackle the vibration due to local modes is a specific question that falls out of the scope of Tasks 1.3 and 1.4.

In summary, shortcomings 3.1.1 and 3.1.2 together are considered as a **key shortcoming** (KS) of SM, to be investigated here. They will be analysed by investigating the influence of (a) the first torsion mode in SS beams; (b) the second bending mode in 2-span continuous bridges; (c) the free vibrations originated by passing loads in beams with partially restrained ends.

- 3.1.3. In general, non-resonant conditions ("valleys" of the response plots) have not been found to be the determinant for bridge assessment as regards the dynamic response. Therefore, shortcoming 3.1.3 will not be considered as a **KS**.

- 3.1.4. The deficiencies for short trains and short subtrains are investigated as a **KS** in this document.

- 3.1.5. The aspect related to irregular train architectures is investigated as a **KS** in this document. Irregularity in the architecture refers here to local variations of the axle distances, differing from a regular pattern.

- 3.1.6. This is related to the transient response that occurs whilst a train is on a bridge, and is investigated here as a **KS**. Since shortcoming 3.1.6 bears a relation with 3.1.5—because a transient response may be originated in an irregular architecture—, in the following shortcoming 3.1.6 will be devoted to irregularity in the axle distances in the end power cars, and 3.1.5 in the rest of cases.

- 3.1.7. Deficiencies of SM in the analysis of short bridges and short wavelengths is investigated here as a **KS**.

- 3.1.8. The fact that 2nd or 3rd terms in Fourier series derivation (DER method) can be significant implies a potential inaccuracy of SM. The DER method as a product of three terms owes its simplicity to the fact that a resonance condition is assumed for the 1st Fourier term of the forcing function. Thus, in passing from section 4.5 to section 5.1 in RP6 (Part A) a number of terms simplify and give rise to the influence line and the signature as we know them. If the 2nd and 3rd Fourier terms are retained, the simplifications associated to resonance (frequency ratio close to one; amplification proportional to $(2\zeta)^{-1}$) will be lost for those terms, with no guarantee that the resulting formulas will be amenable to simple mathematical implementation.

  Moreover, RP6 (Part A) discussed such potential inaccuracy (see section 5.4.3), and proposed (see section 8) that the origin of the problem (null values of the influence line for the 1st Fourier term) could be overcome by using coefficient φ', as it was discussed in section 3.1 in this document. Therefore, the improvements proposed in the RP6 will be implemented and tested in Task 1.4.

- 3.1.9. A number of case studies were analysed in milestone MS4, in relation to this potential shortcoming. However, the subsequent analysis in depth of the variants of PTs and FTs has shown that there exist many possible cases where the train length deviates from an exact multiple of the repeating vehicle length. Therefore, this shortcoming is not studied as an independent KS here, but various suitable

vehicle types will be scrutinised in different sections of this document: coupled units, nonsymmetric trains, and others. In all of them, the train length deviates from an exact multiple of the repeating vehicle length, and the consequences thereof will be investigated.

- 3.1.10. Inaccuracies in the computation of displacements are investigated here as a **KS**.

- 3.1.11. Limitations of SM related to train speed are be investigated here as a **KS**. However, speed cannot be separated from wavelength for a given bridge. Therefore, this shortcoming will be analysed in conjunction with 3.1.7 above.

- 3.1.12. Deficiencies of SM related to lack of symmetry of trains are investigated here as a **KS**.

- 3.1.13. Limitations of SM for analysis of SS decks should also be considered as a **KS**. However, those shortcomings should in principle be revealed from all previous points. Therefore, 3.1.13 will not be considered as a separate limitation in what follows.

- 3.1.14 and 3.1.15 have been discussed in relation to key shortcomings 3.1.1 and 3.1.2.

- 3.1.16. Deficiencies of SM in the analysis of portal frames are investigated as a **KS**, in conjunction with shortcomings 3.1.1 and 3.1.2 mentioned above.

- 3.1.17 The shortcoming mentioned in the RSSB Guideline bears relation also to 3.1.3 and 3.1.7, in the sense that the train signature is not valid to compare trains, particularly at not well-developed resonant conditions. To date, no formulation has been found that allow a comparison of trains with general validity and independently of all bridge characteristics. Instead, from the analysis of the KS mentioned so far, in section 9.2 a novel SM is proposed that can be used for fast calculation of a bridge's response, and shows that the effect of span length L should at least be considered in a train comparison aimed to cover all scenarios.

4.2 Key shortcomings of SM — Summary

Following the review in section 3.1, the following list of key shortcomings (KS) is investigated here. The strategies to analyse the KS and the sections in this document dedicated to each one are summarised in section 5.3:

KS-1 (≡3.1.1+3.1.2+3.1.16). Valid only in **SS bridges where only the first bending mode is considered** [*i.e.* it neglects torsion, and bridge types other than SS (for instance, portal frames or multi-span continuous bridges)]. The influence of higher bending or torsion modes, and local plate modes, is neglected to investigate KS-1.

KS-2 (≡3.1.4). Not valid for **short trains and short subtrains** where dynamic excitation does not arise from fully developed resonance.

KS-3 (≡3.1.5). Not valid for **irregular train architectures**: trains where the spacing of axles varies from the normal pattern within the train (excluding the cases of non-regular distances in the end power cars, which are dealt with in KS-4 below).

KS-4 (≡3.1.6). Inaccurate prediction of **transient forced response**: critical cases that occur whilst a train is on a bridge before the whole length of the train has passed over the bridge (for example the case of an end power car or locomotive with different axle spacings to the remainder of the train).

KS-5 (≡3.1.12). Not valid for **non-symmetric train formations**.

KS-6 (≡3.1.7+3.1.11). Not suitable for comparing the load effects of trains on **short span bridges** or for excitation from **short wavelengths**. Influence of the **speed of trains** in the accuracy of SM to be investigated.

KS-7 (≡3.1.10). Limitations for computing vertical **displacements**.

One final shortcoming is also investigated in, relation to the findings of ERRI D214:

KS-8 (≡2.1(A)+2.2(B)). Inaccuracies arising due to the presence of **heavier front power cars**, specifically at K≈0.5.

The comment about too weak accelerations for $K<1/3$ mentioned in milestone MS4 is not further investigated here. After consideration of that aspect, it was understood that D214 was referring to the problem of the low predicted *minimum* values (at the RIL cancellations), which is a direct consequence of methods DER and LIR: the so-called *zeroes* (ERRI D214 1999). This limitation can only be overcome if the "impact" response is considered as well, in a manner similar to point (B) in section 3.1. Or by the application of other strategies that consider the forced vibration, as will be discussed in section 9.

5 Methodology

5.1 Rolling stock considered for Tasks 1.3 and 1.4

5.1.1 Series of equidistant loads (EQD trains)

EQD "trains" are series of equidistant, 170 kN loads, used for basic analysis of SM.

Three EQD trains are considered: EQD-6, which consists of six loads, EQD-12 with twelve loads, and EQD-18 with eighteen loads. Each EQD train contains 21 series of loads with increasing "coach length" D (distance between consecutive loads), from D=10 m to D=30 m, in steps of 1 m.

5.1.2 General considerations about rolling stock for Tasks 1.3 and 1.4

The train data for the analyses developed here have been retrieved from Task 1.1, coordinated by HUD. Those data include the database inherited from previous projects In2Track2 and In2Track3 (in what follows it will be referred to as "I2T2 database"), plus the database received from the DZSF project.

In the introduction of the ERA Technical Note (ERA, 2022), the following (*in blue italics*) is established about the rolling stock to be considered:

[...] further research to evaluate the dynamic behaviour of the bridges during train passage using the DER method and the time step integration calculation (TSC) for a set of representative bridges together with the following representative train data is needed:

(i) Conventional and articulated Multiple Unit (MU) (for 200km/h - 160 km/h)
(ii) Conventional Double Deck MU (for 200km/h - 160 km/h)
(iii) Conventional and articulated high speed train with similar axle loads (for 320 km/h)
(iv) Loco hauled train pulled and pushed (Railjet for 250 km/h)
(v) Conventional high-speed train with power head (ICE 2 for 280km/h)
(vi) Freight trains with long and short wagons
(vii) 2 more train families (e.g., Talgo-ECx)

Within this document, passenger trains (PT) with maximum operation speed V_{max} > 160 km/h are considered as an excitation for railway bridges, in addition to freight trains (FT). That ensemble of trains comprises the types of rolling stock described in points (*i*) to (*vii*) above. Given that the number of trains considered is large and a wide variety of vehicles is included, the same trains for V_{max} > 160 km/h are also considered as the source of excitation to test the performance of SM for speeds below 160 km/h, in addition to freight trains.

5.1.2.1 Initial filtering of PT trains

An initial filtering of PTs is carried out to remove trains that are very similar among them, considering reference tolerances of 0.10 m in distance, and 7.5 kN in axle load. The reference tolerance in distance is adopted as 10% of the wheelbase of a short, 2.0 m bogie. The reference tolerance in force is adopted as 5% of a 150 kN axle load. In those cases of similarity, the vehicles with higher axle loads are retained.

Trains with max. speeds only slightly above 160 km/h are removed as well (161 to 163 km/h). After the initial filtering, 201 CB trains, 39 AB trains and 40 SA trains are retained which for the PT database considered in this report. Those trains are described in an anonymous manner in Appendix B.

5.1.2.2 Train series and subtypes

PTs of types CB, AB and SA are classified here in *series*, and in *subtypes*. While the series refer to research focussed on particular key shortcomings (shorts, non-symmetric, etc.), the subtypes convey information about the type of (time-history) bridge response that one can expect in principle from a given train.

The selection process was conducted using a hybrid approach, combining algorithmic pre-classification with a manual verification stage to ensure that no train with genuinely distinctive characteristics was inadvertently excluded.

The classification in **four main series (short, symmetric, nonsymmetric, end-transient)** is carried out based on the following criteria:

- Trains with total length below 150 m are considered ***short***, with small margin of few meters to not exclude relevant cases
- Trains are classified in ***symmetric*** or ***nonsymmetric*** with tolerances of 0.10 m, and 7.5 kN. If both tolerances are respected for all axle loads, then the train is classified as "symmetric", otherwise, it is classified as "nonsymmetric".
- Whenever there exists an irregular distance within the last 8 loads of a train (*i.e.* a wheelbase not repetitive in comparison with those in previous carriages) by more than 1.5 m (50% of a long, 3.0 m bogie), then the train is assigned to the series named ***end-transient***.

The classification in subtypes is partially dependent on the train type; therefore it is discussed below separately for CB, AB and SA trains.

5.1.3 Conventional passenger trains (CB trains)

As mentioned previously, the train subtypes convey information about the type of time-history bridge response that one can expect in principle from a given train. For CB trains, the following subtypes are defined in Table 2:

Table 2: List of subtypes for CB trains – No locomotive heavier axles present.

Subtype	Description
RP	Stands for "repetitive pattern", which refers to a train subtype where the pattern of all axle distances (including power cars, if those are present) shows perfect periodicity, with no irregularity in the axle spacings. Small deviations are admitted for this subtype, of the order of 0.30 m. Either the train is a single unit, or it resembles a single unit in practical terms. No heavier (>15%) locomotive axles are present in the front/rear end carriages. Sixty-one (61) trains belong to this category.
MU	"Multiple units", is the case of a CB train that is declared as being a single unit in the I2T2 or DZSF databases, with no heavier (>15%) locomotive axles present in the front and end carriages, and where the 0.30 m tolerance for being classified as RP is not fulfilled. Twenty-eight (28) trains belong to this category.
CMU	"Coupled multiple units", is visually similar to an MU and fulfils the same criteria mentioned above, but in the I2T2 or DZSF databases is declared to have more than one unit. The type of dynamic response in principle may produce transient phenomena similar to MUs. Fifty-six (56) trains belong to this category.

CMU-2-RP	"Coupled multiple units: two RPs". In the I2T2 or DZSF databases is declared to have two units. Both of those units are RPs, and are coupled in the middle of the train formation by an irregular distance so that the vehicle, as a whole, cannot be considered a single RP. Seven (7) trains belong to this category.

5.1.3.1 Loco-hauled trains (regarding axle forces)

Aside from these four basic CB subtypes, there is also a variety of CB loco-hauled trains. In this document, a train is classified as "loco-hauled" if **markedly heavier axle forces** are present in the front and/or rear end carriages. Those heavier axle forces are of interest to analyse the caveats of SM mentioned in section 3.1, point (A). The irregularities in the bridge response due to different **axle distances** in the rear part of a train are discussed additionally by means of the series *end-transient*, as defined in section 5.1.2.2).

Those loco-hauled trains are classified here in subtypes with acronyms that start all of them by "LH". For AB trains, the acronyms start by "ALH" (articulated), and for SA trains they start by "RLH" (regular).

If the locomotive axles are more than 30% heavier than the average of the 4 adjacent loads, then the locomotive is considered "heavy". If the locomotive axles are between 15% and 30% heavier than the average of the 4 adjacent loads, then the locomotive is considered "light". If the locomotive axles are less than 15% heavier than the average of the 4 adjacent loads, then trains is not considered LH/ALH/RLH in this report.

With the considerations above, the following LH subtypes are defined in Table 3:

Table 3: List of subtypes for CB trains – With locomotive heavier axles present.

Subtype	Description
LH-fHL	Loco-hauled with one front heavy locomotive. Eight (8) trains belong to this category.
LH-rHL	Loco-hauled with one rear heavy locomotive. Eight (8) trains belong to this category.
LH-bHL	Loco-hauled with both one front and one rear heavy locomotives. Twelve (12) trains belong to this category.
LH-bLL	Loco-hauled with both one front and one rear light locomotives. Three (3) trains belong to this category.
LH-fHLrLL	Loco-hauled with one front heavy locomotive and one rear light locomotive. Two (2) trains belong to this category.
CLH-bHL	Coupled loco-hauled units, with both one front and one rear heavy locomotives (two power cars, in total). One (1) train belongs to this category.
CLH-mHL	Coupled loco-hauled units, where all units have both one front and one rear heavy locomotives (number of power cars is twice the number of units). Eleven (11) trains belong to this category.
Irregular	Coupled loco-hauled units, where locomotives are multiple, but the front and/or rear ends of the train do not have any power car. Three (3) trains belong to this category.

RP trains belong to all the three PT types: CB, AB and SA; therefore, in each case both the type and subtype will be appropriately specified throughout the document.

Conversely, the rest of subtypes belong only to one type; therefore, by only mentioning the subtype it can be known whether the vehicle is of CB, AB or SA type. Figures 1 to 6 show some representative examples of CB train subtypes (head of the train shown on the left).

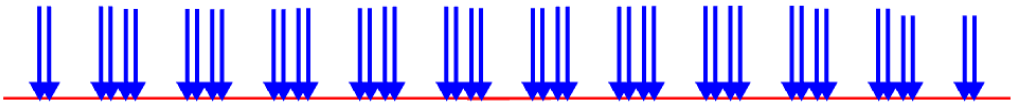

L_{tot} = 258.7 m

D = 23.9 m

P_{max}= 142.0 kN

P_{min} = 125.2 kN

P_{tot} = 6066 kN

Figure 1: Example of a CB, RP train [INB4EU-CB-006].

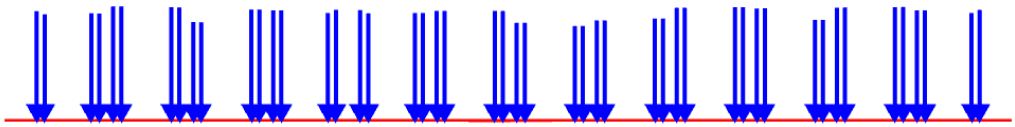

L_{tot} = 293.3 m

D = 24.9 m

P_{max}= 185.3 kN

P_{min} = 150.6 kN

P_{tot} = 8352 kN

Figure 2: Example of a MU train [INB4EU-CB-046].

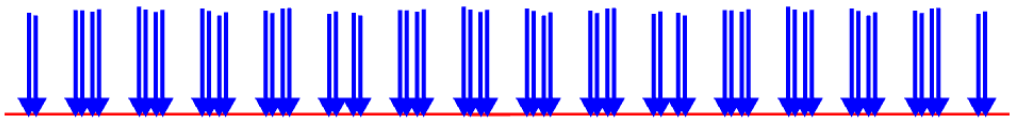

L_{tot} = 390.5 m

D = 25.9 m

P_{max}= 167.3 kN

P_{min} = 151.9 kN

P_{tot} = 9582 kN

Figure 3: Example of a CMU train [INB4EU-CB-128].

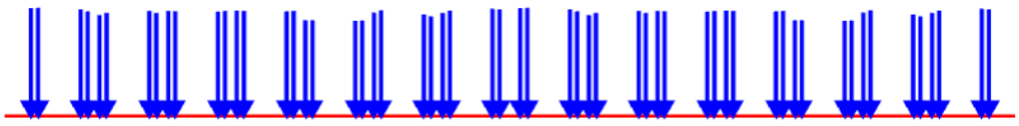

L_{tot} = 365.7 m

D = 26.2 m

P_{max}= 174.1 kN

P_{min} = 151.0 kN

P_{tot} = 9253 kN

Figure 4: Example of a CMU-2RP [INB4EU-CB-052].

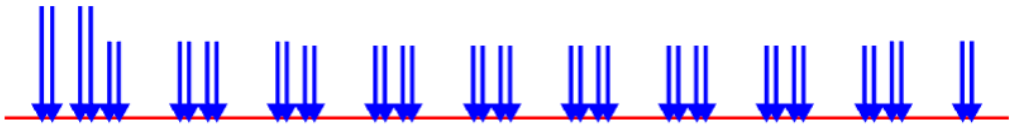

L_{tot} = 251 m
D = 26.4 m
P_{max}= 213.4 kN
P_{min} = 131.8 kN
P_{tot} = 5705 kN

Figure 5: Example of a LH-fHL train.

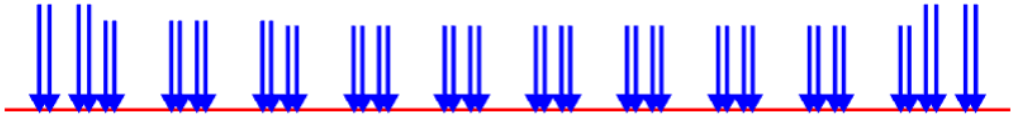

L_{tot} = 271.2 m
D = 26.4 m
P_{max}= 169.2 kN
P_{min} = 131.8 kN
P_{tot} = 6167 kN

Figure 6: Example of a LH-bLL train.

5.1.4 Articulated passenger trains (AB trains)

Since AB train variants are less in number, all the associated subtypes are grouped in Table 4. Few variants of loco-hauled trains are found, in the understanding that locomotives must be either "light" or "heavy" as described in previous subsection. However, some other particularities arise, as described in Table 4. Figures 7 to 10 show some representative examples of AB train subtypes (head of the train shown on the left).

Table 4: List of subtypes for AB trains.

Subtype	Description
RP	Same definition as for CB, RP trains. One (1) train belongs to this category.
ART	"Articulated". ART subtype trains are nearly equal to AB, RP trains, except for the fact that the end carriages are slightly shorter and the 0.30 m tolerance is not fulfilled. Five (5) trains belong to this category.
CART	"Coupled articulated" units, where intermediate distances differ from the RP pattern. Therefore, these trains are more prone to create transient phenomena while some intermediate carriage of the train is crossing the bridge. Twenty-one (21) trains belong to this category.
CART-2-ART	"Coupled articulated units: two ARTs", in a manner analogous to CMU-2-RP subtype defined for RP trains. Five (5) trains belong to this category.
ALH	"Articulated loco-hauled". The train has conventional CB power cars in both ends, not heavier than 15% of the average of the adjacent loads. Three (3) trains belong to this category.
CALH-2-ALH	"Coupled articulated loco-hauled: two ALHs"; in a manner analogous to CMU-2-RP subtype defined for RP trains, these are two identical units coupled. One (1) train belongs to this category.

ALH-fLL	Articulated loco-hauled with one front light locomotive. One (1) train belongs to this category.
ALH-rLL	Articulated loco-hauled with one rear light locomotive. One (1) train belongs to this category.
ALH-bHL	Articulated loco-hauled with both one front and one rear heavy locomotives. One (1) train belongs to this category.

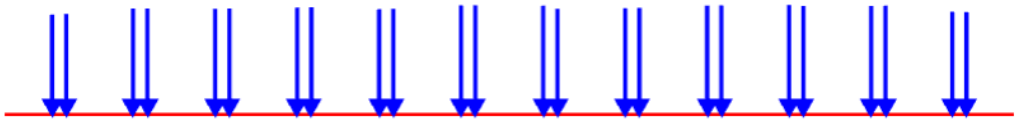

L_{tot} = 192.9 m

D = 17.3 m

P_{max}= 175 kN

P_{min} = 157.8 kN

P_{tot} = 4068 kN

Figure 7: Single case of AB, RP train [INB4EU-AB-001].

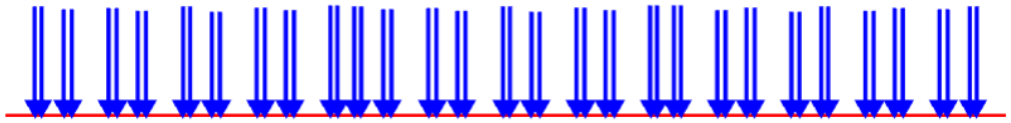

L_{tot} = 324.0 m

D = 10.0 m

P_{max}= 178.9 kN

P_{min} = 167.6 kN

P_{tot} = 9367 kN

Figure 8: Example of a CART train [INB4EU-AB-030].

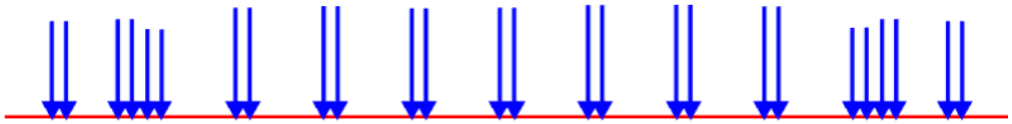

L_{tot} = 193.2 m

D = 19.0 m

P_{max}= 198.4 kN

P_{min} = 151.5 kN

P_{tot} = 4694 kN

Figure 9: Example of a ALH train [INB4EU-AB-004].

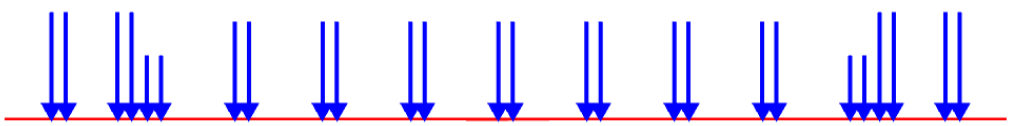

L_{tot} = 193.1 m

D = 19.0 m

P_{max}= 168.6 kN

P_{min} = 93.4 kN

P_{tot} = 3854.3 kN

Figure 10: Single case of ALH-bHL train [INB4EU-AB-008].

5.1.5 Regular passenger trains (SA trains)

Regular PTs are divided into RPs and loco-hauled vehicles. As it happens with both the ALH and CALH-2-ALH subtypes, in this case the power cars of all SA trains are neither "light" nor "heavy"; therefore all of them have axle loads below the 15% threshold defined in section 5.1.3; thus, the subtype acronyms do not have an intermediate "L" or "H" to distinguish "light" from "heavy" locomotives. Nevertheless, the number of variants of loco-hauled regular PTs is rather large (eleven different configurations), therefore not all of them will be considered separately for analysis of SM. However, for completion all subtypes are gathered in Table 5. Figures 11 to 15 show some representative examples of SA subtypes (head of the train shown on the left).

Table 5: List of subtypes for SA trains.

Subtype	Description
RP	Same definition as for CB, RP trains, with a particular consideration of the end bogies typically present in this subtype (see Figure 11). Those bogies are merged into a single axle load at the bogie mid-point, to verify the 0.30 m tolerance mentioned in Table 2. Thirteen (13) trains belong to this category, all of them with coach length of 13.3 m.
RLH-fL	Regular loco-hauled with one front locomotive. Two (2) trains belong to this category.
RLH-2fL	Regular loco-hauled with two front locomotives. Three (3) trains belong to this category.
RLH-3fL	Regular loco-hauled with three front locomotives. One (1) train belongs to this category.
RLH-rL	Regular loco-hauled with one rear locomotive. Two (2) trains belong to this category.
RLH-2rL	Regular loco-hauled with two rear locomotives. Three (3) trains belong to this category.
RLH-3rL	Regular loco-hauled with three rear locomotives. One (1) train belongs to this category.
RLH-bL	Regular loco-hauled with both one front and one rear locomotives. Five (5) trains belong to this category.
RLH-sCbL	Regular loco-hauled with both one front and one rear locomotive, where the car adjacent to the locomotives is shorter. Three (3) trains belong to this category.
RLH-2fLrL	Regular loco-hauled with two front locomotives and one rear locomotive. Three (3) trains belong to this category.
RLH-fL2rL	Regular loco-hauled with one front locomotive and two rear locomotives. Three (3) trains belong to this category.
CRLH-mL	Double unit with multiple locomotives (two RLH-bL units coupled). One (1) train belongs to this category.

For the SA trains, only the loads of the carriage adjacent to a power car are considered to verify the 15% threshold, even if they are in total less than four axles.

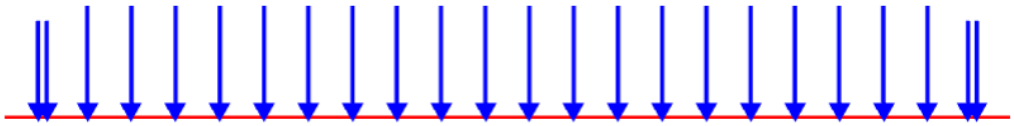

L_{tot} = 282.4 m

D = 13.3 m

P_{max}= 211.9 kN

P_{min} = 181.5 kN

P_{tot} = 4964 kN

Figure 11: Example of a SA, RP train [INB4EU-SA-017].

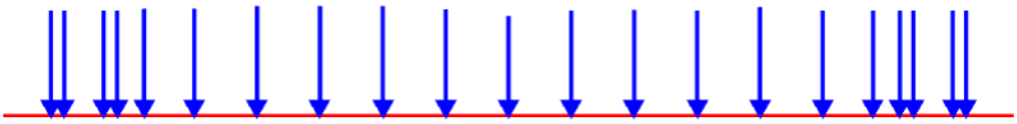

L_{tot} = 191.3 m

D = 13.1 m

P_{max}= 174.6 kN

P_{min} = 157.0 kN

P_{tot} = 3531 kN

Figure 12: Example of a RLH-sCbL train [INB4EU-SA-004].

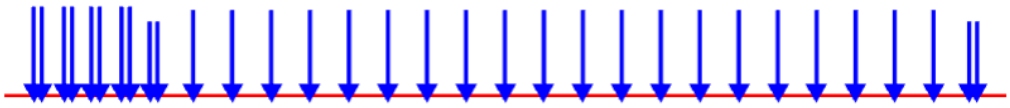

L_{tot} = 321.9 m

D = 13.3 m

P_{max}= 220.7 kN

P_{min} = 181.5 kN

P_{tot} = 6730 kN

Figure 13: Example of a RLH-2fL train [INB4EU-SA-021].

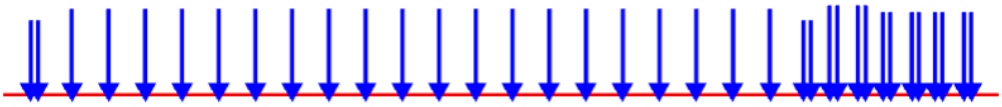

L_{tot} = 340.4 m

D = 13.3 m

P_{max}= 220.7 kN

P_{min} = 181.5 kN

P_{tot} = 7475 kN

Figure 14: Example of a RLH-3rL train [INB4EU-SA-035].

L_{tot} = 395.7 m

D = 13.22 m

P_{max}= 189.3 kN

P_{min} = 164.8 kN

P_{tot} = 7381.0 kN

Figure 15: Single case of CRLH-mL train [INB4EU-SA-040].

5.1.6 Freight trains (FT)

Freight trains considered in this research are a limited subset of those included in the InBridge4EU database compiled by HUD. From the initial 153 FTs in that database, the filtering process applied here is as follows.

Trains with three types of wagon are present in the database: conventional (129 trains), regular (15 trains), and twin wagon conventional (9 trains). For similar values of *D*, with the same type of wagon and a similar number of loads, those trains with the heaviest axles are retained. The aim is to have trains with very few loads, others with an intermediate number of loads around 40-50, and then, moving on to longer trains with even more than 100 loads and up to 600 m in length. In total 22 trains with conventional wagons, 6 trains with regular wagons and 2 trains with twin wagons are retained, for a total of 30 FTs considered in what follows for Tasks 1.3 and 1.4.

Those 30 FTs are ordered by placing the selected two twin wagons trains first, then the six regular wagon trains, and finally the 22 conventional wagon trains. The latter are ordered by placing the five clearly shortest trains first (none exceeding 150 m, arranged in ascending order of loads number and *D*), and then, since the remaining ones are all trains with a minimum length greater than 180 m, they are ordered simply by *D*.

5.1.7 Summarised information about the PTs and FTs for Tasks 1.3 and 1.4

As mentioned before, the PTs are described in an anonymous manner in Appendix B. Then, the FTs are summarised in Appendix C in analogous form.

All the train characteristics can be retrieved from the four accompanying Matlab® files named:

- Conventionals_V_gt_160.mat
- Articulated_V_gt_160.mat
- Regulars_V_gt_160.mat
- Freight_trains_InB4EU.mat

5.1.8 Additional trains for specific analyses

In the sections listed below, additional train models have been considered to study specific aspects of the SM performance. Those models are described in detail in the corresponding sections:

- Section 7.1.2: analysis of short trains (KS-2).
- Section 7.3: train lengths that deviates from an exact multiple of the repeating vehicle length (KS-4).
- Section 7.5: analysis of non-symmetric trains (KS-6).

5.1.9 Load model PT60: a summary of passenger train types, subtypes and series

In previous sections it has been shown that the variety of vehicles included within the three PT types (CB, AB and SA) is wide, and a comprehensive ensemble of dynamic effects (resonance, partial resonance, impact, intermediate transients, end transients) can thus be expected from those PT, for the sake of assessing the limitations of SM.

Besides, the analyses carried out in this document will consider low speeds starting at 50 km/h, therefore the dynamic response at those low speeds and short wavelengths will also be investigated.

For those reasons, a train ensemble—extracted from the full set of PTs—that collects a selection of train configurations as wide as possible is desirable, with a view to test new proposals of SM. Hence, with **model** named here as **PT60** an effort has been done to synthesise, with a limited number of vehicles, the various patterns of axle loads/distances into a single load model, representative of all distinct and relevant potential dynamic effects. Such model is thus a principal means of comparison of the performance of various analysis methods, and particularly new versions of SM vs. TSC methods.

PT60 model has a total of 60 different passenger trains among CB, AB and SA types, will all its main subtypes (including a variety of loco-hauled cases). Both shorter and longer trains have been considered in it, with car lengths D covering a range as wide as possible. The 10 HSLM-A have also been included. Among similar trains, those with stronger signature have been retained. Relevant trains mentioned in discussion with other partners of *InBridge4EU* have been also included.

The organisation of PT60 begins with the trains more regular as regards the axle distances, and gradually incorporates vehicles where the patterns of distances are more irregular, ending with loco-hauled trains and trains with intermediate power cars.

In an anonymous manner, the trains contained in model PT60 are described in Appendix D. A summary of the PT60 vehicles, in the same order as they appear in Appendix D, follows below:

- Ten (10) RPs of CB, AB and SA type, with $13.31 \leq D \leq 28.8$ m (in ascending order of D).
- One (1) ART train with $D = 15.8$ m.
- Two (2) CMU-2-RP trains with $D = 26.2$ m and with $D = 27.2$ m (in ascending order of D).
- One (1) CART-2-ART train with $D = 17.5$ m.
- Four (4) MU trains, with $23.8 \leq D \leq 25.9$ m (in ascending order of D).
- Four (4) CMU trains, with $25.6 \leq D \leq 26.4$ m (in ascending order of D).
- Five (5) CART trains, with either $D = 10.0$ m or $D = 18.5$ m (in ascending order of D).
- One (1) ALH train with $D = 19.0$ m.
- Ten (10) additional ALH trains with $18.0 \leq D \leq 27.0$ m (HSLM-A model).
- Twenty-two (22) trains with various loco-hauled configurations, including the following subtypes in order: CALH-2-ALH, ALH-fLL, LH-fHL, RLH-2fL, LH-rHL, RLH-3rL, RLH-bL, RLH-sCbL, RLH-2fLrL, LH-fHLrLL, ALH-bHL, LH-bHL, CLH-bHL, CRLH-mL, CLH-mHL, Irregular (some subtypes are represented by more than one train, of significantly different D, or total length).

In total, according to the criteria described in section 5.1.2.2:

- Twenty-four (24) trains in model PT60 are symmetric and thirty-six (36) are nonsymmetric.
- Twelve (12) trains in model PT60 are short.
- Thirty-three (33) trains in model PT60 belong to the end-transient series.

5.2 Bridges considered for Tasks 1.3 and 1.4

For the analysis of the eight KS and validation of the proposed improved methods, an ensemble of SS spans from 4.0 m to 40.m will be considered, with a short step in the span length. Regarding bridges of spans shorter than 4.0 m, in (Grunert et al., 2025) it is mentioned that the structural dynamics of such bridges cannot be

accurately unified with those of larger span ranges. Linear masses of the bridges are be selected with low, but realistic values, in order to maximise the dynamic effects. For the same purpose, conservative damping values are taken as stipulated in EN1991-2:2023, section 8.4.6.3.1. Natural frequencies are selected in the lower limit of figure 8.10 in EN1991-2:2023.

As regards the selection of the representative SS, PSC bridges, those considerations are described in detail in (Museros et al., 2021) or (Museros et al., 2024). Following those references, PSC linear mass is

$$m\left(\frac{\text{kg}}{\text{m}}\right) = 4900 + 400 \cdot L \qquad (L \text{ in m}) \tag{11}$$

which has been found to be a reasonable lower bound in comparison to the PSC bridges available in the Project's database. Additionally, for STC bridges, linear mass is adopted from recommendations of DIBRST group (CEN, 2023b) as

$$m\left(\frac{\text{kg}}{\text{m}}\right) = 2000 + 100 \cdot L \qquad (L \text{ in m}) \tag{12}$$

In section 8.1 the linear mass will be incremented by 80%, to consider realistic values for double-track bridges. In sections 8.2, 10.3, 10.4 and 13 the properties of mass, frequency and damping will be extended directly to 2-span continuous beams; given that natural frequencies considered here are low, and linear mass represents in general a lower limit for PSC and STC bridges, such extension is considered a reasonable approximation to investigate the response of 2-span beams. Ad-hoc values of mechanical properties will be adopted in sections 8.3 11 to investigate the behaviour of ERS beams and portal frames.

5.3 Strategies to investigate the key shortcomings

In general, the eight KS are investigated by selecting the most appropriate rolling stock from the types, subtypes and series defined in section 5.1, and conducting comparative studies on the bridges described in section 5.2, to highlight any perceived trends and limitations related to each KS.

As an example, KS-2 is investigated by computing and comparing the error levels of methods DER and LIR when applied to the analysis of corresponding "short" *vs*. "long" sequences of EQD trains and CB RP trains (*i.e*., the most regular rolling stock as regards axle distances). Those error levels are quantified by means of so-called *exceedance maps*—and other associated post-processing techniques explained in section 0.

KS-6 and KS-7 are constant exceptions to this general approach, in the sense that they are investigated alongside each of the other KSs in a transversal manner.

The ranges considered in each exceedance map are: spans L from 4.0 to 40.0 m in steps of 0.1 m; speeds V from 50 to 400 km/h in steps of 1.0 km/h. This gives a total of 126711 (L,V) points per map.

The above-mentioned maps allow an objective measurement of the relative error, both in conservative and non-conservative scenarios, encountered in the prediction of the fundamental outputs of the bridge's response (vertical acceleration and midspan displacement) obtained by any two different approaches. It can mean the error incurred either when comparing a SM *vs*. TSC, a SS bridge *vs*. a 2-span bridge, a SS bridge under bending *vs*. a SS bridge with both bending and torsion considered, etc. Furthermore, these maps capture the dependence of the relative error on L, V, and λ, thus integrating the analysis of KS-6 and KS-7 with the rest of the study.

For further information, the so-called *exceedance analysis* is described in (Museros et al., 2021) or (Museros et al., 2024), and summarized in Appendix A in this document.

Purpose of section 6:

Also of interest to the general approach of this document is that **section 6 presents a basic comparison of DER and LIR performance *vs*. TSC, for five representative types of rolling stock (EQD, RP, CART, loco-hauled and FT), in such a manner that those findings form a basis for the subsequent analysis of KS carried out specifically in sections 7, 8.**

Purpose of section 7:

From the basis obtained in section 6, SM applied to irregular train architectures can be compared to SM applied to RP vehicles (KS-3, see section 7.2), and SM applied to non-symmetric rolling stock can be compared to corresponding symmetric versions of the same trains (KS-5, see section 7.17.4). The approach to KS-2 for analysing short trains was discussed earlier in this section and is developed in section 7.1.

In section 0, KS-4 delves more deeply into the transient phenomena that affect SM, which sometimes (though not always) are because of end power cars, linking that analysis also with effects of initial power cars. Finally, KS-5 is also a more specific investigation of a phenomenon visible in both DER and LIR that will be referred to here as *convex slopes*, and will be discussed later (see section 7.5).

Fundamental assumptions of the analyses in sections 6 and 7:

As mentioned above, the strategy is based on exceedance analyses. Two possibilities are considered: the TSC predicts an acceleration/displacement response higher than a SM by 10% or more in amplitude (therefore such SM is not conservative), or, conversely, the TSC predicts an acceleration/displacement response lower than a SM by 10% or more in amplitude (therefore such SM is excessively conservative). **The first case will be referred to as *negative exceedance*, and the second case as *positive exceedance*[2].** In these two sections only the SS beams in bending mentioned in section 5.2 will be considered, with a view to understand the fundamentals of the phenomena involved.

The first bending mode is considered for this analysis only, given that in SS beams the main resonance situations are typically associated to such mode. In that regard, the considerations mentioned in section 4.1 (*Analysis of the reported shortcomings*) apply here as well.

As for the effects of longitudinal load distribution, they are taken into account by means of reduction factors for a 2.5 long triangular footprint. The correct versions for use with accelerations and displacements were reviewed by Moliner *et al*. (2024).

Purpose of section 8:

Complementing sections 6 and 7, section 8 is instead devoted to investigating KS-1, *i.e*. the limitations of SM in bridges not SS, considering two fundamental structural types where more than one mode is relevant, as well as portal frames. The specific hypotheses considered in section 8 are described therein, along with the previous description of bridges provided in 5.2.

[2] "positive exceedance" cannot be understood as a positive result either because it implies over conservatism; however, for numerical processing it is convenient to distinguish the two possible types of relative errors by means of a ± sign.

5.4 Additional error measures: Z24 plots

To support objective assessment, a zoning strategy (named "Z24" hereafter) and a set of response-based exceedance indicators are introduced, providing summarised interpretations of global dynamic effects.

Z24 strategy is established as a combination of discrete bridge span ranges and train speed ranges (see Table 6). A total of six span ranges and four speed ranges are considered. The velocity classification mimics the approach defined in Table 38 of Appendix E of the TSI Infrastructure (categories P1, P2, P3a, and P3b). However, the prefix "v" adopted in this study indicates that the classification is established exclusively from the train velocity (not axle loads):

Table 6: Distribution of the Z24 matrix.

Velocity/ Span	120–160 km/h	160–200 km/h	200–250 km/h	250–400 km/h
30–40 m	**Z21** Long spans vP3b	**Z22** Long spans vP3a	**Z23** Long spans vP2	**Z24** Long spans vP1
20–30 m	**Z17** Medium - long spans vP3b	**Z18** Medium - long spans vP3a	**Z19** Medium - long spans vP2	**Z20** Medium - long spans vP1
15–20 m	**Z13** Medium spans vP3b	**Z14** Medium spans vP3a	**Z15** Medium spans vP2	**Z16** Medium spans vP1
10–15 m	**Z9** Medium - short spans vP3b	**Z10** Medium - short spans vP3a	**Z11** Medium - short spans vP2	**Z12** Medium - short spans vP1
7–10 m	**Z5** Short spans vP3b	**Z6** Short spans vP3a	**Z7** Short spans vP2	**Z8** Short spans vP1
4–7 m	**Z1** Very short spans Conventional speeds	**Z2** Very short spans vP3a	**Z3** Very short spans vP2	**Z4** Very short spans vP1

The spatial characterization of exceedance within the Z24 domain is described through a set of zone-based indicators, namely the **maximum, mean, binary, and response-weighted mean metrics**, each providing a distinct interpretation of exceedance inside a given zone.

The domain is thus partitioned into zones Z_k, with $k = 1, 2, ..., n_z$, where each zone contains N_k analyzed points. For every point $i \in Z_k$, the exceedance value $e_{i,k}(L,V)$, the binary exceedance condition $b_{i,k}(L,V) \in \{0,1\}$ and the structural acceleration response $a_{i,k}(L,V)$ are defined as functions of the characteristic length L and the train velocity V. Moreover, a response-dependent weighting function $w_{(i,k)}$ is introduced as:

$$w_{(i,k)}(L,V) = f\left[a_{i,k}(L,V)\right];\ 0 \le w_{(i,k)} \le 2 \tag{13}$$

which enables the relevance of structural response to be considered into exceedance assessment.

The **maximum exceedance** indicator reported in zone k is defined as:

$$I_{max}^{(k)}(L,V) = \max_{i \in Z_k} e_{i,k}(L,V) \tag{14}$$

and the **mean or average exceedance** indicator is computed as:

$$I_{mean}^{(k)}(L,V) = \frac{1}{N_k}\sum_{i \in Z_k} e_{i,k}(L,V) \tag{15}$$

thus quantifying the overall exceedance intensity within the zone.

A geometric interpretation of exceedance prevalence is provided by the **binary** indicator as:

$$I_{bin}^{(k)}(L,V) = \frac{100}{N_k}\sum_{i \in Z_k} b_{i,k}(L,V) \tag{16}$$

Finally, bridge response is incorporated through the **weighted mean** indicator as following:

$$I_{wmean}^{(k)}(L,V) = \frac{1}{N_k}\sum_{i \in Z_k} w_{i,k}(L,V) e_{i,k}(L,V) \tag{17}$$

where the weighting function assigns values varying linearly between 0.0 and 2.0 according to the reported bridge acceleration: 0.0 for null acceleration, 2.0 for acceleration equal to 7 m/s^2 or above.

The Z24 framework allows to quantify the levels of error of SM, according to the various potential shortcomings. For instance, Figure 16 shows a binary comparison between standard DER and LIR methods for the PT60 train model. The performance of LIR is found to be advantageous, yet with some excessive errors for the vP2 zones.

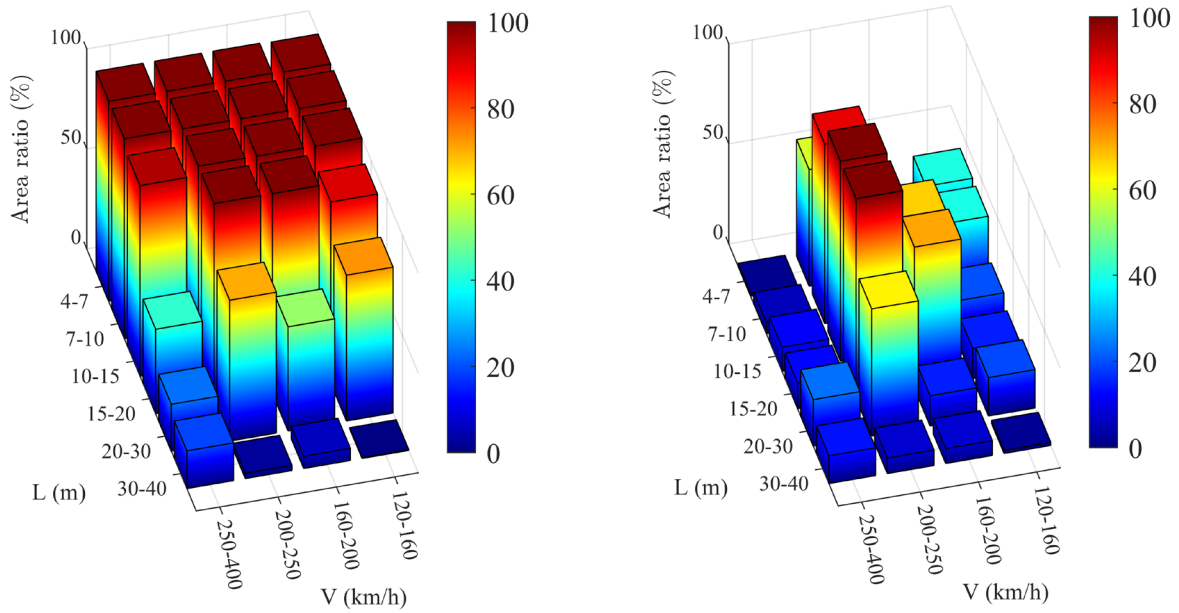

Figure 16: Z24 weighted Δα(−) for RP trains in model PT60: a) DER method; b) LIR method. PSC bridges.

In addition, Figures 17 and 18 illustrate via boxplots the variability of two Z24 indicators among all PT60 trains: DER method analysed with the mean indicator, and LIR method with the maximum indicator,

respectively. The same approach can be applied to any of the other two indicators (binary and weighted), for any train ensemble.

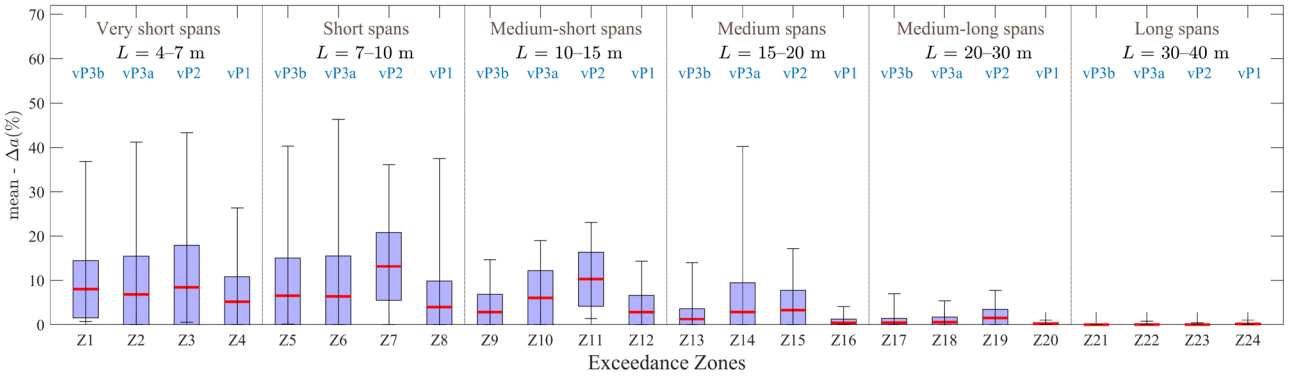

Figure 17: Box plot for DER method: Z24 mean Δa(−) for all trains in model PT60.

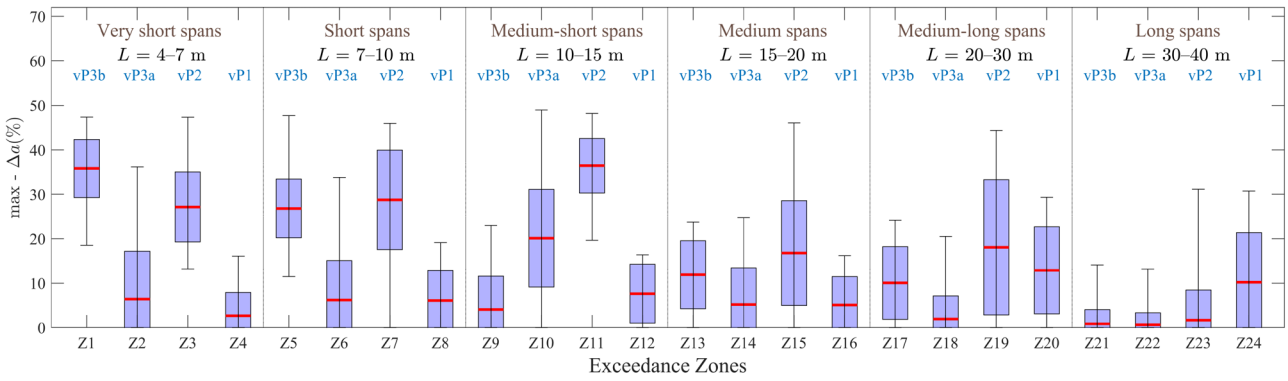

Figure 18: Box plot for LIR method: Z24 max Δa(−) for all trains in model PT60.

6 Comparison of LIR and DER methods in SS bridges

6.1 LIR vs DER methods for EQD trains (equidistant loads)

A basic analysis of the performance of both methods is presented in this section. Given that only single axle loads of 170 kN are used for all values of D, a threshold of 1.0 m/s^2 is chosen for considering acceleration meaningful (dashed horizontal lines in speed envelope plots, see for example Figure 20).

Figure 19 shows the undershooting output of DER and LIR for EQD-18 trains. Only exceedance above 10% in absolute value is shown by default throughout the document. Clear patterns are observed, where the dominant phenomena are the so-called *ascending resonant slopes* (in short, *ascending slopes*). In addition to the constant wavelength lines, discontinuous red lines in exceedance maps indicate the associated nondimensional speed K (**cancellations** K=0.33, 0.2, 0.14; **maxima** K=0.17, 0.25; other values for reference).

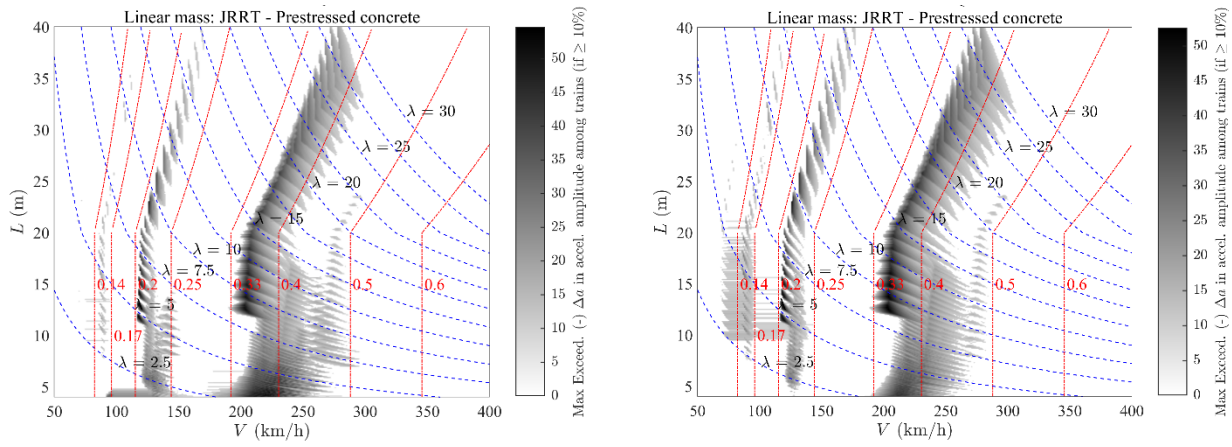

a) *b)*

Figure 19: Maps of Δa(–): a) DER and b) LIR, both vs. TSC. EQD-18 trains. PSC bridges.

Ascending slopes, as can be seen in Figure 19, are related to values of K immediately above main cancellations of the residual influence line. Therefore, they are linked to a combination of resonant and impact behaviour: the loads that have left the beam create a partial resonance, which is complemented by another part of forced vibration; because the influence line is too close to cancellation, the estimation of the partial resonance component is low, and the total predicted response is too weak.

Figure 20 shows that effect in greater detail: subfigure *a*) shows a case close to the cancellation speed K=0.33, where the influence line is close to zero, resulting in very strong undershooting; subfigure *b*), for the same train and wavelength, corresponds to a greater value of K, and, while exceedance is still above 10%, it is much lower than in subfigure *a*).

The effect of ascending slopes is stronger for EQD trains with fewer number of loads (which can be generalised for real trains with fewer number of cars), given that the smaller the number of loads, the wider is the shape of resonant peaks because resonance is developed to a lesser extent[3]. That situation is illustrated in Figure 21, where the response for the same bridge and speed is compared for train #10 of model EQD-18, vs.

[3] This phenomenon can be demonstrated theoretically.

EQD-6, showing a shaper peak for the higher number of loads. As a result, the grey patches in Figure 19 tend to be wider for EQD-12 and EQD-6 trains, which will not be shown here for brevity.

This phenomenon can be more intense for shorter spans, because resonant peaks tend to be wider for higher frequency bridges, when they are plot using the speed as abscissa. The tendency of lower subharmonics (lower values of *i*) to produce wider peaks also has an influence.

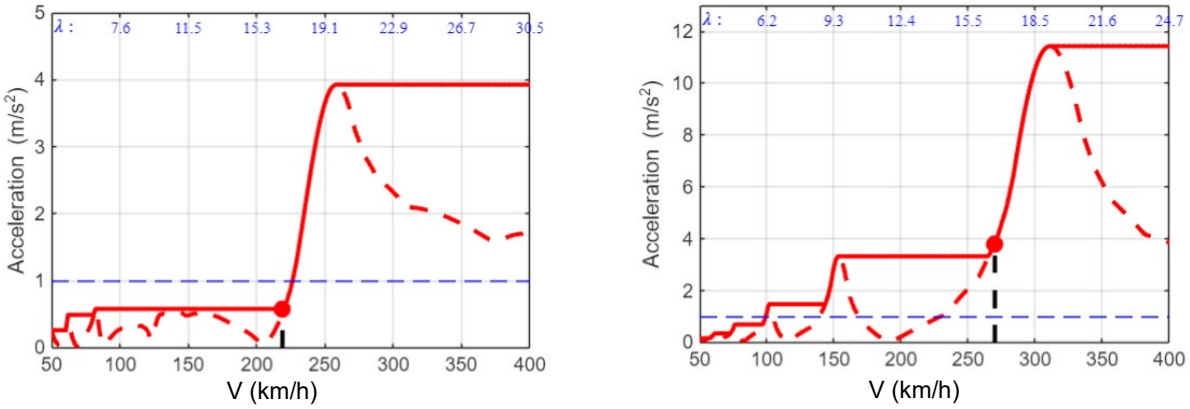

a) *b*)

Figure 20: LIR - EQD-6 train #10 (D=19 m), λ=16.7 m. PSC bridge.
a) L=23.5 m, V=219 km/h, K =0.36, Neg. Exceed = 43.7%.
b) L=17.8 m, V=270 km/h, K =0.47, Neg. Exceed = 11.0%.

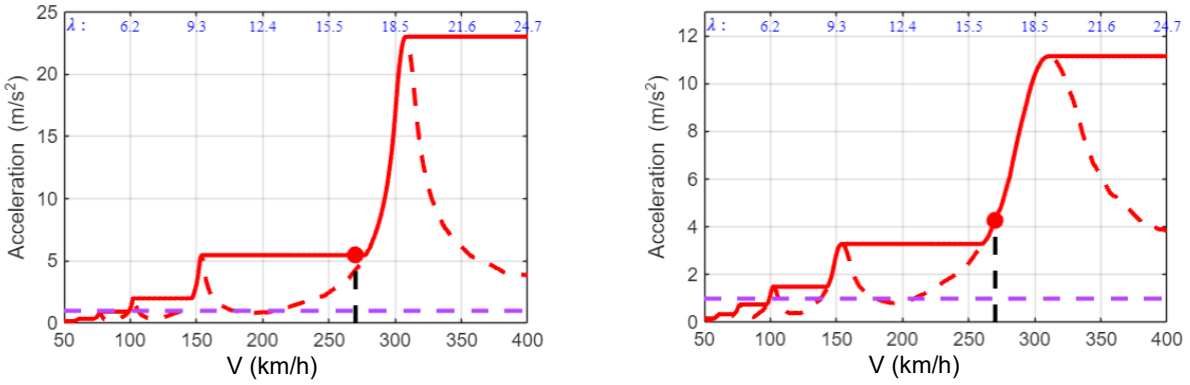

a) *b*)

Figure 21: Duhamel - λ=16.7 m. PSC bridge: L=17.8 m, V=270 km/h, K =0.47
a) EQD-18 train #10 (D=19 m); b) EQD-6 train #10 (D=19 m)

Besides, some overestimation of the LIR method in found in ascending slopes, mostly when the RIL is right after its first local maximum (*K*=0.25 approx.), see Figure 22*b*. That kind of overshooting happens for the first resonant subharmonics. As it can be seen, this effect is somewhat more pronounced when using the DER method (higher subharmonics are also affected, and the second local maximum of the RIL at *K*=0.17 approx.).

With these theoretical EQD trains, DER is also too conservative for the long spans, where long horizontal grey bands are found in Figure 22*a* due to overestimation of peak resonant amplitude, but that phenomenon becomes irrelevant when a higher threshold is set, for instance 2.5 m/s^2 (this is found to happen as well for actual regular RP trains).

Regarding the horizontal, darker grey areas in the rightmost part of both exceedance maps in Figure 22, above *K*=0.5, they obey to the phenomenon of *convex slopes*, (see section 7.5).

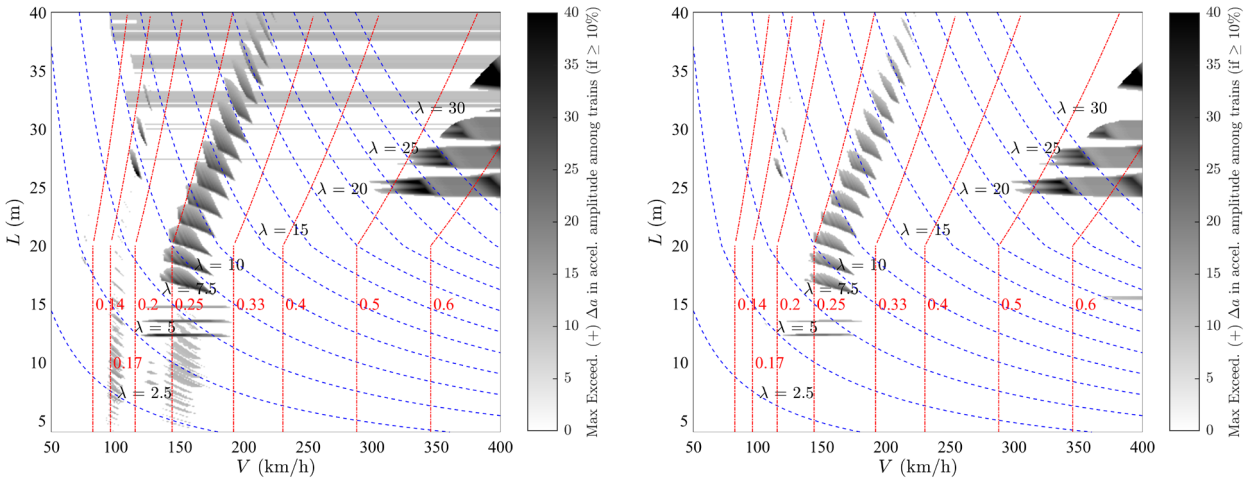

a) *b)*

Figure 22: Maps of Δa(+): a) DER and b) LIR, both vs. TSC. EQD-18 trains. PSC bridges.

The performance of SM for the computation of displacements is affected by the so-called "static contribution" of the bridge deformation. In order to have more realistic values of such contribution, the prediction of vertical displacements is carried out in the next sections, considering real PTs.

6.2 LIR vs DER methods for RP trains (regular patterns – PT)

The analysis of KS in section 4 points out that SM are considered more reliable for trains with regular architectures, which in this report are gathered in subtype named RP (for CB, AB and SA types). Nevertheless, there cases where a SM is inaccurate for a RP train are discussed below.

Negative exceedance in accelerations: Δ*a*(−)

As a first example, Figure 23 shows the case of a CB RP train with coach length D=28.6 m, where undershooting is observed in the application of LIR method, due to phenomena of ascending slopes at the 3rd and 4th subharmonics (λ=9.53 for i=3, and 7.15 m for i=4). A threshold of 2.5 m/s^2 is considered. Such negative exceedance can be expected from the results shown in section 6.1, and is also visible in a smaller area for spans close to L=35 m (1st subharmonic i=1).

However, additionally a resonance peak underestimation occurs at V=180 km/h, for a span L=11.7 m: this is due to a defective approximation of a 4th subharmonic, which in turn is caused by the last bogie of each carriage (see Figure 21). Due to the cumulative response approach used here, peak resonance underestimations (and overestimations) appear in the exceedance maps as horizontal grey patches. Conversely, ascending slopes take the form of patches following a trend closer to the inclination of constant wavelength lines.

In Figure 21, and throughout this report, the following **convention is used for time-history plots:**

Grey triangles (▽) indicate the entrance of the loads in the bridge, and green points (•) represent the values predicted by the SM, depicted at the time instants when the last load of each subtrain leaves the bridge.

Thus, Figure 21 shows that the transient phenomenon that give rise to the underestimated peak takes place when the last bogie of each carriage is still on the bridge (max. response marked as a blue point •). A closer look to that time-history would reveal that the peak takes place approximately when the bogie mid-point is at mid-span (it has crossed 47% of the span).

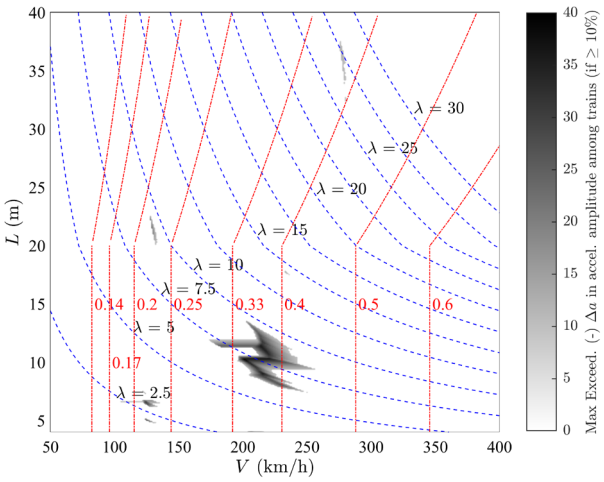

Figure 23: Map of Δa(–): LIR vs. TSC. Train INB4EU-CB-018 (D=28.6 m). PSC bridges.

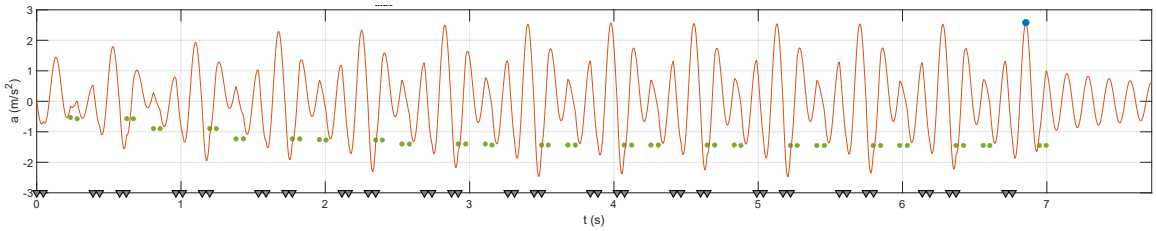

Figure 24: LIR vs. TSC. Δa(–): train INB4EU-CB-018 (D=28.6 m), V=180 km/h, L=11.7 m in Figure 20.

A phenomenon similar to the one shown in Figure 21 happens also for this train at (*L*=10 m, *V*=204 km/h. see Figure 22), which is seen in Figure 23 as well. In principle Figure 22 and Figure 21 look similar because both illustrate a fourth subharmonic. Indeed, in Figure 22 the bogie mid-point is near mid-span too, when the peak is underestimated by LIR; nevertheless, the transient phenomenon is caused by the first bogie of the carriage, and not by the last bogie.

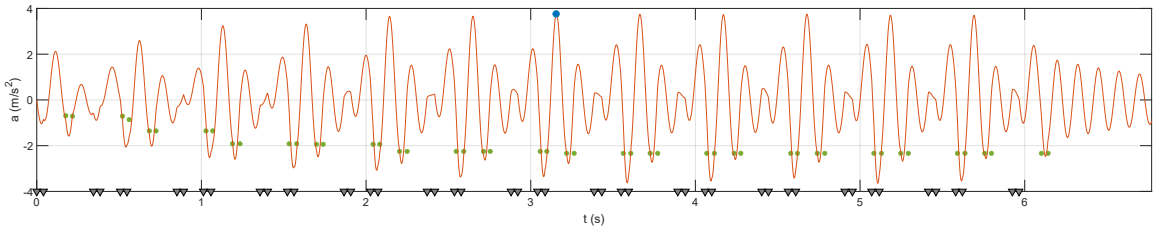

Figure 25: LIR vs. TSC. Δa(–): train INB4EU-CB-018 (D=28.6 m), V=204 km/h, L=10 m in Figure 23.

The fact that a train with regular architecture as a CB RP may produce relevant but different transients from either the front or rear bogies in its carriages—even for similar spans lengths—poses a challenge to classify, in a limited number of categories, the potential cases where SM are inaccurate for the various types of trains. This conclusion arises because one should consider as well:

- The AB RP trains, which have only one shared bogie between cars.
- The various train types with irregular distances as MU, CMU, CART, CMU-2-RP, etc.
- Finally, the numerous variants of loco-hauled trains (see section 5.1).

- All these train subtypes may produce different situations where a transient occurs with fewer of more loads in the bridge, implying one or more than one bogie at the same time, as it will be shown particularly in section 0.
- For the loco-hauled trains, the time instant when the expected transient is more relevant may be difficult to predict, due to: (a) various loads close to each other in the transition from coaches to locomotive; (b) loads of potentially different intensity.

Therefore, because the possibilities of those transient responses creating too a large exceedance are many, the approach adopted here is to combine:

- Detailed graphical information about the error levels of SM, with
- Proposals for improvement in the SM predictions in forced vibration.

The actual shape of the $\Delta a(-)$ maps depends also on the car-body length. Figure 23 shows the case of a CB RP train with D=25.9 m. The undershooting is of ascending slope type for the higher wavelengths and close to K=0.4, also for the 3rd subharmonic (λ=8.63 m, i=3). However peak underestimation close to L=10 m has now moved to L=9 m, in comparison with Figure 23. Besides, peak underestimation close to L=12 m in Figure 23 has now moved to higher K and higher λ, even if the coach length is shorter and the frequency of the bridges remains unmodified for each span in both figures.

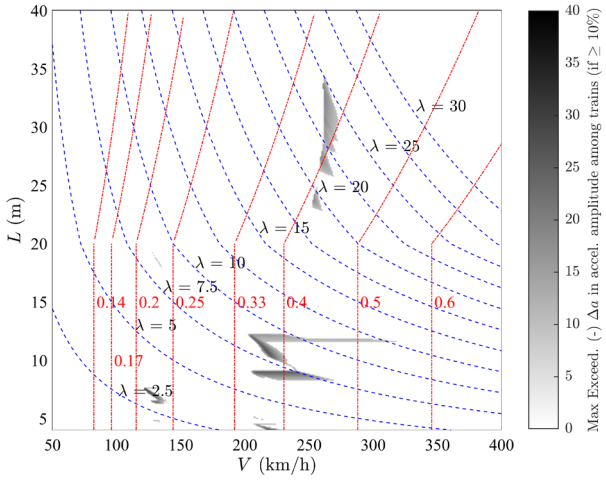

Figure 26: Map of $\Delta a(-)$: LIR vs. TSC. Train INB4EU-CB-011 (D=25.9 m). PSC bridges.

Therefore, in general the $\Delta a(-)$ patterns related to peak underestimations are less predictable. In some cases, they are related to near-maxima points of the RIL, but in some others they are more influenced by the axle loads distribution. This dependence is discussed further in section 0.

As for the performance of DER with RP trains, Figure 24 shows $\Delta a(-)$ for the same two trains discussed previously in this subsection. It can be seen that the performance for spans below some L=10 m is worse. This tendency is general and is observed also for the AB and SA trains. Particularly trains similar to INB4EU-CB-018 show worse performance with the DER method (for additional information about that type of architectures, see train PT60-10 in Appendix E, which is similar to INB4EU-CB-018).

Limitations of exceedance maps and alternative strategies

Exceedance maps provide a useful means of comparing the performance of SM, yet have two limitations:

- They cannot represent tendencies of train ensembles in a single plot because only one value at the time is shown for each (V, L) point. Thus, they can represent an average, maximum, minimum, or standard deviation for an ensemble of trains, but four plots will be required for that purpose.
- If one considers the need to analyse both negative and positive exceedance, for both accelerations and displacements, in PSC as well as in STC bridges, then 32 plots are required to characterise the performance of SM for each train ensemble analysed.

Delivering such large amount of information is indeed feasible and could be incorporated in a revised version of deliverable D1.2. However, at this stage the alternative "Z24" aggregate procedure—described in section 5.4—is adopted for comparing different methods (or trains) among them. Such procedure is complemented with exceedance maps, time-history plots, etc. as required.

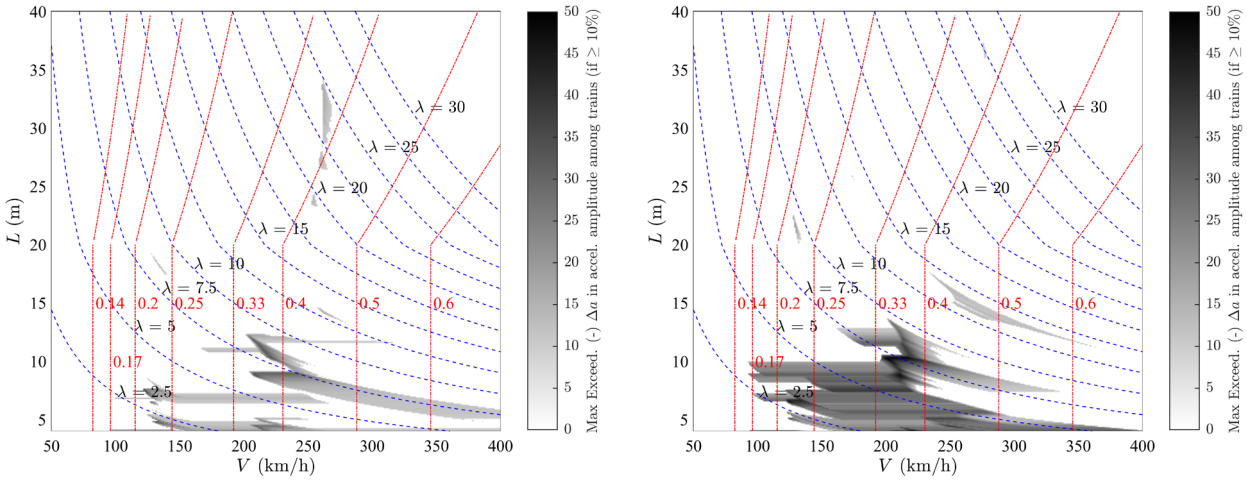

a) *b)*

Figure 27: Maps of Δa(−): DER vs. TSC. a) train INB4EU-CB-011 (D=25.9 m); b) train INB4EU-CB-018 (D=28.6 m). PSC bridges.

Positive exceedance in accelerations: Δa(+)

Figure 28 shows binary $\Delta a_{DER}(+)$ vs. $\Delta a_{LIR}(+)$, for CB RP trains longer[4] than 150 m, in PSC bridges. In total, these are 35 RP trains with $20.4 \leq D \leq 28.9$ m. As it can be seen in the figure, DER has in general a better performance than LIR when both methods are compared through this basic indicator, which computes the bare proportion—area ratio—of (V, L) points in each Z24 zone where at least one train is receiving too a conservative prediction from the SM.

In Figure 28, the very short bridges (4-7 m) for speeds vP1 (>250 km/h) are affected by overshooting in both methods, which may not be too problematic because SS bridges of those spans are not so often used for such high speeds. However, the prediction in general for short bridges is not good, and particularly the medium-long bridges (15-20 m) have also a bad approximation for vP1 speeds.

In Figure 29, a typical exceedance map for both DER and LIR illustrates the reasons behind the too conservative performance shown in Figure 28. All CB RP trains longer than 150 m are considered together in

[4] The influence of short train length is discussed in section 7.1.

Figure 29. It is seen that LIR is more conservative than DER for the shorter spans, which is not so critical for bridge design as the opposite situation (DER is more unconservative for those shorter spans, as mentioned before in this subsection), but isn't convenient for testing train-bridge compatibility either. Conversely, DER is more conservative that LIR for the longer spans (wider horizontal grey areas above some L=30 m spans).

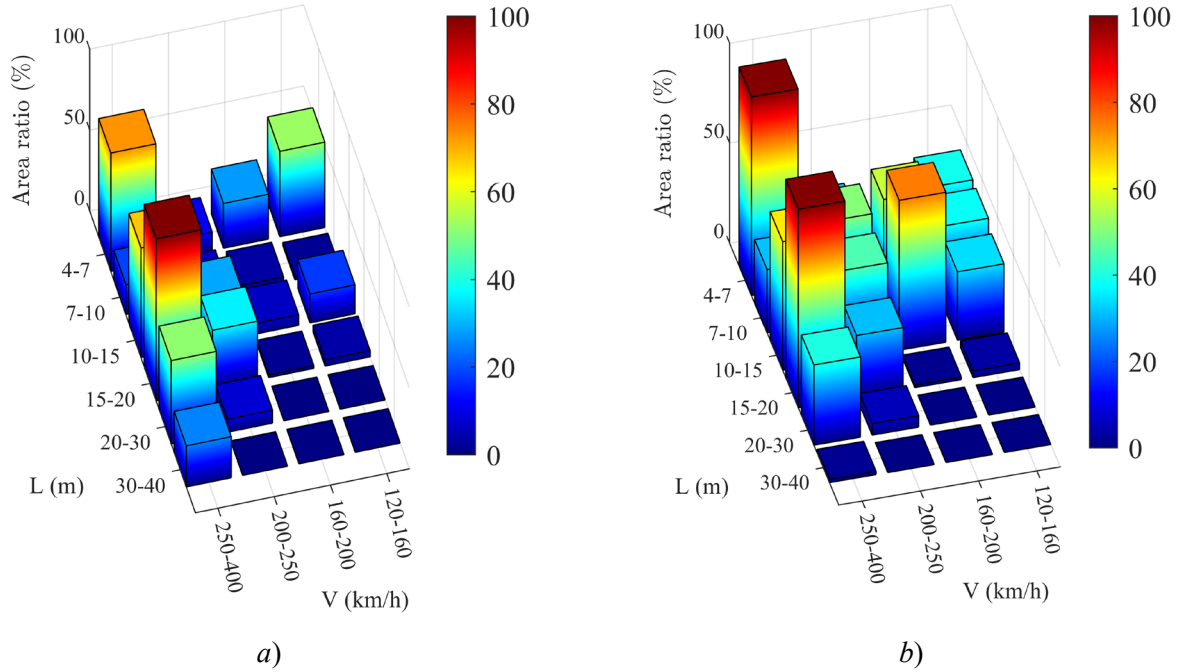

a) *b)*

Figure 28: Z24 plot of binary Δa(+), for CB RP trains longer than 150 m. SM vs. TSC. a) DER; b) LIR. PSC bridges.

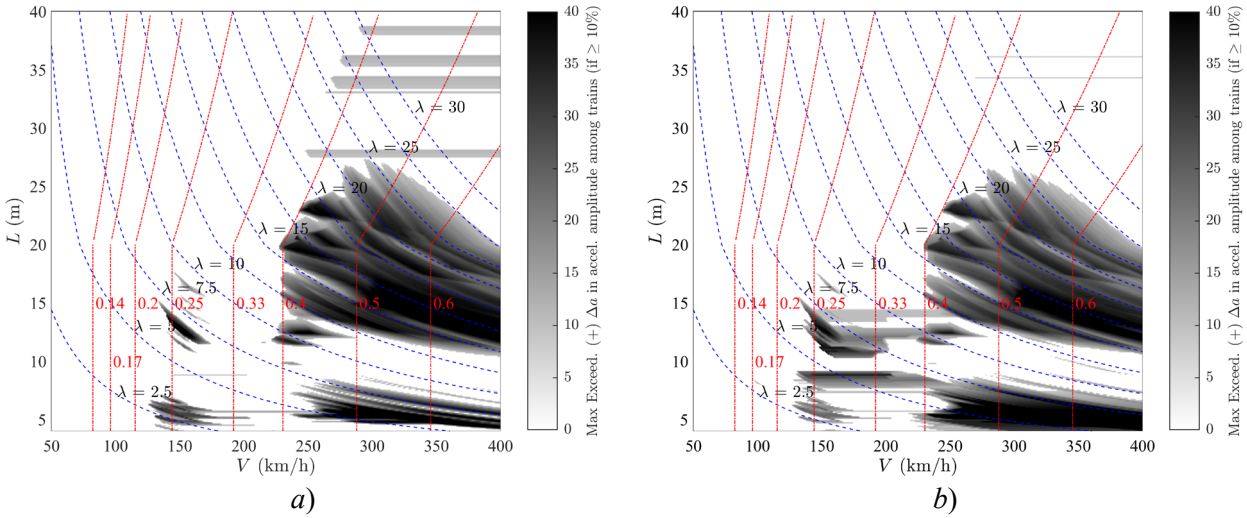

a) *b)*

Figure 29: Maps of Δa(+): a) DER and b) LIR, both vs. TSC. CB RP trains longer than 150 m. PSC bridges.

And notably, there is a wide range between some L=11 and L=26.0 m, for K>0.4, where again the phenomenon of convex slopes mentioned in section 6.1 dominates. That phenomenon is due to overconservative prediction of the effect of the initial carriages (typically 1, 2 or 3 carriages), even if they are not markedly heavier than the rest of the train. It depends to some extent on the train distances and loads, but most RPs suffer from it: CB trains more intensely than AB; as for SA trains, they don't experience this drawback, however it should be recalled that all SA RPs considered here have a particular value D=13.3 m,

which limits exploring the possible influence or the car length. More considerations about this phenomenon are discussed in section 7.5.

In summary, the performance of DER is better than LIR as regards overshooting. The difference is more noticeable for the shorter spans, particularly in very short bridges (4-7 m) for speeds vP1 (>250 km/h) which, as mentioned before, may not be too problematic because SS bridges of those spans are not so often used for such high speeds. A global comparison of both methods is presented in Figures 30 and 31, where box plots show the mean value for each Z24 zone (considering 35 CB, RP trains longer than 150 m): average for all trains, ±1 standard deviation limits, and min./max. values.

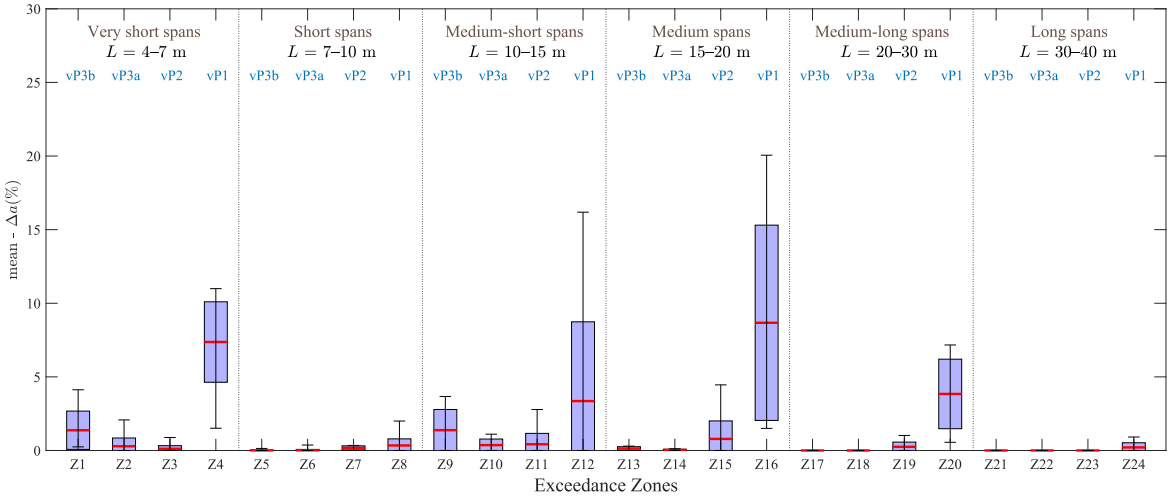

Figure 30: Box plots of Z24 mean Δa(+): DER vs. TSC. CB RP trains longer than 150 m. PSC bridges.

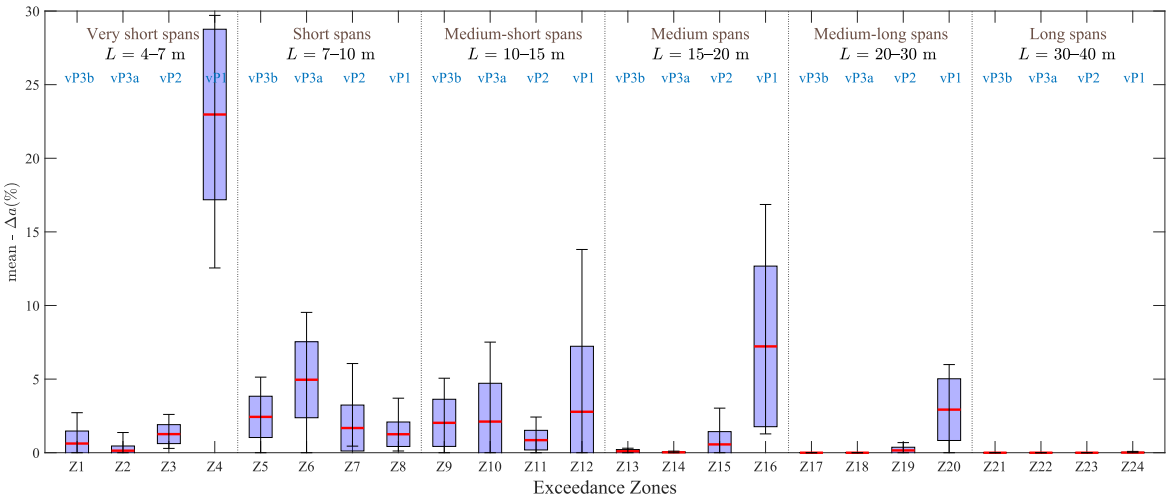

Figure 31: Box plots of Z24 mean Δa(+): LIR vs. TSC. CB RP trains longer than 150 m. PSC bridges.

Negative exceedance in displacements: Δδ(−)

For analysis of displacements in SS beams the threshold of meaningfulness is set on the impact coefficient rather than on acceleration. Given that in bridge design however a dynamic analysis has to be carried out using coefficient φ'=$K/(1-K+K^4)$, for dynamic effects not covered by such φ' to be considered meaningful it is required here that the actual impact factor computed at each speed (difference between

dynamic and static displacement, divided by static displacement) is at least 10% larger than the corresponding φ' at that speed. **In what follows, that criterion is referred to also as the "1.1φ' threshold".**

As it will be discussed later, adopting such criterion has an influence in the shape of some typical exceedance regions, that will be referred to here as the *waterdrop* pattern.

In general, the performance of SM as regards Δδ(−) is good in this case and can be summarised by means of exceedance maps. Few grey areas are found in those maps: Figure 32 shows the exceedance for both methods, where the grey regions are mostly affected by defective ascending slopes—only slightly wider for DER at lower wavelengths. Trains included in Figure 32 are also the 35 CB, RP trains longer than 150 m mentioned previously.

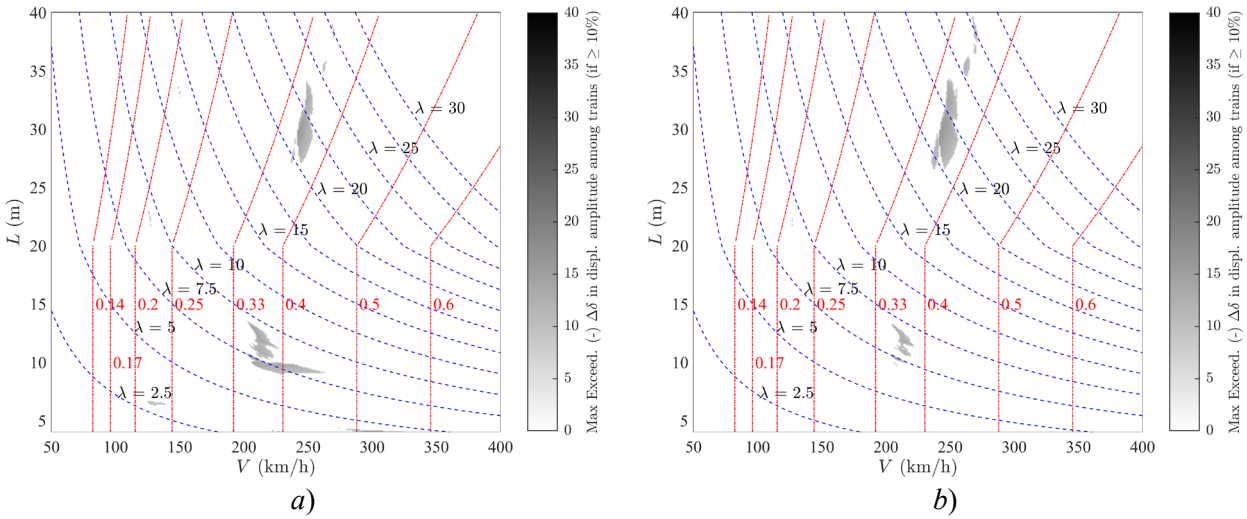

Figure 32: Maps of Δδ(−)*: a) DER and b) LIR, both vs. TSC. CB RP trains longer than 150 m. PSC bridges.*

Positive exceedance in displacements: Δδ(+)

The performance for Δδ(+) is clearly worse, thus the SM are generally conservative as regards the computation of displacements. However, the dependency on the particular train is strong, even within the 35 CB, RP trains longer than 150 m considered here. In general, the exceedance maps for both DER and LIR are similar for each train, though not identical.

For some trains, DER method in the range of spans near L=20 m and above will deliver exceedance slightly above 10%, while for LIR is slightly below, leading to maps which look more different than they actually are; straight horizontal borders in the grey areas typically may correspond to that situation (see for example Figure 33 at L=20 m for V >150 km/h). That situation may also happen for the first resonance when it occurs for K>0.4 approx., in some cases; modifying the tolerance only to 8% or 12% would still change the aspect of Δδ(+) maps in those cases.

As for the types of overshooting, there is a predominance of convex slopes for K>0.4, and also conservative ascending slopes or peak overestimations near the values of K where the RIL is maximum (see some examples in Figures 33 and 34). The maximum levels reached for each train most of the times do not surpass Δδ(+)=20–25%, but there are exceptions where higher overshooting occurs. In a manner similar as it happens with Δa(+), results in very short bridges (4-7 m) for the higher speeds are better for DER; for the rest of the shorter spans, the results of both SM are either similar, or non relevant (Δδ(+)<10%).

Figure 33*a* shows a phenomenon of peak overestimation where the resonant wavelengths create a recognizable exceedance pattern that is referred to in what follows as ***waterdrops***: for example, the third subharmonic at λ=9.6 m (*i*=3) is cancelling at the intersection with values *K*=0.33, 0.20, 0.14, and in between there is an overestimation due to a resonant phenomenon. In general, these patterns are somewhat clearer for DER than for LIR (Figure 33*b*), and in many cases stem from a too strong estimation of the static part of the displacement. Moreover, for other train subtypes they are even more clear. Further insight is given below.

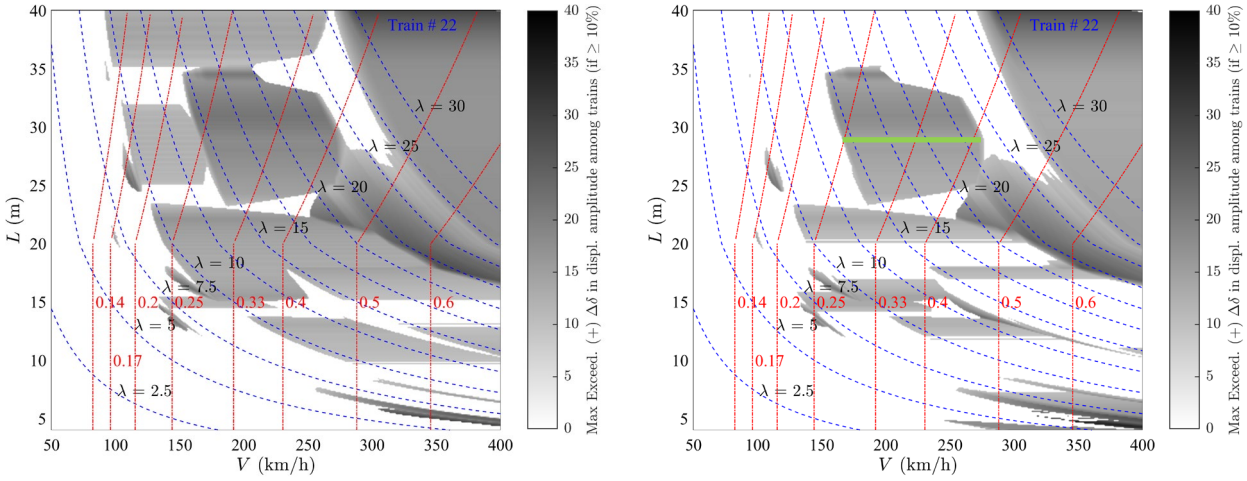

Figure 33: Maps of Δδ(+): DER and LIR, both vs. TSC for train InB4EU-CB-056 (D=28.8 m). a) DER; b) LIR. PSC bridges. "Axis of symmetry" of waterdrop [———]

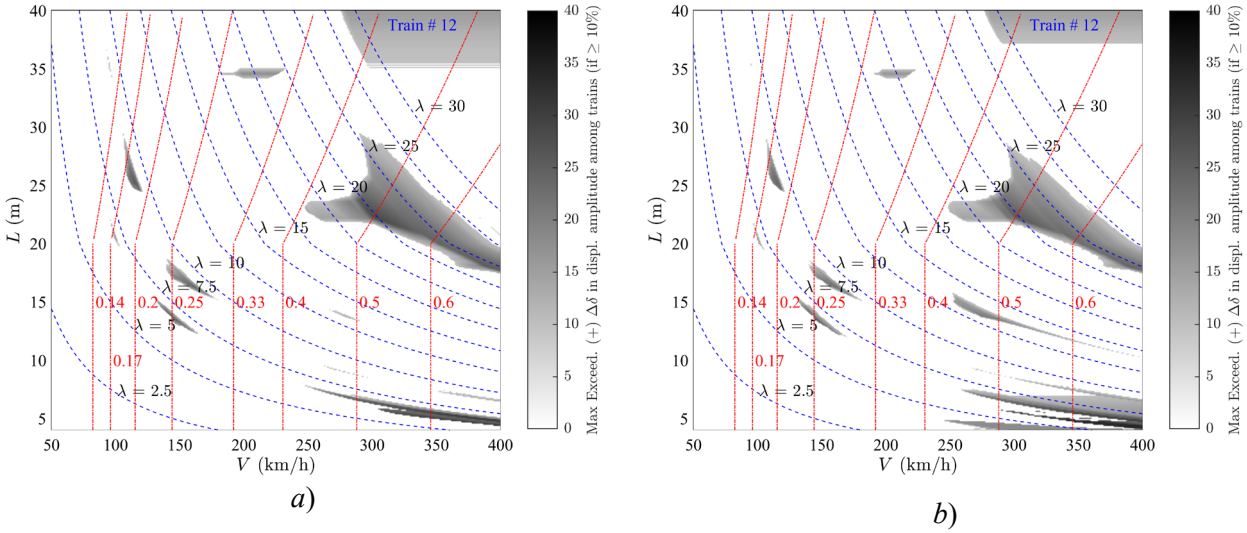

Figure 34: Maps of Δδ(+): DER and LIR, both vs. TSC for train InB4EU-CB-018 (D=28.6 m). a) DER; b) LIR. PSC bridges.

If a too strong estimate of the static part of the displacement has been considered in the SM, and any resonant subharmonic produces a peak displacement that exceeds the reference TSC method by more than 10%, while simultaneously happens to cross the 1.1φ' threshold, then a grey exceedance region appears. But in the closest two cancellation *K* lines the 1.1φ' threshold will not be crossed and exceedance will vanish. And, for increasing speeds, it is recalled that the 1.1φ' threshold gradually increases its value, thus producing the waterdrop form because the (cumulative) peak value is always higher in the horizontal "axis of symmetry" of the waterdrop (green line in Figure 33*b*: originates at *K*=0.25 which is as far as possible from RIL

cancellations). As a conclusion, we can say that $\delta_{st,res}$ is often overestimating the "static" part of the displacement that actually influences the peak response. The concept of static part of the displacement is indeed controversial, because when a train crosses a SS beam the static influence line has maxima and minima, and no theorem exists so far to prove that those maxima are the correct values to be added to the dynamic part of δ obtained from a SM.

For SA RP trains the waterdrop patterns are also visible for DER and LIR, more concentrated around the maximum values of the RIL and away from K=0.33, 0.20, 0.14, see λ=13.3 m (i=1) in Figure 35. It will be seen in section 6.4 that similar patterns occur as well for CART trains—and also in trains with heavy locomotives, but in that case exceedance Δδ due to transients is negative because the static part of the response is underestimated.

A global comparison of both methods is presented in Figures 36 and 37, where box plots of Δδ(+) show results for maximum value for each Z24 zone (considering 35 CB, RP trains longer than 150 m): averages, the ±1 standard deviation limits, and the min./max. values.

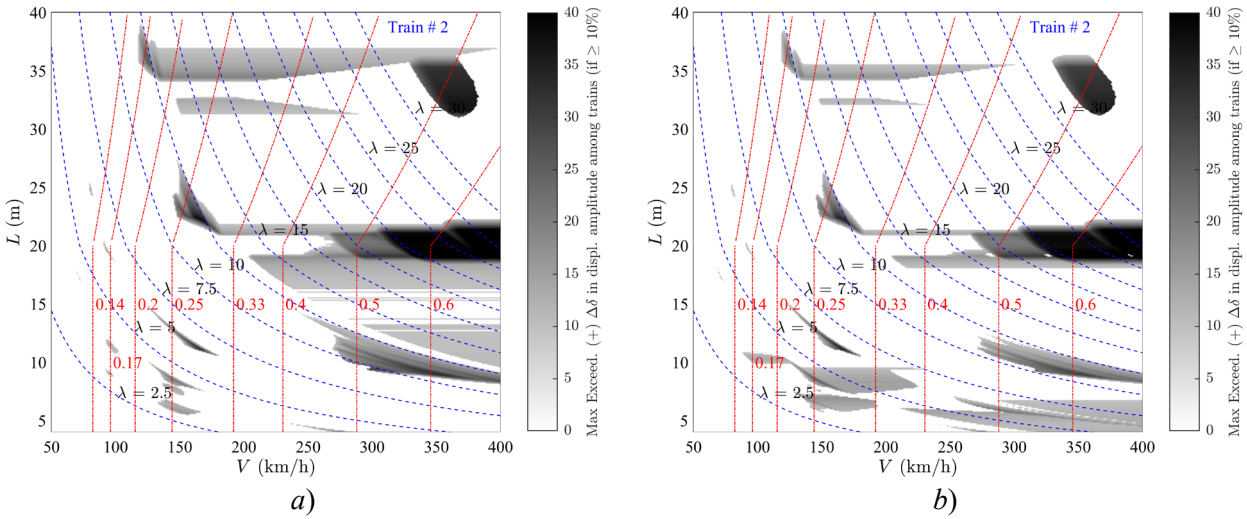

Figure 35: Maps of Δδ(+): DER and LIR, both vs. TSC for train InB4EU-SA-006 (D=13.3 m). a) DER; b) LIR. PSC bridges.

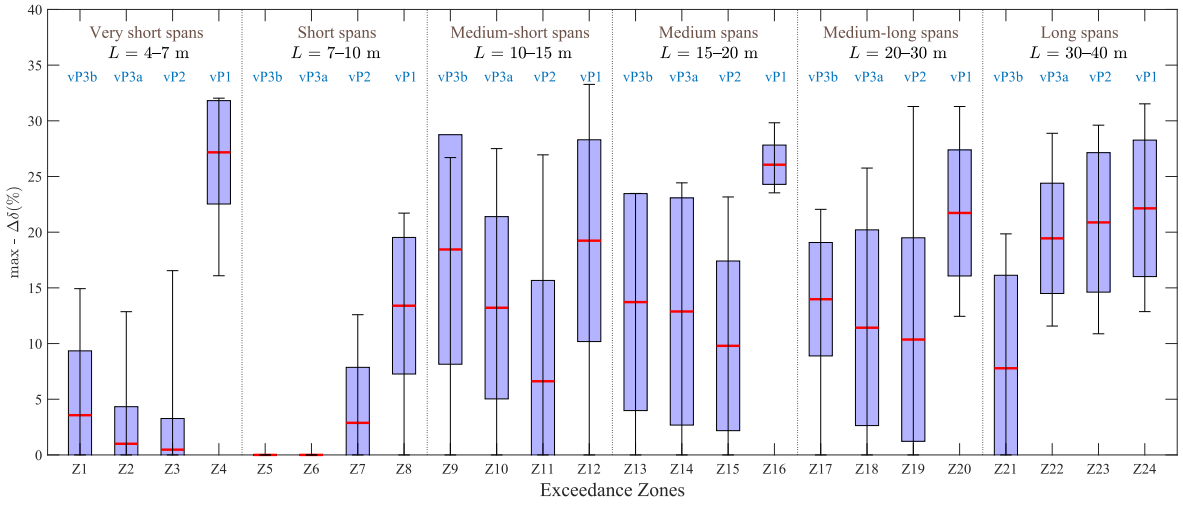

Figure 36: Box plots of max Δδ(+): DER vs. TSC. CB RP trains longer than 150 m. PSC bridges.

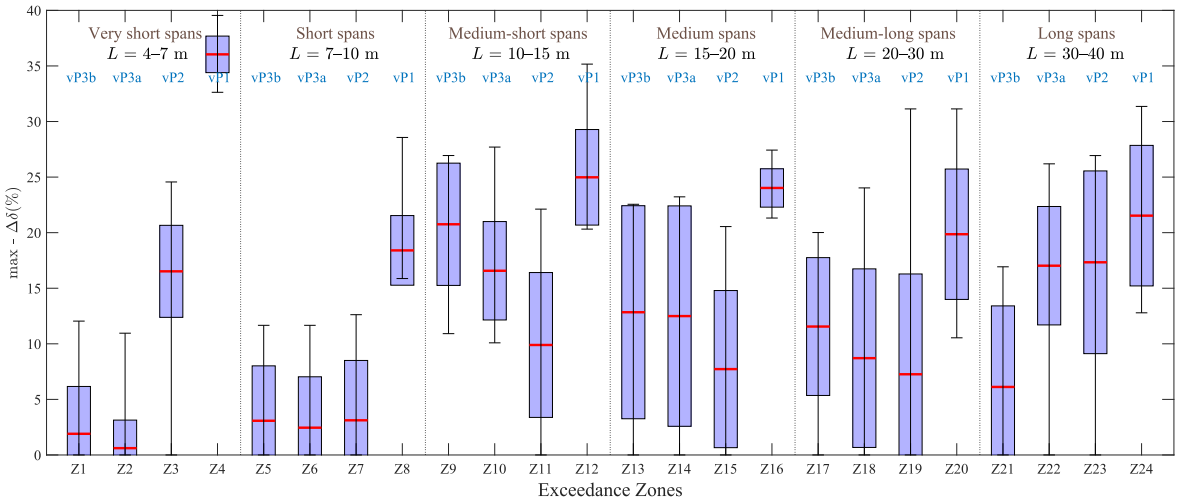

Figure 37: Box plots of max Δδ(+): LIR vs. TSC. CB RP trains longer than 150 m. PSC bridges.

6.3 LIR vs DER methods for CART trains (AB coupled multiple units – PT)

Trains of subtype CART comprise 21 vehicles with coach lengths divided in two clear groups, where either car length *D* is close to 18 m or to a combination 10/15.5 m, approx. These CART vehicles contain two or three coupled units.

Negative exceedance in accelerations: Δ*a*(−)

In general, the performance of both methods is somewhat worse in comparison with the results for RP trains discussed in section 6.2 (for representative cases, see Figure 38*b* in contrast with Figure 23).

It is also confirmed that the performance of both methods is similar for the shortest among the CART trains (the ones with two units). Conversely, for longer CART trains with 3 units, DER results are visibly worse for short spans between *L*=10 and *L*=15 m (see Figure 38*a* in contrast to 38*b*). The irregular architecture, in those cases, is negatively influencing the outputs of DER method in comparison to LIR.

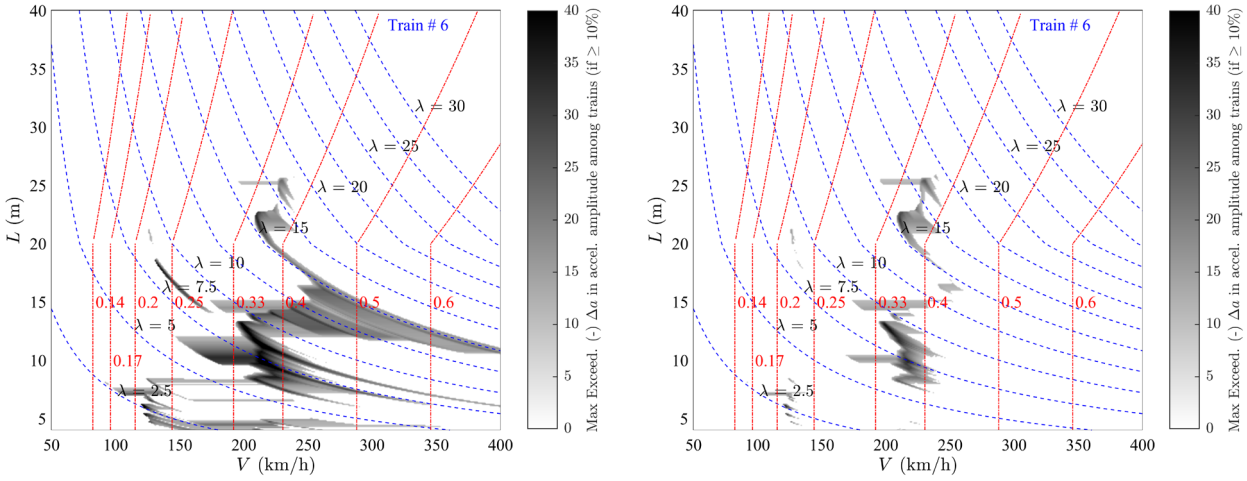

a) *b)*

Figure 38: Maps of Δa(−): DER and LIR, both vs. TSC for train InB4EU-AB-021 (see Figure 39, most frequent D=18.05 m). a) DER; b) LIR. PSC bridges.

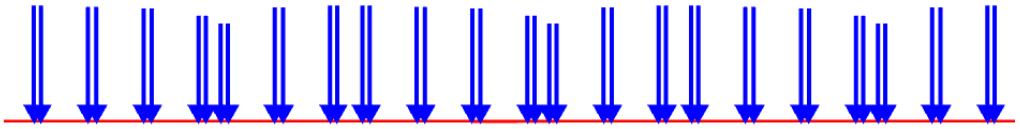

L_{tot} = 319.8 m

D = 18.05 m

P_{max}= 186.0 kN

P_{min} = 154.5 kN

P_{tot} = 7449 kN

Figure 39: Example of a CART train [INB4EU-AB-021].

Positive exceedance in accelerations: $\Delta a(+)$

The convex slopes region typical in spans between some L=11 and L=26.0 m, for K>0.4, present in the RP trains analysed in section 6.2, is less visible for CART trains with D close to 18 m (not shown for brevity). However, it has been confirmed that this does not happen for other coupled units as CMU trains, and it seems thus linked to the car length, given that (*i*) D=18 m is not present for the CMUs and (*ii*) the region of convex slopes becomes again more visible for CART trains with D close to 10/15.5 m (see Figure 40).

Results of $\Delta a(+)$ for both DER and LIR are rather similar for CAR trains with D close to 18 m. For the rest, the main conclusions are similar to those stated in section 6.2: performance of LIR is in general somewhat worse than DER, particularly in very short bridges (4-7 m) for speeds vP1 (>250 km/h), as it can be seen for example in Figure 40.

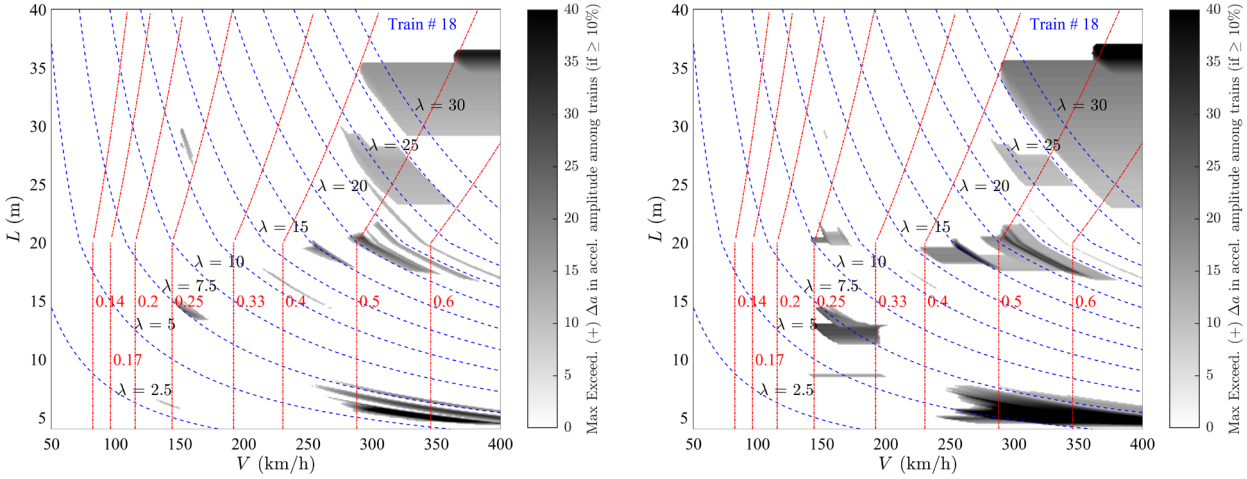

a) *b)*

Figure 40: Maps of $\Delta a(+)$: DER and LIR, both vs. TSC for train InB4EU-AB-033 (most frequent D=10/15.5 m). a) DER; b) LIR. PSC bridges.

Negative exceedance in displacements: $\Delta\delta(-)$

As for the RP trains analysed in section 6.2, the performance is generally good. The only relevant difference appears consistently for trains with D close to 10/15.5 m and three units, where the undershooting of DER is larger in a region where some secondary resonant peaks ($\lambda \approx 10$ m) are underestimated, at speeds immediately below the main resonant peak. The comparison DER *vs*. LIR for one of those trains is shown in Figure 41. The particular speed envelope in that region is shown in Figure 42.

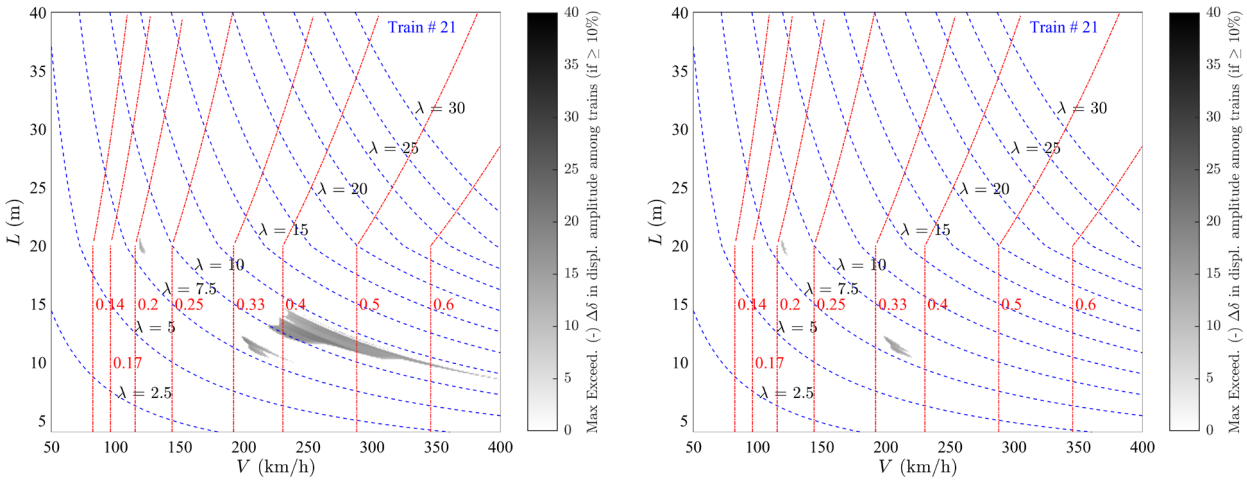

a) *b)*

Figure 41: Maps of Δδ(–): DER and LIR, both vs. TSC for train InB4EU-AB-036 (most frequent D=10/15.5 m). a) DER; b) LIR. PSC bridges.

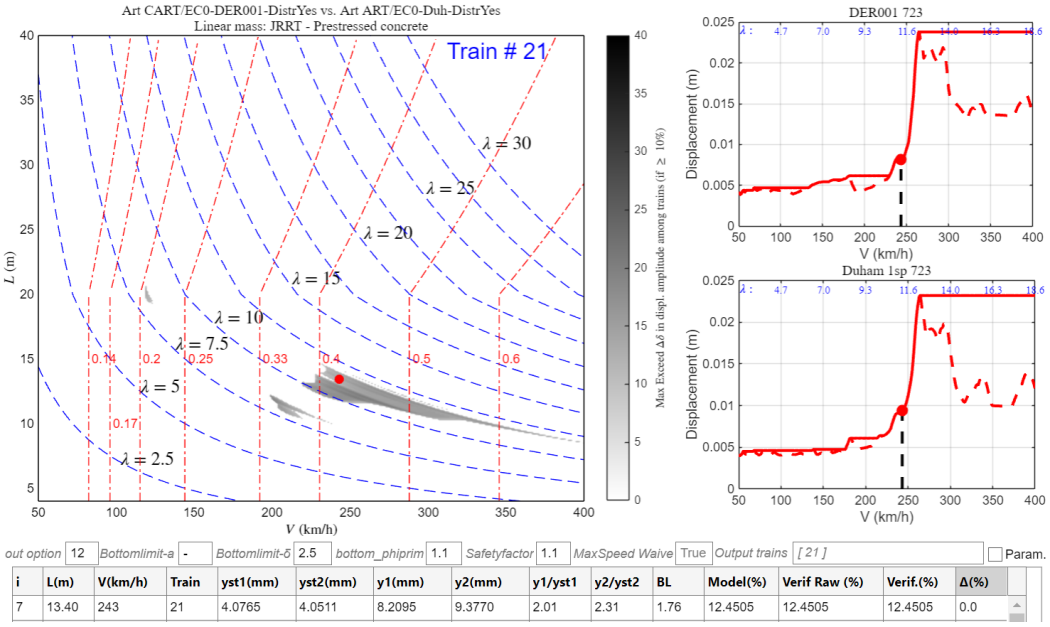

Figure 42: Map of Δδ(–): DER vs. TSC for train InB4EU-AB-036 (most frequent D=10/15.5 m). PSC bridges.

Positive exceedance in displacements: Δδ(+)

As it happened for the CB RP trains, again both methods are generally conservative, with usual values not above 20–25%, but with exceptions in regions of higher exceedance and a marked dependency on the train type. The general aspect of exceedance maps reminds of those in section 6.2 and is not shown for brevity: it includes some cases where it is again visible the overconservative waterdrop pattern (overestimations at resonance peaks that cancel out for the RIL valleys; see for example train PT60-26 in Appendix E).

A global comparison of both methods is presented in Figures 43 and 44, where box plots show the value of those maximum Δδ(+) for each Z24 zone (considering the 21 CART trains): average for all trains, ±1 standard deviation limits, and min./max. values.

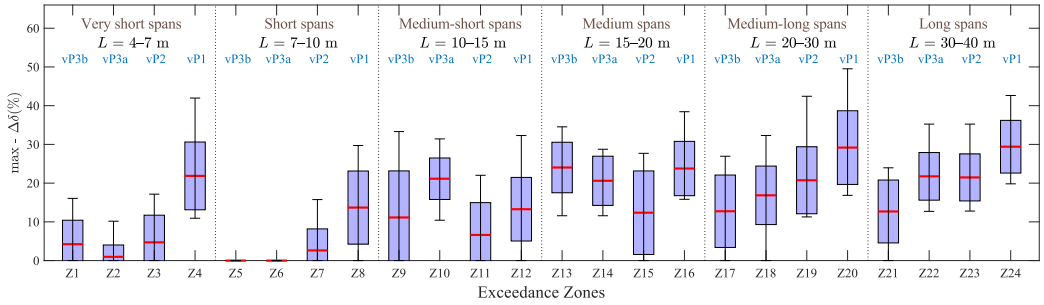

Figure 43: Box plots of max Δδ(+)*: DER vs. TSC. CART trains. PSC bridges.*

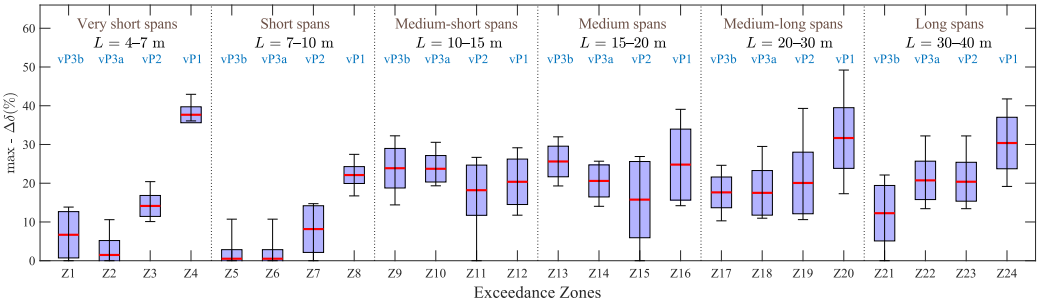

Figure 44: Box plots of max Δδ(+)*: LIR vs. TSC. CART trains. PSC bridges.*

6.4 LIR vs DER methods for loco-hauled trains with two heavy locomotives (PT)

Trains considered here are of subtype LH-bHL, comprising 12 vehicles with (CB) coach lengths between 23.0 and 26.4 m and heavy power cars in both ends.

Negative exceedance in accelerations: Δ*a*(−)

Exceedance Δ*a*(−) for the LIR method is not too different from the one found for the CART trains. Figure 45*b* shows a representative example for a train of subtype LH-bHL. It is seen that performance it is still somewhat worse than for CB RP trains, if compared for instance with Figure 23. For the same train, DER also performs worse than LIR as regards undershooting in acceleration.

Positive exceedance in accelerations: Δ*a*(+)

Exceedance Δ*a*(+) in loco-hauled trains with both heavy locomotives is found rather similar for both DER and LIR, as it happened for the CB RP trains, being in some cases DER again better than LIR for the shorter spans. Some examples are shown in Figure 46.

The trains with D=23.0 m also show a region of worse performance of LIR, when $K > 0.5$ approx. (see Figure 46*b*); that region is particularly worse for LIR in comparison to DER for spans near L=20 m (DER Δ*a*(+) maps are white for those spans, not shown in Figure 46*b*).

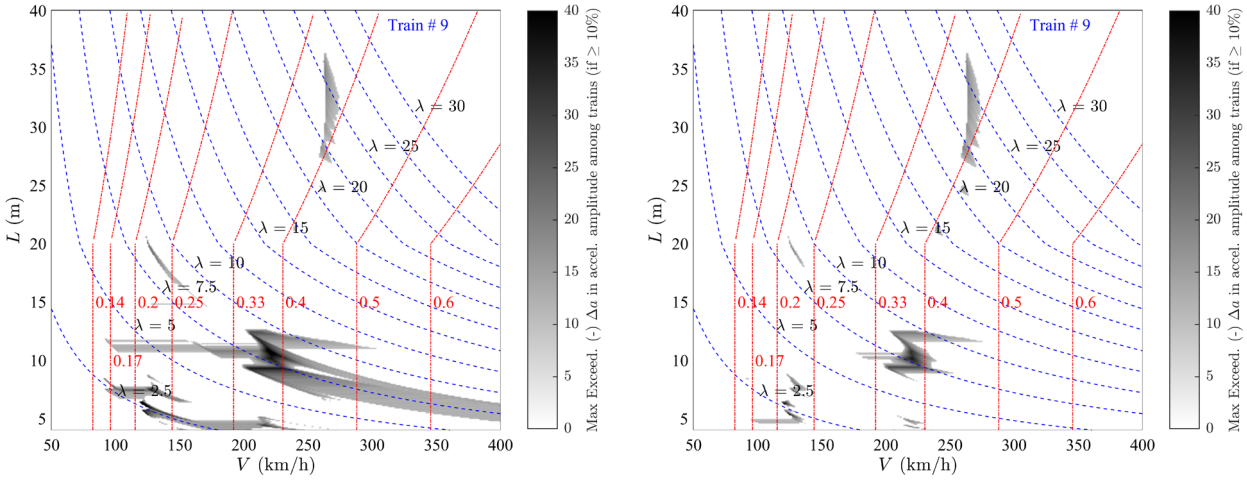

a) *b)*

Figure 45: Maps of Δa(−): DER and LIR, both vs. TSC for train InB4EU-CB-088 (D=26.4 m). a) DER; b) LIR. PSC bridges.

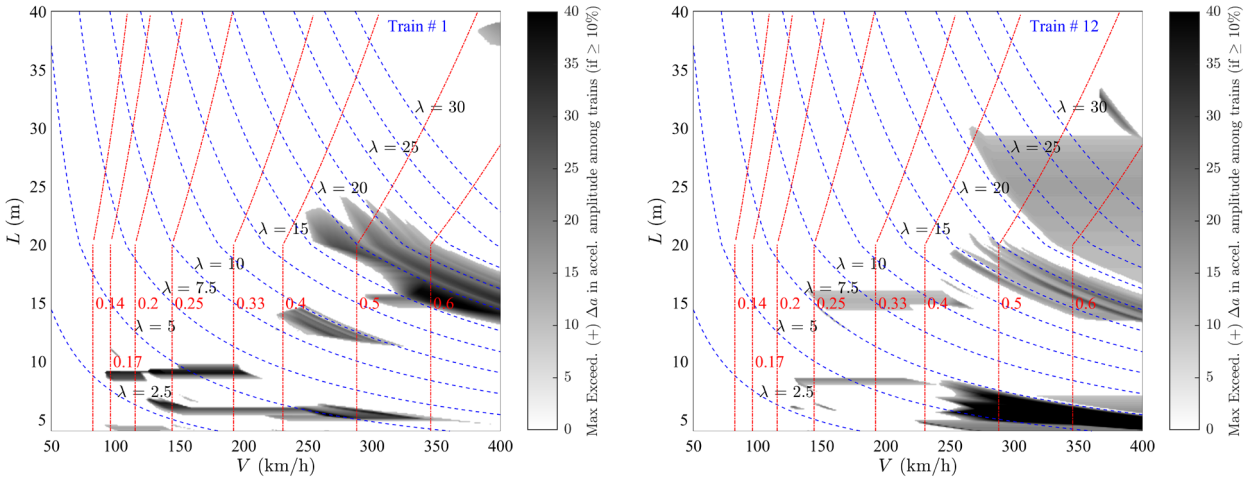

a) *b)*

Figure 46: Maps of Δa(+): DER and LIR, both vs. TSC. a) DER for train InB4EU-CB-013 (D=26.4 m); b) LIR for train InB4EU-CB-125 (D=23.0 m). PSC bridges.

Negative exceedance in displacements: Δδ(−)

Marked differences are found with section 6.2 in this case. The performance is good only for few trains and, conversely, is poor even at low speeds for those trains with the heaviest locomotives in comparison with the rest of cars. Particularly, the third (i=3) and sixth (i=6) subharmonics suffer peak underestimation for K values away from cancellation valleys: see Figure 47*a* for λ=8.7 m, and λ=4.3 for example, where a (non-conservative) waterdrop pattern is visible. The results for LIR are similar, and those cases of Δδ(−) are due to peak underestimation, as it can be seen for LIR in Figure 48.

Conversely, Figure 47*b*, for those trains with not so heavy power car axle loads the performance is better and less peak underestimations are observed.

The phenomenon described in relation to Figures 47*a* and 48 affects a considerable number of loco-hauled trains from model PT-60, including the HSLM-A trains. The reason behind that performance is the way to compute the "static" part of the deflection: while the procedure adopted here following section 3.1(D) in this document (aligned with D214 RP6 – Part A – 6.2) proves convenient for trains where power cars do not contribute significantly to the vertical displacement, in cases where that hypothesis does not hold there is a relevant underestimation and exceedance Δδ(−) arises. This limitation is discussed further in section 0

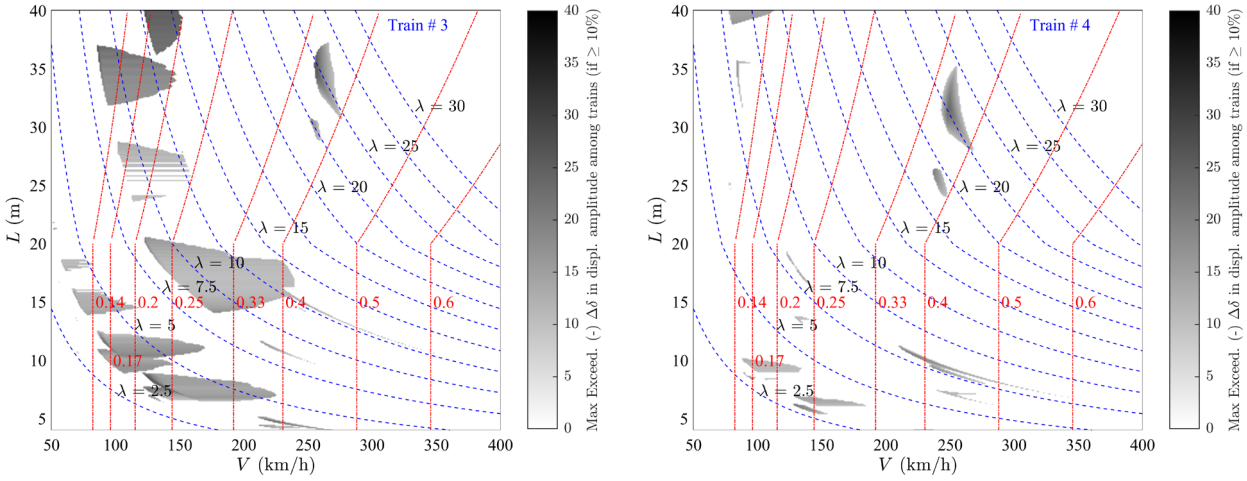

a) *b*)

Figure 47: Maps of Δδ(−): DER vs. TSC. a) train InB4EU-CB-026 (D=26.1 m); b) train InB4EU-CB-030 (D=24.0 m). PSC bridges.

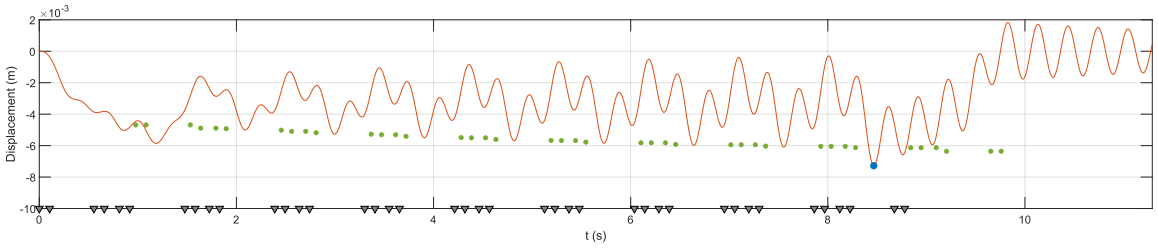

Figure 48: End transient phenomenon due to train InB4EU-CB-026 (D=26.1 m; axle loads in locomotives 55% heavier than in the cars), V=103 km/h, L=28 m in Figure 47a. LIR vs TSC.

Positive exceedance in displacements: Δδ(+)

As it happened for the CB RP trains and CART trains, both methods are generally conservative, with usual values not above 20–25%, but with exceptions in regions of higher exceedance and visible dependency on the train type. The exceedance maps for DER and LIR are similar, and again the most frequent difference lies in the very short bridges (4-7 m) for speeds vP1 (>250 km/h), where LIR behaves worse. Figure 49 shows some representative examples.

It is found that the waterdrop pattern of overestimations is not present in the case of these trains with heavier power car axles, and overeshooting concentrates mostly in the region of convex slopes for K>0.45 approx. This could be expected, given that for those trains understimation is ocurring, as discussed earlier in this subsection. Section 0 includes further information about these effects, discussing the interaction of Δδ(+) and

Δδ(−) in cases where heavy locomotives are present, depending on how the static part of the deflection is taken into account.

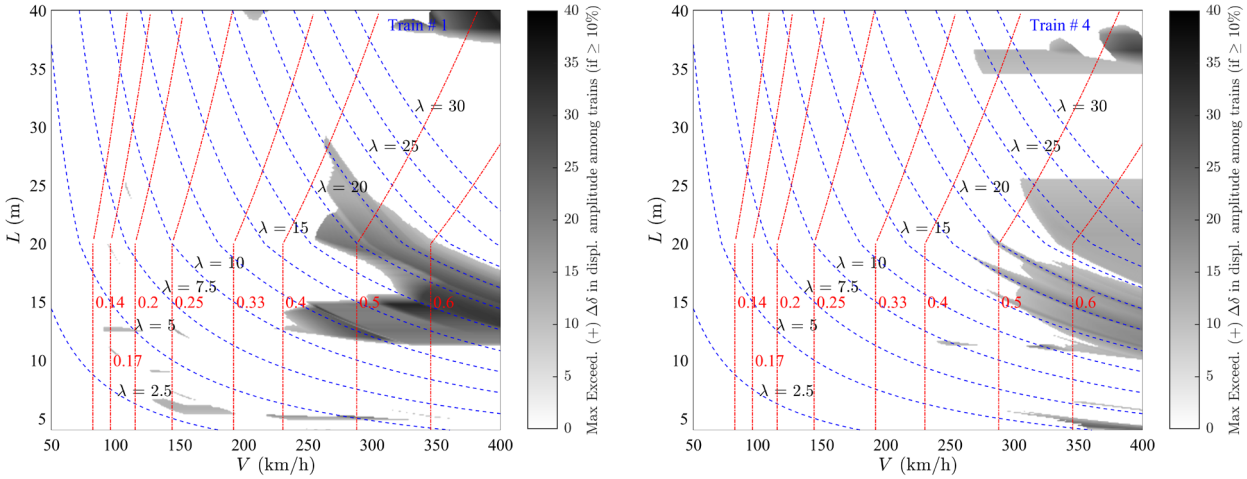

a) *b*)

Figure 49: Maps of Δδ(+)*: DER and LIR, both vs. TSC. a) DER for train InB4EU-CB-013 (D=26.4 m); b) LIR for train InB4EU-CB-030 (D=24.0 m). PSC bridges.*

6.5 LIR vs DER methods for freight trains (FT)

For the analysis of FT the speed limits have been restricted to $50 \le V \le 180$ km/h. Therefore, the global assessment with the Z24 strategy and the associated box plots are not available in this case. To illustrate the overall performance of SM, a particular type of multiple plot is used instead (see Figure 50 as an example).

Negative exceedance in accelerations: Δ*a*(−)

Regarding Δ*a*(−), the DER method performs significantly worse than the LIR method, and the range of bridges with spans less than approximately L=20 m is not usable with DER. Figures 50 and 51 present a comparison of both methods for the first fifteen FT described in Appendix C. As for the LIR method, the results are more usable, but in any case, limitations due to ascending slopes and peak underestimation arise, which requires the method to be used with caution.

The LIR results are completed with Figure 52, for the fifteen remaining FT described in Appendix C. In general, the ascending slopes are in this case located in the subharmonics of those bridges that happen to take place after the second cancellation of the RIL, i.e. for values of K slightly above 0.2 (the first cancellation K=0.33 will not be reached for $V \le 180$ km/h). The transients, as it will be discussed in section 0, are less predictable and more train-dependent.

While in some cases spans up to $L \le 20$ m are affected, overall the range of more defective bridges are those with $L \le 15$ m approx.

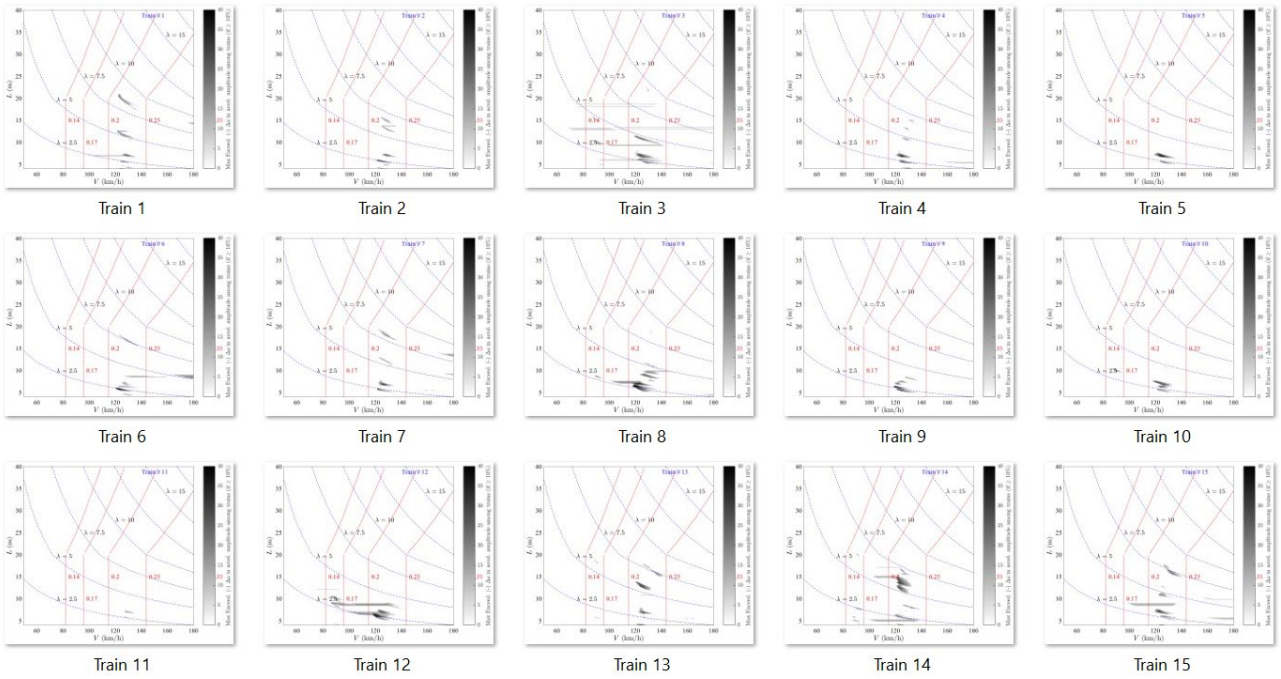

Figure 50: Maps of Δa(–): LIR vs. TSC. Fifteen first freight trains in Appendix C. PSC bridges.

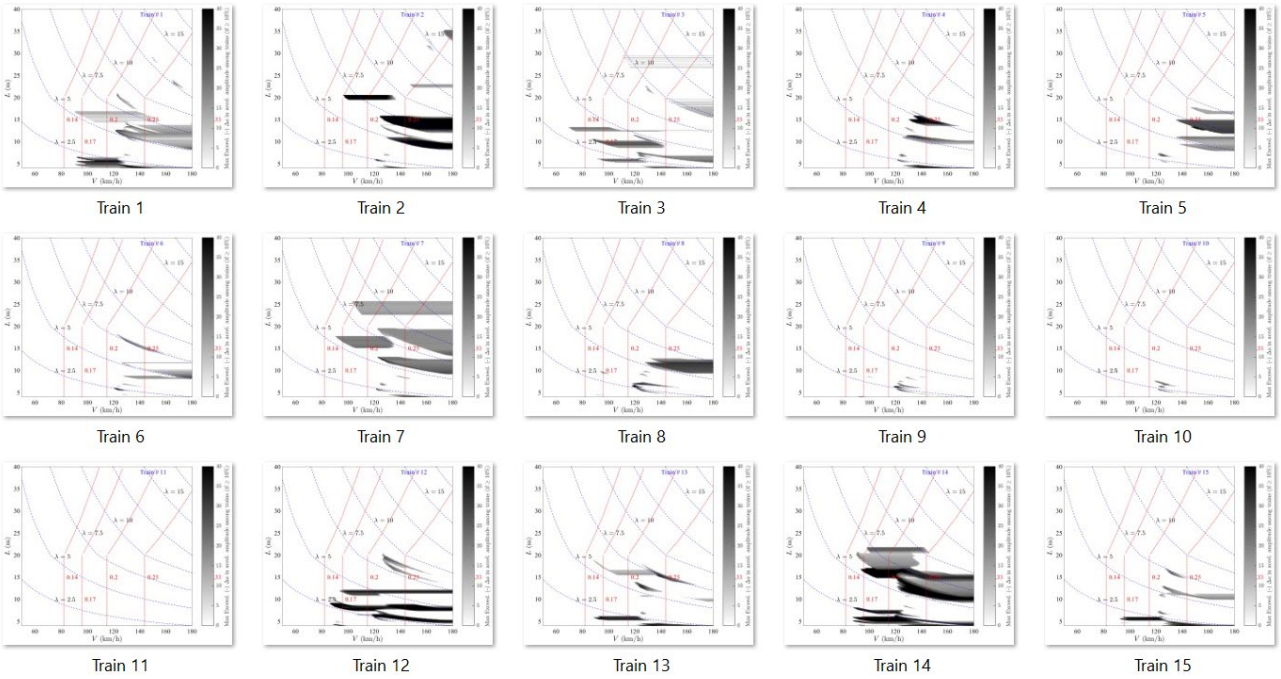

Figure 51: Maps of Δa(–): DER vs. TSC. Fifteen first freight trains in Appendix C. PSC bridges.

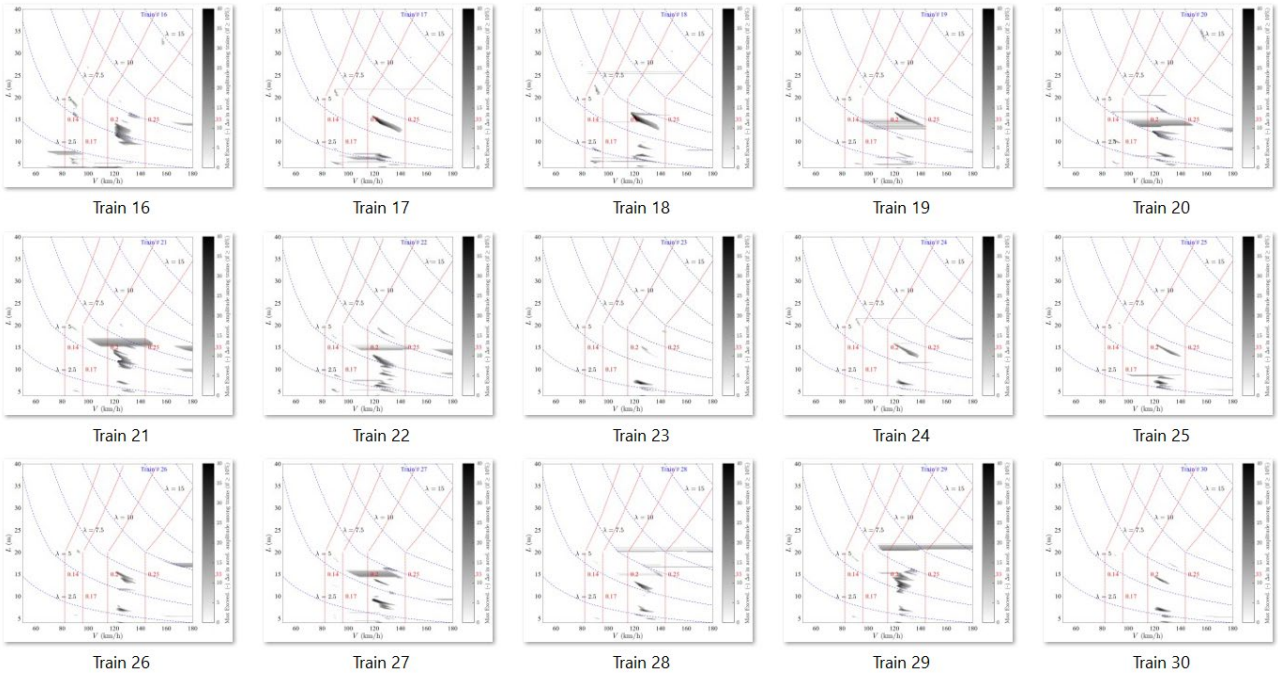

Figure 52: Maps of Δa(–): LIR vs. TSC. Fifteen last freight trains in Appendix C. PSC bridges.

Positive exceedance in accelerations: Δ*a*(+)

As it happens with Δ*a*(–), in the analysis of Δ*a*(+) the DER method performs consistently worse than LIR (compare Figures 53 and 54). Therefore, DER method is not recommended for the prediction of acceleration due to FT at speeds below 180 km/h.

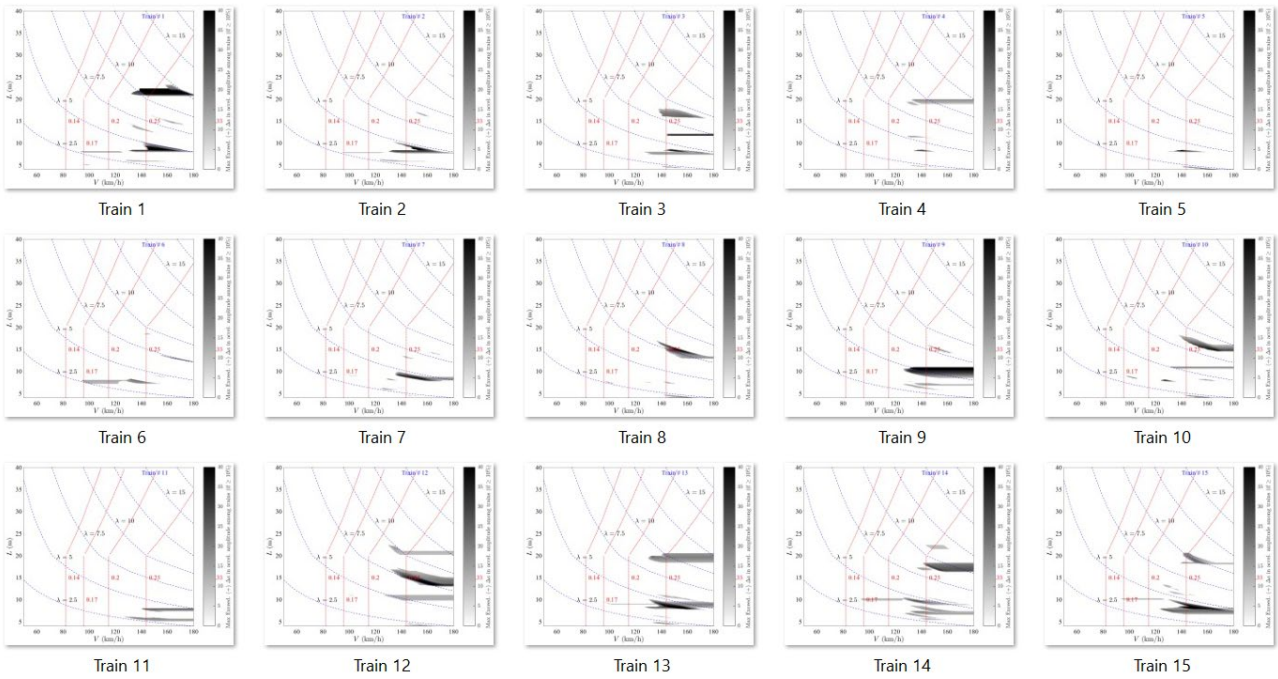

Figure 53: Maps of Δa(+): LIR vs. TSC. Fifteen first freight trains in Appendix C. PSC bridges.

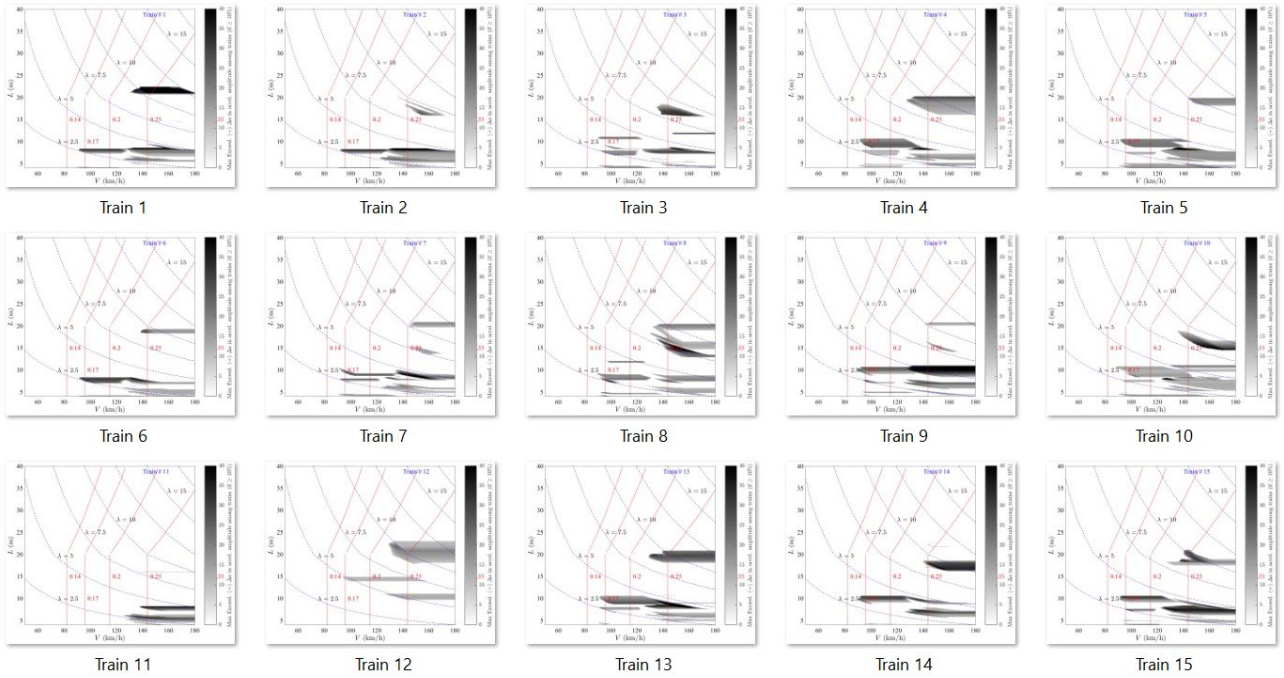

Figure 54: Maps of Δa(+): DER vs. TSC. Fifteen first freight trains in Appendix C. PSC bridges.

As for the results from the LIR, it is not easy to find tendencies, given the variety of train architectures. The most notorious pattern is that overestimation usually happens for K>0.225 approx., and affects more intensely discrete spans values below L=20 m, that are not identical for each train. A classification of FT in subtypes could help to identify those trends in the future, however priorities should be defined first on what FT subtypes are more relevant to that purpose.

The tendencies described above for Δa(−) and Δa(+) get somewhat worse for STC bridges, given that more cases exceed the 2.5 m/s^2 threshold, and then particularly more transient phenomena leading to peak misestimation become visible.

Negative exceedance in displacements: Δδ(−)

In general, this type of exceedance is very low; it is only noticeable as a waterdrop pattern for trains that have clearly heavier initial locomotives, because the weight of those axles is being eliminated for the calculation of $\delta_{st,\mathrm{res}}$, but if such weight were included, this type of exceedance would vanish.

An example of such cases is given below. The train INB4EU-FT-008 has four front axles of approx. P=205 kN approx. (see Figure 55). For a PSC bridge of span L=9.8 m, at speed V=98 km/h, the dynamic response is slightly above the φ' impact coefficient: 1.25 *vs*. 1.21, which is due to a certain resonance noticeable during the passage of the power cars (see Figure 56).

The results obtained with DER are similar, only worse than for LIR in some particular trains (INB4EU-FT-002, INB4EU-FT-012 and more visibly INB4EU-FT-016).

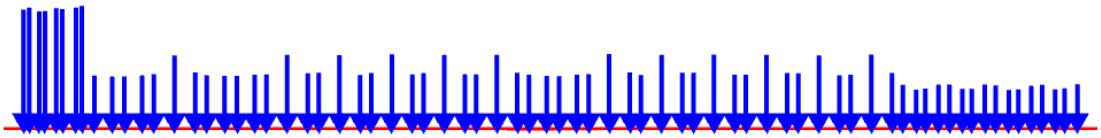

Figure 55: Load pattern of train INB4EU-FT-008.

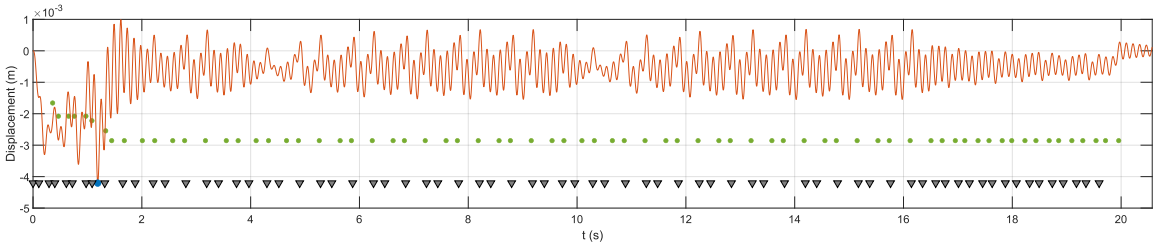

Figure 56: LIR vs. TSC. Δδ(–): Vertical displacement due to train INB4EU-FT-008; PSC bridge of span L=9.8 m, at speed V=98 km/h.

Positive exceedance in displacements: Δδ(+)

Except for a few specific trains, error levels are similar between DER and LIR. As mentioned for Δ*a*(+), it is not easy to identify patterns that apply to all trains. In some cases, these patterns are seemingly identifiable, but they do not exist in other trains of a similar type. A prior classification into subtypes would therefore be necessary to draw clearer conclusions. Figure 57 shows one of the few recognizable patterns, comparing (subfigure *a*) *vs*. *b*)) a train with *twin conventional* wagons to one with *conventional* wagons. The results for the former are clearly more conservative. The waterdrop pattern tends to appear in Figure 57*a*, indicating that resonance is indeed occurring, but adding the static deflection at resonance is excessive. In most cases, the error level does not exceed 20-25%, so the results can still be considered usable, although overly conservative.

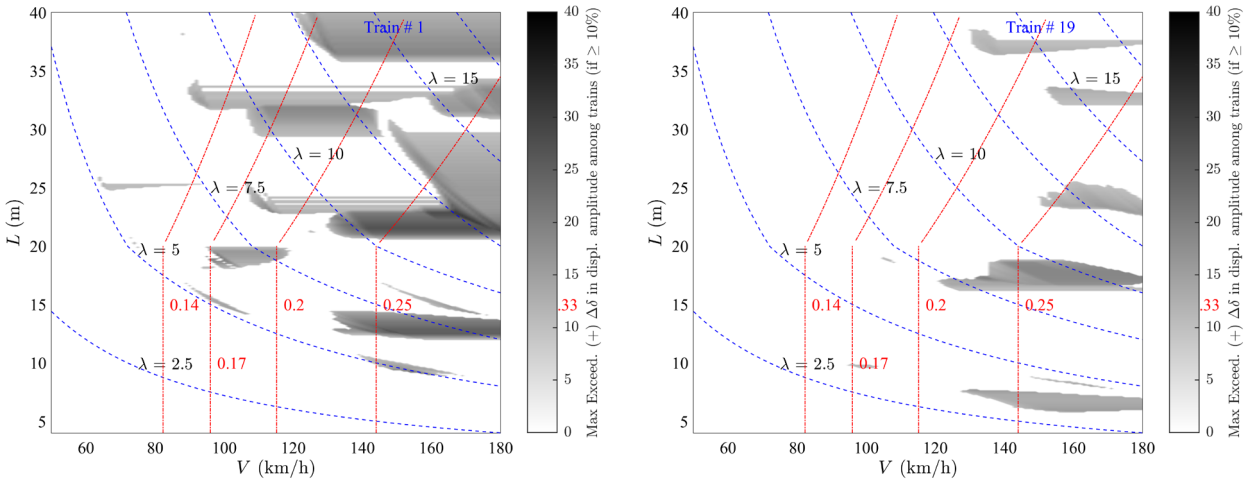

a) *b)*

Figure 57: Maps of Δδ(+): LIR vs. TSC. a) train InB4EU-FT-001 (D=26.4 m, twin wagon); b) train InB4EU-FT-019 (D=14.1 m, conventional wagon). PSC bridges.

The case of the train INB4EU-FT-001 with twin conventional wagons (Figure 57*a*) is analysed in more detail in Figures 58 to 60. Such train has several heavy axles in the front section, with average loads of some *P*=200 kN. These are the axles used to calculate the static deflection at resonance, as it is not logical to assume they are all locomotive axles (and therefore remove them). For a PSC bridge, with *L*=28.2, at a speed *V*=157

km/h, there is significant dynamic amplification (factor 1.85) due to a second subharmonic resonant peak (see Figures 59 and 60). However, the maximum resonant response receives a LIR conservative estimate of 12.5%. Simple addition of the static deflection at resonance plus the resonant term computed with the SM may induce such kind of errors, which in some cases lead to waterdrop patterns either fully or partially developed.

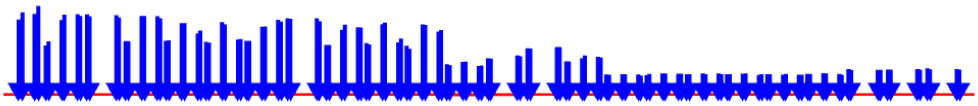

Figure 58: Load pattern of train INB4EU-FT-001.

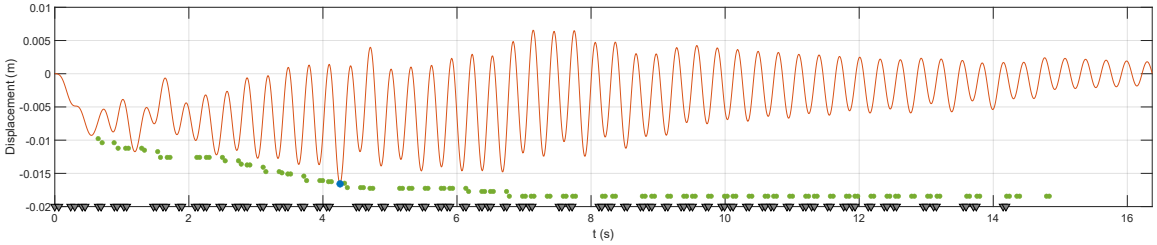

Figure 59: LIR vs. TSC. Δδ(+): Vertical displacement due to train INB4EU-FT-001; PSC bridge of span L=28.2 m, at speed V=157 km/h.

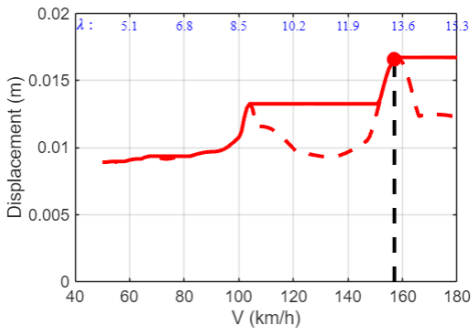

Figure 60: TSC. Vertical displacement due to train INB4EU-FT-001; PSC bridge of span L=28.2 m. Dynamic amplification = 1.85.

7 Limitations of SM in SS bridges

As the previous section, this one is also dedicated to the use of SM in SS bridges exclusively. Section 8 is devoted instead to the limitations of SM in those cases where more than one mode is relevant—including torsion effects and multi-span bridges—, as well as in portal frames.

7.1 Limitations in the analysis of short trains

This section is dedicated to investigating the limitations of SM in relation to KS-2.

7.1.1 Error levels for short EQD trains (equidistant loads)

Negative exceedance in accelerations: $\Delta a(-)$

Some of the figures shown here have already been presented in section 6.1, but are now compared *vs*. shorter trains, with only 6 equidistant loads instead of 18. As indicated in section 6.1, the results are analyzed exclusively for vertical accelerations. Regarding $\Delta a(-)$, it can be seen in Figures 61 and 62 that both SM yield similar conclusions: the shorter trains demonstrate moderately worse results for ascending slopes of the first cancellation (K=0.33), with somewhat wider grey areas, but those with longer cars (top of those figures) seem to deliver somewhat better results instead for ascending slopes of subsequent cancellations (K=0.20 and 0.14). However, this is largely due to the fact that the 1.0 m/s² threshold chosen for this study eliminates the grey areas of those subsequent cancellations. Therefore, in conclusion, it can be said that the main difference in behavior lies in the ascending slopes associated with K=0.33 (approx.), with the SM performing somewhat worse for shorter loading sequences. This influence was anticipated in section 6.1.

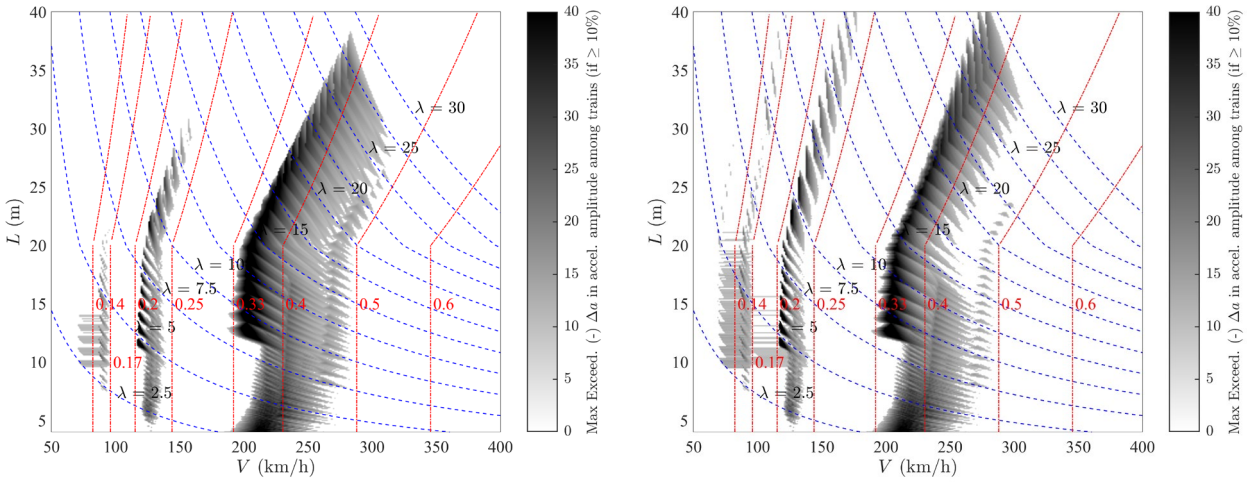

a) *b*)

Figure 61: Maps of $\Delta a(-)$: LIR vs. TSC. a) EQD-6 and b) EQD-18 trains. PSC bridges.

Positive exceedance in accelerations: $\Delta a(+)$

Regarding $\Delta a(+)$, both SM clearly show poorer performance with short loading sequences in the convex slope zone above K=0.45 (see Figures 63 and 64).

Specifically with the DER method, there are significantly more overestimations of resonant peaks at low speeds and short-to-medium spans with short sequences. For longer sequences, the problem shifts instead to

the longer spans. It should be noted, however, that this conclusion is linked to the low threshold of significant acceleration chosen for this comparative study (1.0 m/s^2).

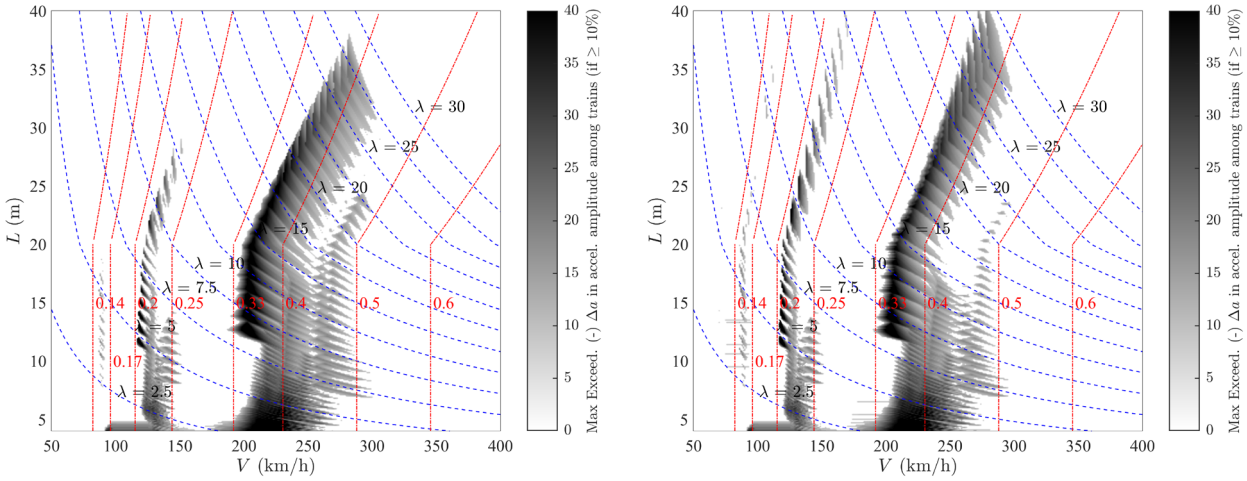

a) *b*)

Figure 62: Maps of Δa(−): DER vs. TSC. a) EQD-6 and b) EQD-18 trains. PSC bridges.

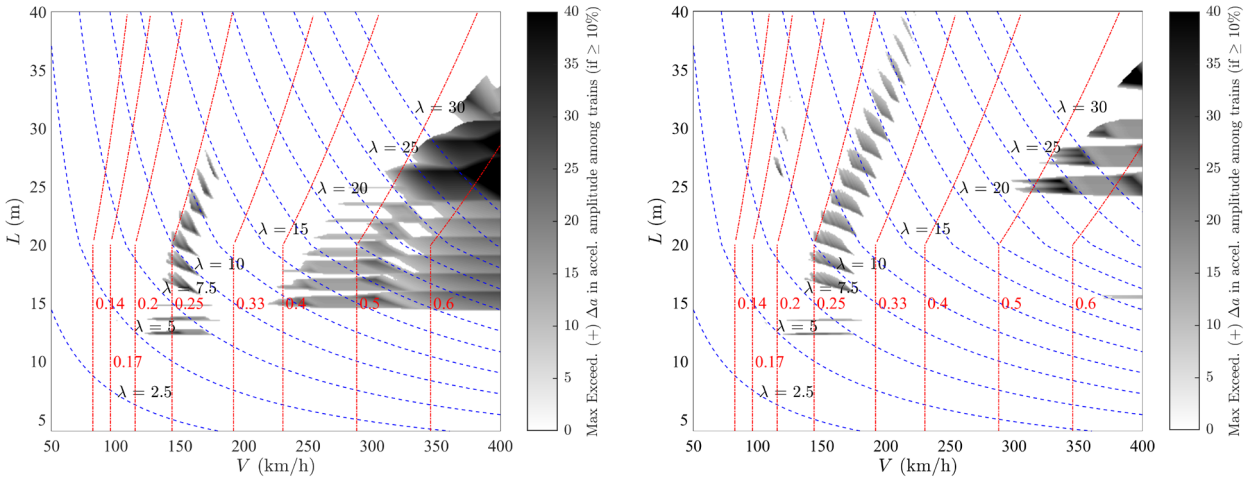

a) *b*)

Figure 63: Maps of Δa(+): LIR vs. TSC. a) EQD-6 and b) EQD-18 trains. PSC bridges.

7.1.2 Error levels for short conventional RP trains (short regular patterns – PT)

To obtain further conclusions about the performance of SM with short trains, in this section actual PTs are considered. The particular rolling stock used for this purpose consists in a series of 23 CB RP trains, of length greater that 200 m, as described in Table 7. Some of those trains are not symmetric because of the axle load intensities, but are however labelled RP because their axle distances follow the repetitive, regular pattern described in section 5.1.3. Some of the trains are inversed or mirrored versions of other trains in the same Table 7.

All those 23 trains being longer than 200 m, their corresponding short ("half-length") versions are created by removing 50% of their carriages. In case of an uneven number of carriages N, 50% of (N–1) of them are removed.

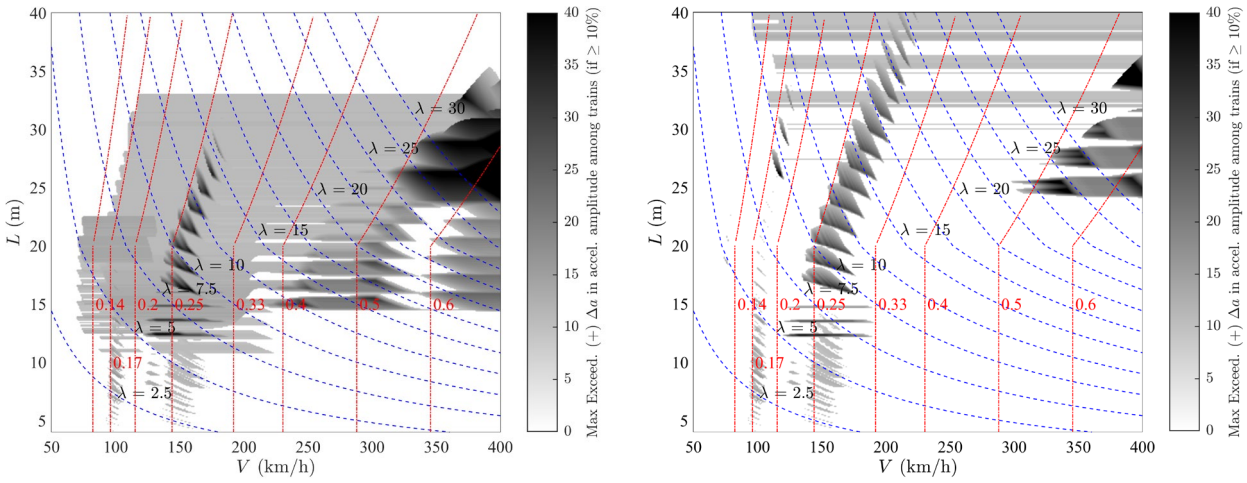

a) *b*)

Figure 64: Maps of Δa(+): DER vs. TSC. a) EQD-6 and b) EQD-18 trains. PSC bridges.

Table 7: List of trains selected for post-processing CB, RP vehicles of length > 200 m vs. half-length versions. Trains in blue font are mirrored versions of the previous train in the table.

CB (L_{tot} in meters)		
INB4EU-CB-005 (210.9 m)	INB4EU-CB-113 (338.05 m)	INB4EU-CB-096 (395.55 m)
INB4EU-CB-083 (210.9 m)	INB4EU-CB-018 (338.05 m)	INB4EU-CB-058 (395.63 m)
INB4EU-CB-071 (228.4 m)	INB4EU-CB-092 (338.05 m)	INB4EU-CB-111 (395.63 m)
INB4EU-CB-120 (228.4 m)	INB4EU-CB-028 (366.8 m)	INB4EU-CB-059 (395.63 m)
INB4EU-CB-011 (228.9 m)	INB4EU-CB-095 (366.8 m)	INB4EU-CB-060 (395.63 m)
INB4EU-CB-006 (258.7 m)	INB4EU-CB-079 (391.9 m)	INB4EU-CB-061 (395.63 m)
INB4EU-CB-084 (258.7 m)	INB4EU-CB-127 (391.9 m)	INB4EU-CB-112 (395.63 m)
INB4EU-CB-062 (338.05 m)	INB4EU-CB-029 (395.55 m)	—

The comparison of error levels of the SM for the half-length versions of the trains in Table 7, *vs*. the original trains in that table, is discussed below in terms of negative and positive exceedances.

Negative exceedance in accelerations: $\Delta a(-)$

The differences when using the LIR method in PSC bridges are minimal, with only small variations, as can be seen for example in Figure 65. This conclusion applies to all trains in Table 7, and also when considering STC bridges, although in this type of bridge more exceedance areas appear because more part of the response is above the 2.5 m/s² threshold for acceleration (see, for example, Figure 66 for the same train as in Figure 65).

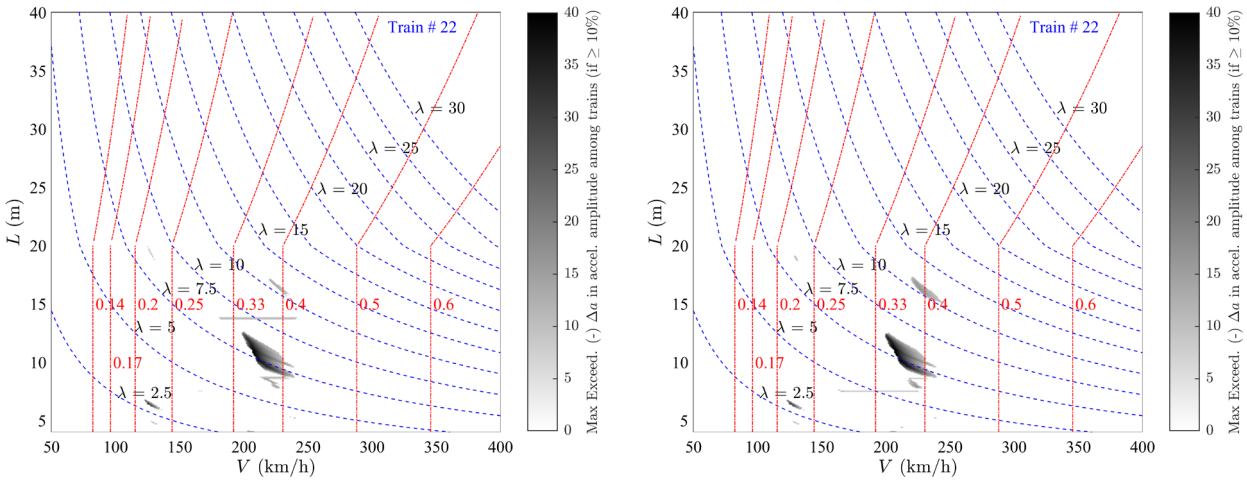

a) *b)*

Figure 65: Maps of Δa(–): LIR vs. TSC for original and half-length CB RP trains in Table 7. a) original INB4EU-CB-120; b) half-length INB4EU-CB-120. PSC bridges.

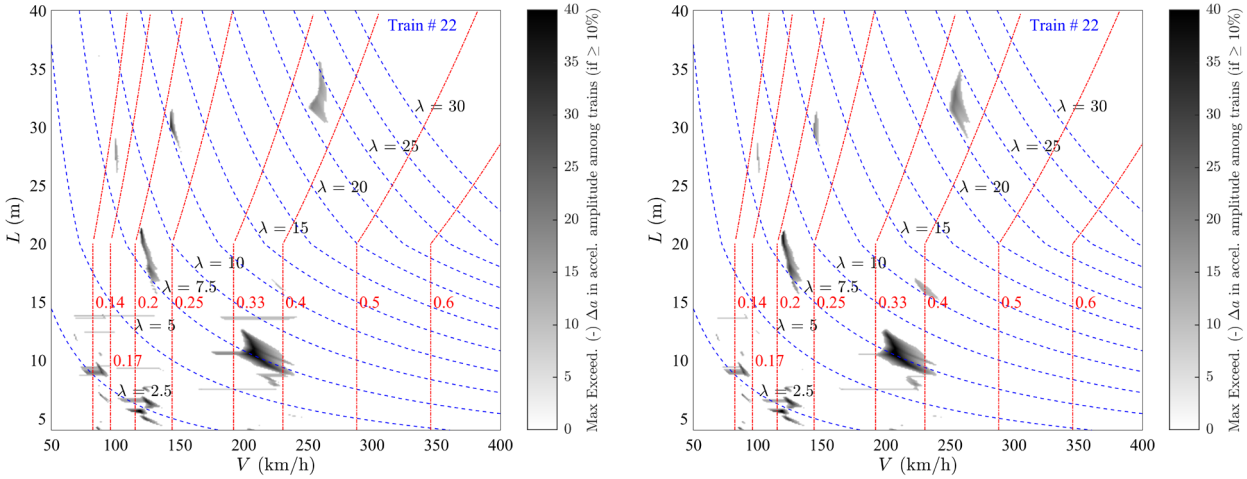

a) *b)*

Figure 66: Maps of Δa(–): LIR vs. TSC for original and half-length CB RP trains in Table 7. a) original INB4EU-CB-120; b) half-length INB4EU-CB-120. STC bridges.

In contrast, not all trains exhibit the same response with DER method. In some, there are few differences between the half-length and original versions, but in others the differences are more pronounced. Among those in Table 7, those that were already shorter originally show greater sensitivity, and, unexpectedly, when the half-length version is created, the DER prediction improves. This is shown in Figure 67 for the same train as in Figure 65.

The situation becomes more complex for STC bridges analysed with DER method. More short spans and short wavelengths are affected by the original trains, in comparison with the half-length trains, as shown in Figure 68. The conclusions from Figures 67 and 68 are influenced by the 10% limit set for considering meaningful an exceedance value. If that limit is increased to 15%, then subplots *a*) and *b*) in those figures become more similar.

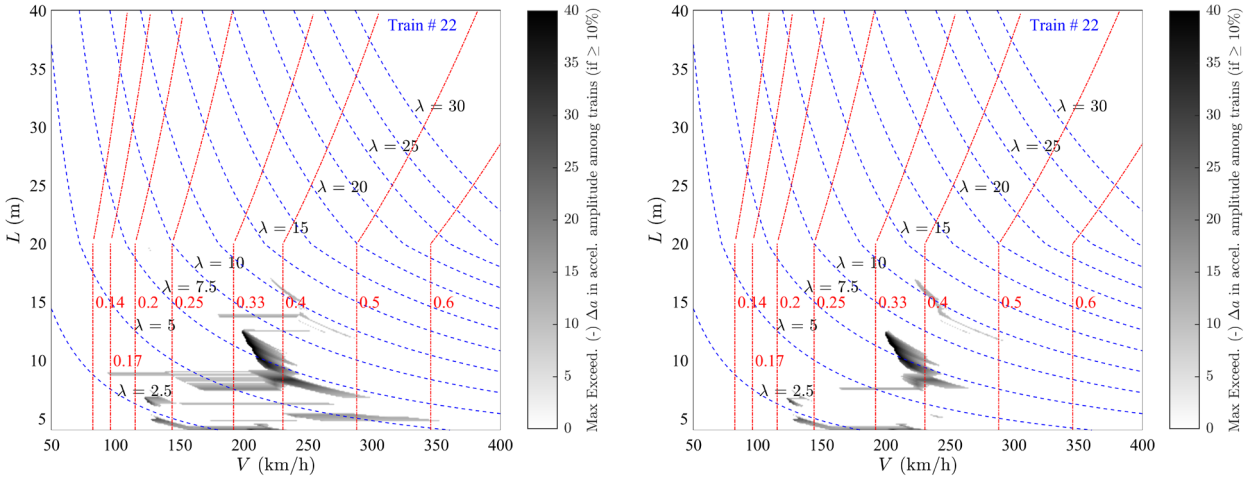

a) *b)*

Figure 67: Maps of Δa(−): DER vs. TSC for original and half-length CB RP trains in Table 7. a) original INB4EU-CB-120; b) half-length INB4EU-CB-120. PSC bridges.

Nevertheless, in certain cases the entire range of short spans and short wavelengths is defective and presents Δ*a*(−) greater than 10%, which in this case happens for the trains in Table 7 with the greatest original length, and without so much dependence between half-length and original versions of the vehicle, as shown in Figure 69; this can be attributed to an unsatisfactory performance of the DER for that range of spans and wavelengths on STC bridges.

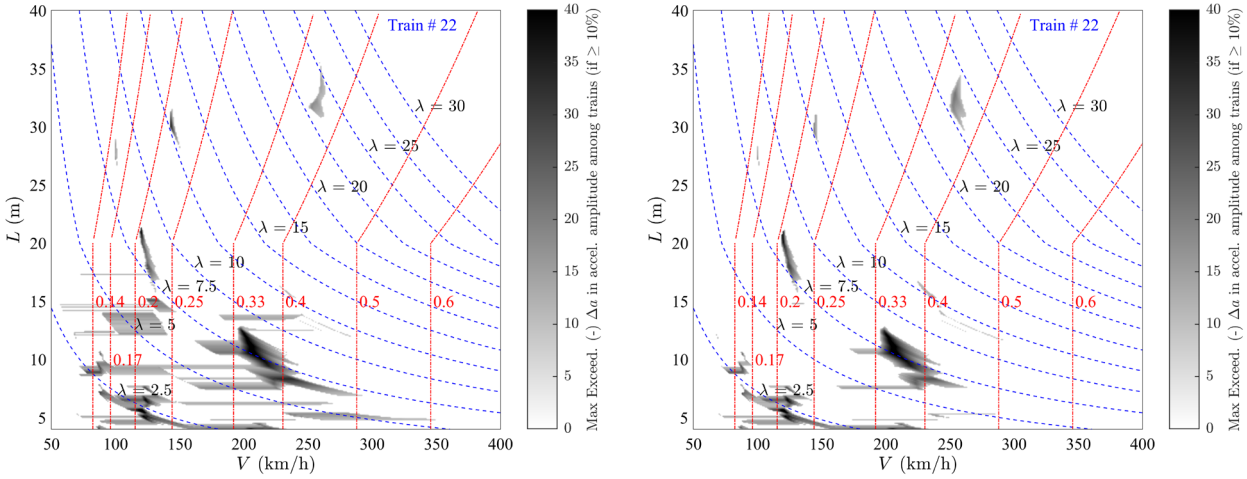

a) *b)*

Figure 68: Maps of Δa(−): DER vs. TSC for original and half-length CB RP trains in Table 7. a) original INB4EU-CB-120; b) half-length INB4EU-CB-120. STC bridges.

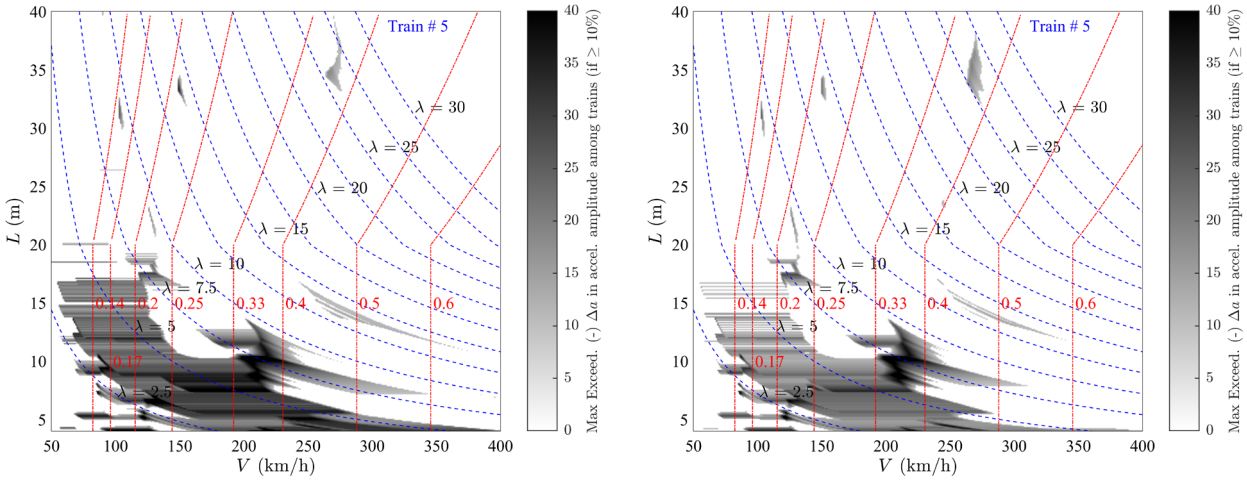

a) *b)*

Figure 69: Maps of Δa(−): DER vs. TSC for original and half-length CB RP trains in Table 7. a) original INB4EU-CB-028; b) half-length INB4EU-CB-028. STC bridges.

Positive exceedance in accelerations: Δ*a*(+)

On PSC bridges, the convex slopes area above *K*=0.45 approx. changes shape slightly, although not too significantly, see for example Figure 70. Otherwise, the Δ*a*(+) maps are quite similar for the original trains and their half-length versions, for both DER and LIR.

For STC bridges there are more variations between the original trains and their half-length versions. Although the overall appearance is largely similar, for most trains, specific areas appear where Δ*a*(+) worsens as the train length is reduced, which occurs with both methods (see Figure 71 for example). Due to the lower mass and damping, more regions of the response exceed the acceleration threshold and are affected by the too conservative prediction areas.

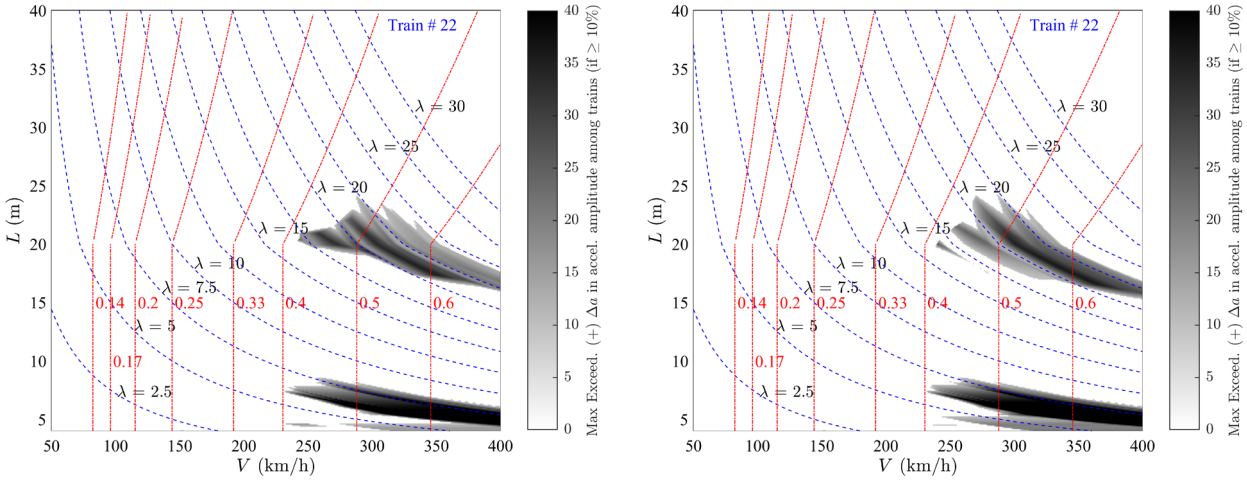

a) *b)*

Figure 70: Maps of Δa(+): LIR vs. TSC for original and half-length CB RP trains in Table 7. a) original INB4EU-CB-120; b) half-length INB4EU-CB-120. PSC bridges.

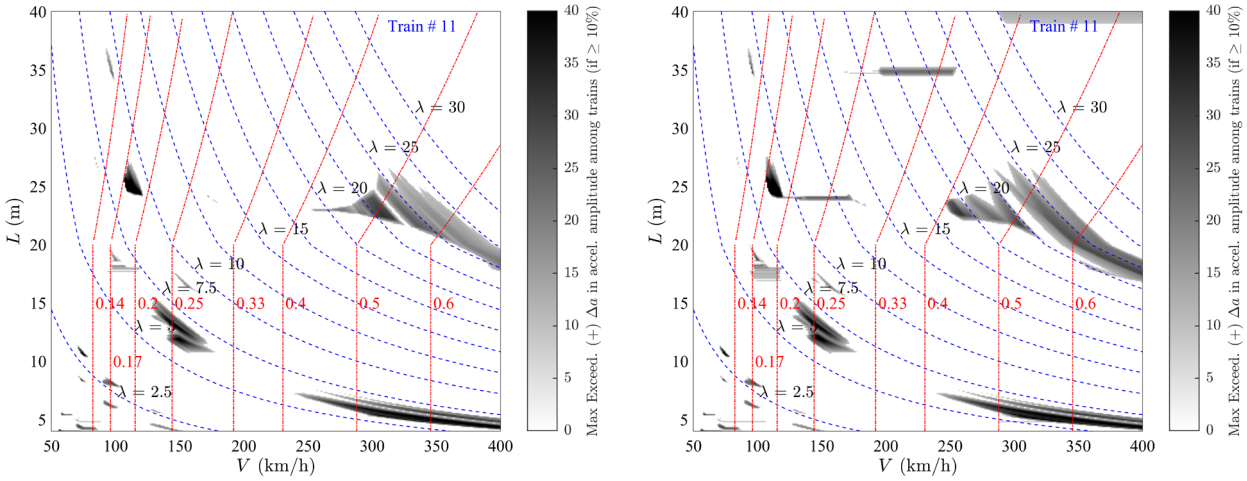

Figure 71: Maps of Δa(+): DER vs. TSC for original and half-length CB RP trains in Table 7. a) original INB4EU-CB-062; b) half-length INB4EU-CB-062. STC bridges.

Negative exceedance in displacements: Δδ(−)

It is recalled that for analysis of displacements in SS bridges the threshold is set on the impact coefficient rather than on acceleration. That cancels the influence of the bridge mass, and thus the aspect of exceedance maps for displacements in PSC and STC bridges are more similar than for accelerations.

As mentioned in section 6.2, in general, the performance of SM as regards Δδ(−) is good and few grey areas are found in the exceedance maps. Besides, a negligible influence is observed when the length of the vehicle is halved, therefore the maps are not shown for brevity. The few grey regions are mostly affected by defective ascending slopes—only slightly wider for DER at lower wavelengths (see section 6.2).

Positive exceedance in displacements: Δδ(+)

Finally, in PSC bridges, Δδ(+) worsens in most cases when the train length is halved. However, for some trains the opposite occurs (compare Figures 72 and 73), which is also linked to the permissible 10% tolerance, as discussed, for example, in section 6.2.

Trains with carriages below D=26 m are somewhat less affected by the deterioration in subharmonics above the first one. In general, the most recognizable pattern is that of overconservative waterdrops; however, this pattern is filtered in some areas by the 10% tolerance, as mentioned before. These conclusions are held for STC bridges, with some areas more affected by Δδ(+) at medium and low wavelengths.

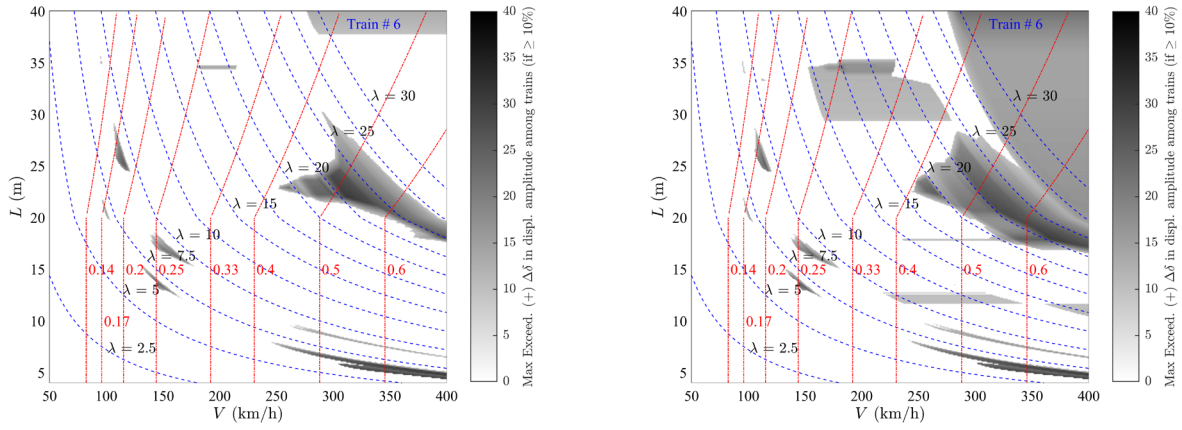

a) *b)*

Figure 72: Maps of Δδ(+): DER vs. TSC for original and half-length CB RP trains in Table 7. a) original INB4EU-CB-029; b) half-length INB4EU-CB-029. PSC bridges.

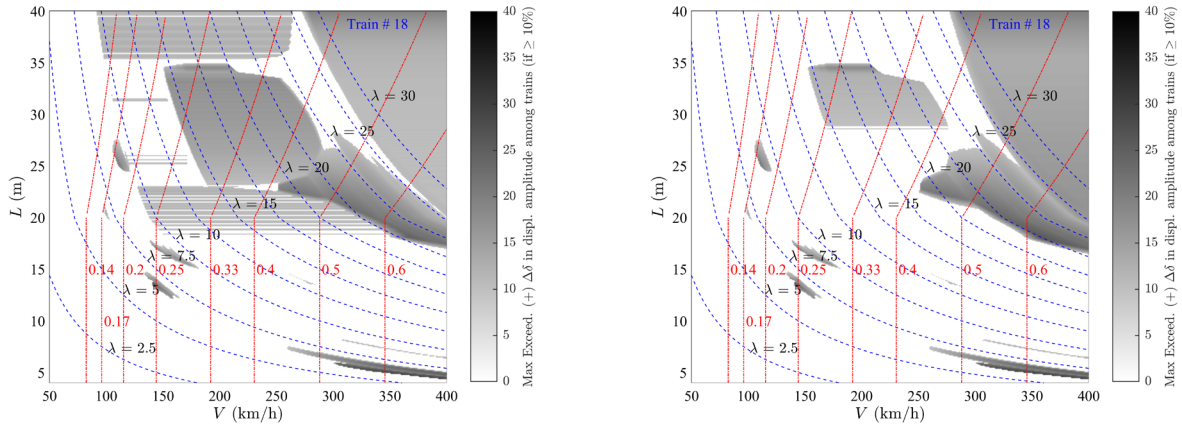

a) *b)*

Figure 73: Maps of Δδ(+): DER vs. TSC for original and half-length CB RP trains in Table 7. a) original INB4EU-CB-096; b) half-length INB4EU-CB-096. PSC bridges.

7.2 Limitations in the analysis of trains with irregular architectures

This section is dedicated to investigating the limitations of SM in relation to KS-3.

7.2.1 Error levels for CMU trains (coupled multiple units – PT)

CMU trains are a large subtype, with 56 vehicles, although all of them have a car length very close to D=26.0 m and three units, resulting in a certain homogeneity in some of the results discussed below.

Negative exceedance in accelerations: $\Delta a(-)$

The $\Delta a(-)$ results for CMU trains are similar to those shown for CART trains in the section 6.3. The DER method continues to perform worse than LIR for short spans below L=12.5 m approx., at the third subharmonic (i=3) or higher, and on PSC bridges. Both methods perform worse than for CB RP trains. When analysing STC bridges, more problematic spans emerge, as more cases exceed the acceleration response threshold (2.5 m/s²): the affected spans comprise up to approximately L=20 m with the DER method, and the LIR method also shows some further underestimations of resonant peaks, although to a lesser extent (see Figure 74).

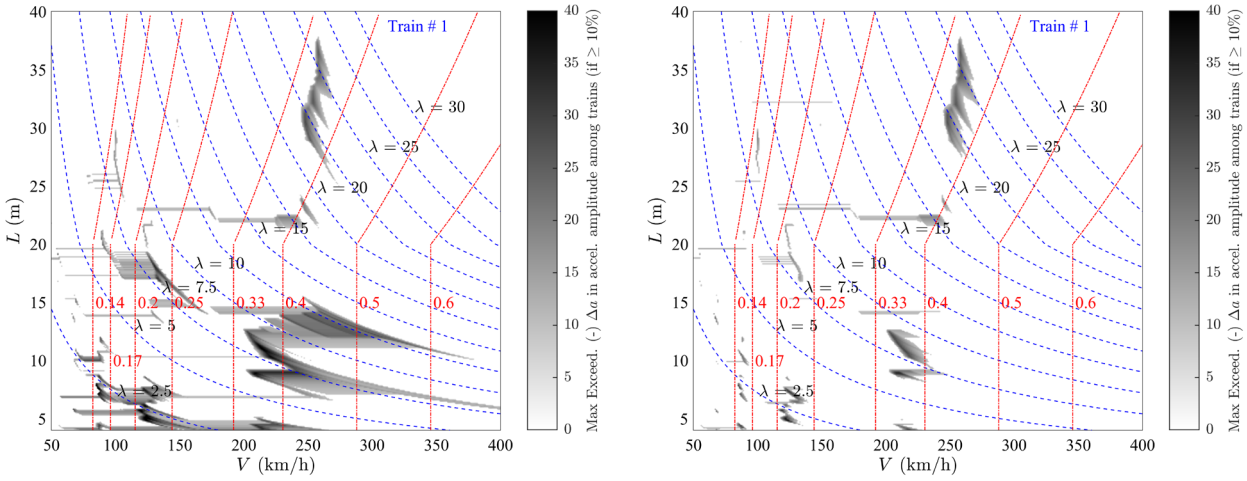

a) *b*)

Figure 74: Maps of $\Delta a(-)$: DER and LIR, both vs. TSC for train InB4EU-CB-128 (D=25.9 m). a) DER; b) LIR. STC bridges.

Positive exceedance in accelerations & negative exceedance in displacements: $\Delta a(+)$ and $\Delta\delta(-)$

The remaining conclusions for CMU trains are little affected by the type of bridge, whether PSC or STC.

Regarding the $\Delta a(+)$ maps, these conclusions can be summarized as being very similar to those of the CB RP trains (see section 6.2). The same applies to the $\Delta\delta(-)$ exceedance.

Positive exceedance in displacements: $\Delta\delta(+)$

Finally, for $\Delta\delta(+)$, the shortest trains in the group (total length between 160 and 240 m) show worse performance for spans 20 m $\leq L \leq$35 m approx., in the first subharmonic (i=1). In those cases there happens a very similar resonance in both these trains and the longer ones, but SM are less accurate in the shorter trains. The pattern of overconservative waterdrops is typically not present here. Two representative cases for CMU trains are shown in Figure 75: subfigure *a*) with total length close to 400 m, and subfigure *b*) with total length close to 200 m.

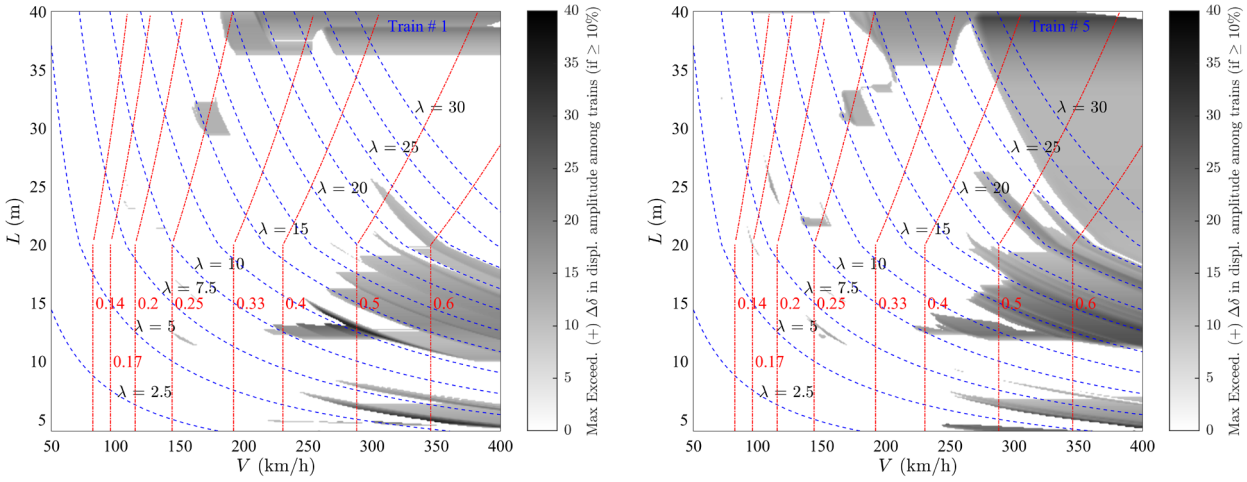

a) *b)*

Figure 75: Maps of Δδ(+)*: LIR vs. TSC. a) train InB4EU-CB-128 (D=25.9 m). b) train InB4EU-CB-132 (D=26.4 m). STC bridges.*

7.2.2 Error levels for double RP units (PT)

In contrast with the CMU subtype, CMU-2-RP trains are a smaller group that contains 7 vehicles with car lengths $25.9 \le D \le 27.2$ m and two equal units, coupled in the middle of the train where it appears an irregularity in the pattern of axle distances.

Negative exceedance in accelerations: $\Delta a(-)$

For the LIR method, in general, the coupling in the middle of the train does not lead to significant worsening, when results are compared to those of CB RP trains (section 6.2): the CMU-2-RP that have an equivalent RP vehicle (of approximately half length), produce very similar $\Delta a(-)$ maps, and the ones that do not have such an equivalent vehicle produce $\Delta a(-)$ maps qualitatively quite similar to the ones in section 6.2.

Conversely, for the DER method a worsening is observed for those CMU-2-RP that have an equivalent RP vehicle; Figure 76 shows a representative example. And overall, the $\Delta a(-)$ maps show larger areas of exceedance than the ones in section 6.2.

Positive exceedance in accelerations: $\Delta a(+)$

In general, as for the $\Delta a(-)$ results, for the LIR method the coupling in the middle of the train does not lead to significant worsening, when results are compared to those of CB RP trains (section 6.2). Regarding the DER method, somewhat better performance is indeed found for the CMU-2-RP, particularly the grey areas of convex slopes above K=0.45 approx. become less dense.

Negative exceedance in displacements: $\Delta\delta(-)$

Regarding the values of $\Delta\delta(-)$, for both SM the conclusions are very similar to those of previous sections: little grey areas are found in the exceedance maps and good performance is observed for the CMU-2-RP trains.

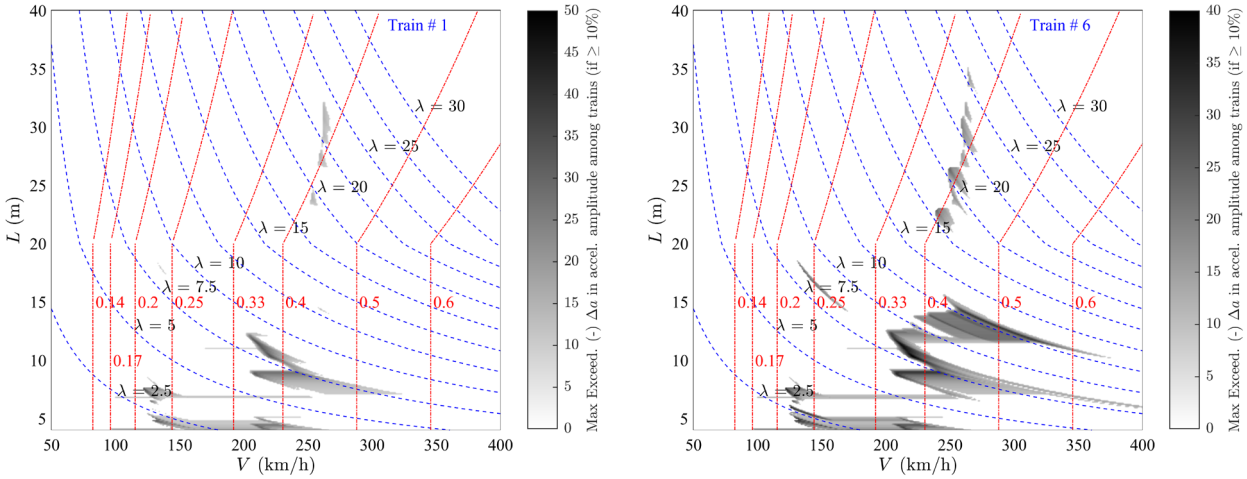

a) *b*)

Figure 76: Maps of Δa(–): DER vs. TSC. a) train CB RP InB4EU-CB-001 (D=25.9 m); b) corresponding CMU-2-RP train InB4EU-CB-001 (D=25.9 m). PSC bridges.

Positive exceedance in displacements: Δδ(+)

Finally, as it happens with the CMU trains (section 7.2.1), the shortest trains in the group show worse performance for spans 20 m $\leq L \leq$ 35 m approx., in the first subharmonic (i=1). The pattern of overconservative waterdrops is not usually present either. Two representative cases of CMU-2-RP trains are shown in Figure 77: subfigure *a*) with total length close to 400 m, and subfigure *b*) with total length close to 200 m. In that figure the waterdrop pattern is slightly visible, but the overestimations are not strong enough to exceed the 10% threshold.

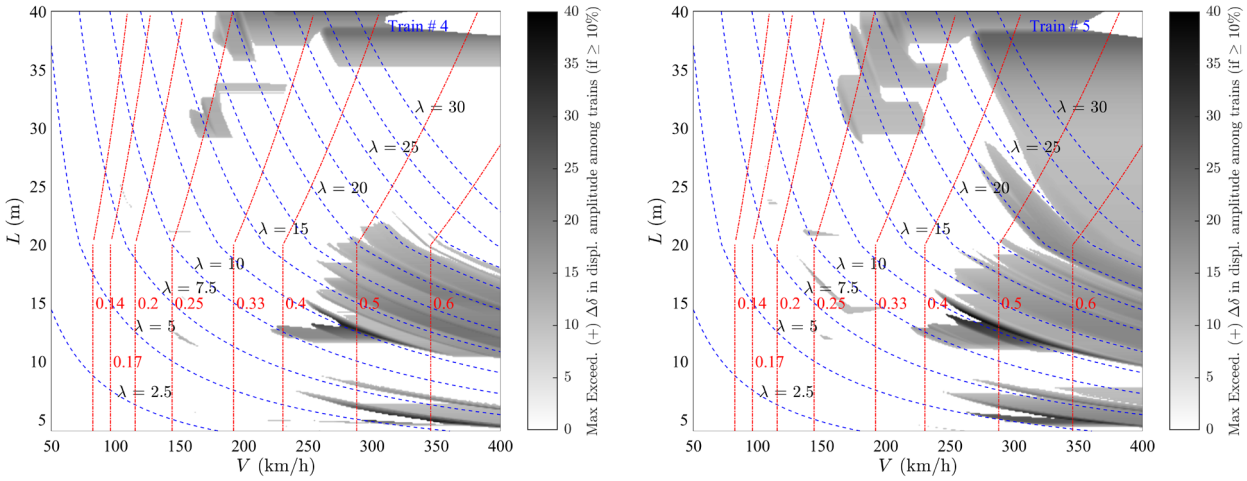

a) *b*)

Figure 77: Maps of Δδ(+): LIR vs. TSC. a) train InB4EU-CB-108 (D=25.9 m). b) train InB4EU-CB-141 (D=25.8 m). PSC bridges.

7.3 Limitations due to end-transient and locomotive transient response

This section is dedicated to investigating the limitations of SM in relation to KS-4.

General assessment:

In general, for trains classified as end-transient, the prediction of vertical acceleration worsens somewhat due to the occurrence of those transient phenomena. The mean exceedance indicators for each Z24 increase for $\Delta a(-)$ in areas where, with CB RP type trains, they were very low (compare Figures 78 *vs*. 79). This overall assessment also applies to $\Delta a(+)$.

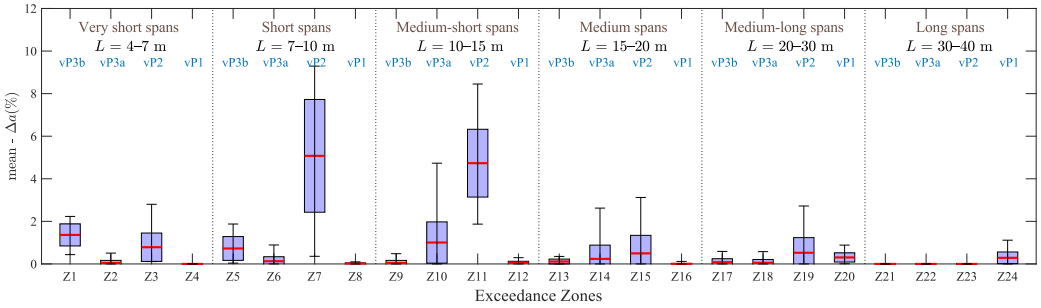

Figure 78: Box plots of Z24 mean $\Delta a(-)$: LIR vs. TSC. End-transient trains. PSC bridges.

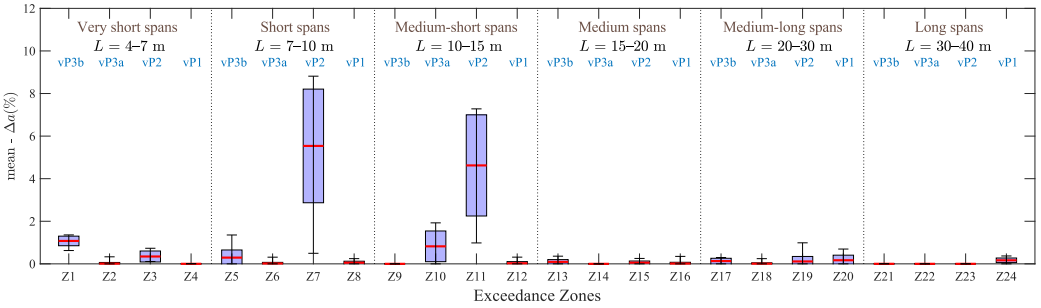

Figure 79: Box plots of Z24 mean $\Delta a(-)$: LIR vs. TSC. CB RP trains longer than 150 m. PSC bridges.

Regarding $\Delta\delta(-)$ and analysing the variety of PT60 model trains, it is observed that trains #28 to #40, which are of AB type with locomotives (also train #52), suffer from an underestimation of the peaks because the locomotive axles are removed for computing the *static deflection at resonance*. The weight of the power car in the transition to the passenger cars has a clear influence, and when the locomotive axles are removed the static part of the deflection is underestimated.

The same occurs for SA trains with RLH-bL, numbers #47 and #48; RLH-sCbL, number #49; and RLH-2fLrL, number #50; and CRLH-mL, number #57, which is a double-unit with four locomotives.

The problem appears as the already mentioned (non-conservative) waterdrop pattern that implies peak underestimations that cancel out at the RIL valleys, and its origin is the same in all those cases. Therefore, an alternative procedure would be *not to remove the locomotive axles* to compute the static part of the deflection for AB and SA loco-hauled trains.

Train #41 is instead a CB without a rear locomotive, and therefore gives better results for $\Delta\delta(-)$, as does train #42. Train #43 is an RLH-2fL and performs slightly worse in some areas due to initial transients from the two front power cars.

From train #44 onwards, CB trains with heavier rear locomotives appear, so the resonance peaks are again underestimated in the final transients leading to Δδ(−) regions, following the waterdrop pattern. The same applies to trains numbered #45, #46 (RLH-3rL), #51, #53, #54 (only slightly, because the locomotives are lighter than on other trains), #55, #56, #58 (the transient occurs in the intermediate locomotives), #59 (same), and #60 (the transient sometimes occurs in the last locomotive, sometimes in the intermediate one).

However, the prediction for these trains, being less conservative, produces fewer Δδ(+) zones than for the PT60 trains that are not loco-hauled (the ones up to and including train #27). Therefore, if the alternative procedure mentioned above is tested, the Δδ(+) behaviour worsens and may lead to the opposite pattern. Five trains from model PT60 are tested to investigate that possibility, and effectively Δδ(+) is found to increase visibly (compare Figures 80 and 81). Therefore, it remains to decide which option is preferable in each use, though in principle it is advisable to keep the axles of rear and intermediate power cars, for AB and SA trains, and also for CB trains if those axles are heavier, whenever a non-conservative prediction is to be avoided in the computation of static displacement for usage with DER/LIR.

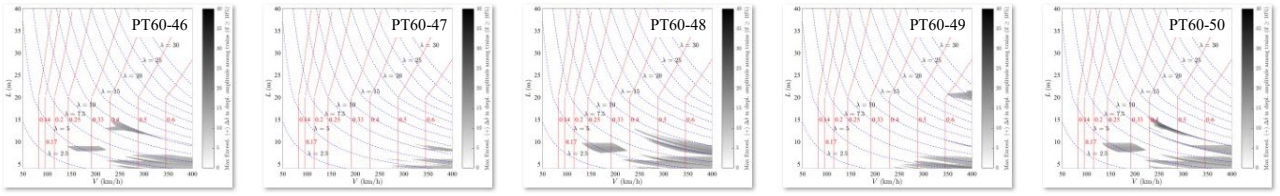

Figure 80: Δδ(+) for five loco-hauled trains from model PT60. Static part of the displacement computed removing the axles of locomotives (i.e. basic SM formulation used in deliverable D1.2). PSC bridges.

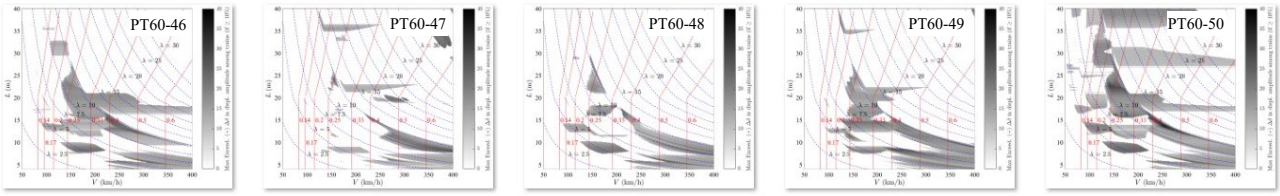

Figure 81: Δδ(+) for five loco-hauled trains from model PT60. Static part of the displacement computed without removing the axles of locomotives. PSC bridges.

Analysis of the transient phenomena: Δ*a*(−)

Section 6.2 presented examples of transients that can cause errors in the prediction of the DER or LIR, where the effect was due either to the first or second bogie of conventional train cars with regular wheelbases (CB RP). This section shows other relevant cases originating from end transients and locomotive transients (whether located at the end of the train or not).

Figure 82 shows a case where a Δ*a*(−) occurs due to an LH-bHL subtype train, when the centre of the penultimate bogie is located over the end abutment of the bridge. This differs from the cases mentioned in section 6.2, where the bogie responsible for the transient was located near the centre of the span. In this case, there is only one load acting on the bridge.

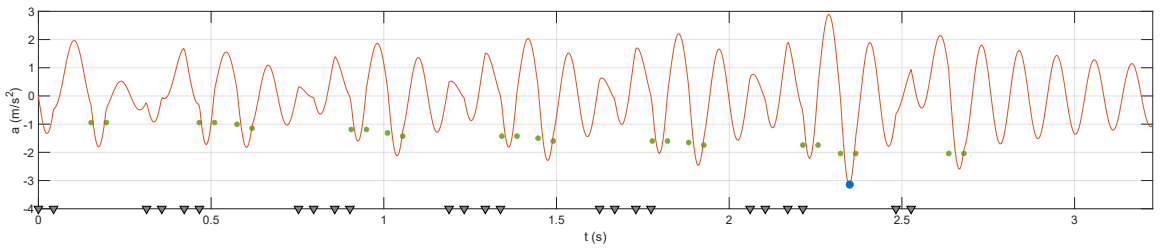

Figure 82: LIR vs. TSC. Negative exceedance: train INB4EU-CB-030 (D=24.0 m; LH-bHL), V=205 km/h, L=8.7 m, PSC bridge. Δa(−)=20.8%

Conversely, Figure 83 shows a case where a Δ*a*(−) occurs due to an LH-fHL subtype train, despite not having a final heavy locomotive. The end-transient peak occurs now when the first load of the third-to-last bogie has just entered the span, being therefore very close to the first abutment, and this load is also the only one on the bridge.

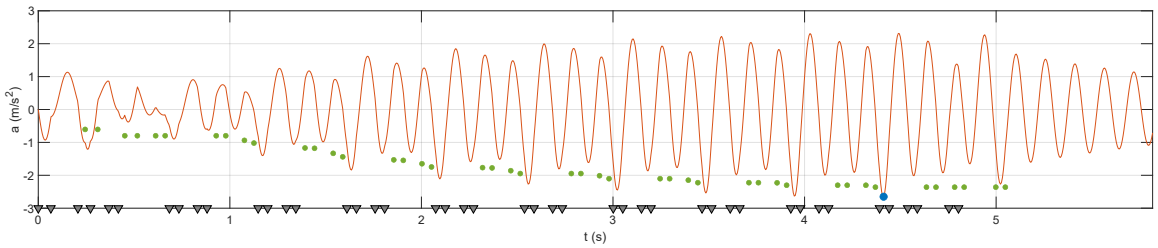

Figure 83: LIR vs. TSC. Negative exceedance: train INB4EU-CB-075 (D=23.3 m; LH-fHL), V=181 km/h, L=12.3 m, PSC bridge. Δa(−)=10.7%

Figure 84 shows another final transient due to the last bogie of a CMU train on a longer bridge (*L*=25.2 m), but which experiences a negative Δ*a*(−) when the last bogie passes approximately through the centre of the span. This figure should be compared with another transient on a bridge of similar length (L = 24.2 m), where another CMU creates a transient, but this time an intermediate one—not a final one—, in which four loads act simultaneously on the span (Figure 85). That is, the greater length of the bridge allows for other variations of the transient phenomenon to appear.

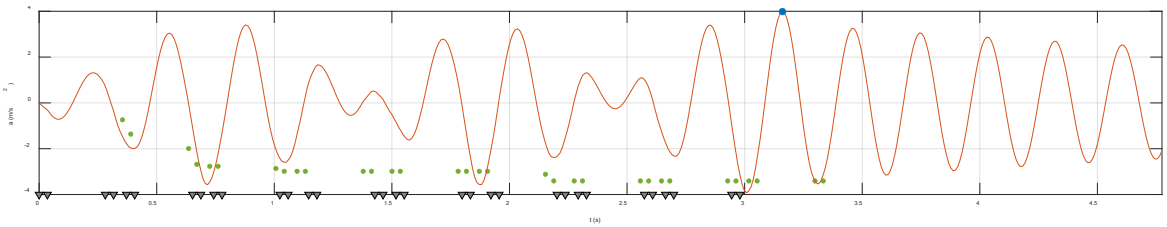

Figure 84: LIR vs. TSC. Negative exceedance: train INB4EU-CB-134 (D=26.4 m; CMU), V=256 km/h, L=25.2 m, PSC bridge. Δa(−)=14.2%

A final example of interest regarding Δ*a*(−) is shown in Figure 86, where the transient is again of the "end" type, occurring while the first load of the last bogie and the last load of the penultimate bogie are both acting on the structure. The train is of type CLH-bHL.

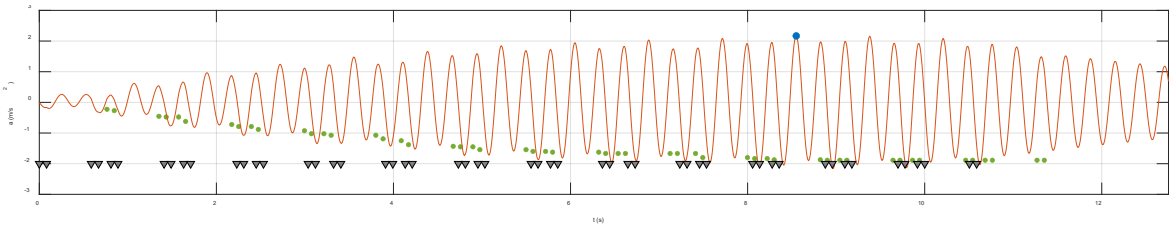

Figure 85: LIR vs. TSC. Negative exceedance: train INB4EU-CB-154 (D=25.6 m; CMU), V=114 km/h, L=24.2 m, PSC bridge. Δa(−)=10.2%

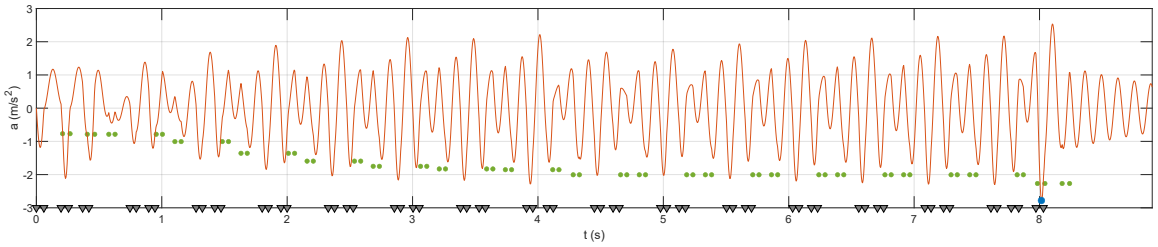

Figure 86: LIR vs. TSC. Negative exceedance: train INB4EU-CB-138 (D=26.5 m; CLH-bHL), V=181 km/h, L=10.5 m, PSC bridge. Δa(−)=16.4%

In addition to the variations just shown, it should be noted that, in cases with multiple loads on the span, their intensity will affect the response: if a relevant transient may be predicted for one load combination, for others with same axle distances but different load values, an erroneous prediction could be reached.

Furthermore, it can be observed that in some of the cases discussed above the resonant peak implies positive acceleration, while in others it implies negative acceleration. This requires, if combined with any kind of forced response correction, to consider the phase of the maximum free vibrations. The only strategy that could be suggested a priori is to correct the peak value given by the DER/LIR, both positively and negatively, with such forced term, thus accounting for both scenarios. This adds further complexity to the attempt to provide a limited number of recommendations for correcting the peak value predictions given by current SM.

In summary, the ensemble of factors to consider for predicting a relevant transient in the evaluation of response peaks using SM should be, for CB trains:

- That both bogies of a car may cause the transient when it is due to them passing approximately through the centre of the span.
- That loads located near any of the supports may also cause a transient.
- That on longer bridges, two bogies can be simultaneously on the bridge, acting approximately centred.
- If the loads are not all of them of equal value, the peak of the response will occur earlier or later, depending on which loads are heavier.
- Sometimes, even a single load on each bogie may cause the transient phenomenon.
- Scenarios of positive or negative acceleration peaks must be considered.

It should also be remembered that, as seen in previous sections, the DER method generally produces more transients that affect the calculation of $\Delta a(-)$.

Analysis of the transient phenomena: $\Delta a(+)$

Regarding $\Delta a(+)$, the behaviour of the HSLM-A trains is analysed as an example. Their geometric variations are easy to remember, as they all have locomotives with identical spacing patterns and all loads within each train are constant.

For the HSLM-A1 train (P=170 kN), Figure 87 shows a transient due to the first locomotive, where the overestimation occurs because the peak generated when the first passenger car bogie is departing is not calculated correctly. There is only one load on the bridge, near its second abutment.

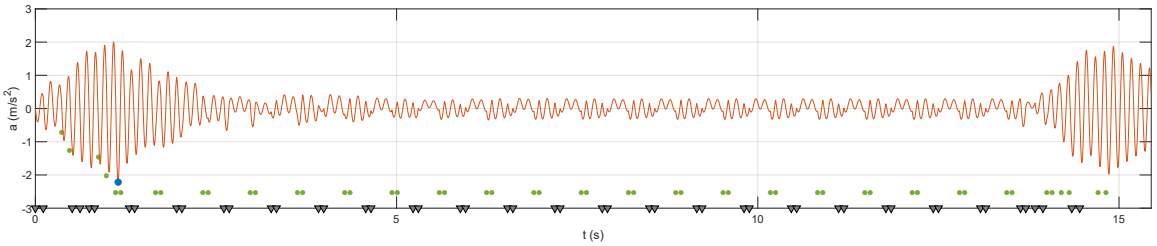

Figure 87: LIR vs. TSC. Positive exceedance: train HSLM-A1 (D=18.0 m; ALH), V=99 km/h, L=10.0 m, PSC bridge. Δa(+)=14.2%

In trains similar to HSLM-A1, this type of transient does not appear for HLSM-A2 (P=200 kN) or HSLM-A4 (P =190 kN), both with slightly heavier loads than HSLM-A1, but conversely it does appear in HSLM-A3 (P =180 kN), which shows the difficulty in predicting the phenomenon.

For HLSM-A2 (P=200 kN), it can be seen in Figure 88 that the relevant transient has shifted to the las passenger car bogie, immediately before the rear power car enters the span. That bogie is acting nearly mid-span, but in this case it does not increment the response and it diminishes the acceleration instead. As for Train HSLM-A4 (P=190 kN), it does not suffer from any of these relevant transients.

The later trains of the HSLM-A model exhibit similar behaviour to the A1 and A3 for these short bridges, primarily affecting the fifth subharmonic (i=5), with greater intensity for DER than LIR, in the $6.5 \leq L \leq 8.0$ m range and also at around L=10 m. However, train A8 hardly suffers from these problems. These transient phenomena, therefore, prove difficult to characterize using simple *a priori* rules.

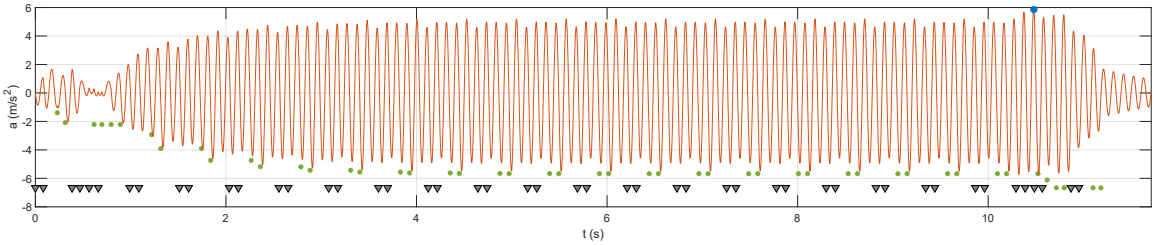

Figure 88: LIR vs. TSC. Positive exceedance: train HSLM-A02 (D=19.0 m; ALH), V=136 km/h, L=8.4 m, PSC bridge. Δa(+)=10.9%

Regarding the longer wavelengths of the first subharmonic (i=1), Appendix E shows an affected area for the longer HSLM-A trains and spans above some 30 m, where the final response to the passing train, immediately after the free vibration begins, is overestimated by approx. +12% with both DER and LIR (see Figure 89 for the HSLM-A7, where the transients for short bridges are also visible).

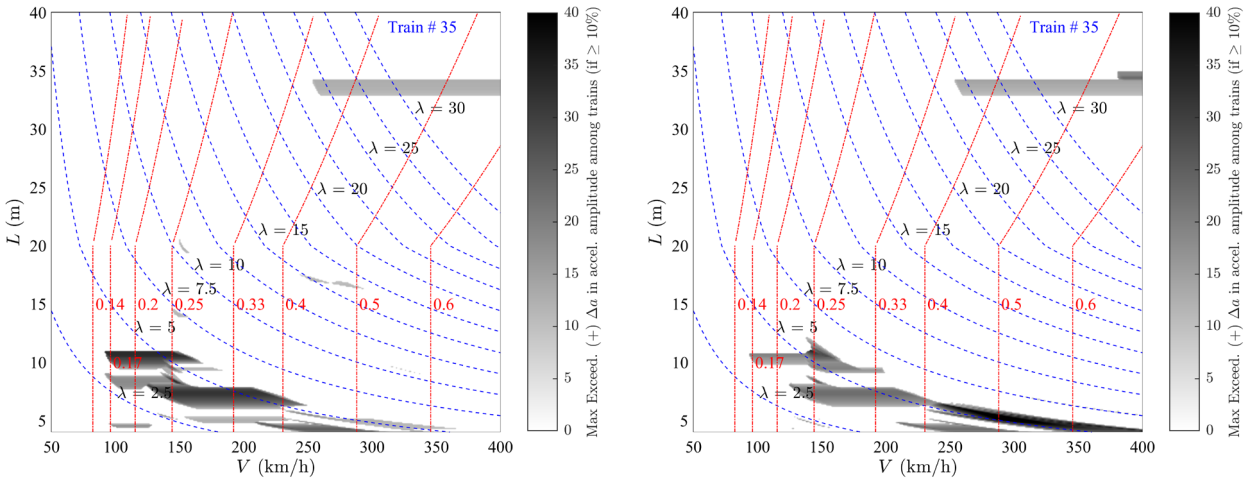

a) *b)*

Figure 89: Maps of Δa(+): LIR and DER, both vs. TSC for HSLM-A7. a) DER; b) LIR. PSC bridges.

Conclusions about transient phenomena:

The possibility of incorporating all the variants of transients described above into a limited number of *a priori* rules, applicable to the European rolling stock, does not appear feasible at present. A line of research could be opened to explore, first and foremost, specific vehicle variants such as regular or articulated RP trains with constant loads. This would eliminate the uncertainty introduced by the greater number of bogies in CB trains and the potential variability in the intensity of loads close to one another. Depending on the success of such line of research, the complexity of extending it to other rolling stock could be assessed, although this currently offers limited guarantee.

On the other hand, similar problems arise in displacement calculations, with the added complication that the static effect of locomotives may or may not be relevant depending on their weight, as described before in this section. Therefore, the manner to consider the static contribution combined with resonance introduces an additional source of uncertainty for vehicles with heavy locomotives.

In any case, the perception that resonant peaks are augmented or diminished by the forced response suggests a line of work that has been reflected in this report in the proposal of the new HLIR method, which is presented in section 9.2. HLIR method locates these resonant maxima in time, and then straightforwardly adds the correction of the forced response to obtain a significantly improved prediction.

7.4 Limitations in the analysis of non-symmetric trains

This section is dedicated to investigating the limitations of SM in relation to KS-5.

To study the influence of symmetry on the load patterns, conventional trains were selected whose axle load shows small scatter in terms of amplitude, but which belong to the *nonsymmetric series* defined in section 5.1.2.2, due to irregular axle distances. This comprises 44 trains of MU and CMU subtypes, in which no locomotives appear significantly heavier than the passenger cars. Car lengths *D* of those trains are on the order of 24–26 m, and total lengths are between 290 and 420 m approximately. This set of vehicles will henceforth be referred to as the "nonsym-B" model. Table 8 collects all trains comprised in such model.

From these, a series of 44 shorter trains is constructed, in which the minimum car length is close to 18 m, simply multiplying the wheelbases of nonsym-B model by a factor 18/24, while maintaining the bogies to have

a realistic wheelbase: this is "nonsym-A" model. And finally, another series of 44 longer trains is generated, in which the minimum car length is approximately 27 m, by multiplying the wheelbases by 27/24 but also maintaining the same number of bogies (model "nonsym-C").

To compare the nonsym-A/B/C models with comparable but symmetrical ones, three train sets named "sym-A/B/C" are generated as follows: the first car of each train in the corresponding nonsymmetric models is considered, the distance between its last axle and the first axle of the second car is determined, and with this data, a CB RP pattern is constructed to define the wheelbases of the entire new symmetrical train, keeping the total number of cars identical between the corresponding symmetrical and nonsymmetric trains. Finally, it is verified that the total length of the corresponding nonsymmetric and symmetrical trains remains similar.

Table 8: List of 44 CB trains selected for post-processing nonsymmetric transient phenomena (MU and CMU).

Model *nonsym-B*		
INB4EU-CB-045	INB4EU-CB-158	INB4EU-CB-180
INB4EU-CB-046	INB4EU-CB-160	INB4EU-CB-181
INB4EU-CB-047	INB4EU-CB-161	INB4EU-CB-183
INB4EU-CB-048	INB4EU-CB-162	INB4EU-CB-184
INB4EU-CB-049	INB4EU-CB-164	INB4EU-CB-185
INB4EU-CB-050	INB4EU-CB-165	INB4EU-CB-187
INB4EU-CB-100	INB4EU-CB-167	INB4EU-CB-188
INB4EU-CB-101	INB4EU-CB-168	INB4EU-CB-190
INB4EU-CB-102	INB4EU-CB-170	INB4EU-CB-191
INB4EU-CB-103	INB4EU-CB-171	INB4EU-CB-193
INB4EU-CB-104	INB4EU-CB-173	INB4EU-CB-194
INB4EU-CB-105	INB4EU-CB-174	INB4EU-CB-196
INB4EU-CB-154	INB4EU-CB-175	INB4EU-CB-197
INB4EU-CB-155	INB4EU-CB-177	INB4EU-CB-198
INB4EU-CB-157	INB4EU-CB-178	—

For the sake of conciseness, the discussion is limited to PSC bridges. Regarding $\Delta a(-)$, in Figure 90, for some representative vehicles of the different models, it can be observed that the lack of symmetry causes some additional transient phenomena (Figures 90*a,* 90*c,* 90*d,* in contrast to 90*b,* 90*d,* 90*e*), although without significant differences compared to the corresponding symmetric trains. The region after the first cancellation (K=0.33) is the most affected in the third and fourth subharmonics (i=3, 4), and the first subharmonic (i=1) is more affected by the problem of ascending slopes for trains with shorter cars (Figures 90*a* and 90*b*). In CB trains, the second subharmonic (i=2) is not usually determinant when calculating the cumulative response due to the *car factor*, as is known (Museros *et al*. 2024). The DER method is not analysed in this case, as it has typically proven to be less accurate than the LIR method with respect to $\Delta a(-)$.

Regarding $\Delta a(+)$, as with the LIR method, there are still no excessively marked differences. For trains with shorter cars, in general, the lack of symmetry worsens the results at some specific spans for MU trains, but curiously, the opposite is true for CMU trains, in spans below L=10 m. For trains of intermediate coach length,

the trend is the same, although there are no major differences, with these being observed more frequently in the form of peak overestimations around K=0.25. In trains with longer cars, these overestimations affect more nonsymmetric trains, always for spans below approximately 15 m. Therefore, it is difficult to draw conclusions of general applicability. These results are not shown here for brevity; instead, the results of the DER for $\Delta a(+)$ are analyzed below. This method, as discussed in previous sections, generally produces peak overestimations less frequently than the LIR for short spans.

Reviewing the DER results for $\Delta a(+)$, in short-car trains there is similar behavior for symmetric and nonsymmetric MUs; although it is somewhat worse for CMUs and short spans when those trains are symmetric (see Figures 91*a* and 91*b*). With medium-length cars, nonsymmetric MUs give somewhat worse results for some spans (Figures 91*c* and 91*d*), but, in general, in the larger exceedance areas (which are not excessively affected in their shape), the error levels are worse with symmetrical trains than with asymmetrical ones, which was not expected a priori (again see Figures 91*c* and 91*d*). This last conclusion extends to longer-car trains (Figures 91*e* and 91*f*). Therefore, drawing general conclusions is again not easy.

As for $\Delta\delta(-)$, this error is usually very small or practically zero for all trains, as mentioned in various previous sections. Therefore, the corresponding graphs are omitted for brevity. Only for the trains with longer cars is a slight negative influence of non-symmetry in the DER observed, for some trains, in the form of peak underestimation in the fourth subharmonic (i=4). This affects spans below approximately L=10 m, with an error level of around 15%. However, this does not occur for other very similar trains of the same nonsym-C model, which again highlights the difficulty in predicting transient effects in advance.

Finally, regarding exceedance $\Delta\delta(+)$, in the LIR model, the nonsym-A trains exhibit slightly higher error levels than their symmetric counterparts for spans between approximately $20 \le L \le 25$ m when K=0.25, although the error intensity for the symmetric trains is slightly greater for short spans at high speed (see Figures 92*a* and 92*b*). In any case, these are not substantial differences in the SM prediction. Similar behaviour is seen for the nonsym-B vs. sym-B trains (Figures 92*c* and 92*d*), and for the nonsym-C vs. sym-C model (Figures 92*e* and 92*f*). It can therefore be concluded that lack of symmetry worsens the prediction in this case, although not excessively. With the DER method, however, the situation is more balanced, as the MU trains perform similar or slightly better when they are symmetric, and the CMU trains when they are nonsymmetric, in terms of $\Delta\delta(+)$ levels; those figures are omitted for brevity.

The conclusions of this study are summarized in sections 15 and 16.

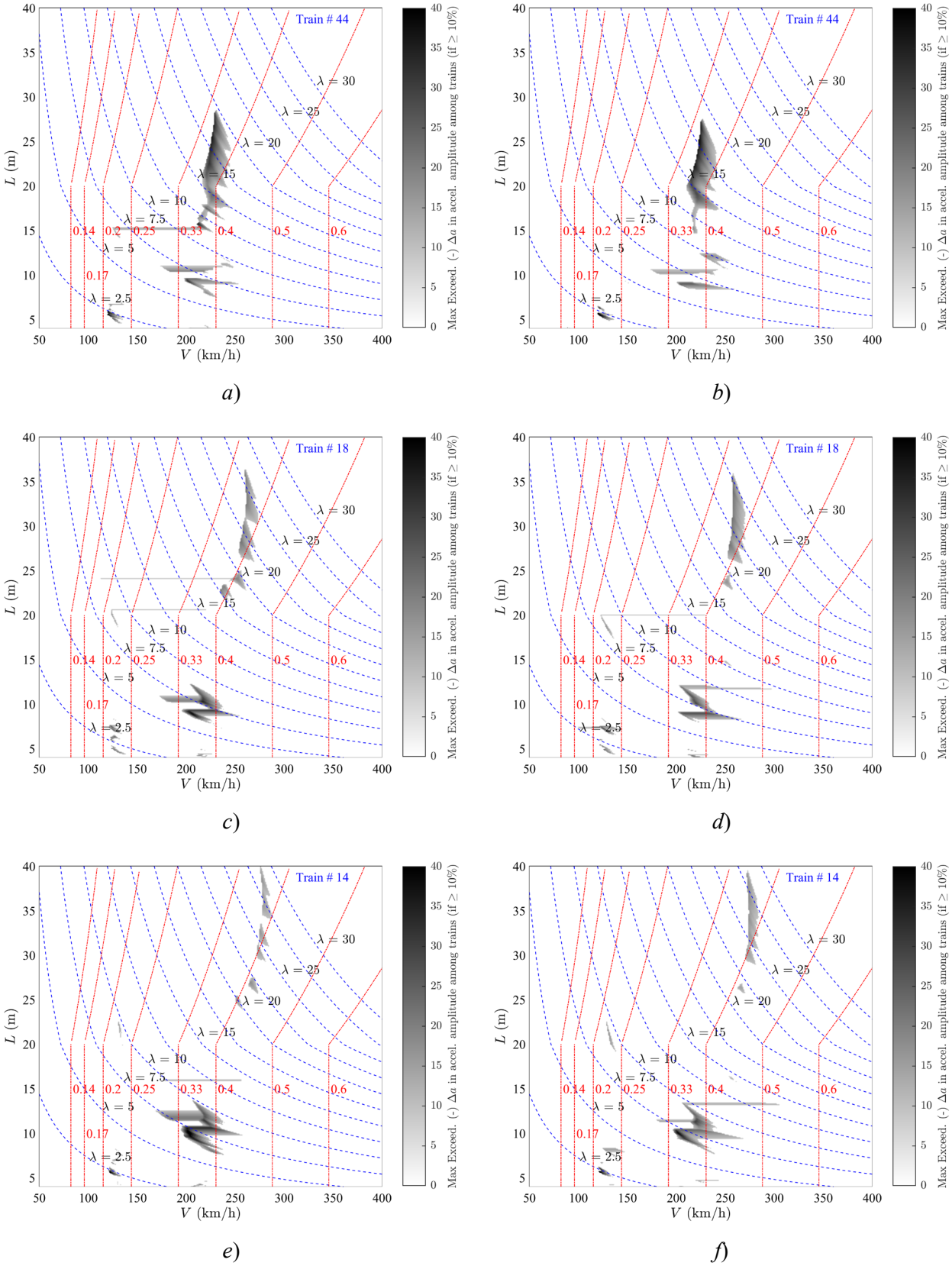

Figure 90: Maps of Δα(–): LIR vs. TSC. a) nonsym-A (train #44); b) sym-A (train #44); c) nonsym-B (train #18); d) sym-B (train #18); e) nonsym-C (train #14); f) sym-C (train #14). PSC bridges.

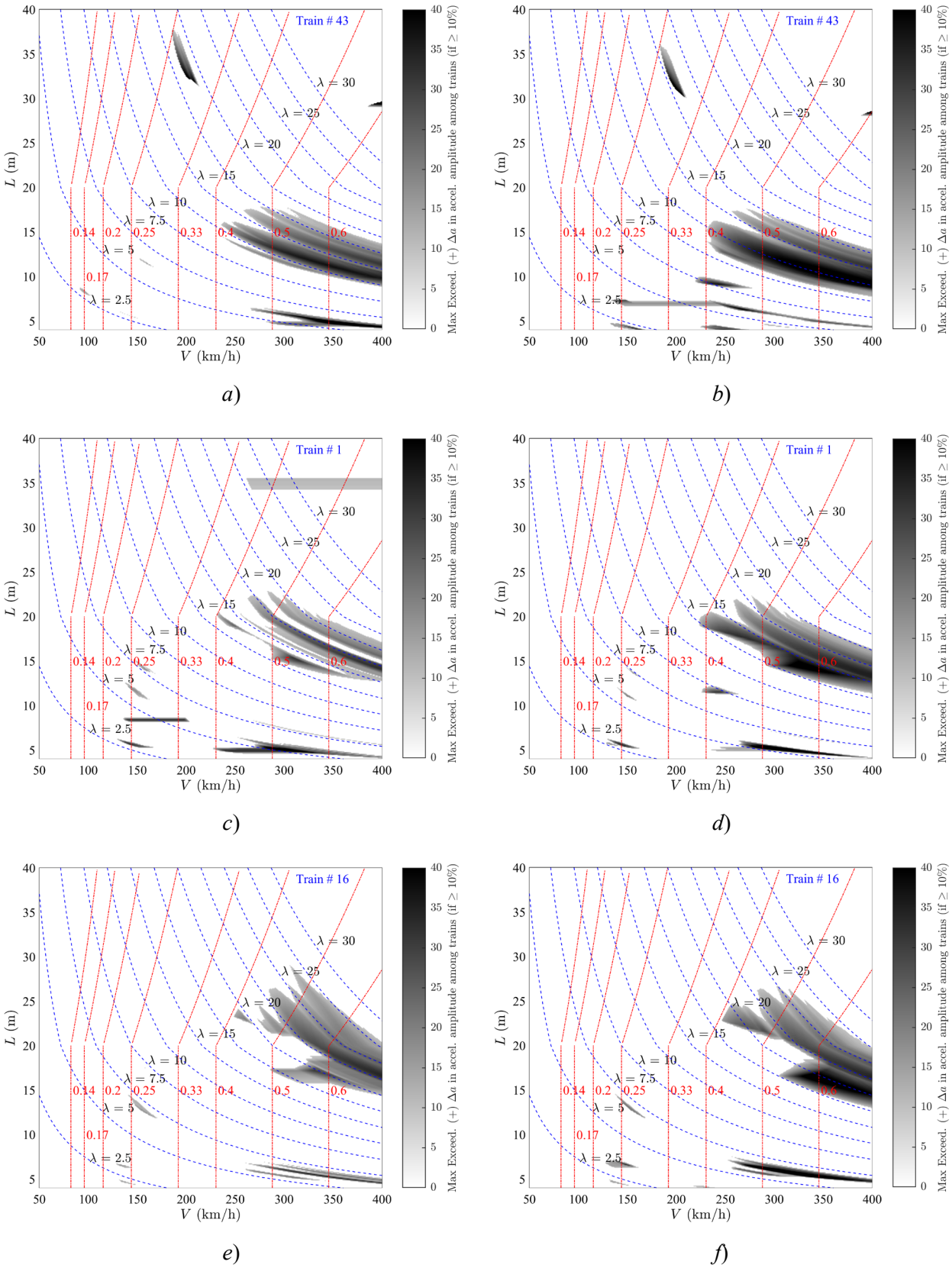

Figure 91: Maps of Δα(+): DER vs. TSC. a) nonsym-A (train #43); b) sym-A (train #43); c) nonsym-B (train #1); d) sym-B (train #1); e) nonsym-C (train #16); f) sym-C (train #16). PSC bridges.

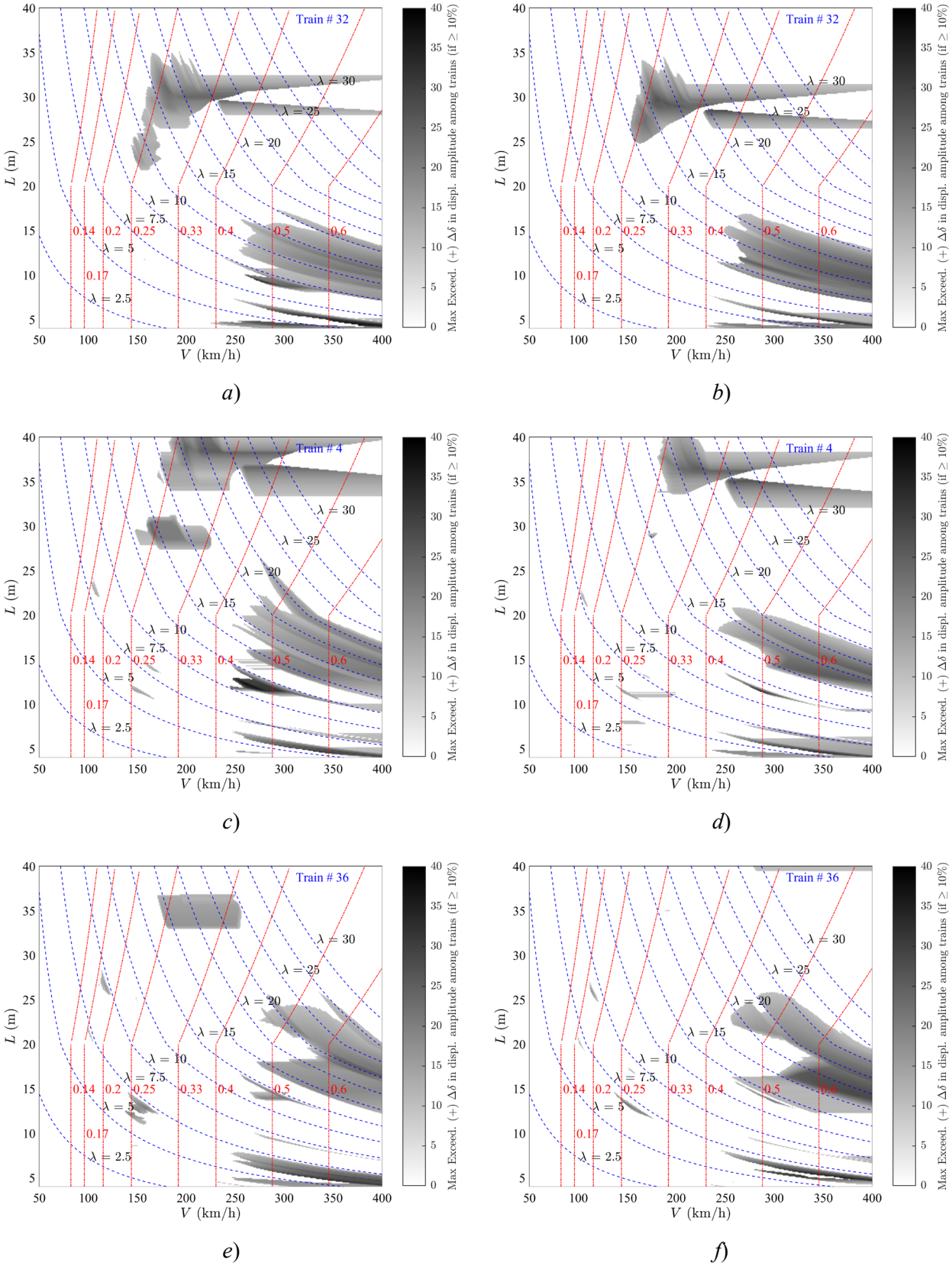

Figure 92: Maps of Δδ(+): LIR vs. TSC. a) nonsym-A (train #32); b) sym-A (train #32); c) nonsym-B (train #4); d) sym-B (train #4); e) nonsym-C (train #36); f) sym-C (train #36). PSC bridges.

7.5 Limitations due to heavier front power cars for $K \geq 0.5$: convex slopes

This section is dedicated to investigating the limitations of SM in relation to KS-8.

When nondimensional speed K reaches above 0.45 approx., the values of the RIL tend to their maxima and the free vibration response increases monotonically with the speed, until $K \approx 0.73$. Therefore, in that region the prediction of the free vibration (see Eq. (8)) can be predominant, particularly if some transient effect reduces that free vibration (forced and free vibration in counter-phase) and results in a total response which is less that the one predicted by the LIR method.

Those situations may happen because, for bridges with low or medium frequencies, the region of high K values is actually reached, particularly for spans below some 25 m. Figure 93 shows one example, for a sequence of equidistant loads evenly spaced at D = 10 m (train #1 from model EQD-12). In the prediction of LIR, which is seen in the right-top part of the figure, **the typical convex aspect of the RIL is observed**; however, the TSC calculation (Duhamel) yields a lower response, as it can be seen in the right-bottom plot. In the left part of the figure, the red point indicates that the case corresponds to V=337 km/h, for a span L=15.5 m. $\Delta a(+)$ = 15.4% in that case.

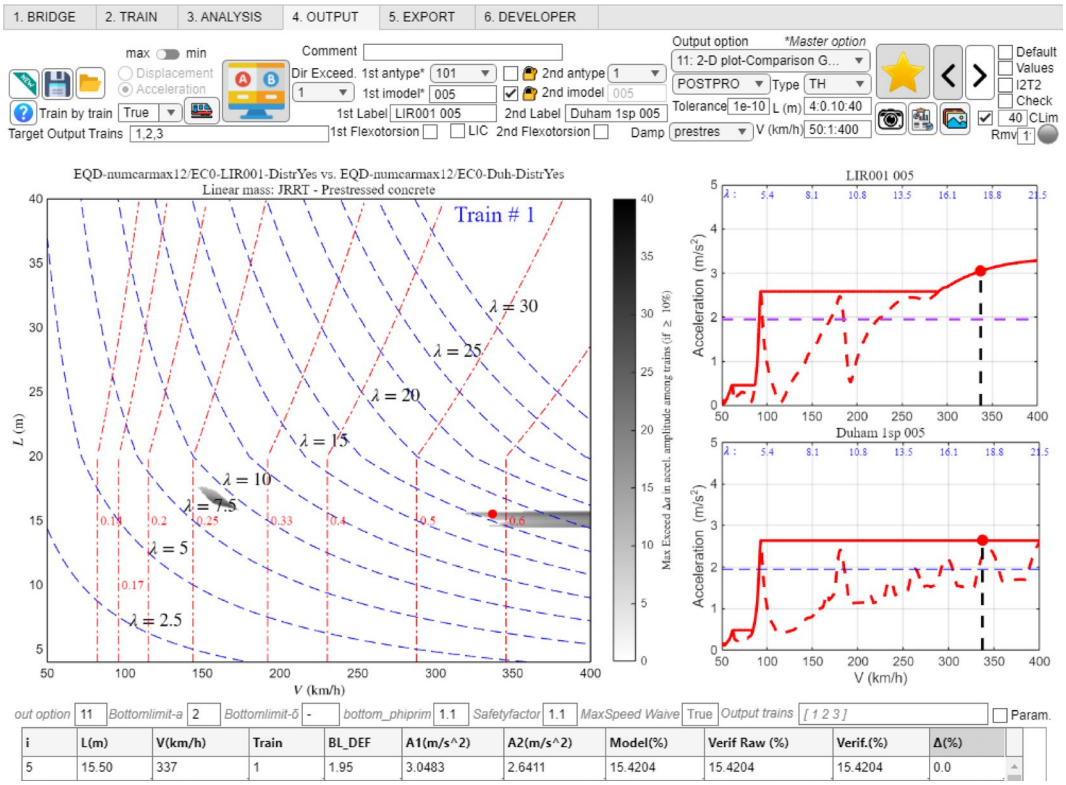

Figure 93: LIR vs. TSC. Map of Δa(+): train #1 from model EQD-12 (D=10 m). PSC bridges.

Figure 94 shows the time-history response of the case described above in Figure 93. It is seen that the maximum acceleration due solely to the first load (curve where the maximum is the red point •) is almost identical to the values predicted by the LIR method (green points •). But the true maximum acceleration is clearly lower, because a transient phenomenon due to the entrance of the second load is in counter-phase with the first load, and thus the response immediately after the entrance of the second load decreases.

That effect gives rise to the "convex slopes", that appear also to some extent in the DER method, and may be even more relevant in both methods when there is a heavy first locomotive, because then the prediction from the first subtrains will be predominant.

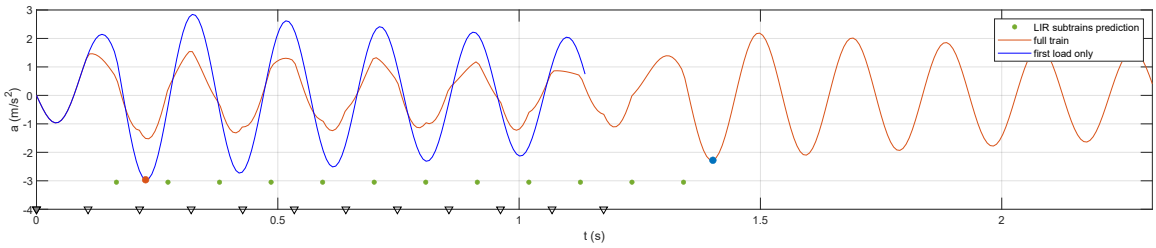

Figure 94: Time-history corresponding to case described in Figure 93. True max. acceleration = ●; max. acceleration due to solely first load = ●; entrance of first load = ▽ ; entrance of rest of loads = ▽ .

However, it is not necessary for the locomotives to be particularly heavy for this type of initial transient, which falls on the safe side in terms of prediction, to occur. The drawback is that such a prediction can, in fact, be too conservative—even when heavy locomotives are not present.

As an illustrative example, one of the trains used to generate Figure 29, the CB RP identified as INB4EU-CB-005, is analyzed below. Figures 95, 96 and 97 correspond to K values of 0.49, 0.61, and 0.64, respectively, for a PSC bridge of L=16 m, crossed by this train. It can be observed in Figure 95 how the prediction of the subtrain formed by the first four loads is excessive, since when the first bogie of the second car enters, the maximum response does not reach the level predicted by the LIR (4.6 m/s² *vs*. 6.2 m/s²).

However, Figure 96 shows that at higher speeds, on the same bridge, the conservative prediction originates in the subtrain formed by the first eight loads (8.9 m/s² *vs*. 11.0 m/s²), since the first bogie of the third car slightly attenuates the response after its entry into the span.

Similarly, Figure 97 shows that at even higher speeds, also on the same bridge, the conservative prediction originates from the subtrain formed by the first twelve loads (11.5 m/s² *vs*. 14.0 m/s²), because the first bogie of the fourth car slightly attenuates the response after entering the span.

The convex slope problem occurs for both the DER and LIR methods, as shown in Figure 29, and is a consequence of considering the initial subtrains to compute the signature in the range K>0.45 approx.

A possible solution, therefore, was proposed by D214 in its RP6, consisting of eliminating the axles of the heavy initial locomotives. This solution is analysed in sections 9.1.2 and particularly 9.1.4, using the methods referred to here as DER3 and LIR3. In any case, given that the phenomenon can occur not only because of the first four axles, but also because of the first 8 or even 12 axles, the strategy of eliminating the sub-trains of the first locomotive does not seem to guarantee a valid solution in general a priori.

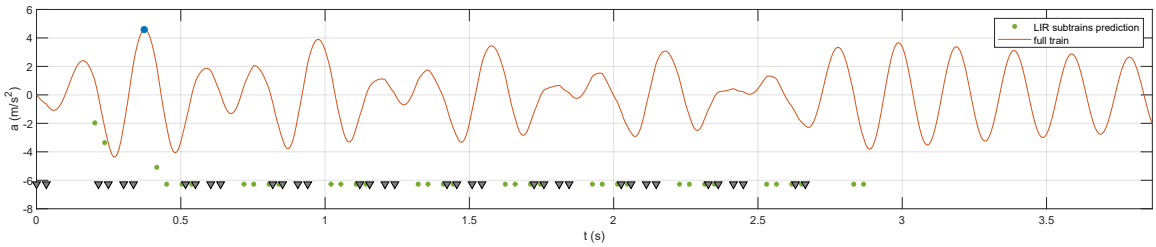

Figure 95: Time-history for train INB4EU-CB-005, V=285 km/h (K=0.49), L=16 m, PSC bridge. True max. acceleration = ●

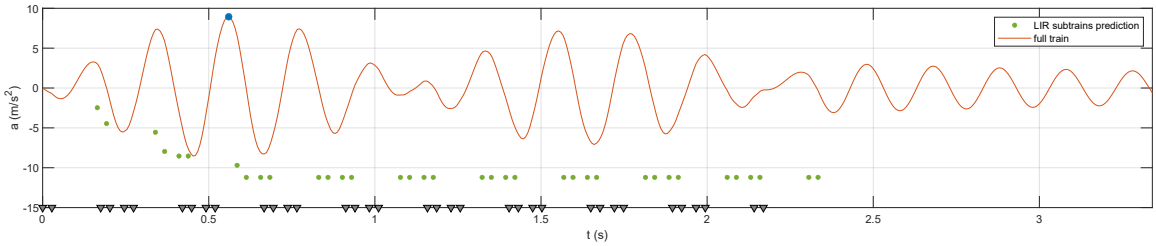

Figure 96: Time-history for train INB4EU-CB-005, V=350 km/h (K=0.61), L=16 m, PSC bridge. True max. acceleration = ●

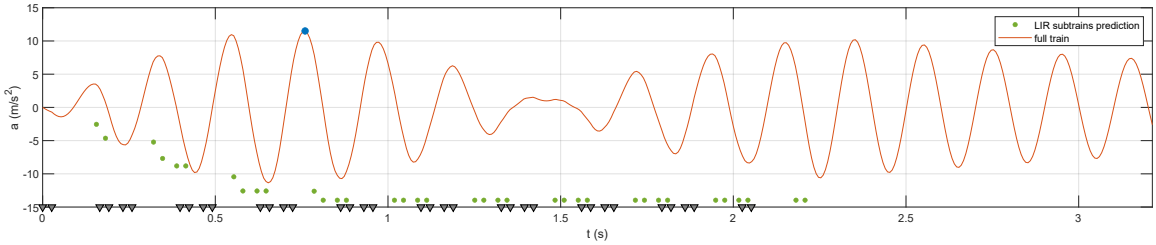

Figure 97: Time-history for train INB4EU-CB-005, V=370 km/h (K=0.64), L=16 m, PSC bridge. True max. acceleration = ●

8 Limitations of SM in bridges not SS: cases where more than one mode is relevant and portal frames

8.1 Bridges with relevant torsion effects

8.1.1 Formulation of torsional vibration: analogy with bending vibration

The formulation considered for analysis of torsion is that of a simple, uniform beam of span L, where the centre of gravity of the cross section coincides with the shear centre, so that no coupled lateral bending-torsion occurs.

If coupled lateral bending-torsion were relevant for the bridge behaviour, the first frequency and mode of vibration of such kind of motion should be determined with a suitable numerical model, along with the modal mass for a corresponding mode shape of unit maximum amplitude. Then, the modal mass can be transformed into an equivalent I_p (polar mass moment of inertia per unit length), by assuming a sinusoidal mode shape with only one half-wave.

The following dynamic parameters define the differential equation of motion:

- I_p = inertial term, equal to the polar mass moment of inertia per unit length (kg·m^2/m).
- $k_T = \sqrt{\frac{I_p}{m}}$ = torsion mass radius of gyration (m), where m is the linear mass of the bridge (kg/m).
- n_{0T} = first torsion natural frequency = $n_0 \cdot n_{0R}$, where n_{0R} is the ratio between torsion and bending first natural frequencies, expressed in Hz or rad/s.
- e = eccentricity of axle loads = eccentricity of the track (m).
- e_m= eccentricity of the measurement point (m); it is usual to consider $e_m = e$.

With ω_{0T} being the torsion frequency in rad/s, the differential equation of motion is

$$\frac{I_p L}{2}\ddot{\theta}(t) + 2\zeta\omega_{0T}\frac{I_p L}{2}\dot{\theta}(t) + \omega_{0T}^2\frac{I_p L}{2}\theta(t) = -F \cdot e \cdot \sin\frac{\pi V t}{L} \qquad 0 \le t \le L \tag{18}$$

$$\ddot{\theta}(t) + 2\zeta\omega_{0T}\dot{\theta}(t) + \omega_{0T}^2\theta(t) = -\frac{2\,F\,e}{I_p L}\sin\frac{\pi V t}{L} \qquad 0 \le t \le L \tag{19}$$

$$\ddot{\theta}(t) + 2\zeta\omega_{0T}\dot{\theta}(t) + \omega_{0T}^2\theta(t) = -\frac{2}{mL}\frac{F\,e}{k_T^2}\sin\frac{\pi V t}{L} \qquad 0 \le t \le L \tag{20}$$

where the amplitude of the mode of vibration is $\theta(t)$, and the mode shape considered is sinusoidal with only one half-wave, and unit maximum value at mid-span. Therefore, the associated vertical displacement is computed simply as the product $e_m \cdot \theta(t)$, negative in downwards sense.

From Eq. (20) it can be seen that the solution of the torsion equation is formally identical to the bending equation, by simply adjusting the frequency of vibration and multiplying the axle loads by $\frac{e}{k_T^2}$. Therefore, all predictions of the SM conservative/non conservative performance in relation to torsion are the same as for pure bending, by simply adjusting the wavelength (or the nondimensional speed, alternatively). The amplitude of the response and its meaningfulness in comparison to the assumed lower bound thresholds will be affected by factor $\frac{e \cdot e_m}{k_T^2}$. Estimates of the eccentricities are in the order of 2.5 m or slightly below. Estimates of the radius of gyration are between 2.5 and 3.5 m (see section 8.1.2). Therefore, in general $\frac{e \cdot e_m}{k_T^2} < 1$.

As for the static response, one has, in absolute value

$$\theta_{st} = \frac{2}{mL\omega_{0T}^2}\frac{F\,e}{k_T^2} = y_{st}\,\frac{e}{n_{0R}^2 k_T^2} \quad \Longrightarrow \quad y_{st,\text{tors}} = y_{st}\,\frac{e\cdot e_m}{n_{0R}^2 k_T^2} \tag{21}$$

where y_{st} is the static vertical deflection of the fundamental bending mode, and typically the deflection due to the torsion mode will be clearly smaller than the bending one.

As it is known, the fundamental bending frequency is $n_0 = \frac{\pi}{2L^2}\sqrt{\frac{EI_z}{m}}$, where E is the modulus of elasticity (N/m^2) and I_z is the second moment of area with respect to the beam horizontal, principal inertia axis. The stiffness term $\omega_{0T}^2\frac{I_p L}{2}$ in Eq. (18) can be demonstrated to be equal to $\frac{\pi^2}{L^2}GJ\frac{L}{2}$, and $G = \frac{E}{2(1+\nu)}$, with ν being Poisson's ratio, therefore

$$J = 2(1+\nu)\left(k_T\, n_{0R}\frac{\pi}{L}\right)^2 I_z \tag{22}$$

Since the fundamental torsion frequency is $n_{0T} = \frac{1}{2L}\sqrt{\frac{GJ}{I_p}}$, in order for n_{0T} to be actually reached Eq. (22) can be interpreted as follows: while the bending frequency n_0 is proportional to $\pi/2L^2$, the torsion frequency n_{0T} is proportional to $1/2L$, thus the torsional constant J—proportional to n_{0T} squared— is dimished by a factor $\left(\frac{\pi}{L}\right)^2$ with respect to I_z; conversely, J is to be incremented by a factor n_{0R}^2 in comparison to I_z; finally, I_z is also modified proportionally to the torsional inertia, according to k_T^2 —if $k_T^2 > 1$ for example, then the constant J has to be incremented in the same amount if n_{0T} is to be obtained.

For implementation in a FE software using a simple beam model with homogeneous material, it should be considered that typically[5]

- $I_p = \rho I_{pA}$, where I_{pA} is the polar area moment of inertia (m^4), and ρ is the material density (kg/m^3).
- $I_{pA} = I_y + I_z$, being I_y the second moment of area with respect to the vertical principal inertia axis of the cross section.
- $I_{pA} = k_T^2\, A$, where A is the cross-sectional area (m^2). Therefore, the mass radius of gyration is the same as the area radius of gyration, which is not true due at least to the presence of dead weights (ballast, etc.).
- In order to correct that discrepancy, for given values of the equivalent beam $\{E, \nu, \rho, L, m, n_0, n_{0R}, k_T\}$ the procedure should follow the steps below:

  (1) Obtain $A = m/\rho$, and then compute I_z by imposing the formula for n_0.

  (2) Adjust $I_y = (k_T^2 m - \rho I_Z)/\rho$, which will fix the torsional inertia.

  (3) Compute $G = \frac{E}{2(1+\nu)}$ and adjust J using Eq. (22), which will fix the torsional frequency.

[5] Depending on the particular software.

8.1.2 Evaluation of the influence of torsion: pure bending vs. combined bending & torsion

In current standards it is mentioned that eigenmodes for bending are sufficient if the condition $n_{0R} = n_{0T}/n_0 > 1.2$ is satisfied (CEN, 2023 | section 8.4.4). This subsection presents an analysis of such clause, for PSC SS bridges. Whenever the combined bending/torsion response is significantly higher than the pure bending response, current SM—based solely on bending—will fail to predict the bridge response.

The hypothesis of the study are the following:

- An exceedance analysis is carried out for PSC, SS bridges, considering individually whether the max. displacements or max. accelerations at mid-span are significantly larger (more than 10%) for the combined bending/torsion analysis, in comparison to the analysis of pure bending.
- To that end, nonconservative $\Delta a_T(-)$ or $\Delta \delta_T(-)$ are defined here as the situations where the combined bending/torsion response exceeds the sole bending response.
- Three different frequency ratios are considered: $n_{0R} = n_{0T}/n_0$ = [1.1, 1.2, 1.3], and three different values of the radius of gyration, typical of double-track bridges with ballasted track: k_T = [2.5, 3.0, 3.5] m. For a ballast bed of some 9.0 m width, the radius of gyration is approximately k_T = 2.6 m; therefore, for ballasted tracks k_T = 2.5 m is a suitable lower limit for a sensitivity analysis. As for the upper limit, k_T = 3.5 m is also a reference value for a large box girder concrete bridge with deck height of approximately 4.5 m.
- $e_m = e$ = 2.35 m.
- To consider the presence of two tracks on the deck, the linear masses considered for the bridges are 80% higher than the ones described in Eq (11).; the fundamental natural frequencies and damping ratios remain unmodified.
- Longitudinal load distribution is considered by means of a triangular footprint with a length of 2.5 m.
- The rolling stock used corresponds to model PT60.

Some representative results are discussed below. Figures 98, 99 and 100 show the error levels $\Delta a_T(-)$ derived from neglecting the torsional contribution in the response, in scenarios where the frequency ratio is n_{0T} = 1.3, for three different trains. Each of those figures gathers the results for the three values k_T = [2.5, 3.0, 3.5] m. While the trains analysed in Figures 98, 99 and 100 all of them have some kind of power cars, it can be stated that the response is not too different for other trains without power cars; therefore, the results shown here are considered meaningful.

It is emphasized that the thresholds used for meaningful acceleration and displacement (or rather, impact coefficient) are the same as in the preceding sections: 2.5 m/s^2 and +10% above φ'.

The main conclusion obtained from this analysis is that, even for n_{0T} = 1.3>1.2, the contribution of torsion for checking the serviceability acceleration limit can be significant by more than 10%, for certain spans lengths and some values of the radius of gyration. When the radius of gyration increases, the effect of torsion is seen to decrease markedly. The same tendency is observed for increasing span length. However, values of $k_T \approx 3.0$ m are realistic for double-track bridges, and therefore the results presented here point out that the n_{0T} >1.2 rule given in (CEN, 2023 | section 8.4.4) could require further specification of its range of validity, as a function of [L, k_T], and some suitable parameter as K or λ.

These results have been obtained by means of an analytic mode shape approach, using Duhamel's integral as TSC method, and double-checked with independent FEM analysis, which has been satisfactory in all examples selected for validation.

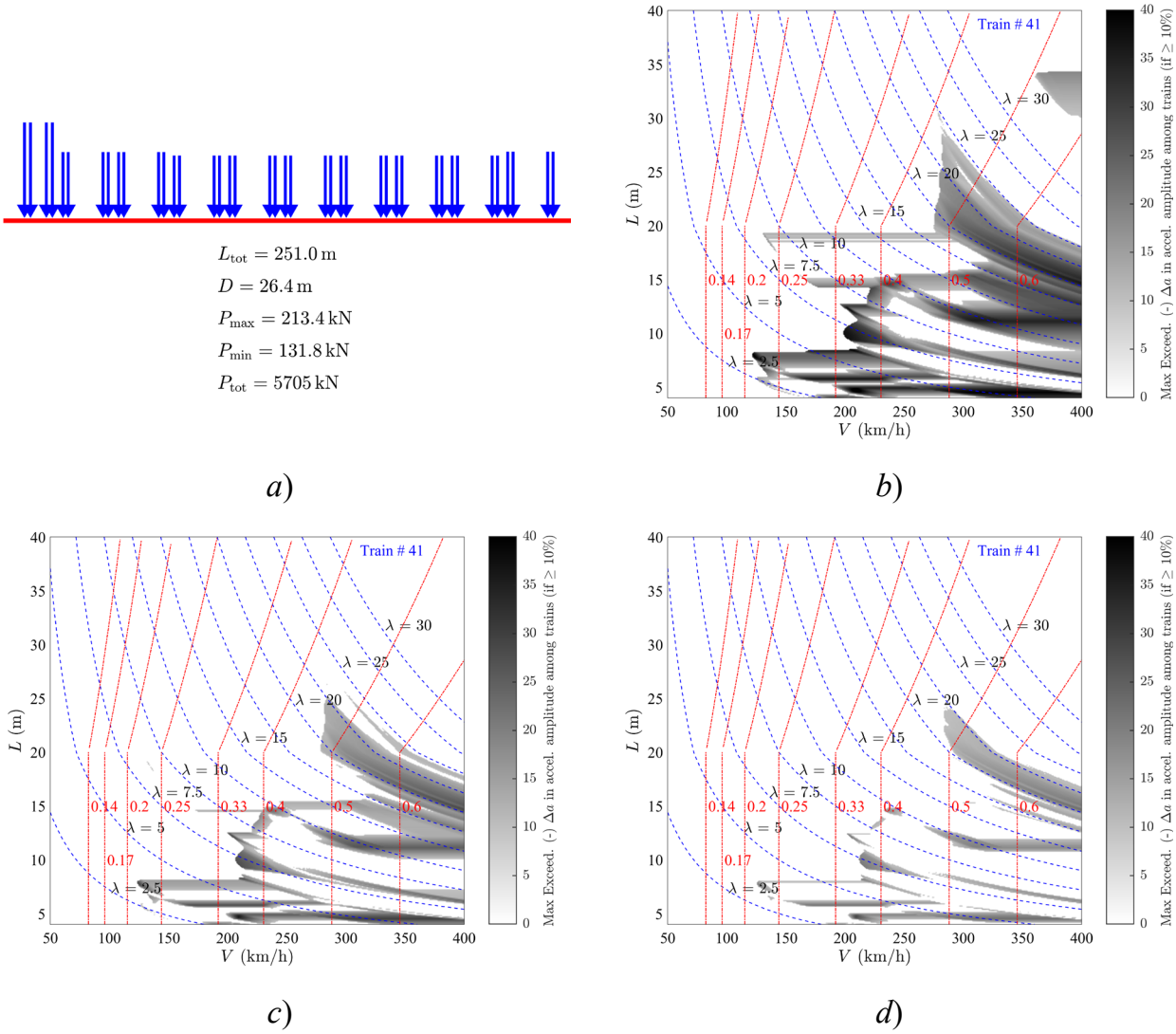

Figure 98: $\Delta a_T(-)$ bending vs. bending+torsion. Train PT60-41 [INB4EU-CB-003]. n_{0T}=1.3. a) train definition; b) k_T=2.5 m; c) k_T=3.0 m; d) k_T=3.5 m. PSC bridges.

Figures 98, 99 and 100 show that spans above some 20–25 m are less affected, and for K<0.45 approx. the influence of torsion is negligible for those longer spans.

While it is questionable that bridges of span close to 5–7 m and below can be analysed accurately with beam models, the figures in this section (and in the rest of this document) include those spans as a lower limit, which enables to show the tendencies of the response for the shorter SS bridges.

For example, a double track, filler beam bridge of span L=10 m is a realistic case that could be considered included in Figures 98, 99 and 100 (providing that its frequency ratio were close to n_{0T} = 1.3). Without a detailed evaluation of the radius of gyration in such case, the assessment carried out to set out the sensitivity analysis in this section suggests that k_T could be near 3.0 m or below for such bridge type.

Thought not shown here for brevity, the results for frequency ratios equal to 1.2 and 1.1 confirm that the influence of torsion in those cases would be visibly higher than for n_{0T} = 1.3, as it could be expected (particularly for n_{0T} = 1.1).

Figures 101 and 102 show a summarized comparison of how the effect of the radius of gyration influences the relevance of bending+torsion compared to sole bending, in the prediction of maximum vertical acceleration. The binary Z24 indicators show the area ratio of each zone affected by exceedance as an average value, standard deviation, max and min.

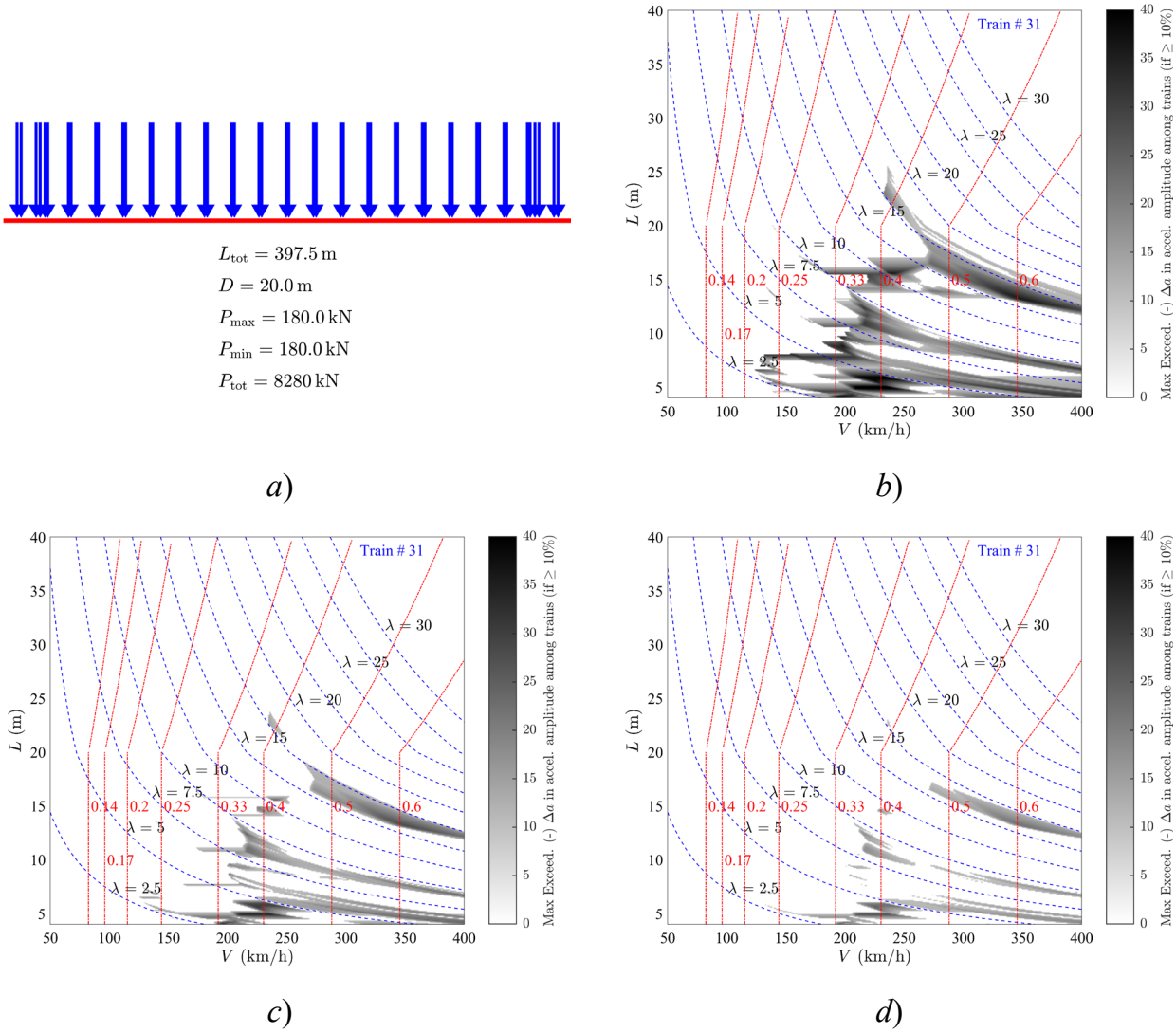

Figure 99: $\Delta a_T(-)$ bending vs. bending+torsion. Train PT60-31 [HSLM-A3]. n_{0T}=1.3. a) train definition; b) k_T=2.5 m; c) k_T=3.0 m; d) k_T=3.5 m. PSC bridges.

As regards the influence of torsion vibrations in the computation of vertical displacements, an example of how relevant that effect could be at some particular speeds is shown first in Figure 103. In that example, the response of the bending mode is far from resonance notwithstanding the high speed of circulation, and instead the torsion mode is experiencing resonance in its first subharmonic. This is one of the examples considered here for verification of the global exceedance analysis *vs*. FEM results.

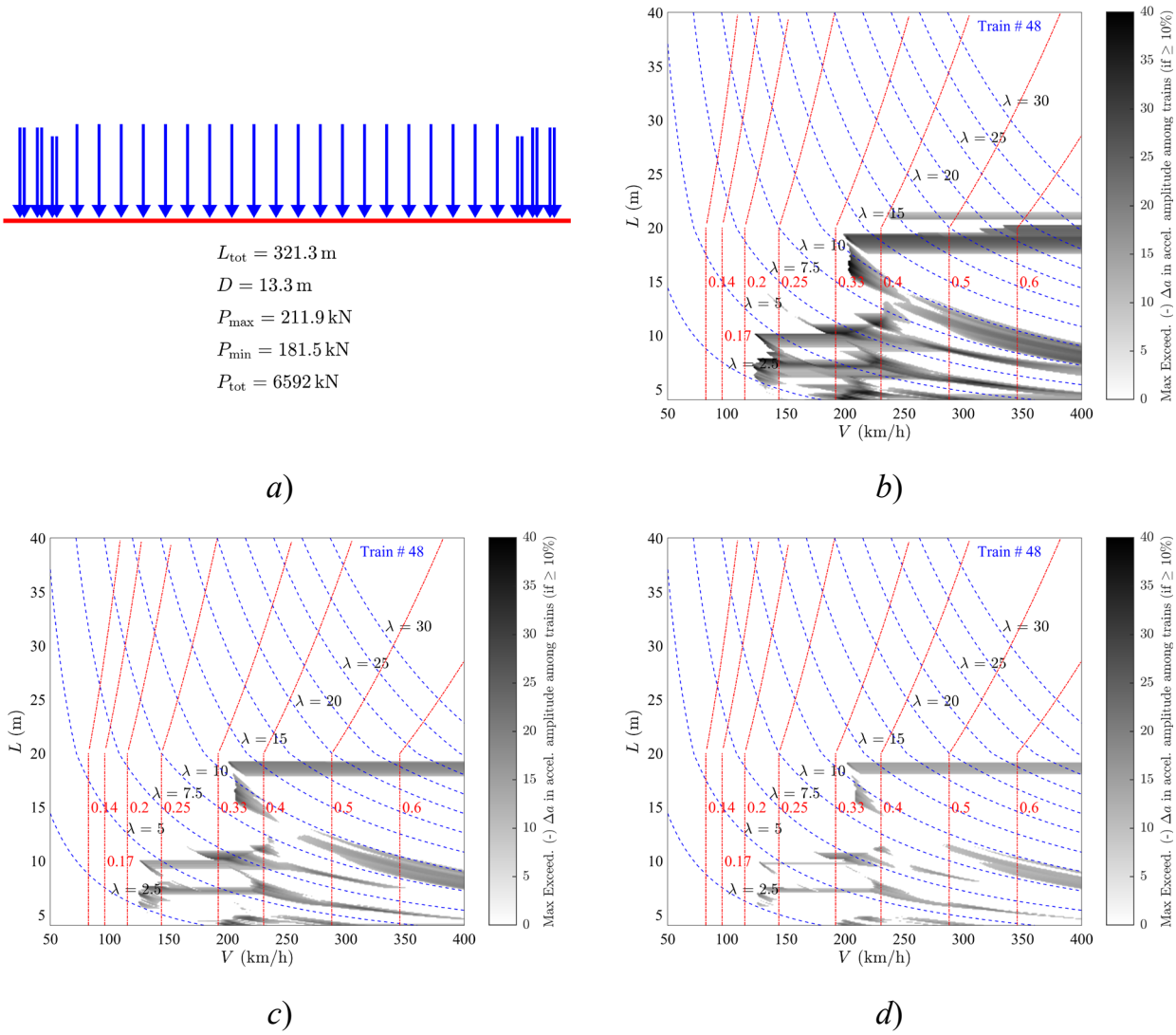

Figure 100: $\Delta a_T(-)$ bending vs. bending+torsion. Train PT60-48 [INB4EU-SA-022]. n_{0T}=1.3. a) train definition; b) k_T=2.5 m; c) k_T=3.0 m; d) k_T=3.5 m. PSC bridges.

Only the shortest trains, and those with heavy front locomotives, produce somewhat different phenomena than the rest. This is mainly because when they cross the 1.1φ' threshold for the exceedance calculation, it is not necessarily due to a resonance phenomenon (which is the frequent case in longer trains or those with rear locomotives). The remaining trains, that is, the vast majority of the PT60 model, generate a pattern again with a waterdrop appearance (see for example Figure 104), which tends to diminish with higher values of k_T due to the smaller static deflection associated (see Eq.(21)), and is due to the following. At the wavelengths of the bending resonance subharmonics, when these λ isolines do not intersect the cancellation K lines, resonance occurs. Then, the 1.1φ' threshold is normally exceeded, and, when the static torsional deflection is added to the bending mode effect, even without torsional resonance occurring, the 10% threshold is crossed and a gray exceedance zone appears. If the bending resonance was not too strong (because it was closer to cancellation at the subharmonic intersection), the effect is mitigated sooner by increasing the speed and the overall increase in the bridge's response, resulting in a waterdrop shape. And for exceedance values close to the 10% limit, in some spans, the transition occurs to a level immediately below that limit (say 9.9%), and the area becomes white.

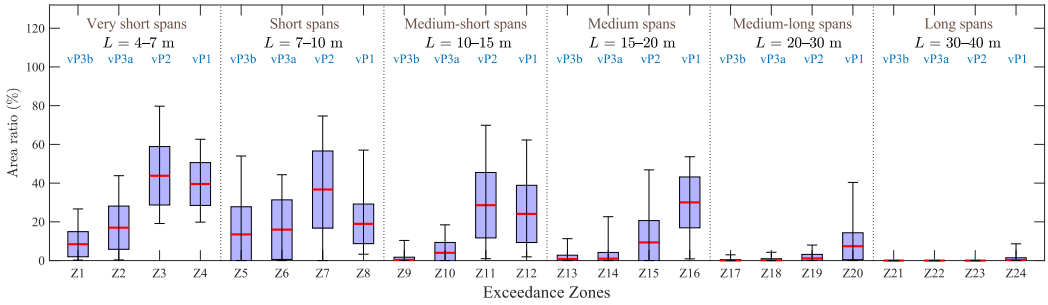

Figure 101: Box plots of Z24 binary $\Delta a_T(-)$ bending vs. bending+torsion. PT60 model. n_{0T}=1.3, k_T=3.0. PSC bridges.

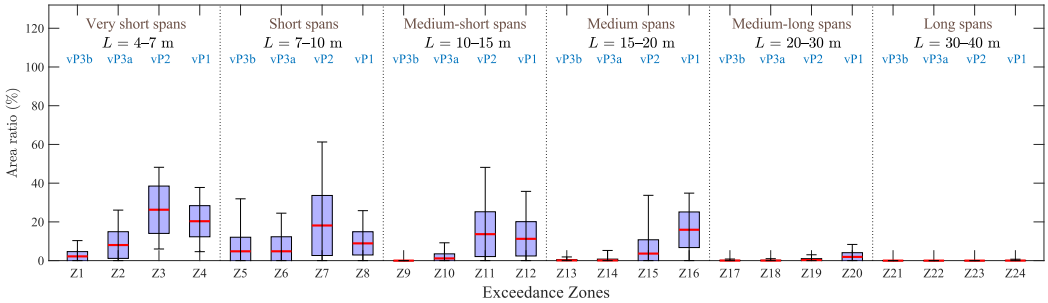

Figure 102: Box plots of Z24 binary $\Delta a_T(-)$ bending vs. bending+torsion. PT60 model. n_{0T}=1.3, k_T=3.5. PSC bridges.

Subsequent torsional resonance peaks exceeding the bending peaks in total displacement are not usually detected. The fact that torsional and bending resonances do not interact as significantly as in acceleration calculations is partly due to the usual ω^2 factor, which increases the weight of the second mode in accelerations. Furthermore, the stronger static deflection due to bending introduces an initial offset favoring this type of response in the overall deflection calculation (see for example the initial instants in Figure 103).

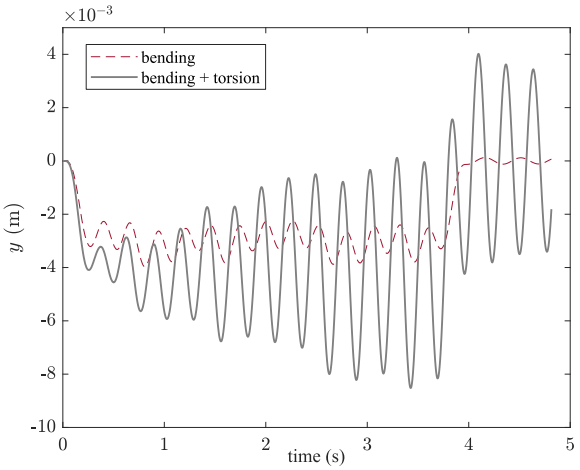

Figure 103: FEM+TSC analysis. Bending vs. bending+torsion. Train PT60-10 [INB4EU-CB-111]. L=35.7 m, V=390 km/h, n_{0T}=1.3, k_T=3.0 m. PSC bridge.

Moreover, if the impact coefficient obtained from the maximum combined bending and torsion deflection is to be applied to amplify, for example, the effects of an eccentric live load (a static train on one of the tracks of a double-track bridge deck), it should be noted that this would be inconsistent from a structural analysis viewpoint. As these analyses have shown, the maximum amplification of displacements computed in a cumulative sense is often due to bending, not torsion. Therefore, the effects of both components of the static load should not be amplified equally in bridge design.

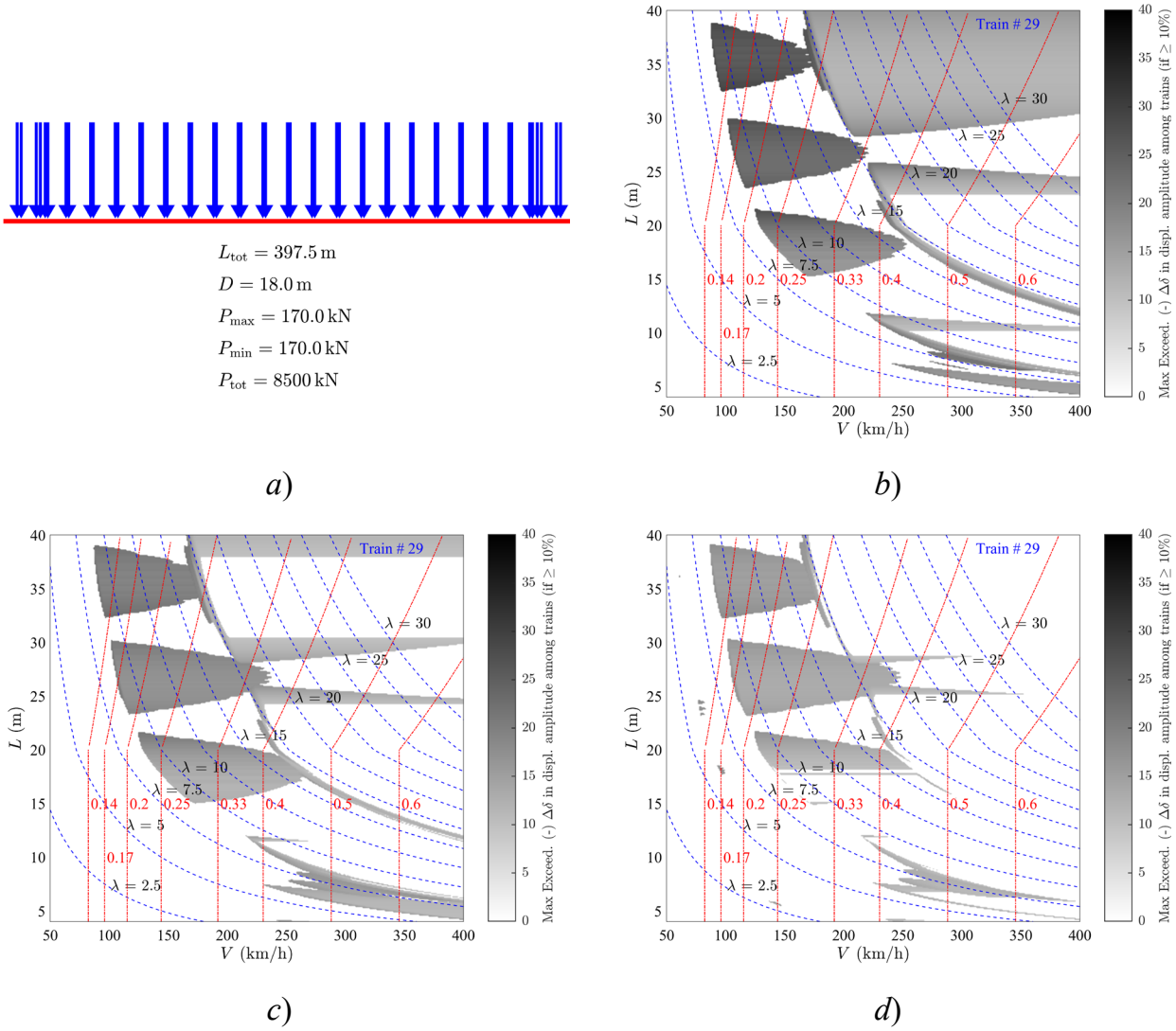

Figure 104: $\Delta\delta_T(-)$ bending vs. bending+torsion. Train PT60-29 [HSLM-A1]. n_{0T}=1.3. a) train definition; b) k_T=2.5 m; c) k_T=3.0 m; d) k_T=3.5 m. PSC bridges.

It was mentioned in the beginning of this subsection that, whenever the combined bending/torsion response is significantly higher than the pure bending response, current SM—based solely on bending—will fail to predict the bridge response. However, from the results presented in this section, the possibility arises that a simple addition of the torsion static deflection could help to fix a good number of cases, for the computation of the vertical displacements. Such hypothesis could be suitably tested in the future.

8.2 Continuous multi-span bridges

From a structural engineering perspective, the comparison between single-span (Figure 105*a*) and 2-span beams (Figure 105*b*) under moving loads not only enables a quantitative assessment of differences in dynamic response but also reveals qualitative changes in the amplification behavior. Within the LIR framework, this comparison becomes particularly relevant, as the transition from an isostatic to a continuous configuration introduces additional effects associated with load redistribution, structural continuity, and modal interaction.

The main goal of this section is to analyse whether, on a general basis, a relevant number of trains can induce a dynamic response of 2-span beams that is significantly higher than the response of an identical structure of a simple span. If that were the case, the analysis of 2-span continuous bridges with current SM

will prove no be not on the safe side, if performed out with SS models for its greater simplicity. The analysis is restricted to the response in terms of vertical accelerations.

To take into account the spatial variability of railway loads, a triangular load distribution with a characteristic spacing of 2.5 m was adopted. This idealization is particularly effective in representing the interaction between consecutive axles and their coupling with the structural vibration modes. In this context, the analysis performed on the 60 trains of the PT60 model allows the exploration of a wide spectrum of loading configurations, ranging from highly regular to strongly irregular trains.

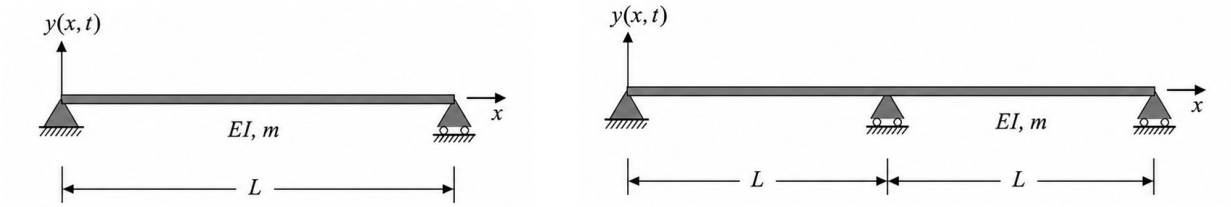

a) *b)*

Figure 105: considered models: a) one-span model; b) 2-span model.

The comparison between the response of the SS beam model with respect to the 2-span beam model was conducted to identify when the latter exceeds the former. For both cases, closed-form mode shapes were use, integrated with Duhamel's method as TSC. The comparison was made using the PT60 model. For each train the exceedance map of the comparison was obtained. As an example, Figure 106*a* shows the axle load distribution of train PT60-01, and Figure 106*b* shows train PT60-31.

In the acceleration exceedance map for the PT60-01, Figure 106*a*, three non-zero exceedance zones (grayscale) and a fourth elongated zone that coincides with a length of 9.3 m for speeds between 206 and 280 km/h can be observed. However, this section will emphasize the two large zones that exceed 40% exceedance. The zone appearing leftmost at $\lambda = 10$ will be referred to as Z_1, and the zone appearing from $\lambda = 20$ will be referred to as Z_2. In both of them, the maps indicate that the response of the 2-span structure is higher.

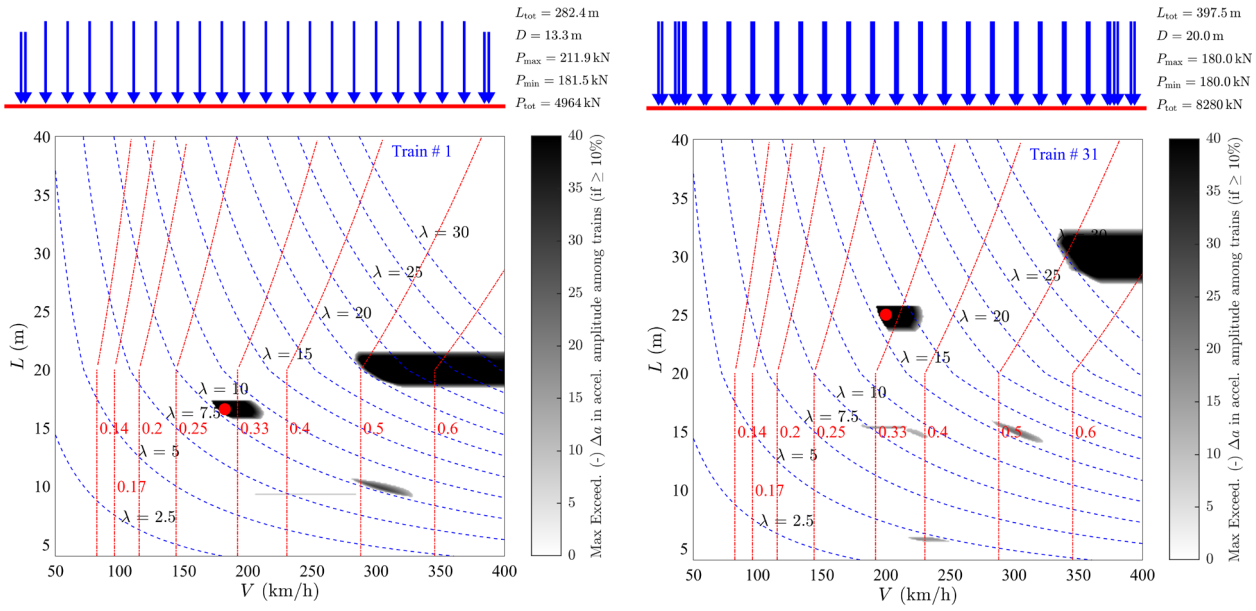

a) *b)*

Figure 106: Maps for the 2-span versus one-span configurations: a) PT60-01 train; b) PT60-31 train.

A point within Z_1 was selected for analysis, which has $L = 16.6\,m$, associated with a beam frequency of ($n_0 = 4.82\,Hz$). Since the PT60-01 train has a coach length of $D = 13.3\,m$, it presents resonance speeds $V_{1i}^{(1s)}$ of 230, 115, and 77 km/h, for i = 1, 2, and 3, where the subscript represents the i-th subharmonic of the first mode and the superscript (1s) refers to the one-span beam model. The first harmonic and third subharmonic are observed in the envelope curve of Figure 107*a*. However, the second subharmonic speed of 115 km/h is located near the second cancellation, which nullifies its contribution to the envelope (Museros *et al*. 2013).

When extending this analysis to 2-span beams, it is emphasized that they present the same natural frequency for the first vibration mode, given that the flexural stiffness and linear mass properties are purposely conserved between both models. Therefore, the eigenvalue and eigenvector analysis of both systems makes them share this frequency and mode shape between the single-span beam and one of the spans of the 2-span beam. Thus, this 2-span model has the same resonance speeds previously described, in addition to those from the second vibration mode, which correspond to $V_{2i}^{(2s)}$ = 360, 180 and 90 km/h, where the subscript represents the i-th subharmonic of the second mode and the superscript (2s) refers to the 2-span beam model. These speeds can be traced in the envelope curve of Figure 107*b*.

The combination of both vibration modes in the 2-span model causes the second subharmonic of the second vibration mode to stand out in the vicinity of $V = 180$ km/h, significantly exceeding the response of the 1-span model, which shows no resonance in that train passing speed. This condition exceeds the threshold set at 2.5 m/s^2 and also exceeds 10% exceedance, even reaching an increase of up to 60%. This behavior is maintained when comparing the cumulative acceleration of both models and does not cease until both models reach the first resonance of the first mode, where increasing their response together causes the exceedance to fall below the permitted threshold, thus bringing the exceedance zone to an end.

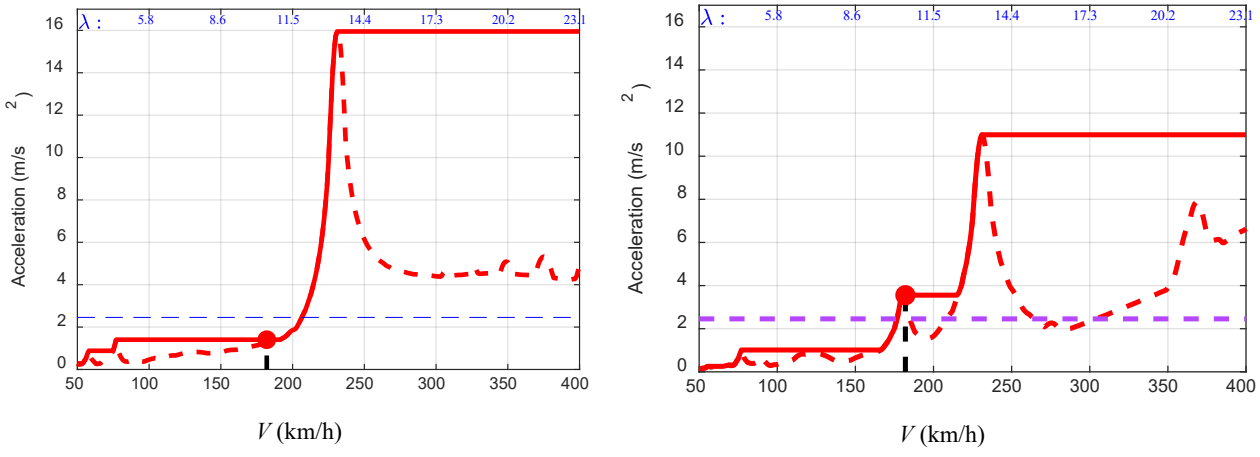

Figure 107: Acceleration envelope for exceedance zon Z_1: a) one-span model; b) 2-span model.

Subsequently, a point to be analyzed within Z_2 was selected also for train PT60-01, which corresponded to a beam length of $L = 20\,m$ and a speed of $V = 300$ km/h. The resonance speeds are $V_{1i}^{(1s)}$ = 192, 96, and 64 km/h, while $V_{2i}^{(2s)}$ = 299, 149.5, and 99.7 km/h. This comparison shows that the cumulative acceleration response of the 2-span beam exceeds that of the SS beam at the first resonance of the second mode. This occurs because the SS beam cannot exhibit resonances at the mentioned speed; moreover, its first resonance is located close to the first cancellation, and the amplitude of its 2nd subharmonic is insufficient to reach the response levels attained by the 2-span beam. This behavior reaches exceedance values of up to 58% and extends starting

from a speed of 299 km/h. Meanwhile, for lower speeds, the SS model maintained a higher cumulative acceleration than the 2-span model; therefore, it showed no exceedance for values below $V = 290$ km/h ($<$ 299 km/h). For beam lengths slightly longer and slightly shorter than $L = 20\ m$, the local resonant peaks of the last bogie prevail, which gives Z_2 the width shown in the exceedance map. Outside this sensitive zone as a function of L, and for speeds equal to or greater than 300 km/h, the first resonance of the SS beam does not cancel out, allowing its response to exceed that of the 2-span model, causing the Z_2 region to disappear.

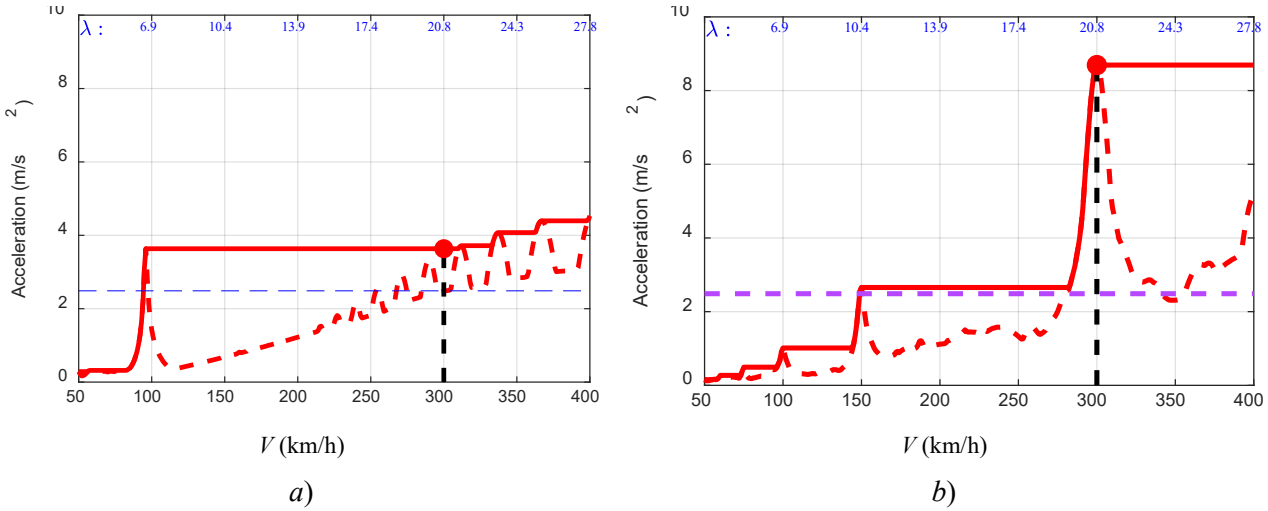

Figure 108: Acceleration envelope for exceedance zone M_2: a) one-span model; b) 2-span model.

The PT60-31 train illustrated in Figure 106*b* presents a higher value of D, which also increases the λ value where the previously described non-trivial exceedance map zones occur. Both trains present a rather regular distribution of their loads. In this sense, an analysis similar to the one applied to the PT60-01 train can be applied on this train, identifying that the non-zero exceedance zones occur at the wavelengths corresponding to 31.2 and 15.6. It is worth mentioning that the frequency ratio between the second and first vibration modes of the 2-span beam corresponds to 1.56, and that the aforementioned wavelengths are calculated with respect to the SS beam wavelength scale.

To identify the regions with the greatest effects of the 2-span beam with respect to the SS beam, an analysis was implemented using the area ratio or binary indicator in terms of the Z24 values, as shown in Figure 109. That figure considers all trains in the PT60 model. It was found that the difference introduced by the 2-span configuration is more widely visible from medium to long spans. Furthermore, the occurrence of exceedance increases with velocity for the first three velocity categories, whereas the last category may exhibit a slight reduction in the expected binary exceedance trend.

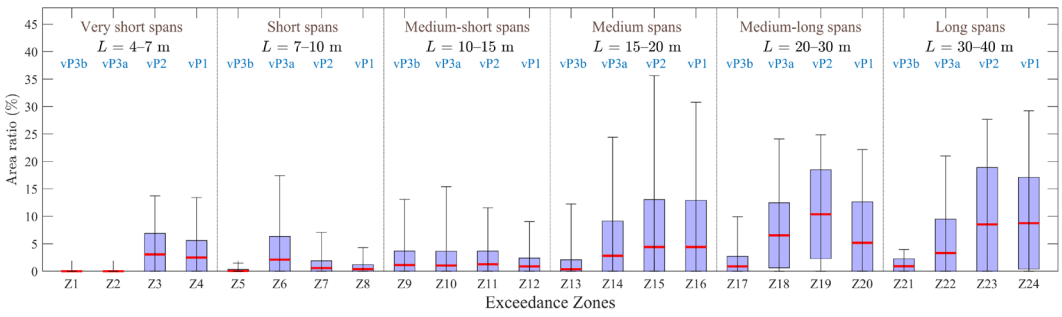

Figure 109: Box plots of Z24 binary $\Delta a(-)$: one-span vs 2-span beams under the PT60 train model. PSC bridges.

Although the binary indicator suggests a moderate to medium overall effect, the maximum-value analysis reveals significantly larger differences, with max. exceedances consistently above 30% and extreme cases approaching 80% (Z20, Z24), as shown in Figure 110. Thus, the Z24 box-plot analysis indicates that this influence is widely distributed across the analyzed regions, particularly at intermediate and high train speeds, and becomes more pronounced in medium, medium-long, and long bridges.

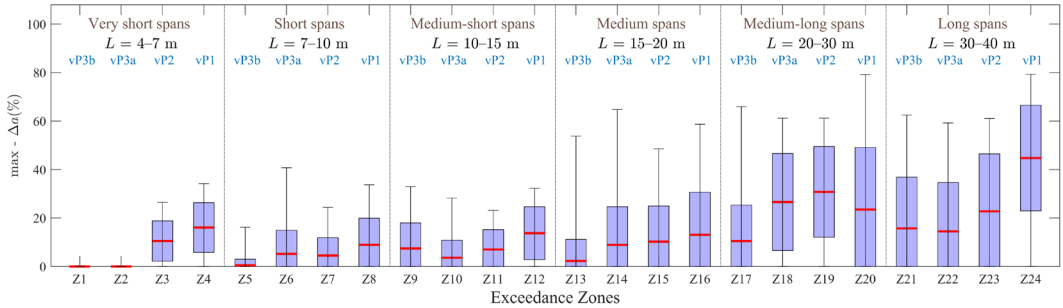

Figure 110: Box plots of Z24 max Δa(−): one-span vs 2-span beams under the PT60 train model. PSC bridges.

As it could be expected it was identified that the regions with nonzero exceedance shift as a function of the L/D ratio, progressively moving until the grey regions leave the analysis domain. This effect is easily visible for the trains of the HSLM-A model (PT60-29 to PT60-38), shown in Figure 111, where this shifting pattern of the regions can be clearly observed.

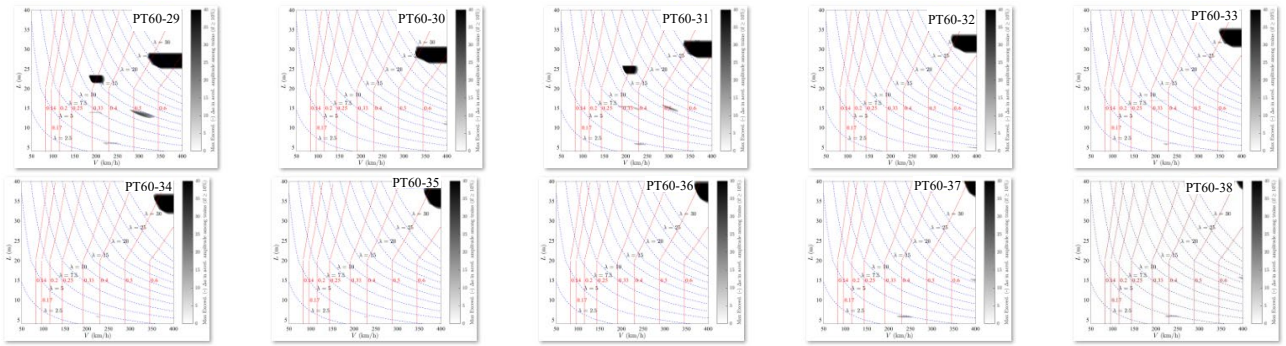

Figure 111: Δa(+) for trains PT60-29 - PT60-38. PSC bridges.

Among the particular cases, the following train-specific behaviours were identified:

- It was observed that the PT60-08 train, due to its short length, does not activate the exceedance regions identified in the other trains.
- Similar exceedance maps were found for loco-hauled trains PT60-43 and PT60-46 to PT60-50, since these SA trains share a wagon length of $D = 13\,m$ and a load distribution with a certain degree of regularity.
- Another similar subgroup comprises CB loco-hauled trains PT60-51, PT60-53, PT60-56, and PT60-60, all of them with D=26.0 m.

These findings demonstrate that the simplified use of SS models to predict the maximum vibration (acceleration) level may lead to significant underestimations of the response in continuous bridges, especially in scenarios where load regularity induces sustained resonance phenomena.

8.3 Portal frames

Figure 112 presents the comparison of the acceleration envelope response between a SS beam and a portal frame structure where the frequency ratio with the equivalent SS beam is 2.0. In part *a*) of the figure, a span length $L = 20$ m was considered for both the beam and the portal-frame, together with an equidistant train model characterized by a coach length $D = 10$ m. Under these conditions, the response of the SS beam clearly exceeds that of the portal frame over the entire velocity range, providing an initial indication of the substantial dynamic differences between both structural systems.

However, when the same coach length is maintained while reducing the span to $L = 15$ m, it is observed that the portal frame is capable of exceeding the SS beam response at the first harmonic resonance, as shown in part *b*) of the figure. Cancellation of the first subharmonic takes place in one but not in the other. In this representation, L is a normalised wavelength equal to λ/D.

It should be noted that, for the subharmonic resonances identified in both examples, the SS beam generally exhibits a higher response than the portal frame, which is consistent with the geometric and structural characteristics of the latter system. These observations indicate that the dynamic behaviour of portal frame structures cannot be adequately represented using formulations originally derived for simply supported beams, since the associated mode shapes differ significantly. Consequently, the results highlight the need for a new formulation specifically adapted to portal frame configurations. In the first example, a natural frequency of 4 Hz was considered for the SS beam, whereas in the second example a frequency of 5.3 Hz was adopted, following the lower limit of figure 8.10 in EN1991-2:2023. In both cases, the portal frame system was assumed to have a natural frequency twice that of the corresponding SS beam example.

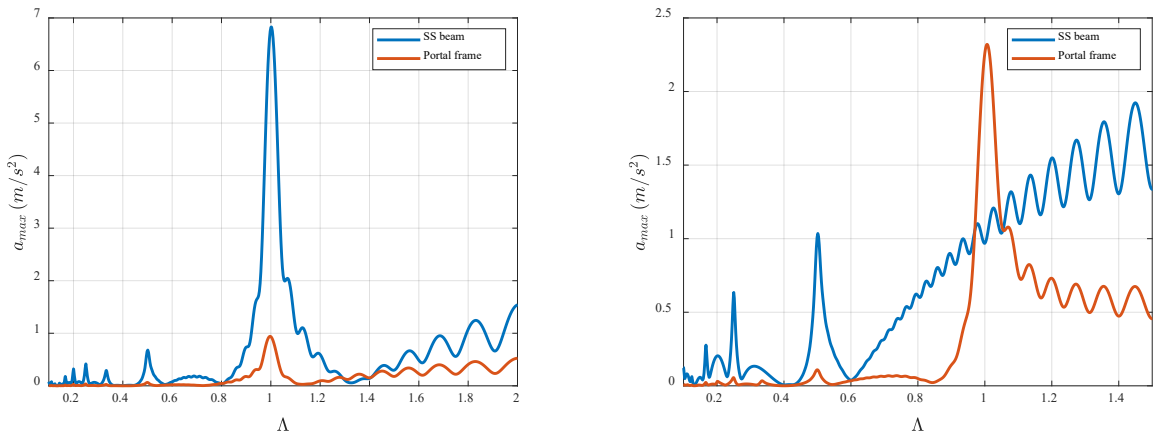

a) *b*)

Figure 112: Acceleration envelope comparison between SS beams and equivalent portal-frame structures.

9 Improved SM capable of assessing resonance and impact scenarios in SS bridges

9.1 Analysis of the improvements to SM proposed by ERRI D214 (SS bridges)

From the considerations in sections 3.1 and 3.2, points (A), (B), (C), (E), (I), (J), the following variants of the SM are proposed. Point (D) had already been incorporated in the basic versions of DER and LIR. All these variants are tested considering train model PT60:

9.1.1 DER2 method

Incorporates to the basic DER the improvements mentioned in points (B) and (E) of section 3.1 (consideration of both the impact displacement and acceleration, as minimum output values of those response variables).

As regards the error levels in $\Delta a(-)$, no worsening is observed when the method is compared with the basic DER version. That could be expected in negative exceedance computation, because the predicted response is taken as the maximum between the classic DER formula and the impact acceleration. Some small improvements are found, mostly in ascending slopes (K right above 0.33), though in some trains of model PT60 there is little influence. Overall, the performance of DER2 in this type of indicator is still not satisfactory, mostly for short spans and short wavelengths, as has been discussed in sections 6 and 7.

In relation to $\Delta a(+)$, worsening is observed for spans below some 12–15 m; these could be expected to some extent because DER2 method is setting a lower bound to the predicted response, in comparison to basic DER. Particularly unsatisfactory behaviour is observed for train PT69-08 (with only 8 loads). Another representative example is shown in Figure 113.

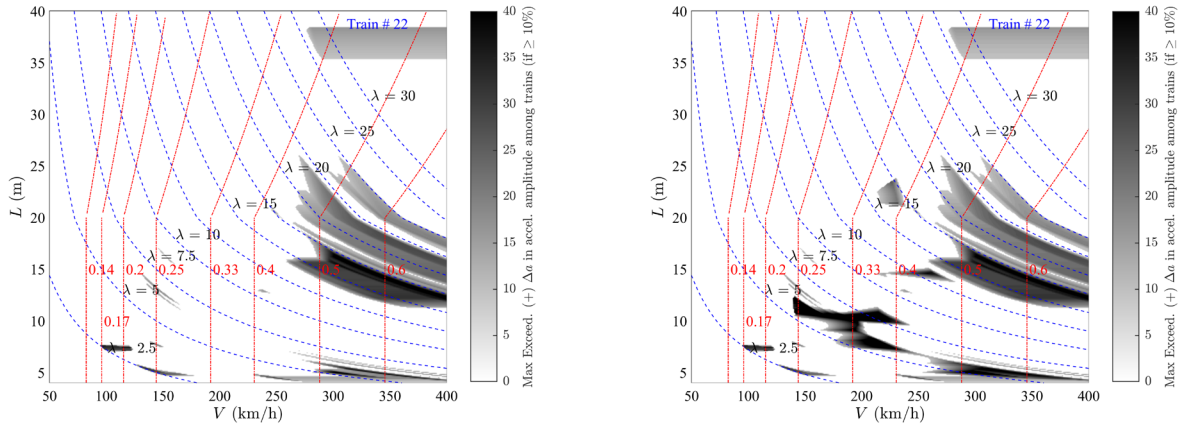

Figure 113: Maps of Δa(+): DER and DER2, both vs. TSC for train PT60-22[INB4EU-CB-130] (D=26.4 m). a) DER; b) DER2; PSC bridges.

Regarding the error levels in $\Delta\delta(-)$, again no worsening is to be be expected. A limited but interesting improvement is found for those trains where the undershooting was associated to a too small estimation of $\delta_{st,res}$ (typically, nonconservative waterdrop patterns). Figure 114 illustrates that performance, with one of the HSLM-A trains.

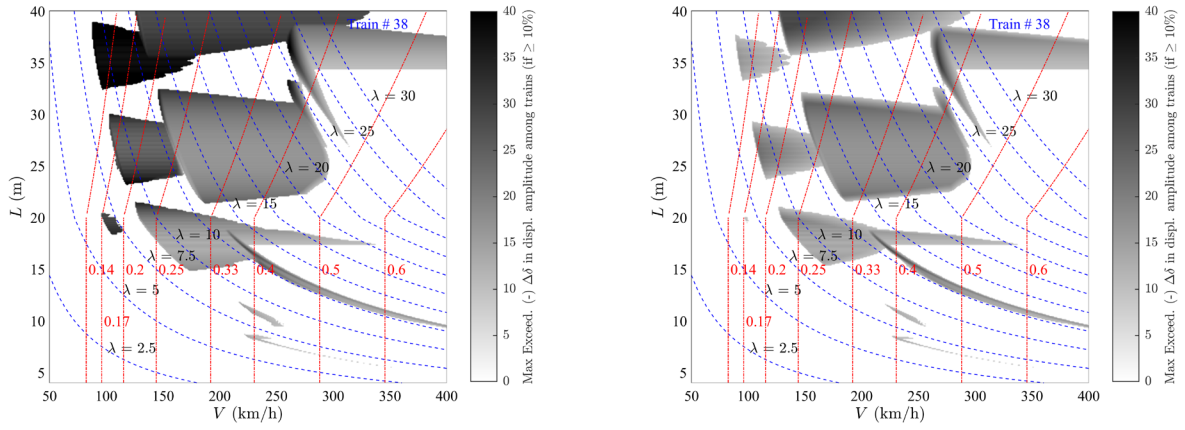

a) *b)*

Figure 114: Maps of Δδ(–): DER and DER2, both vs. TSC for train PT60-38[HSLM-A10] (D=27.0 m).

Finally, as regards exceedance Δδ(+), no worsening is observed, which is a positive conclusion given that in the computation of accelerations the opposite was seen to happen—for Δ*a*(+). Some improvements are found, particularly for trains with only front, heavy locomotives (PT60-41 and PT60-42); and few minor improvements for other loco-hauled vehicles.

Overall, the performance for accelerations is not consistently satisfactory, but the tendencies for the computation of displacement are positive, with advantages particularly for the loco-hauled trains. This conclusion should be considered along with the analysis presented for LIR2 in section 9.1.3 below.

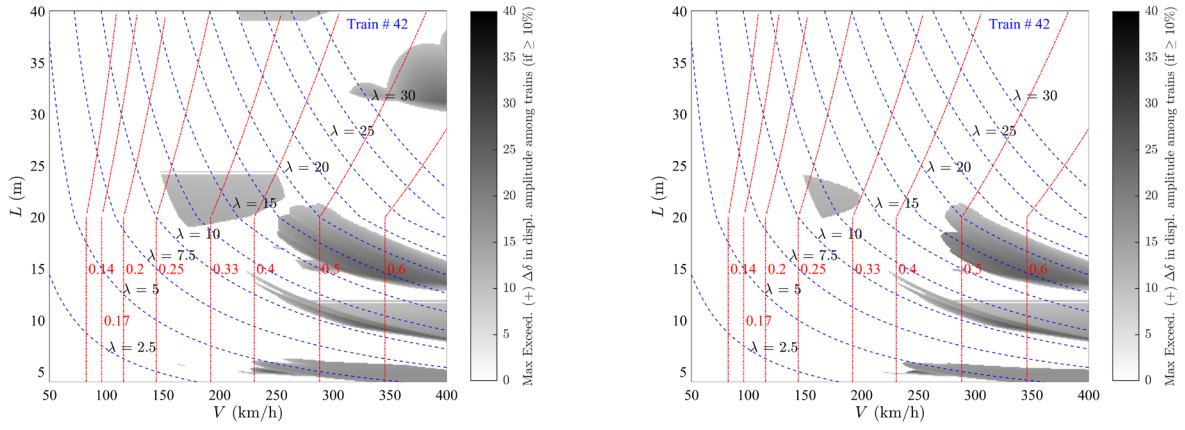

a) *b)*

Figure 115: Maps of Δδ(+): DER and DER2, both vs. TSC for train PT60-42[INB4EU-CB-075] (D=23.3 m).

9.1.2 DER3 method

In this approach the first 4 loads are removed to calculate the response through the signature, only for the first 4 subtrains (section 3.1, points (A) and (C)). That implies that those subtrains are nullified. Regarding this potential improvement, it has been seen in the section 7.6 that even the first 8 or 12 loads can cause a similar *convex* effect; therefore it is a priori likely that the problem of convex slopes cannot be solved completely in this manner.

Given that DER has proved in general to perform worse in undershooting (nonconservative predictions) and somewhat better in overshooting (except for FT), in section 9.1 testing of LIR3 version is preferred to DER3. Both methods implement the same idea, as section 9.1.4 explains. However, to verify the degree of improvement, in what follows all methods tested in section 9.1 compare $\Delta a(-)$ *vs*. LIR variants, and $\Delta a(+)$ *vs*. DER variants—with the exception of LIR2 which is the simplest improvement of basic LIR.

For consistency, a similar strategy is followed to test for vertical displacements. In general, both methods DER and LIR, in its basic versions, have proved to be similar as regards $\Delta\delta(-)$, and with small areas of advantage for each of them as regards $\Delta\delta(+)$.

9.1.3 LIR2 method (analogous to DER2)

Incorporates to the basic LIR the improvements mentioned in points (B) and (E) of section 3.1 (consideration of both the impact displacement and acceleration, as minimum output values of those response variables).

As it was mentioned for DER2 method, regarding $\Delta a(-)$, no worsening is observed when the method is compared with the basic LIR version, as it should happen. Some small improvements are found, mostly in ascending slopes (K right above 0.33), though in some trains of model PT60 there is little influence. An illustrative example is shown in Figure 116.

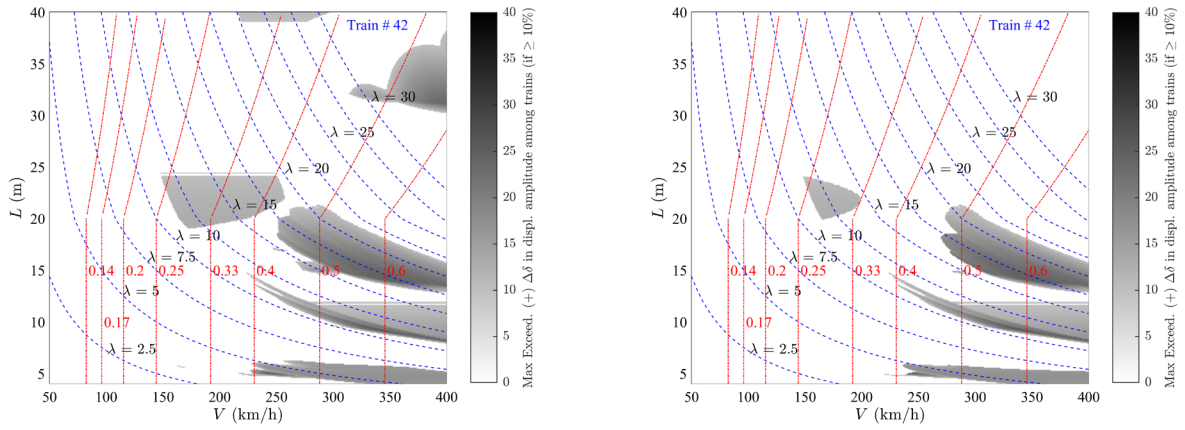

Figure 116: Maps of $\Delta\delta(-)$: LIR and LIR2, both vs. TSC for train PT60-22[INB4EU-CB-130] (D=26.4 m).

In relation to $\Delta a(+)$, worsening is observed as for DER2 method for spans below some 12–15 m. Particularly unsatisfactory behaviour is observed for train PT69-08 (with only 8 loads). Other representative examples are similar to the one for DER2 in Figure 113.

The conclusions for $\Delta\delta(-)$ and $\Delta\delta(+)$ are the same as for method DER2 too. In conclusion, the performance is not consistent enough for the computation of accelerations, but the tendencies for vertical displacements are positive, with advantages particularly for the loco-hauled trains. It was mentioned in section 0 that it remains to decide which option is preferable for computing the static deflection at resonance for each train type; it was advised that, in principle, one should keep the axles of rear and intermediate power cars, for AB and SA trains, and also for CB trains if those axles are heavier, whenever a non-conservative prediction is to be avoided in the computation of static displacement for usage with SM. It is pointed out as future research here to understand whether that option is or not preferable, if LIR2 or DER2 are used instead of basic DER and LIR.

9.1.4 LIR3 method (analogous to DER3)

In this approach the first 4 loads are eliminated to calculate the response through the signature, only for the first 4 subtrains (section 3.1, points (A) and (C)).

In relation with $\Delta a(-)$, almost identical results in comparison with LIR2 are obtained, with only few subtle differences found. However, the main interest of LIR3 and DER3 methods is to limit overshooting for K>0.45 approx. (region of convex slopes). Those main aspects are discussed below.

As for overconservative exceedance $\Delta a(+)>10\%$, the improvement observed in Figure 117 is found in some trains, though not in the majority of them. Aside from the example in such figure, also for trains with heavy locomotive front axles experience some improvement, as it was mentioned by D214, but only partial (see Figure 118).

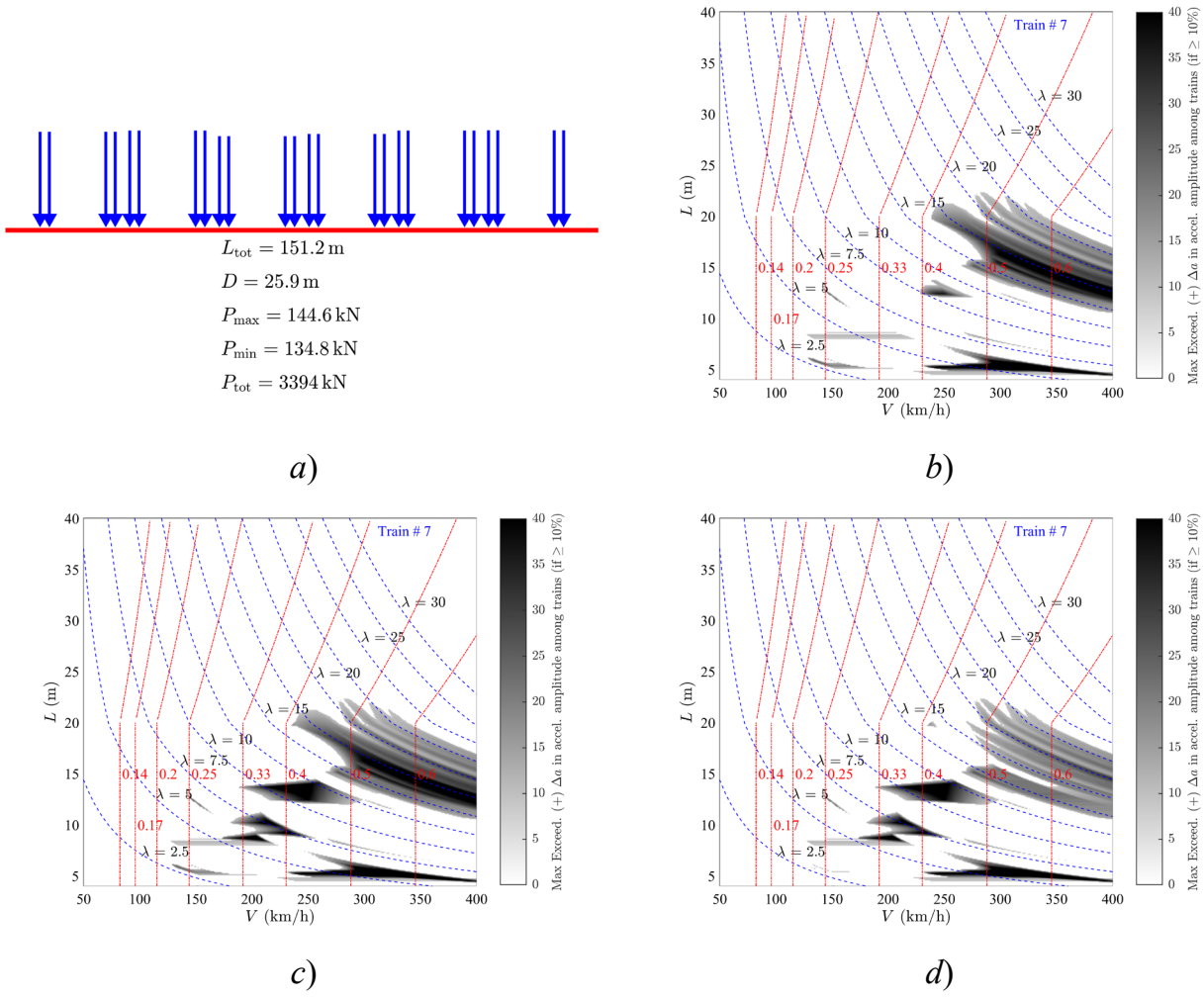

Figure 117: $\Delta a(+)$ SM vs. TSC. Train PT60-07 [INB4EU-CB-001]. a) train definition; b) LIR; c) LIR2; d) LIR3. PSC bridges.

Therefore, it is seen that the expected improvement does not cover the entire region the convex slopes, so the problem is not solved in a general manner, as it was anticipated in section 7.5.

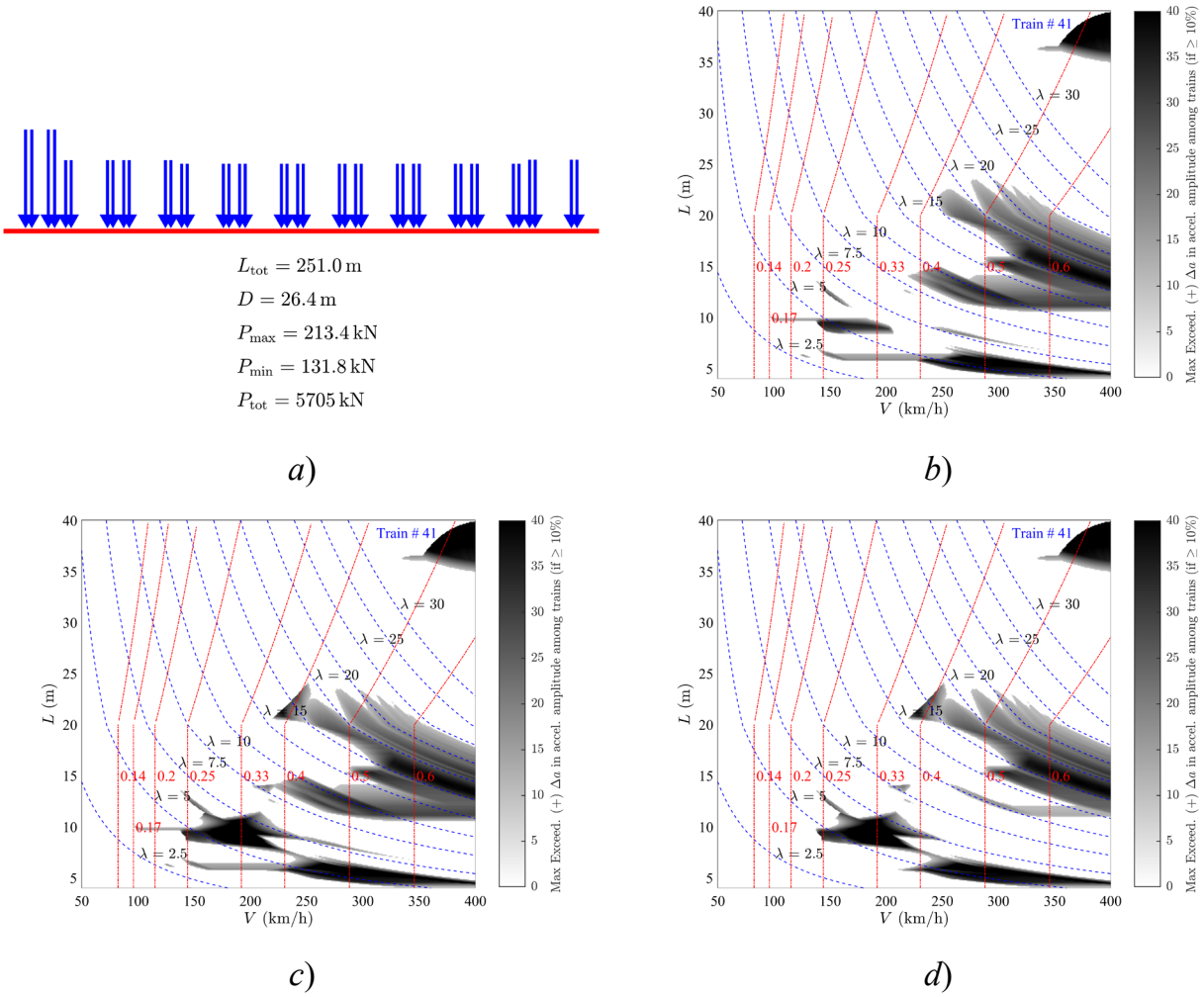

Figure 118: Δa(+) SM vs. TSC. Train PT60-41 [INB4EU-CB-003]. a) train definition; b) LIR; c) LIR2; d) LIR3. PSC bridges.

As regards Δδ(+), almost identical results than with LIR2 are obtained. Finally, regarding Δδ(+), in some trains there is an improvement for a limited range of spans, at K>0.45 approx. Typically the trains with only heavy front locomotives are in this ensemble, but few more within all PT60 model. Therefore, as mentioned above, we cannot conclude that this method is a solution generally valid to avoid the convex slopes region

9.1.5 LIF$_{h1}$ method (basic implementation of homogeneous forced influence line, FIL$_h$)

Section 7.1 in Partie – B of RP6 from D214 (ERRI D214 1999) mentions the possibility of taking into account the effects of the loads on the bridge (homogeneous forced influence line, FIL$_h$), to avoid the undershooting due to the cancellation valleys in the RIL. The method proposed is basic, since it neglects the particular solution and simply uses the signature times the FIL$_h$. Subsequently, the maximum acceleration between FIL$_h$ and classical LIR is retained. An implementation of such idea is tested here to analyse whether it can improve the estimates of vertical acceleration.

For each subtrain that has left the bridge and is already in the RIL, the possible remaining loads that are still acting on the bridge are considered. The rearmost one is placed at a position where the maximum of the FIL$_h$ is achieved (1/4 period after the load enters the bridge, approx.), and the remaining ones that fit on the bridge are combined with it using the classical signature.

It should be emphasised that this method makes the treatment of the train loads no longer independent of the span length.

LIR005 vs LIR001-PT60-512-Prestres-BL 2_5-Accel(-)

In relation to $\Delta a(-)$, almost identical predictions in comparison with LIR, with only marginal differences found. Therefore, the problems of ascending slopes does not seem to be solved with this implementation. And relation to $\Delta a(+)$, results are fully identical compared to LIR. Such inexistent difference poses doubts on the correct implementation of the method, which will be reviewed for the definitive version of this deliverable.

For the calculation of displacements, this method follows the same approach of LIR2.

9.1.6 LIF_{h2} method (refined implementation of homogeneous forced influence line, FIL_h)

With a view to estimate the maximum acceleration, method LIF_{h1} described in previous subsection considers the homogeneous forced vibration in a simplified manner. Additionally, Section 7.2 in Partie – B of RP6 from D214 (ERRI D214 1999) proposes a more refined implementation (named here as LIF_{h2}) which is discussed and tested in this section.

Section 7.2 in Partie – B of RP6 points out that for a (zero damping) case of a single load, the RIL equation takes null value for the fictitious time instant corresponding to the mid-span section. This can be proven to be truth regardless the value of K; moreover, the sign of the RIL slope at that point changes at the cancellation speeds (K=0.33, 0.20, 0.14, etc.). So, it is possible to sum both the RIL and the FIL_h, taking into account the phase, however D214 does not seem to discuss some questions that follow.

A load must be either in the RIL or in the FIL_h, both situations being mutually exclusive. Therefore, combining the RIL and the FIL_h solutions for each load would be erroneous. It would make sense to try to combine out-of-phase the RIL solution for *all loads* placed in the RIL, with the FIL_h solution for *all loads* placed in the FIL_h, but that would need to consider the relative distances between the loads in each influence line, which is not mentioned in 7.2 Partie – B of RP6. Instead, the formulation described in there seems to propose the following direct implementation:

9.1.6.1 Direct implementation of LIF_{h2} method

- Compute the RIL term as usual, *i.e.* using the standard LIR formulation (term named "A").
- Compute the FIL_h term as explained in 7.1 Partie – B of RP6, which will make use of the distances between the loads acting just on the span (term named "B"). See previous section 9.1.5 here.
- Instead of simply taking the maximum among them as mentioned in 7.1 Partie – B of RP6, combine them out-of-phase with expression

$$\sqrt{A^2 + B^2 + 2\,A\,B\,\cos\frac{\pi}{2K}} \tag{23}$$

which does not take into account the relative distances between the loads in each influence line. Thus, lack of physical basis seems to be accepted in favour of simplicity.

9.1.6.2 Advanced implementation of LIF_{h2} method

Or perhaps here we are misunderstanding what D214 tries to convey. Another possibility would be to try to take into account the relative distances between loads in the RIL and loads in the FIL_h by casting all of them into the same computed signature, while previously multiplying each of them by the corresponding influence

line. If that were done so, the damping term in such modified signature should be also adjusted, because both sets of loads don't enter each influence line on a common time reference; that aspect isn't mentioned either in RP6.

Finally, the terms A and B should be separated in the above computations, and Eq. (23) applied to consider the essential out-of-phase condition between RIL and FIL_h.

9.1.6.3 Conclusions about the implementation of LIF_{h2} method and further methods proposed by D214

It is seen that there are uncertainties about the proper way to implement 7.2 Partie – B of RP6. In this document Eq. (23) is adopted as described in section 9.1.6.1. In doing so, the analysis is no longer independent of the bridge span, as it was previously mentioned for method LIF_{h1}.

Moreover, the further methods described in section 7.3 Partie – B of RP6 which try to include the particular solution of the FIL (FIL_p) are also dependent on the bridge span.

Given that such dependence on the span makes it no longer possible to have a signature completely independent of the bridge, and considering that the results discussed below for method LIF_{h2} are not positive overall, in the next section a hybrid method is proposed that will integrate the ideas discussed in this section with a suitable mathematical treatment of the phases of the RIL, FIL_h, and FIL_p.

9.1.6.4 Results of LIF_{h2} method

From Eq. (23) it is seen that the term $\cos\frac{\pi}{2K}$ will act in some cases as an amplifier of the prediction, while in other will diminish the output result. Particularly, near the range K=0.25 one can expect such amplification, and near K=0.5 a de-amplification. Some representative results shown in the following plots confirm these expectations.

Figure 119 shows negative exceedance in acceleration, comparing the LIR and LIF_{h2} predictions. It is seen that in the range K=0.5, for spans below L=15 m, the prediction worsens. Though a benefit is observed in the transient phenomenon that takes place at some 170 km/h for L=15 m ("horizontal" grey patch), this is at the expense of worsening in other regions (K=0.17 as well, where again $\cos\frac{\pi}{2K} = -1$). Similar performance is found for many other trains from PT60 model. The intended improvement, therefore, is not consistent as regards $\Delta a(-)$.

Figure 120 shows positive exceedance in acceleration, comparing the DER and LIF_{h2} predictions. It is seen that in the region of convex response (range K>0.45 approx.), the prediction is improved for both trains considered in that figure. Therefore, the part of the forced response that characterises the convex slopes (see section 7.5) is being better estimated. However, this is also at the expense of a clear worsening in all transients that start at K=0.25 approx., where the response is neatly overestimated. Moreover, it can be said that such worsening is rather usual for all trains in model PT60 (sometimes affecting shorter spans, many times for spans up to some L=20 m), but the improvement for the region K>0.5 is more irregular among the various trains. The overall improvement obtained with the implementation of LIF_{h2}, therefore, is not consistent either as regards $\Delta a(+)$.

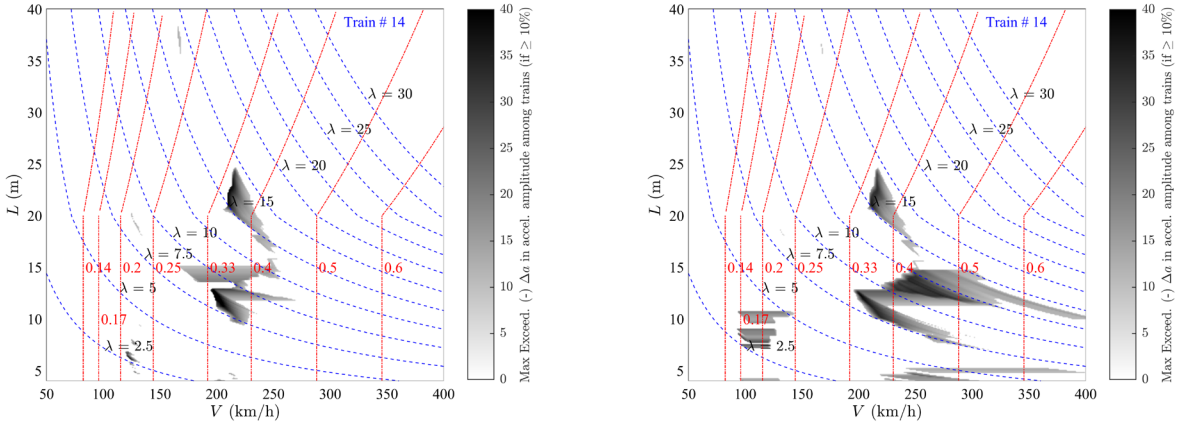

a) *b)*

Figure 119: Maps of Δa(−): LIR and LIF$_{h2}$, both vs. TSC for train PT60-14[INB4EU-AB-013] (D=17.5 m). a) LIR; b) LIF$_{h2}$; PSC bridges.

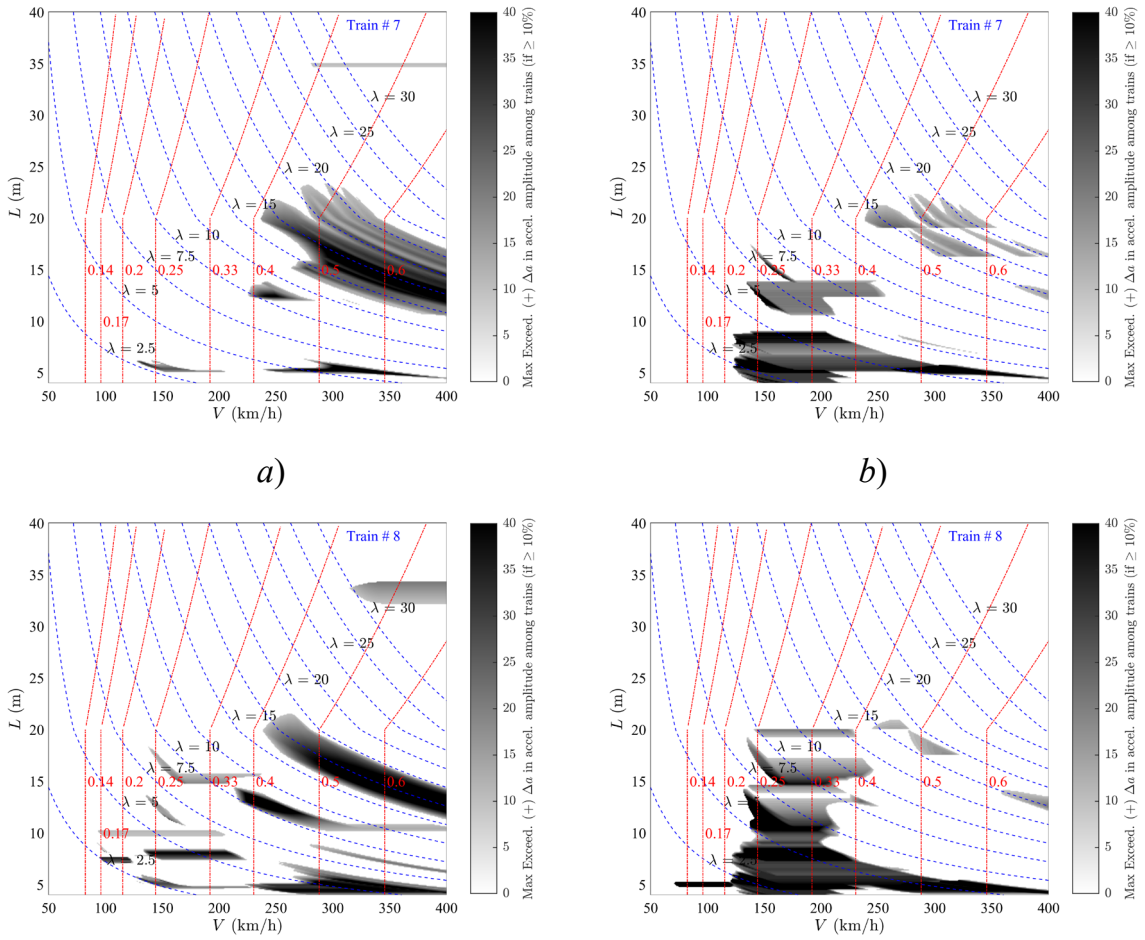

a) *b)*

c) *d)*

Figure 120: Maps of Δa(+): DER and LIF$_{h2}$, both vs. TSC, for trains PT60-07[INB4EU-CB-001] (D=25.9 m) and PT60-08[INB4EU-CB-007] (D=26.4 m). a) DER PT60-07; b) LIFh2 PT60-07; c) DER PT60-08; d) LIF$_{h2}$ PT60-08 PSC bridges.

9.2 Hybrid LIR method for SS bridges (HLIR)

The method presented in this section considers the following assumptions:

- While in many cases resonance is determinant for bridge design, in previous sections it has been shown that in other cases only partial resonance is developed, where forced response has also a relevant contribution—either adding or subtracting a significant part of the response.
- A promising alternative is thus to capture exactly the instant when the maximum free vibration occurs for each subtrain, and then combine it in closed form (considering the phase in a suitable manner) with the forced response of the loads on the bridge (homogeneous plus particular).
- With this alternative, all cases of partial resonance can be better approximated than with the methods previously discussed. That approach is presented first and subsequently is complemented with the treatment of other types of transient response.
- An *a priori* advantage, inherent to this strategy, is that it does eliminate positive exceedance altogether, both for $\Delta a(+)$ and $\Delta\delta(+)$, thus being aligned with the demand in the *ERA Technical Note* (ERA, 2022) in relation to "*not overestimate the load effects of the existing trains that are operating*".

9.2.1.1 HLIR method for partial resonance cases

Because the combination of RIL and FIL equations is phase-dependent and trigonometric functions present intervals with strong slopes, it is important not to neglect any damping term in a first formulation of the method, particularly as regards the computation of phase angles. That is also relevant to satisfy the target level of accuracy in the Project (–10%). Therefore, several expressions from a previous publication will be used here, valid for general viscous damping in SS bridges (Museros and Moliner 2017).

The exact expression of the RIL that predicts the normalised initial amplitude of the free vibration due to a single load is (Museros and Moliner 2017):

$$R(K,\zeta)=\frac{K}{\sqrt{1-\zeta^2}\sqrt{(1-K^2)^2+(2\zeta K)^2}}\sqrt{1+e^{-2\zeta\pi/K}+2\,e^{-\zeta\pi/K}\cos\left(\frac{\pi}{K}\sqrt{1-\zeta^2}\right)} \tag{24}$$

The initial phase angle of the free vibration is dependent on the initial conditions of the RIL given also in (Museros and Moliner 2017), and can be computed as follows in interval [–π/2, +π/2]:

$$\varphi_0=\tan^{-1}\left(\frac{-\xi_0\sqrt{1-\zeta^2}}{\xi_0\zeta+\dot{\xi}_0}\right) \tag{25}$$

$$\xi_0=2\zeta+e^{-\zeta\pi/K}\left(\frac{2\zeta^2+K^2-1}{\sqrt{1-\zeta^2}}\sin\left(\frac{\pi}{K}\sqrt{1-\zeta^2}\right)+2\zeta\cos\left(\frac{\pi}{K}\sqrt{1-\zeta^2}\right)\right) \tag{26}$$

$$\dot{\xi}_0=K^2-1+e^{-\zeta\pi/K}\left(\frac{\zeta(1+K^2)}{\sqrt{1-\zeta^2}}\sin\left(\frac{\pi}{K}\sqrt{1-\zeta^2}\right)+(1-K^2)\cos\left(\frac{\pi}{K}\sqrt{1-\zeta^2}\right)\right) \tag{27}$$

It is recalled that $K=\frac{\lambda}{2L}$, thus $R(K,\zeta)$ and φ_0 depend on the wavelength, span length and damping ratio only.

Knowing the phase φ_0 of the free vibration $y_j(t)$ of a single jth load, the equation of the RIL due to a series of k_s>1 loads from a subtrain can be expressed mathematically as follows, where positive displacement is measured upwards. The bridge has linear mass m, and fundamental frequency ω; only the contribution of the first bending mode is retained for the moment:

$$y_f(t) = \sum_{j=1}^{k_s} y_j(t) = \frac{-2}{mL\omega^2} R(K,\zeta)\, Z\, e^{-\zeta\omega t} \sin\left(\omega_d t + \beta_y\right) \tag{28}$$

$$Z = \sqrt{\left(\sum_{j=1}^{k_s} P_j\, e^{\zeta\omega d_j/V} \sin\left(\omega_d\, d_j/V\right)\right)^2 + \left(\sum_{j=1}^{k_s} P_j\, e^{\zeta\omega d_j/V} \cos\left(\omega_d\, d_j/V\right)\right)^2} \tag{29}$$

$$\beta_y = (\pi - \varphi_0) + \tan^{-1}\left(\frac{-\sum_{j=1}^{k_s} P_j\, e^{\zeta\omega d_j/V} \sin(\omega_d d_j/V)}{\sum_{j=1}^{k_s} P_j\, e^{\zeta\omega d_j/V} \cos(\omega_d d_j/V)}\right) \quad \text{(four quadrant arc tangent)} \tag{30}$$

In the Eq. (28) time is measured from the instant when the first load of the subtrain leaves the bridge, but such equation is only valid when the full subtrain is in the RIL.

By differentiation, the acceleration RIL due to the k_s>1 loads from the subtrain can now be expressed as

$$a_f(t) = \sum_{j=1}^{k_s} a_j(t) = \frac{2}{mL} R(K,\zeta)\, Z\, e^{-\zeta\omega t} \sin(\omega_d t + \beta_a) \tag{31}$$

$$\beta_a = \beta_y + \tan^{-1}\left(\frac{2\zeta\sqrt{1-\zeta^2}}{1-2\zeta^2}\right) \tag{32}$$

The terms of type are $\omega_d\, d_j/V$ are well known, since they appear in the usual signature, only modified here by damping:

$$\omega_d\, d_j/V = \frac{\omega d_j}{V}\sqrt{1-\zeta^2} = \frac{2\pi d_j}{\lambda}\sqrt{1-\zeta^2} \tag{33}$$

Those terms depend then on the train configuration, plus the wavelength and damping ratio. Given that Eqs. (29) and (30) depend on the train configuration, and $K = \frac{\lambda}{2L}$, thus Eqs. (28) and (31) for the RIL as a function of time depend on the wavelength, train configuration, damping ratio and span length, except for the first constant term $\frac{2}{mL\omega^2}$ or $\frac{2}{mL}$.

Certainly, to obtain a time-history using Eqs. (28) and (31), particular values of ωt and $\omega_d t$ must be employed, which make those expressions frequency dependent. However, when particularised for the time instants of interest discussed below, it will be seen that both frequency and time dependency vanish.

The new formulation is now tested satisfactorily for a set of five loads. The correspondence in acceleration, Eq. (31), is excellent (see Figure 121). Same conclusion is obtained for displacements, Eq. (28), not shown for conciseness. The input data for the simulation are the following:

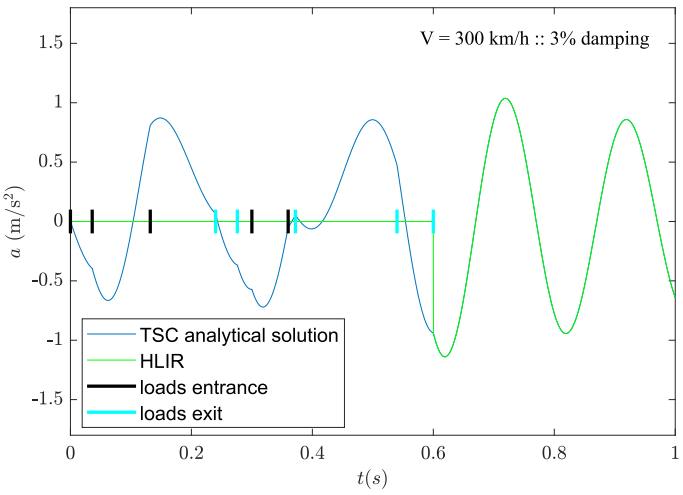

Figure 121: HLIR validation vs. TSC. Exact mid-span time-history of the residual influence line (RIL).

In order to obtain the instants of maximum free acceleration, one must differentiate and equate to zero:

$$\dot{a}_f(t) = \frac{2}{mL} R(K,\zeta)\, Z \left[-\zeta\omega\, e^{-\zeta\omega t} \sin(\omega_d t + \beta_a) + \omega_d\, e^{-\zeta\omega t} \cos(\omega_d t + \beta_a)\right] = 0 \tag{34}$$

$$\tan(\omega_d t^a_{max} + \beta_a) = \frac{\sqrt{1-\zeta^2}}{\zeta} \;\Rightarrow\; \omega_d t^a_{max} = \varphi^a_{max} = \tan^{-1}\left(\frac{\sqrt{1-\zeta^2}}{\zeta}\right) - \beta_a \geq \frac{\omega_d d_{k_S}}{V} \tag{35}$$

Previous inequality arises from the fact that the RIL expression is only valid when the last load of the subtrain (k_s-th load) has left the beam, but time was set to zero when the first load left the beam. Therefore, the solution to the arc tangent is to be found by adding $n\pi$ as follows:

$$\varphi^a_{max} = \varphi^a_{max,0} + n\pi - \beta_a \geq \frac{\omega_d d_{k_S}}{V} \;\Rightarrow\; n \geq \frac{1}{\pi}\left(\beta_a - \varphi^a_{max,0} + \frac{2\pi d_{k_S}}{\lambda}\sqrt{1-\zeta^2}\right) \quad \text{where} \quad n \geq 0 \tag{36}$$

$$\text{and} \quad \varphi^a_{max,0} = \tan^{-1}\left(\frac{\sqrt{1-\zeta^2}}{\zeta}\right) \qquad \text{comprised in interval } [0,\, \pi/2] \tag{37}$$

The minimum possible value has to be retained for n, to capture the first maximum of the RIL. In modern software such value of n is obtained with a "*ceil*" or analogous ceiling function. It can be seen that n and φ^a_{max} depend on the train configuration, wavelength, span length and damping ratio [train, λ, L, ζ].

Once the correct n has been found, it could be checked that the phase φ^a_{max} is such that load $(k_s + 1)$ has not left the bridge yet, i.e., n could be disregarded and the next subtrain then be processed if

$$\varphi^a_{max} = \varphi^a_{max,0} + n\pi - \beta_a > \frac{\omega_d d_{(k_S+1)}}{V} \tag{38}$$

However, that is not an optimal way to consider various free cycles of interest, as will be discussed below.

A similar development may be followed to obtain the time of maximum displacement, by using β_y instead of β_a, but it suffices to add the relative phase delay between displacement and acceleration as follows:

$$\varphi^y_{max} = \varphi^a_{max} + \tan^{-1}\left(\frac{2\zeta\sqrt{1-\zeta^2}}{1-2\zeta^2}\right) \tag{39}$$

In order to process various free cycles, the subsequent maxima/minima of the RIL are also of interest. Therefore, a discrete number l of phase angles can be considered to get the RIL extreme values, each one incrementing the phase in one half-cycle:

$$\varphi^a_{max,l} = \varphi^a_{max} + (l-1)\,\pi \qquad l = 1, 2, 3, \ldots l_{max} \tag{40}$$

Parameter l_{max} should allow to consider the possibility of a predefined number of free cycles. Those free cycles are related to what is usually known as number of subhamonics i, which in this context are the (complete) cycles of the RIL of interest to combine with subsequent forced vibration. Those cycles are of interest because while they take place for each subtrain, subsequent loads may enter the bridge and create a relevant transient.

Therefore, if one wants to consider $i = 4$ for example:

$$l_{max} = 2i = 8 \tag{41}$$

However, if the coach length[6] and the speed are such that a lower index (i) of the maximum subharmonic

[6] The minimum coach length should be used preferably.

is expected, then one can use a smaller value of l_{max}. Considering again a "ceil" function:

$$l_{max} = \min\left\{2i\,;\ \text{ceil}(\tfrac{D}{\lambda})\right\} \geq 1 \tag{42}$$

In summary, HLIR is a hybrid method than combines RIL and FIL equations and exploits the following informed guessing about the critical instants of the response:

- Eqs. (36), (37), (40) and (42) predict the phases (time instants) of interest to combine free plus forced acceleration response, considering that various cycles of free vibration may take place before a relevant forced effect adds or subtracts to the free vibration. Those four equations provide phases which depend on parameters [train, λ, L, ζ].
- The phases are given in the form of l_{max} products for each subtrain, of the kind $\varphi^a_{max,l} = \omega_d t^a_{max,l}$.
- Eq. (39) allows to transfer the results for obtaining the maximum displacements.

At this point, it remains only to add the known forced solution for those loads acting on the bridge at the desired time instants. That addition can also be proved to depend on [train, λ, L, ζ], except for the same constant terms $\frac{2}{mL\omega^2}$ or $\frac{2}{mL}$. Following this approach, no overestimation (positive exceedance) is present in the results, and very good overall performance is achieved for the large majority of vehicles and speeds. Moreover, the method is at early stages of development and can be optimised in a number of ways in the future.

In that regard, a final comment refers to any loads which could have exit the bridge between the time when load k_s (*i.e.* subtrain k_s) did left the bridge, and any of the phases from Eq. (36) is reached. For those loads, instead of adding the forced solution, it is straightforward to add simply the free vibration, using Eq. (31), or Eq. (28) particularised for a single load.

The nondimensional version of the forced response (FIL_p plus FIL_h) of the fundamental mode of vibration under a single load, valid for general viscous damping, is provided below for completeness:

$$y_{\text{forced}}(t) = \frac{y_{\text{stat}}}{(1-K^2)^2+(2\zeta K)^2}\{(1-K^2)\sin(K\omega t) - 2\zeta K\cos(K\omega t) + \\ + Ke^{-\zeta\omega t}\left[\frac{2\zeta^2+K^2-1}{\sqrt{1-\zeta^2}}\sin\left(\omega\sqrt{1-\zeta^2}\,t\right) + 2\zeta\cos\left(\omega\sqrt{1-\zeta^2}\,t\right)\right]\} \tag{43}$$

where, for an acting force F, the static deflection is $y_{\text{stat}} = \frac{-2F}{mL\omega^2}$. The forced acceleration is obtained by differentiation:

$$a_{\text{forced}}(t) = \frac{-2F}{mL}\frac{K^2}{(1-K^2)^2+(2\zeta K)^2}\{(K^2-1)\sin(K\omega t) + 2\zeta K\cos(K\omega t) + \\ + \frac{e^{-\zeta\omega t}}{K}\left[\frac{1+2\zeta^2K^2-K^2}{\sqrt{1-\zeta^2}}\sin\left(\omega\sqrt{1-\zeta^2}\,t\right) - 2\zeta K^2\cos\left(\omega\sqrt{1-\zeta^2}\,t\right)\right]\} \tag{44}$$

Typically for any phase $\varphi^a_{max,l}$, the arguments in the trigonometric functions in Eqs. (43) and (44) for a generic load k become, after adding L/V to transform to global time

$$K\omega\, t^a_{max,l} = K\omega\left(\frac{\varphi^a_{max,l}}{\omega\sqrt{1-\zeta^2}} + \frac{L}{V} - \frac{d_k}{V}\right) = \frac{\lambda\,\varphi^a_{max,l}}{2L\sqrt{1-\zeta^2}} + \pi\left(1-\frac{d_k}{L}\right) \tag{45}$$

$$\omega\sqrt{1-\zeta^2}\, t^a_{max,l} = \omega\sqrt{1-\zeta^2}\left(\frac{\varphi^a_{max,l}}{\omega\sqrt{1-\zeta^2}} + \frac{L}{V} - \frac{d_k}{V}\right) = \varphi^a_{max,l} + \frac{2\pi(L-d_k)}{\lambda}\sqrt{1-\zeta^2} \tag{46}$$

which confirms the dependency on [train, λ, L, ζ]. Therefore, as mentioned previously in sections 9.1.5 and 9.1.6.3, complete independence of the bridge is not possible to take the forced vibration into account.

9.2.1.2 HLIR method for initial transient cases

In sections 6.5, 0 and 7.5, some cases were illustrated where the response due to the initial axles or subtrains of the train is predominant. In those cases, little or even no free vibration has been originated yet, and the basic formulation of HLIR presented in previous subsection may not be suitable to predict the maximum forced response.

However, simple strategies can be adopted to cover those cases satisfactorily. A first approximation is to sample the forced response exclusively at the time instants when the mid-point of the initial bogies (or single axles) crosses the mid-span section. That guess of the critical time instant can also be improved if necessary.

In that way, Eqs. (43) and (44) can be used, and again a dependency on parameters [train, λ, L, ζ] is obtained, since the total number of loads on the bridge will depend on the span length. The computational cost is minimal, given that only few additional points have to be computed.

9.2.1.3 3D train spectrum

In sections 9.2.1.1 and 9.2.1.2 the dependency of the response on parameters [train, λ, L, ζ], with exception of multiplicative constants, has been emphasised. While that fact is known from nondimensional formulations of the equations of motion presented by previous researchers, and is contained also in the *similarity formulas* proposed by ERRI D214, it opens the door to producing 3D spectra that actually allow to compare different trains. Today's computational resources make it feasible in a reasonable time, by just assuming constant values of linear mass and natural frequency for each span length.

HLIR method can provide optimal computational efficiency for such spectra, given that the points sampled are minimal, and optimisation of the method is only at its earliest stage.

The consideration of damping must however be individual in each spectrum, since subharmonics due to different trains could be either covered or non-covered by other trains, if they do not belong to the same resonant order (same value of i).

9.2.1.4 HLIR: summary of results

To demonstrate the capabilities of the HLIR method, a series of time history results are shown below, corresponding to phenomena that current SM were unable to predict accurately. These results are representative of the main shortcomings analyzed in the sections of this document. This validation is further supported by graphs that globally demonstrate the significant improvement in accuracy achieved by the HLIR method.

First, regarding acceleration calculations, Figure 122 shows a case where the initial exceedance was $\Delta a(+) = 19.2\%$, due to a convex slope caused by a short train of only eight loads. The phenomenon is correctly simulated using HLIR, with an l_{max} parameter of 2.

Then Figure 123 shows how HLIR also improves upon one of the frequent cases of ascending slopes, where the response exhibits some resonant characteristics, but the vibration does not accumulate in phase, and therefore the response peak does not necessarily occur towards the end of the train's passage. Using $l_{max}=2$ again, initial exceedance was $\Delta a(-)=41.3\%$ and HLIR reduces it to 7.2%.

On the other hand, Figure 124 shows an end-transient captured excellently by HLIR with $l_{max}=2$, where the initial exceedance was $\Delta a(-)=13.3\%$, which HLIR reduces to zero.

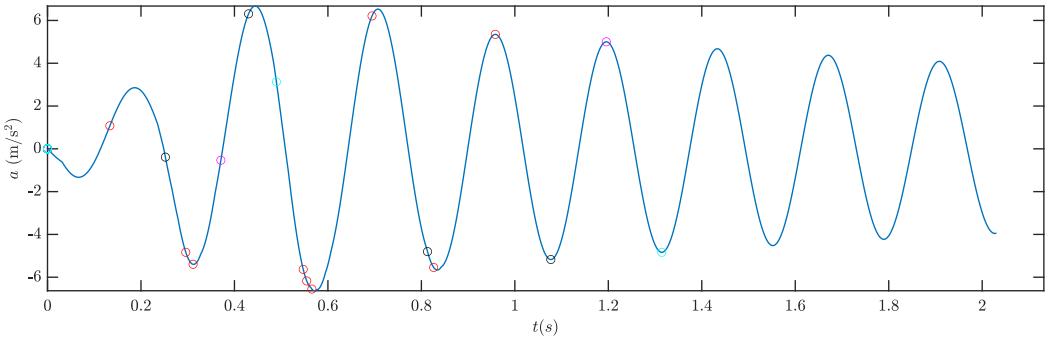

Figure 122: HLIR vs. LIR and TSC. Train PT60-08[INB4EU-CB-007] (D=26.4 m, only 8 loads), V=290 km/h, L=19.0 m, PSC bridge. TSC = _____ ; HLIR values = ∘(various colours).

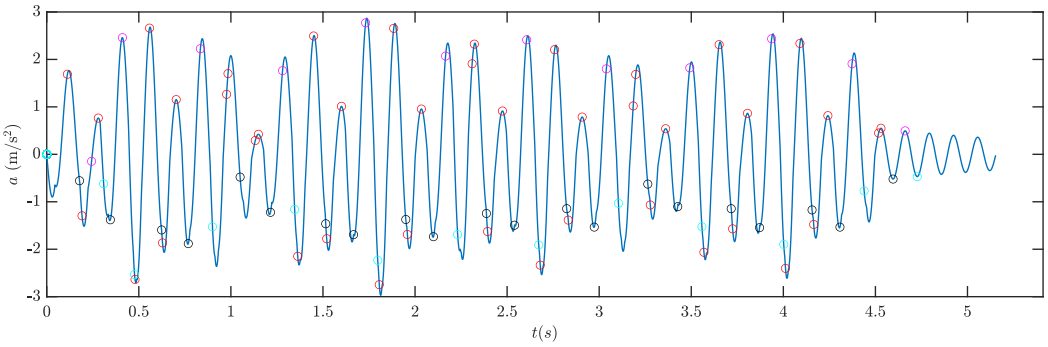

Figure 123: HLIR vs. LIR and TSC. Train PT60-18[INB4EU-CB-073] (D=25.9 m), V=210 km/h, L=10.5 m, PSC bridge. TSC = _____ ; HLIR values = ∘(various colours).

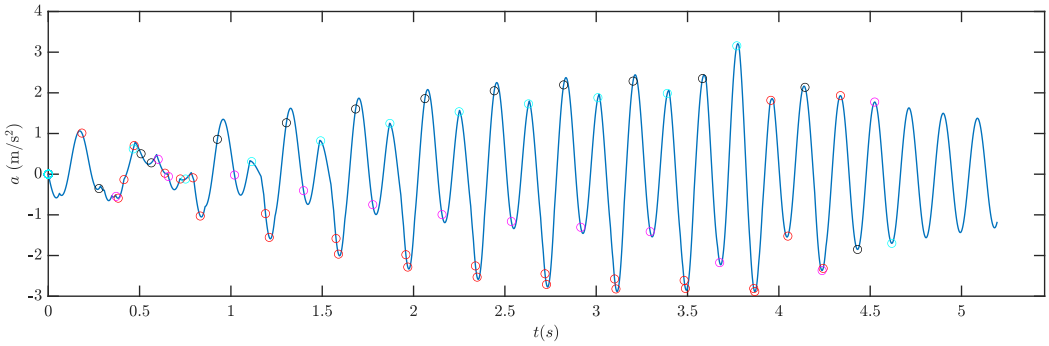

Figure 124: HLIR vs. LIR and TSC. Train PT60-28[INB4EU-AB-004] (D=19.0 m), V=176 km/h, L=15.0 m, PSC bridge. TSC = _____ ; HLIR values = ∘(various colours).

Regarding intermediate transients in irregular vehicles, Figure 125 shows the case of a CRLH-mL type loco-hauled train, a double unit with four power cars. Again, with l_{max}=2, the initial exceedance $\Delta a(-)$=12.2% is reduced to zero.

As a last example related to accelerations, Figure 126 shows the response to a CRLH-2fL train with two front locomotives, at very short wavelength λ=2.5. If longitudinal reduction factors are considered, max. acceleration falls to 2.54 m/s^2. This phenomenon happens at a 5th subharmonic speed, which implies more unloaded cycles between loads, therefore, it is seen indeed that not all peaks are captured with l_{max}=2. In those cases one would need up to l_{max}=5 or 6 if all transients were to be obtained, which opens an interesting area to optimise HLIR and adapt it to any situation occurring at the shortest wavelengths.

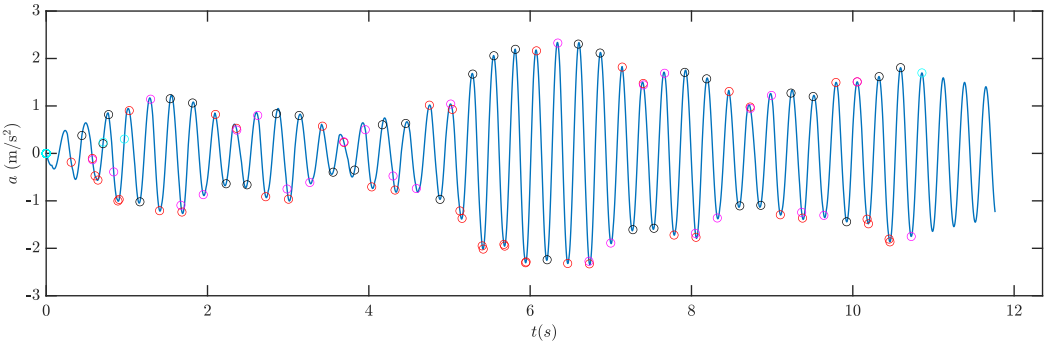

Figure 125: HLIR vs. LIR and TSC. Train PT60-57[INB4EU-SA-040] (D=13.2 m), V=144 km/h, L=22.0 m, PSC bridge. TSC = _____ ; HLIR values = ∘(various colours).

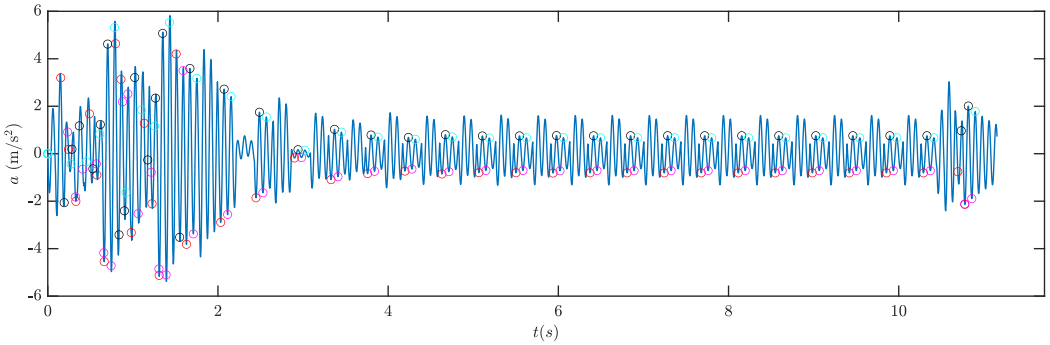

Figure 126: HLIR vs. LIR and TSC. Train PT60-43[INB4EU-SA-021] (D=13.3 m), V=110 km/h, L=6.5 m, PSC bridge. TSC = _____ ; HLIR values = ∘(various colours).

Now a number of relevant examples are shown, related to the computation of displacements. Figure 127 shows a complex case of a CMU train where an intermediate transient occurs, with an original exceedance Δδ(+) = 30.0%, which HLIR cuts down to 9.4%. This is one of the points with the highest exceedance for this type of train (see maps in Appendix E).

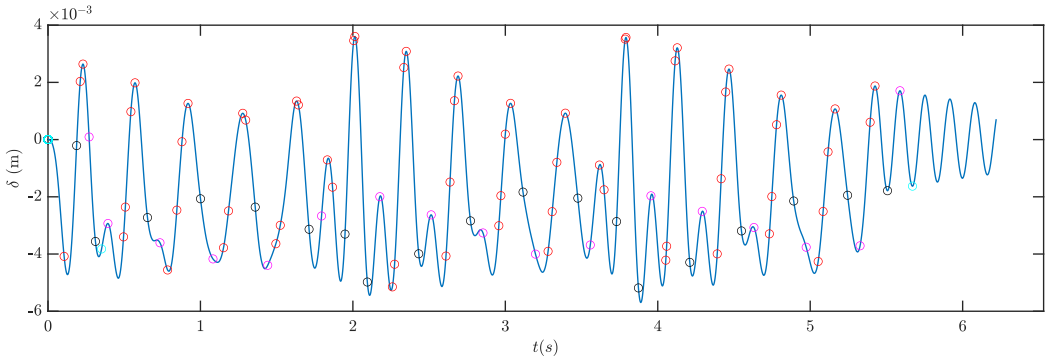

Figure 127: HLIR vs. LIR and TSC. Train PT60-21[INB4EU-CB-128] (D=25.9 m), V=269 km/h, L=13.1 m, PSC bridge. TSC = _____ ; HLIR values = ∘(various colours).

Turning the attention to cases of the usual waterdrop patterns, Figure 128 shows a case of second resonance, where each unloaded cycle is captured using l_{max}=2. The final transient is approximated with high accuracy, in a low-speed resonant phenomenon that slightly exceeds the 1.1φ' threshold (reaching a dynamic amplification

of 30%). The two initial locomotives produce a negligible effect compared to the final transient after the resonance created by the passenger cars. The initial exceedance was Δδ(−)=13.6%, which HLIR eliminates.

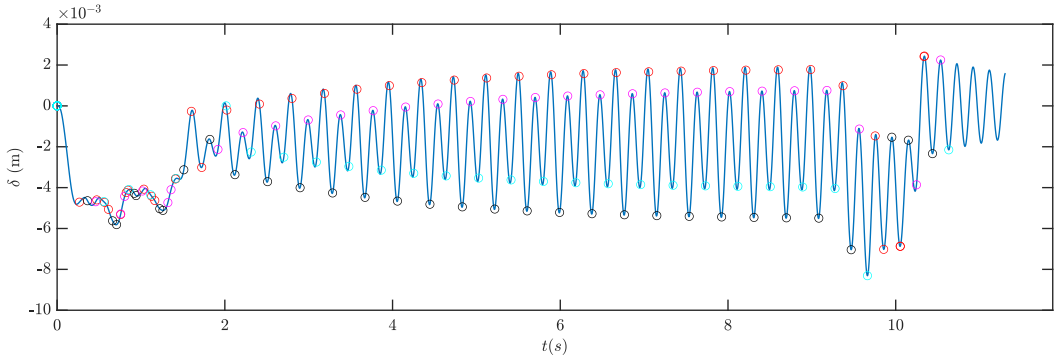

Figure 128: HLIR vs. LIR and TSC. Train PT60-50[INB4EU-SA-029] (D=13.3 m), V=124 km/h, L=15.5 m, PSC bridge. TSC = _____ ; HLIR values = ∘(various colours).

Finally, Figure 129 shows a more challenging resonance in a higher-order subharmonic occurring at very low speed (only 69 km/h), but which also slightly exceeds the 1.1φ‘ threshold (reaching a dynamic amplification of 22%). The train has a clearly heavier rear locomotive, which generates a transient that in this case requires l_{max}=3 to be captured, due to the greater number of unloaded cycles between peaks. The initial exceedance was Δδ(−)=11.5%, which the HLIR eliminates.

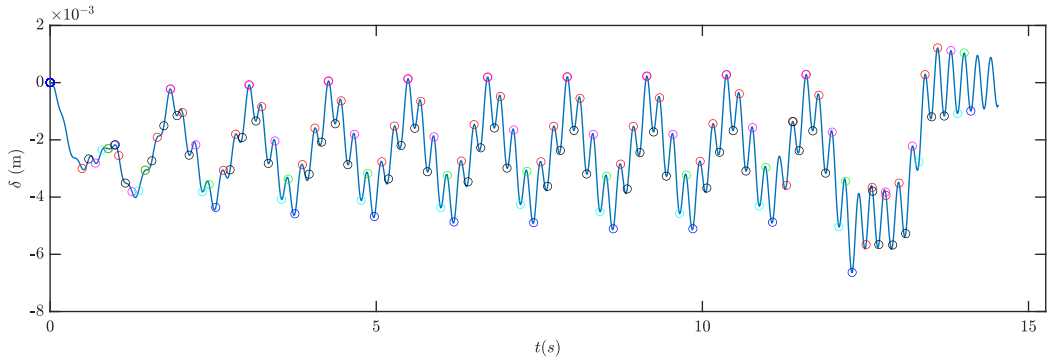

Figure 129: HLIR vs. LIR and TSC. Train PT60-45[INB4EU-SA-124] (D=23.4 m), V=69 km/h, L=16.3 m, PSC bridge. TSC = _____ ; HLIR values = ∘(various colours).

The overall assessment of HLIR can be broken down into displacements and accelerations. Regarding displacements, the formulation proposed in section 9.2.1.1, where l_{max} is calculated using Eq. (42), provides optimal results, and hardly any exceedance zones are observed in the maps, not even for STC bridges. The results are not included here as they probably are not necessary (boxplots and exceedance values of zero except for a few residual cases).

Regarding accelerations, Figure 130 compares a typical train calculated with LIR and with HLIR. This train is representative of the error levels obtained usually with LIR for the PT60 model. In some specific trains of this model, the error levels are somewhat higher, and in others, lower or practically zero. In any case, there is always a significant improvement compared to the LIR results. The aggregate comparison is shown in Figures 131 and 132, where the binary indicator (proportion affected in each Z24 area) is contrasted between LIR and HLIR for all PT60 trains, revealing the notable advantage of the latter.

These results, which still require improvement in certain small areas where HLIR shows some exceedance, are indeed reduced to far fewer cases than with current SMs. This opens the possibility of undertaking an

optimization process in the immediate future to achieve (a) the best accuracy and (b) optimal coding in terms of calculation times. All this, while bearing in mind that HLIR method does not suffer from over-conservatism.

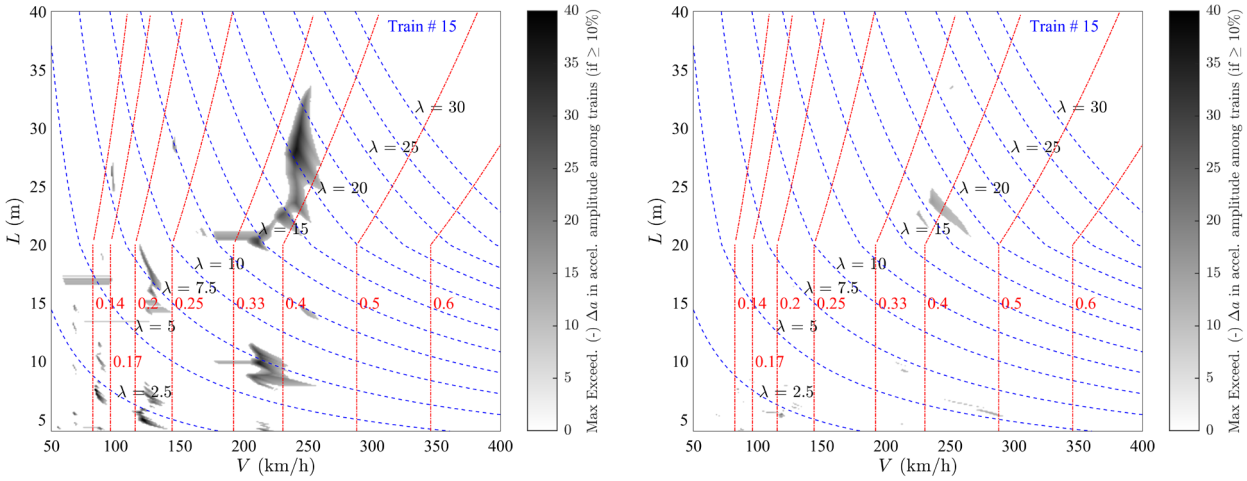

Figure 130: Maps of Δa(–): LIR and HLIR, both vs. TSC for train PT60-15[INB4EU-CB-098]. a) LIR; b) HLIR. STC bridges.

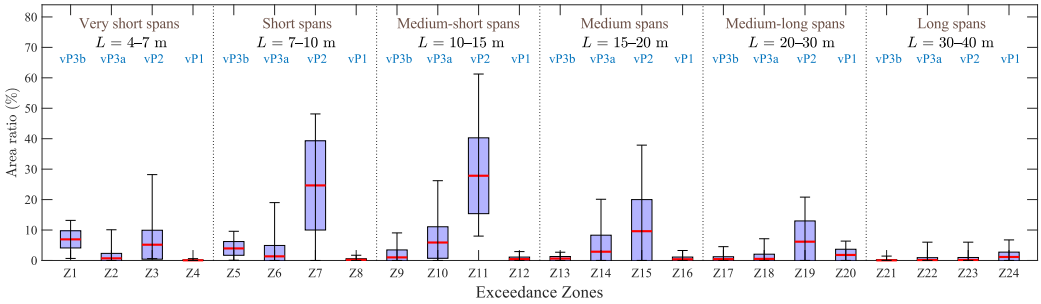

Figure 131: Box plots of Z24 binary Δa(–): LIR vs TSC. PT60 model. STC bridges.

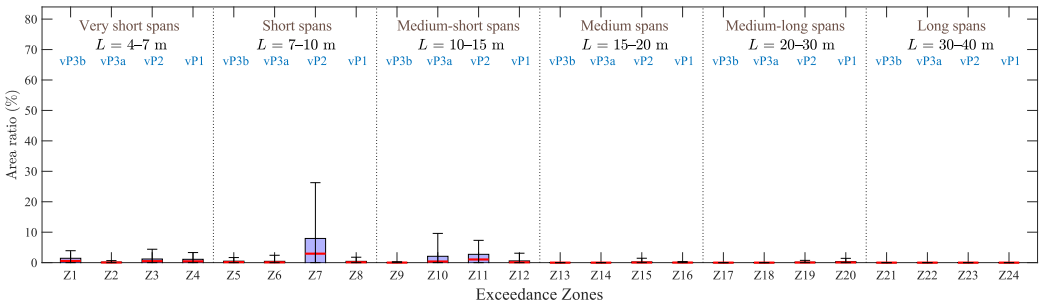

Figure 132: Box plots of Z24 binary Δa(–): LIR vs TSC. PT60 model. STC bridges.

10 Improved SM for cases where more than one mode is relevant

10.1 Hybrid LIR method for SS bridges with torsion

From the approaches presented in sections 8.1.1 and 9.2, it is deduced that HLIR method can be extended to analyse torsional vibration with few modifications. To that end, in the corresponding expressions in section 9.2:

- Use torsion wavelength $\lambda_T = \frac{V}{n_{0T}} = \frac{\lambda}{n_{0R}}$, instead of $\lambda = \frac{V}{n_0}$ (alternatively, use $K_T = \frac{K}{n_{0R}} = \frac{V}{2n_{0T}\,L} = \frac{\lambda_T}{2L}$).
- Parameters [train (axles distances), L, ζ] remain unmodified.
- Multiply the train loads by $\frac{e \cdot e_m}{k_T^2}$.

With that approach, the phases (time instants) to estimate the max. response in torsion are obtained again by means of Eqs. (28), (29), (32) and (34), with Eq. (31) to correct for evaluation of vertical displacement due to torsion.

The combination of those results with bending to have an estimate of the total maximum response is straightforward. It suffices to compute the max. response in bending as described in section 9.2, and then add the torsion response for the same phases, and vice-versa.

Such procedure opens in turn the possibility to produce 3D spectra that consider torsion effects, for any given values of $[e, e_m, n_{0R}, k_T]$.

10.2 LIR and DER formulations for the torsion mode

From the approach presented in section 8.1.1 it is also deduced that the same formulations usually employed for approximating the beam bending response with current LIR and DER methods (see section 3) can be used straightforwardly for the torsion mode. To that end:

- Use torsion wavelength $\lambda_T = V/n_{0T}$ to compute the train signature and DER influence line.
- Use torsion nondimensional speed $K_T = \frac{V}{2n_{0T}\,L}$ to compute the LIR influence line.
- Multiply the train signature by $\frac{e \cdot e_m}{k_T^2}$.

Though such an approximation is mathematically valid, its use would still be limited by the same shortcomings of LIR and DER demonstrated in sections 6 and 7 for SS bridges. Therefore, if better accuracy is desired, it is recommended to proceed as explained in section 10.1.

10.3 LIR approach for continuous multi-span bridges

While simply supported (SS) bridges generally present well-separated natural frequencies that allow admissible predictions using the fundamental vibration mode, continuous multi-span bridges exhibit clustered modal distributions that produce a more coupled and complex dynamic response, as it was discussed in section 8.2. Within this framework, a combined analytical–numerical formulation based on the LIR approach is proposed here to estimate the dominant resonant response of continuous railway bridges. The methodology is developed for bridges whose modal behaviour is characterized by a first cluster of two coupled modes, although the formulation can be extended to structures with a larger number of spans.

At is current stage, the formulation is based on a modal decomposition strategy in which the contribution of each vibration mode is evaluated independently and later combined using classical modal combination procedures such as the Square Root of the Sum of the Squares (SRSS) and the Complete Quadratic Combination (CQC). Though being defective for general application when error target is 10% (see section 10.4), those well–known procedures can provide an initial estimate, which is amenable to improvement as it will be mentioned in the conclusions in this section.

For the first mode, a closed-form analytical expression of the damped LIR method is derived in terms of nondimensional parameters, whereas the second mode contribution is obtained numerically through a normalized response map in the (K, ζ) parameter space. The resulting response surface can later be evaluated by interpolation, allowing rapid estimation of the modal contribution without repeatedly solving the full dynamic problem. Furthermore, the formulation adopts a proportionality-based framework that permits extension to higher modes and bridges with an arbitrary number of spans.

The proposed methodology is validated through comparisons with analytical and semi-analytical solutions considering a limited set of train–bridge configurations. For this excitation set, the method achieved accuracies exceeding 95% in the prediction of resonance peaks. Typical discrepancies observed in cancellation valleys were found to have limited practical significance, since bridge design is mainly controlled by peak response quantities.

The methodology proved particularly suitable for preliminary design studies, parametric analyses, and network-level screening applications, where numerous train–bridge configurations must be evaluated efficiently. Nevertheless, although the obtained results were admissible for a reduced number of trains exhibiting mainly regular loading patterns, larger discrepancies were identified when more realistic and irregular train configurations were considered. These limitations highlight the need for enhanced formulations capable of capturing the phase information of the dynamic system more accurately.

In this regard, the HLIR approach appears as a promising extension, since previous sections have demonstrated its capability to substantially improve the estimation of train-induced responses in SS bridges. Owing to its enhanced treatment of phase information, it is anticipated that similar improvements in accuracy may also be achieved in the dynamic analysis of continuous multi-span railway bridges.

10.3.1 Two-span continuous bridges

The dynamic behaviour of 2-span continuous bridges has been studied using a modal decomposition that combines an analytical description of the first mode shape with a numerical, nondimensionalised treatment of the second mode shape, as shown in Figure 133. A detailed development can be found in (Cueva, 2025).

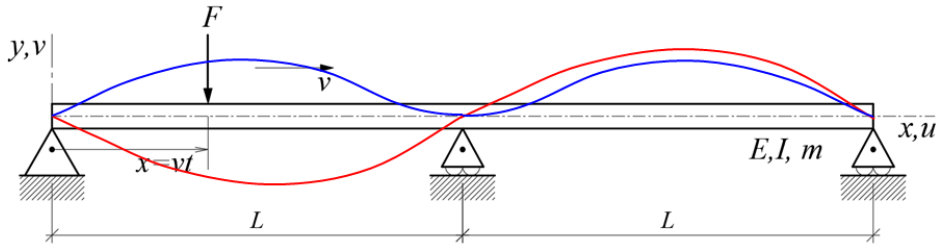

Figure 133: Two-span beam representation with the first and second mode shapes.

For the first mode, a novel closed-form analytical expression of the damped LIR method is obtained in terms of nondimensional parameters as described in Eq. (47), whose associated terms are defined in Eqs. (48-51).

$$\Gamma_1(K,\zeta,R) = RK\sqrt{T_1(K,\zeta)^2 + T_2(K,\zeta)^2} \tag{47}$$

where:

$$T_1(K,\zeta) = e^{-\frac{2\zeta\pi}{K}}[(1-K^2)\,sin\,\alpha - 2\zeta\,cos\,\alpha] + 2\zeta \tag{48}$$

$$T_2(K,\zeta) = e^{-\frac{2\zeta\pi}{K}}[\zeta(1+K^2)\,sin\,\alpha + (1-K^2)\,cos\,\alpha] - (1-K^2) \tag{49}$$

$$R = y_{st}/[(1-K^2)^2 + (2\zeta K)^2] \tag{50}$$

$$\alpha = 2\pi/K \tag{51}$$

K is the nondimensional velocity, ζ is the damping ratio of the bridge, α is inversely proportional to K with a proportionality factor of 2π, and R is a dynamic amplification factor.

Besides, the second mode contribution is determined using a numerical procedure based on the prior construction of a normalised response map, $\tilde{\Gamma}_2$, in the (K,ζ) parameter space, as shown in Figure 134. In this figure m, $\tilde{m}_2$ and L represent the linear mass, the modal mass of the second mode, and the beam length, respectively. It is worth noting that the modal mass of the second mode, $\tilde{m}_2$, is proportional to the term mL, with a proportionality factor of 0.878 characteristic of 2-span bridges. Nevertheless, this proportionality-based approach can be extended to any number of modes and to bridges with an arbitrary number of spans.

Thus, the resulting surface is later evaluated by interpolation, enabling rapid estimation of modal contribution without repeatedly solving the full dynamic problem.

Eq. (52) defines the new spectral method for a 2-span continuous bridge. This method is based on the LIR approach and on the previously described combined procedure, which enables efficient estimation of the bridge dynamic response.

In the following equation, Γ_1 and $\tilde{\Gamma}_2$ represent the influence line and the response map of the corresponding modes, G denotes the train signature, $\omega_{1,2}$ are the natural frequencies of the modes of interest, and $f(.)$ is the function that combines the modal contributions to obtain the maximum bridge acceleration, amax.

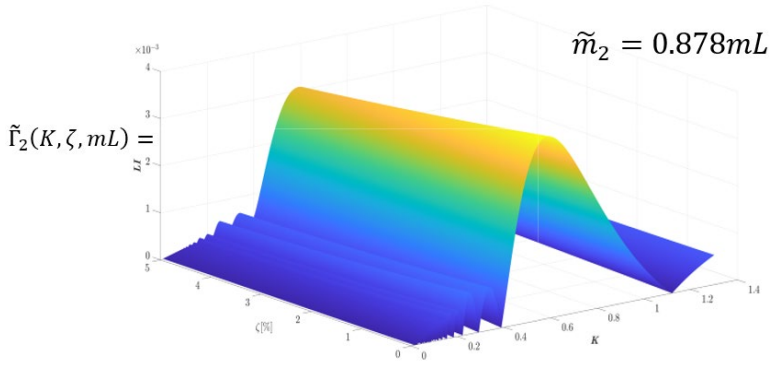

Figure 134: Response map (influence line) for the second mode.

$$a_{max} = f(\omega_1^2 \cdot \Gamma_1(K,\zeta,R) \cdot G(F_i,d_i,\lambda_1,\zeta)\,,\ \omega_2^2 \cdot \Gamma_2(K,\zeta,R) \cdot G(F_i,d_i,\lambda_2,\zeta)\,) \tag{52}$$

As an example, Figure 135 shows the maximum acceleration response of a 2-span bridge with a length of $L = 10\ m$ per span, and a damping ratio of 1.7%, subjected to Train #9 of the HSLM-A model. In this case,

it is observed that the new LIR method for 2-span bridges can reproduce the dynamic effects of this type of bridge with good accuracy, as detailed in (Cueva, 2025).

It is particularly important to highlight the precision achieved in the assessment of resonance. This acceptable level of accuracy has been obtained both with the Complete Quadratic Combination (CQC) and Square Root of the Sum of the Squares (SRSS) methods as combination functions, $f(.)$. However, such good accuracy cannot be expected in all cases, as it will be explained in next section.

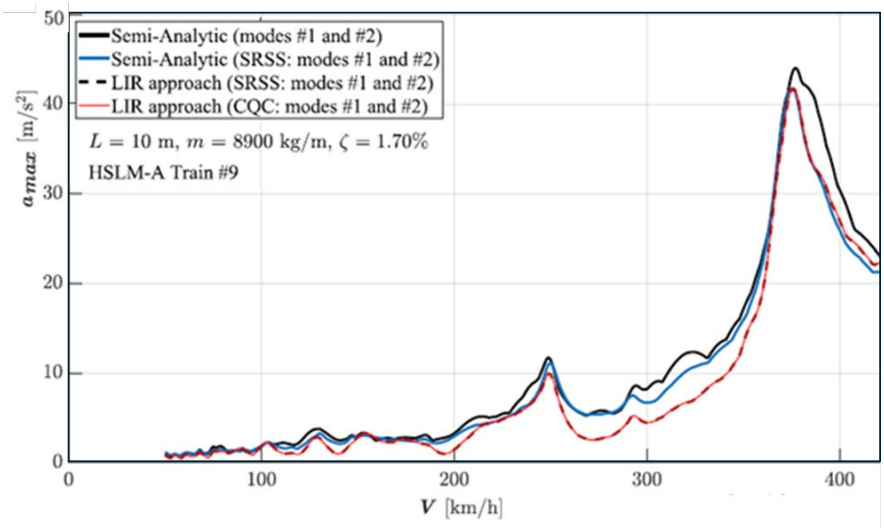

Figure 135: Comparison of the dynamic acceleration response obtained from the semi-analytical method and the LIR method for a bridge with span L = 10 m under the HSLM-A9 train (PT60-37).

From this new formulation, the main results and conclusions are:

- A simplified methodology has been developed for the dynamic analysis of continuous 2-span railway bridges under moving loads, combining an analytical formulation for the first mode with a semi-analytical/numerical treatment for the second one.
- The extension of the LIR approach to a multimodal framework enables the estimation of the dominant resonant response without requiring full time-domain integration, achieving acceptable accuracy in the resonance peaks.
- The proposed formulation is based on a proportionality framework that enables its extension to higher modes and to bridges with an arbitrary number of spans, highlighting its adaptability to a wide range of practical applications.
- Among the limitations of the approach is the prediction of cancellation regions, where larger discrepancies are observed. Nevertheless, this issue has limited practical significance, since structural design criteria are primarily governed by peak response quantities.
- The results obtained have been acceptable for a reduced number of trains exhibiting mainly regular loading patterns. However, when considering a larger set of real train configurations, the LIR method has shown significant differences with respect to the exact solutions.
- The identified limitations provide an ideal framework for exploring the efficiency of the HLIR method, which has been shown to substantially improve the estimation of the response in SS bridges. Furthermore, due to its capability to accurately capture the phase information of the dynamic system, it is anticipated that this level of precision can also be maintained in multi-span bridge analyses.

10.4 Performance of CQC method in cases where more than one mode is relevant

In recent years, various studies on improvements to the well-known SRSS and CQC methods have been published in scientific journals. Those articles more closely related to the objectives of InBridge4EU are discussed below.

Two years ago, *Deep learning-based response spectrum analysis method for building structures* (Kim et al. 2024) was published. This article builds upon both classic methods and proposes an improvement consisting of a modal combination rule based on deep learning, introducing modal contribution coefficients generated by a neural network. The authors claim that this improves the prediction of responses affected by higher vibration modes, which they demonstrate through simulations on building frames of different types.

Last year, *Generalized CQC method for evaluating coupled structural responses under multiple excitations* (Feng et al. 2025) was also published. The proposed methodology attempts to account for the stochastic characteristics of multiple vibration sources in structures, such as wind action at different heights in a skyscraper. It can therefore simultaneously consider multiple correlated vibration sources—and non-proportional damping. However, the approach is of the random vibration type, where, knowing the PSD and cross-power spectra of the different excitations, a statistical estimate of displacements and internal forces can be obtained. This does not seem to be an optimal approach for the analysis of railway bridges, where current practices are based in considering the excitation due to axle load fundamentally as a deterministic action.

Therefore, without resorting to the im plementation of ad-hoc neural networks, which is beyond the scope of Task 1.4, the most suitable option seems to be to verify the possibility of using the CQC method in cases where a significant influence of more than one vibration mode has been detected, to analyse whether this method is capable of predicting it correctly.

10.4.1 Evaluation of the bending response of continuous 2-span bridges with CQC method

To that end, a relevant case where the influence of various modes simultaneously has been observed is the response of 2-span continuous bridges, analysed in previous section 8.2.

Particularly, the proximity of the resonant speeds of the second subharmonic of the first mode, and the third subharmonic of the second mode, has been found to have an influence in a number of cases. That situation is explained because the quotient of wavelengths in a continuous bridge with two identical spans is $\left(\frac{V}{f_1}\right)/\left(\frac{V}{f_2}\right) = \left(\frac{V}{f_1}\right)/\left(\frac{V}{1.5625 \cdot f_1}\right) = 1.5625 \approx \frac{3}{2}$; therefore, the third resonant peak of the second mode appears at speed only slightly above the second resonant peak of the first mode.

Many situations where CQC performs defectively can be explained with the rule of the ratio of subharmonic wavelengths just mentioned, which will take place as well with the 4th one in bending plus the 6th one in torsion.

In those cases, the coupling of both modes takes place strongly enough that the CQC method underestimates the output. And, as a result, almost invariably with all trains of model PT60, the outputs from CQC are not on the safe side when the difference with TSC exceeds 10%; see a representative example of mode coupling in Figure 136, where the two close resonant peaks can be observed. Only in few isolated cases has an overconservative prediction of CQC larger than 10% been observed, in a very narrow range of spans (not shown for brevity).

However, other situations are found as well where CQC is non-conservative. Figure 137 shows a case of a 2nd subharmonic resonant peak of the second bending mode, which is not coupled with the first mode because

that is not possible given the frequency ratios, but still the response is underestimated in comparison with TSC, because the CQC rule in this case does not get the peak value correctly.

Overall, it can be said that the performance of CQC for predicting the acceleration has been found unsatisfactory for all trains in model PT60, mostly for the range K>0.25 and spans up to some 25–30 m.

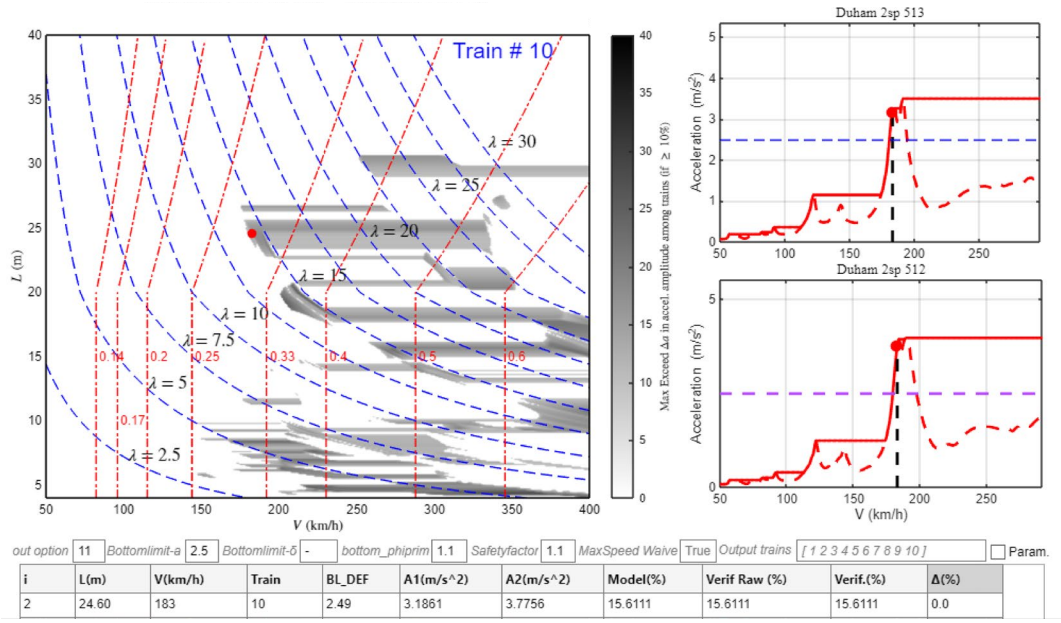

i	L(m)	V(km/h)	Train	BL_DEF	A1(m/s^2)	A2(m/s^2)	Model(%)	Verif Raw (%)	Verif.(%)	Δ(%)
2	24.60	183	10	2.49	3.1861	3.7756	15.6111	15.6111	15.6111	0.0

Figure 136: CQC vs. TSC in 2-span bridge of L=24.6 m, for train PT60-10[INB4EU-CB-111] (D=28.8 m). PSC bridges. TSC exceeds CQC in acceleration by 15.6%.

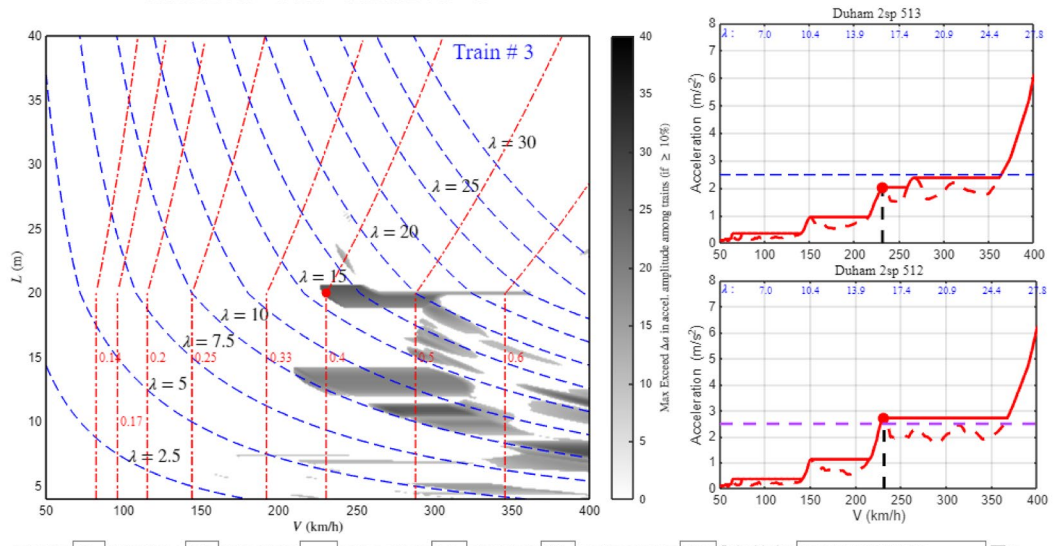

i	L(m)	V(km/h)	Train	BL_DEF	A1(m/s^2)	A2(m/s^2)	Model(%)	Verif Raw (%)	Verif.(%)	Δ(%)
3	20.10	231	3	2.49	2.0194	2.7085	25.4412	25.4412	25.4412	-0.0

Figure 137: CQC vs. TSC in 2-span bridge of L=20.1 m, for train PT60-03[INB4EU-CB-069] (D=20.0 m). PSC bridges. TSC exceeds CQC in acceleration by 25.4%.

As regards the computation of displacements, in section 8.1.2 it was concluded that a simple addition of the torsion static deflection could help fix a good number of cases of combined bending-torsion response, and it was pointed out that such hypothesis could be tested in the future. A similar conclusion could be reached for the quantification of vertical displacement by CQC method in 2-span continuous beams: Figure 138 shows

again a waterdrop pattern for a conventional CMU train; the key point in one of the waterdrops is also examined in the subplots on the right, and it is found that a 3rd subharmonic resonance takes place for the first mode at λ=8.8 m; no coupling with the second mode exists in this case but, however, the second mode has actually a static contribution that is not well estimated by CQC (similar to the SRSS rule in this case), and it is likely that a direct addition (or absolute value sum) will have proved more convenient.

It is recalled here that waterdrop patterns arise when a resonant subharmonic produces a peak displacement that exceeds the reference TSC method, and simultaneously crosses the 1.1φ' threshold; then, in the closest two cancellation *K* lines the threshold is not crossed and exceedance vanishes and, for increasing speeds the 1.1φ' threshold gradually increases, and produces the waterdrop form given that the (cumulative) peak value is always higher in the horizontal axis of symmetry of the waterdrop.

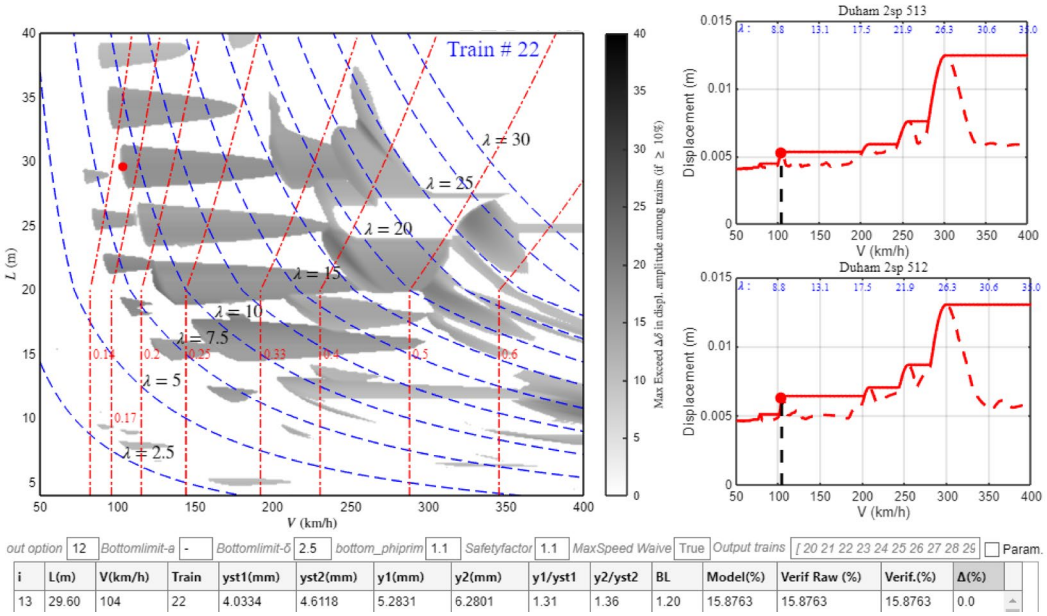

i	L(m)	V(km/h)	Train	yst1(mm)	yst2(mm)	y1(mm)	y2(mm)	y1/yst1	y2/yst2	BL	Model(%)	Verif Raw (%)	Verif.(%)	Δ(%)
13	29.60	104	22	4.0334	4.6118	5.2831	6.2801	1.31	1.36	1.20	15.8763	15.8763	15.8763	0.0

Figure 138: CQC vs. TSC in 2-span bridge of L=29.6 m, for train PT60-22[INB4EU-CB-130] (D=26.4 m). PSC bridges. TSC exceeds CQC in displacements by 15.9%.

11 Improved SM for portal frames

11.1 LIR approach for beams with rotational elastic restraints (ERS beams)

While the LIR method was originally developed for SS beams, working with a beam with elastically restrained supports (ERS beam, see Figure 139) makes it possible to evaluate the entire spectrum of boundary conditions from SS to fully embedded (*i.e.* beam rigidly supported, or RS beam), including any intermediate stiffness level, as illustrated in Figure 140.

The ERS-LIR formulation has been developed during Task 1.4 of the Project and tested for single-span bridges. This approach can be useful to analyse those bridge configurations where the deck presents complex boundaries. This method was developed on the analytical solution of the symmetric mode, which is described in Eq. (53), and depends on the terms given in Eqs. (54)-(57).

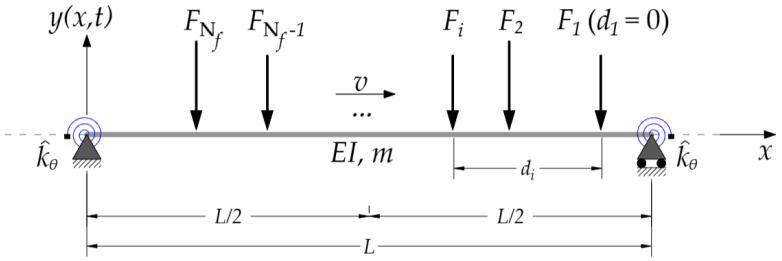

Figure 139: Physical model of a beam with elastic rotational supports ("ERS beam") under a stream of moving loads.

$$\xi^s(t) = y_{st}\left\{\frac{\eta(N_1+N_2)}{(1-(\gamma K)^2)^2+(2K\gamma\zeta_s)^2}+\frac{(\eta-1)(N_4-N_3)}{(1+(\gamma K)^2)^2-(2K\gamma\zeta_s)^2}\right\}, t \le 2\bar{t} = \frac{L}{v} \tag{53}$$

Where:

$$N_1 = (1-(\gamma K)^2)\left\{\cos\left(\frac{\lambda}{2}(t/\bar{t}-1)\right) - e^{-\zeta_s\omega_s t}\left[\cos(\omega_{sd}t)\,c_\lambda + \sin(\omega_{sd}t)\left(\frac{\zeta_s c_\lambda + \gamma K s_\lambda}{\sqrt{1-\zeta_s^2}}\right)\right]\right\} \tag{54}$$

$$N_2 = 2K\gamma\zeta_s\left\{\sin\left(\frac{\lambda}{2}(t/\bar{t}-1)\right) + e^{-\zeta_s\omega_s t}\left[\cos(\omega_{sd}t)\,s_\lambda + \sin(\omega_{sd}t)\left(\frac{\zeta_s s_\lambda - \gamma K c_\lambda}{\sqrt{1-\zeta_s^2}}\right)\right]\right\} \tag{55}$$

$$N_3 = (1+(\gamma K)^2)\left\{\cosh\left(\frac{\lambda}{2}(t/\bar{t}-1)\right) - e^{-\zeta_s\omega_s t}\left[\cos(\omega_{sd}t)\,c_{h\lambda} + \sin(\omega_{sd}t)\left(\frac{\zeta_s c_{h\lambda} - \gamma K s_{h\lambda}}{\sqrt{1-\zeta_s^2}}\right)\right]\right\} \tag{56}$$

$$N_4 = 2K\gamma\zeta_s\left\{\sinh\left(\frac{\lambda}{2}(t/\bar{t}-1)\right) + e^{-\zeta_s\omega_s t}\left[\cos(\omega_{sd}t)\,s_{h\lambda} + \sin(\omega_{sd}t)\left(\frac{\zeta_s s_{h\lambda} - \gamma K c_{h\lambda}}{\sqrt{1-\zeta_s^2}}\right)\right]\right\} \tag{57}$$

In the context of the ERS beam's dynamic response, the dimensionless parameter K is defined as the ratio between the train-induced load frequency and the bridge's natural frequency of interest. Then, K is further modulated by γ, where γ^2 represents the ratio of the ERS beam's natural frequency to that of its simply supported counterpart. The parameters ζ_s, ω_s and ω_{sd} correspond to the damping ratio and the natural and damped frequency of the symmetry mode of the ERS systems. Other coefficients are defined as described in Eq. (58).

$$c_\lambda = \cos\left(\frac{\lambda}{2}\right),\ s_\lambda = \sin\left(\frac{\lambda}{2}\right),\ c_{h\lambda} = \cosh\left(\frac{\lambda}{2}\right),\ s_{h\lambda} = \sinh\left(\frac{\lambda}{2}\right) \tag{58}$$

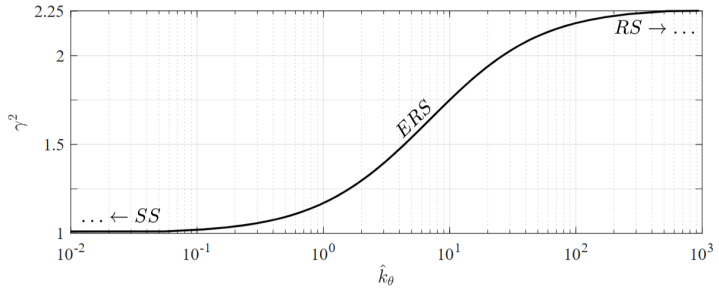

Figure 140: Variation of the ERS to SS frequency ratio in function of the normalized rotational stiffness.

The ERS-LIR formulation to estimate the maximum acceleration levels is then given by Eq. (59):

$$\Gamma_{max} = y_{st} \cdot \eta_\gamma \cos\left(\frac{\gamma\pi}{2}\right) \cdot |\bar{p}| \cdot \frac{\gamma K}{1-(\gamma K)^4} \cdot \sqrt{1 + e^{-\zeta\frac{\pi}{K}}\left\{e^{-\zeta\frac{\pi}{K}} + 2\cos\left[\frac{\pi}{K} - \Theta\right]\right\}} \tag{59}$$

where:

$$\bar{p} = P + iQ \tag{60}$$

$$\Theta = \angle \bar{p}^2 \tag{61}$$

$$P = \tanh\left(\frac{\gamma\pi}{2}\right)[(\gamma K)^2 - 1] - \tan\left(\frac{\gamma\pi}{2}\right)[(\gamma K)^2 + 1] \tag{62}$$

$$Q = 2\gamma K \tag{63}$$

$$\eta_\gamma = \frac{\cosh\left(\frac{\gamma\pi}{2}\right)}{\left[\cos\left(\frac{\gamma\pi}{2}\right) - \cosh\left(\frac{\gamma\pi}{2}\right)\right]} \tag{64}$$

In this formulation, P and Q, as described in Eqs. (62) and (63), respectively, define a complex parameter $\bar{p}$, Eq. (60), whose magnitude $|\bar{p}|$ phase angle Θ, given in Eq. (61), govern the critical zones along the ERS beam's influence line Γ_{max} defined in Eq. (59). Finally, η_γ is introduced as the parameter that calibrates the ERS beam's mode shape, as shown in Eq. (64). Furthermore, verification analysis confirms that as the rotational stiffness at the ends approaches zero, the ERS-LIR formulation converges to the classical LIR approach for the SS beam.

This improved SM has been tested for a variety of practical cases (see Figure 141), with very accurate results, which demonstrates its capabilities.

Furthermore, this novel formulation is extended in next section in a view to encompass a variety of SM applications to portal frame bridges.

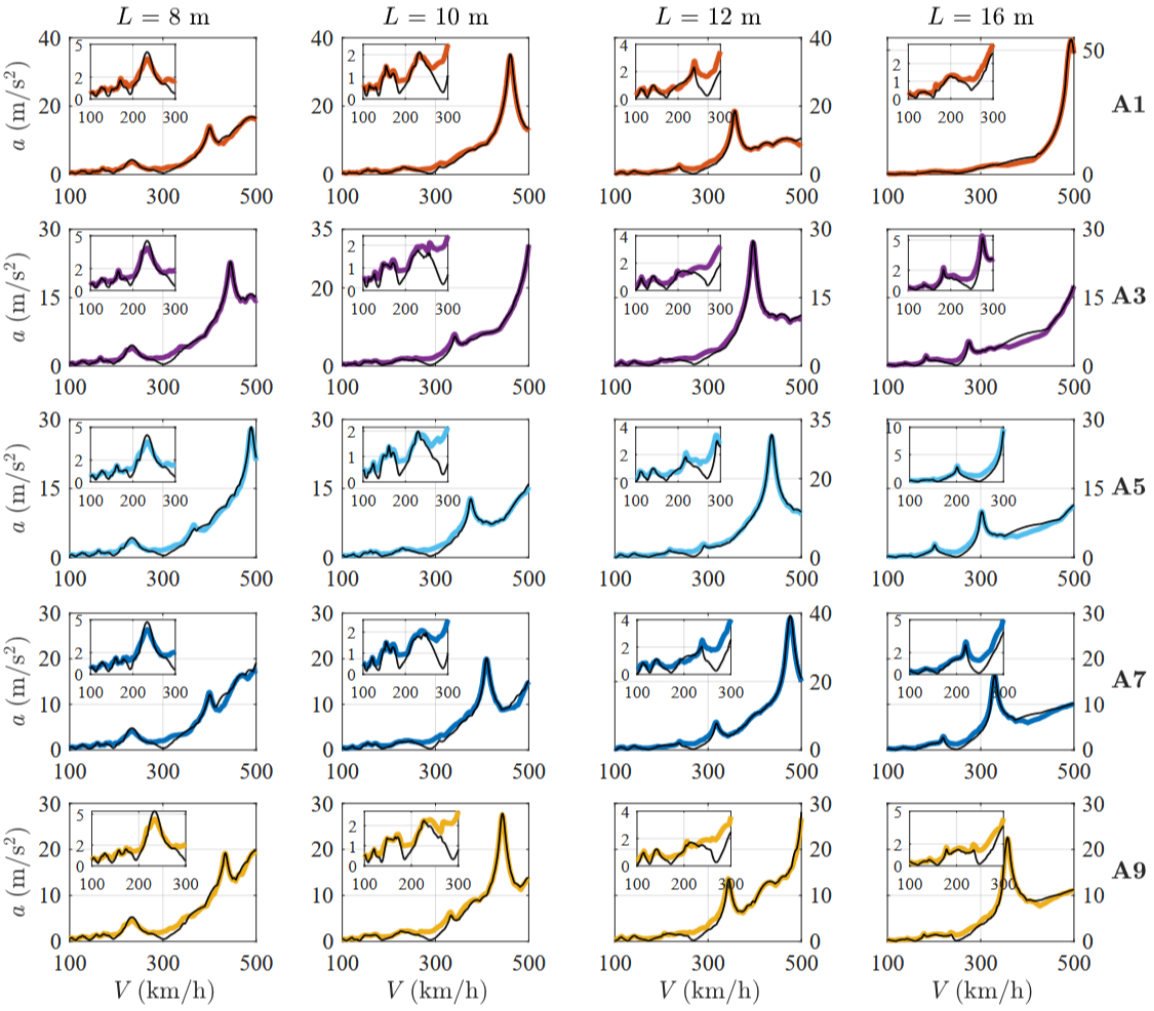

Figure 141: Application of a new LIR-based method for beams resting on elastic rotational supports. Case of beams where the elastic supports double their fundamental frequency, under the passage of five trains from the HSLM-A model.

11.2 LIR approach for portal frames

Portal frames constitute one of the structural configurations considered in this work for extending the applicability of SM. Their inclusion is particularly relevant within the objectives of Task 1.4. The motivation for this extension comes from the mathematical exact coincidence between the symmetric mode shape of an equivalent ERS beam and that of a portal frame.

In both cases, the first symmetric mode is described by a combination of *cosine* and *hyperbolic cosine* functions. That same mathematical expression allows the exact response of a portal frame to be obtained from the new solution of the ERS beam under moving load presented in previous section 11.1. By means of a suitable equivalence of few parameters, the response of the portal frame can be computed very accurately.

In this section, a portal frame is defined as a structural system in which the upper beam is vertically restrained at its ends, while the lateral walls provide continuity with the ground. These walls exhibit additional stiffness due to the surrounding soil, which is modelled using a Winkler-type representation, as shown in Figure 142*a*. Therefore, the upper member is neither treated as a strictly simply supported beam nor as a fully clamped–clamped beam. Instead, it will be proved to be mathematically equivalent to an ERS beam, as shown

in Figure 142*b*, where the rotational stiffness at the ends represents the contribution of the lateral members to the dynamic behaviour of the upper beam, and the modal mass is suitably adapted.

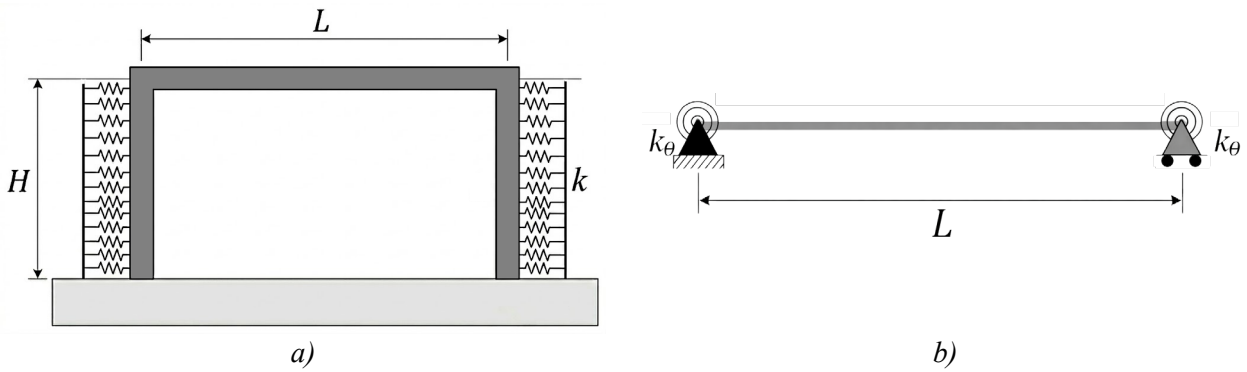

Figure 142: Schematic representation of portal frame and beam systems: a) portal frame and b) ERS equivalent beam.

A fundamental aspect of the proposed approach is that the first symmetric mode shape has a direct dependency on the eigenvalue of the system in both structural types. This dependency allows the proportionality of the loading function to be preserved when moving from the portal frame to the ERS model.

This correspondence can be observed in Eq. (65), which presents the equation of motion associated with the fundamental symmetric mode of the ERS model. In this expression, the superscript s denotes the first symmetric mode shape. The equation has been normalized by the generalized modal mass M_b, so that the amplitude of the external forcing term is initially expressed as F_0/M_b.

$$\ddot{\xi}^s(t) + 2\zeta_s\omega_s\dot{\xi}^s(t) + \omega_s^2\,\xi^s(t) = \frac{F_0}{M_b}\phi^s\left(\frac{L}{2}(t/\bar{t}-1)\right), \qquad 0 \le t \le 2\bar{t} = L/v \tag{65}$$

However, when transitioning from the ERS idealization to the equivalent portal-frame representation, M_b is affected by the contribution of the lateral walls. These members do not only modify the effective mass of the system; they also influence its effective stiffness and, consequently, its natural frequency and static flexibility. For this reason, the forcing amplitude can be more conveniently reformulated in terms of the static deflection y_{st} and the natural frequency ω_s, as shown in Eq. (66).

Both quantities (y_{st}, ω_s) can be obtained conveniently from a FEM model of the portal frame (or other analytical formulations for this type of structures), allowing the ERS-based formulation to capture exactly the dynamic contribution of the lateral walls without requiring a reformulation of the moving-load solution.

$$\ddot{\xi}^s(t) + 2\zeta_s\omega_s\dot{\xi}^s(t) + \omega_s^2\,\xi^s(t) = y_{st}\,\omega_s^2\,\phi^s\left(\frac{L}{2}(t/\bar{t}-1)\right),\ 0 \le t \le 2\bar{t} = L/v \tag{66}$$

Thus, the value of y_{st} for a portal frame can be obtained from:

- FEM static analysis,
- FEM low-amplitude dynamic analysis using just one mode, or
- Closed-form expressions;

and ω_s can be obtained simply from a FEM modal analysis. If the static displacement is obtained from pure static analysis (FEM or closed-form expressions), which is more convenient, then a small error will be introduced, since the displacement will be slightly different from the static displacement due to the first mode. However, that error is negligible for practical purposes (of the order of 2–3% in the examples presented below).

In conclusion, the new proposed method does not require reformulating either the closed-form ERS moving-load solution or its LIR formulation, but just obtain (y_{st}, ω_s) by any other analysis procedure, and feed it into the ERS solutions given in section 11.1.

For verification purposes, two FEM-based numerical examples are introduced to investigate the analytical response of the portal frame. The frame was modelled using the following material properties:

- Concrete density ($\rho = 2500$ kg/m^3)
- Young's modulus (E = 36 GPa)
- Poisson's ratio ($\nu = 0.2$)
- Lateral Winkler stiffness (k = 74 MN/m^2).

The reference spans (L) considered in the examples were 16 m and 8 m. The lineal mass was taken as m = 9700 kg/m, while the damping ratio was set equal to ζ = 1.56%. The height of the lateral walls was fixed as H = 5 m. The FEM mesh was discretized using 96 elements, in a manner similar to in Figure 143.

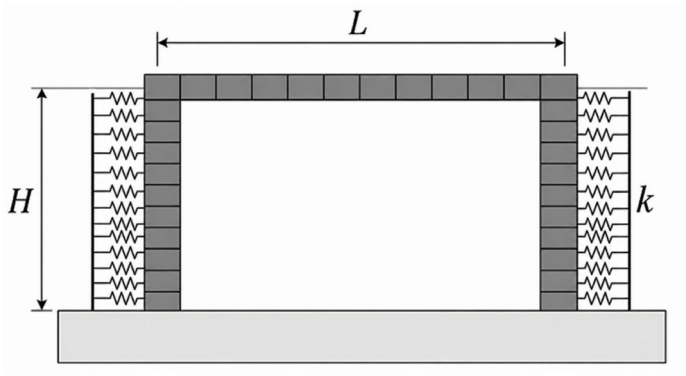

Figure 143: Portal frame FEM model.

- The first example considers a train of 12 equally spaced moving loads of 170 kN distributed over a total length of 110 m and travelling at constant velocity. This case provides a regular loading pattern suitable for verifying the consistency of the proposed formulation under idealized conditions.
- The second example considers a shorter and more irregular train, in which both the axle distances and the load magnitudes vary. This second case is more demanding because it evaluates whether the formulation can capture the response produced by a non-uniform moving load sequence. The adopted train model has a total length of 85 m. The axle loads range from 120 to 250 kN, as shown in Figure 144.

Figure 144: Irregular train for verification of portal frame formulation as equivalent ERS beam.

The velocity considered in the numerical examples is V = 144 km/h. For each case, the response of the portal frame is first obtained from the FEM model with static, modal and transient analysis. The y_{st} for the

ERS solution is calibrated from the static result (*i.e.* the FEM value is fed into Eq. (66)), and then the transient response of the portal frame is compared with the ERS analytical solution.

The results show that the proposed calibration strategy enables the ERS model to reproduce the portal-frame response accurately. For the equidistant train, the analytical response agrees closely with the reference FEM solution, confirming that the dominant symmetric mode of the frame can be effectively represented using the same functional structure adopted for the equivalent beam. This agreement is also maintained for the irregular train pattern, demonstrating that the method is not limited to uniform load configurations. In both cases, the ERS formulation captures the forced vibration induced by the axle loads, the subsequent free-vibration intervals, and their superposition during the complete train passage. Despite the complexity of the resulting time histories, the displacement response is accurately described, as shown in Figures 145 and 146.

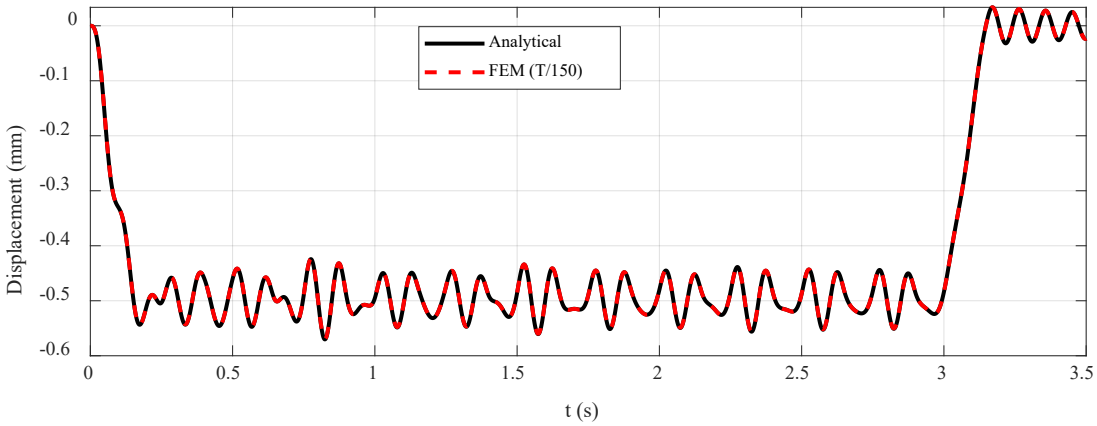

Figure 145: Portal frame response comparison under equidistant train.

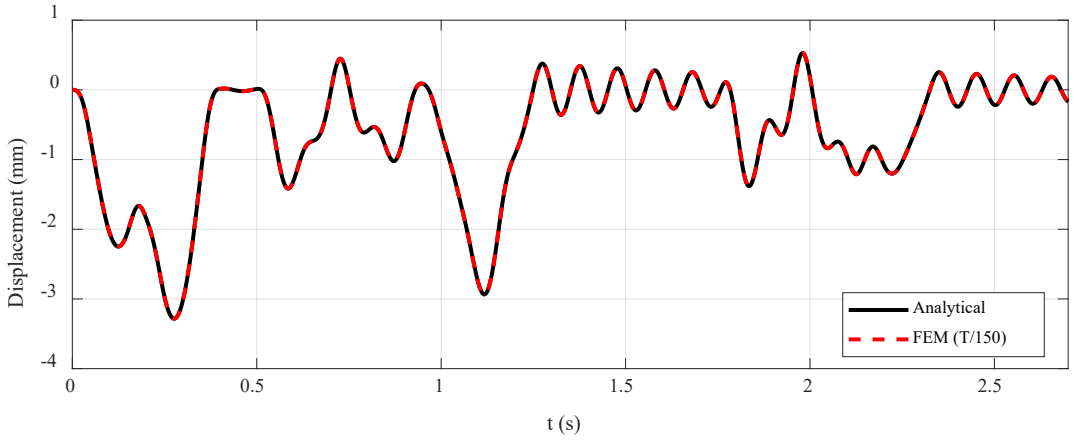

Figure 146: Portal frame response comparison under irregular train.

These new results confirm that the proposed ERS approach can be extended beyond idealized beam configurations. Its application only requires the identification of two fundamental parameters: one static parameter, related to the global flexibility of the system, and one dynamic parameter, associated with its fundamental frequency of vibration. Once these quantities are calibrated, the moving-load formulation remains formally unchanged, making the approach fully compatible with proposals such as the ERS-LIR method. Consequently, the dynamic response can be obtained at a significantly lower computational cost than that required by full FEM simulations. This makes the approach suitable for:

- Preliminary analyses

- Sensitivity studies
- Network screening purposes
- Applications where repeated evaluations under different moving-load configurations are required.

The structure of the solution obtained in the previous subsection for the time-domain response of the symmetric mode of vibration of an ERS beam, which has subsequently been extended here to compute the response of portal frames, is formally analogous to the solutions for SS beams, characterized by the particular solution due to the forced effect of load transfer, plus the homogeneous solution.

This opens possibilities for extending the HLIR approach to both ERS beams and portal frames, which is considered of interest for the Project, given the gain in accuracy and the lack of positive exceedance shown by HLIR in the analysis of SS bridges.

12 SM approach based on random vibrations

In 2022, a method for predicting the dynamic response of high-speed bridges was investigated at KTH University, following an approximation based on defining railway excitation in the form of a power spectral density (PSD) (Ciku and Gavriliuk, 2022). That idea is in line with the purpose of developing a SM in the frequency domain based on theory of random vibrations. Therefore, some fundamental aspects of that previous document are discussed below.

The study focused on a simply supported railway bridge with span L=20 m, modelled as a single-degree-of-freedom (SDOF) system. In its Annex A.5, three additional spans [17.5, 22.5, 25.0] m were also tested. The excitation applied to those bridges were the ten HSLM-A trains.

The authors demonstrate that the train signature can be combined with the bridge influence line and transformed into a PSD to predict the dynamic response of high-speed railway bridges. A verification is obtained from the FFT of the modal load, and its subsequent conversion to PSD by means of the periodogram estimate. If the input spectral density and the system's transfer function are known, it is possible to obtain the output PSD, thus, by integrating this spectral density, the RMS value of the response can be estimated. In the case of this work the main focus is on the values of vertical acceleration.

However, as of today RMS values of acceleration are not suitable for verifying the limited states required by current standards. Therefore, a steady-state assumption is subsequently adopted to transform RMS values into peak values ($a_{RMS} = a_{peak}/\sqrt{2}$), which are additionally corrected by a factor that takes into account the number of cycles required for steady-state to be reached (see section 4.3.1 in (Ciku and Gavriliuk, 2022)).

This overall innovative method should be considered in the framework of the objectives of this Project, which aims to develop SM that can be accurate to 10% for each train individually, at resonant speeds and also away from resonance—thus taking transient phenomena into account—, in comparison with TSC.

With that perspective, the following remarks are considered:

- The authors point out in their conclusions that the method underestimates the response away from resonant and subresonant speeds. That can be relevant in the prediction of cumulative response in the ascending slopes of the (sub)resonant peaks, as has been discussed in various sections of this deliverable. Those regions are in fact underestimated in various figures in A.5 from (Ciku and Gavriliuk, 2022).
- They point out as well that the subtrains of the train models can lead to higher peak response. Indeed, the figures in A.5 from (Ciku and Gavriliuk, 2022) show areas where some minor peaks around 300 km/h are not accurately approximated (considering the 10% requirement). This may seem insignificant, but for bridges with a mass lower than that considered in section A.5.3 (for example, steel and composite bridges), the values could approach 3.5 m/s² and become relevant for individual train assessment.
- Furthermore, in this deliverable a variety of transient phenomena greater than initially expected has been found. Those transients tipically lead to inaccurate predictions from the traditional SM because those methods are based on the resonance assumption, which is equivalent to the steady-state assumption in (Ciku and Gavriliuk, 2022). Therefore, doubts arise about how this random-based method could deal with RMS-to-peak value conversion, in transient cases where a relevant difference with the steady-state occurs. The authors do not mention how this gap could be closed—which they also discuss in relation to end-transients observed from HSLM-A power cars with higher damping values.

- In this deliverable fairly frequent transient phenomena for spans below 17.5 m have been found, which is the shortest bridge length considered in (Ciku and Gavriliuk, 2022). In fact, most peak misestimations do occur for those shorter spans.
- Moreover, a relevant number of the transients described in sections 6 and 7 are generated by CB trains, which were not considered in (Ciku and Gavriliuk, 2022). This point, along with the limitation of the study to spans above 17.5 m, poses additional concerns about the performance of the random-based method for other spans and rolling stock.
- Finally, for the calculation of displacements, since the proposed method relies on a steady-state assumption to transform RMS values into peak values, then the quasi-static component of the deflection should be added. When performing this type of operation, the limitations described in sections 6 and 7 (conservative or non-conservative waterdrop patterns, etc.) should also be dealt with, which will probably result in non-straightforward developments.

Though recognising its innovative approach, and the benefit that a purely spectral definition of the train excitation would bring along, as of today the uncertainties found in the examination of the random/spectral approach proposed by (Ciku and Gavriliuk, 2022) are considerable. Moreover, the dependency of the transients on the span length has been showcased in various sections of this document, which is another difficulty that the proposed method did not discuss.

A substitute alternative in the frequency domain that overcomes these challenges has not been formulated so far. Therefore, while the research priorities have been set in the remaining objectives of Task 1.4, the methodology based on random vibrations is not investigated further in this document.

13 SM and reduction factors for longitudinal load distribution

13.1 Introduction: reduction factors in SS bridges

Several studies have investigated the relevant effect of longitudinal load distribution on the dynamic response of railway bridges. Its major importance to obtain a more realistic prediction of vertical accelerations and displacements, particularly for short wavelength values, make them an indispensable tool to combine with the use of SM, for a fast and reliable prediction of the bridge response. Little will be gained with the use of SM, if the overall process is complicated by an increased multiplicity of axle loads, arising from longitudinal load distribution schemes.

An optimal solution to the problem relies on introducing reduction factors through simplified formulations applied to simply supported (SS) single-span beam models (Jin *et al.*, 2018; Moliner *et al*., 2024), as illustrated in Eq. (67). Among these contributions, the work of Jin *et al.* (2018) is particularly relevant, since it established a mathematical relationship between the reduction factor and the wavelength associated with the bridge acceleration response. Their study showed that, when the first three modal contributions are considered, the longitudinally distributed load filters out more than 80% of the second- and third-mode acceleration response due to a low-pass filtering effect induced by the load distribution.

Similarly, Moliner *et al*. (2024) analysed the influence of longitudinal load distribution on both acceleration and displacement responses by adopting a triangular distributed load over a characteristic length of 2.5 m, corresponding to a ballast depth of 0.65 m and bounded within the upper and lower load distribution limits. Based on this approach, a simplified data-driven formulation was proposed for displacement reduction in single-span bridges, retaining wavelength and impact factor as governing parameters and considering a separation threshold of λ=6.8 m, as presented in Eq. (68). The coefficients of this formulation are detailed in Table 9.

$$\Psi_{\text{UIC},3.0} = -0.000113\lambda^4 + 0.00527\lambda^3 - 0.0830\lambda^2 + 0.570\lambda \qquad (67)$$

$$0.14 \leq \Psi_{\text{UIC},3.0} \leq 1 \qquad \lambda < 10\ m$$

$$\left(\lambda, \frac{\delta}{\delta_s}\right) = C_1 + C_2.Ln(\lambda) + C_3.Ln\left(\frac{\delta}{\delta_s}\right) + C_4.(Ln(\lambda))^2 + C_5.Ln(\lambda).Ln\left(\frac{\delta}{\delta_s}\right) \quad 2.0 \leq \lambda \leq 6.8\ \text{m} \qquad (68)$$

$$\psi\left(\lambda, \frac{\delta}{\delta_s}\right) = \min\left[C_6 + C_7.Ln(\lambda) + C_8.Ln\left(\frac{\delta}{\delta_s}\right), 1\right] \quad 6.8 \leq \lambda \leq 10\ \text{m}$$

Table 9: Coefficients of the reduction factor ψ for displacement (Moliner et al. 2024).

$2.0 \leq \lambda \leq 6.8$ m					$6.8 \leq \lambda \leq 10$ m		
C_1	C_2	C_3	C_4	C_5	C_6	C_7	C_8
0.55	0.58	−0.65	−0.19	0.32	0.68	0.145	−0.026

13.2 Reduction factors in continuous multi-span bridges

The previous advances on reduction factors have primarily focused on single-span bridge configurations, while the influence of longitudinal load distribution on continuous 2-span bridges remains less explored. In

this context, this section investigates the effect of longitudinal load distribution on the vibratory response of short- and medium-span 2-span railway bridges.

Dynamic analyses were implemented using modal superposition and transient analysis techniques, considering 20 different trains, including both real and normative trains. The study focuses on span lengths of $L = 7.5\,m, 10\,m$, and $12.5\,m$, representative of short-span railway bridges where load distribution effects are particularly relevant.

Initially, the critical regions associated with maximum acceleration and displacement in each span were identified through the first modal cluster, dominated by the first and second vibration modes. Subsequently, each modal contribution and its associated frequency were analysed using both concentrated loads and longitudinally distributed triangular loads over 2.5 m. This approach enabled the representation of acceleration and displacement responses as a function of the modal wavelength.

Based on the resonant speeds obtained from the concentrated-load models, reduction factors for acceleration and displacement were computed as the ratio between the distributed-load response and the corresponding concentrated-load response at the same speed. These results were then compared with existing reference formulations: for accelerations, the model proposed by the International Union of Railways (UIC) for a 3.0 m load distribution (see Eq. (67)), and for displacements, the formulation developed by Moliner *et al*. (2024) for single-span bridges (see Eq. (68)).

In this regard, Figure 147 focuses on the comparison for a bridge with span $L = 7.5\,m$. Parts *a*) and *b*) of that figure illustrate the performance of the first and second bending modes in terms of acceleration response, while parts *c*) and *d*) present the corresponding displacement responses. The results demonstrate that the simplified approach based on current reduction factors (Eqs. (67) and (68)) provides an excellent approximation to the distributed load model.

It is also noteworthy that significant reductions are observed when compared to the point-load model. At the same time, the simplified approach based on reduction factors retains a substantially lower computational cost, making it particularly attractive for practical engineering applications.

This analysis was subsequently extended to the three previously mentioned bridge lengths and to the complete set of train typologies. The comparison against the reference formulations for displacement and acceleration reduction is presented in Figure 148. To provide a quantitative assessment of the obtained results, the agreement between the actual reduction coefficients Ψ, ψ and the theoretical ones $\hat{\Psi}, \hat{\psi}$ was evaluated using the Mean Absolute Percentage Error (MAPE) and the Root Mean Square Error (RMSE) for both acceleration and displacement responses. Eqs. (69) and (70) formulate these statistical indicators for the acceleration.

$$MAPE = \frac{100}{N}\sum_{i=1}^{N}\left|\frac{\hat{\Psi}-\Psi}{\Psi}\right| \tag{69}$$

$$RMSE = \sqrt{\frac{\sum_{i=1}^{N_{test}}(\hat{\Psi}-\Psi)^2}{\Psi}} \tag{70}$$

Where $\hat{\Psi}$ is the reduction factor obtained from Eq. (67), Ψ is the actual reduction coefficient derived from the 2.5 m triangular distributed load model, and N represents the total number of data points. In addition, the maximum relative error (ϵ_r) evaluated for the most critical cases of each bridge span, was defined as the variation between the estimated and the actual reduction factors with respect to the latter (see Eq. (71)).

$$\epsilon_r = \frac{\Psi-\hat{\Psi}}{\Psi}x100 \tag{71}$$

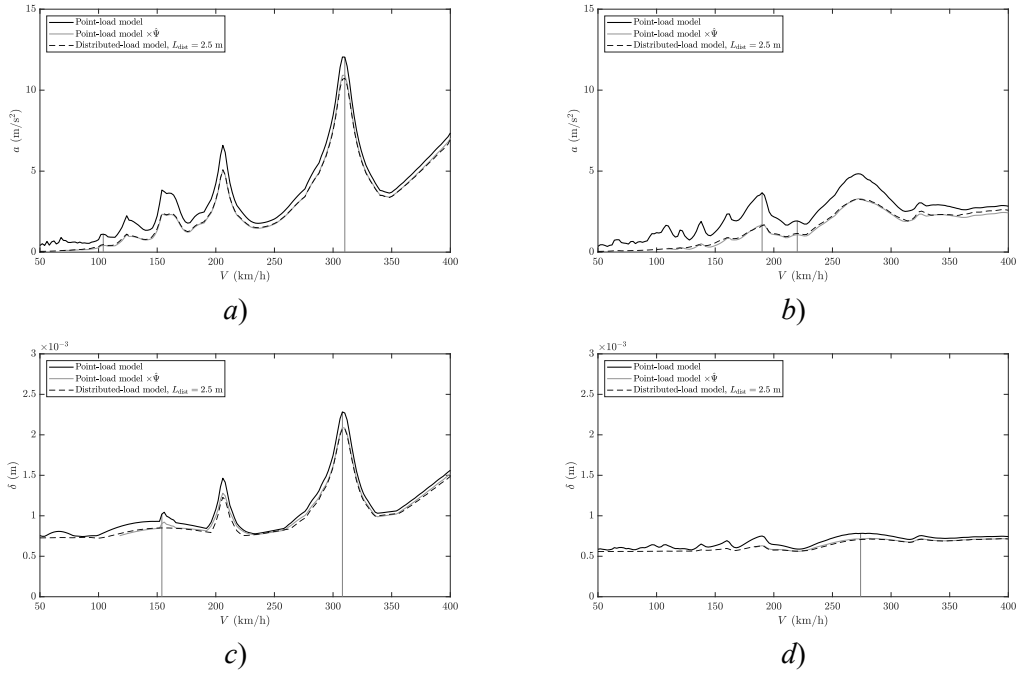

Figure 147. *Acceleration for a) 1st mode and b) 2nd mode; displacement for c) 1st mode and d) 2nd mode.*

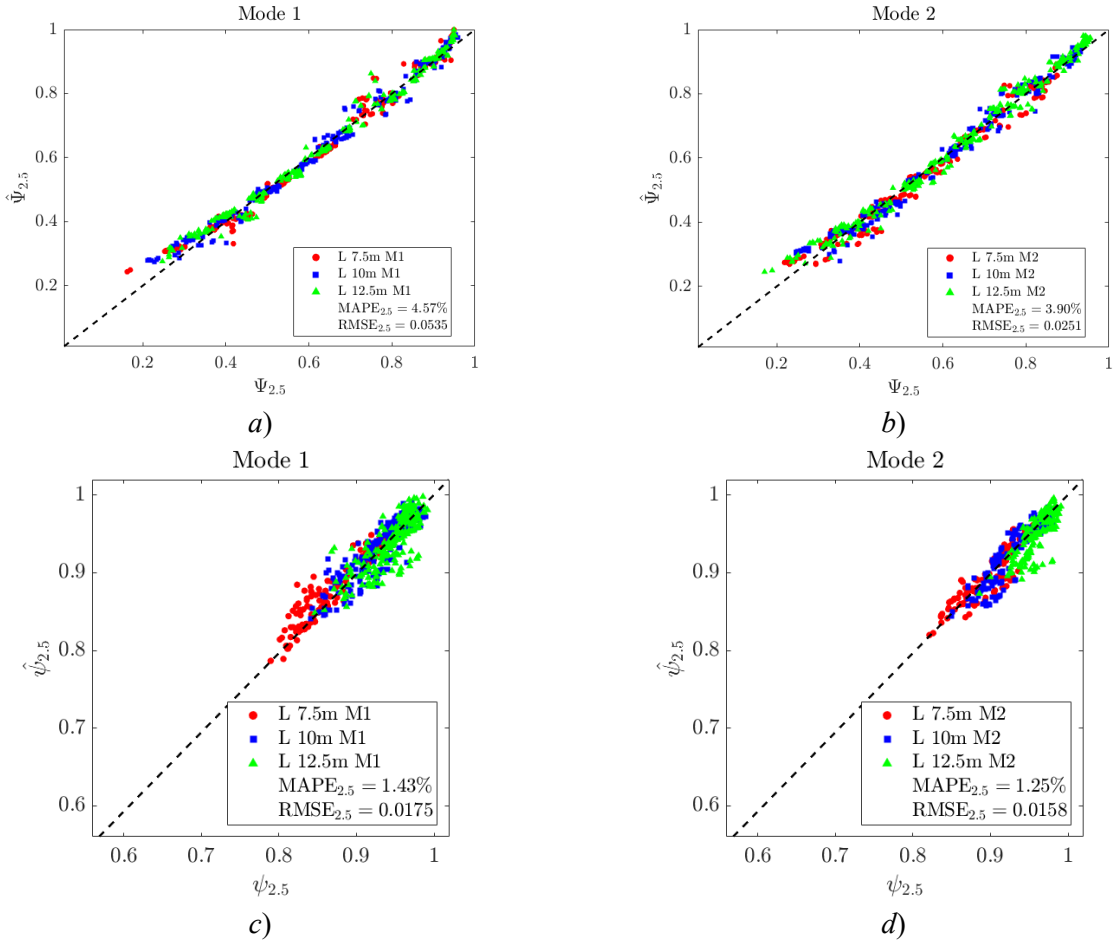

Figure 148. *Accel. comparison for a) 1st mode and b) 2nd mode; displacement comparison for c) 1st mode and d) 2nd mode.*

Regarding the statistical assessment of the acceleration reduction factors using Eq. (69), the MAPE was found to be below 5%, while the RMSE showed deviations lower than 0.06 for each modal component. Focusing on the envelope corresponding to the most critical case (i.e., the most unfavorable safety margin), the ϵ_r was generally below 15% for the first mode and 20% for the second mode. However, these errors were mainly associated with low train speeds, where the bridge acceleration, even in the worst-case scenario, generally remained below 1 m/s^2.

On the other hand, for the displacement reduction factors, the simplified displacement formulation, $\hat{\psi}(\lambda, \delta/\delta_s)$, was evaluated considering a minimum wavelength threshold of 2.5 m. In this case, the MAPE remained below 1.5%, while the RMSE showed deviations lower than 0.02 for each modal component. Similarly, the most critical case exhibited maximum relative errors generally below 15% for the first mode and 6% for the second mode. As in the acceleration results, these discrepancies were predominantly associated with low-speed scenarios.

The theoretical formulations used to estimate the reduction coefficients $(\hat{\Psi}, \hat{\psi})$ for each vibration mode within the first modal cluster (first and second modes), considering their corresponding vibration frequencies, followed trends similar to the actual reduction coefficients (Ψ, ψ) within the wavelength ranges of ($\lambda < 10$m for acceleration and $2.5\text{m} \leq \lambda \leq 10\text{m}$ for displacement. This behavior is consistent with the equivalent low-pass filtering phenomenon demonstrated by Jin *et al*. (2018) for single-span bridges, where wavelength associated with the fundamental frequency was identified as the governing parameter. However, the present study confirms that the same principle also governs the response of the first modal cluster in 2-span bridges.

Moreover, the analysis of 2-span bridges can be suitably complemented with the use of current reduction factors, Eqs. (67) and (68), to take into account its response attenuation due to longitudinal load distribution. A Master's Thesis is currently being finished at UPV, where an extended version of these findings is presented and discussed.

13.3 Reduction factors: applicability to other bridge types

As a relevant consequence of the research presented in this section, particular interest is to be recognized to the article by Jin *et al*. (2018), which has found, with the above mentioned Master's Thesis, a remarkable confirmation of its results for the first two vibration modes of a 2-span continuous beam.

Indeed, the property of the longitudinal load distribution acting as a low-pass filter appears to be consolidated for this type of beams, making the UIC formulation, Eq. (67), very promising for use in ERS beams and portal frames, thus contributing to optimizing the analysis of these bridge types.

14 Dissemination

- A one-page abstract entitled “Influence of nonsymmetric train loading in the dynamics of high-speed bridges” was presented at the conference COMPDYN 2025 (June 2025, Rhodes Island, Greece). Such contribution analyses the influence of non-symmetrical train loading in the response of high-speed railway bridges.
- A paper where the ERS-LIR formulation was presented was submitted to JSV. The journal editor required some initial modifications before the paper could be accepted for full review process. Those modifications are being implemented and the paper is to be re-submitted shortly.
- A one-page abstract entitled “Dynamic Characterization of the La Yedra Masonry Arch Railway Bridge” was presented at the 16th International Conference on Vibration Problems (ICOVP-2025) and the 11th International Conference on Wave Mechanics and Vibrations (WMVC-2025), held in Lisbon, Portugal, in September 2025. Such contribution analyses the dynamic behaviour of masonry arch railway bridges.
- A conference paper entitled “Screening analysis of continuous beams under moving loads by Residual Influence Line (LIR) methods: a Matlab toolbox implementation” has been accepted for presentation at the EURODYN 2026 conference (September–October 2026, Hannover, Germany). Such contribution presents an efficient methodology and a MATLAB toolbox for the rapid dynamic screening of continuous railway bridges subjected to moving loads, based on LIR methods and modal combination strategies.
- A conference paper related to model PT60 and its usage is ready to be submitted in June 2026 to RAILWAYS 2026 conference (August 2026, Budapest, Hungary).
- A Master’s Thesis entitled “Dynamic behaviour analysis of continuous two-span railway bridges under railway traffic: application to the Lödge River Bridge” was completed within the MSc in Structural and Geotechnical Engineering (September 2025, Universitat Politècnica de València, Spain). Such contribution developed and validated a simplified Residual Influence Line (LIR) methodology for predicting the resonant response of continuous railway bridges subjected to high-speed railway traffic.
- A number of results presented in this document are amenable also to dissemination in scientific and professional forums.

15 Summary

General approach:

- Reviewing the available literature, eight key shortcomings (KS) of current SM have been identified. These are described in section 4.2 to avoid repetition here. While the first KS concerns the types of bridges for which SM are valid (SS beams, continuous beams, bridges undergoing torsion, portal frames), the others focus on different types of vehicles (short, non-symmetric, irregular) traveling on SS bridges, as well as the SM's shortcomings in analyzing certain ranges of SS spans, wavelengths, and particularly in calculating displacements.
- The study of the SM limitations was based on a categorization of PT and FT available in the InBridge4EU database. Specifically, regarding PT for speeds exceeding 160 km/h, 201 CB trains, 39 AB trains, and 40 SA trains were selected. These were categorized into four series (short, symmetric, non-symmetric, end-transient), which are associated a priori with certain SM limitations. Furthermore, they have been classified into subtypes that indicate the type of temporal response that can be expected, based on the axle spacing pattern: regular patterns (RP), multiple units (MU), coupled multiple units (CMU), quasi-regular articulated (ART), certain variants of loco-hauled trains, and others. For the FT, 30 representative units of the different wagon types, wagon lengths, and overall lengths have been retained.
- Based on the use of *exceedance maps*, comparative studies have been conducted with different types of rolling stock to analyze the limitations of the superstructures. The results of SM have been compared with Duhamel's integral as reference TSC. The ranges considered in each exceedance map are: spans (L) from 4.0 to 40.0 m in 0.1 m increments; speeds (V) from 50 to 400 km/h in 1.0 km/h increments. This yields a total of 126711 (L,V) points per map.
- The exceedance analysis is based on a cumulative response approach. An error level below 10% is considered acceptable, and in such case the (L,V) point appears white in the map. Otherwise, it appears as a variable intensity grey point. Before each (L,V) point is tested to determine whether the 10% error level is crossed, a meaningfulness threshold is set to remove cases of limited practical interest. For accelerations, that threshold is 2.5 m/s^2. For displacements, the dynamic amplification with respect to the bride static respose under the same vehicle must be at least 10% above φ'; in short, this is called *1.1φ' threshold*, and is responsible for some geometrical patterns found in the exceedance maps.
- For each span, reduced but realistic values for linear mass, frequency, and damping rate were selected. The first modes of vibration for bending and, where applicable, torsion were used in the analysis (the first two modes for continuous 2-span bridges). Response reduction was considered due to a longitudinal triangular load distribution 2.5 meters long.
- Primarily, the structural type used most often to analyse the KS is the PSC bridge. Than implies higher linear mass and damping in comparison with STC bridges. The main effect when considering STC bridges is that, due to their lower damping, a greater number of cases exceed the meaningfulness thresholds. Consequently, a greater number of situations arise where the relative error criterion of less than 10% is not met. This is further affected by the lower mass associated with STC bridges, which, in the acceleration analysis, also contributes to the larger number of cases exceeding the 2.5 m/s² threshold. However, except in particular cases mentioned below, considering PSC or STC bridges to analyse the performance of SM does not lead to significantly different conclusions.

- Relative errors of SM can appear in four different manners: nonconservative prediction of acceleration $\Delta a(-)$, conservative prediction of acceleration $\Delta a(+)$, nonconservative prediction of displacement $\Delta\delta(-)$, conservative prediction of displacement $\Delta\delta$ (+). All of them are computed as a percentage with respect to the max. absolute value obtained wih the TSC method. $\Delta a(-)$ and $\Delta\delta(-)$ are referred to as *negative exceedances*; $\Delta a(+)$ and $\Delta\delta(+)$ are referred to as *positive exceedances*.

Limitations of Spectral Methods DER and LIR related to rolling stock variants (SS bridges):

⇒ **Train model PT60**

- This train model contains 60 PT that are representative of different CB, AB, SA trains and loco-hauled variants, of various coach lengths and total lengths. Their exceedance maps for DER an LIR are collected in Appendix E, for PSC bridges. Appendix E is therefore a useful source of information to obtain an estimate of the error levels of SM for current european rolling stock. STC bridges are not included in current version of D1.2 to fulfill the max. 50 Mb size for the submission; however UPV will try to include them as well in the final version of this deliverable.

⇒ **Sequences of equidistant loads**

- Analysed for sequences of equidistant loads, both LIR and DER methods present areas of negative and positive exceedance, related mostly to the values of nondimensional speed K, when the cancellations K=1/3, 1/5, etc. or maxima $K\approx$1/4, 1/6, etc. of the RIL (respectively) coincide with the beginning of the ascending slope of a resonant peak. Both situations entail a limitation of the SM to deal with a combined response which is not fully, but only partially resonant.
- In those cases, the negative exceedance affects more clearly various resonant subharmonics, and that is an important pattern referred to here as (defective) ***ascending slopes***. Such pattern is found in most $\Delta a(-)$ maps, also for real PT and FT, in the form of grey areas that initiate at K slightly above cancellation, for a wavelength somewhat below the corresponding subharmonic, and prolongate to higher speeds following a curved shape that mimics the constant λ lines.

⇒ **RP trains**

- For CB RP trains, the performance of DER in $\Delta a(-)$ is worse in comparison to LIR, for spans below some L=10 m. This conclusion holds for SA RP trains, for spans below some L=14 m. The performance for AB RP trains is similar. And, for STC bridges, results from DER are unusable for long CB RP trains in spans below some L=15 m for λ<10 m.
- For CB RP trains, DER is somewhat better than LIR as regards $\Delta a(+)$. The difference is more noticeable for the shorter spans, particularly in very short bridges (4-7 m) for speeds vP1 (>250 km/h), which may not be too problematic because SS bridges of those spans are not so often used for such high speeds. In both cases, the range between some L=11 and L=26.0 m, for K>0.4, is affected by the phenomenon of convex slopes.
- Previous conclusion holds for AB RP trains, where the results of DER and LIR in $\Delta a(+)$ are rather similar. For SA RP trains, the convex slopes do not appear, and DER behaves slightly worse for the shortest spans and wavelengths: L<8 m and λ<4 m.

- For CB RP trains, the performance of SM as regards Δδ(−) is good, and few grey areas are found in the exceedance maps. Conclusions for AB RP and SA RP trains are similar in this case. This is largely due to the "static part of the displacement" being somewhat overestimated.
- Therefore, for CB RP trains the performance of SM as regards Δδ(+) is generally conservative, with usual values not above 20–25%, but with exceptions in regions of higher exceedance and a marked dependency on the train type. There is a predominance of convex slopes for K>0.4, and also conservative ascending slopes or resonance peak overestimations that cancel out near the valleys of the RIL—with a recognizable "waterdrop" pattern that is even more often found in other train subtypes. DER is again somewhat better than LIR for the shorter spans, particularly in very short bridges (4-7 m) for speeds vP1 (>250 km/h). Conversely, LIR is equal or better than DER for spans above 20 m. Main conclusions for AB RP and SA RP trains are similar.
- The concept of "static part of the displacement" is controversial. When a train crosses a SS beam the static influence line has maxima and minima, and no theorem exists so far to prove that those maxima are the correct values to be added to the dynamic part of δ obtained from a SM. This is a subject of interest for future research.
- The waterdrop pattern arises when areas of displacement exceedance above 10% are filtered and thus reshaped by the 1.1φ' threshold.

⇒ **CART trains**

- In general the performance of both methods as regards Δa(−) is similar for the shorter CART trains, which are the ones with two units; and is somewhat worse in comparison with RP trains. The same behaviour is observed for loco-hauled trains with both heavy power cars. For CART trains with 3 units the performance of DER becomes visibly worse for short spans between L=10 and L=15 m, due to their irregular architecture.
- As for Δa(+), the main conclusions are similar to those stated for RP trains: performance of LIR is in general somewhat worse than DER, particularly in very short bridges (4-7 m) for speeds vP1 (>250 km/h).
- Regarding Δδ(−), the results of LIR are very similar as for CB RP trains. Only DER method behaves somewhat worse for secondary resonant peaks in some cases.
- Finally, as regards Δδ(+), again both methods are generally conservative, with usual values not above 20–25%, but with exceptions in regions of higher exceedance and a marked dependency on the train type. General aspect of exceedance maps is similar to those of RP trains, including in some cases patterns of resonance peak overestimations that cancel out near the valleys of the RIL (as for CB RP trains, this is the waterdrop pattern).

⇒ **Loco-hauled trains with one heavy locomotive at each end**

- Exceedance Δa(+) in loco-hauled trains with both heavy locomotives is found rather similar for DER and LIR, as it happened for the CB RP trains, again being in some cases DER better than LIR for the shorter spans. Trains of this subtype with D=23.0 m also show a region of worse performance of LIR for spans near L=20 m, when K > 0.5 approx.
- Regarding Δδ(−), in loco-hauled trains with both heavy locomotives the performance is clearly worse for those trains with the heavier locomotive axles, where frequent peak underestimations are found for

both DER and LIR at several subharmonics, when K is away from cancellation. This phenomenon shows up again as a (nonconservative) waterdrop pattern, and is due to the static part of the displacement being underestimated because it is computed without the power cars (in D214 convention, that is the *static displacement at resonance* = $\delta_{st,\mathrm{res}}$).

- Finally, as regards $\Delta\delta(+)$, the pattern is similar for both DER and LIR, as it happened for the RP and CART trains, with the difference that waterdrop patterns of overestimations are not present in loco-hauled trains with both heavy locomotives, for the reasons mentioned in previous conclusion.

⟹ **Freight trains**

- In the analysis of freight trains, accelerations are found to be significantly better predicted using the LIR method than the DER method, and the latter is not recommended for this type of rolling stock at speeds below 180 km/h. Especially for spans below 15-20 m, the LIR method should also be used with caution, as underestimation or overestimation can occur for discrete values of the spans, with errors exceeding 10%.
- Regarding displacement calculations for freight trains, the conclusions mentioned above for the *loco-hauled trains with one heavy locomotive at each end* suggest that the initial heavy locomotive axles be not removed when calculating $\delta_{st,\mathrm{res}}$.Providing that approach is adopted, the prediction is generally good in terms of $\Delta\delta(-)$. However, it can be an overly conservative prediction, leading to $\Delta\delta(+)$ typically by 20-25%, which affects trains with conventional wagons more (the most affected range is above approximately K=0.225), and twin wagon trains particularly in their different subharmonics, even at speeds lower than K=0.225.

⟹ **Short trains**

- For shorter *vs*. longer sequences of equidistant loads, the main difference in performance as regards $\Delta a(-)$ lies in the ascending slopes associated with K=0.33 (approx.), with both SM showing somewhat wider exceedance areas for shorter loading sequences (6 loads *vs*. 18 loads). Regarding $\Delta a(+)$, both SM clearly show poorer performance with short loading sequences in the convex slope zone above K=0.45.
- The dependence on train length has also been explored with suitable rolling stock: all CB RP vehicles of 200 m or more are considered, by halving their length and performing a comparison with the original ones.
- $\Delta a(-)$ is more strongly dependent on train length in calculations with DER, especially for STC bridges, with wavelengths below approximately 10 m being most affected on bridges with spans of less than 15–20 m. Those trains that were shorter in their original vesions show greater sensitivity, and, unexpectedly, when the half-length version is created, the DER prediction improves. Also contrary to the general belief, $\Delta a(-)$ has shown a non significant dependency on train length when using LIR. $\Delta a(+)$ is not much affected by train length either, and only on STC bridges do some specific cases of deterioration appear when the train length is halved.
- Regarding $\Delta\delta(-)$, a negligible influence is observed when the length of the vehicle is halved. A more complex case to analyse is that of $\Delta\delta(+)$, since in most cases this type of exceedance worsens when the train length is halved; however, in some trains, the opposite occurs. Trains with carriages below D=26 m are found to be somewhat less affected by the deterioration in higher subharmonics (i=2, 3,…). In general, the most recognizable pattern is of the waterdrop type; however, this pattern is filtered out in some areas by the 10% tolerance.

⟹ **Trains with irregular architectures: CMU**

- The $\Delta a(-)$ results for CMU trains are similar to those shown for CART trains. The DER method continues to perform worse than LIR for short spans below L=12.5 m approx., at the third subharmonic (i=3) or higher, and on PSC bridges. Both methods perform worse than for CB RP trains. When analysing STC bridges, more problematic spans emerge.
- Regarding the $\Delta a(+)$ maps, these conclusions can be summarized as being very similar to those of the CB RP trains. The same applies to $\Delta\delta(-)$. There is no significant dependence on the bridge type (PSC or STC).
- Finally, for $\Delta\delta(+)$, the shortest trains in the group show worse performance for spans 20 m $\leq L \leq$ 35 m approx., in the first subharmonic (i=1). That being said, the general behaviour is not too different that for CB RP trains. Overconservative waterdrop patters are hardly visible.

⟹ **Trains with irregular architectures: CMU-2-RP**

- When a single CB RP is transformed into a CMU-2-RP, $\Delta a(-)$ results are visibly less affected for LIR than for DER. In general, the maps for LIR are similar to those observed for CB RP trains, and are worse for the DER method instead.
- The conclusions for $\Delta a(+)$ are analogous than for CMU trains, except that DER results are slightly better for CMU-2-RPs than for CB RPs—that conclusion was a priori unexpected.
- Regarding $\Delta\delta(-)$, the performance is good, as it was for CB RPs or CMUs. The small, more defective areas observed for the CART subtype with DER method do not even appear here.
- Regarding $\Delta\delta(+)$, the conclusions are the same as for CMU trains.

⟹ **Symmetric vs. nonsymmetric trains**

- As for the short trains, particular rolling stock is considered here. It comprises 44 trains belonging to the MU and CMU subtypes, with no locomotives significantly heavier than the passenger cars. Car lengths D of those trains are on the order of 24–26 m. That first ensemble is replicated five times: two initial times where the car length is either shortened by 18/24 or elongated by 27/24; three more times to create symmetrical versions of the three preceding ensembles. From there:
- The LIR method is slightly negatively affected by lack of train symmetry, which is most evident for exceedance $\Delta a(-)$, as well as for $\Delta\delta(+)$ with some nuances. Regarding $\Delta\delta(-)$, there is hardly any error in any case; and regarding $\Delta a(+)$, the lack of symmetry is sometimes detrimental, but not always.
- The DER method has not been considered in relation to the evaluation of $\Delta a(-)$, due to is usual worse performance in that aspect. With respect to $\Delta a(+)$, the lack of symmetry of trains has also a nonuniform influence, as with LIR. Furthermore, in certain isolated vehicles, it negatively affects $\Delta\delta(-)$ for short bridges, but not in other very similar cases. Finally, while the $\Delta\delta(+)$ error is similar or somewhat smaller in MU trains when they are symmetric, the contrary happens in CMU trains: it is smaller when they are nonsymmetric.
- The two previous conclusions do not support that a lack of train symmetry generally worsens the predictions of the SM, except regarding the underestimation of acceleration with the LIR.

Limitations of Spectral Methods DER and LIR due to transients (SS bridges): resonant peak misestimation

- Exceedance due to peak misestimation is less predictable than for ascending slopes. Considering trains of different car length, it may take place for bridges of the same length, or for bridges of different length. In general, if the (near) maximum of a free vibration happens simultaneously with a bogie acting near mid-span, one can have peak underestimation, but that will also be influenced by the possibility of more than one bogie on the span at the same time (strongly dependent on the train architecture, and on the bridge span); or in shorter spans, even by the possibility of a single load from a bogie near mid-span being more critical than the full bogie. Even if one restricted the train architectures to a limited number, in order to predict when peak underestimation may happen, then an estimate of the error level should be obtained to be able to correct the prediction of LIR or DER.
- The possibility of incorporating all variants of transients found here (see section 0) into a limited number of a priori rules, applicable to the European rolling stock, does not appear feasible at present. A line of research could be opened to explore, first and foremost, specific vehicle variants such as regular or articulated RP trains with constant loads. This would eliminate (*a*) the uncertainty introduced by the greater number of bogies in CB trains and (*b*) the potential variability in the intensity of loads close to one another. Depending on the success of such line of research, the complexity of extending it to other rolling stock could be assessed, although this currently offers limited guarantee.
- On the other hand, similar problems arise in displacement calculations, with the added complication that the static effect of locomotives may or may not be relevant depending on their weight compared to the passenger cars. Therefore, the manner to consider the static contribution combined with resonance introduces an additional source of uncertainty for vehicles with heavy locomotives.
- In any case, the perception that resonant peaks are augmented or diminished by the forced response suggests a line of work that has been reflected in this report in the proposal of the new HLIR method, which has been presented in section 9.2. HLIR method locates these resonant maxima in time, and then straightforwardly adds the correction of the forced response to obtain a significantly improved prediction.

Limitations of Spectral Methods DER and LIR for short-span bridges and short wavelengths (SS bridges):

- It is observed that acceleration prediction is typically compromised, to a greater extent, on short bridges below approximately L=15 m. Regarding $\Delta a(-)$ with LIR, this is partly due to the ascending slopes of the subharmonics immediately after cancellations K=0.33 or K=0.2, with a greater number of them concentrated in the short-span range (although this partly depends on the vehicle's length D). It is also due to the transients that occur in these same areas more or less often, almost always more frequently than for longer beams. As for DER, the conclusion is the same but with worse results, and in a considerable number of vehicles that results are practically unusable, as shown in Appendix E. The wavelength ranges most affected are below approximately 8-10 m.
- Regarding $\Delta a(+)$, the situation doesn't improve, although for both methods it also tends to shift at higher speeds with the same wavelength (and therefore to increasingly shorter bridges), where the RIL takes on higher values and produces positive exceedance. It's worth remembering that, typically, an affected area of intermediate spans also appears, above approximately K=0.45. Finally, the transients that arise in this case imply overestimation, and therefore usually appear near RIL maxima K=0.25 or K=0.17.

- The displacement calculation, in general, is no worse for shorter spans or wavelengths than for higher values of these parameters; if anything, it's better, with the exception of very short bridges at very high speeds (a case of limited practical interest). The displacement calculation is mainly affected by the ability to predict a correct value for the "static effect" to add to the SM output, which, as discussed in previous sections, results in either conservative or nonconservative predictions (see comments related to LIR2 method below).

Improvements to Spectral Methods for SS bridges: methods proposed by D214

- Method DER2 adds the impact displacement and impact acceleration (computed through φ′ factor) as minimum output values of DER. The same idea applies to method LIR2.
- Overall, the performance of DER2 for computation of accelerations is not consistently satisfactory, but the tendencies for the computation of displacement are instead positive, with advantages particularly for the loco-hauled trains. This conclusion should be considered along with those for method LIR2 below.
- In general, the performance of LIR2 is similar to DER2, with better predictions as regards overshooting in accelerations. Its behaviour in displacement computation is equivalent to DER2. As regards how to consider the *static displacement at resonance*, $\delta_{st,\mathrm{res}}$), it remains to decide which option is preferable for each train type; it is advised that, in principle, one should keep the axles of rear and intermediate power cars, for AB and SA trains, and also for CB trains if those axles are clearly heavier than the carriages, whenever a non-conservative prediction is to be avoided in the computation of static displacement for usage with SM. It is pointed out as future research to determine whether that option is or not preferable, if LIR2 or DER2 are used instead of basic DER and LIR.
- The problem of conservative response prediction in the range K>0.45 approx. (*convex slopes*) occurs for both the DER and LIR methods, and is a consequence of considering the initial subtrains to compute the signature.
- A possible solution was proposed by D214 in its RP6, consisting of eliminating the axles of the heavy initial locomotives. This solution was analyzed here using the methods referred to as DER3 and, more specifically, LIR3. In any case, given that the phenomenon may occur not only because of the first four axles, but also because of the first 8 or even 12 axles, the strategy of eliminating the four first sub-trains does not guarantee a valid solution in general a priori
- As a consequence, in the computation of accelerations the improvement expected from method LIR3 does not cover the entire region the convex slopes and the problem is not solved in a general manner, as it could be anticipated. The same conclusion holds for vertical displacements; moreover, the benefit is limited to only trains with heavy front locomotives, and few more vehicles within all PT60 model. It cannot be concluded that removing the first axles of a train is a solution generally valid to avoid the convex slopes region, which is seen to affect many train types and not only those with heavier power cars.
- Method LIF_{h1}, though being of simpler implementation than LIF_{h2} has delivered results which cannot be fully trusted at this stage, given that they are almost identical to those of basic LIR. Its correct coding and postprocessing will be reviewed before the final version of D1.2 is submitted.
- Method LIF_{h2} proposed by D214 to improve the computation of vertical accelerations has been implemented. This method implements an out-of-phase combination of the estimates of free and forced

acceleration response. However, some doubts arise as to how the relative phase of the RIL and FIL should be handled. With the implementation adopted here, the improvements in some regions of the exceedance maps are obtained at the expense of worsening in other regions. Therefore, the improvement is not consistent overall and the method cannot be recommended in this version.

- Moreover, its implementation is not as straightforward as a simple formula. Therefore, to assume that further complexity to obtain a limited benefit (for example, in the region K>0.45 for some train types) does not seem justified.

Improvements of Spectral Methods for SS bridges: HLIR method

- To date, no formulation exists that allows a comparison of trains with general validity and independently of all bridge characteristics. Instead, a novel SM named HLIR is proposed here that can be used for fast calculation of a bridge's response, and shows that the effect of span length L should at least be considered in a train comparison aimed to cover all scenarios.
- The method predicts the phases (time instants) of interest to combine free plus forced response. It is proved that those phases depend on four parameters: [train, λ, L, ζ]. Then the known forced solution for those loads acting on the bridge at the desired time instants is added. That addition can be proved to depend also on [train, λ, L, ζ], except for the same constant terms $\frac{2}{mL\omega^2}$ or $\frac{2}{mL}$ as the free response.
- While that dependency is known from nondimensional formulations of the equations of motion presented by previous researchers, and is implicit also in the similarity formulas proposed by ERRI D214, it opens the door to producing 3D spectra that actually allow to compare different trains. HLIR method can provide optimal computational efficiency for such spectra, given that the points sampled are minimal, and optimisation of the method is only at its earliest stage.
- The overall assessment of HLIR can be broken down into displacements and accelerations. Regarding displacements, the formulation proposed here provides optimal results, and hardly any exceedance zones are observed in the maps, not even for STC bridges.
- Regarding accelerations, there is always a very significant improvement compared to the LIR results, though some minor areas remain in the exceedance maps. These results, which require a final improvement in those small areas where HLIR shows some exceedance, are reduced to far fewer cases than with current SMs. This opens the possibility of undertaking an optimization process in the immediate future to achieve (*a*) the best accuracy and (*b*) optimal coding in terms of calculation times.
- All this, with the notable advantage also that HLIR method does not suffer from any kind of over-conservatism.

Limitations and improvements of Spectral Methods in 2-span continuous bridges

- The comparative analysis between SS and continuous 2-span railway bridges demonstrated that structural continuity introduces significant modal interaction effects capable of substantially amplifying the dynamic response under moving loads. The results of a wide analysis based on model PT60 showed that the second vibration mode of continuous bridges may generate exceedances above 40% and reaching values close to 80% with respect to equivalent SS configurations, particularly for medium and long spans. Furthermore, the location of the exceedance regions was found to depend strongly on the

(L/D) ratio. These findings confirm that simplified SS representations may significantly underestimate the response of continuous railway bridges. Consequently, the incorporation of multimodal and continuity effects is essential for reliable dynamic assessment and for the development of efficient bridge screening methodologies.

- To that end, a simplified LIR-based methodology for the dynamic assessment of continuous 2-span railway bridges has been proposed. The formulation combines a closed-form analytical representation of the first vibration mode with a numerical treatment of the second mode through a normalized response map in the (K,ζ) parameter space, and proportionality rules of general application. This multimodal framework enables the estimation of dominant resonant responses without the need of TSC. Furthermore, the proportionality-based formulation enables its extension to higher modes and bridges with an arbitrary number of spans. Although larger discrepancies were observed in cancellation regions, these differences are of limited practical importance since bridge design is governed primarily by peak acceleration responses.
- Nevertheless, the results obtained for SS bridges indicate that the accuracy of the LIR approach decreases when complex and irregular real train configurations are considered. These limitations highlight the need for enhanced formulations capable of incorporating phase information more accurately. In this regard, the HLIR method emerges as a promising alternative for future developments in combination with the new methods for 2-span beams proposed here..

Assessment of the CQC method for multi-mode combination

- Taking as a benchmark application the prediction of response in 2-span continuous beams, where the first two modes have been found to interact significantly in certain cases, the accuracy of method CQC has been evaluated.
- The performance of such method for predicting accelerations has been found unsatisfactory for all trains in model PT60, mostly for the range $K > 0.25$ and spans up to some 25–30 m.
- As regards the computation of displacements, and similarly to what has been observed regarding the influence of torsion, it should be verified whether a simple addition of the static deflection from the non-resonant mode could improve the quantification of vertical displacement by CQC method in 2-span continuous beams.

Limitations and improvements of Spectral Methods in portal frames

- Examples have been provided that the difference in the predicted response of a beam with rotational, elastic end restraints (ERS beam) and an equivalent SS beam is evident. A fact that stems from the differences in the fundamental bending mode shapes of both structural types.
- The ERS-LIR formulation proposed here constitutes a significant extension of the classical Residual Influence Line approach by enabling the dynamic assessment of ERS beams, thus covering the complete spectrum of boundary conditions between simply supported and clamped-clamped beams. The complete analytic solution provided for the first symmetric vibration mode enables also such subsequent LIR formulation. It is demonstrated that the influence of rotational stiffness can be incorporated through a nondimensional framework governed by the following parameters: nondimensional velocity K, ERS to SS frequency ratio γ^2, and damping ratio ζ_s. The formulation preserves the physical interpretation and

computational efficiency of the original LIR method while substantially increasing its applicability to practical railway bridge configurations with complex support conditions.

- Furthermore, the research undertaken for portal frames has demonstrated that the proposed ERS-based strategy provides a sistematic way to extend the SM formulation beyond conventional beam idealizations. By exploiting the similarity between the symmetric modal response of the portal frame and that of an ERS beam, the dynamic contribution of the lateral walls and soil interaction can be incorporated through only two calibrated quantities: the static deflection (y_{st}) and the fundamental natural frequency (ω_s). The comparison with FEM results confirms that the reduced formulation accurately captures the forced response, the free-vibration intervals, and their superposition during train passage. This agreement indicates that the method preserves the essential dynamic behaviour of the portal-frame system without requiring a reformulation of the closed-form moving-load solution or its LIR-based implementation. Consequently, the approach represents a practical alternative for preliminary design, parametric analyses, and repeated evaluations of portal-frame structures subjected to moving loads.
- Finally, these novel formulations for ERS beams and portal frames offer also possibilities to be integrated in a HLIR strategy, to consider the combination of free and forced vibration in an optimal computational scheme.

Limitations and improvements of Spectral Methods in bridges subjected to torsion:

- A suitable formulation of the torsional vibration has been presented, that adds parameters n_{0T} (frequency ratio) and k_T (mass radius of gyration) to the bending problem, in addition to the eccentricities. Those parameters can be easily calculated or calibrated from FEM models of actual bridges. The proposed fomulation has enabled a large sensitivity analysis for realistic ranges of n_{0T} and k_T.
- Regarding the torsional behaviour, even for a frequency ratio n_{0T} = 1.3>1.2, the contribution of torsion for checking the serviceability acceleration limit can be significant by more than 10%, for certain spans lengths and some values of the radius of gyration. When the radius of gyration increases, the effect of torsion is seen to decrease markedly. These results point out that the n_{0T} >1.2 rule given in (CEN, 2023 | section 8.4.4) could require further specification of its range of validity, as a function of [L, k_T], and some suitable parameter as K or λ.
- For the cases mentioned in the conclusion above, classical SM will therefore fail to estimate the vertical acceleration of a bridge deck because they neglect torsion.
- For the same cases discussed above, the contribution of torsion to the max. vertical displacement, considering the cumulative response approach adopted here, is most times quasi-static. This opens the possibility that it may be added to the vertical bending displacement as a means of simplified calculation.
- The formulation of the torsion problem is identical to that of the bending problem, except for some constant factors and the need to adapt wavelengths and nondimensional speeds. With that perspective, all improvements to SM based on bending behaviour can be directly extrapolated to torsion, as, for example, the HLIR formulation.

Reduction factors for longitudinal load distribution in 2-span beams and other bridge types

- Considering the effect of longitudinal load distribution in numerical models through expansion in a larger number of smaller loads is more computationally demanding. Besides, it becomes also more involved for the purpose of SM implementation, if one intends to considered the various sub-trains included in the signatures. Therefore, the use of response reduction factors as the one proposed by UIC for accelerations after the works by D214 can be of great benefit for combined use with SM.
- To that end, current existing reduction factors, which are known to work well in SS bridges, have been tested in 2-span continuous beams, in contrast to TSC calculations where the distribution is accurately implemented as a a triangular footprint of 2.5 m.
- The equivalent low-pass filtering effect established by Jin et al. (2018) is found to be also valid for 2-span bridges. This result indicates that reduction coefficients for the acceleration (for example, the ones proposed by UIC) will deliver good results in 2-span beams, and should be evaluated as a function of the wavelength associated with each vibration mode individually.
- This is a good indicator that the UIC reduction coefficient could be probably used with benefit for other bridge types such as portal frames, since the low-pass filtering effect does not depend on the mode shape.
- The logarithmic formulation proposed by Moliner et al. (2024) for predicting displacement reduction factors showed trends similar to those obtained using the 2.5 m triangular longitudinal load distribution. Therefore, its use with each vibration mode individually currently shows good perspectives as well in 2-span beams.

16 Conclusions

- The principal conclusions of Tasks 1.3 and 1.4 are gathered in this section. It is advised to consider subsection "*General approach*", under previous section 15, for a summary of the hypotheses involved regarding rolling stock, bridge properties, and analysis methods.
- The limit of 10% for the maximum relative error assumed as an objective in InB4EU is a demanding goal for a simplified method that deals with a large variety of rolling stock and span lengths. Therefore, and also due to the multiplicity of train variants, the number of regions with unacceptable error level in the exceedance maps have been found to be more numerous that initially expected.
- It is often mentioned that current SM are not suitable for comparing the load effects of trains on short span bridges or for excitation from short wavelengths. As regards the vertical accelerations, that statement is largely correct. It is observed that acceleration predictions from LIR are typically compromised in a nonconservative manner, to a greater extent, on short bridges below approximately L=15 m, at speeds after cancellations K=0.33 or K=0.2. As for DER, the conclusion is the same but with worse results, and in a considerable number of vehicles that results are practically unusable, as shown in Appendix E. The wavelength ranges most affected are below approximately 8-10 m.
- Regarding the too conservative predictions of acceleration, the situation doesn't improve for the shorter spans, although for both methods it tends to shift at higher speeds with the same wavelength (and therefore to increasingly shorter bridges), where the RIL takes on higher values and produces positive exceedance. The errors in peak values in this case imply overestimation, and therefore usually appear near RIL maxima K=0.25 or K=0.17.
- The displacement calculation, in general, is no worse for shorter spans or wavelengths than for higher values of these parameters; if anything, it's better, with the exception of very short bridges at very high speeds (a case of limited practical interest). The displacement calculation is mainly affected by the ability to predict a correct value for the "static effect" to add to the SM output, which is discussed below.
- For most trains, the performance of DER in negative acceleration exceedance $\Delta a(-)$ is worse in comparison to LIR, for spans below some L=15 m. As mentioned above, in a relevant number of cases the results of DER cannot be exploited for wavelengths below λ=10 m approx. Both methods perform slightly worse for trains with more irregular architectures, and, when analysing STC bridges, more problematic spans emerge. Typically a region of defective resonant *ascending slopes* is found near the first subharmonic after cancellation K=0.33 and close to K=0.4, affecting a range of spans in that area. Loco-hauled trains also tend to originate transient phenomena (peak underestimation) for spans below some L=15 m, when K is above RIL maxima K=0.25 or K=0.17 but approaching cancellations.
- As for the positive acceleration exceedance $\Delta a(+)$ performance of LIR is in general somewhat worse than DER, particularly in very short bridges (4-7 m) for speeds above 250 km/h—which probably has few implications from a practical point of view. The range between some L=10.0 and L=26.0 m, for K>0.4–0.45, is typically affected by the so-called here phenomenon of *convex slopes,* in both methods.
- The calculation of displacements is significantly influenced by how the *static part* of it is evaluated, which is typically added directly to the results obtained from the (signature × RIL × constant) product. However, the concept of the static part of the displacement is controversial: when a train crosses a SS beam, the static influence line has maxima and minima, and no theorem exists to prove that these

maxima values are the correct values to be added to the dynamic part of δ obtained from a static impact measurement. This is a subject of interest for future research.

- Consequently, if the recommendation in RP6 of D214, Part A, is followed, and the *static displacement at resonance* is added (calculated without locomotives), the result is usually too conservative for trains where the locomotives do not have much influence on the static line (Δδ(+) appears, Δδ(−) is very small), either because they are lightweight or nonexistent.
- Conversely, the result is not on the safe side in cases where the presence of the locomotives is relevant for the static calculation (Δδ(−) appears, Δδ(+) remains mostly in the area of convex slopes). Therefore, it is advised that, in principle, one should keep the axles of rear and intermediate power cars, for AB and SA trains, and also for CB trains if those axles are clearly heavier than the carriages, whenever a nonconservative prediction is to be avoided in computing a static displacement for usage with SM.
- Contrary to the general belief, performance of current **SM for short trains** has not consistently shown to be worse than for versions of the same trains twice as long, so length itself does not appear to be a determining factor. The analysis has been based on the more regular and periodic CB RP trains. With them, DER method shows greater sensitivity than LIR in accelerations, but with results that worsen for longer trains, which was not expected either. In displacements, nonconservative predictions are little affected, and conservative predictions are more affected, but not always in favor of longer trains.
- The possibility of incorporating all variants of transients found during this research into a limited number of a priori rules, applicable to the European rolling stock, does not appear feasible at present. A line of research could be opened to explore, first and foremost, specific vehicle variants such as regular or articulated RP trains with constant loads. This would eliminate (*a*) the uncertainty introduced by the greater number of bogies in CB trains and (*b*) the potential variability in the intensity of loads close to one another. Depending on the success of such line of research, the complexity of extending it to other rolling stock could be assessed, although this currently offers limited guarantee.
- On the other hand, similar problems arise in displacement calculations, with the added complication that the static effect of locomotives may or may not be relevant depending on their weight compared to the passenger cars.
- Nevertheless, the perception that resonant peaks are augmented or diminished by the forced response suggests a line of work that has been reflected in this report in the proposal of the new HLIR method. HLIR method locates these resonant maxima in time, and then straightforwardly adds the correction of the forced response to obtain a significantly improved prediction.
- The lack of train symmetry does not generally worsens the predictions of the SM in a general manner, except regarding the underestimation of acceleration with the LIR. That behaviour has been investigated with trains that initially were nonsymmetric, of subtypes MU and CMU.
- In the analysis of freight trains, accelerations are significantly better predicted using the LIR method than the DER method, and the latter is not recommended for this type of rolling stock at speeds below 180 km/h. Especially for spans below 15-20 m, the LIR method should also be used with caution, as underestimation or overestimation can occur for discrete values of the spans, with errors exceeding 10%.
- Regarding displacement calculations for freight trains, it is suggested that the initial heavy locomotive axles be not removed when calculating $\delta_{st,\mathrm{res}}$.Providing that approach is adopted, the prediction is generally good in terms of Δδ(−). However, it can be an overly conservative prediction, leading to Δδ(+)

typically by 20-25%, which affects trains with conventional wagons more (the most affected range is above approximately K=0.225), and twin wagon trains particularly in their different subharmonics, even at speeds lower than K=0.225.

- Several methods proposed by D214 in its RP6 to improve the basic formulation of DER and LIR have been implemented and thoroughly tested using exceedance maps and the PT60 model. In general, these methods have not shown a consistent improvement in prediction that would validate their generic use for any bridge, train, and speed. Only some partial improvements, described in previous sections, have been achieved, at the expense of worsening performance in other areas of the map. The only more widespread improvement has been observed for DER2 and LIR2 methods—which incorporate impact displacement as the minimum output value—with advantages particularly for loco-hauled trains. In any case, this improvement could interfere with the calculation of the *static displacement at resonance*, so it should be re-evaluated based on the strategies adopted for both aspects of the procedure.
- Method named here as LIF_{h1} has yielded results that cannot be fully trusted at this stage, given that they are almost identical to those of basic LIR. Its correct coding and postprocessing will be reviewed before the final version of D1.2 is submitted.
- To date, no formulation exists that allows a comparison of trains with general validity and independently of all bridge characteristics. A novel SM named HLIR is proposed here that can be used for fast calculation of a bridge's response, and shows that the effect of span length L should at least be considered in a train comparison aimed to cover all scenarios. This method is also free from over-conservatism.
- The method predicts the phases (time instants) of interest to combine free plus forced response. It is proved that those phases depend on four parameters: [train, λ, L, ζ]. Then the known forced solution for those loads acting on the bridge at the desired time instants is added.
- While that global dependency, except for mass/stiffnes constants, is known from nondimensional formulations by previous researchers, it opens the door to producing 3D spectra that actually allow to compare different trains. HLIR method can provide optimal computational efficiency for such spectra.
- Regarding displacements, HLIR provides optimal results, and hardly any exceedance zones are observed in the maps, not even for STC bridges.
- Regarding accelerations, there is always a very significant improvement compared to the LIR/DER results, though some minor small areas remain in the exceedance maps. This opens the possibility of undertaking an optimization process in the immediate future to achieve (a) the best accuracy for HLIR method and (b) its optimal coding in terms of calculation times.
- It has been shown that structural continuity in 2-span railway bridges introduces significant multimodal amplification effects that may substantially exceed the response of equivalent SS models. Moreover, the exceedance regions strongly depend on the L/D ratio, highlighting the importance of considering continuity and modal interaction effects.
- The proposed multimodal LIR-based methodology enables the efficient dynamic assessment of continuous 2-span railway bridges by combining analytical and numerical modal formulations without requiring full time-domain integration. The approach reproduced resonance peaks with high accuracy while substantially reducing computational cost, demonstrating strong potential for preliminary bridge screening and future extensions to more complex multi-span configurations.

- Also, the CQC method applied to 2-span continuous beams has ben found to perform unsatisfactorily for the computation of vertical accelerations. As for the vertical displacements, a direct quasi-static addition of the non-resonant mode could be explored as an alternative in the future.
- Beams with end conditions other than SS require specific formulations of closed-form solutions and derived SM. The ERS-LIR formulation proposed here provides a complete, analytic solution to the equation of motion, and extends the classical LIR method to beams with elastically restrained supports, enabling the assessment of the full spectrum of boundary conditions between SS and clamped-clamped beams. The method preserves the computational efficiency of the original formulation while providing accurate prediction of resonance peaks in railway bridge applications with complex support conditions.
- Of interest for practical applications in portal frames is the fact that the proposed ERS-based strategy enables a straightforward extension of the SM formulation to such structures by incorporating the effects of lateral walls and soil interaction through two simple, calibrated modal parameters: natural frequency and static deflection. Comparisons with FEM results confirmed that the reduced formulation accurately reproduces the dynamic response under moving loads while significantly reducing computational effort.
- Regarding the torsional behaviour, even for a frequency ratio n_{0T} = 1.3>1.2, the contribution of torsion to vertical accelerations can be significant by more than 10%, for certain spans lengths and some values of the radius of gyration. When the radius of gyration increases, the effect of torsion decreases markedly. These results point out that the n_{0T} >1.2 rule given in (CEN, 2023 | section 8.4.4) could require further specification of its range of validity, as a function of [L, k_T], and some suitable parameter as K or λ.
- For the cases mentioned in the conclusion above, classical SM will therefore fail to estimate the vertical acceleration of a bridge deck because they neglect torsion.
- For the same cases discussed above, the contribution of torsion to the max. vertical displacement, considering the cumulative response approach adopted here, is most times quasi-static. As mentioned for the CQC methods, this opens the possibility that it may be added to the vertical bending displacement as a means of simplified calculation.
- All new formulations proposed here for torsion, 2-span beams, and portal frames, are amenable in the near future to be casted into an HLIR strategy for optimal computational performance with minimum error (and null overshooting).
- The study of the reduction-factors for longitudinal load distribution demonstrated that the existing formulations, previously developed for SS bridges, can be successfully extended to continuous 2-span bridges when wavelength is considered mode by mode (also the *impact coefficient*, in the case of displacements). Furthermore, the proposed simplified approaches reproduced the trends obtained from detailed FEM analyses with good accuracy while considerably reducing computational effort.
- Previous attempts to deliver a method based on the theory of random vibrations have encountered a number of difficulties which Task 1.3 of this Project has deemed of practical relevance: inaccuracies to estimate the response in the ascending resonant slopes, reliance on steady-state hypothesis to obtain peak values—which cannot be combined with local transient phenomena—; lack of validation in short spans and for bridges with low mass and damping; lack of validation for CB trains or irregular architectures. Given that all those aspects have been proven to be significant during Task 1.3, the methods based on random vibration have not been explored further and research priorities have focused in the remaining objectives of Task 1.4.

REFERENCES

Ciku, A. & Gavriliuk V. (2022). *Spectral density approach for dynamic analysis of high-speed railway bridges* [Master's thesis, Kungliga Tekniska Högskolan]. Publications KTH. https://kth.diva-portal.org/smash/record.jsf?pid=diva2%3A1677115&dswid=-9532.

European Committee for Standardization / CEN. (2023). Eurocode 1 – Actions on structures – Part 2: Traffic loads on bridges and other civil engineering works (EN1991-2:2023).

European Committee for Standardization / CEN / TC250/SC1/WG03 "Dynamic interface between bridges and rolling stock (DIBRST)". (2023 - DRAFT). Dynamic interface between Railway Bridges and Rolling Stock — State of the art report.

European Rail Research Institute (D-214 Committee, ERRI D214). (1999). RP6 – Calculation for bridges with simply-supported beams during the passage of a train. Utretch.

European Rail Research Institute (D-214.2 Committee, ERRI D214.2). (2002). Use of universal trains for the dynamic design of railway bridges. Summary of results of D214. Utretch.

European Union Agency for Railways. (2022). ERA technical note on work needed for closing TSI open point on bridge dynamics. ERA1193-TD-01-2022 V 1.0

Feng, X., Xu, J., Wang, C., Chen, C., Wang, J. & Chen, T. (2025). Generalized CQC method for evaluating coupled structural responses under multiple excitations. *Structures*, 82, 110683. https://doi.org/10.1016/j.istruc.2025.110683

Grunert, G., Grunert, D., Behnke, R., Schäfer, S., Liu, X. & Reddy, S. (2025). A Machine Learning-Based Algorithm for the Prediction of Eigenfrequencies of Railway Bridges. *International Journal of Structural Stability and Dynamics*, 25(24), 2540016. https://doi.org/10.1142/S0219455425400164

In2Track2 project. (2021). *Deliverable "Tunnel and Bridge I2T2 Report". Report: "High-speed low cost bridges, background report" (D5.2.5).* Trafikverket, KTH, UPORTO

Jin, Z., Huang, B., Ren , J. & Pei, S. (2018). Reduction of Vehicle-Induced Vibration of Railway Bridges due to Distribution of Axle Loads through Track. *Shock and Vibration*, 2018, 2431980. https://doi.org/10.1155/2018/2431980

Kim, T., Kwon, O.S. & Song, J. (2024). Deep learning-based response spectrum analysis method for building structures. *Earthquake Engineering & Structural Dynamics,* 53, 1638–1655. https://doi.org/10.1002/eqe.4086

Martínez-Rodrigo, M.D., Andersson, A., Pacoste, C. & Karoumi, R. (2020). Resonance and cancellation phenomena in two-span continuous beams and its application to railway bridges. *Engineering Structures*, 222, 111103. https://doi.org/10.1016/j.engstruct.2020.111103

Moliner, E., Museros, P. & Allahvirdizadeh, R. (2024). Track–bridge interaction effects in the acceleration and displacement response of high-speed railway bridges: Simplified vs refined modelling. *Engineering Structures*, 314, 118304. https://doi.org/10.1016/j.engstruct.2024.118304

Museros, P., Moliner E. & Martínez-Rodrigo, M.D. (2013). Free vibrations of simply-supported beam bridges under moving loads: Maximum resonance, cancellation and resonant vertical acceleration. *Journal of Sound and Vibration*, 332, 326–345. http://dx.doi.org/10.1016/j.jsv.2012.08.008

Museros, P. & Moliner, E. (2017). Comments on "Vibration of simply supported beams under a single moving load: A detailed study of cancellation phenomenon" by C.P. Sudheesh Kumar, C. Sujatha, K. Shankar [Int. J.

Mech. Sci. 99(2015) 40–47,doi:10.1016/j.ijmecsci.2015.05.001]. *International Journal of Mechanical Sciences*, 128-129, 709–713. http://dx.doi.org/10.1016/j.ijmecsci.2016.07.005

Museros, P., Andersson, A., Martí, V. & Karoumi, R. (2021). Dynamic behaviour of bridges under critical articulated trains: Signature and bogie factor applied to the review of some regulations included in EN 1991-2. *Proceedings of the Institution of Mechanical Engineers, Part F: Journal of Rail and Rapid Transit*, 235(5), 655–675. https://doi.org/10.1177/0954409720956476

Museros, P., Andersson, A. & Pinazo, B. (2023). High-speed trains derived from Annex E/EN 1991-2. *Mendeley Data (V3)*. https://doi.org/10.17632/hdr6dd5xv2.3

Museros, P., Andersson, A. & Pinazo, B. (2024). Dynamic behaviour of bridges under critical conventional and regular trains: Review of some regulations included in EN 1991-2. *Proceedings of the Institution of Mechanical Engineers, Part F: Journal of Rail and Rapid Transit*, 238(8), 977–988. https://doi.org/10.1177/09544097241245150

Rail Safety and Standards Board / RSSB. (2024). Guidance on Evaluating Excessive Dynamic Effects in Underline Bridges (Rail Industry Guidance Note GEGN8616 | Issue One).

Zangeneh, A., Museros, P., Pacoste, C. & Karoumi, R. (2021). Free vibration of viscoelastically supported beam bridges under moving loads: Closed-form formula for maximum resonant response. *Engineering Structures*, 244, 112759. https://doi.org/10.1016/j.engstruct.2021.112759

Appendix A — Comparison of dynamic effects from different trains or from different analysis methods: Definition of exceedance and required speed increase

The methodology summarised here is further described in (Museros et al., 2021) or (Museros et al., 2024). The comparison of the dynamic effects arising from either two different trains, or two different load models (a "load model" is understood as an ensemble of several trains), or two different analysis methods as well, can be carried out on the basis of two indicators referred to as ***exceedance*** and ***required speed increase*** (RSI) as explained below.

It should be emphasised that the comparisons are performed here in terms of **cumulative response**, given that the operating speed of a track section may be reduced to lower values for particular reasons. Therefore, for a given design speed of the line V, the highest peak response at any speed lower than V is determinant for bridge design. Figure 61 is used to explain this concept, by showing the comparison of a model formed several conventional trains ("Model 101" see (Museros et al., 2023)), *vs*. model HSLM-A.

Figure 61 shows that the cumulative response in terms of acceleration—the same applies to displacements—is marked by "steps", where the various trains from the Model 101 and the HSLM-A create successive resonant or subresonant peaks. So, each new peak causes a higher step in the cumulative response. Three main cases can be considered where such kind of comparative plots can be applied:

Application A.1: Simply as Figure 61 shows, two different trains or two different load models can be compared in terms of the cumulative maximum acceleration (or displacement) that they create on a bridge. Typically: (a) one of the two elements of the comparison will be a normative train, or a normative load model as HSLM-A, while (b) the other element of the comparison will be a real (or realistic) train, or real (or realistic) train model.

Application A.2: The same type of cumulative response plot can be produced when a single train or a single load model is analysed by two different methods (namely, a TSC and a SM). Therefore, the concept of "exceedance" is also useful to reveal which of the two methods is more conservative. In this case, the concept of RSI (described further below) may not always be exploitable.

Application A.3: Similarly, the exceedance can be used to compare a given real train, *vs*. a variant of such train: for instance, it can be used to compared a non-symmetric train *vs*. its mirrored version, in order to examine if there is a difference between the responses induced in a bridge when the train is running either in *push* or in *pull mode*. In this case, the concept of RSI (described further below) will typically not be of interest.

For brevity and greater generality, the description below is based solely in "Application A.1" as defined above. From an analysis as shown in Figure 61, first the exceedance in acceleration is defined —for each speed V— as

$$\Delta a(V) = max\left[100\,\frac{a_{max,REAL}(V) - a_{max,HSLMA}(V)}{a_{max,HSLMA}(V)};\ 0\right] \qquad (72)$$

were subscript REAL implies that response is computed for a load model of a "real" train (for instance, a conventional train model as "Model 101"). The definition given in Eq. (46) above applies to vertical displacements as well by simply replacing each $a(V)$ by $\delta(V)$.

If an exceedance $\Delta a(V=V_0)$ or $\Delta\delta(V=V_0)$ is found to be below an acceptable limit, that acceleration or displacement in excess of the response computed with HSLM-A is not to be deemed relevant. Following ERRI D214.2 (2002), a threshold of 10% will be generally adopted.

Conversely, if $\Delta a(V=V_0) > 10\%$, the RSI value (represented by ΔV) is then computed as follows, for the vertical accelerations (the treatment of displacements is identical). When comparing a real train model (as Model 101) vs. a normative load model as HSLM-A (*i.e.* in case of "Application A.1"), the situation where $\Delta a(V=V_0)>10\%$ does not necessarily imply by itself that the real train model is not duly covered; the important reason behind it is that the effects of HSLM-A may (or not) increase strongly for V only slightly larger than V_0 and, in such situation, the safety factor "design speed"/"operational speed" >1 would suffice for HSLM-A to exceed the real train again. That situation can be observed in Figure 61, for instance, at speed V=100 km/h.

Therefore, the RSI or predicted speed increase required for HSLM-A to cover a real train ΔV is defined as the minimum difference in speed (as a percentage) that is needed to reach, from the dominant peak of the real train response, the response curve of the HSLM-A with identical amplitude, but at higher speed. Figure 61 also illustrates that concept: in that example, the RSI at V=109 km/h is (143−109)/109 = 0.31 →ΔV = 31%.

It is important to mention that RSI is typically not considered relevant below 20%, following the prescriptions of Eurocode EN 1991-2. Such code establishes that the standard increase of design speed to be assigned to HSLM-A model for bridge dynamic analysis is precisely 20%.

In summary, Figure 61 shows an example where the exceedance $\Delta a(V$=109 km/h) is clearly above 10%, and such neat exceedance is maintained during an ample interval of speed, from 109 to 143 km/h. Since ΔV=31%, the RSI is above 20% and the lack of coverage in this situation is relevant.

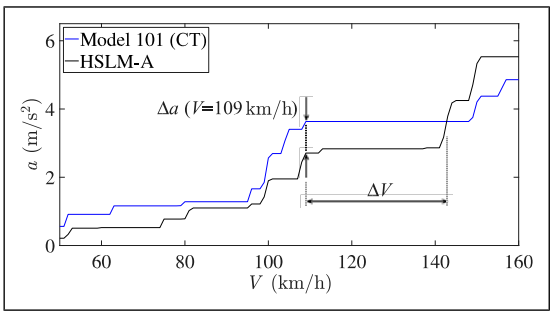

Figure 149: Cumulative response in acceleration for a bridge of span L = 25.2 m: definition of exceedance Δa and required speed increase ΔV.

NOTE: As mentioned earlier, it is recalled that for "Application A.2" the concept of RSI may not always be exploitable. And for "Application A.3", such concept will typically be not needed.

In a comprehensive fashion, Figure 62 shows an so-called *exceedance map*, which is the result of plotting the exceedance analysis (performed as described by Figure 61) for a large number of different span lengths. In Figure 62, the range of spans covers from 4 to 40 m. Lines of equal wavelength are superimposed for completeness. The left plot in Figure 62 shows the exceedance Δa, whenever it is above some given threshold (10% in this case). Then, the right plot shows the RSI value (ΔV), whenever it is above some other threshold (20% in this case).

It should be emphasised that comparisons are typically carried out with the second dataset (HSLM-A, in Figure 61) taken as a reference for comparison. Then, what Figure 62 shows are those cases where the first

dataset exceeds the second dataset. But the opposite situation could also be displayed, *i.e.* when the second dataset exceeds the first one. Both types of analysis may be of interest, depending on the objectives of the study.

In general, in this document the first case is referred to as ***negative exceedance***, because it is the reference dataset which is exceeded—which typically will be associated to a non-conservative situation (negative situation). Therefore, we can state that Figure 62 displays a map of negative exceedance.

The opposite situation will be referred to here in general as ***positive exceedance***, i.e. when the reference results are more conservative than those of the first dataset (positive situation—providing that they are not too conservative).

Finally, in certain studies, plots similar to Figure 62(left) may be convenient as well where any exceedance, either positive or negative, is displayed whenever its value is above some fixed threshold. We call those maps of ***bidirectional exceedance***. Application A.2 may benefit from that kid of maps, given that the accuracy of an approximate method should be tested in that way, allowing, for instance, a maximum deviation of 10% between two response curves, in absolute value: one response curve would be obtained from an "exact" analysis method, and another one would be obtained from an approximate method (as an Spectral Method, for instance).

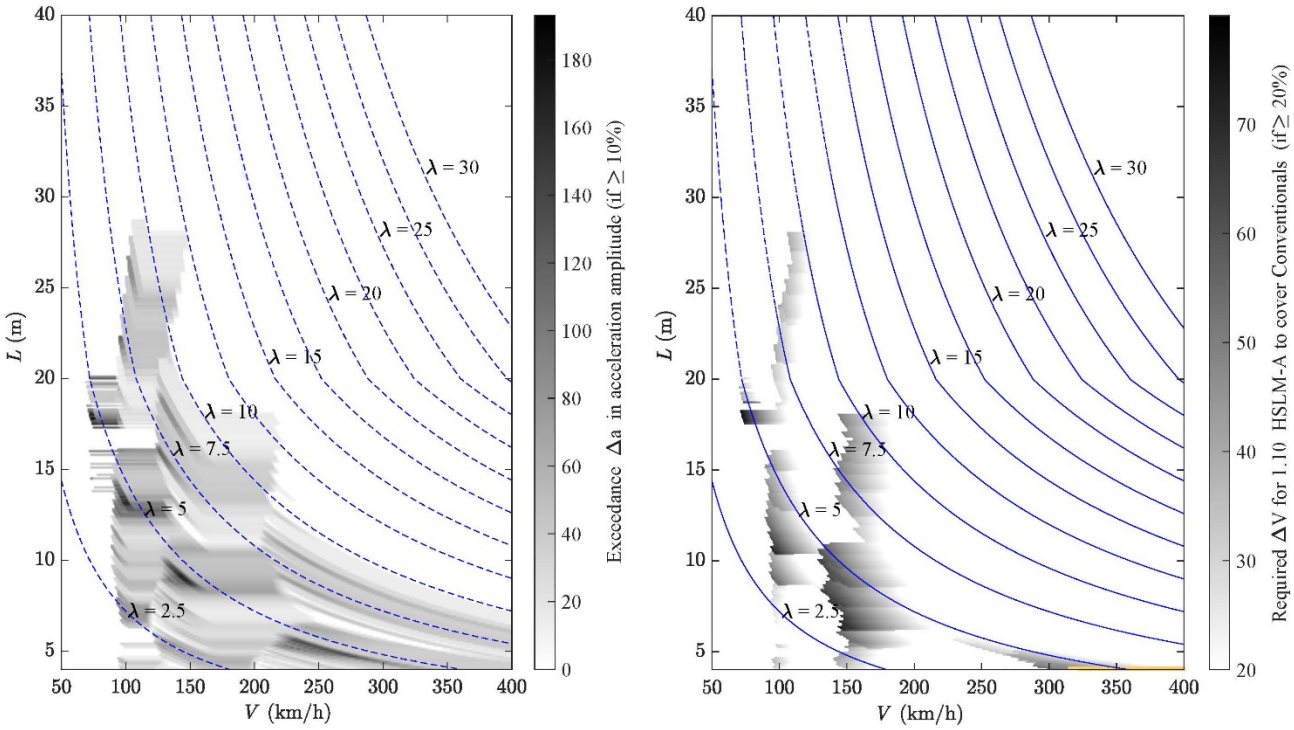

Figure 150: Example of corresponding maps of exceedance Δa and required speed increase ΔV.

Appendix B — Passenger trains: anonymous description

Conventional trains (CB)

Anony. Name	ID	D [m]	U [-]	V [km/h]	N [-]	d_{max} [m]	P [kN]	Series				Subtype
								Symm	NonSymm	Short	EndTr	
INB4EU-CB-001	10	25.90	1	220	24	151.2	3394.2	1		1		RP
INB4EU-CB-002	12	26.40	1	200	44	271.2	6166.8		1		1	LH-bLL
INB4EU-CB-003	13	26.40	1	200	40	251.0	5705.5		1			LH-fHL
INB4EU-CB-004	14	26.40	1	200	40	251.5	5725.1		1			LH-fHL
INB4EU-CB-005	15	23.90	1	220	36	210.9	4951.1		1			RP
INB4EU-CB-006	16	23.90	1	220	44	258.7	6065.5		1			RP
INB4EU-CB-007	17	26.40	1	200	8	48.9	1620.1		1	1		RP
INB4EU-CB-008	18	26.40	1	200	12	75.3	2398.2		1	1		RP
INB4EU-CB-009	86	27.16	1	200	16	103.1	2572.0		1	1		RP
INB4EU-CB-010	93	25.90	1	230	20	125.3	3194.1		1	1		RP
INB4EU-CB-011	125	25.90	1	200	36	228.9	5035.8	1				RP
INB4EU-CB-012	128	25.90	1	200	12	73.5	1660.2	1		1		RP
INB4EU-CB-013	230	26.40	1	280	56	350.5	8921.3		1		1	LH-bHL
INB4EU-CB-014	233	26.40	1	280	64	403.3	10129.4		1		1	LH-bHL
INB4EU-CB-015	236	26.02	1	200	16	99.7	2481.4	1		1		RP
INB4EU-CB-016	238	26.40	1	280	32	198.3	4731.7		1			LH-fHL
INB4EU-CB-017	241	24.78	1	330	32	193.3	5125.5	1				RP
INB4EU-CB-018	275	28.60	1	250	48	338.1	7674.3		1			RP
INB4EU-CB-019	278	26.50	1	230	32	199.0	4764.4		1			LH-fHL
INB4EU-CB-020	316	26.40	1	220	32	198.7	5170.7		1			LH-fHL
INB4EU-CB-021	317	26.40	1	220	52	323.1	8485.3	1			1	LH-fHLrLL
INB4EU-CB-022	324	24.80	1	350	16	93.8	2536.2	1		1		RP
INB4EU-CB-023	325	24.80	1	350	32	193.0	4662.9		1			RP
INB4EU-CB-024	328	25.78	1	250	16	99.1	2700.2	1		1		RP
INB4EU-CB-025	338	25.90	1	220	24	151.4	2930.2	1		1		RP
INB4EU-CB-026	339	26.10	1	300	40	251.2	5029.3	1			1	LH-bHL
INB4EU-CB-027	340	25.50	1	250	24	148.0	3355.0	1		1		RP
INB4EU-CB-028	346	28.75	1	265	52	366.8	8363.7		1			RP
INB4EU-CB-029	347	28.75	1	265	56	395.6	8892.5		1			RP
INB4EU-CB-030	390	24.04	1	200	24	143.9	3143.8	1		1	1	LH-bHL
INB4EU-CB-031	391	24.04	1	200	16	94.2	2242.9	1		1	1	LH-bHL
INB4EU-CB-032	393	25.29	1	200	24	152.1	3297.2		1	1	1	LH-bHL
INB4EU-CB-033	394	25.29	1	200	16	99.1	2325.7	1		1	1	LH-bHL
INB4EU-CB-034	464	25.63	1	200	16	98.8	2649.2	1		1		MU
INB4EU-CB-035	465	25.62	1	200	20	124.8	3277.2	1		1		MU
INB4EU-CB-036	466	25.62	1	200	24	150.8	3904.4	1		1		MU
INB4EU-CB-037	467	25.63	1	200	16	100.0	2649.2	1		1		MU
INB4EU-CB-038	468	25.62	1	200	20	126.6	3277.2	1		1		MU
INB4EU-CB-039	469	25.62	1	200	24	153.2	3904.4	1		1		MU
INB4EU-CB-040	473	24.04	1	200	24	143.9	3761.8	1		1	1	LH-fHLrLL
INB4EU-CB-041	474	23.80	1	200	16	93.1	2815.9		1	1		MU
INB4EU-CB-042	475	23.80	1	200	16	93.1	2815.9		1	1		MU
INB4EU-CB-043	476	24.90	1	200	32	192.7	5536.5		1			MU
INB4EU-CB-044	477	24.90	1	200	32	192.7	5536.5		1			MU
INB4EU-CB-045	480	24.90	1	200	48	293.3	8352.4		1			MU
INB4EU-CB-046	481	24.90	1	200	48	293.3	8352.4		1			MU
INB4EU-CB-047	482	24.90	1	200	48	293.3	8352.4		1			MU
INB4EU-CB-048	483	24.90	1	200	48	293.3	8352.4		1			MU
INB4EU-CB-049	484	24.90	1	200	48	293.3	8352.4		1			MU
INB4EU-CB-050	486	24.90	1	200	48	293.3	8352.4		1			MU

Anony. Name	ID	D [m]	U [-]	V [km/h]	N [-]	d_{max} [m]	P [kN]	Series				Subtype
								Symm	NonSymm	Short	EndTr	
INB4EU-CB-051	506	26.20	1	250	28	178.9	4626.7		1			RP
INB4EU-CB-052	509	26.20	2	250	56	365.7	9253.4		1			CMU-2-RP
INB4EU-CB-053	511	25.90	1	250	28	177.1	4520.0	1				RP
INB4EU-CB-054	512	26.40	1	250	64	402.5	10280.0	1			1	LH-bLL
INB4EU-CB-055	513	25.90	2	250	56	361.5	8135.1		1			CMU-2-RP
INB4EU-CB-056	514	28.75	1	250	28	194.3	5202.8		1			RP
INB4EU-CB-057	515	28.90	1	250	28	194.3	5202.8		1			RP
INB4EU-CB-058	516	28.75	2	250	56	395.6	10405.6		1			CMU-RP
INB4EU-CB-059	517	28.75	2	250	56	395.6	10405.6	1				CMU-RP
INB4EU-CB-060	518	28.75	2	250	56	395.6	10405.6	1				CMU-RP
INB4EU-CB-061	519	28.75	2	250	56	395.6	10405.6		1			CMU-RP
INB4EU-CB-062	521	28.75	1	250	48	338.1	9053.4		1			RP
INB4EU-CB-063	567	23.10	1	163	20	110.8	2403.6	1		1		RP
INB4EU-CB-064	570	26.10	1	200	20	124.0	2544.6		1	1		RP
INB4EU-CB-065	581	23.20	1	196	44	241.3	5270.2		1		1	LH-rHL
INB4EU-CB-066	607	23.00	1	202	20	110.7	3014.4		1	1		RP
INB4EU-CB-067	616	23.00	1	192	20	110.4	2468.1		1	1		RP
INB4EU-CB-068	620	22.90	1	178	16	86.9	2120.3		1	1		RP
INB4EU-CB-069	627	20.00	1	219	24	116.8	2840.3		1	1		RP
INB4EU-CB-070	639	20.40	1	162	32	159.6	3605.8		1			RP
INB4EU-CB-071	647	26.00	1	200	36	228.4	4511.4		1			RP
INB4EU-CB-072	652	26.00	1	164	20	123.6	2527.4	1		1		RP
INB4EU-CB-073	667	25.90	1	197	40	251.8	4981.0		1			MU
INB4EU-CB-074	680	23.00	1	186	20	110.5	2759.2		1	1		RP
INB4EU-CB-075	686	23.30	1	179	44	241.5	5440.1		1		1	LH-fHL
INB4EU-CB-076	692	23.40	1	201	44	242.8	5705.4		1		1	LH-fHL
INB4EU-CB-077	697	23.00	1	163	36	191.6	3855.1		1		1	LH-bHL
INB4EU-CB-078	704	26.00	1	200	40	253.4	5079.7		1			MU
INB4EU-CB-079	706	24.80	1	224	64	391.9	9884.4		1			RP
INB4EU-CB-080	724	26.40	1	200	44	271.2	6166.8		1		1	LH-bLL
INB4EU-CB-081	725	26.40	1	200	40	251.0	5705.5		1		1	LH-rHL
INB4EU-CB-082	726	26.40	1	200	40	251.5	5725.1		1		1	LH-rHL
INB4EU-CB-083	727	23.90	1	220	36	210.9	4951.1		1			RP
INB4EU-CB-084	728	23.90	1	220	44	258.7	6065.5		1			RP
INB4EU-CB-085	729	26.40	3	200	8	48.9	1620.1		1	1		CMU-RP
INB4EU-CB-086	730	26.40	3	200	12	75.3	2398.2		1	1		CMU-RP
INB4EU-CB-087	735	25.90	2	230	20	125.3	3194.1		1	1		CMU-RP
INB4EU-CB-088	777	26.40	1	280	56	350.5	8921.3		1		1	LH-bHL
INB4EU-CB-089	780	26.40	1	280	64	403.3	10129.4		1		1	LH-bHL
INB4EU-CB-090	781	26.40	1	280	32	198.3	4731.7		1		1	LH-rHL
INB4EU-CB-091	783	24.78	1	330	32	193.3	5125.5	1				RP
INB4EU-CB-092	784	28.60	1	250	48	338.1	7674.3		1			RP
INB4EU-CB-093	786	26.50	1	230	32	199.0	4764.4		1		1	LH-rHL
INB4EU-CB-094	800	26.40	1	220	32	198.7	5170.7		1		1	LH-rHL
INB4EU-CB-095	815	28.75	1	265	52	366.8	8363.7		1			RP
INB4EU-CB-096	816	28.75	1	265	56	395.6	8892.5		1			RP
INB4EU-CB-097	819	25.29	1	200	24	152.1	3297.2		1	1	1	LH-bHL
INB4EU-CB-098	825	23.80	1	200	16	93.1	2815.9		1	1		MU
INB4EU-CB-099	826	24.90	1	200	32	192.7	5536.5		1			MU
INB4EU-CB-100	828	24.90	1	200	48	293.3	8352.4		1			MU

Anony. Name	ID	D [m]	U [-]	V [km/h]	N [-]	d_{max} [m]	P [kN]	Series				Subtype
								Symm	NonSymm	Short	EndTr	
INB4EU-CB-101	829	24.90	1	200	48	293.3	8352.4		1			MU
INB4EU-CB-102	830	24.90	1	200	48	293.3	8352.4		1			MU
INB4EU-CB-103	831	24.90	1	200	48	293.3	8352.4		1			MU
INB4EU-CB-104	832	24.90	1	200	48	293.3	8352.4		1			MU
INB4EU-CB-105	834	24.90	1	200	48	293.3	8352.4		1			MU
INB4EU-CB-106	848	26.20	1	250	28	178.9	4626.7		1			RP
INB4EU-CB-107	850	26.20	2	250	56	365.7	9253.4		1			CMU-2-RP
INB4EU-CB-108	851	25.90	2	250	56	361.5	8135.1		1			CMU-2-RP
INB4EU-CB-109	852	28.75	1	250	28	194.3	5202.8		1			RP
INB4EU-CB-110	853	28.90	1	250	28	194.3	5202.8		1			RP
INB4EU-CB-111	854	28.75	2	250	56	395.6	10405.6		1			CMU-RP
INB4EU-CB-112	855	28.75	2	250	56	395.6	10405.6		1			CMU-RP
INB4EU-CB-113	857	28.75	1	250	48	338.1	9053.4		1			RP
INB4EU-CB-114	881	23.20	1	196	44	241.3	5270.2		1		1	LH-fHL
INB4EU-CB-115	893	23.00	1	202	20	110.7	3014.4		1	1		RP
INB4EU-CB-116	899	23.00	1	192	20	110.4	2468.1		1	1		RP
INB4EU-CB-117	901	22.90	1	178	16	86.9	2120.3		1	1		RP
INB4EU-CB-118	906	20.00	1	219	24	116.8	2840.3		1	1		RP
INB4EU-CB-119	915	20.40	1	162	32	159.6	3605.8		1			RP
INB4EU-CB-120	921	26.00	1	200	36	228.4	4511.4		1			RP
INB4EU-CB-121	931	25.90	1	197	40	251.8	4981.0		1			MU
INB4EU-CB-122	938	23.00	1	186	20	110.5	2759.2		1	1		RP
INB4EU-CB-123	943	23.30	1	179	44	241.5	5440.1		1		1	LH-rHL
INB4EU-CB-124	948	23.40	1	201	44	242.8	5705.4		1		1	LH-rHL
INB4EU-CB-125	951	23.00	1	163	36	191.6	3855.1		1		1	LH-bHL
INB4EU-CB-126	956	26.00	1	200	40	253.4	5079.7		1			MU
INB4EU-CB-127	957	24.80	1	224	64	391.9	9884.4		1			RP
INB4EU-CB-128	985	25.90	3	230	60	390.5	9582.3		1			CMU
INB4EU-CB-129	999	26.40	3	200	24	159.1	4860.3		1		1	CMU
INB4EU-CB-130	1001	26.40	3	200	28	185.5	5638.4		1			CMU
INB4EU-CB-131	1007	26.40	3	200	28	185.5	5638.4		1		1	CMU
INB4EU-CB-132	1009	26.40	3	200	32	211.9	6416.4		1			CMU
INB4EU-CB-133	1031	26.40	3	200	28	185.5	5638.4		1		1	CMU
INB4EU-CB-134	1033	26.40	3	200	32	211.9	6416.4		1			CMU
INB4EU-CB-135	1039	26.40	3	200	32	211.9	6416.4		1		1	CMU
INB4EU-CB-136	1041	26.40	3	200	36	238.3	7194.5		1			CMU
INB4EU-CB-137	2062	26.50	2	230	64	404.1	9528.7		1			Irregular
INB4EU-CB-138	2063	26.50	2	230	64	403.8	9528.7	1			1	CLH-bHL
INB4EU-CB-139	2064	26.50	2	230	64	404.5	9528.7	1				Irregular
INB4EU-CB-140	2065	26.50	2	230	64	404.1	9528.7		1		1	Irregular
INB4EU-CB-141	2839	25.78	2	250	32	206.5	5400.4	1				CMU-2-RP
INB4EU-CB-142	2915	24.04	2	200	48	293.9	6287.5	1			1	CLH-mHL
INB4EU-CB-143	2916	24.04	2	200	40	244.2	5386.7		1		1	CLH-mHL
INB4EU-CB-144	2918	24.04	2	200	40	244.2	5386.7		1		1	CLH-mHL
INB4EU-CB-145	2919	24.04	2	200	32	194.6	4485.9	1			1	CLH-mHL
INB4EU-CB-146	2924	25.29	3	200	64	418.9	8920.2		1		1	CLH-mHL
INB4EU-CB-147	2926	25.29	3	200	64	418.9	8920.2		1		1	CLH-mHL
INB4EU-CB-148	2928	25.29	3	200	56	365.9	7948.6		1		1	CLH-mHL
INB4EU-CB-149	2934	25.29	3	200	64	418.9	8920.2		1		1	CLH-mHL
INB4EU-CB-150	2936	25.29	3	200	56	365.9	7948.6		1		1	CLH-mHL

Anony. Name	ID	D [m]	U [-]	V [km/h]	N [-]	d_{max} [m]	P [kN]	Series				Subtype
								Symm	NonSymm	Short	EndTr	
INB4EU-CB-151	2940	25.29	3	200	56	365.9	7948.6		1		1	CLH-mHL
INB4EU-CB-152	2942	25.29	3	200	48	313.0	6977.1	1			1	CLH-mHL
INB4EU-CB-153	2956	25.63	3	200	48	309.3	7947.6	1				CMU
INB4EU-CB-154	2957	25.63	3	200	52	335.3	8575.6		1			CMU
INB4EU-CB-155	2958	25.63	3	200	56	361.3	9202.8		1			CMU
INB4EU-CB-156	2959	25.63	3	200	52	335.3	8575.6	1				CMU
INB4EU-CB-157	2960	25.63	3	200	56	361.3	9203.6		1			CMU
INB4EU-CB-158	2961	25.63	3	200	60	387.3	9830.8		1			CMU
INB4EU-CB-159	2962	25.63	3	200	56	361.3	9202.8	1				CMU
INB4EU-CB-160	2963	25.63	3	200	60	387.3	9830.8		1			CMU
INB4EU-CB-161	2964	25.63	3	200	64	413.3	10458.0		1			CMU
INB4EU-CB-162	2965	25.63	3	200	52	335.3	8575.6		1			CMU
INB4EU-CB-163	2966	25.63	3	200	56	361.3	9203.6	1				CMU
INB4EU-CB-164	2967	25.63	3	200	60	387.3	9830.8		1			CMU
INB4EU-CB-165	2968	25.63	3	200	56	361.3	9203.6		1			CMU
INB4EU-CB-166	2969	25.62	3	200	60	387.3	9831.6	1				CMU
INB4EU-CB-167	2970	25.63	3	200	64	413.3	10458.8		1			CMU
INB4EU-CB-168	2971	25.63	3	200	60	387.3	9830.8		1			CMU
INB4EU-CB-169	2972	25.63	3	200	64	413.3	10458.8	1				CMU
INB4EU-CB-170	2973	25.63	3	200	56	361.3	9202.8		1			CMU
INB4EU-CB-171	2974	25.63	3	200	60	387.3	9830.8		1			CMU
INB4EU-CB-172	2975	25.63	3	200	64	413.3	10458.0	1				CMU
INB4EU-CB-173	2976	25.63	3	200	60	387.3	9830.8		1			CMU
INB4EU-CB-174	2977	25.63	3	200	64	413.3	10458.8		1			CMU
INB4EU-CB-175	2978	25.63	3	200	64	413.3	10458.0		1			CMU
INB4EU-CB-176	2979	25.63	3	200	48	313.2	7947.6	1				CMU
INB4EU-CB-177	2980	25.63	3	200	52	339.8	8575.6		1			CMU
INB4EU-CB-178	2981	25.63	3	200	56	366.4	9202.8		1			CMU
INB4EU-CB-179	2982	25.63	3	200	52	339.8	8575.6	1				CMU
INB4EU-CB-180	2983	25.63	3	200	56	366.4	9203.6		1			CMU
INB4EU-CB-181	2984	25.63	3	200	60	393.0	9830.8		1			CMU
INB4EU-CB-182	2985	25.63	3	200	56	366.4	9202.8	1				CMU
INB4EU-CB-183	2986	25.63	3	200	60	393.0	9830.8		1			CMU
INB4EU-CB-184	2987	25.63	3	200	64	419.6	10458.0		1			CMU
INB4EU-CB-185	2988	25.63	3	200	52	339.8	8575.6		1			CMU
INB4EU-CB-186	2989	25.63	3	200	56	366.4	9203.6	1				CMU
INB4EU-CB-187	2990	25.63	3	200	60	393.0	9830.8		1			CMU
INB4EU-CB-188	2991	25.63	3	200	56	366.4	9203.6		1			CMU
INB4EU-CB-189	2992	25.62	3	200	60	393.0	9831.6	1				CMU
INB4EU-CB-190	2993	25.62	3	200	64	419.6	10458.8		1			CMU
INB4EU-CB-191	2994	25.63	3	200	60	393.0	9830.8		1			CMU
INB4EU-CB-192	2995	25.62	3	200	64	419.6	10458.8	1				CMU
INB4EU-CB-193	2996	25.63	3	200	56	366.4	9202.8		1			CMU
INB4EU-CB-194	2997	25.63	3	200	60	393.0	9830.8		1			CMU
INB4EU-CB-195	2998	25.63	3	200	64	419.6	10458.0	1				CMU
INB4EU-CB-196	2999	25.63	3	200	60	393.0	9830.8		1			CMU
INB4EU-CB-197	3000	25.62	3	200	64	419.6	10458.8		1			CMU
INB4EU-CB-198	3001	25.63	3	200	64	419.6	10458.0		1			CMU
INB4EU-CB-199	3007	25.90	2	220	48	310.1	6788.3	1				CMU-2-RP
INB4EU-CB-200	3012	27.16	2	200	32	212.3	5144.0		1			CMU-2-RP
INB4EU-CB-201	3016	26.02	3	200	48	313.1	7444.2	1				CMU

Articulated trains (AB)

Anony. Name	ID	D [m]	U [-]	V [km/h]	N [-]	d_{max} [m]	P [kN]	Series				Subtype
								Symm	NonSymm	Short	EndTr	
INB4EU-AB-001	5	17.30	1	300	24	192.9	4068.0	1				RP
INB4EU-AB-002	82	18.50	1	200	14	101	2483.1		1	1		CART
INB4EU-AB-003	85	18.50	1	200	20	156.5	3575.5		1			CART
INB4EU-AB-004	132	18.98	1	320	26	193.15	4694.1	1			1	ALH
INB4EU-AB-005	282	10.02	1	200	18	104.13	3122.3		1	1		CART
INB4EU-AB-006	341	18.98	1	320	48	386.68	6852.4		1		1	ALH-rLL
INB4EU-AB-007	342	18.97	1	320	20	154.17	3362.0		1		1	ALH
INB4EU-AB-008	343	18.97	1	320	26	193.14	3854.3	1			1	ALH-bHL
INB4EU-AB-009	398	17.50	1	250	24	193.6	4292.4		1			ART
INB4EU-AB-010	463	15.75	1	200	14	98.7	2362.2		1	1		ART
INB4EU-AB-011	497	17.50	2	250	48	395.6	8671.6		1			CART-2-ART
INB4EU-AB-012	501	17.50	1	250	24	193.6	4375.8		1			ART
INB4EU-AB-013	503	17.50	2	250	48	395.6	8751.6	1				CART-2-ART
INB4EU-AB-014	734	18.50	3	200	14	101	2483.1		1	1		CART
INB4EU-AB-015	790	10.02	2	200	18	104.13	3122.3		1	1		CART
INB4EU-AB-016	811	18.98	1	320	48	386.68	6852.4		1		1	ALH-fLL
INB4EU-AB-017	812	18.97	1	320	20	154.17	3362.0		1		1	ALH
INB4EU-AB-018	820	17.50	1	250	24	193.6	4292.4		1			ART
INB4EU-AB-019	821	15.75	1	200	14	98.7	2362.2		1	1		ART
INB4EU-AB-020	844	17.50	2	250	48	395.6	8671.6		1			CART-2-ART
INB4EU-AB-021	969	18.50	3	200	42	319.8	7449.4		1		1	CART
INB4EU-AB-022	970	18.50	3	200	42	319.8	7449.4		1			CART
INB4EU-AB-023	971	18.50	3	200	42	319.8	7449.4		1		1	CART
INB4EU-AB-024	972	18.50	3	200	42	319.8	7449.4		1			CART
INB4EU-AB-025	973	18.50	3	200	42	319.8	7449.4		1		1	CART
INB4EU-AB-026	974	18.50	3	200	42	319.8	7449.4		1			CART
INB4EU-AB-027	975	18.50	3	200	42	319.8	7449.4		1		1	CART
INB4EU-AB-028	976	18.50	3	200	42	319.8	7449.4		1			CART
INB4EU-AB-029	2504	10.02	3	200	54	323.95	9367.0		1		1	CART
INB4EU-AB-030	2505	10.02	3	200	54	323.95	9367.0		1		1	CART
INB4EU-AB-031	2512	10.02	3	200	54	323.95	9367.0		1		1	CART
INB4EU-AB-032	2513	10.02	3	200	54	323.95	9367.0		1		1	CART
INB4EU-AB-033	2568	10.02	3	200	54	323.95	9367.0		1		1	CART
INB4EU-AB-034	2569	10.02	3	200	54	323.95	9367.0		1		1	CART
INB4EU-AB-035	2576	10.02	3	200	54	323.95	9367.0		1		1	CART
INB4EU-AB-036	2577	10.02	3	200	54	323.95	9367.0		1		1	CART
INB4EU-AB-037	2951	17.50	2	250	48	395.6	8584.7		1			CART-2-ART
INB4EU-AB-038	2954	17.50	2	250	48	395.6	8584.7		1			CART-2-ART
INB4EU-AB-039	3014	18.98	2	320	52	393.34	9388.2	1			1	CALH-2-ALH

Regular trains (SA)

Anony. Name	ID	D [m]	U [-]	V [km/h]	N [-]	d_{max} [m]	P [kN]	Series				Subtype
								Symm	NonSymm	Short	EndTr	
INB4EU-SA-001	273	13.22	1	330	21	193.8	3690.5		1		1	RLH-bL
INB4EU-SA-002	330	13.14	1	250	20	175.2	3358.9		1		1	RLH-sCbL
INB4EU-SA-003	331	13.14	1	250	22	176.9	3822.0		1		1	RLH-sCbL
INB4EU-SA-004	332	13.14	1	300	21	191.3	3530.6		1		1	RLH-sCbL
INB4EU-SA-005	522	13.30	1	230	12	122.8	2421.1	1		1		RP
INB4EU-SA-006	523	13.30	1	230	13	136.1	2633.0	1		1		RP
INB4EU-SA-007	524	13.31	1	230	14	149.4	2844.9	1		1		RP
INB4EU-SA-008	525	13.31	1	230	15	162.7	3056.8	1				RP
INB4EU-SA-009	526	13.31	1	230	16	176.0	3268.7	1				RP
INB4EU-SA-010	527	13.31	1	230	17	189.3	3480.6	1				RP
INB4EU-SA-011	528	13.31	1	230	18	202.6	3692.5	1				RP
INB4EU-SA-012	529	13.31	1	230	19	215.9	3904.4	1				RP
INB4EU-SA-013	530	13.31	1	230	20	229.2	4116.3	1				RP
INB4EU-SA-014	531	13.31	1	230	21	242.5	4328.2	1				RP
INB4EU-SA-015	532	13.31	1	230	22	255.8	4540.1	1				RP
INB4EU-SA-016	533	13.31	1	230	23	269.1	4752.0	1				RP
INB4EU-SA-017	534	13.31	1	230	24	282.4	4963.9	1				RP
INB4EU-SA-018	535	13.30	1	230	28	301.8	5778.1		1			RLH-fL
INB4EU-SA-019	536	13.30	1	230	28	302.2	5846.8		1			RLH-fL
INB4EU-SA-020	537	13.30	1	230	32	320.7	6592.3		1			RLH-2fL
INB4EU-SA-021	538	13.30	1	230	32	321.9	6729.7		1			RLH-2fL
INB4EU-SA-022	539	13.30	1	230	32	321.3	6592.3	1			1	RLH-bL
INB4EU-SA-023	540	13.30	1	230	32	322.1	6729.7	1			1	RLH-bL
INB4EU-SA-024	541	13.30	1	230	32	321.5	6661.0		1			RLH-2fL
INB4EU-SA-025	542	13.30	1	230	36	340.4	7475.2		1			RLH-3fL
INB4EU-SA-026	543	13.30	1	230	32	321.7	6661.0		1		1	RLH-bL
INB4EU-SA-027	544	13.30	1	230	36	340.6	7475.2		1		1	RLH-2fLrL
INB4EU-SA-028	545	13.30	1	230	36	341.0	7475.2		1		1	RLH-2fLrL
INB4EU-SA-029	546	13.30	1	230	36	340.6	7475.2		1		1	RLH-2fLrL
INB4EU-SA-030	861	13.30	1	230	28	301.8	5778.1		1		1	RLH-rL
INB4EU-SA-031	862	13.30	1	230	28	302.2	5846.8		1		1	RLH-rL
INB4EU-SA-032	863	13.30	1	230	32	320.7	6592.3		1		1	RLH-2rL
INB4EU-SA-033	864	13.30	1	230	32	321.9	6729.7		1		1	RLH-2rL
INB4EU-SA-034	865	13.30	1	230	32	321.5	6661.0		1		1	RLH-2rL
INB4EU-SA-035	866	13.30	1	230	36	340.4	7475.2		1		1	RLH-3rL
INB4EU-SA-036	867	13.30	1	230	32	321.7	6661.0		1		1	RLH-bL
INB4EU-SA-037	868	13.30	1	230	36	340.6	7475.2		1		1	RLH-fL2rL
INB4EU-SA-038	869	13.30	1	230	36	341.0	7475.2		1		1	RLH-fL2rL
INB4EU-SA-039	870	13.30	1	230	36	340.6	7475.2		1		1	RLH-fL2rL
INB4EU-SA-040	3017	13.22	2	330	42	395.7	7381.0		1		1	CRLH-mL

Appendix C — Freight trains: anonymous description

Anony. Name	ID	D [m]	N [-]	d_{max} [m]	P [kN]	Wagon
INB4EU-FT-001	100230	26.44	128	618.81	13562.8	Twin_Wagon_conv
INB4EU-FT-002	106059	29.64	124	633.81	12941.9	Twin_Wagon_conv
INB4EU-FT-003	115039	9.64	84	400.07	15144.3	Regular
INB4EU-FT-004	126087	13.50	52	331.31	6394.7	Regular
INB4EU-FT-005	121754	13.52	122	629.60	7566.3	Regular
INB4EU-FT-006	115943	15.49	92	694.83	11604.9	Regular
INB4EU-FT-007	125137	16.70	40	296.31	6234.1	Regular
INB4EU-FT-008	116551	36.94	72	533.45	7146.8	Regular
INB4EU-FT-009	96529	13.87	8	29.73	1669.5	Conventional
INB4EU-FT-010	87184	16.08	8	32.16	1667.6	Conventional
INB4EU-FT-011	41339	20.57	12	64.06	1268.8	Conventional
INB4EU-FT-012	38902	15.84	28	122.22	5912.2	Conventional
INB4EU-FT-013	85438	23.37	28	154.28	5961.8	Conventional
INB4EU-FT-014	85483	8.41	62	287.60	11274.1	Conventional
INB4EU-FT-015	60020	9.68	64	310.27	6572.5	Conventional
INB4EU-FT-016	117	11.95	138	497.51	29086.0	Conventional
INB4EU-FT-017	74471	13.13	76	250.62	14422.8	Conventional
INB4EU-FT-018	19416	13.51	100	346.36	21474.7	Conventional
INB4EU-FT-019	88801	14.12	52	183.60	8970.6	Conventional
INB4EU-FT-020	13057	15.40	92	360.85	17769.9	Conventional
INB4EU-FT-021	42722	15.55	56	243.70	10986.0	Conventional
INB4EU-FT-022	80713	16.89	48	195.45	10089.7	Conventional
INB4EU-FT-023	5132	17.51	88	449.57	7388.6	Conventional
INB4EU-FT-024	34854	19.85	92	450.50	16017.9	Conventional
INB4EU-FT-025	75696	19.91	44	219.84	7115.9	Conventional
INB4EU-FT-026	40048	20.00	120	592.13	16204.2	Conventional
INB4EU-FT-027	13364	21.63	92	464.44	18399.5	Conventional
INB4EU-FT-028	42440	22.42	60	328.33	12242.9	Conventional
INB4EU-FT-029	59970	23.37	92	516.46	19926.0	Conventional
INB4EU-FT-030	74931	24.29	114	649.39	14649.8	Conventional

Appendix D — Definition of PT60 trains

PT60 model has a total of 60 different passenger trains among CB, AB and SA types, will all its main subtypes (including a variety of loco-hauled cases). Both shorter and longer trains have been considered in it, with car lengths D covering a range as wide as possible. The 10 HSLM-A have also been included. Among similar trains, those with stronger signature have been retained. Relevant trains mentioned in discussion with other partners of *InBridge4EU* have been also included.

The organisation of PT60 begins with the trains more regular as regards the axle distances, and gradually incorporates vehicles where the patterns of distances are more irregular, ending with loco-hauled trains and trains with intermediate power cars.

In an anonymous manner, the trains contained in model PT60 are described here. A summary of the PT60 vehicles follows:

- Ten (10) RPs of CB, AB and SA type, with $13.31 \le D \le 28.8$ m (in ascending order of D).
- One (1) ART train with $D = 15.8$ m.
- Two (2) CMU-2-RP trains with $D = 26.2$ m and with $D = 27.2$ m (in ascending order of D).
- One (1) CART-2-ART train with $D = 17.5$ m.
- Four (4) MU trains, with $23.8 \le D \le 25.9$ m (in ascending order of D).
- Four (4) CMU trains, with $25.6 \le D \le 26.4$ m (in ascending order of D).
- Five (5) CART trains, with either $D = 10.0$ m or $D = 18.5$ m (in ascending order of D).
- One (1) ALH train with $D = 19.0$ m.
- Ten (10) additional ALH trains with $18.0 \le D \le 27.0$ m (HSLM-A model).
- Twenty-two (22) trains with various loco-hauled configurations, including the following subtypes in order: CALH-2-ALH, ALH-fLL, LH-fHL, RLH-2fL, LH-rHL, RLH-3rL, RLH-bL, RLH-sCbL, RLH-2fLrL, LH-fHLrLL, ALH-bHL, LH-bHL, CLH-bHL, CRLH-mL, CLH-mHL, Irregular (some subtypes are represented by more than one train, of significantly different D, or total length).

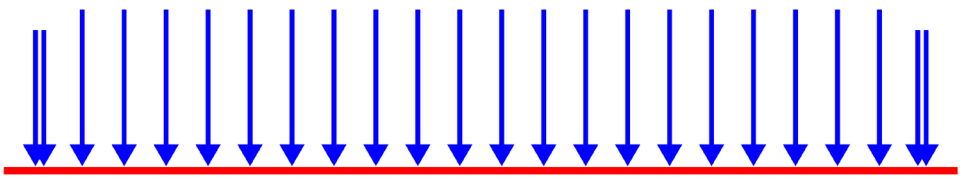

$L_{tot} = 282.4\,m$
$D = 13.3\,m$
$P_{max} = 211.9\,kN$
$P_{min} = 181.5\,kN$
$P_{tot} = 4964\,kN$

Figure Train PT60-01 [INB4EU-SA-017]

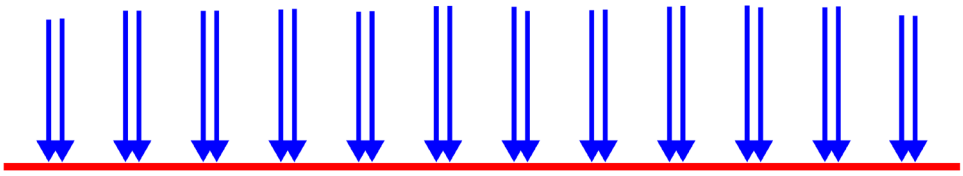

$L_{tot} = 192.9\,m$
$D = 17.3\,m$
$P_{max} = 175.0\,kN$
$P_{min} = 157.8\,kN$
$P_{tot} = 4068\,kN$

Figure Train PT60-02 [INB4EU-AB-001]

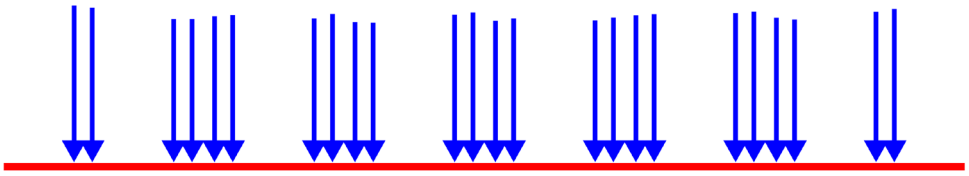

$L_{tot} = 116.8\,m$
$D = 20.0\,m$
$P_{max} = 127.4\,kN$
$P_{min} = 112.1\,kN$
$P_{tot} = 2840\,kN$

Figure Train PT60-03 [INB4EU-CB-069]

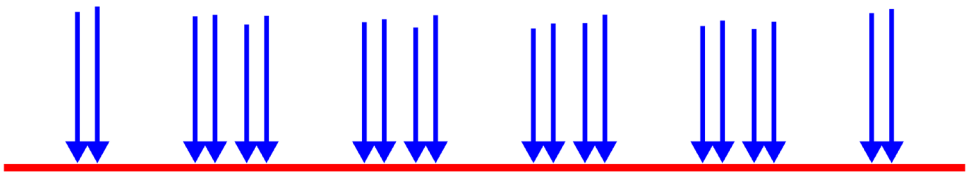

$L_{tot} = 110.7\,m$
$D = 23.0\,m$
$P_{max} = 165.4\,kN$
$P_{min} = 139.3\,kN$
$P_{tot} = 3014\,kN$

Figure Train PT60-04 [INB4EU-CB-066]

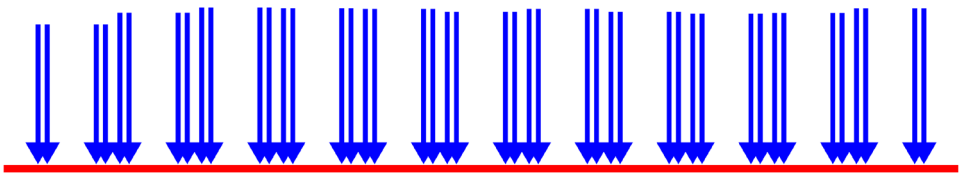

$L_{tot} = 258.7\,m$
$D = 23.9\,m$
$P_{max} = 142.0\,kN$
$P_{min} = 125.2\,kN$
$P_{tot} = 6065\,kN$

Figure Train PT60-05 [INB4EU-CB-084]

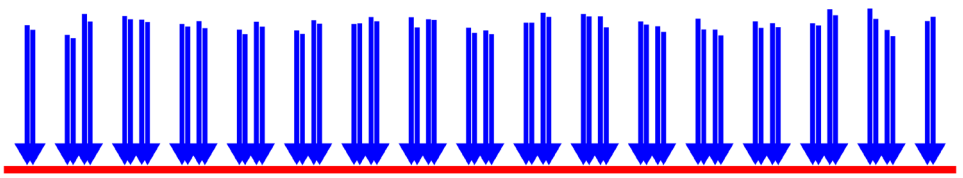

$L_{tot} = 391.9\,m$
$D = 24.8\,m$
$P_{max} = 173.0\,kN$
$P_{min} = 137.0\,kN$
$P_{tot} = 9884\,kN$

Figure Train PT60-06 [INB4EU-CB-127]

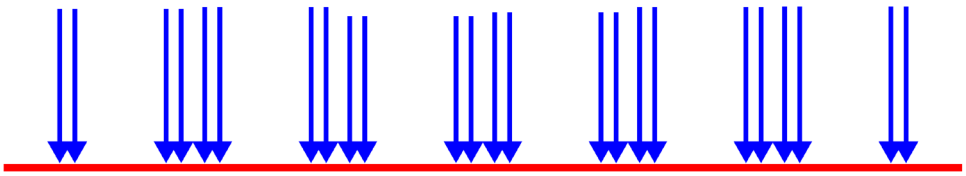

$L_{tot} = 151.2\,m$
$D = 25.9\,m$
$P_{max} = 144.6\,kN$
$P_{min} = 134.8\,kN$
$P_{tot} = 3394\,kN$

Figure Train PT60-07 [INB4EU-CB-001]

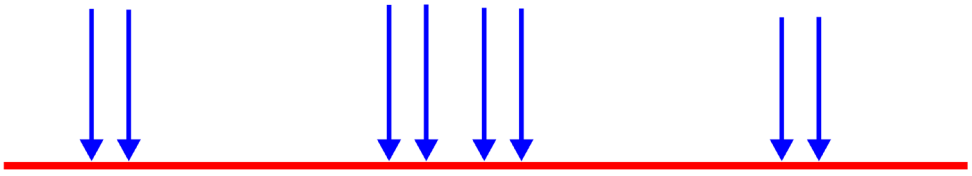

$L_{tot} = 48.9\,m$
$D = 26.4\,m$
$P_{max} = 210.3\,kN$
$P_{min} = 191.4\,kN$
$P_{tot} = 1620\,kN$

Figure Train PT60-08 [INB4EU-CB-007]

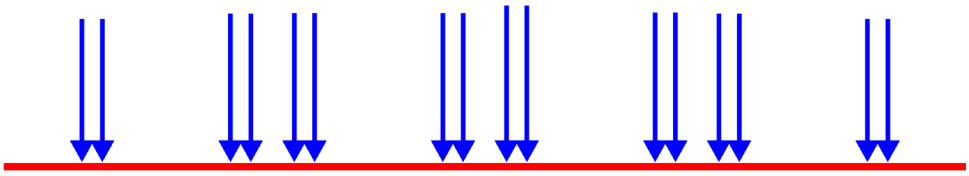

$L_{tot} = 103.1\,m$
$D = 27.2\,m$
$P_{max} = 170.4\,kN$
$P_{min} = 154.4\,kN$
$P_{tot} = 2572\,kN$

Figure Train PT60-09 [INB4EU-CB-009]

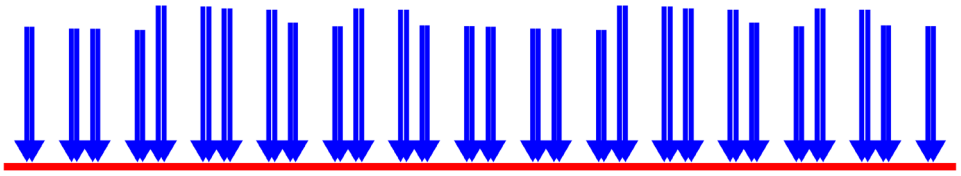

$L_{tot} = 395.6\,m$
$D = 28.8\,m$
$P_{max} = 204.8\,kN$
$P_{min} = 169.6\,kN$
$P_{tot} = 10406\,kN$

Figure Train PT60-10 [INB4EU-CB-111]

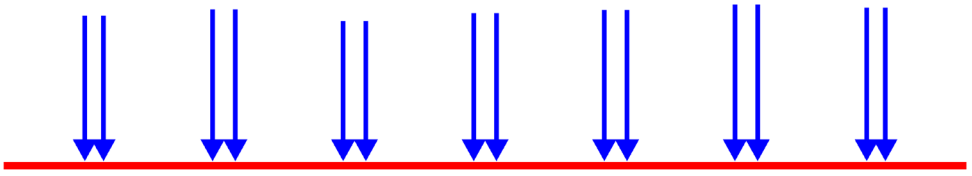

$L_{tot} = 98.7\,m$
$D = 15.8\,m$
$P_{max} = 177.6\,kN$
$P_{min} = 157.0\,kN$
$P_{tot} = 2362\,kN$

Figure Train PT60-11 [INB4EU-AB-019]

$L_{tot} = 365.7\,m$
$D = 26.2\,m$
$P_{max} = 174.1\,kN$
$P_{min} = 151.0\,kN$
$P_{tot} = 9253\,kN$

Figure Train PT60-12 [INB4EU-CB-052]

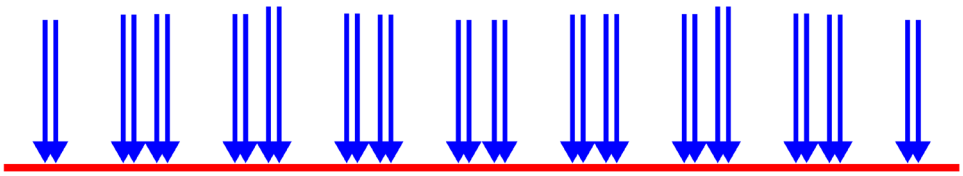

$L_{tot} = 212.3\,m$
$D = 27.2\,m$
$P_{max} = 170.4\,kN$
$P_{min} = 154.4\,kN$
$P_{tot} = 5144\,kN$

Figure Train PT60-13 [INB4EU-CB-200]

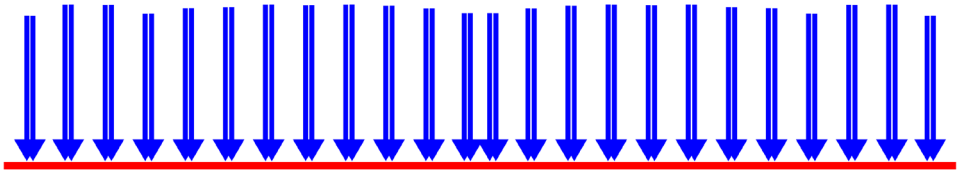

$L_{tot} = 395.6\,m$
$D = 17.5\,m$
$P_{max} = 186.9\,kN$
$P_{min} = 172.2\,kN$
$P_{tot} = 8752\,kN$

Figure Train PT60-14 [INB4EU-AB-013]

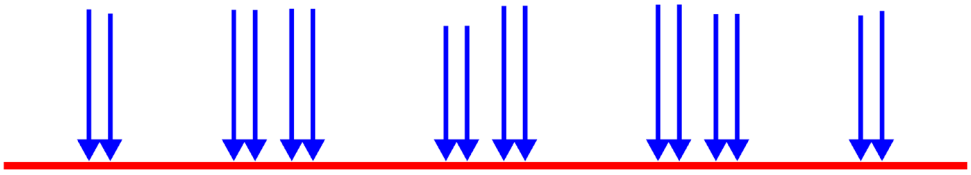

$L_{tot} = 93.1\,m$
$D = 23.8\,m$
$P_{max} = 185.3\,kN$
$P_{min} = 157.3\,kN$
$P_{tot} = 2816\,kN$

Figure Train PT60-15 [INB4EU-CB-098]

$L_{tot} = 293.3\,m$
$D = 24.9\,m$
$P_{max} = 185.3\,kN$
$P_{min} = 150.6\,kN$
$P_{tot} = 8352\,kN$

Figure Train PT60-16 [INB4EU-CB-102]

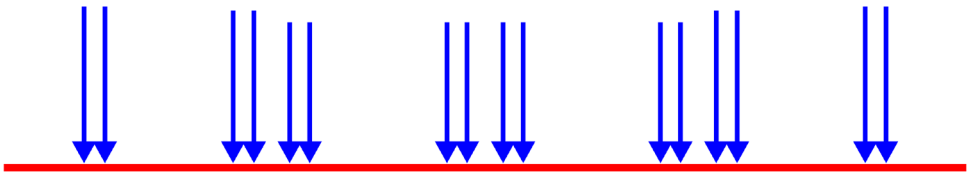

$L_{tot} = 100.0\,m$
$D = 25.6\,m$
$P_{max} = 176.6\,kN$
$P_{min} = 157.0\,kN$
$P_{tot} = 2649\,kN$

Figure Train PT60-17 [INB4EU-CB-037]

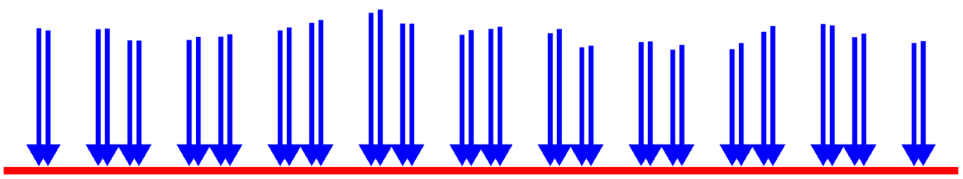

$L_{tot} = 251.8\,m$
$D = 25.9\,m$
$P_{max} = 149.2\,kN$
$P_{min} = 107.0\,kN$
$P_{tot} = 4981\,kN$

Figure Train PT60-18 [INB4EU-CB-073]

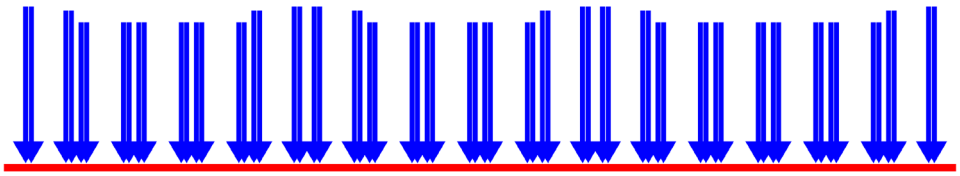

$L_{tot} = 419.6\,m$
$D = 25.6\,m$
$P_{max} = 176.6\,kN$
$P_{min} = 157.0\,kN$
$P_{tot} = 10459\,kN$

Figure Train PT60-19 [INB4EU-CB-190]

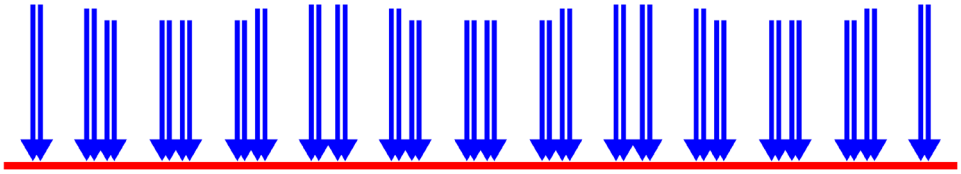

$L_{tot} = 309.3\,m$
$D = 25.6\,m$
$P_{max} = 176.6\,kN$
$P_{min} = 157.0\,kN$
$P_{tot} = 7948\,kN$

Figure Train PT60-20 [INB4EU-CB-153]

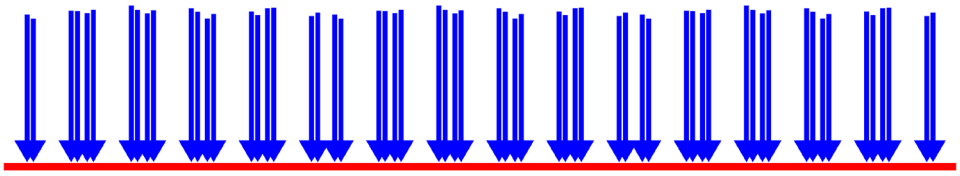

$L_{tot} = 390.5\,m$
$D = 25.9\,m$
$P_{max} = 167.3\,kN$
$P_{min} = 151.9\,kN$
$P_{tot} = 9582\,kN$

Figure Train PT60-21 [INB4EU-CB-128]

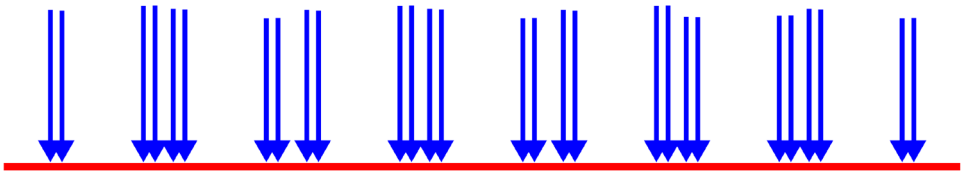

$L_{tot} = 185.5\,m$
$D = 26.4\,m$
$P_{max} = 210.3\,kN$
$P_{min} = 191.4\,kN$
$P_{tot} = 5638\,kN$

Figure Train PT60-22 [INB4EU-CB-130]

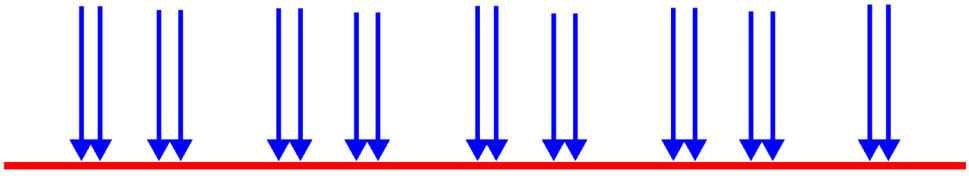

$L_{tot} = 104.1\,m$
$D = 10.0\,m$
$P_{max} = 178.9\,kN$
$P_{min} = 167.6\,kN$
$P_{tot} = 3122\,kN$

Figure Train PT60-23 [INB4EU-AB-05]

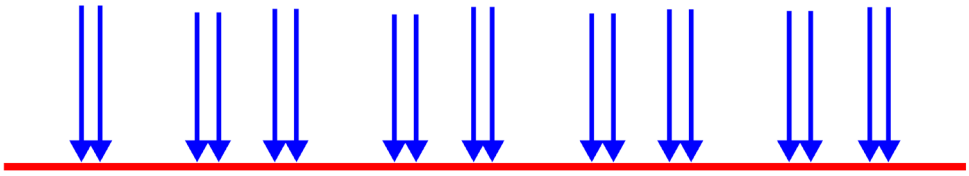

$L_{tot} = 104.1\,m$
$D = 10.0\,m$
$P_{max} = 178.9\,kN$
$P_{min} = 167.6\,kN$
$P_{tot} = 3122\,kN$

Figure Train PT60-24 [INB4EU-AB-015]

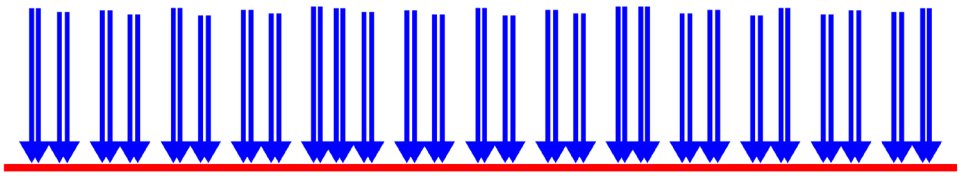

$L_{tot} = 324.0\,m$
$D = 10.0\,m$
$P_{max} = 178.9\,kN$
$P_{min} = 167.6\,kN$
$P_{tot} = 9367\,kN$

Figure Train PT60-25 [INB4EU-AB-030]

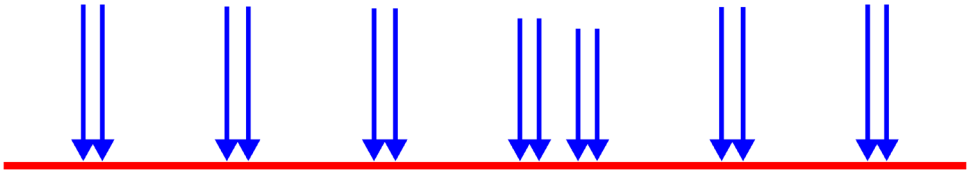

$L_{tot} = 101.0\,m$
$D = 18.5\,m$
$P_{max} = 186.0\,kN$
$P_{min} = 154.5\,kN$
$P_{tot} = 2483\,kN$

Figure Train PT60-26 [INB4EU-AB-002]

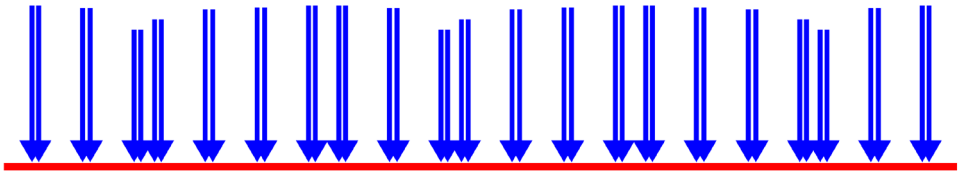

$L_{tot} = 319.8\,m$
$D = 18.5\,m$
$P_{max} = 186.0\,kN$
$P_{min} = 154.5\,kN$
$P_{tot} = 7449\,kN$

Figure Train PT60-27 [INB4EU-AB-027]

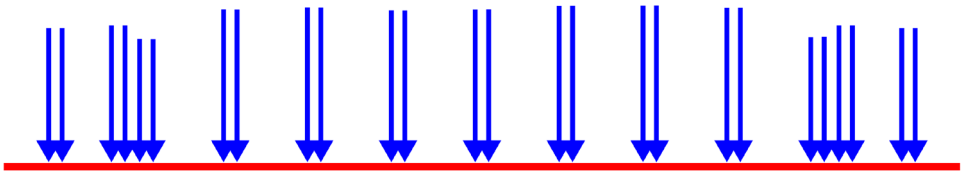

$L_{tot} = 193.2\,m$
$D = 19.0\,m$
$P_{max} = 198.4\,kN$
$P_{min} = 151.5\,kN$
$P_{tot} = 4694\,kN$

Figure Train PT60-28 [INB4EU-AB-004]

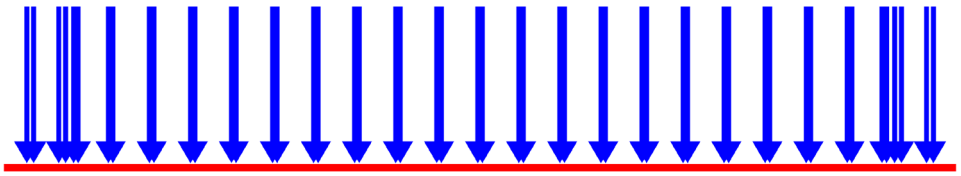

$L_{tot} = 397.5\,m$
$D = 18.0\,m$
$P_{max} = 170.0\,kN$
$P_{min} = 170.0\,kN$
$P_{tot} = 8500\,kN$

Figure Train PT60-29 [HSLM-A1]

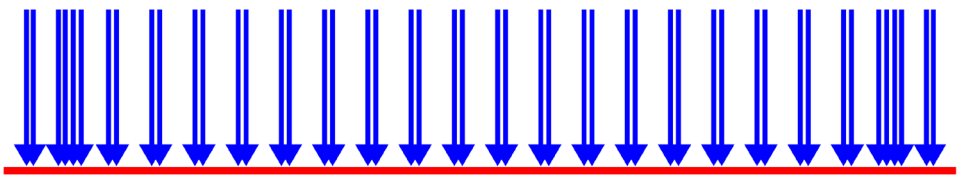

$L_{tot} = 398.5\,m$
$D = 19.0\,m$
$P_{max} = 200.0\,kN$
$P_{min} = 200.0\,kN$
$P_{tot} = 9600\,kN$

Figure Train PT60-30 [HSLM-A2]

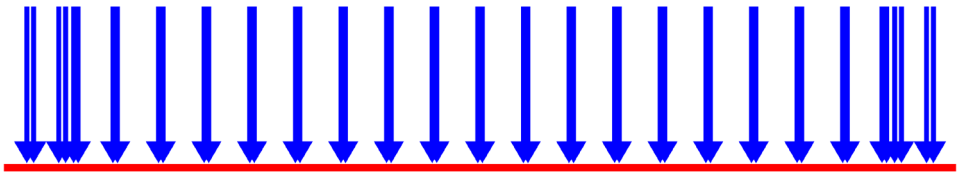

$L_{tot} = 397.5\,\text{m}$
$D = 20.0\,\text{m}$
$P_{max} = 180.0\,\text{kN}$
$P_{min} = 180.0\,\text{kN}$
$P_{tot} = 8280\,\text{kN}$

Figure Train PT60-31 [HSLM-A3]

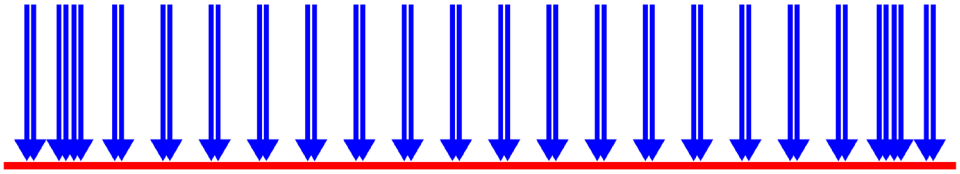

$L_{tot} = 394.5\,\text{m}$
$D = 21.0\,\text{m}$
$P_{max} = 190.0\,\text{kN}$
$P_{min} = 190.0\,\text{kN}$
$P_{tot} = 8360\,\text{kN}$

Figure Train PT60-32 [HSLM-A4]

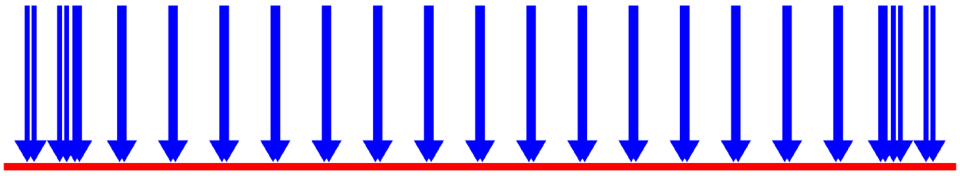

$L_{tot} = 389.5\,\text{m}$
$D = 22.0\,\text{m}$
$P_{max} = 170.0\,\text{kN}$
$P_{min} = 170.0\,\text{kN}$
$P_{tot} = 7140\,\text{kN}$

Figure Train PT60-33 [HSLM-A5]

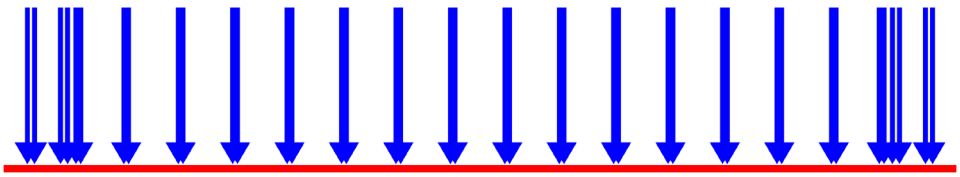

$L_{tot} = 382.5\,\text{m}$
$D = 23.0\,\text{m}$
$P_{max} = 180.0\,\text{kN}$
$P_{min} = 180.0\,\text{kN}$
$P_{tot} = 7200\,\text{kN}$

Figure Train PT60-34 [HSLM-A6]

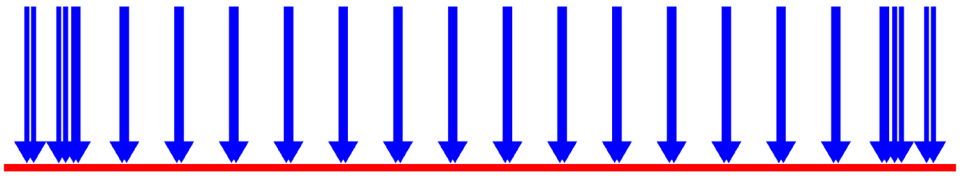

$L_{tot} = 397.5\,\text{m}$
$D = 24.0\,\text{m}$
$P_{max} = 190.0\,\text{kN}$
$P_{min} = 190.0\,\text{kN}$
$P_{tot} = 7600\,\text{kN}$

Figure Train PT60-35 [HSLM-A7]

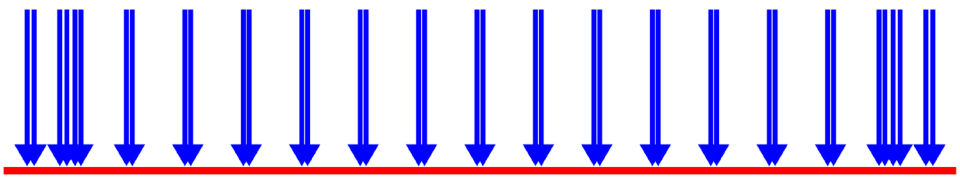

$L_{tot} = 387.5\,\text{m}$
$D = 25.0\,\text{m}$
$P_{max} = 190.0\,\text{kN}$
$P_{min} = 190.0\,\text{kN}$
$P_{tot} = 7220\,\text{kN}$

Figure Train PT60-36 [HSLM-A8]

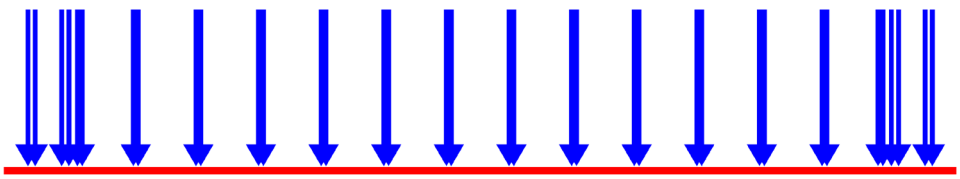

$L_{tot} = 375.5\,m$
$D = 26.0\,m$
$P_{max} = 210.0\,kN$
$P_{min} = 210.0\,kN$
$P_{tot} = 7560\,kN$

Figure Train PT60-37 [HSLM-A9]

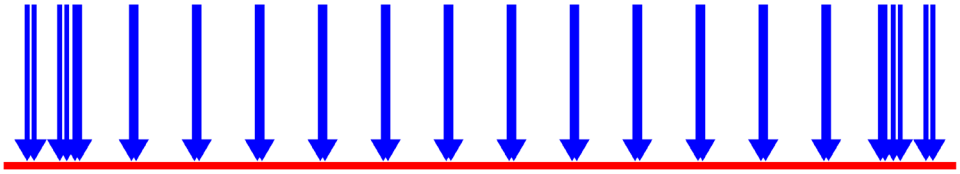

$L_{tot} = 388.5\,m$
$D = 27.0\,m$
$P_{max} = 210.0\,kN$
$P_{min} = 210.0\,kN$
$P_{tot} = 7560\,kN$

Figure Train PT60-38 [HSLM-A10]

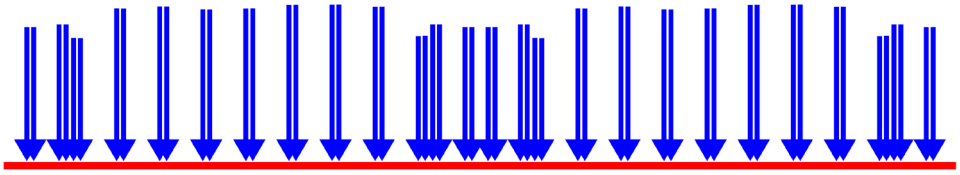

$L_{tot} = 393.3\,m$
$D = 19.0\,m$
$P_{max} = 198.4\,kN$
$P_{min} = 151.5\,kN$
$P_{tot} = 9388\,kN$

Figure Train PT60-39 [INB4EU-AB-039]

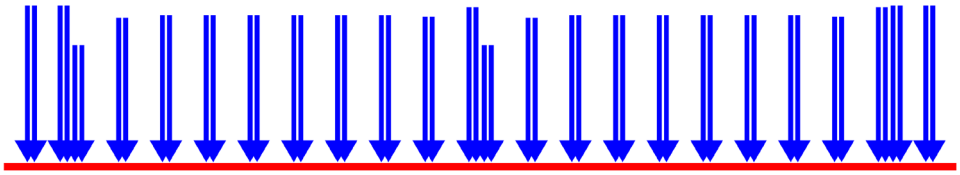

$L_{tot} = 386.7\,m$
$D = 19.0\,m$
$P_{max} = 153.8\,kN$
$P_{min} = 111.0\,kN$
$P_{tot} = 6852\,kN$

Figure Train PT60-40 [INB4EU-AB-016]

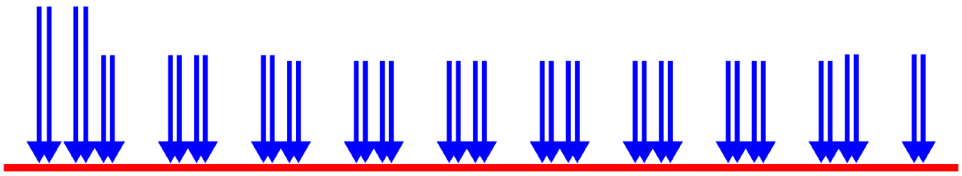

$L_{tot} = 251.0\,m$
$D = 26.4\,m$
$P_{max} = 213.4\,kN$
$P_{min} = 131.8\,kN$
$P_{tot} = 5705\,kN$

Figure Train PT60-41 [INB4EU-CB-003]

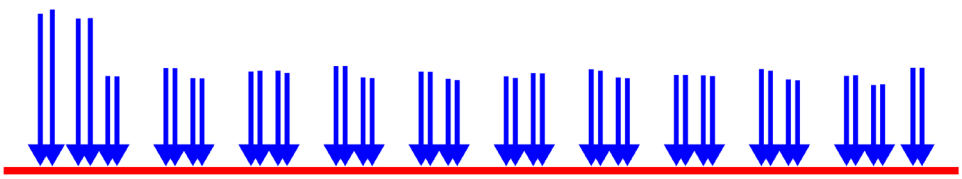

$L_{tot} = 241.5\,m$
$D = 23.3\,m$
$P_{max} = 212.5\,kN$
$P_{min} = 99.5\,kN$
$P_{tot} = 5440\,kN$

Figure Train PT60-42 [INB4EU-CB-075]

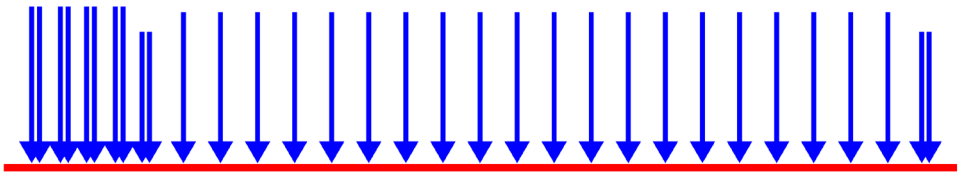

$L_{tot} = 321.9\,m$
$D = 13.3\,m$
$P_{max} = 220.7\,kN$
$P_{min} = 181.5\,kN$
$P_{tot} = 6730\,kN$

Figure Train PT60-43 [INB4EU-SA-021]

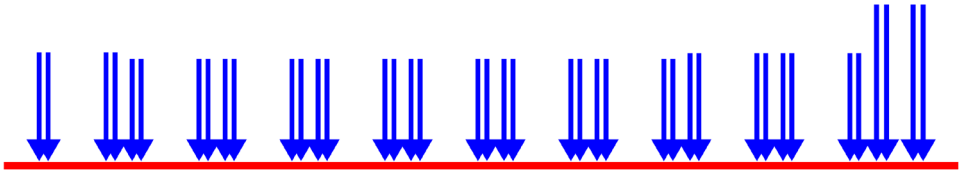

$L_{tot} = 251.0\,m$
$D = 26.4\,m$
$P_{max} = 213.4\,kN$
$P_{min} = 131.8\,kN$
$P_{tot} = 5705\,kN$

Figure Train PT60-44 [INB4EU-CB-081]

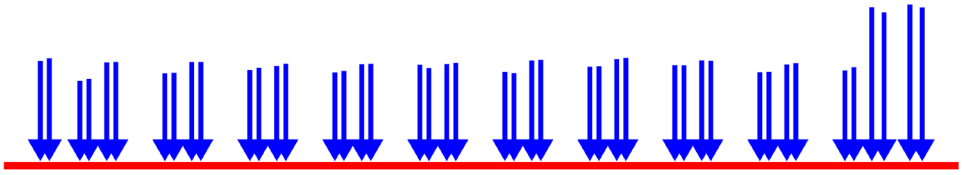

$L_{tot} = 242.8\,m$
$D = 23.4\,m$
$P_{max} = 214.9\,kN$
$P_{min} = 99.5\,kN$
$P_{tot} = 5705\,kN$

Figure Train PT60-45 [INB4EU-CB-124]

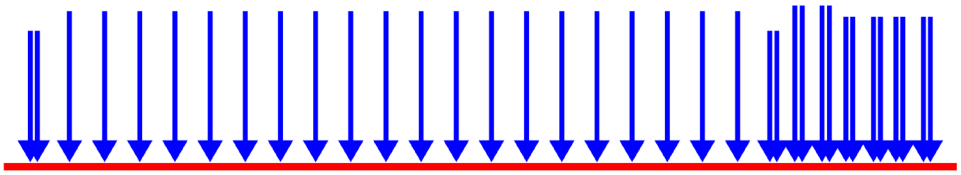

$L_{tot} = 340.4\,m$
$D = 13.3\,m$
$P_{max} = 220.7\,kN$
$P_{min} = 181.5\,kN$
$P_{tot} = 7475\,kN$

Figure Train PT60-46 [INB4EU-SA-035]

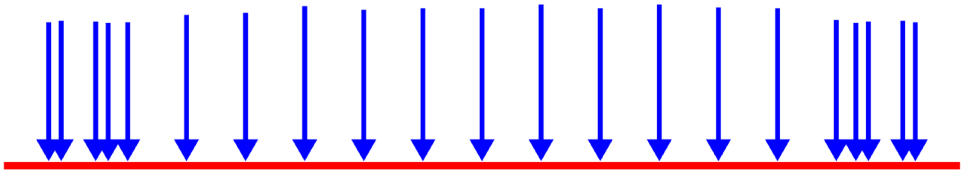

$L_{tot} = 193.8\,m$
$D = 13.2\,m$
$P_{max} = 189.3\,kN$
$P_{min} = 164.8\,kN$
$P_{tot} = 3691\,kN$

Figure Train PT60-47 [INB4EU-SA-001]

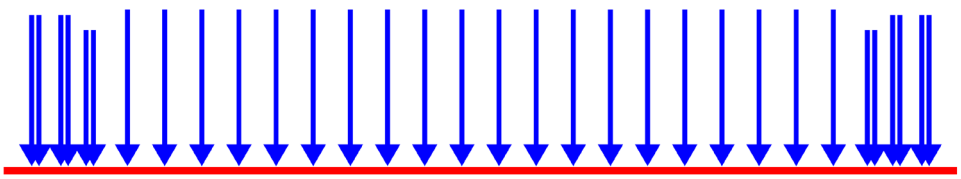

$L_{tot} = 321.3\,m$
$D = 13.3\,m$
$P_{max} = 211.9\,kN$
$P_{min} = 181.5\,kN$
$P_{tot} = 6592\,kN$

Figure Train PT60-48 [INB4EU-SA-022]

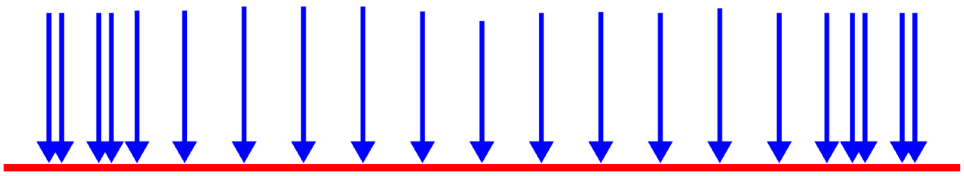

$L_{tot} = 191.3\,m$
$D = 13.1\,m$
$P_{max} = 174.6\,kN$
$P_{min} = 157.0\,kN$
$P_{tot} = 3531\,kN$

Figure Train PT60-49 [INB4EU-SA-004]

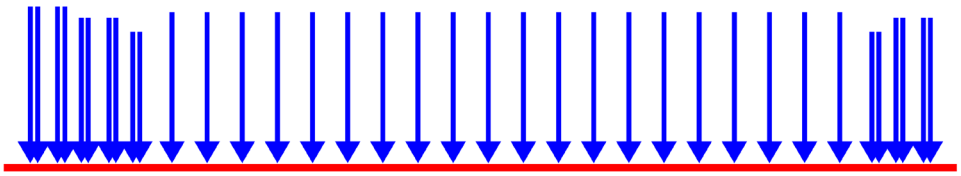

$L_{tot} = 340.6\,m$
$D = 13.3\,m$
$P_{max} = 220.7\,kN$
$P_{min} = 181.5\,kN$
$P_{tot} = 7475\,kN$

Figure Train PT60-50 [INB4EU-SA-029]

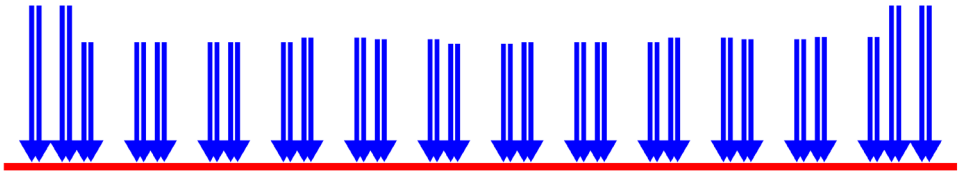

$L_{tot} = 323.1\,m$
$D = 26.4\,m$
$P_{max} = 206.0\,kN$
$P_{min} = 150.6\,kN$
$P_{tot} = 8485\,kN$

Figure Train PT60-51 [INB4EU-CB-021]

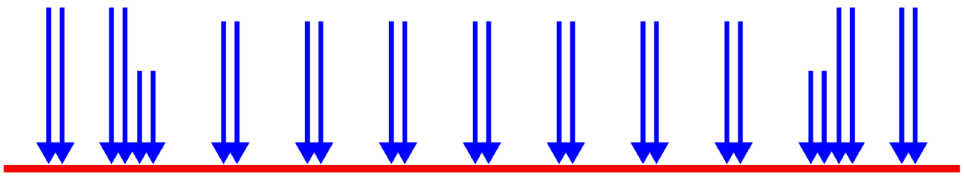

$L_{tot} = 193.1\,m$
$D = 19.0\,m$
$P_{max} = 168.6\,kN$
$P_{min} = 93.4\,kN$
$P_{tot} = 3854\,kN$

Figure Train PT60-52 [INB4EU-AB-008]

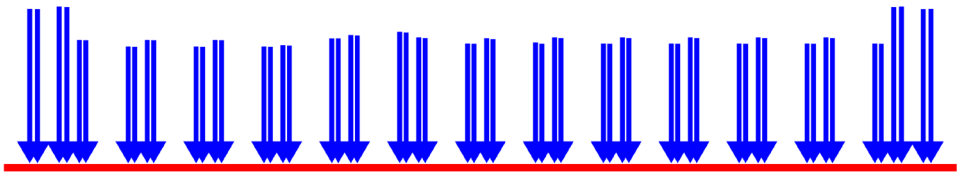

$L_{tot} = 350.5\,m$
$D = 26.4\,m$
$P_{max} = 201.4\,kN$
$P_{min} = 144.1\,kN$
$P_{tot} = 8921\,kN$

Figure Train PT60-53 [INB4EU-CB-013]

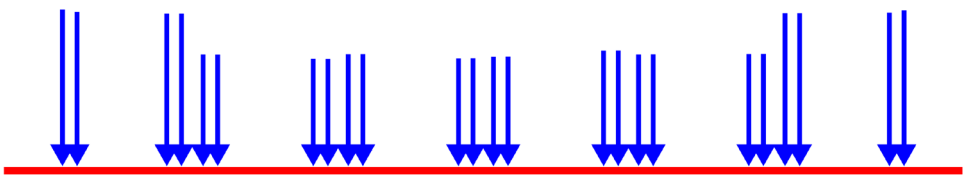

$L_{tot} = 143.9\,m$
$D = 24.0\,m$
$P_{max} = 168.0\,kN$
$P_{min} = 109.8\,kN$
$P_{tot} = 3144\,kN$

Figure Train PT60-54 [INB4EU-CB-030]

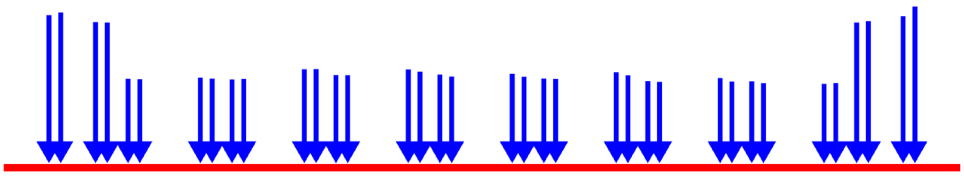

$L_{tot} = 191.6\,m$
$D = 23.0\,m$
$P_{max} = 179.7\,kN$
$P_{min} = 82.0\,kN$
$P_{tot} = 3855\,kN$

Figure Train PT60-55 [INB4EU-CB-077]

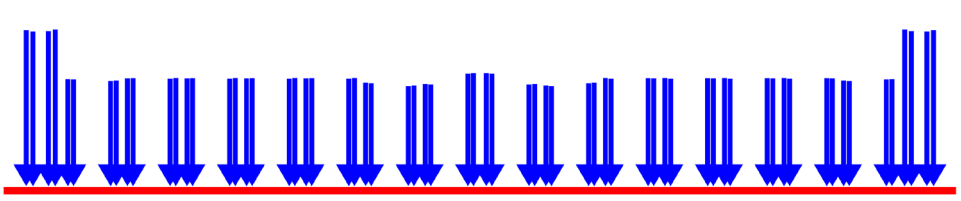

$L_{tot} = 403.8\,m$
$D = 26.5\,m$
$P_{max} = 215.2\,kN$
$P_{min} = 129.5\,kN$
$P_{tot} = 9529\,kN$

Figure Train PT60-56 [INB4EU-CB-138]

$L_{tot} = 395.7\,m$
$D = 13.2\,m$
$P_{max} = 189.3\,kN$
$P_{min} = 164.8\,kN$
$P_{tot} = 7381\,kN$

Figure Train PT60-57 [INB4EU-SA-040]

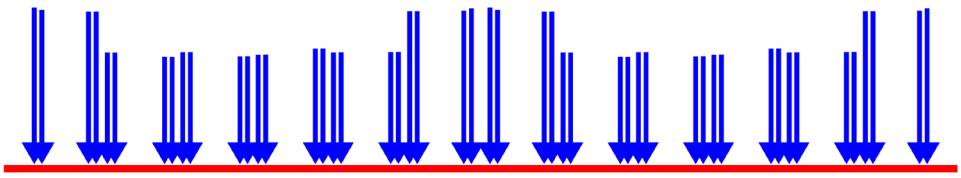

$L_{tot} = 293.9\,m$
$D = 24.0\,m$
$P_{max} = 168.0\,kN$
$P_{min} = 109.8\,kN$
$P_{tot} = 6288\,kN$

Figure Train PT60-58 [INB4EU-CB-142]

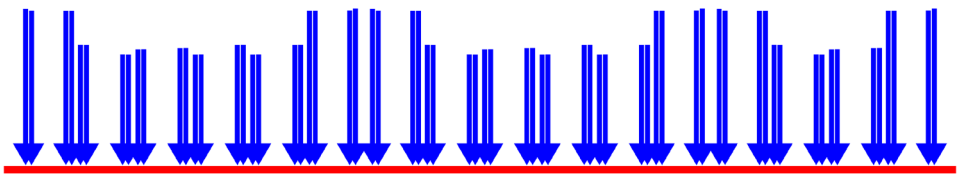

$L_{tot} = 418.9\,m$
$D = 25.3\,m$
$P_{max} = 170.8\,kN$
$P_{min} = 115.6\,kN$
$P_{tot} = 8920\,kN$

Figure Train PT60-59 [INB4EU-CB-146]

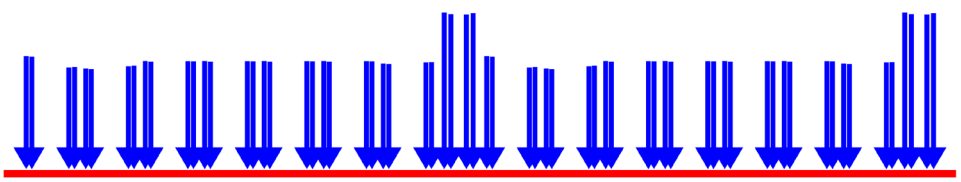

$L_{tot} = 404.1\,m$
$D = 26.5\,m$
$P_{max} = 215.2\,kN$
$P_{min} = 129.5\,kN$
$P_{tot} = 9529\,kN$

Figure Train PT60-60 [INB4EU-CB-140]

Appendix E — Exceedance maps for PT60 trains

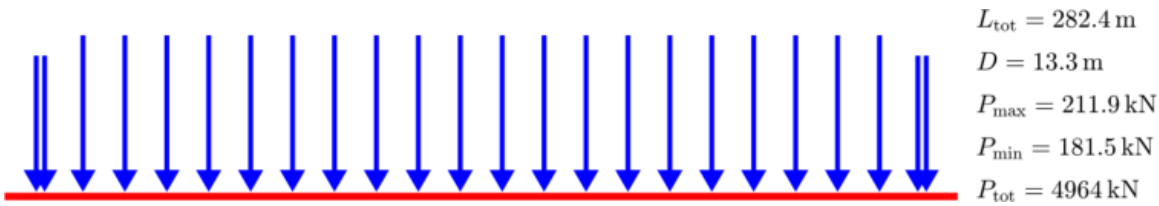

Figure Train PT60-01 [INB4EU-SA-017]

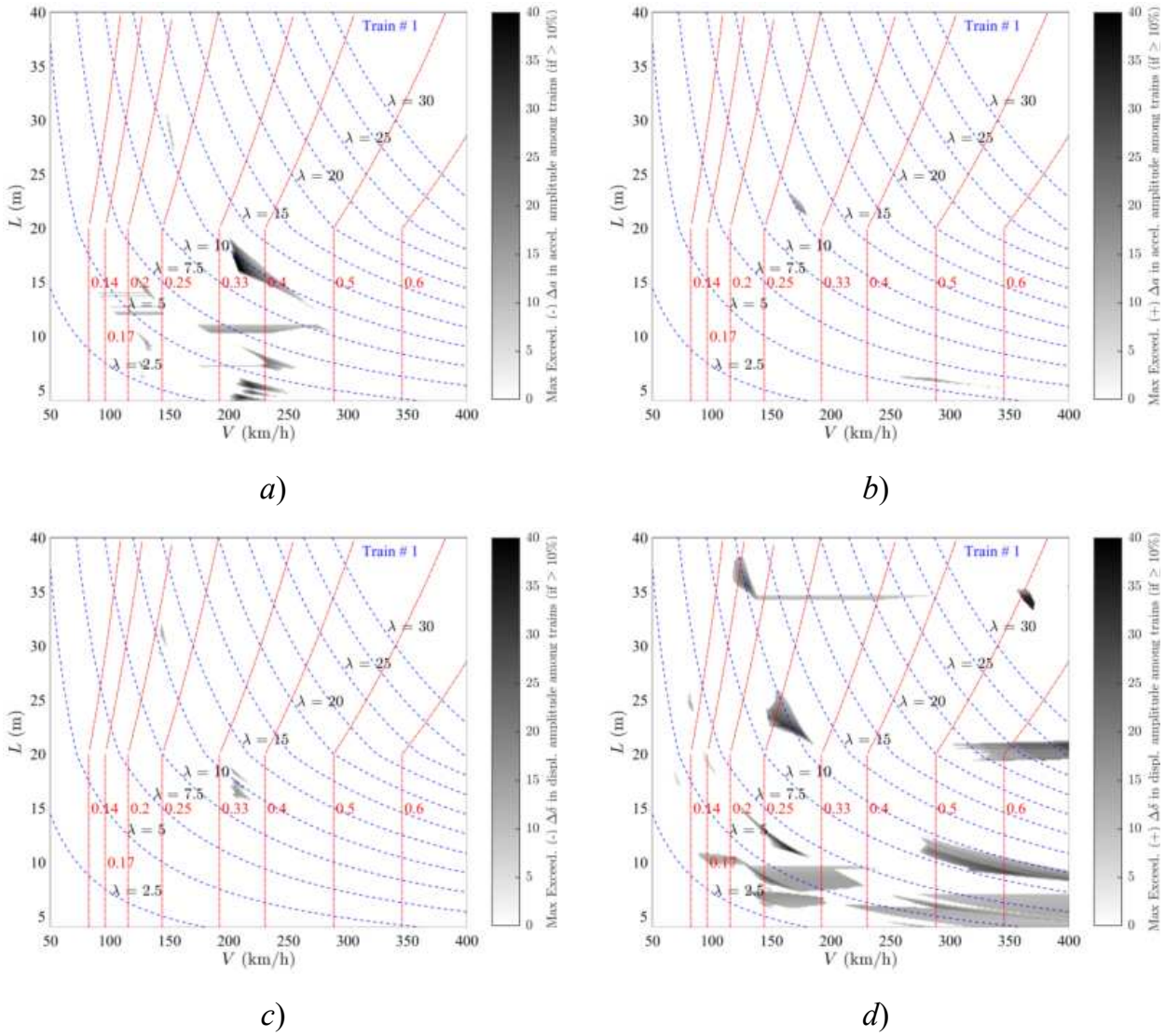

Figure 1. Exceedance Maps Train PT60-01 LIR vs Duhamel: a) Δa(–); b) Δa(+); c) Δδ(–); d) Δδ(+). PSC bridges.

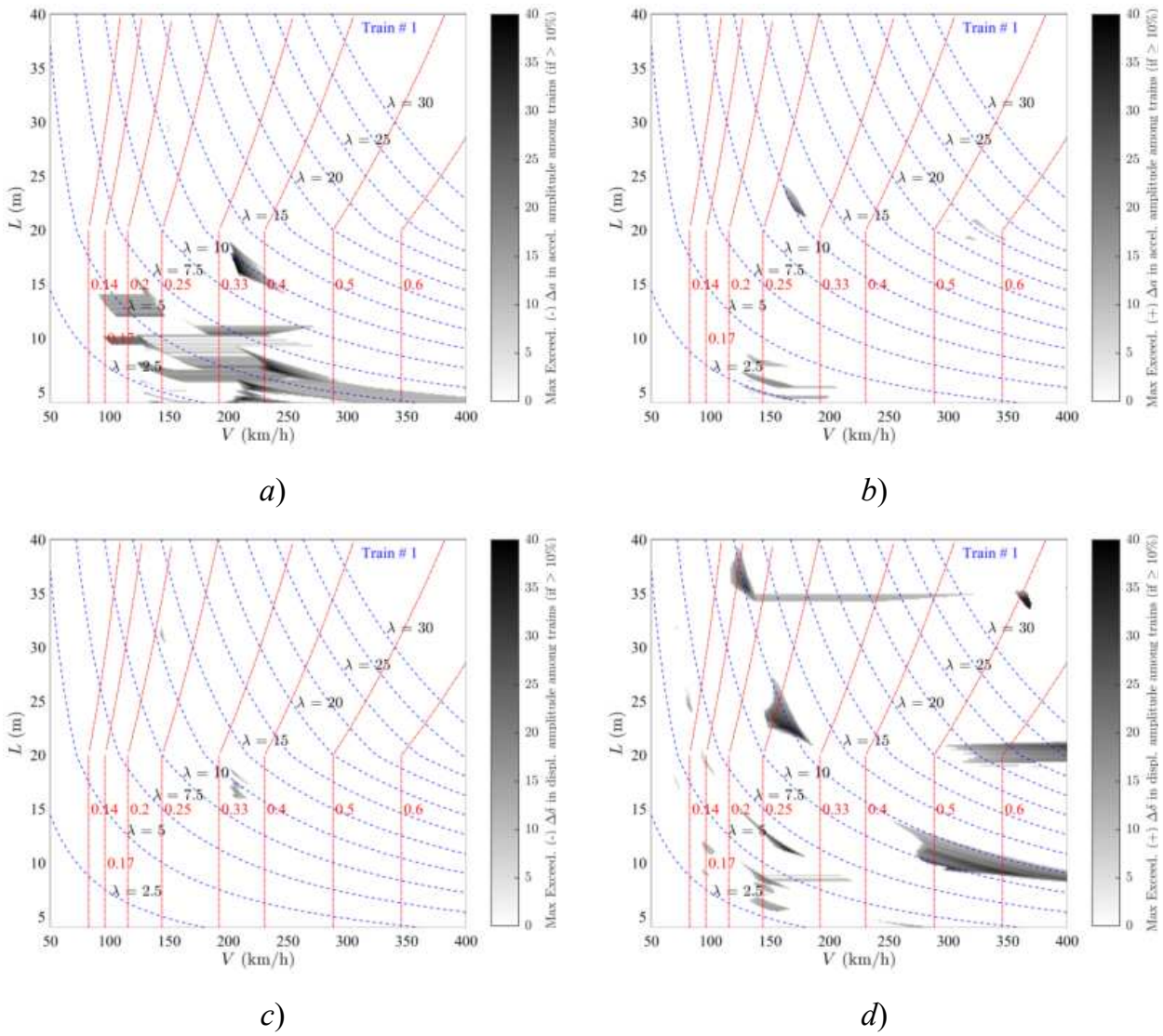

Figure 2. Exceedance Maps Train PT60-01 DER vs Duhamel: a) Δa(−); b) Δa(+); c) Δδ(−); d) Δδ(+). PSC bridges.

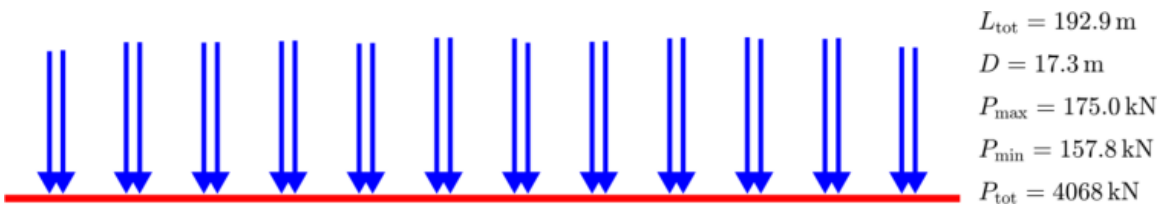

Figure Train PT60-02 [INB4EU-AB-001]

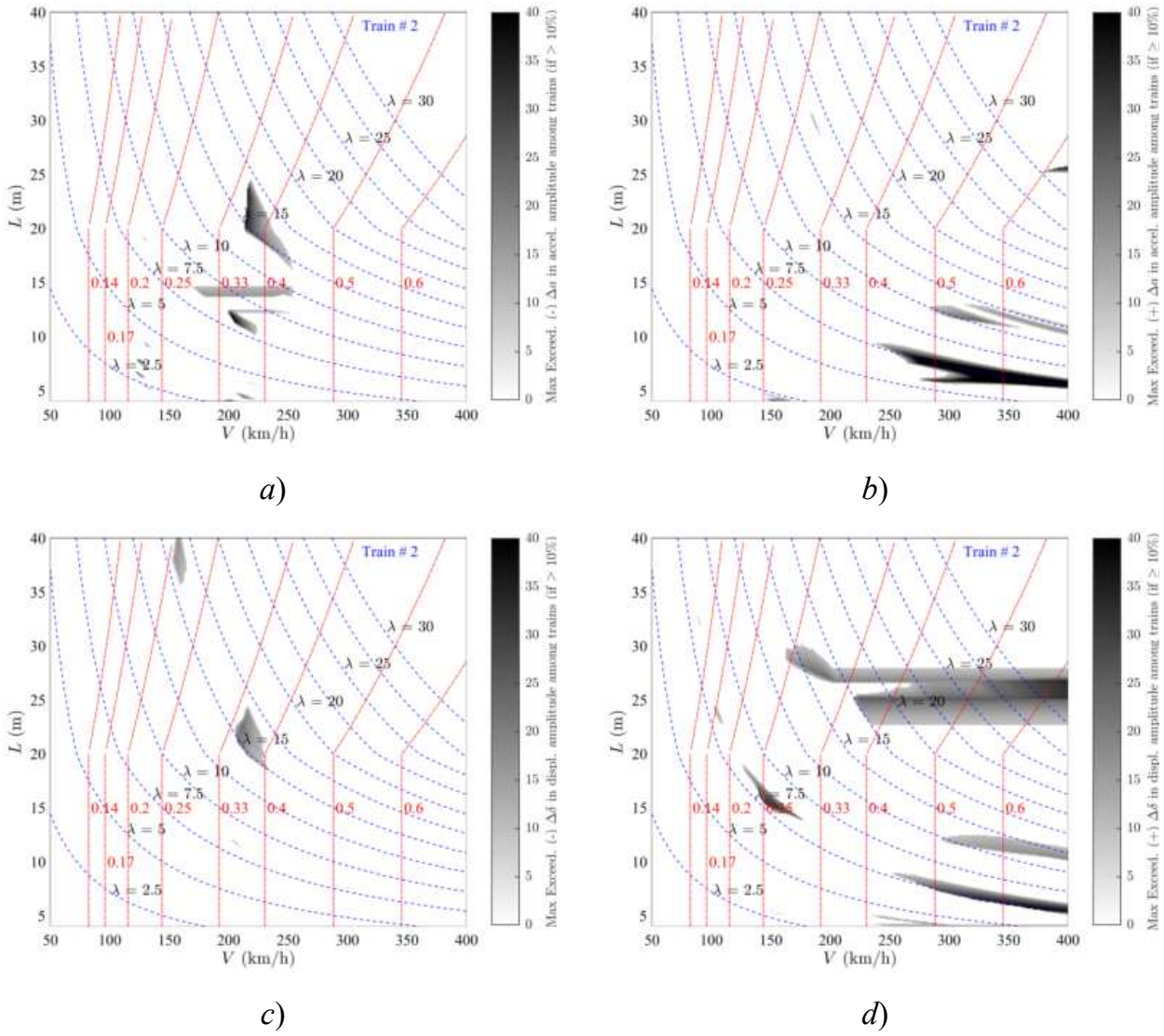

Figure 3. Exceedance Maps Train PT60-02 LIR vs Duhamel: a) Δa(–); b) Δa(+); c) Δδ(–); d) Δδ(+). PSC bridges.

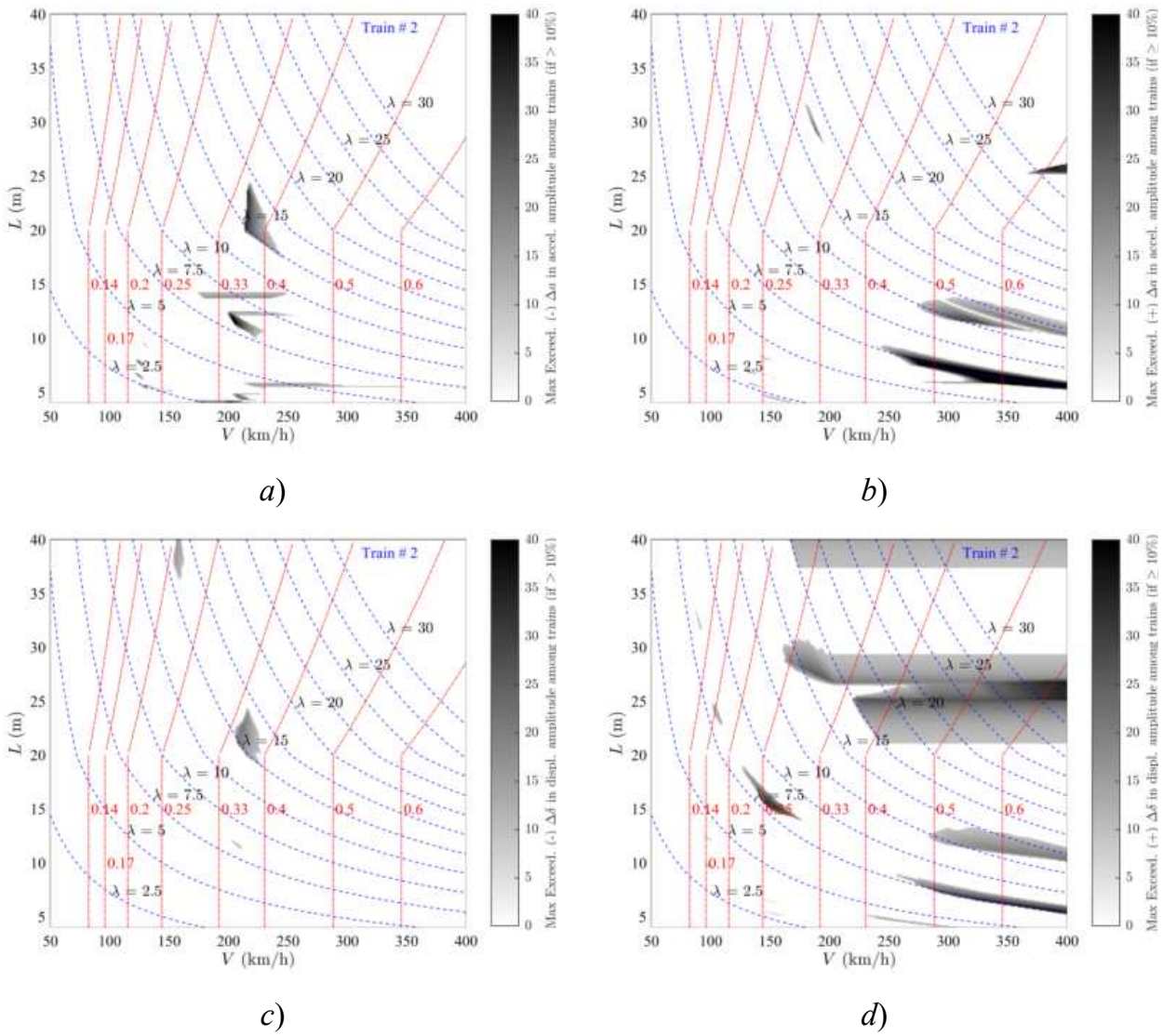

Figure 4. Exceedance Maps Train PT60-02 DER vs Duhamel: a) Δa(–); b) Δa(+); c) Δδ(–); d) Δδ(+). PSC bridges.

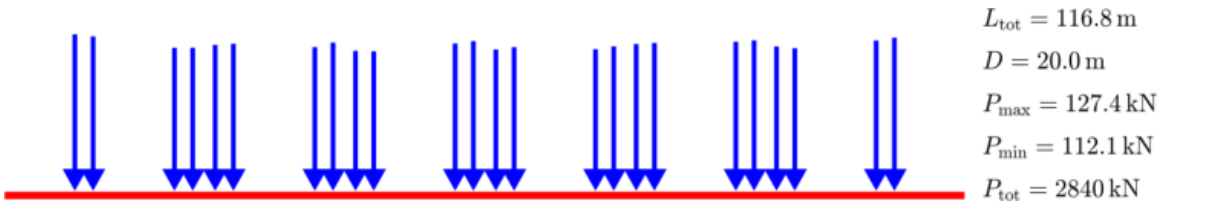

Figure Train PT60-03 [INB4EU-CB-069]

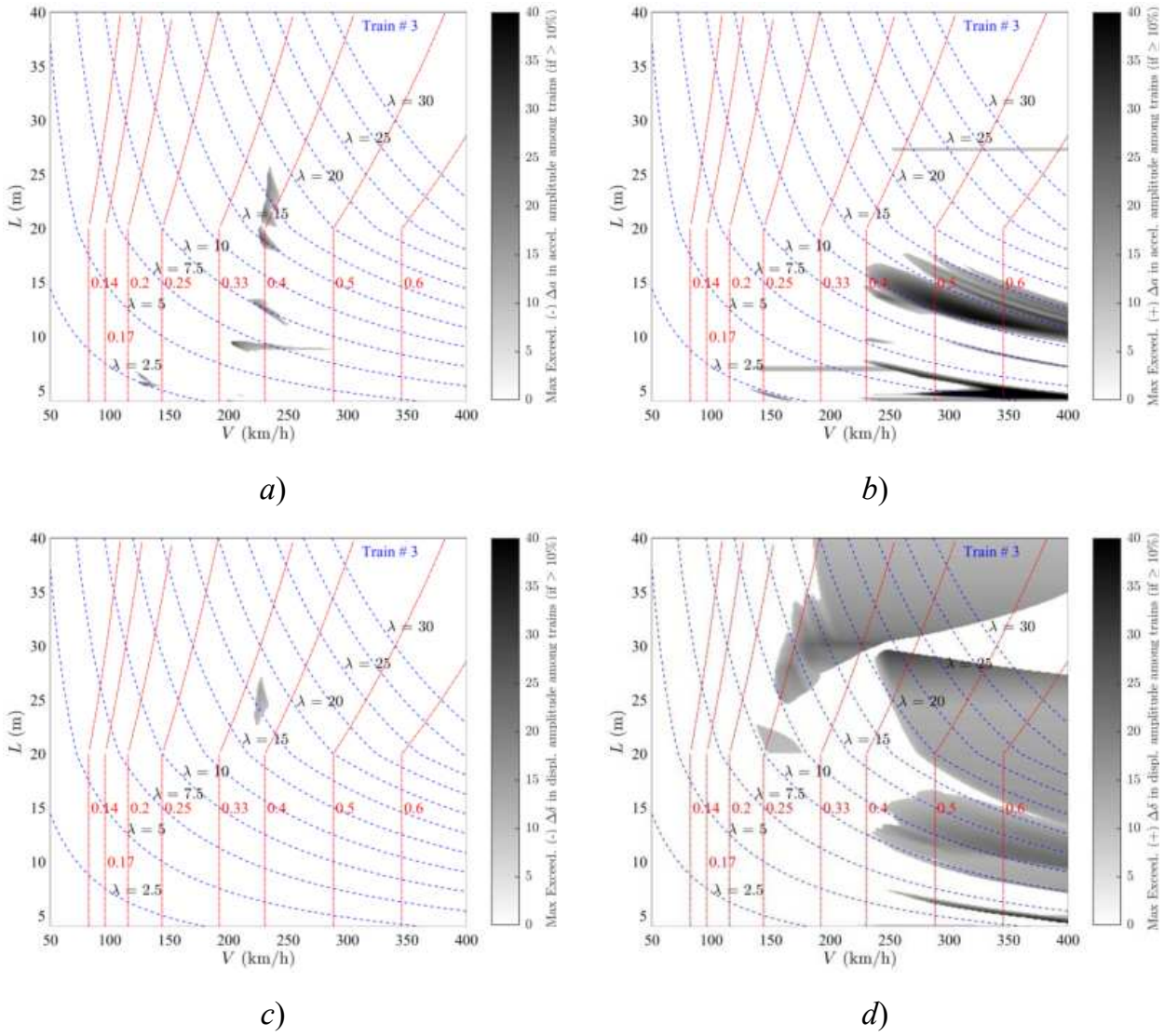

Figure 5. Exceedance Maps Train PT60-03 LIR vs Duhamel: a) Δa(–); b) Δa(+); c) Δδ(–); d) Δδ(+). PSC bridges.

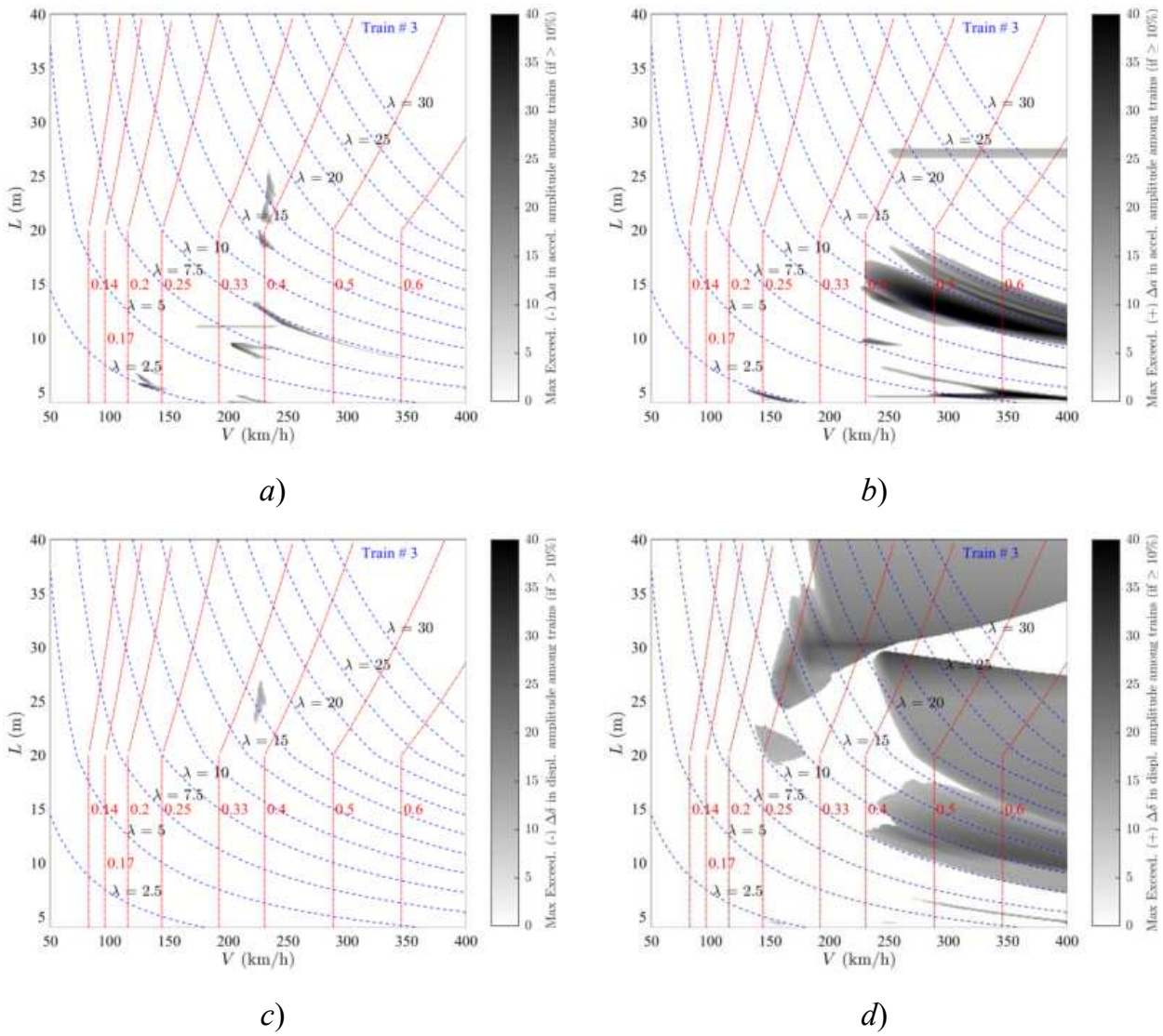

Figure 6. Exceedance Maps Train PT60-03 DER vs Duhamel: a) Δa(–); b) Δa(+); c) Δδ(–); d) Δδ(+). PSC bridges.

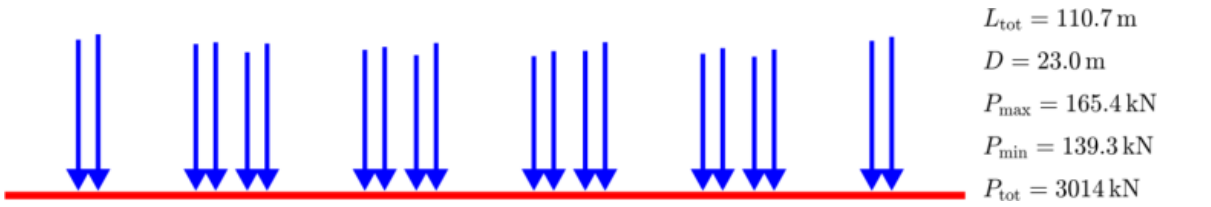

Figure Train PT60-04 [INB4EU-CB-066]

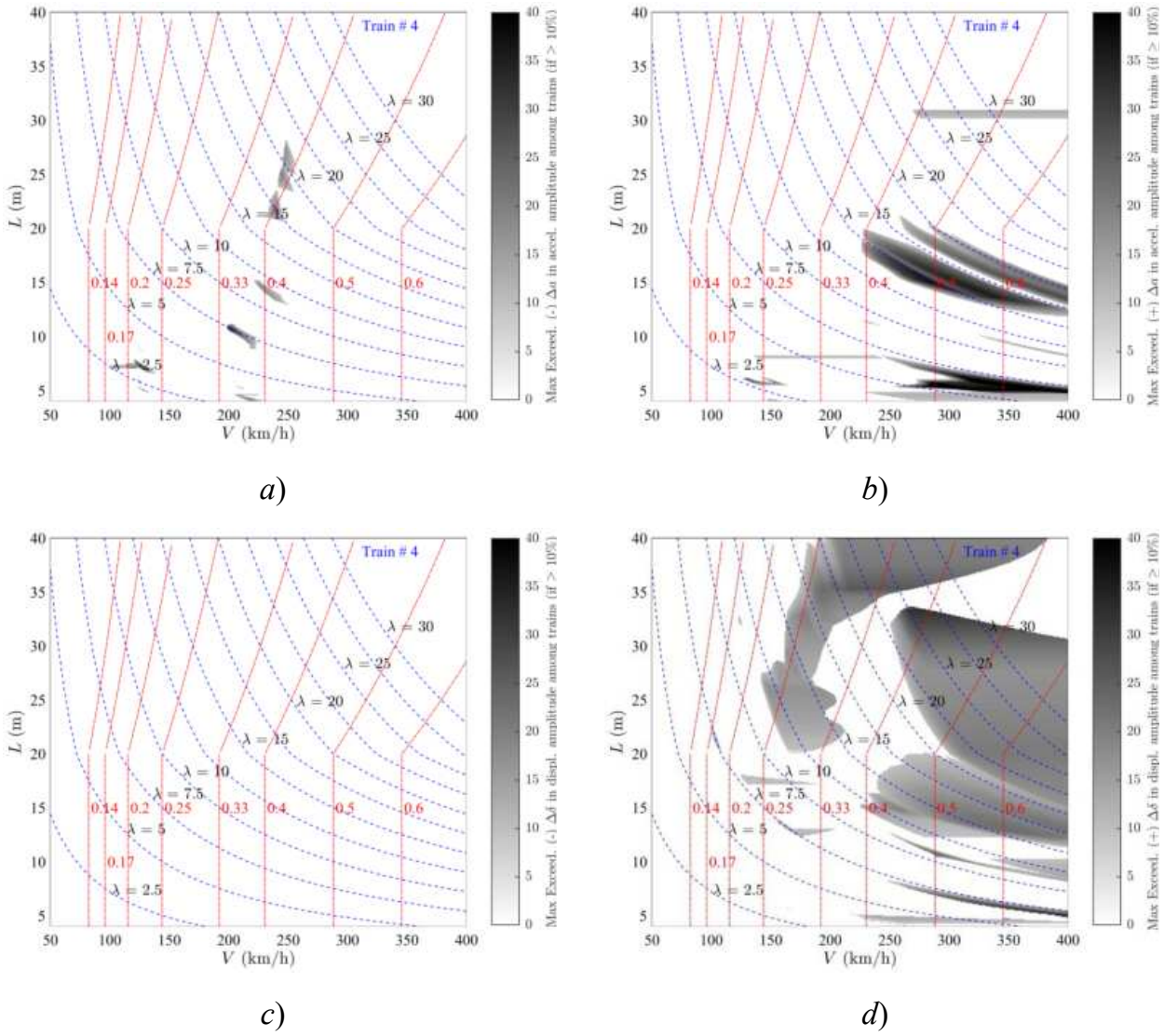

Figure 7. Exceedance Maps Train PT60-04 LIR vs Duhamel: a) Δa(–); b) Δa(+); c) Δδ(–); d) Δδ(+). PSC bridges.

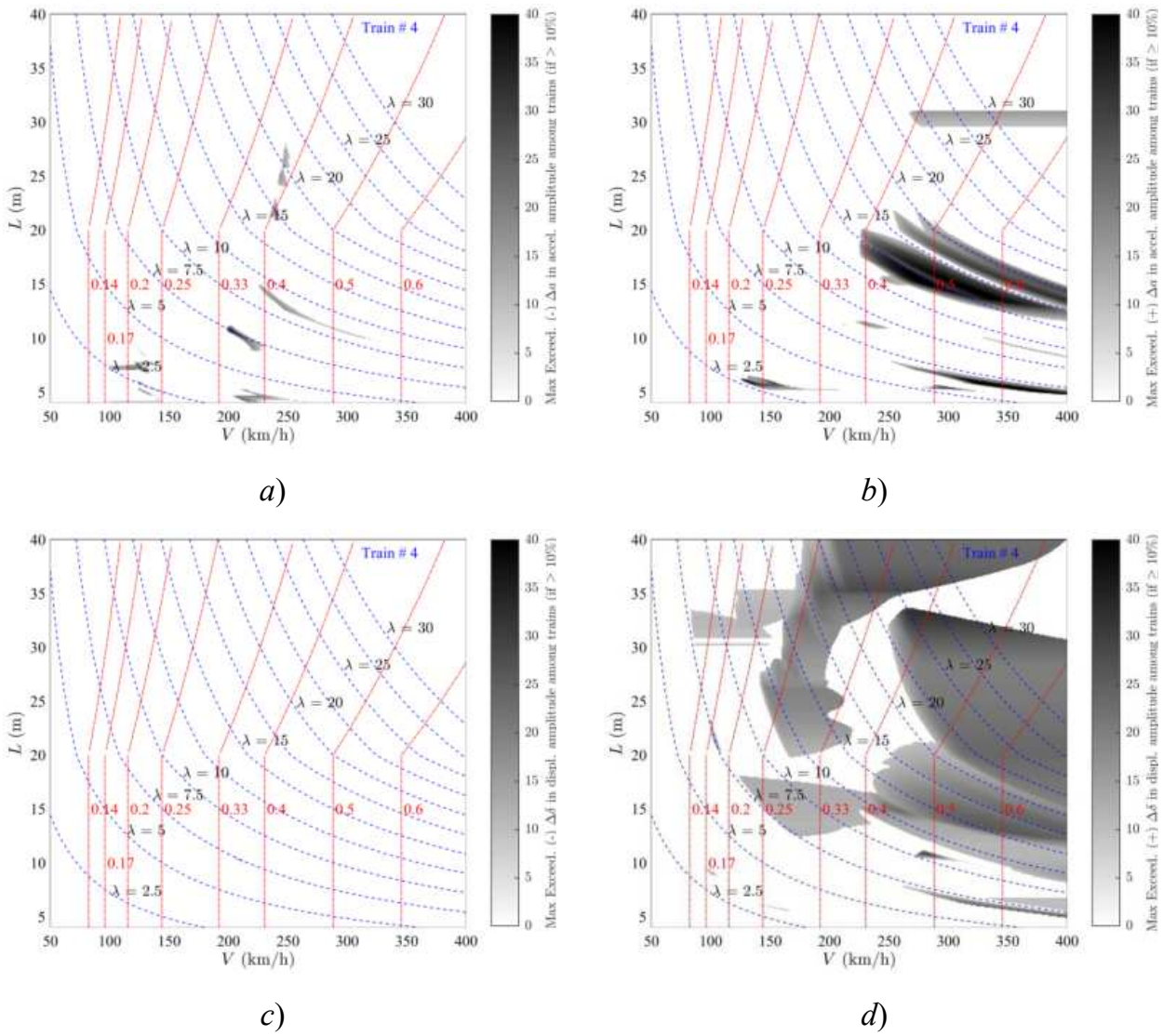

Figure 8. Exceedance Maps Train PT60-04 DER vs Duhamel: a) Δa(–); b) Δa(+); c) Δδ(–); d) Δδ(+). PSC bridges.

Figure Train PT60-05 [INB4EU-CB-084]

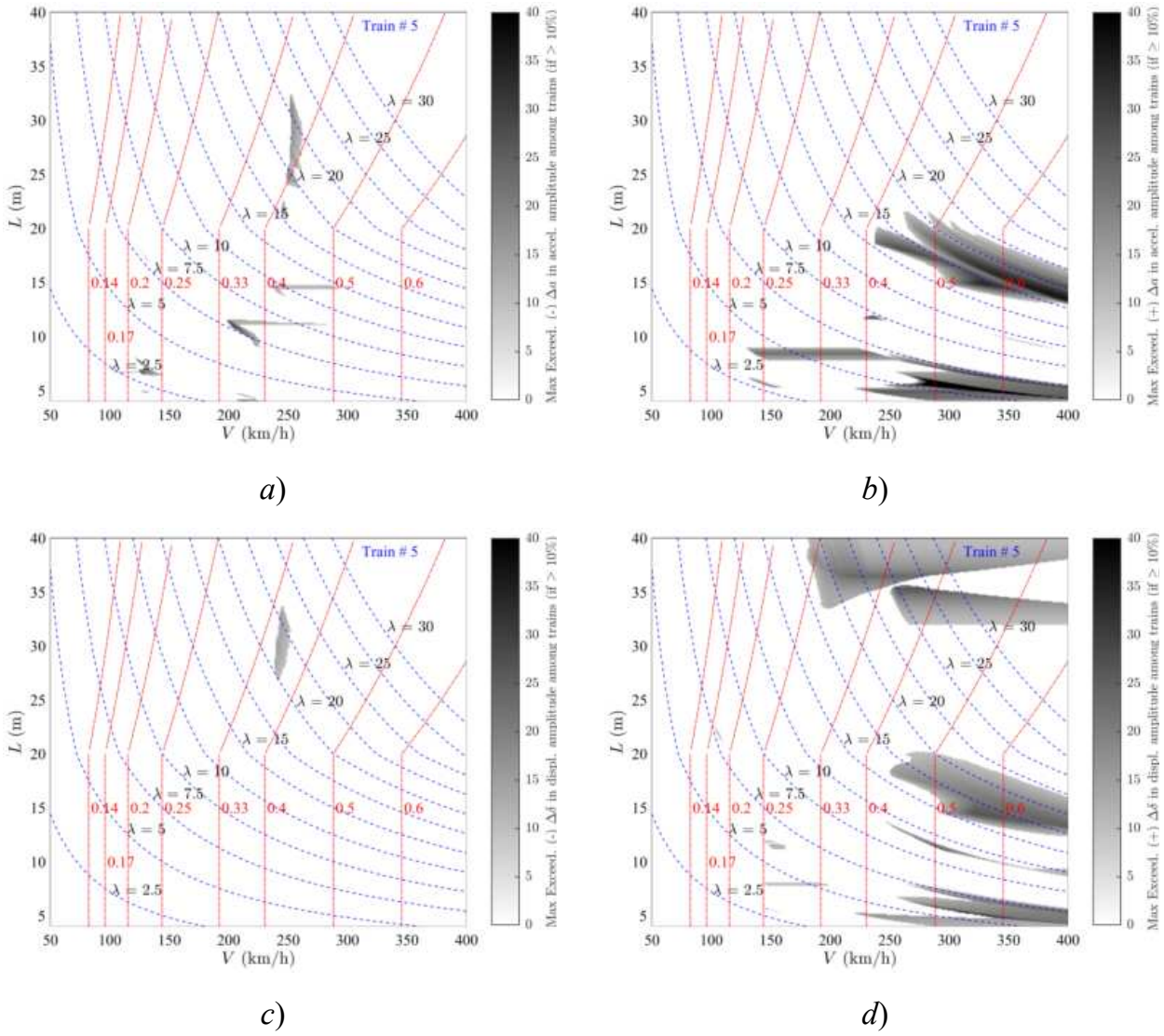

Figure 9. Exceedance Maps Train PT60-05 LIR vs Duhamel: a) Δa(–); b) Δa(+); c) Δδ(–); d) Δδ(+). PSC bridges.

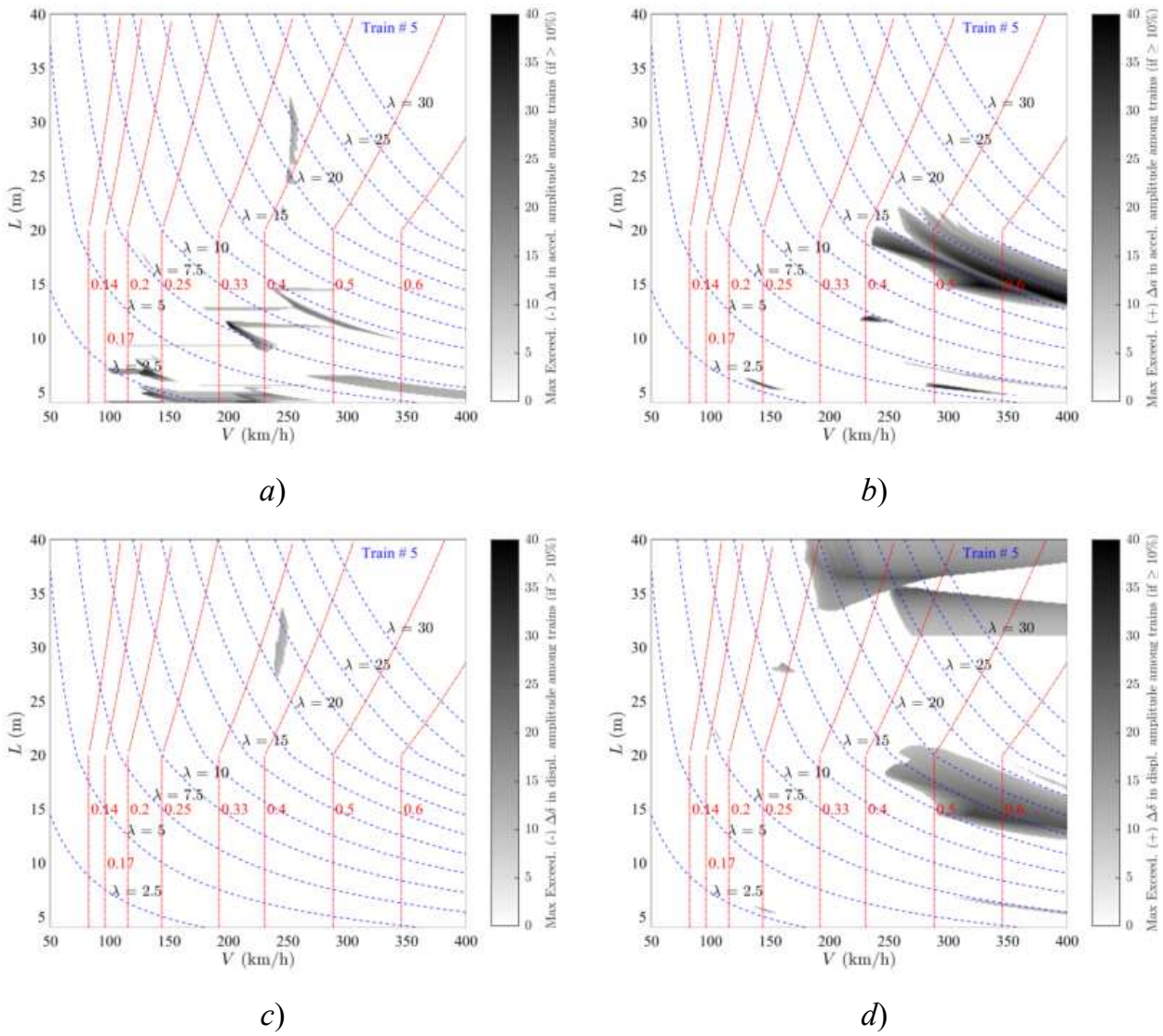

Figure 10. Exceedance Maps Train PT60-05 DER vs Duhamel: a) Δa(–); b) Δa(+); c) Δδ(–); d) Δδ(+). PSC bridges.

Figure Train PT60-06 [INB4EU-CB-127]

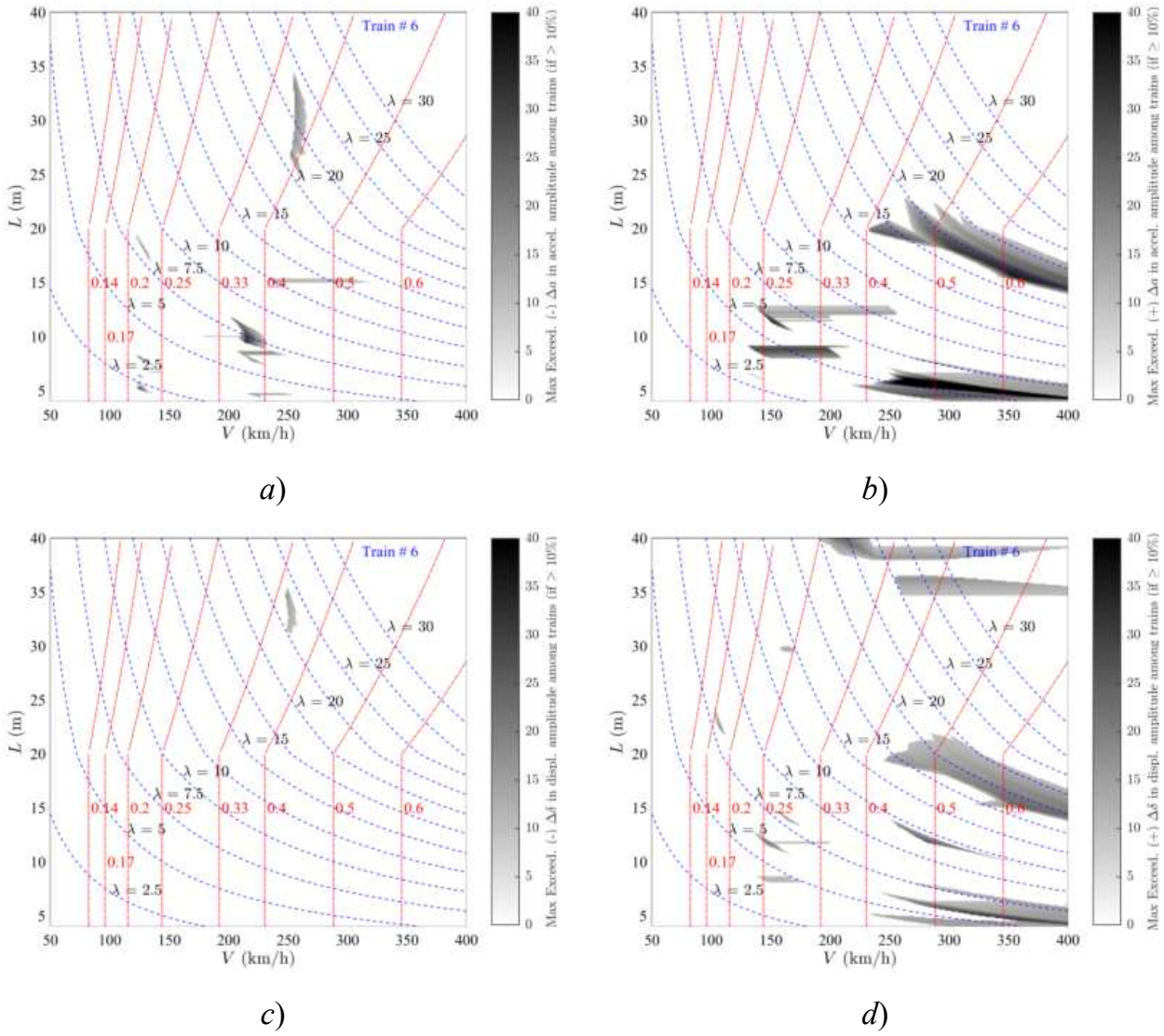

Figure 11. Exceedance Maps Train PT60-06 LIR vs Duhamel: a) Δa(–); b) Δa(+); c) Δδ(–); d) Δδ(+). PSC bridges.

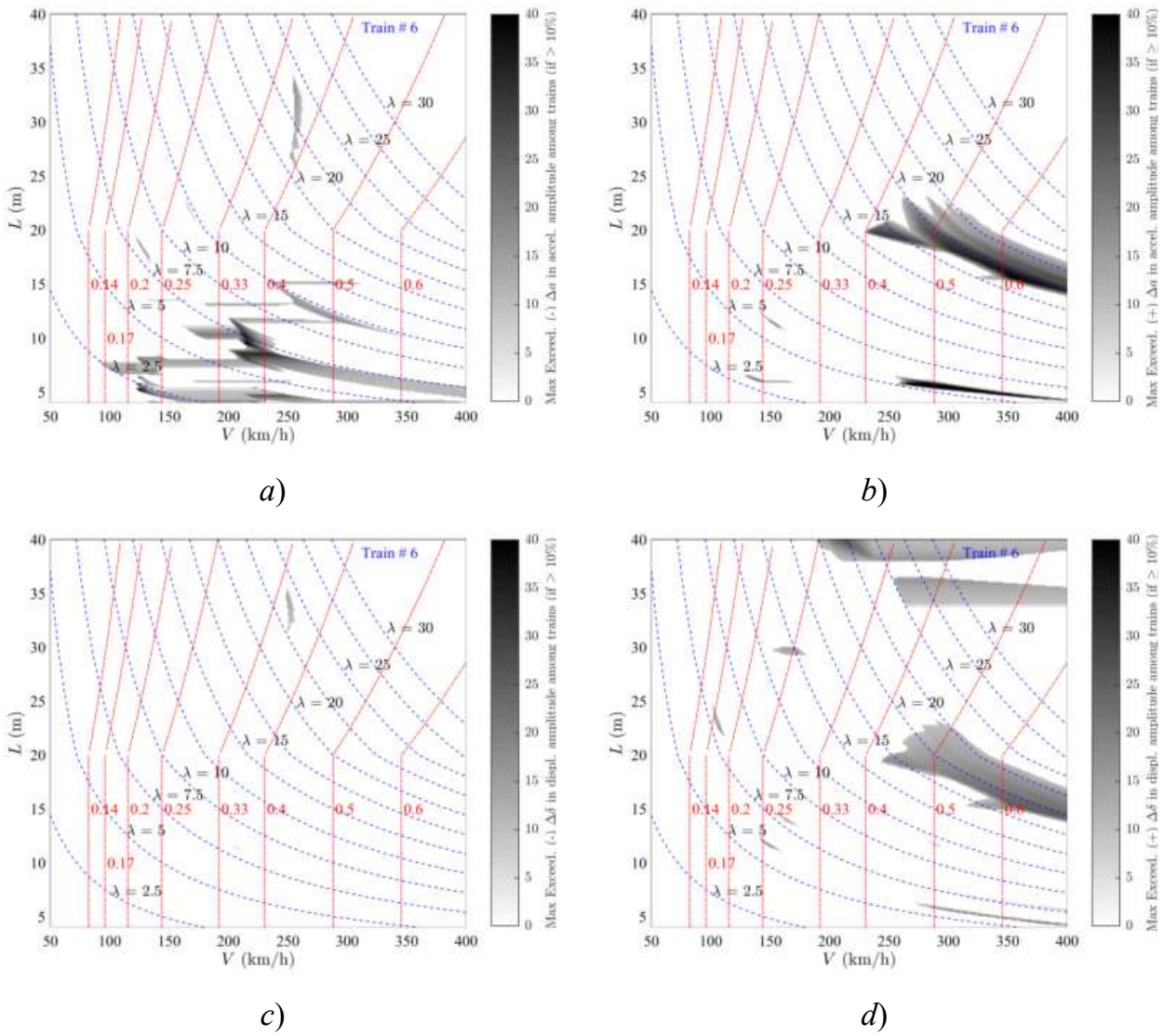

Figure 12. Exceedance Maps Train PT60-06 DER vs Duhamel: a) Δa(–); b) Δa(+); c) Δδ(–); d) Δδ(+). PSC bridges.

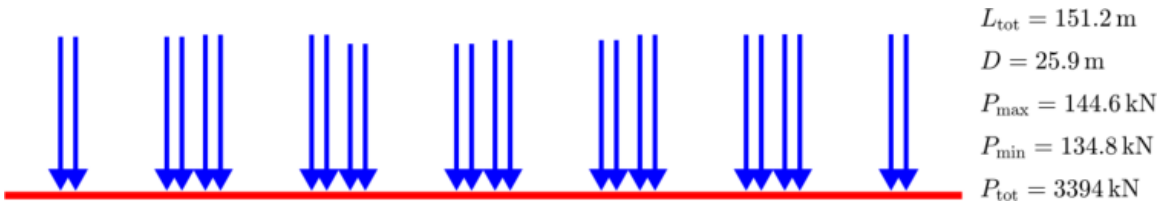

Figure Train PT60-07 [INB4EU-CB-001]

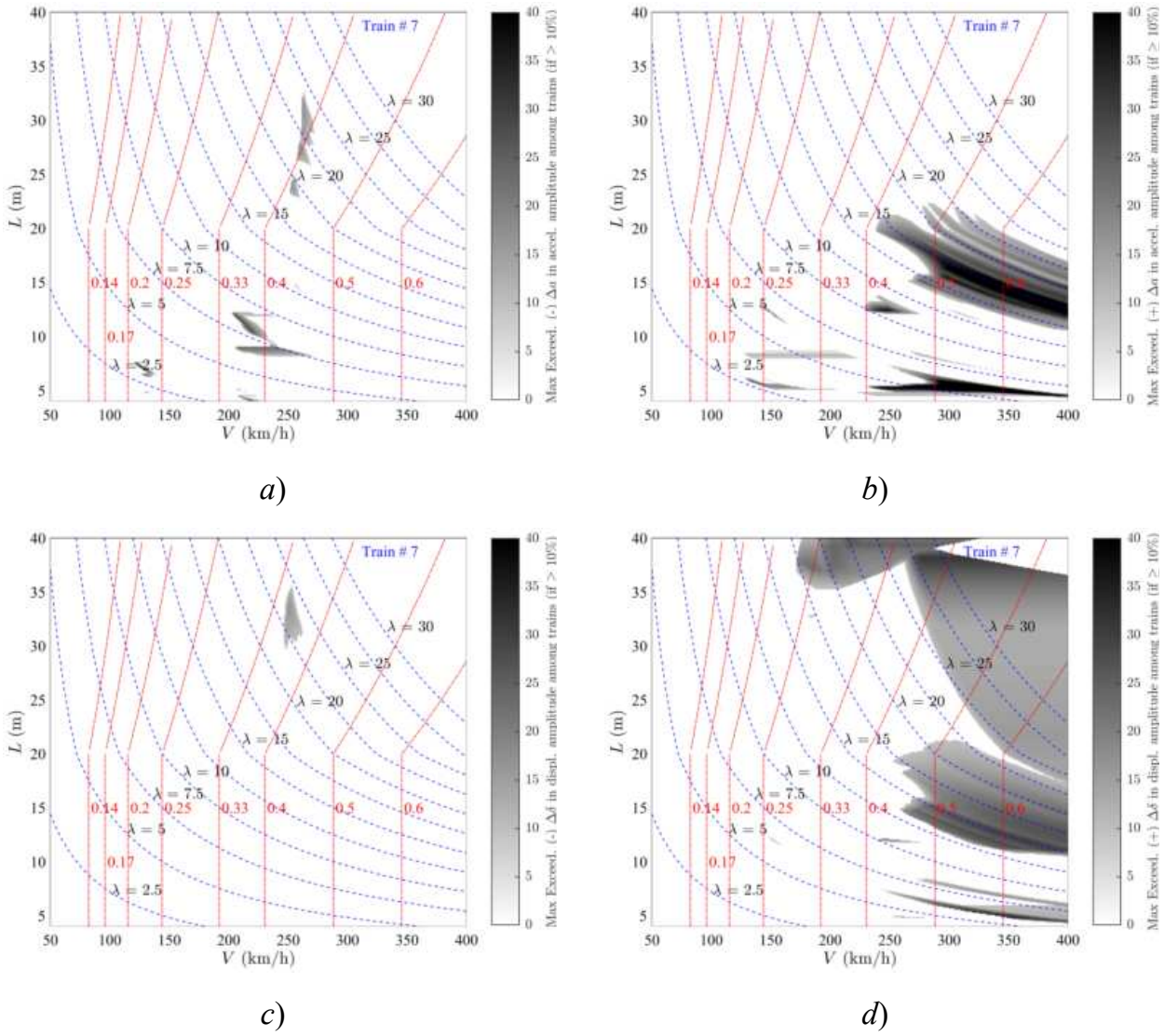

Figure 13. Exceedance Maps Train PT60-07 LIR vs Duhamel: a) Δa(–); b) Δa(+); c) Δδ(–); d) Δδ(+). PSC bridges.

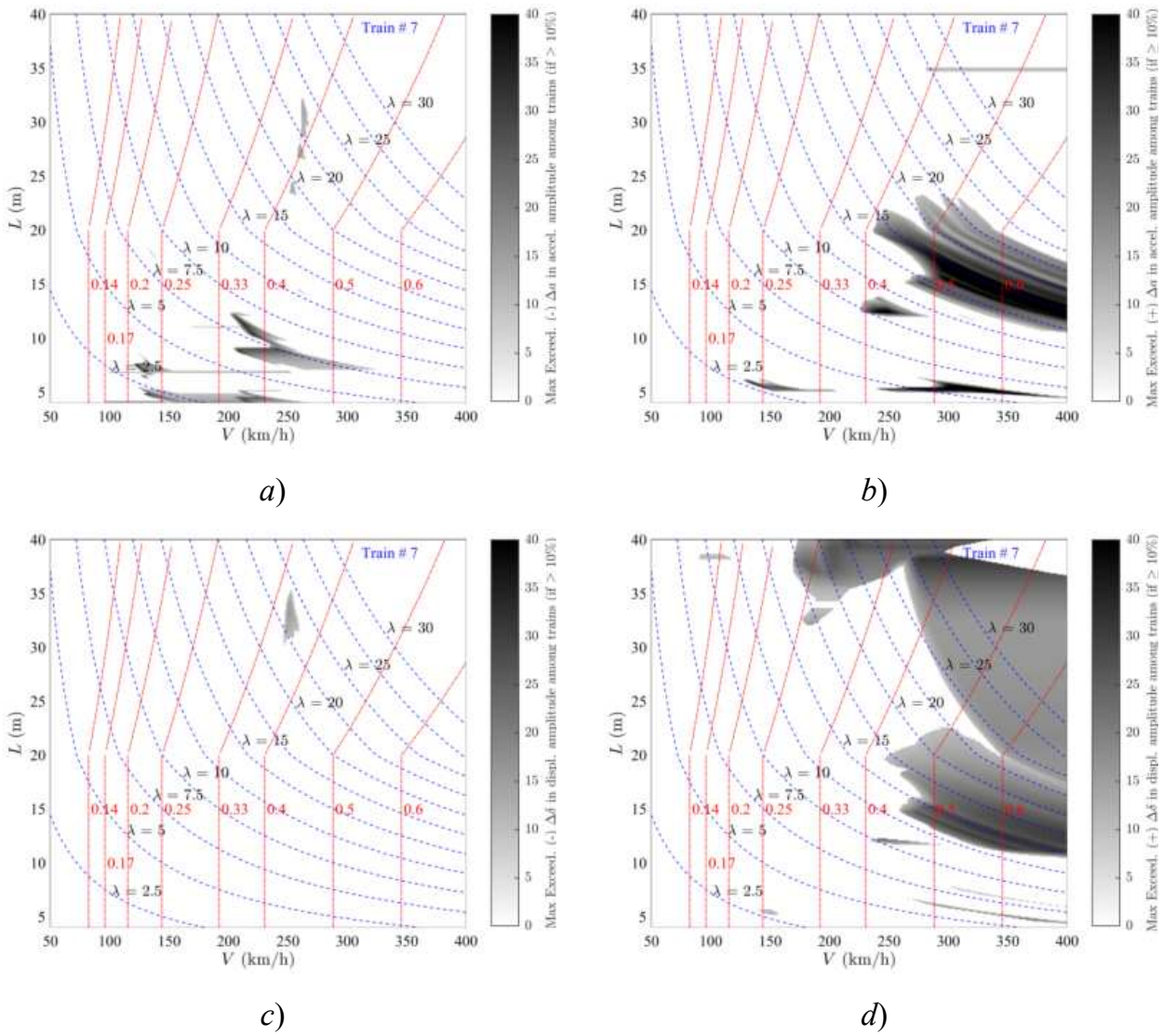

Figure 14. Exceedance Maps Train PT60-07 DER vs Duhamel: a) Δa(–); b) Δa(+); c) Δδ(–); d) Δδ(+). PSC bridges.

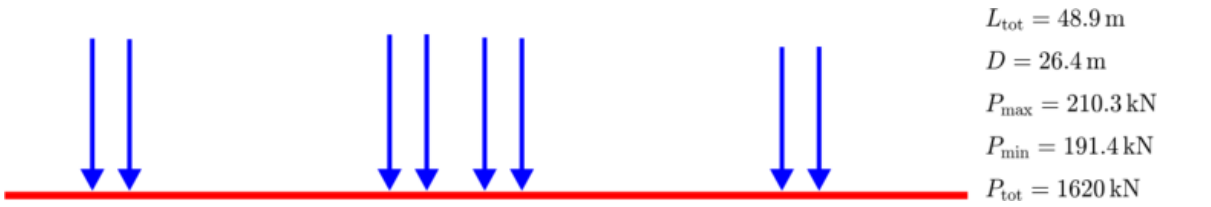

Figure Train PT60-08 [INB4EU-CB-007]

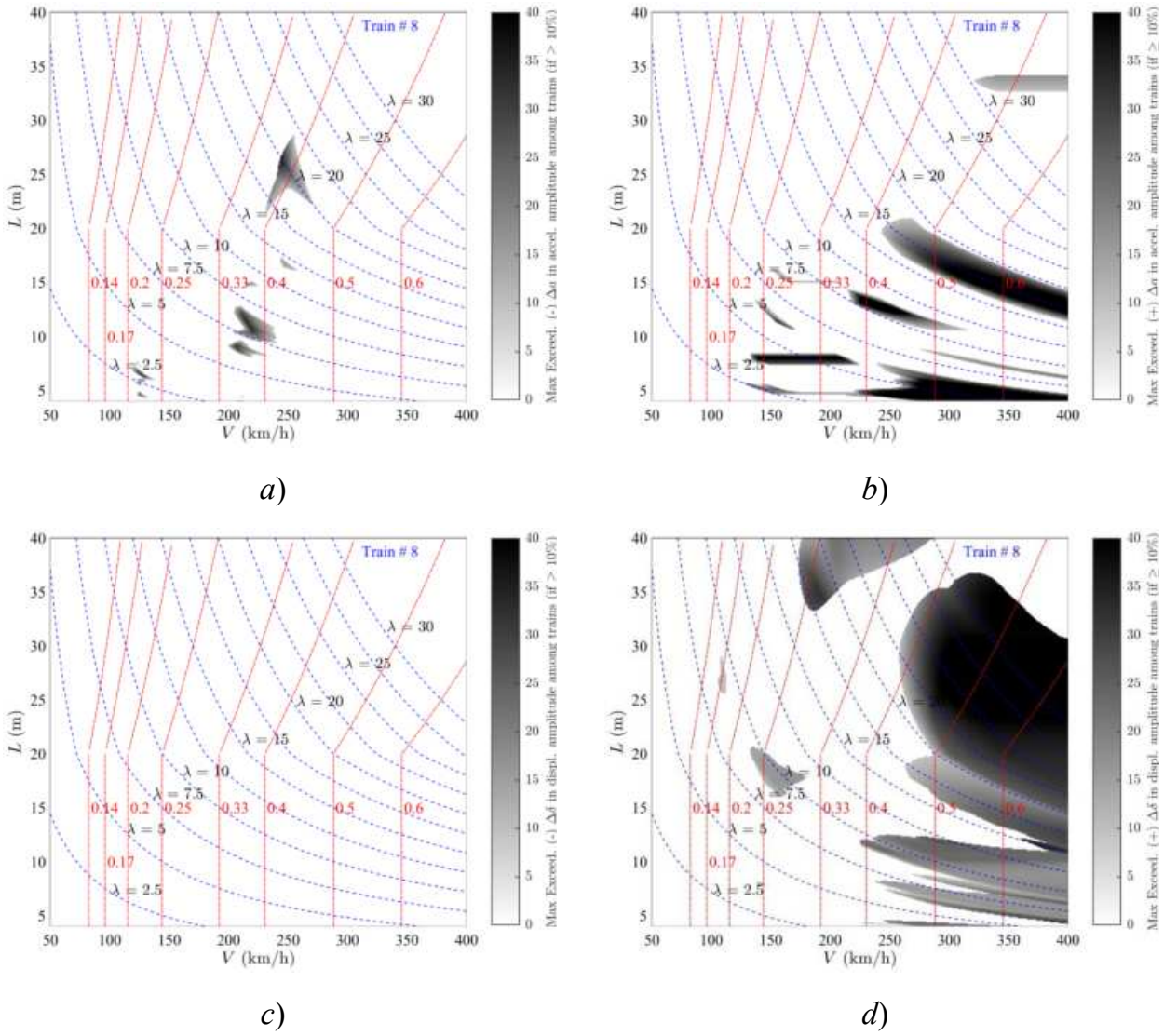

Figure 15. Exceedance Maps Train PT60-08 LIR vs Duhamel: a) Δa(–); b) Δa(+); c) Δδ(–); d) Δδ(+). PSC bridges.

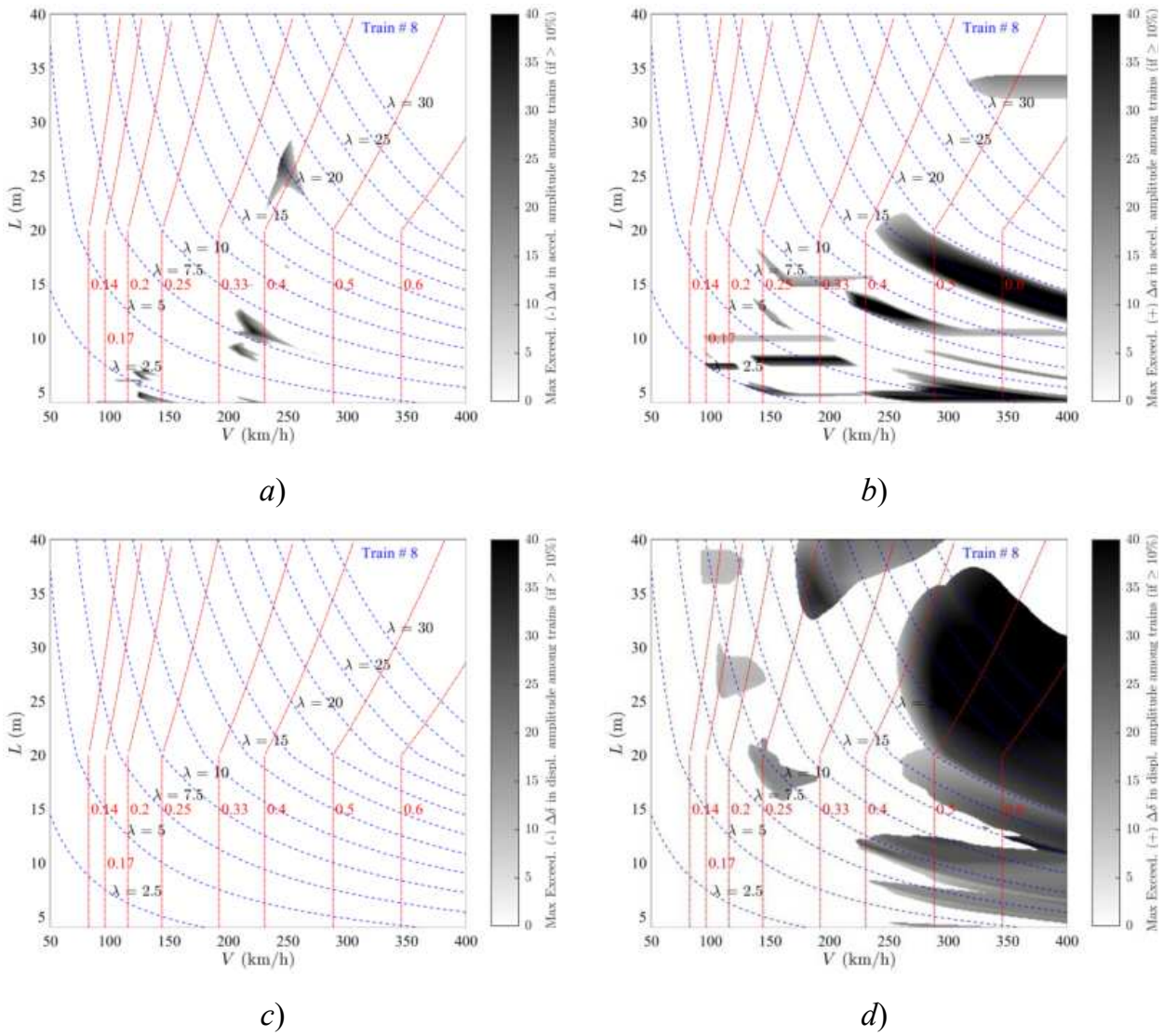

Figure 16. Exceedance Maps Train PT60-08 DER vs Duhamel: a) Δa(−); b) Δa(+); c) Δδ(−); d) Δδ(+). PSC bridges.

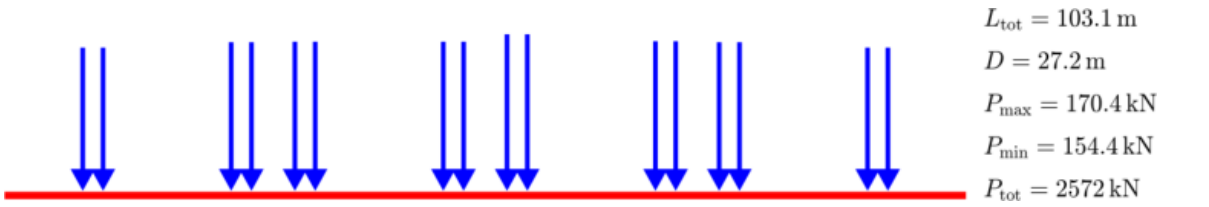

Figure Train PT60-09 [INB4EU-CB-009]

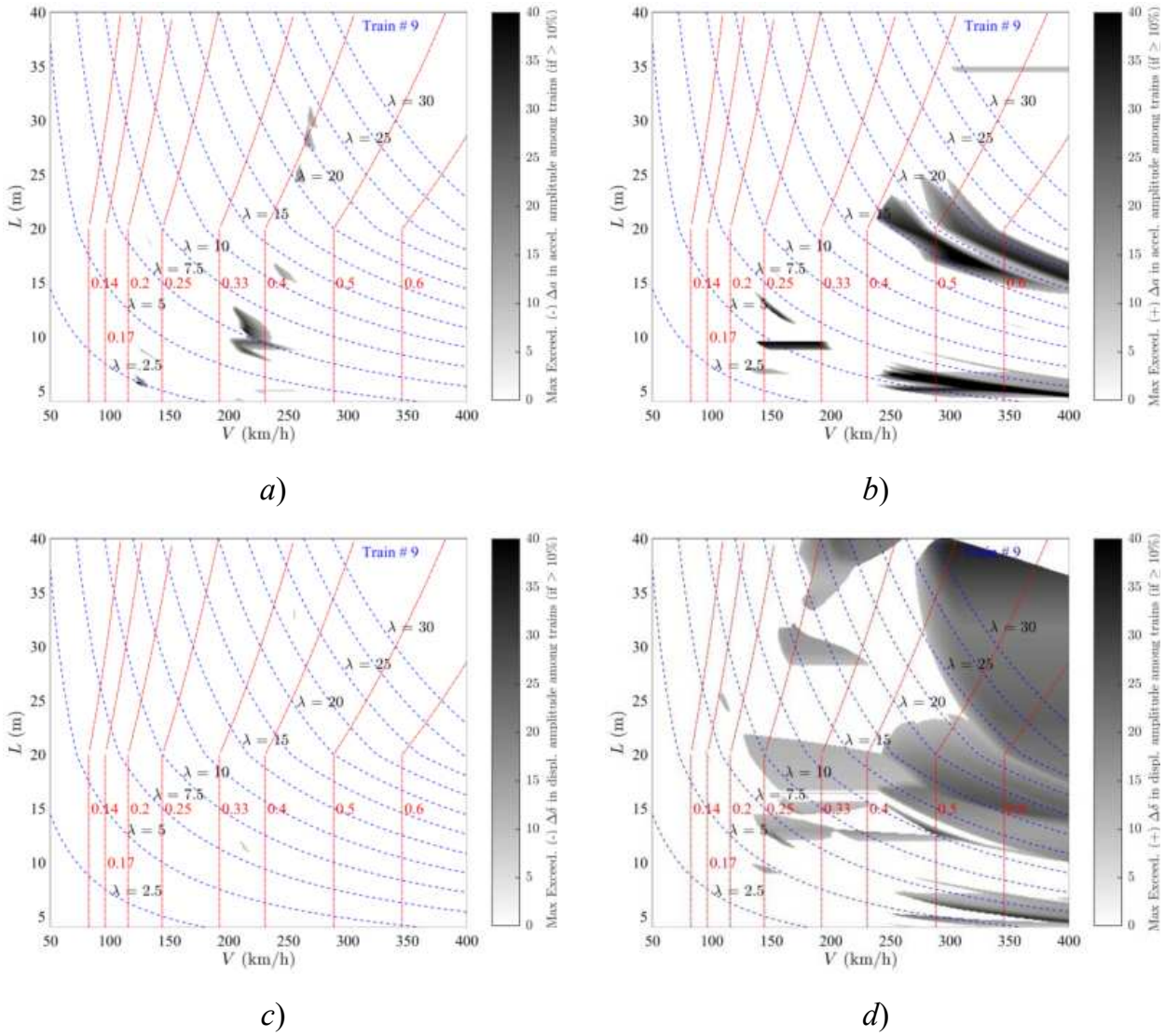

Figure 17. Exceedance Maps Train PT60-09 LIR vs Duhamel: a) Δa(–); b) Δa(+); c) Δδ(–); d) Δδ(+). PSC bridges.

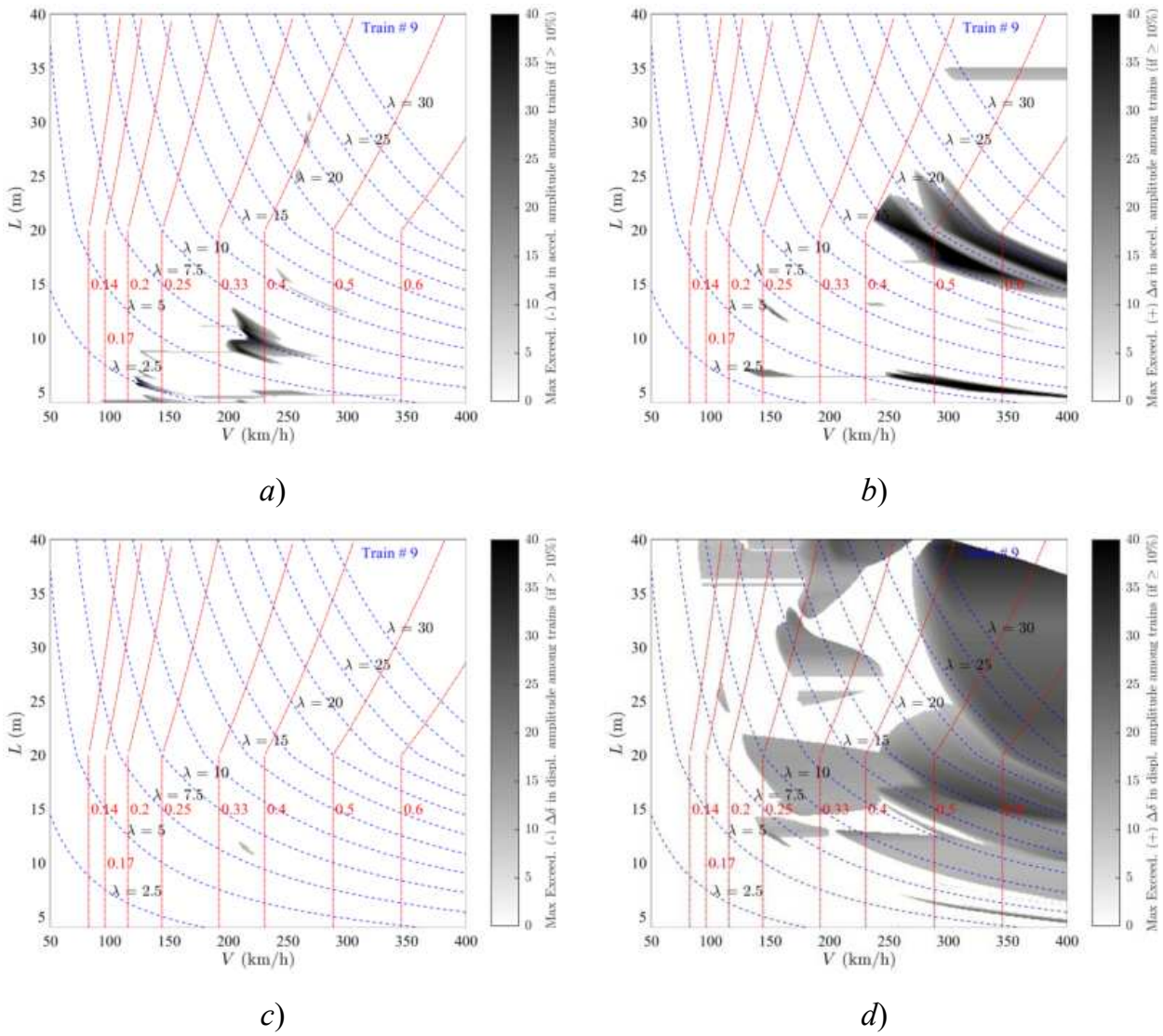

Figure 18. Exceedance Maps Train PT60-09 DER vs Duhamel: a) Δa(–); b) Δa(+); c) Δδ(–); d) Δδ(+). PSC bridges.

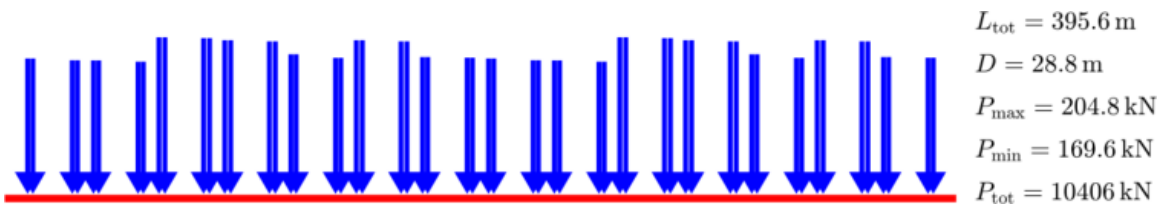

Figure Train PT60-10 [INB4EU-CB-111]

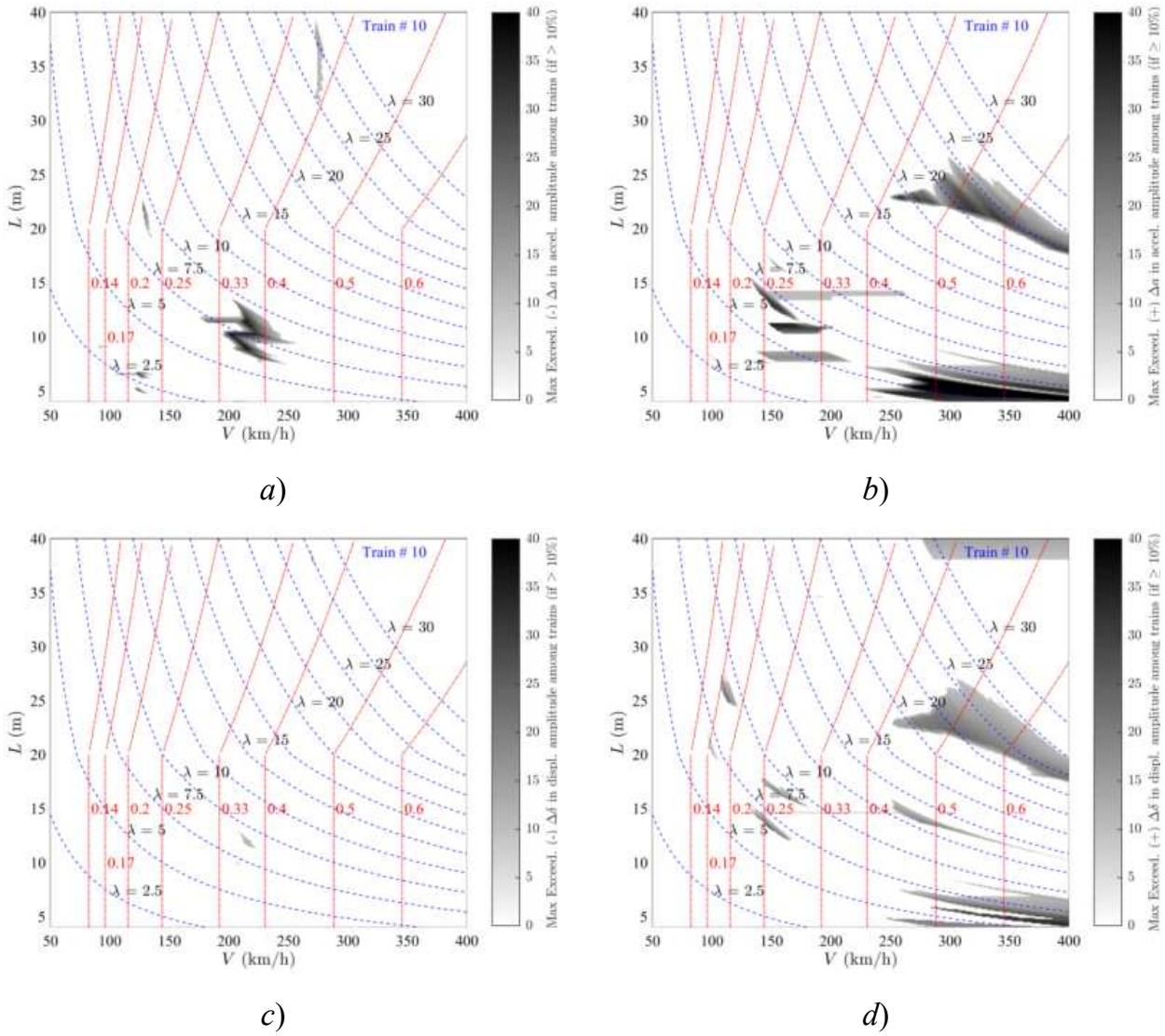

Figure 19. Exceedance Maps Train PT60-10 LIR vs Duhamel: a) Δa(–); b) Δa(+); c) Δδ(–); d) Δδ(+). PSC bridges.

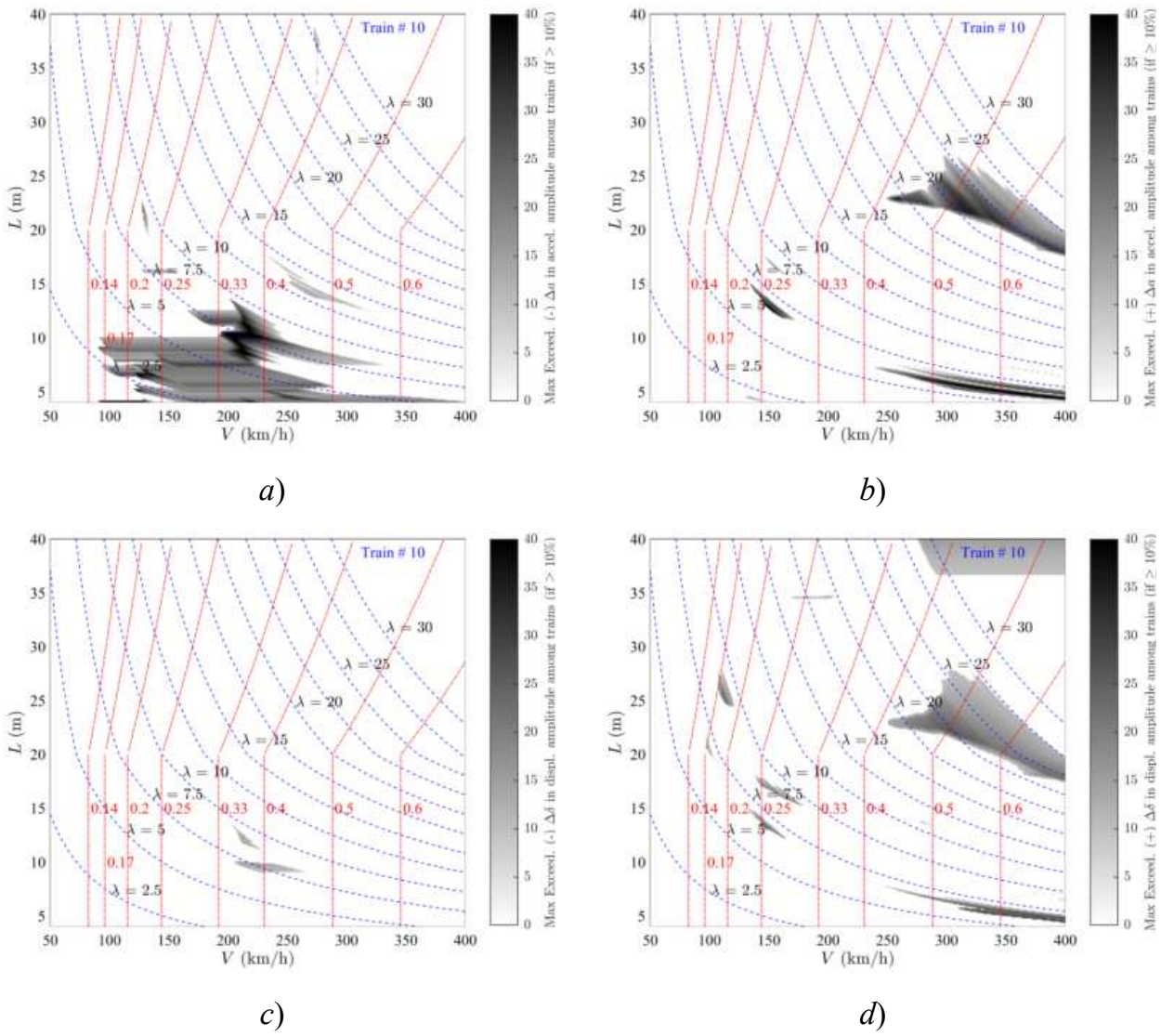

Figure 20. Exceedance Maps Train PT60-10 DER vs Duhamel: a) Δa(–); b) Δa(+); c) Δδ(–); d) Δδ(+). PSC bridges.

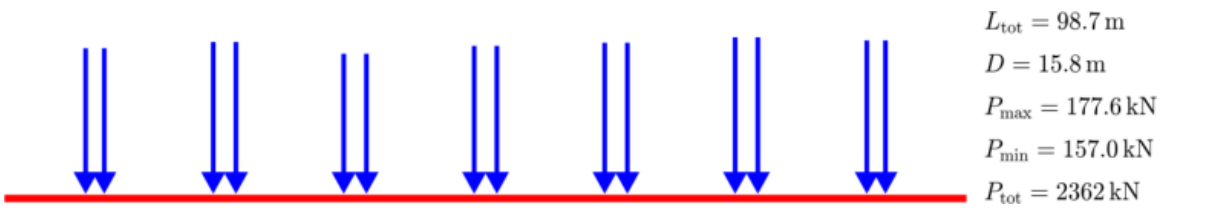

Figure Train PT60-11 [INB4EU-AB-019]

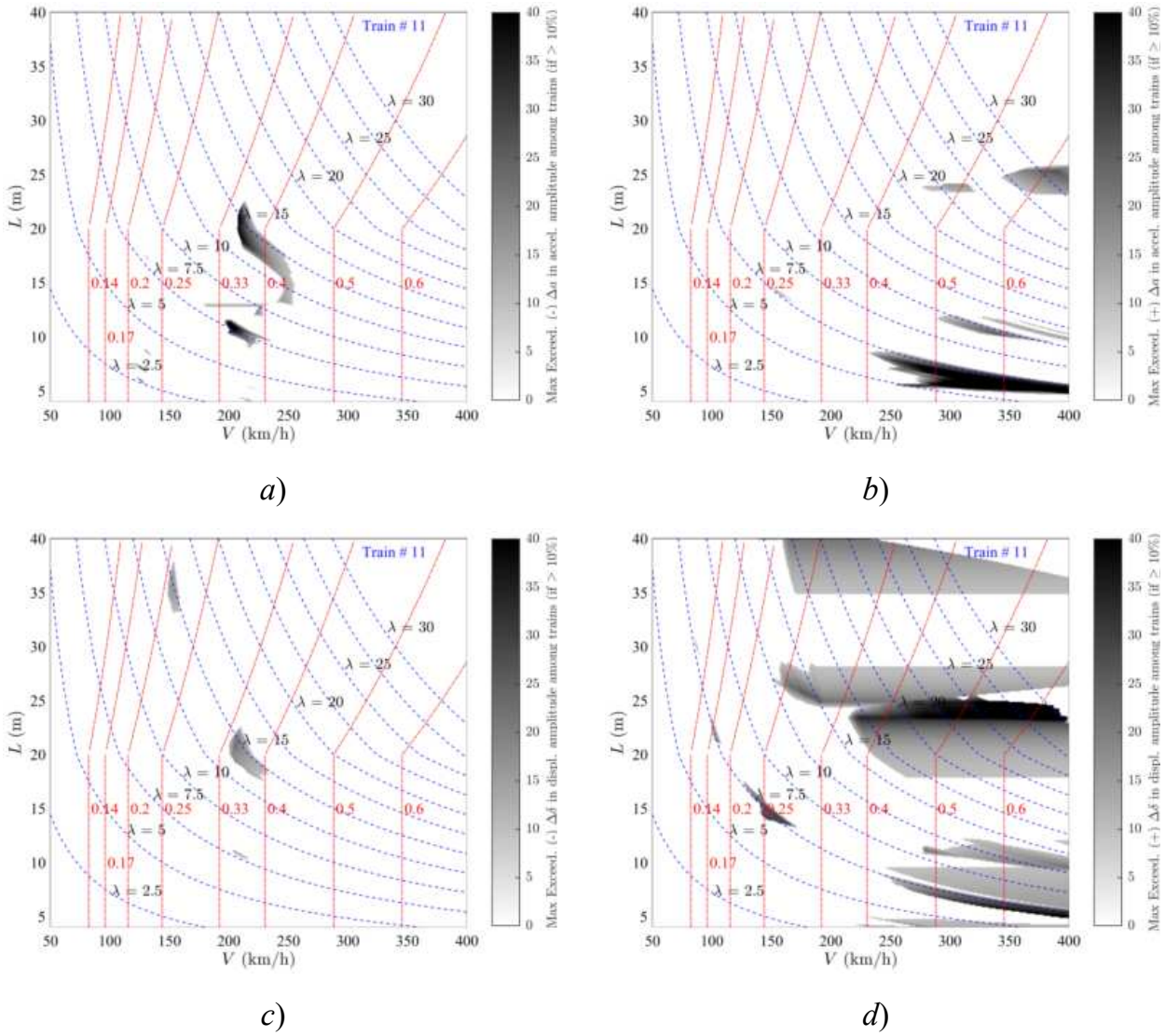

Figure 21. Exceedance Maps Train PT60-11 LIR vs Duhamel: a) Δa(–); b) Δa(+); c) Δδ(–); d) Δδ(+). PSC bridges.

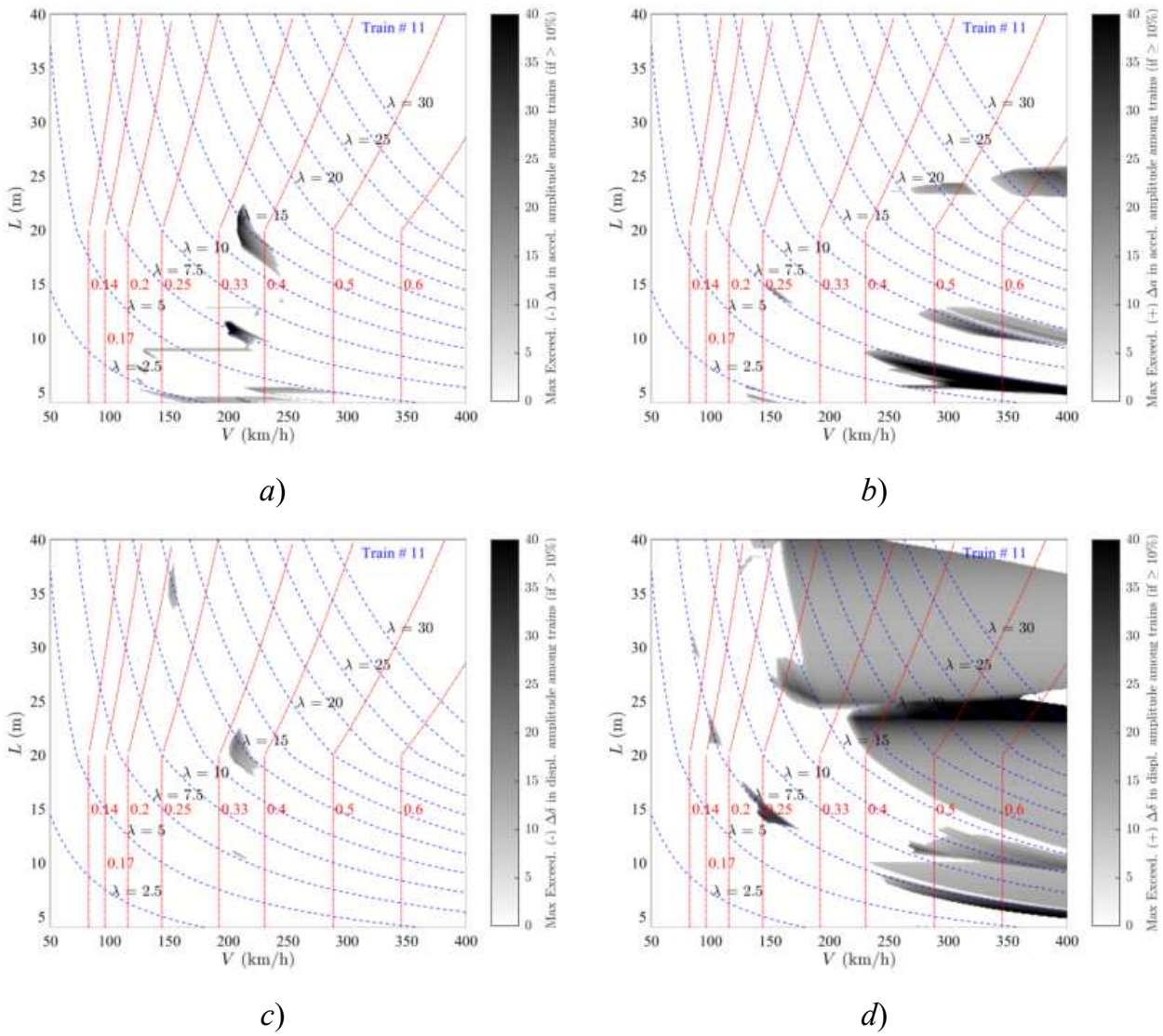

Figure 22. Exceedance Maps Train PT60-11 DER vs Duhamel: a) Δa(–); b) Δa(+); c) Δδ(–); d) Δδ(+). PSC bridges.

Figure Train PT60-12 [INB4EU-CB-052]

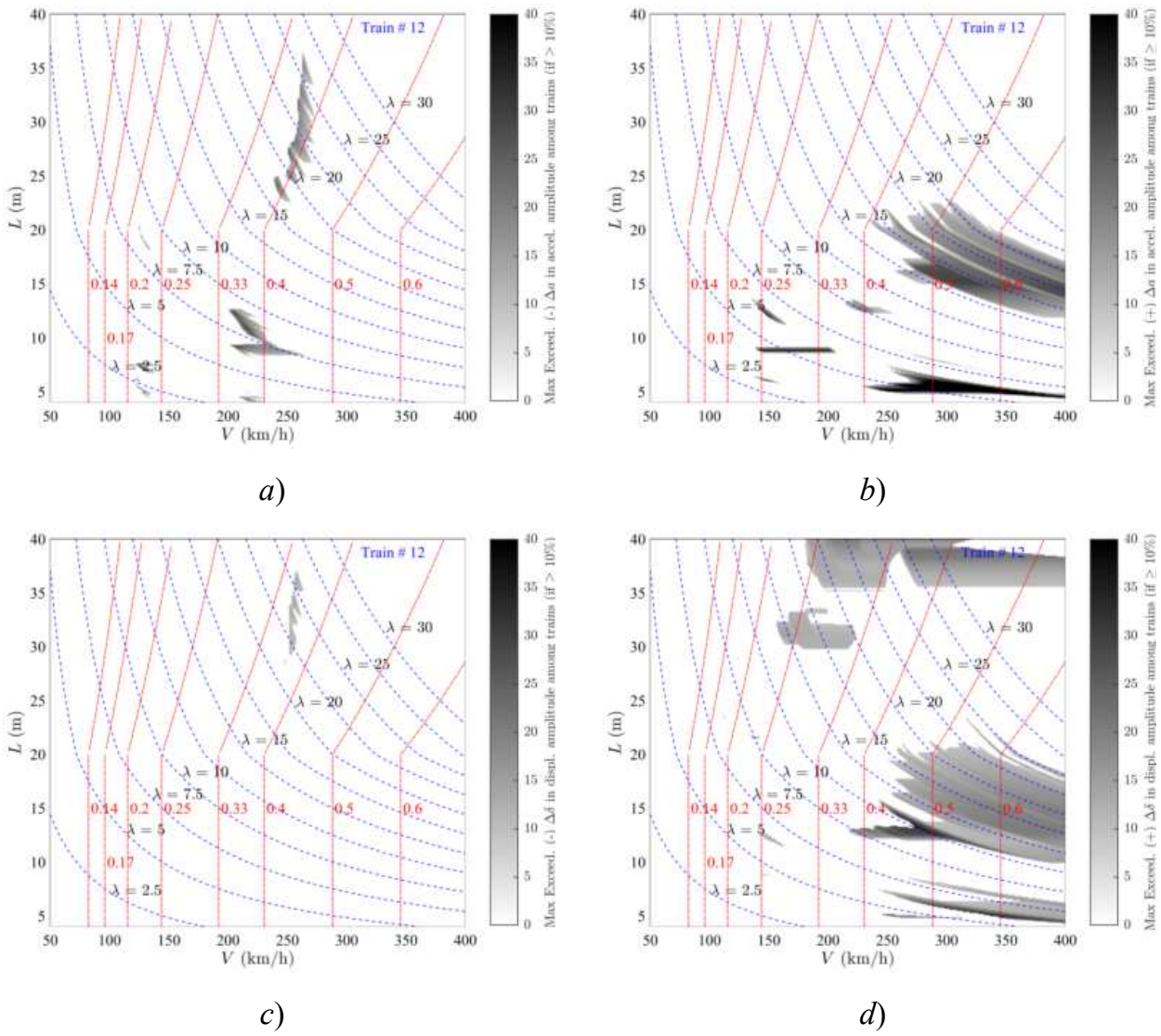

Figure 23. Exceedance Maps Train PT60-12 LIR vs Duhamel: a) Δa(–); b) Δa(+); c) Δδ(–); d) Δδ(+). PSC bridges.

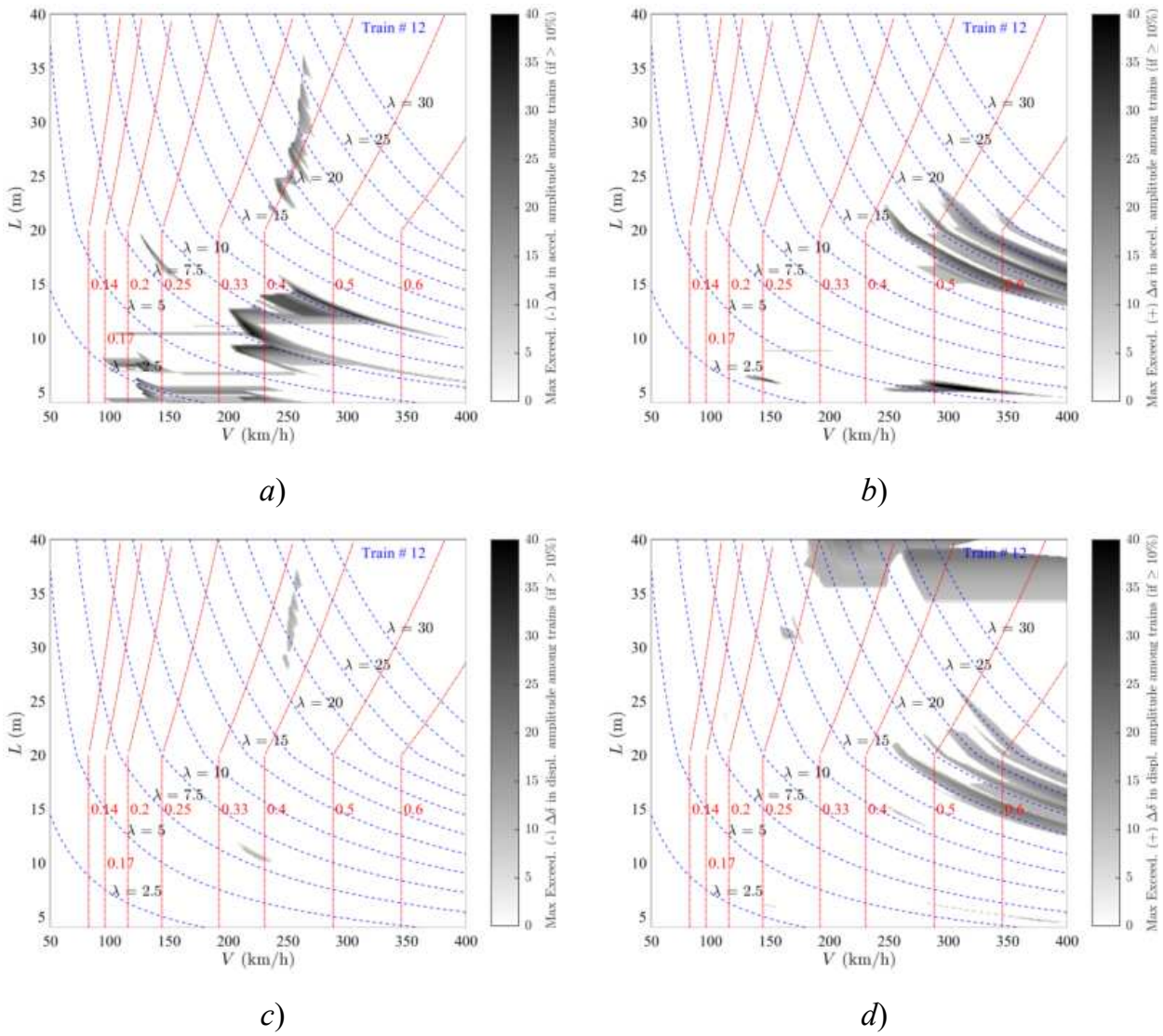

Figure 24. Exceedance Maps Train PT60-12 DER vs Duhamel: a) Δa(−); b) Δa(+); c) Δδ(−); d) Δδ(+). PSC bridges.

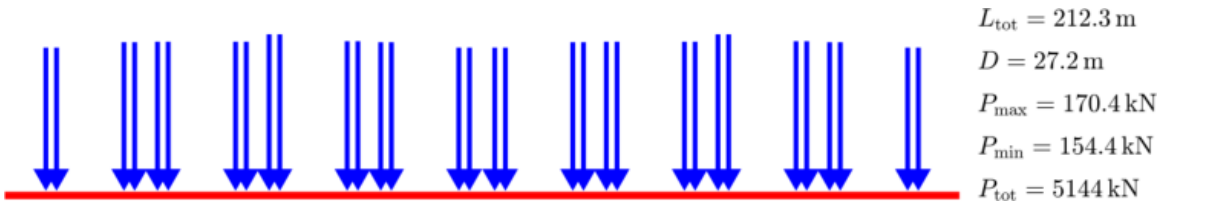

Figure Train PT60-13 [INB4EU-CB-200]

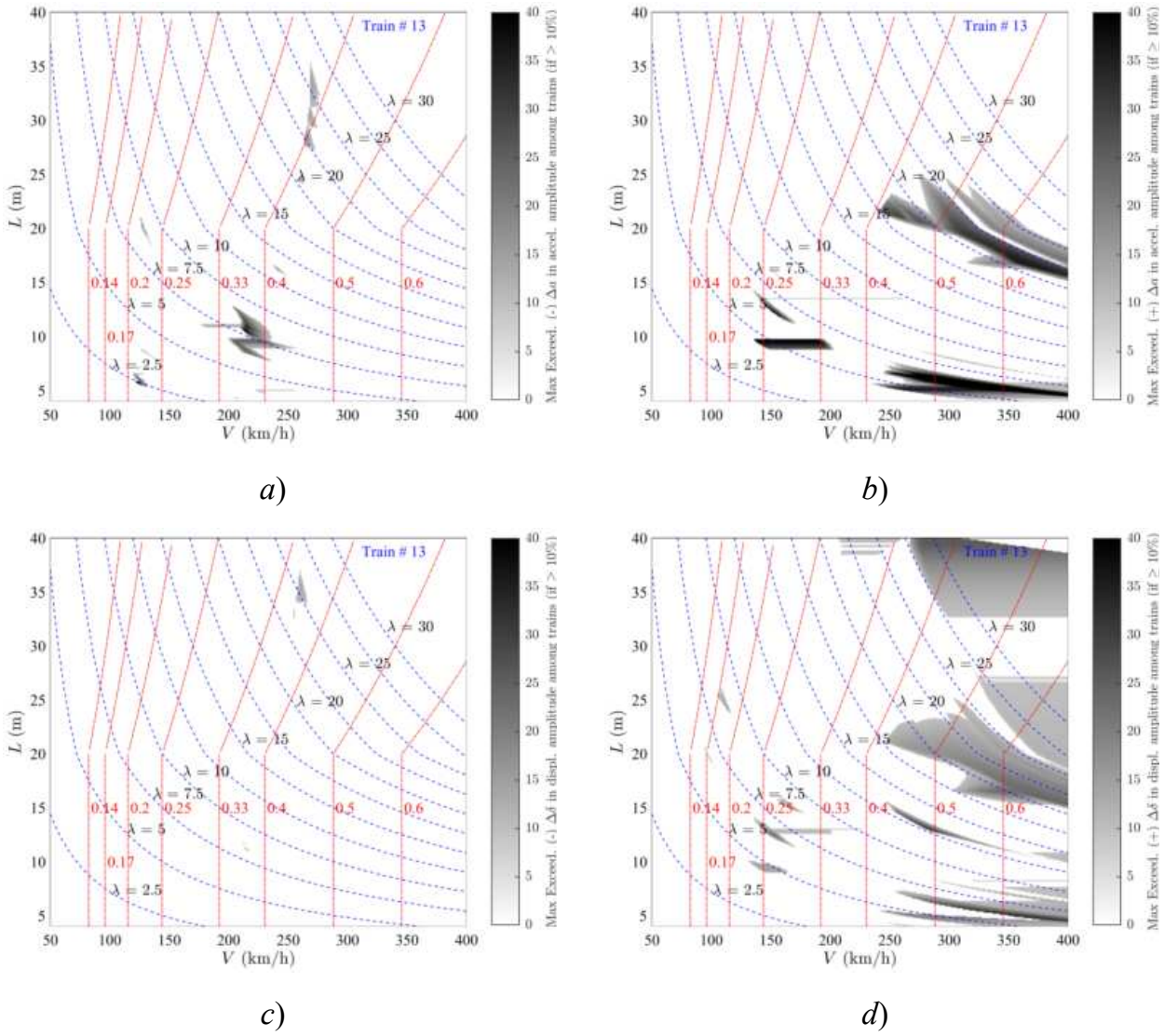

Figure 25. Exceedance Maps Train PT60-13 LIR vs Duhamel: a) Δa(–); b) Δa(+); c) Δδ(–); d) Δδ(+). PSC bridges.

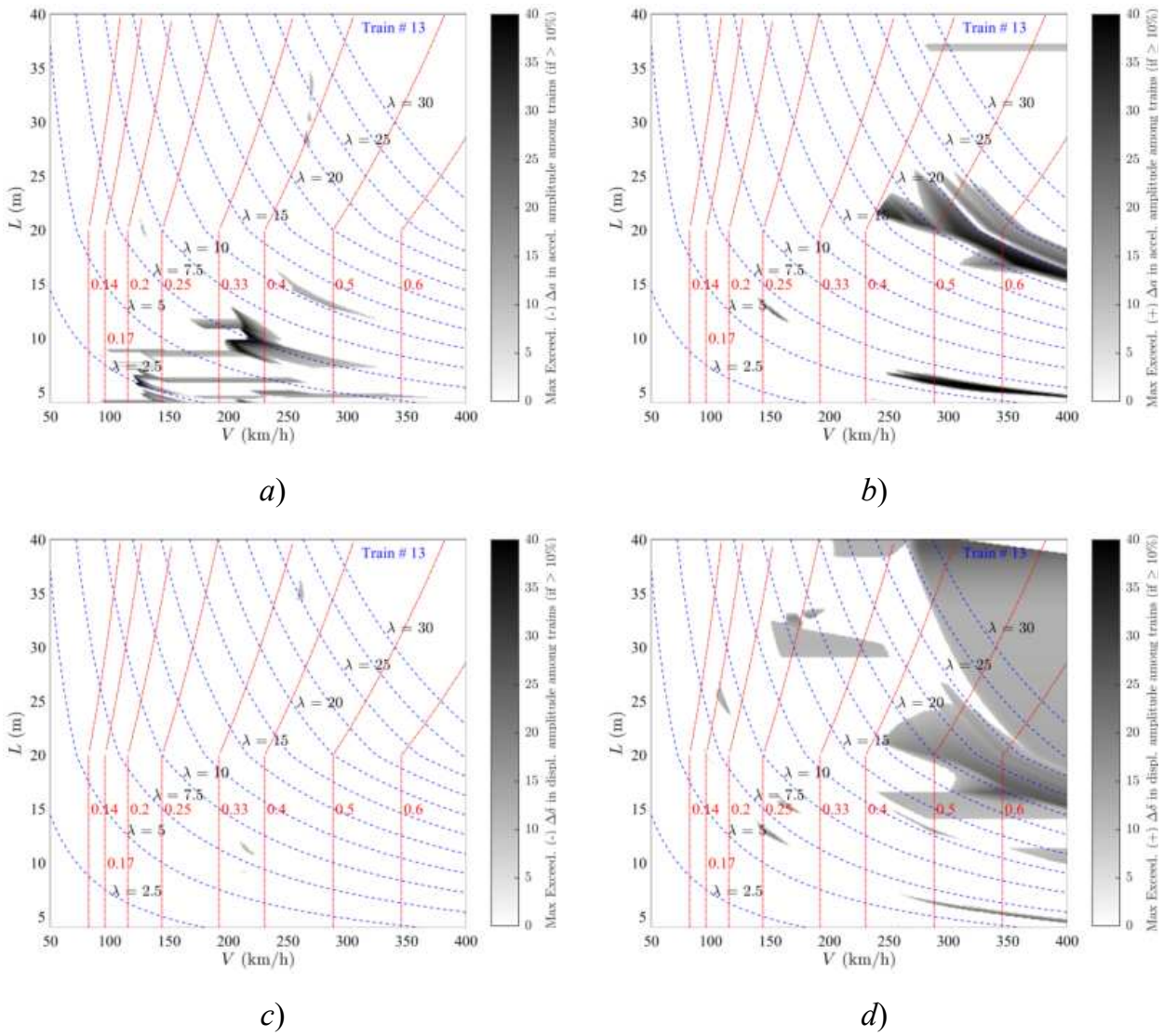

Figure 26. Exceedance Maps Train PT60-13 DER vs Duhamel: a) Δa(–); b) Δa(+); c) Δδ(–); d) Δδ(+). PSC bridges.

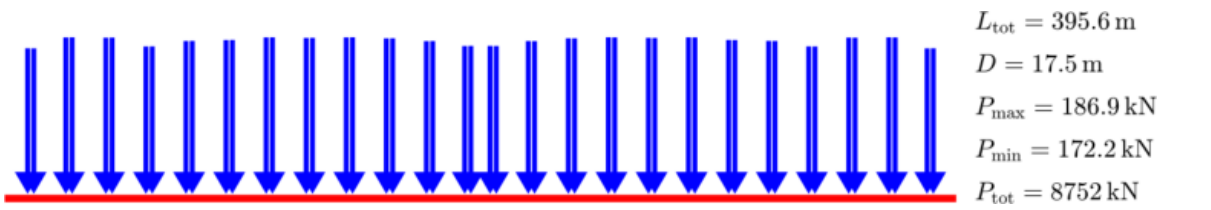

Figure Train PT60-14 [INB4EU-AB-013]

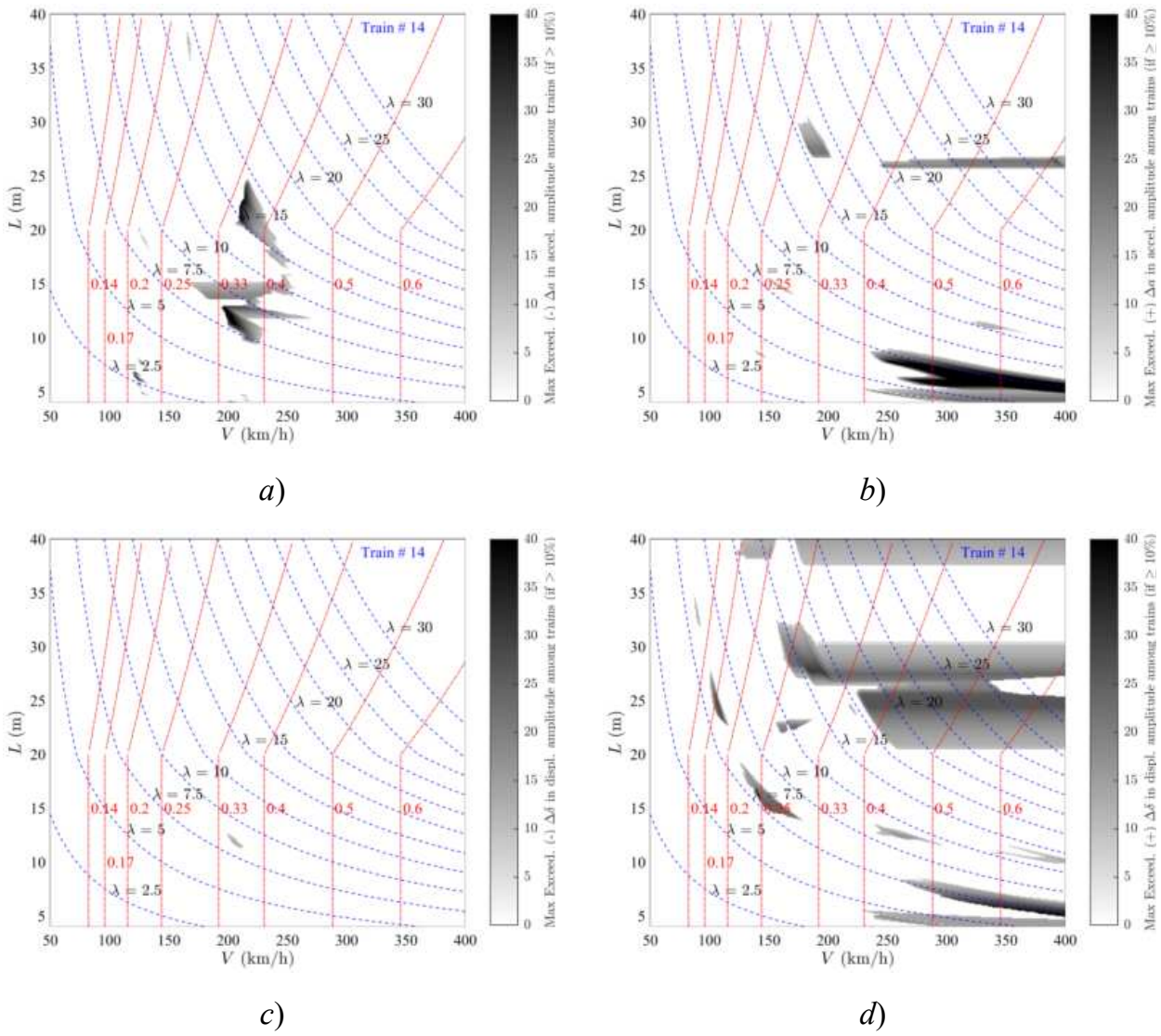

Figure 27. Exceedance Maps Train PT60-14 LIR vs Duhamel: a) Δa(–); b) Δa(+); c) Δδ(–); d) Δδ(+). PSC bridges.

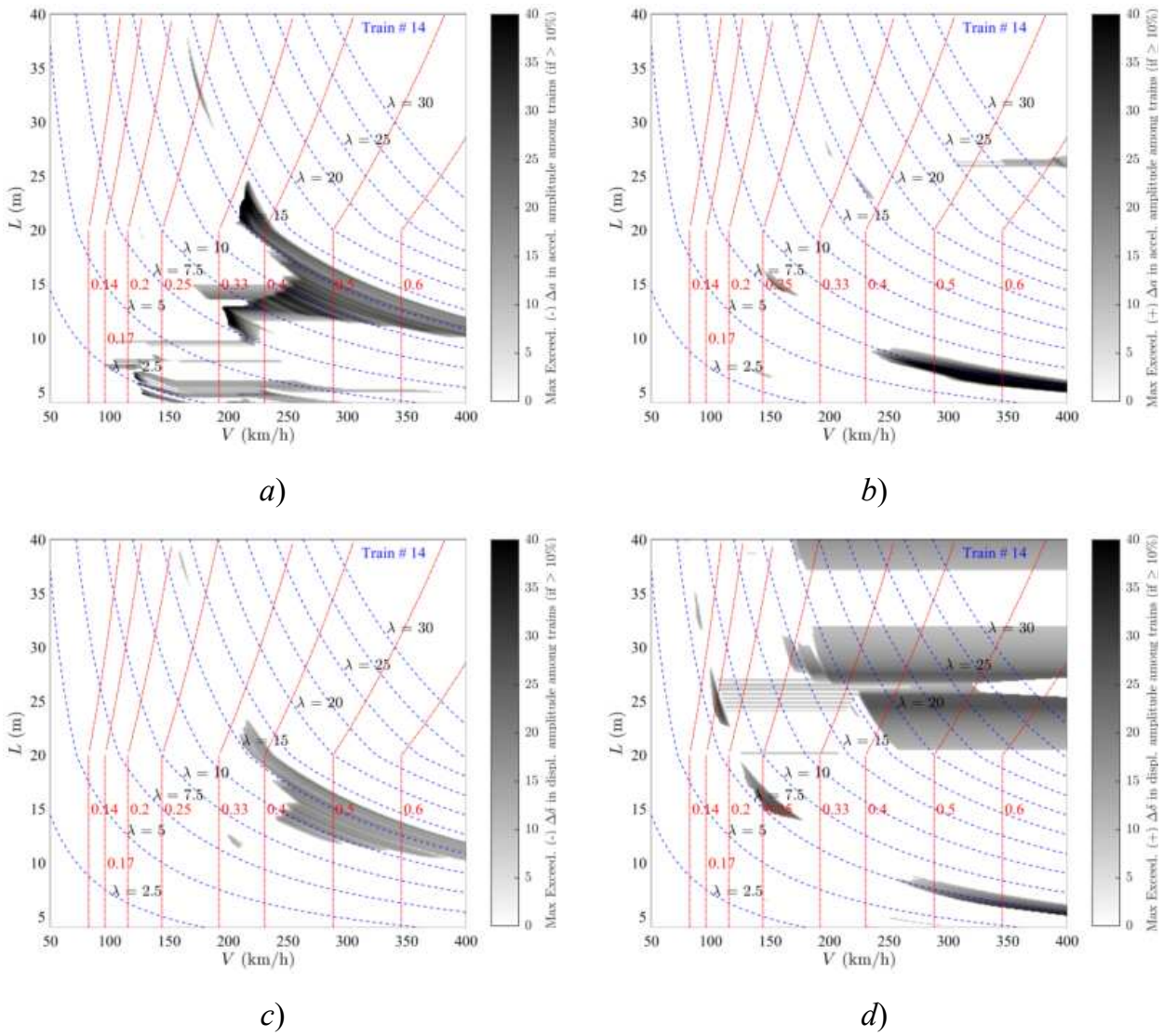

Figure 28. Exceedance Maps Train PT60-14 DER vs Duhamel: a) Δa(−); b) Δa(+); c) Δδ(−); d) Δδ(+). PSC bridges.

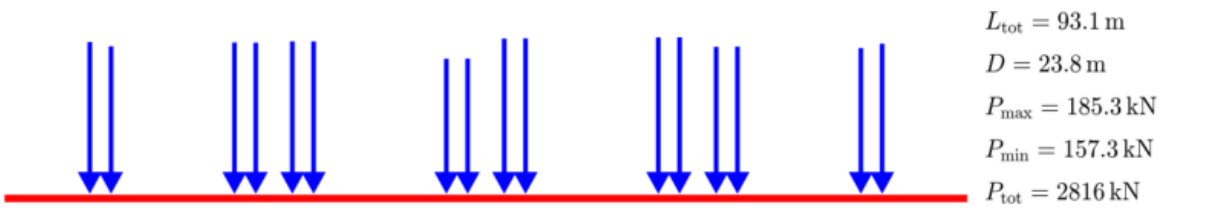

Figure Train PT60-15 [INB4EU-CB-098]

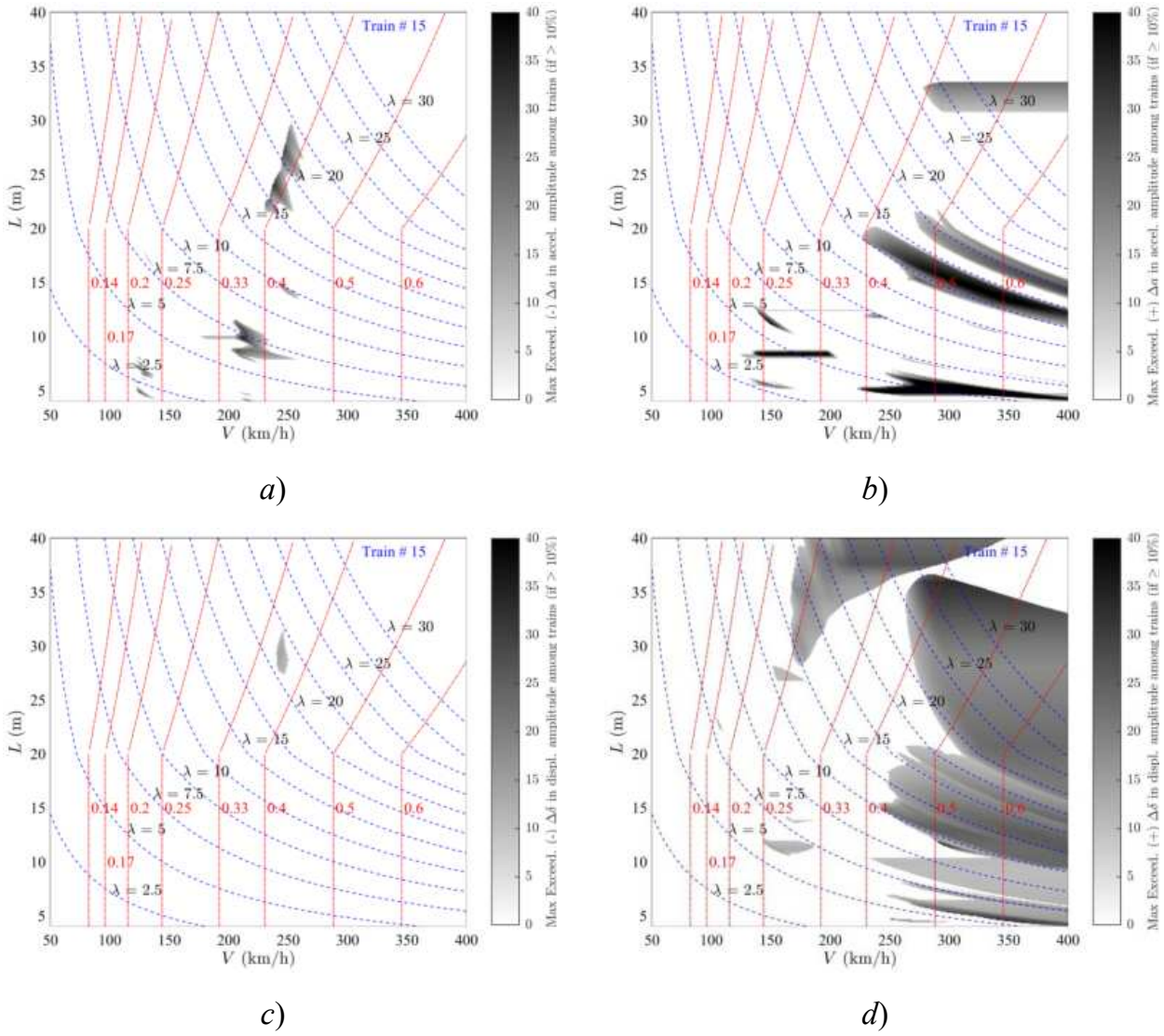

Figure 29. Exceedance Maps Train PT60-15 LIR vs Duhamel: a) Δa(–); b) Δa(+); c) Δδ(–); d) Δδ(+). PSC bridges.

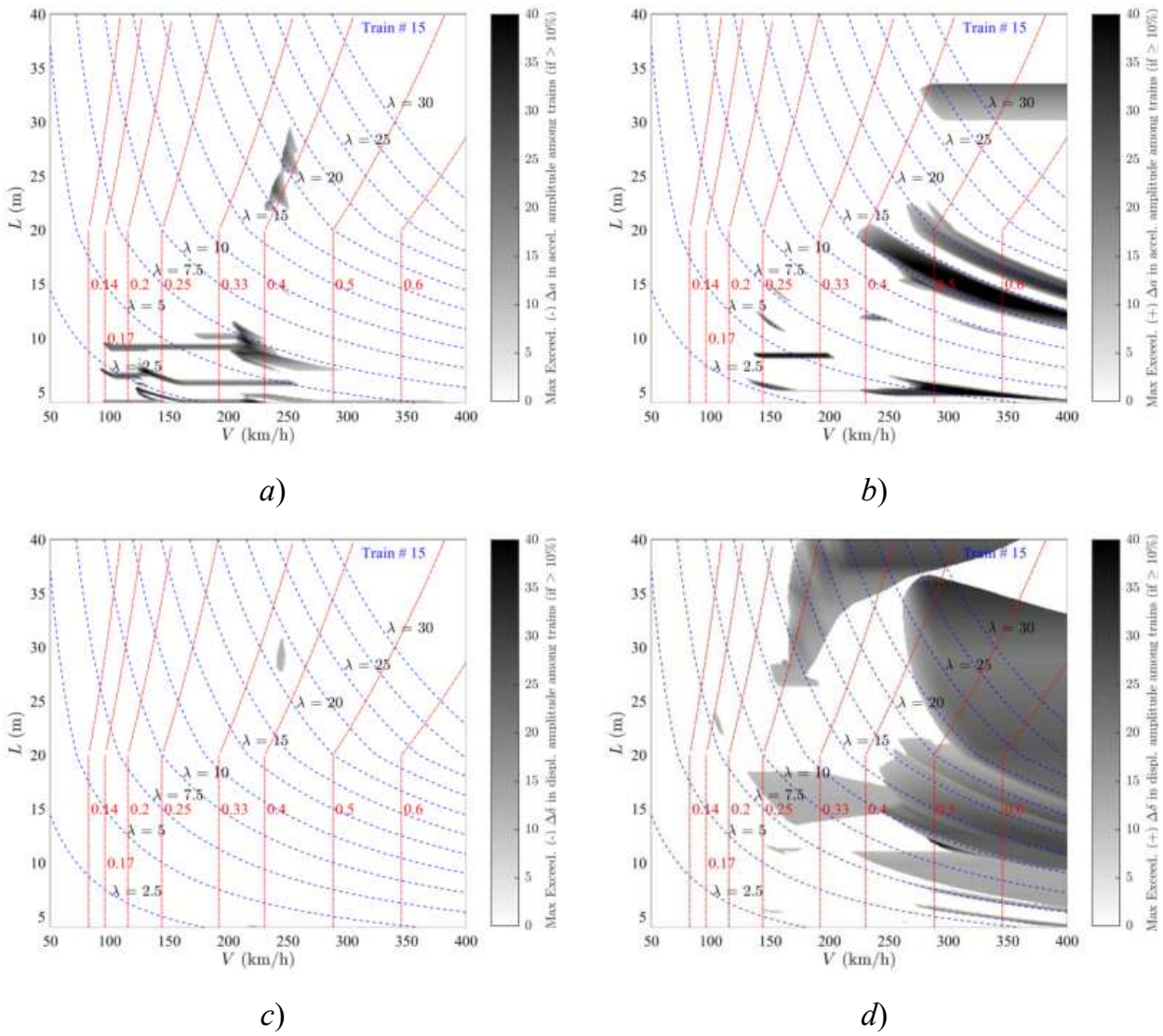

Figure 30. Exceedance Maps Train PT60-15 DER vs Duhamel: a) Δa(–); b) Δa(+); c) Δδ(–); d) Δδ(+). PSC bridges.

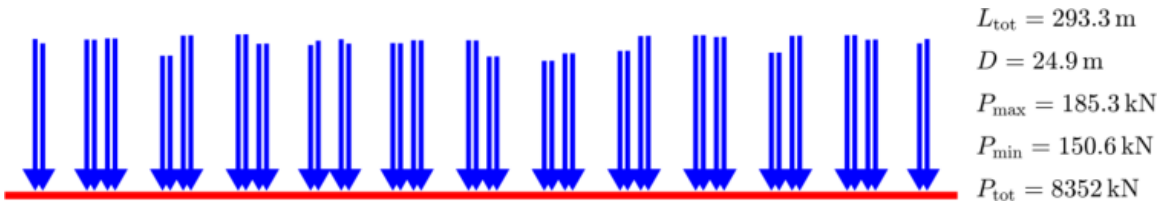

Figure Train PT60-16 [INB4EU-CB-102]

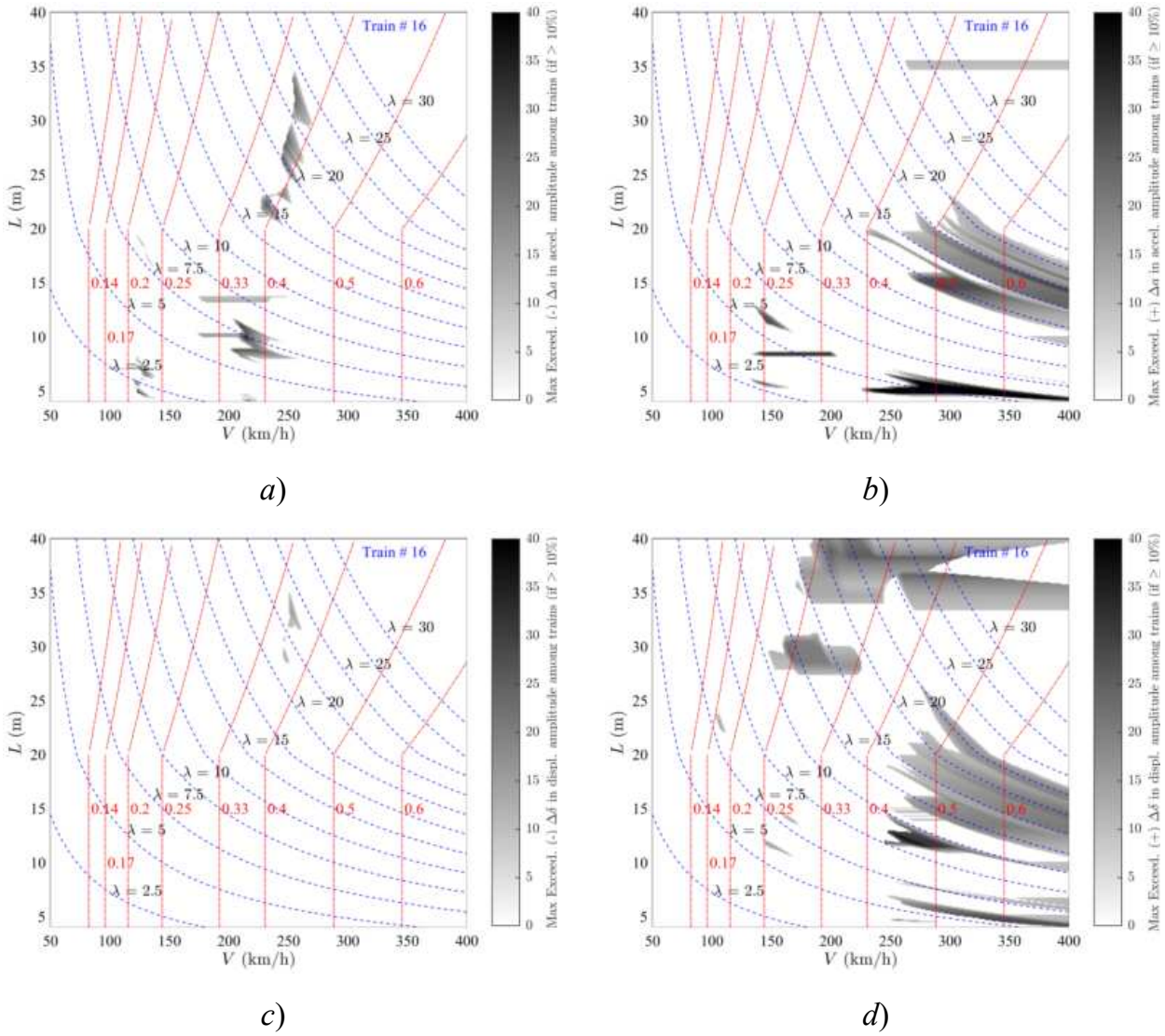

Figure 31. Exceedance Maps Train PT60-16 LIR vs Duhamel: a) Δa(–); b) Δa(+); c) Δδ(–); d) Δδ(+). PSC bridges.

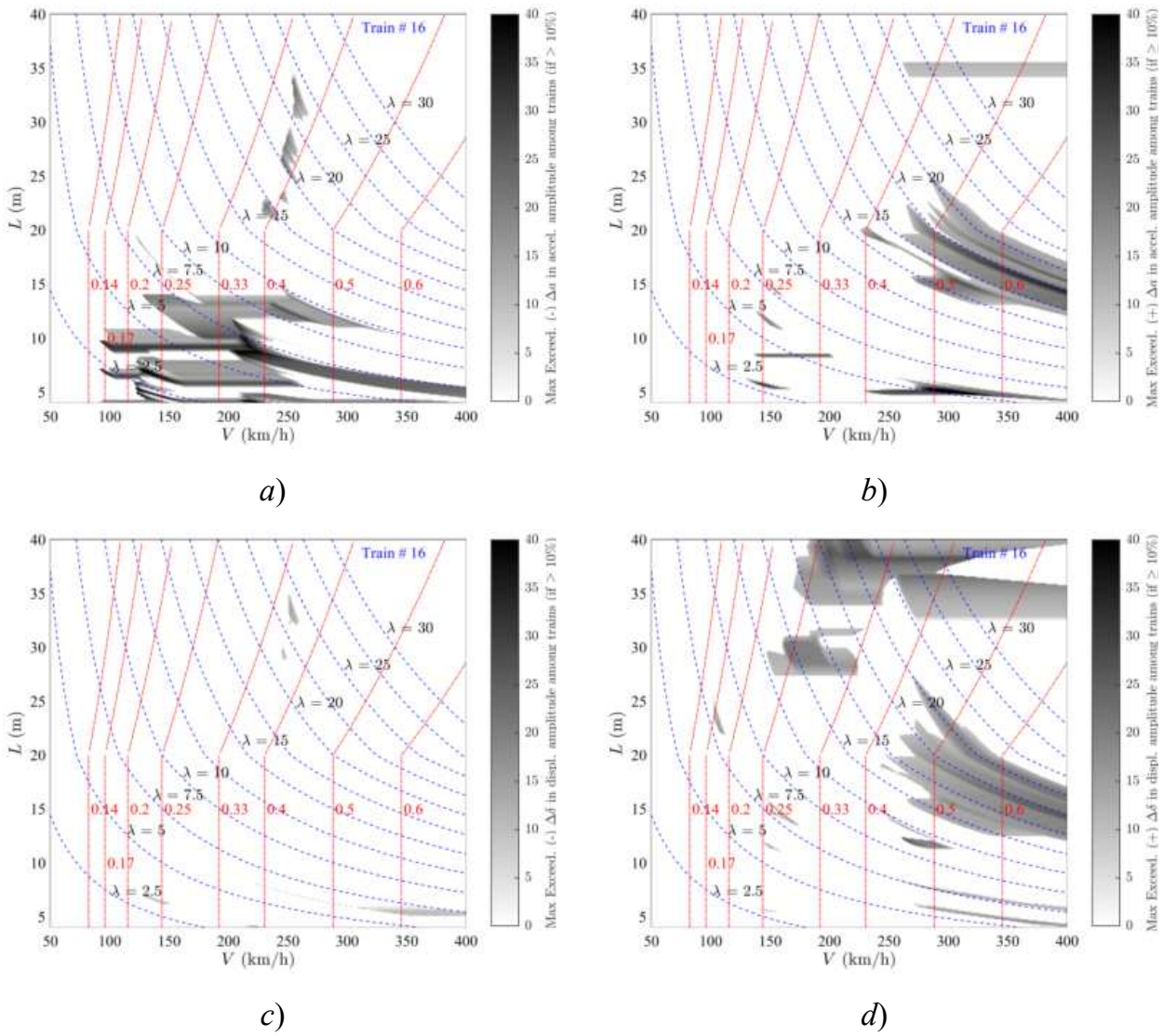

Figure 32. Exceedance Maps Train PT60-16 DER vs Duhamel: a) Δa(–); b) Δa(+); c) Δδ(–); d) Δδ(+). PSC bridges.

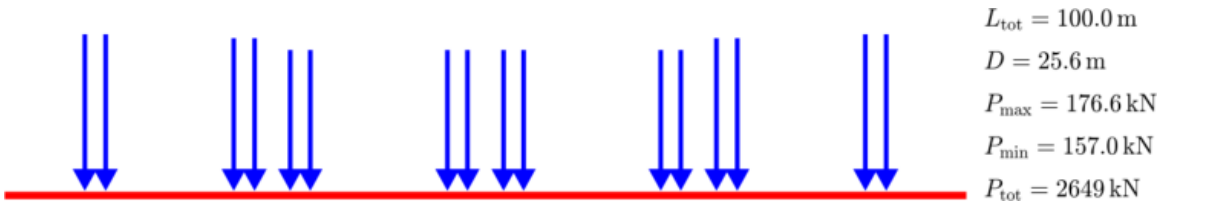

Figure Train PT60-17 [INB4EU-CB-037]

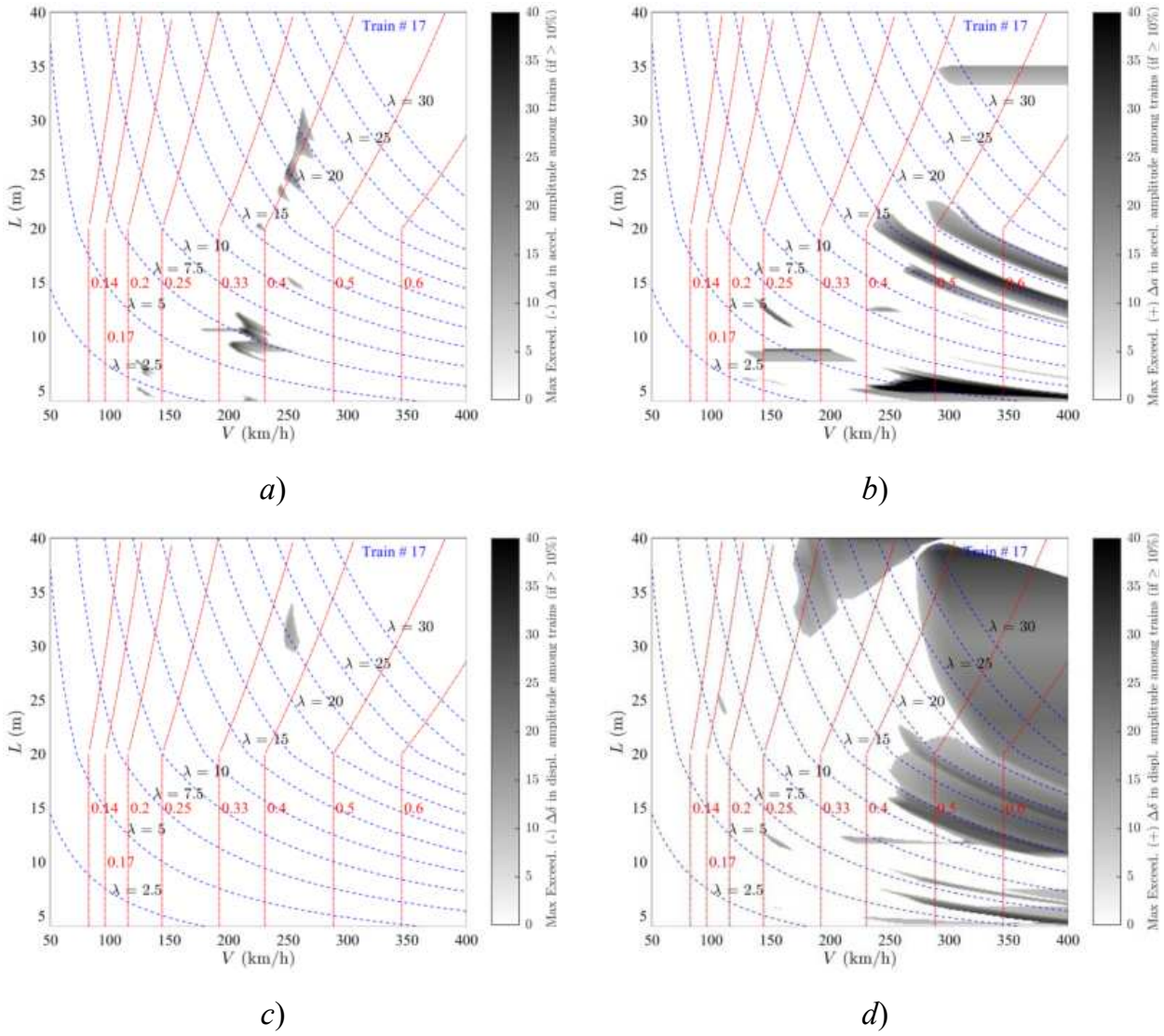

Figure 33. Exceedance Maps Train PT60-17 LIR vs Duhamel: a) Δa(–); b) Δa(+); c) Δδ(–); d) Δδ(+). PSC bridges.

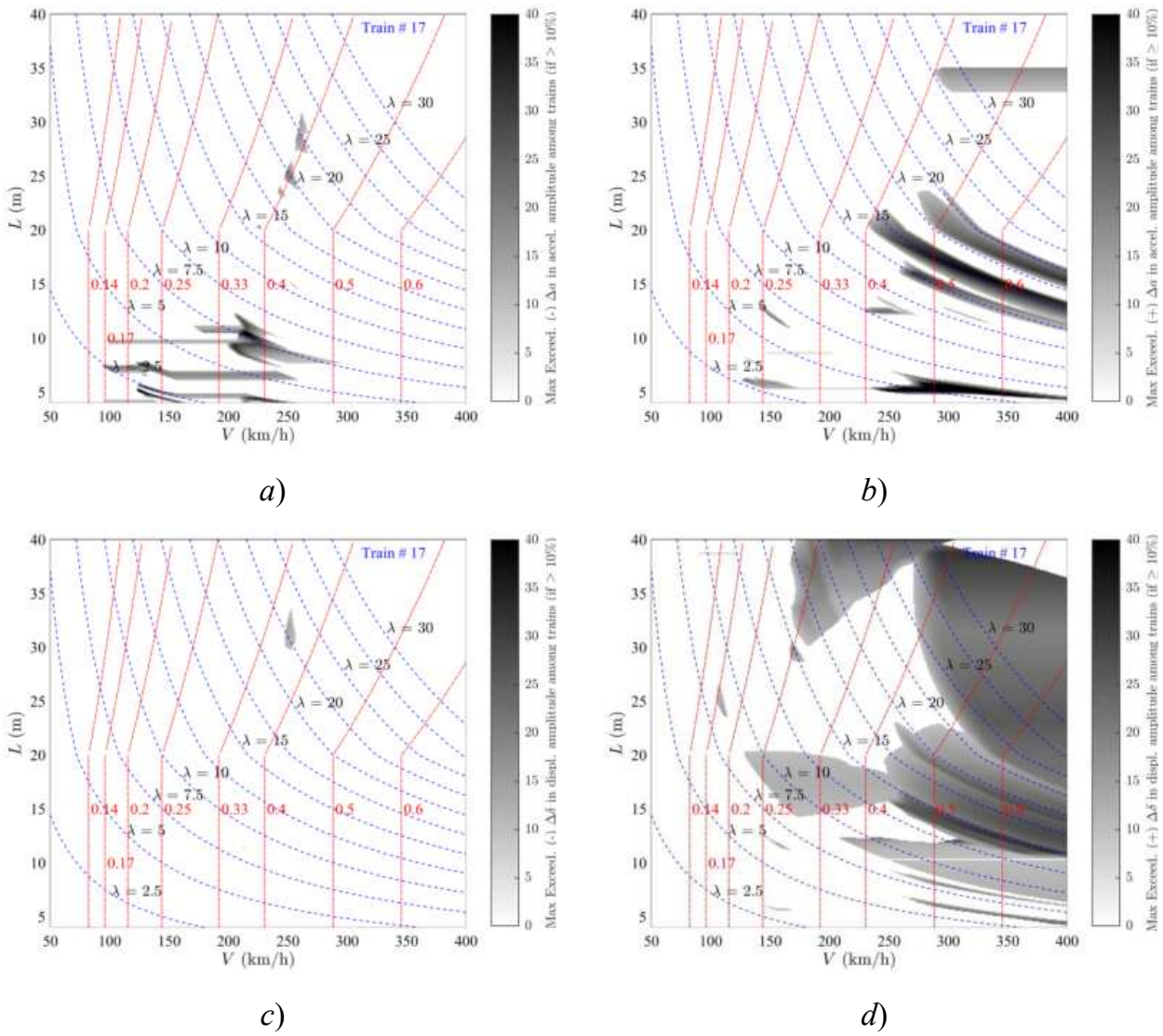

Figure 34. Exceedance Maps Train PT60-17 DER vs Duhamel: a) Δa(−); b) Δa(+); c) Δδ(−); d) Δδ(+). PSC bridges.

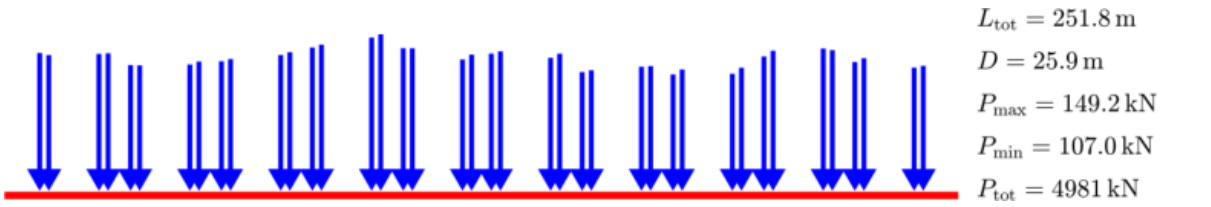

Figure Train PT60-18 [INB4EU-CB-073]

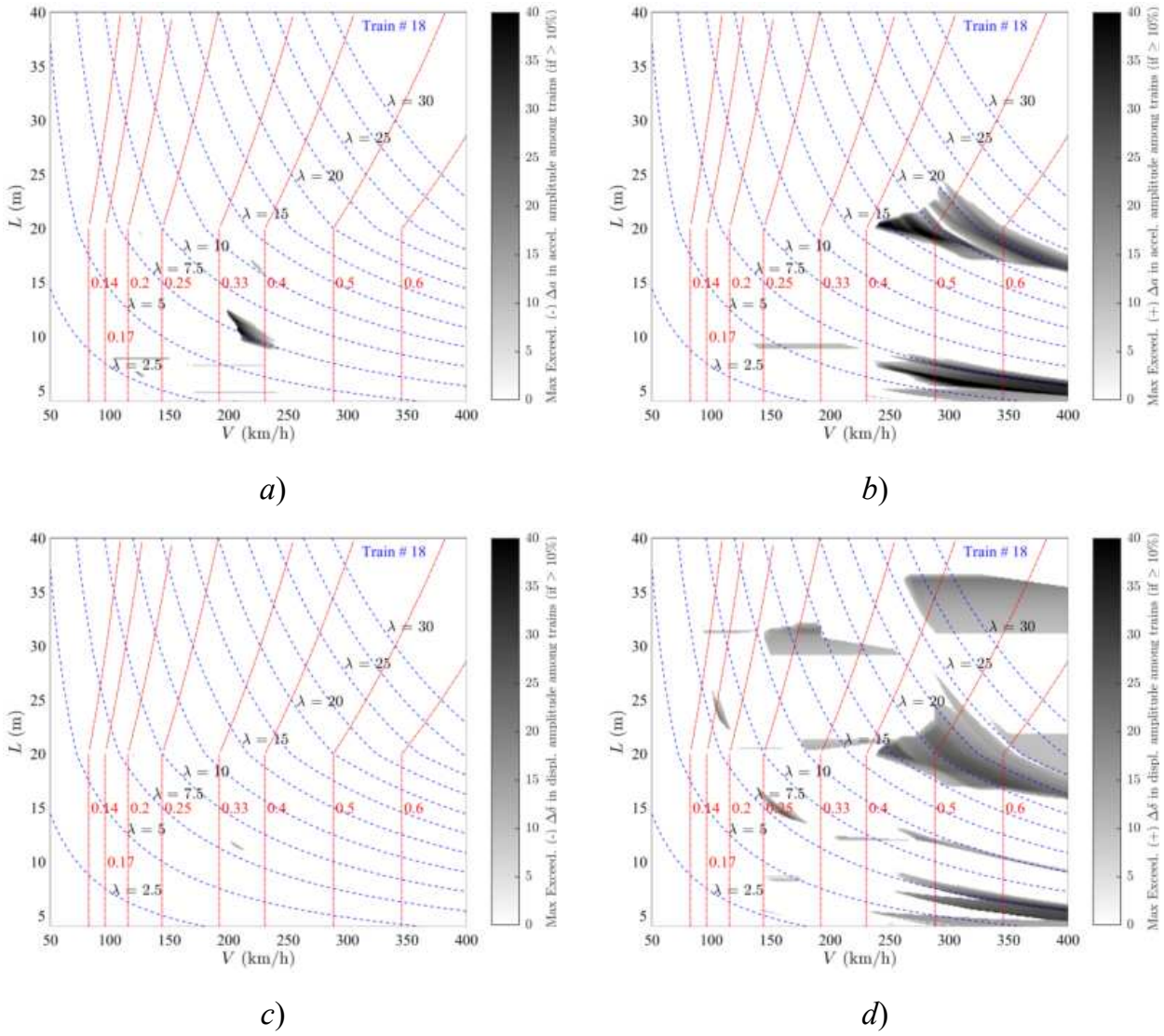

Figure 35. Exceedance Maps Train PT60-18 LIR vs Duhamel: a) Δa(–); b) Δa(+); c) Δδ(–); d) Δδ(+). PSC bridges.

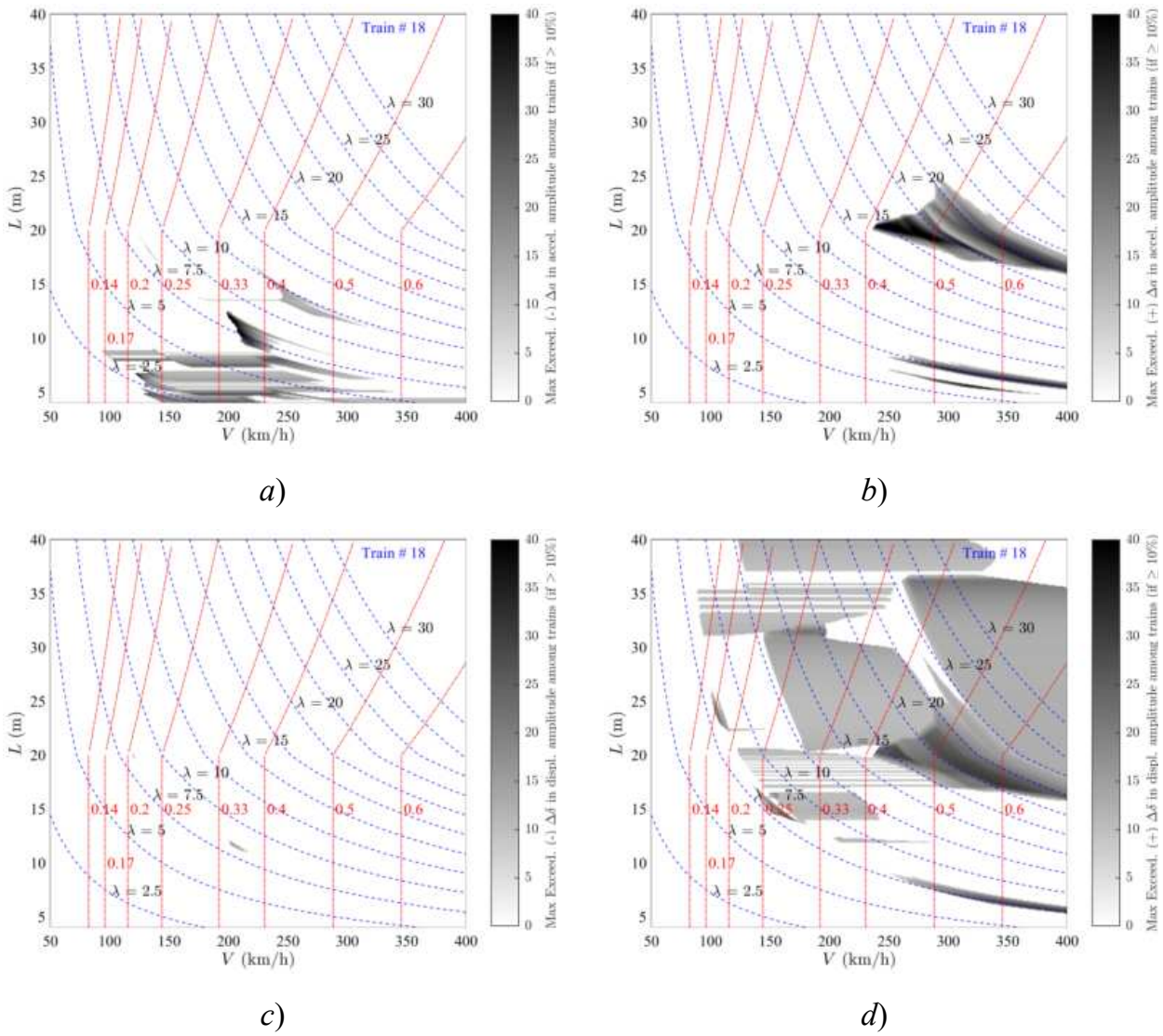

Figure 36. Exceedance Maps Train PT60-18 DER vs Duhamel: a) Δa(–); b) Δa(+); c) Δδ(–); d) Δδ(+). PSC bridges.

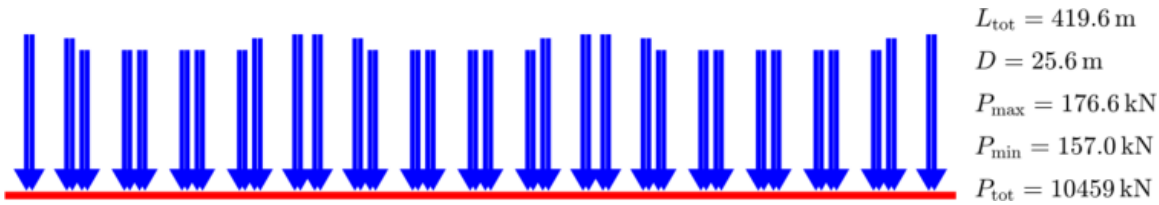

Figure Train PT60-19 [INB4EU-CB-190]

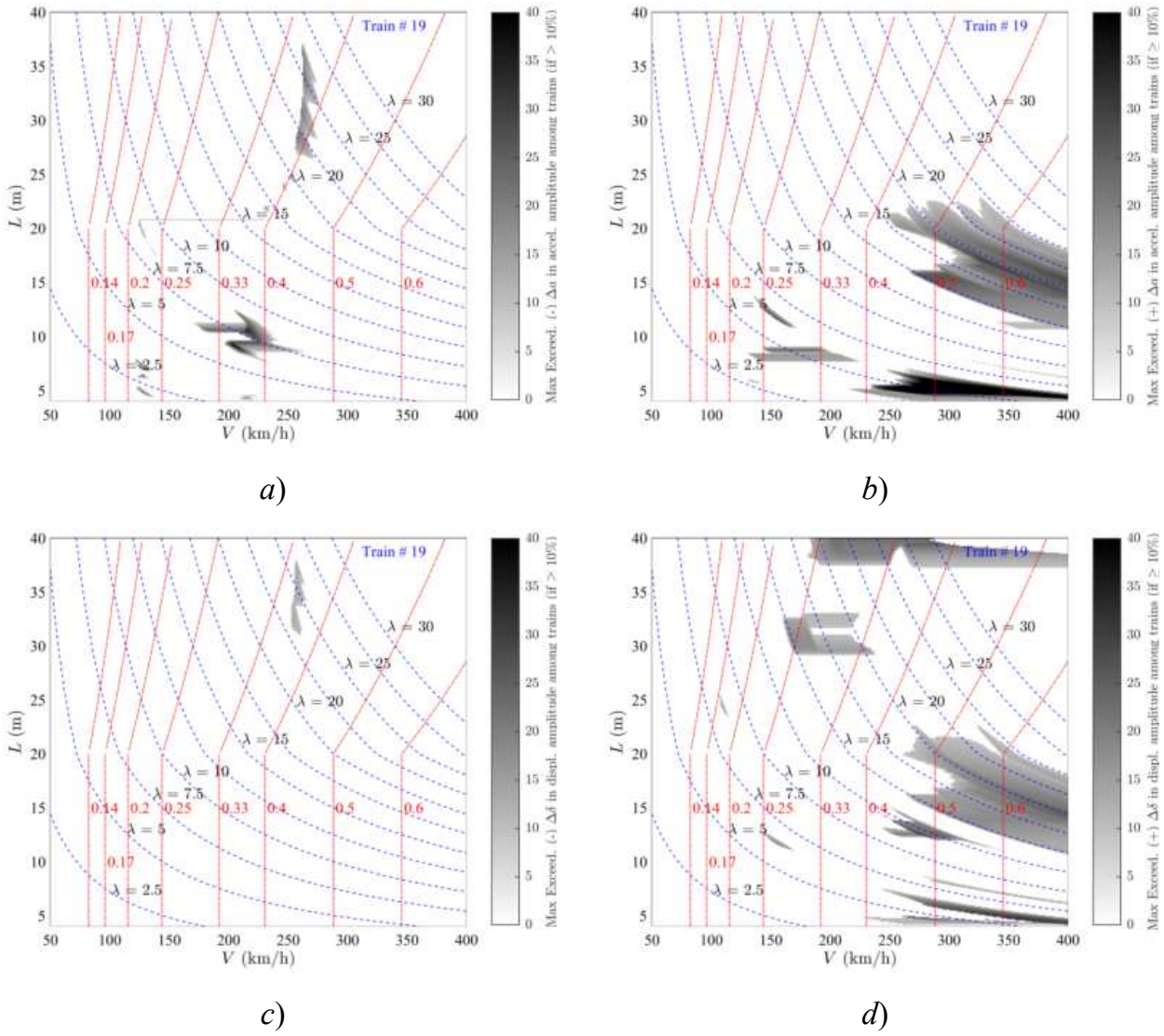

Figure 37. Exceedance Maps Train PT60-19 LIR vs Duhamel: a) Δa(–); b) Δa(+); c) Δδ(–); d) Δδ(+). PSC bridges.

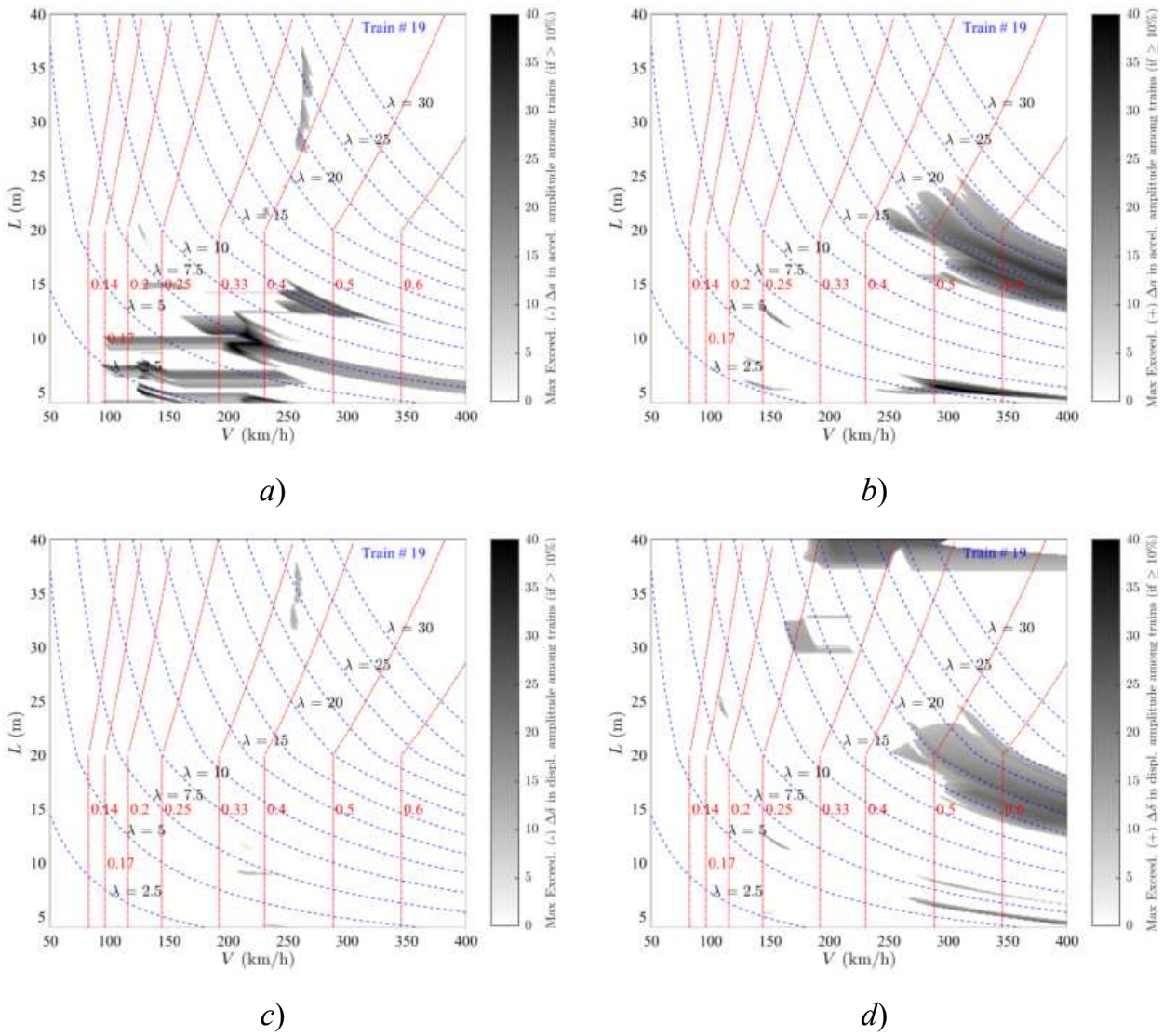

Figure 38. Exceedance Maps Train PT60-19 DER vs Duhamel: a) Δa(–); b) Δa(+); c) Δδ(–); d) Δδ(+). PSC bridges.

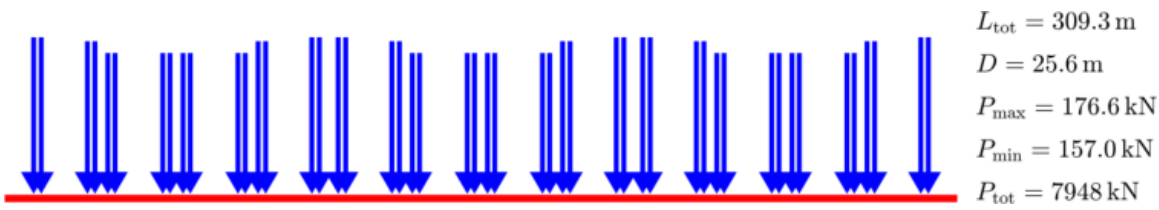

Figure Train PT60-20 [INB4EU-CB-153]

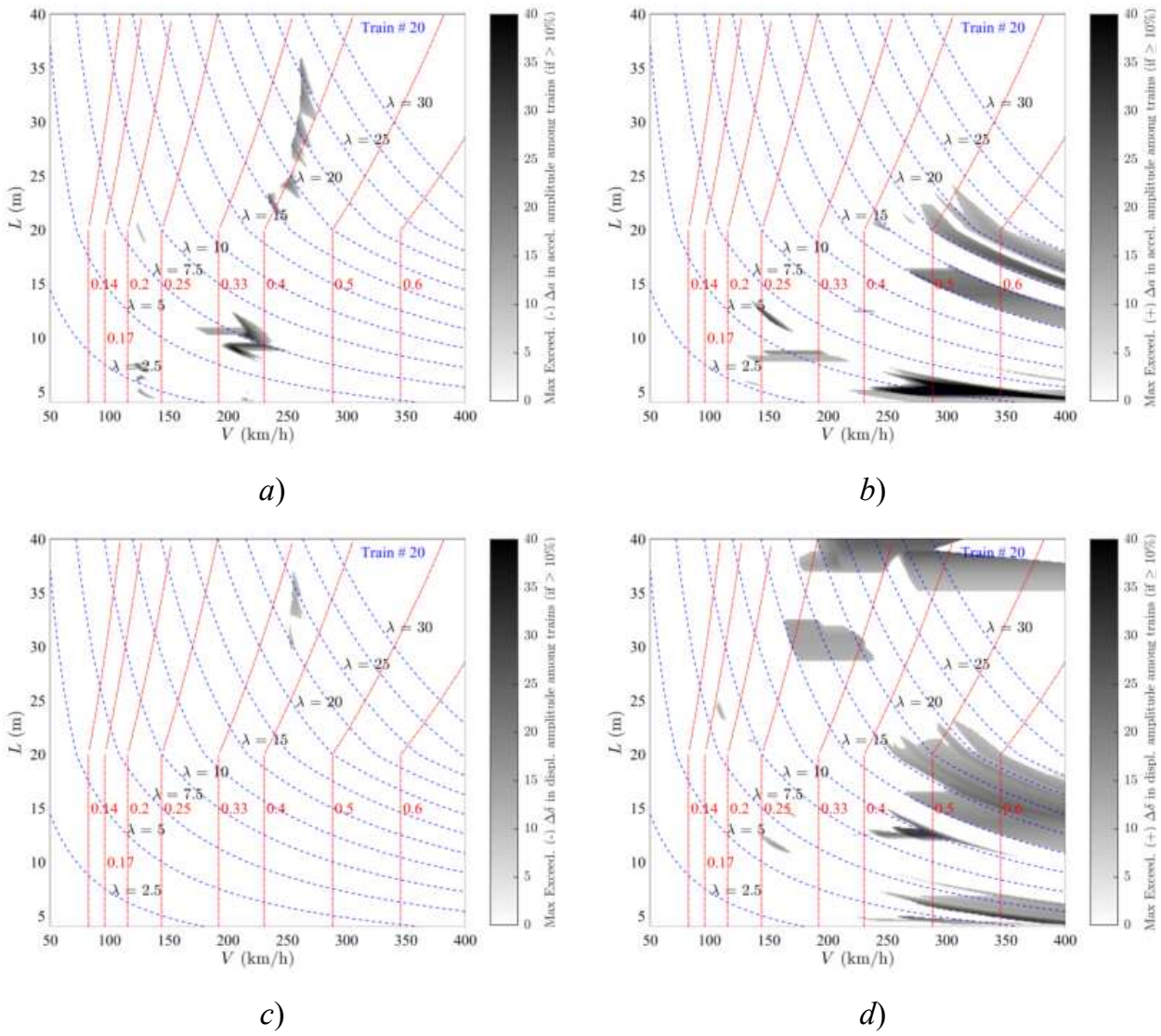

Figure 39. Exceedance Maps Train PT60-20 LIR vs Duhamel: a) Δa(–); b) Δa(+); c) Δδ(–); d) Δδ(+). PSC bridges.

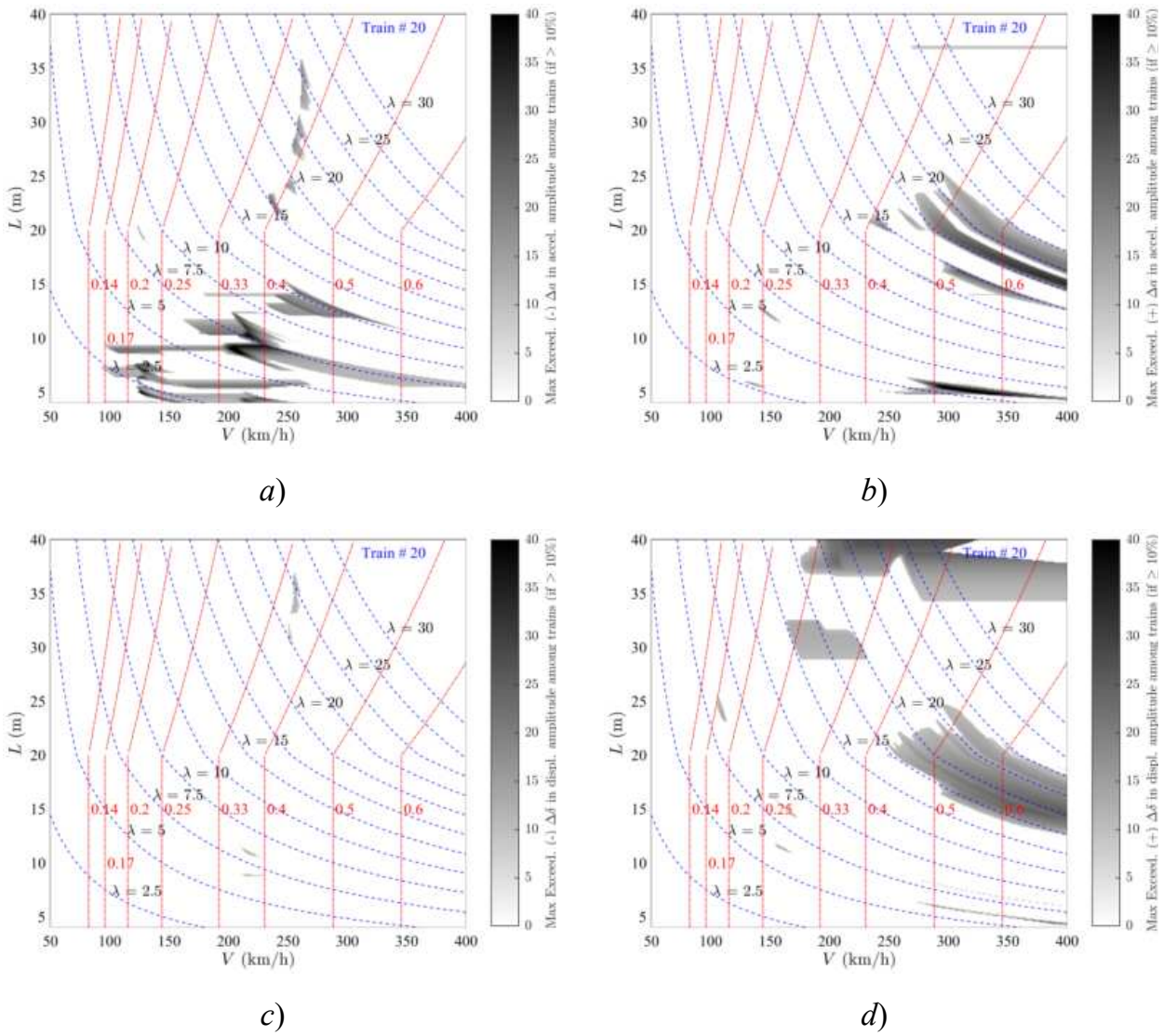

Figure 40. Exceedance Maps Train PT60-20 DER vs Duhamel: a) Δa(−); b) Δa(+); c) Δδ(−); d) Δδ(+). PSC bridges.

Figure Train PT60-21 [INB4EU-CB-128]

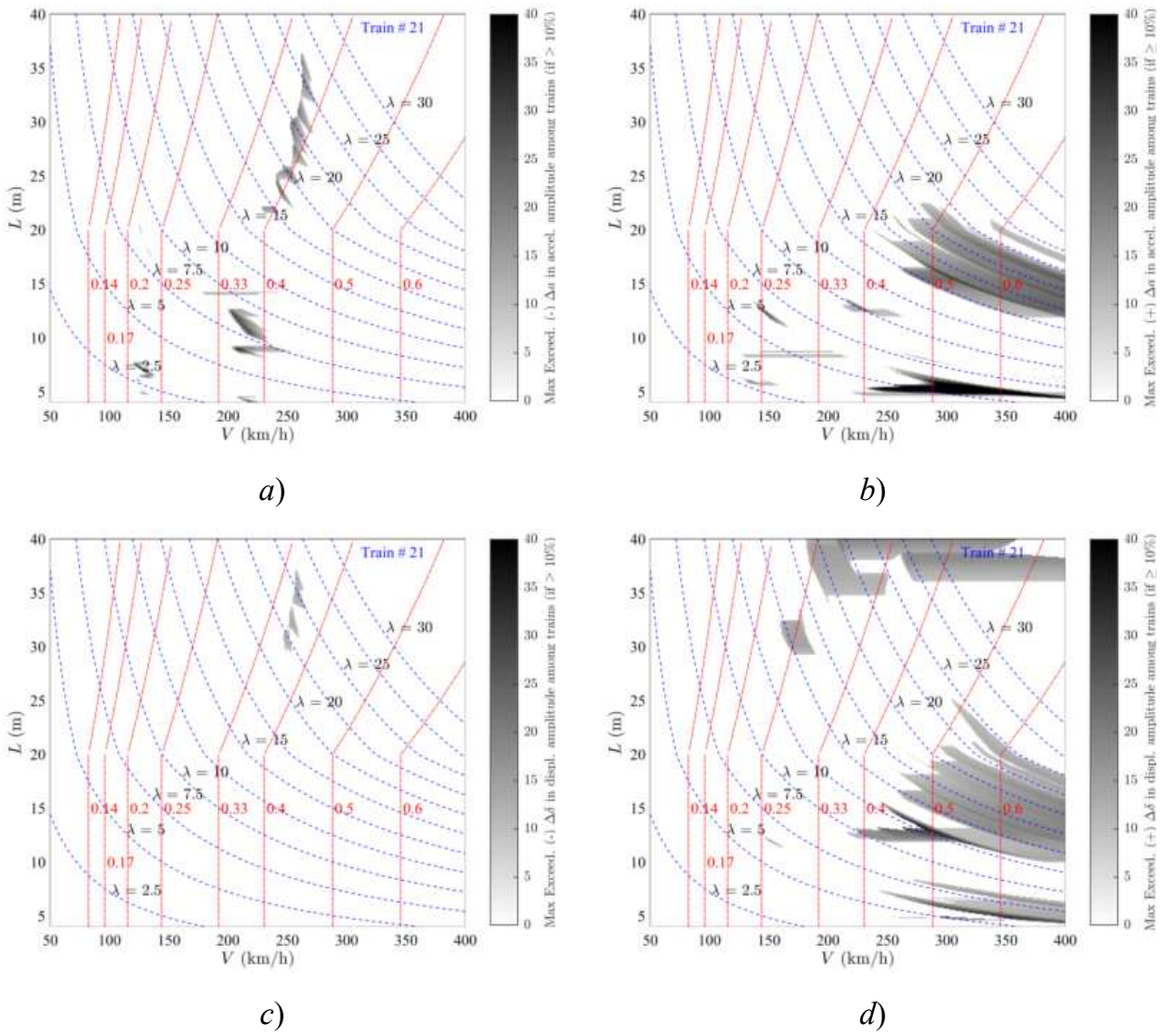

Figure 41. Exceedance Maps Train PT60-21 LIR vs Duhamel: a) Δa(–); b) Δa(+); c) Δδ(–); d) Δδ(+). PSC bridges.

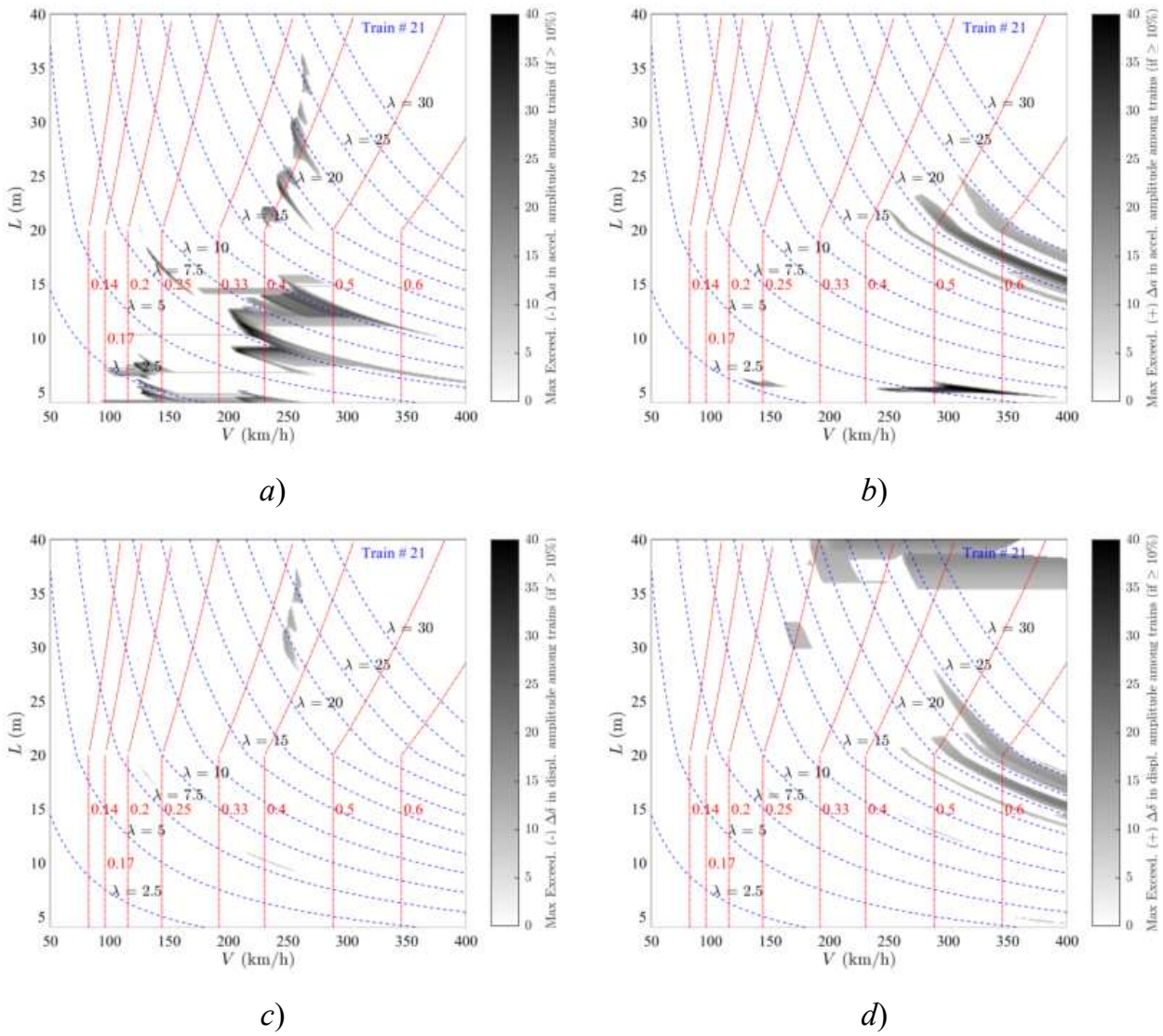

Figure 42. Exceedance Maps Train PT60-21 DER vs Duhamel: a) Δa(−); b) Δa(+); c) Δδ(−); d) Δδ(+). PSC bridges.

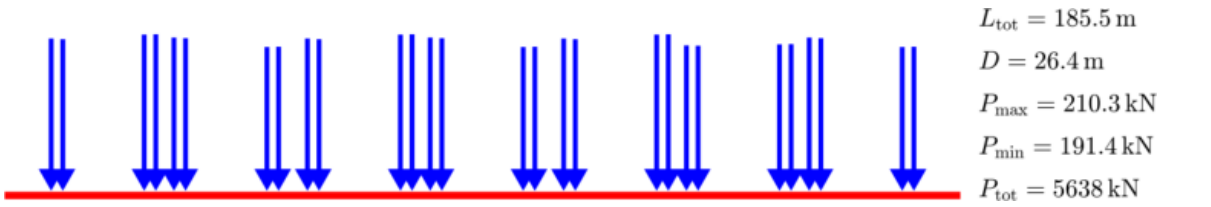

Figure Train PT60-22 [INB4EU-CB-130]

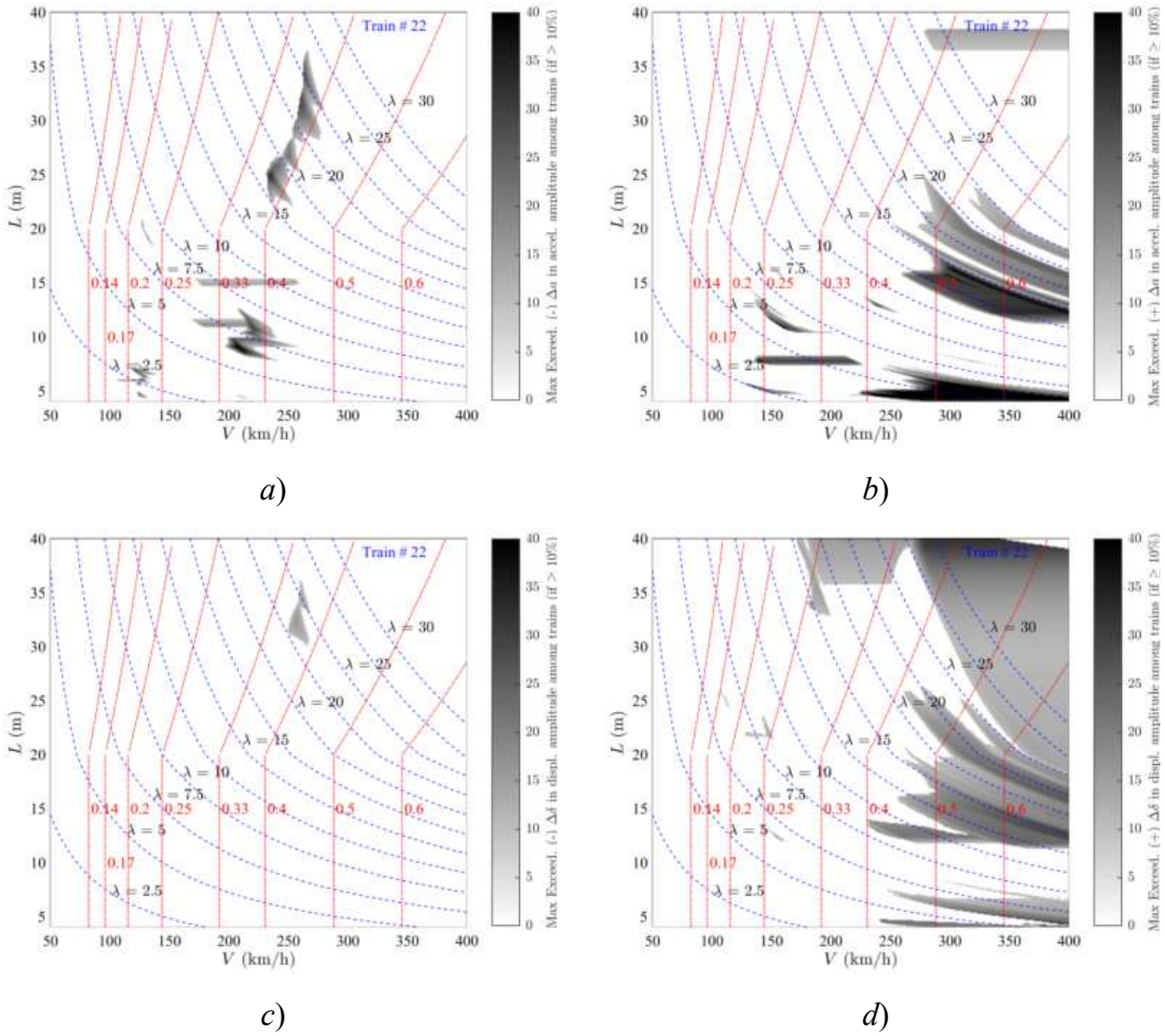

Figure 43. Exceedance Maps Train PT60-22 LIR vs Duhamel: a) Δa(–); b) Δa(+); c) Δδ(–); d) Δδ(+). PSC bridges.

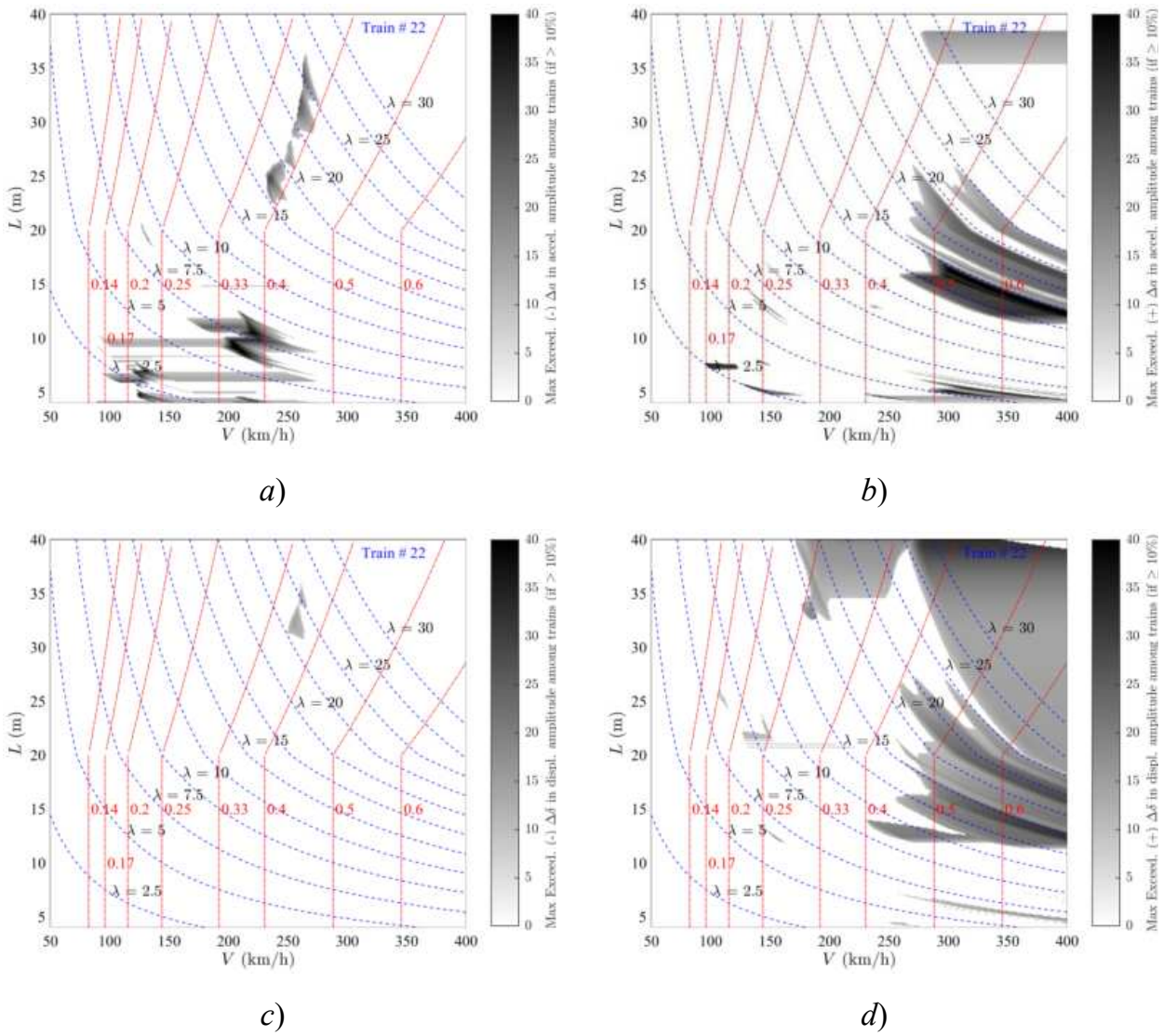

Figure 44. Exceedance Maps Train PT60-22 DER vs Duhamel: a) Δa(–); b) Δa(+); c) Δδ(–); d) Δδ(+). PSC bridges.

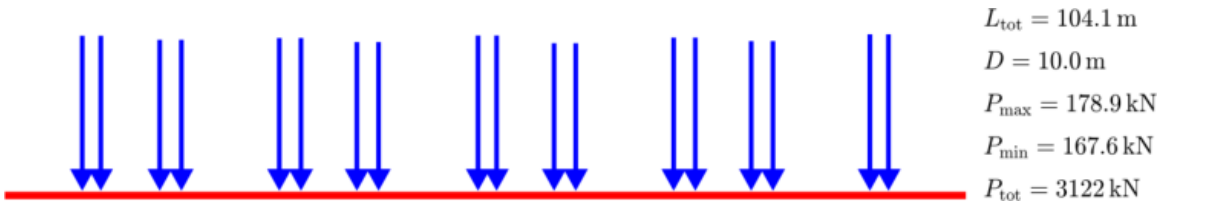

Figure Train PT60-23 [INB4EU-AB-05]

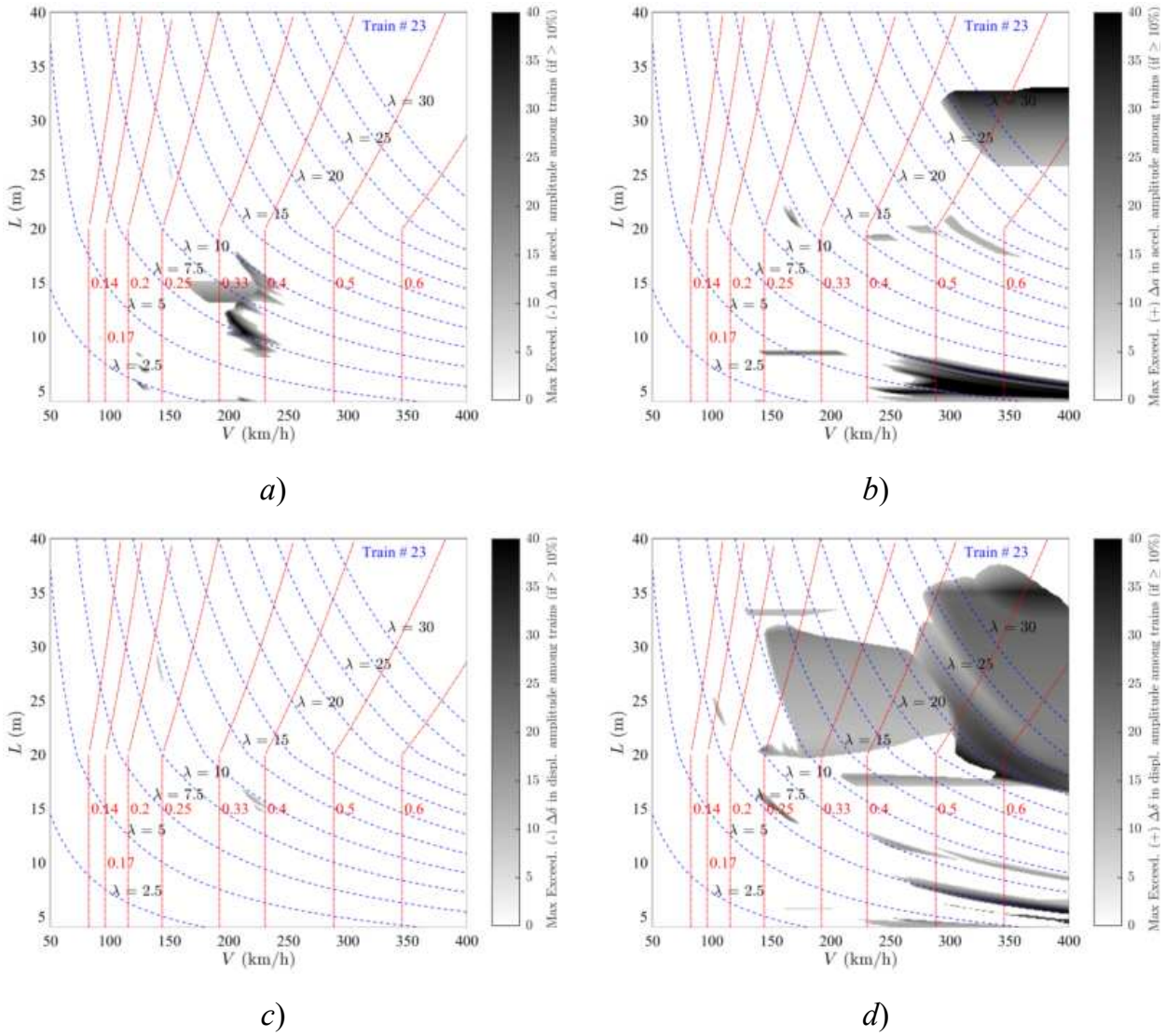

Figure 45. Exceedance Maps Train PT60-23 LIR vs Duhamel: a) Δa(–); b) Δa(+); c) Δδ(–); d) Δδ(+). PSC bridges.

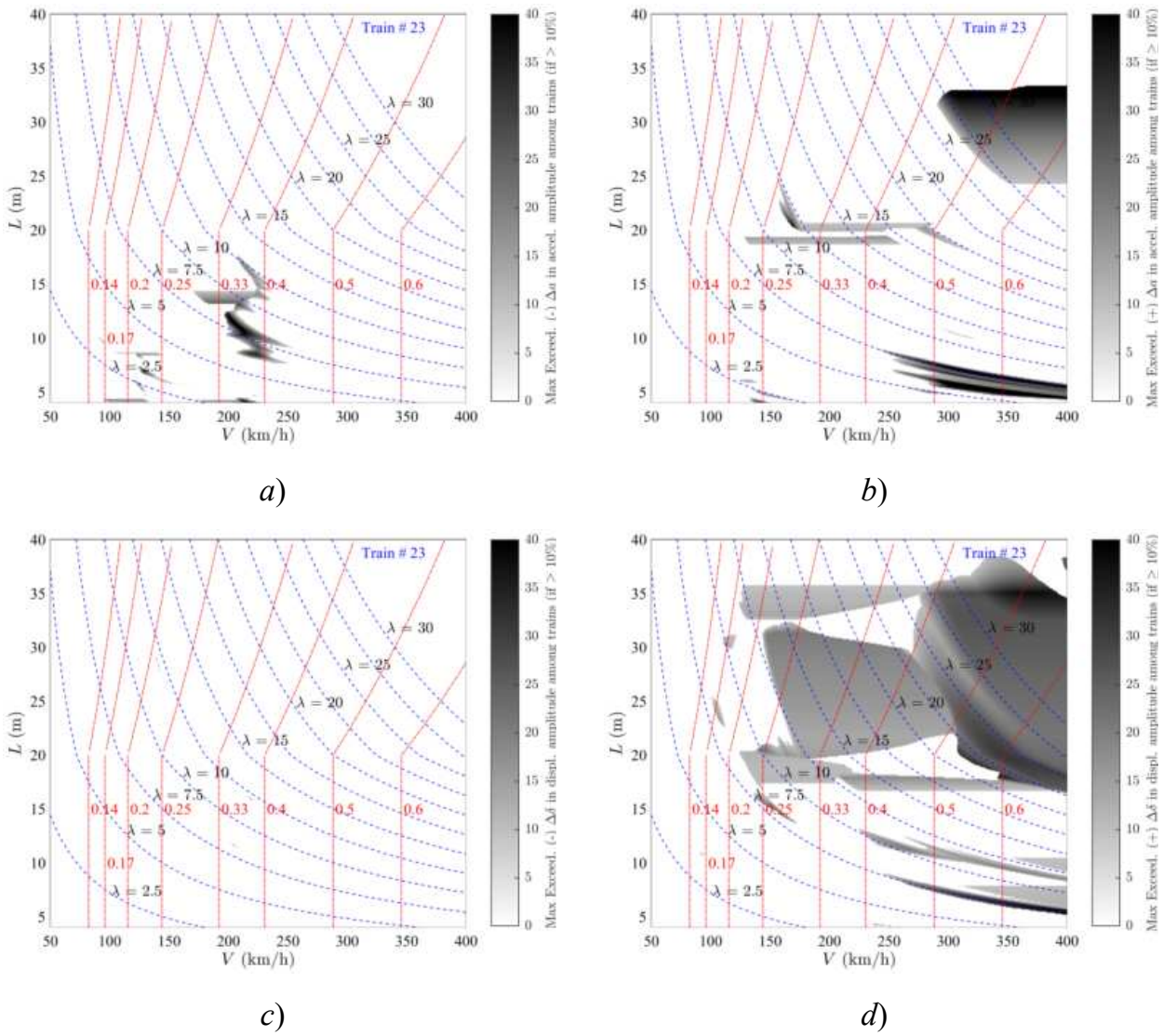

Figure 46. Exceedance Maps Train PT60-23 DER vs Duhamel: a) Δa(−); b) Δa(+); c) Δδ(−); d) Δδ(+). PSC bridges.

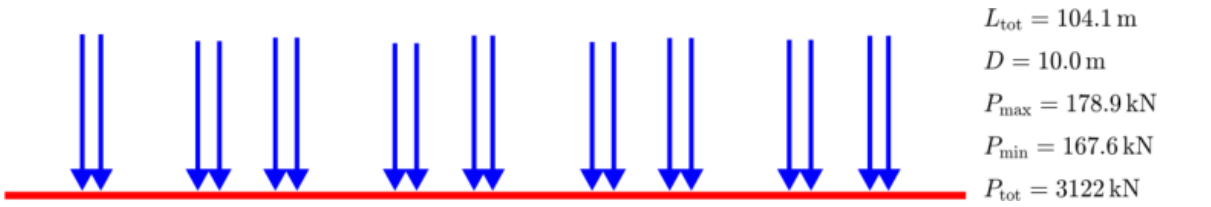

Figure Train PT60-24 [INB4EU-AB-015]

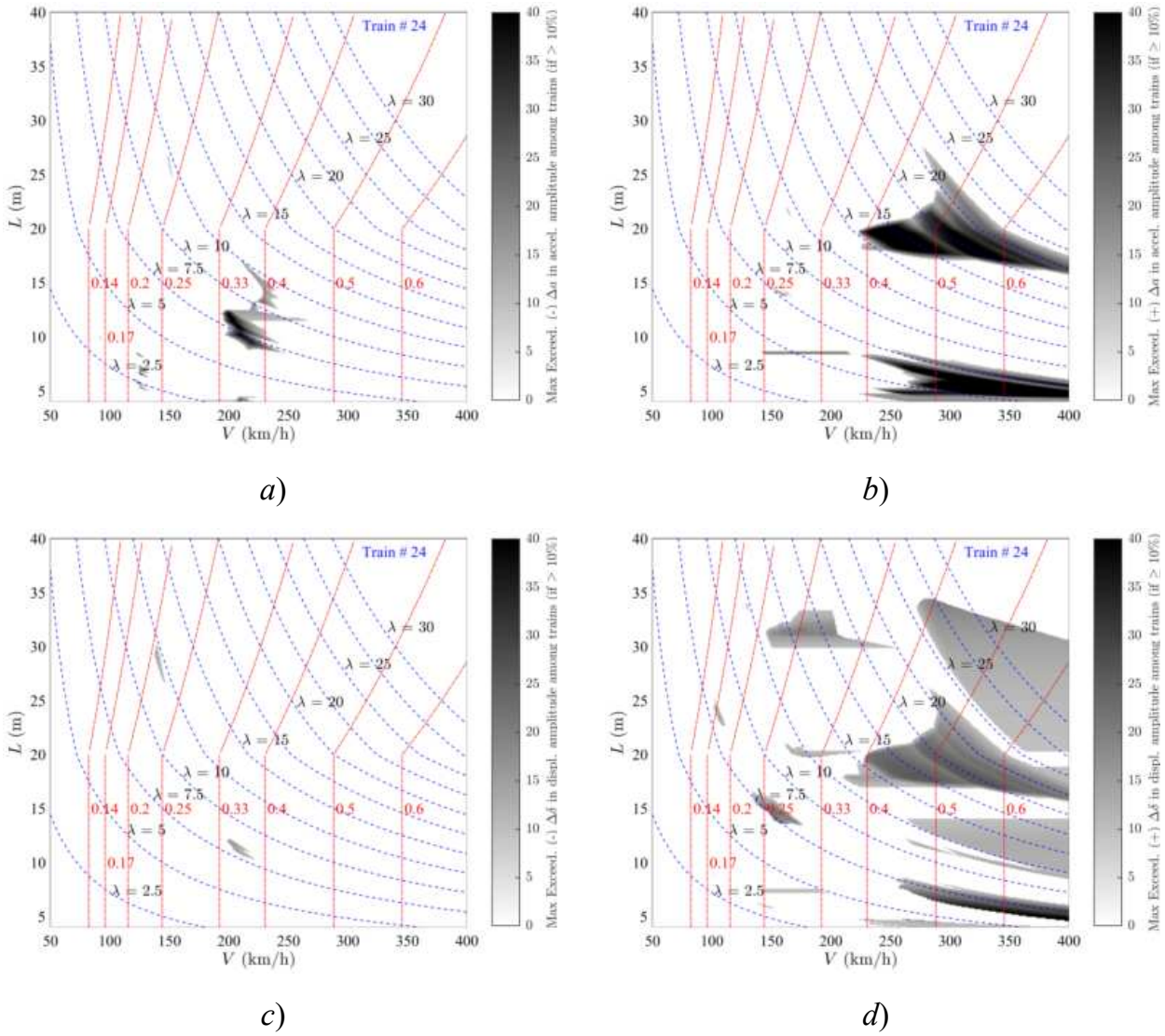

Figure 47. Exceedance Maps Train PT60-24 LIR vs Duhamel: a) Δa(–); b) Δa(+); c) Δδ(–); d) Δδ(+). PSC bridges.

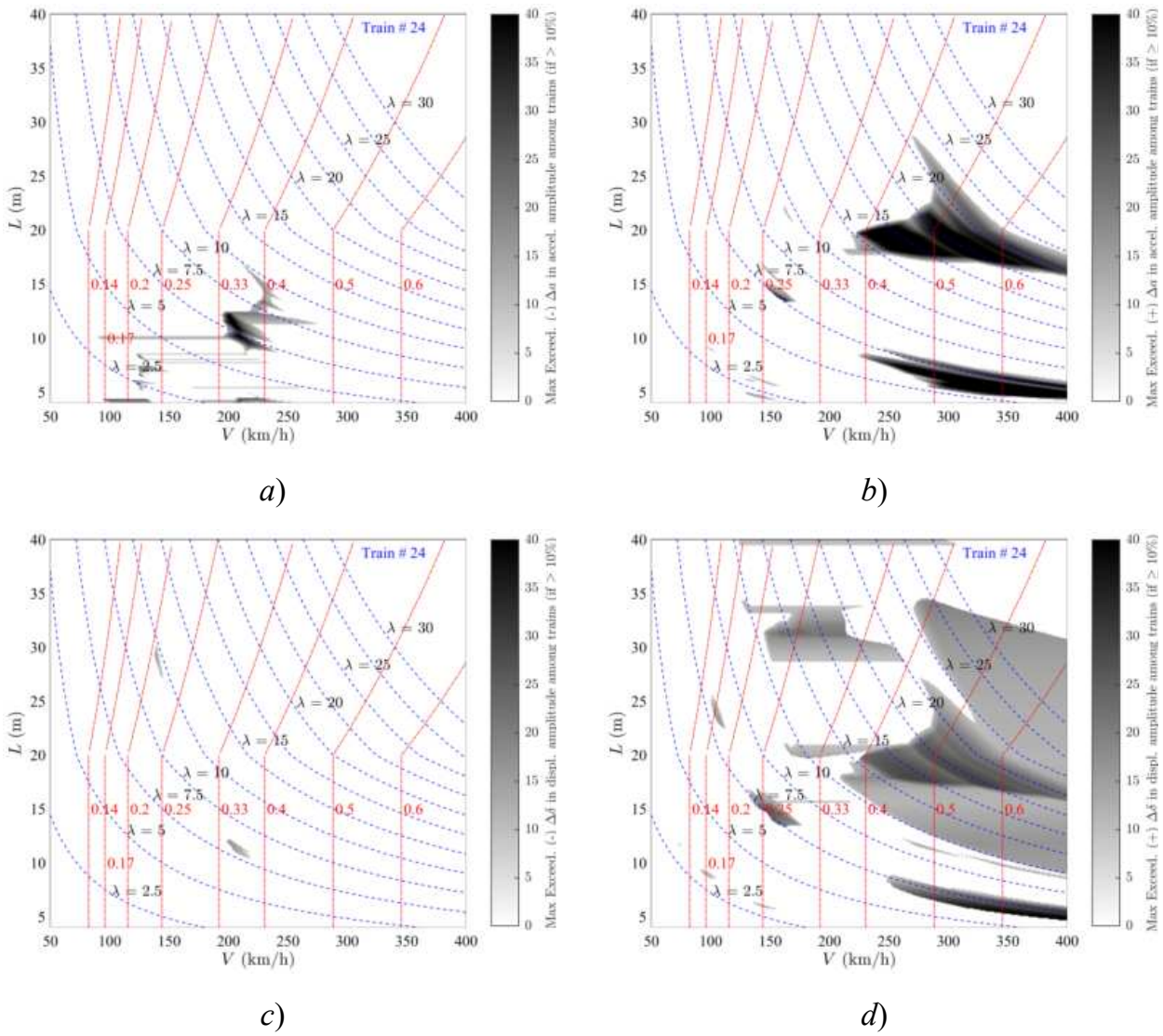

Figure 48. Exceedance Maps Train PT60-24 DER vs Duhamel: a) Δa(−); b) Δa(+); c) Δδ(−); d) Δδ(+). PSC bridges.

Figure Train PT60-25 [INB4EU-AB-030]

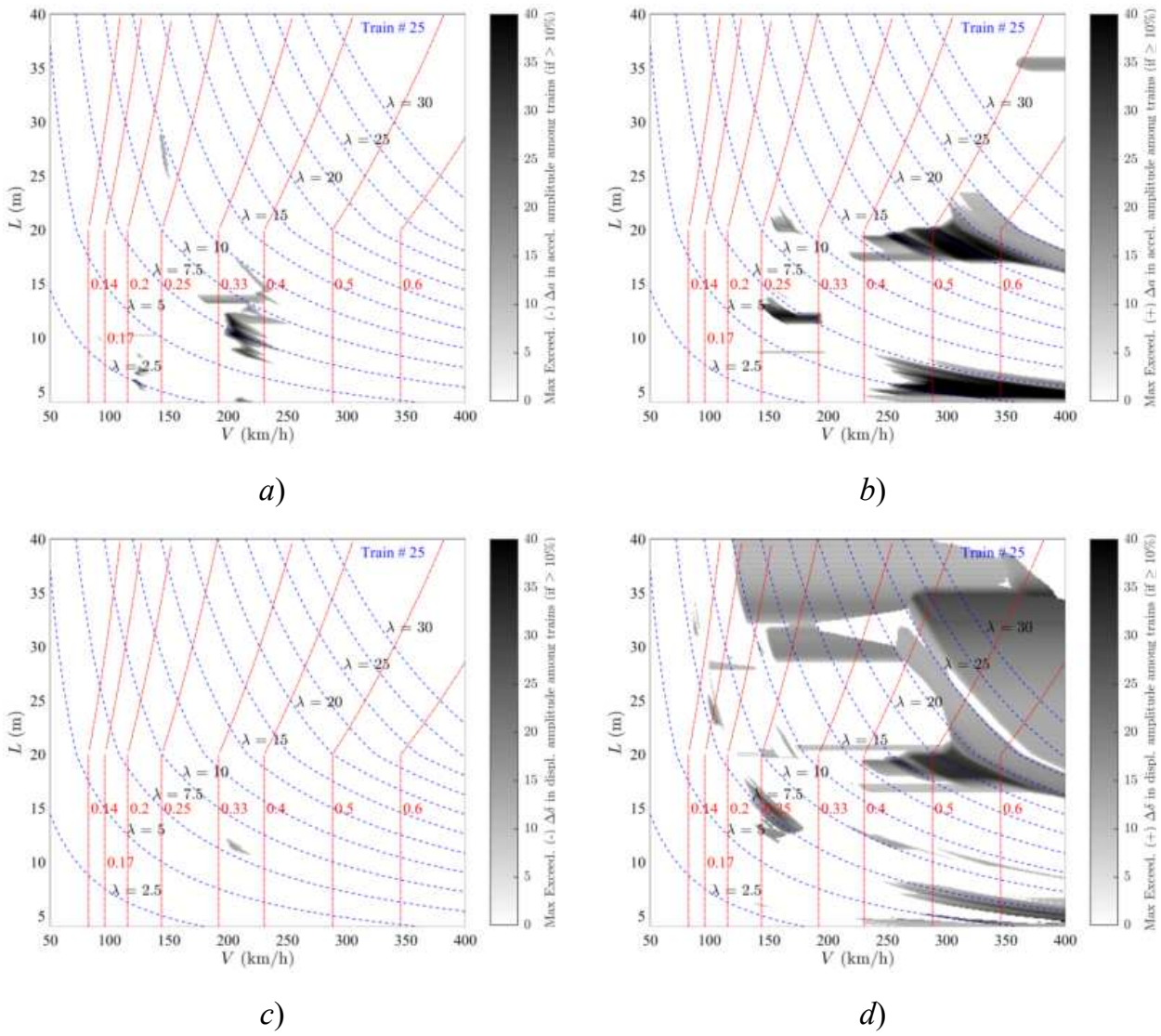

Figure 49. Exceedance Maps Train PT60-25 LIR vs Duhamel: a) Δa(–); b) Δa(+); c) Δδ(–); d) Δδ(+). PSC bridges.

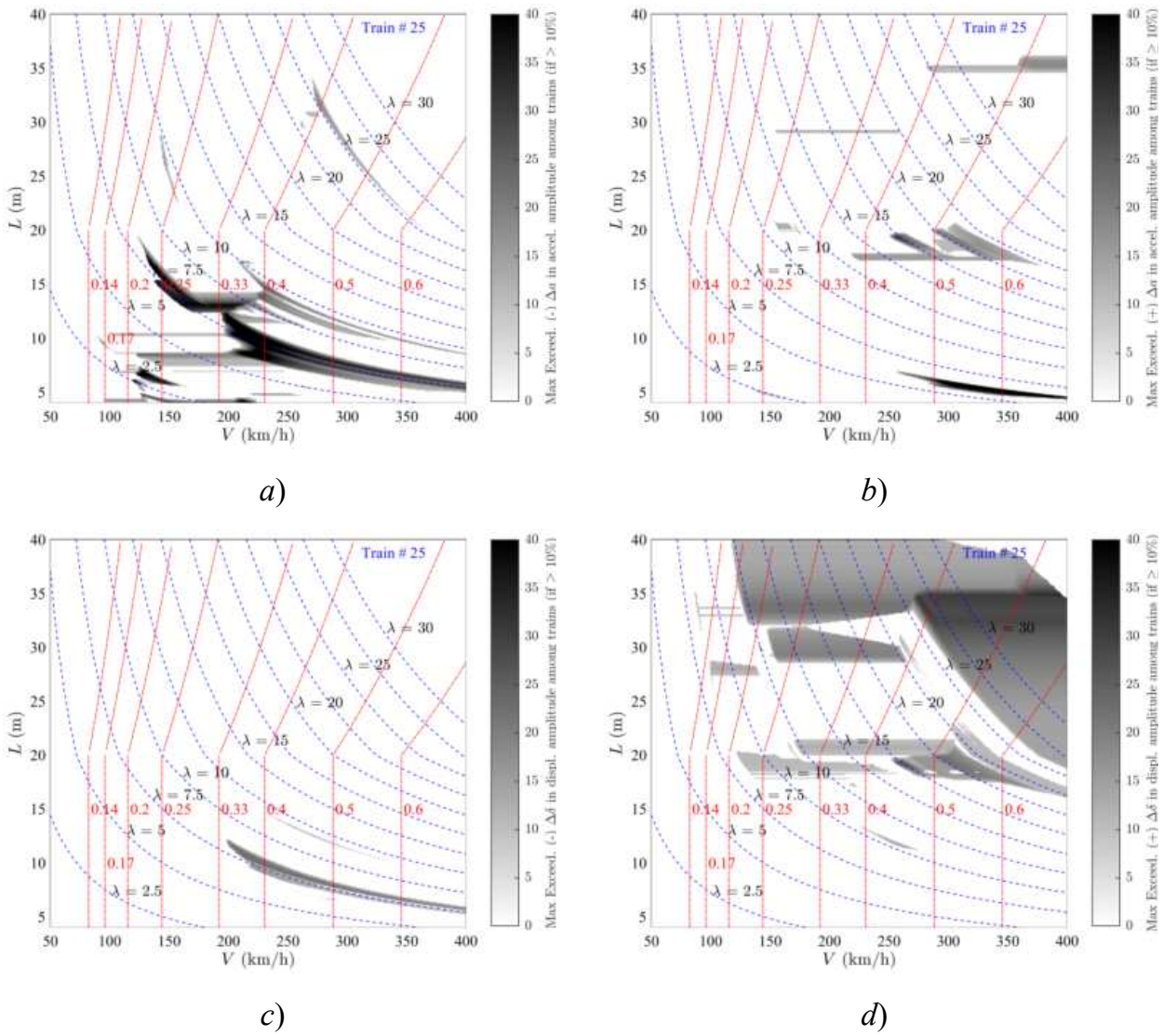

Figure 50. Exceedance Maps Train PT60-25 DER vs Duhamel: a) Δa(–); b) Δa(+); c) Δδ(–); d) Δδ(+). PSC bridges.

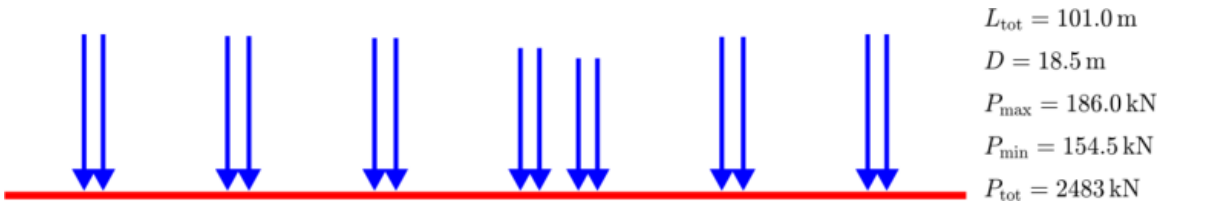

Figure Train PT60-26 [INB4EU-AB-002]

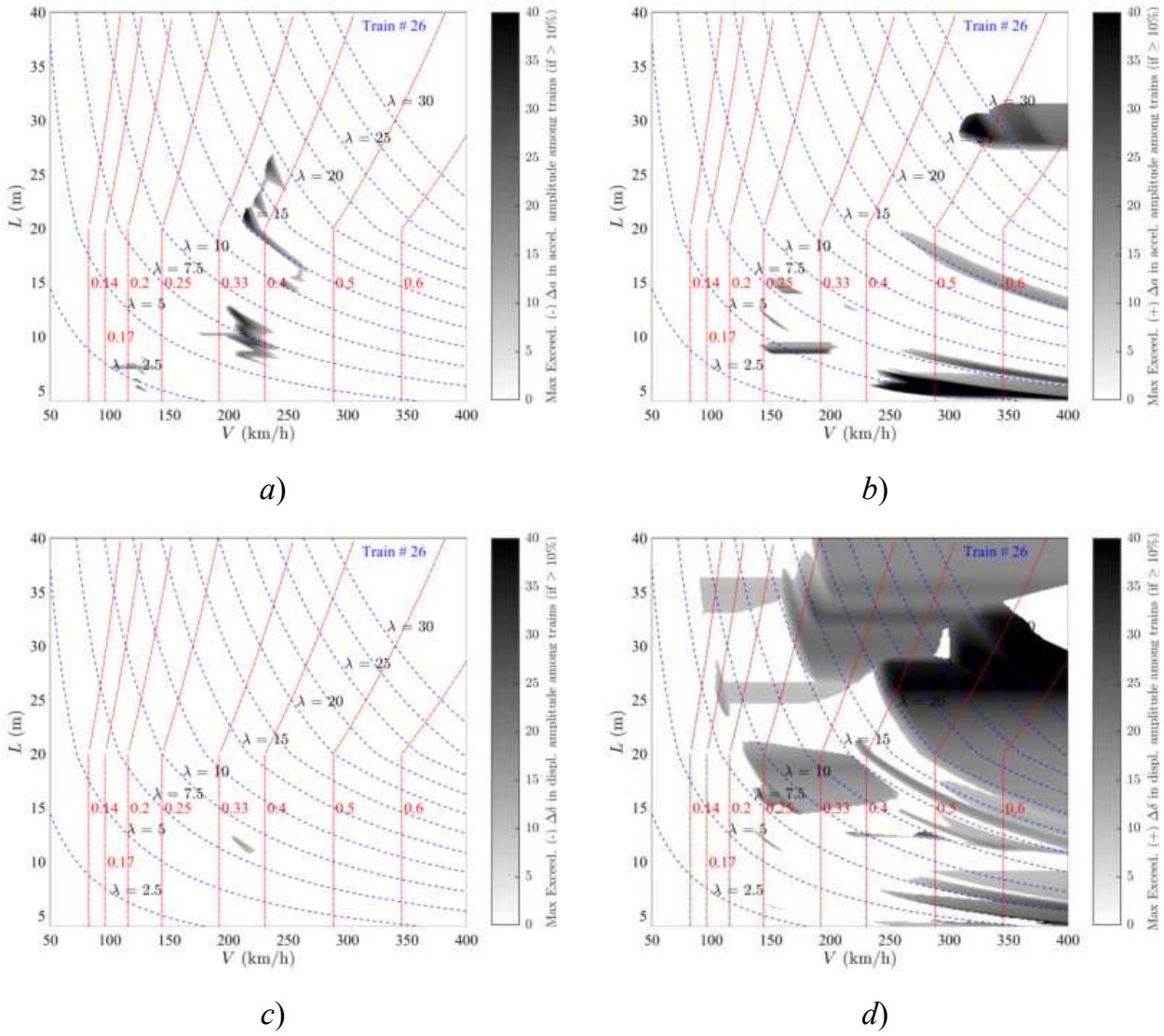

Figure 51. Exceedance Maps Train PT60-26 LIR vs Duhamel: a) Δa(–); b) Δa(+); c) Δδ(–); d) Δδ(+). PSC bridges.

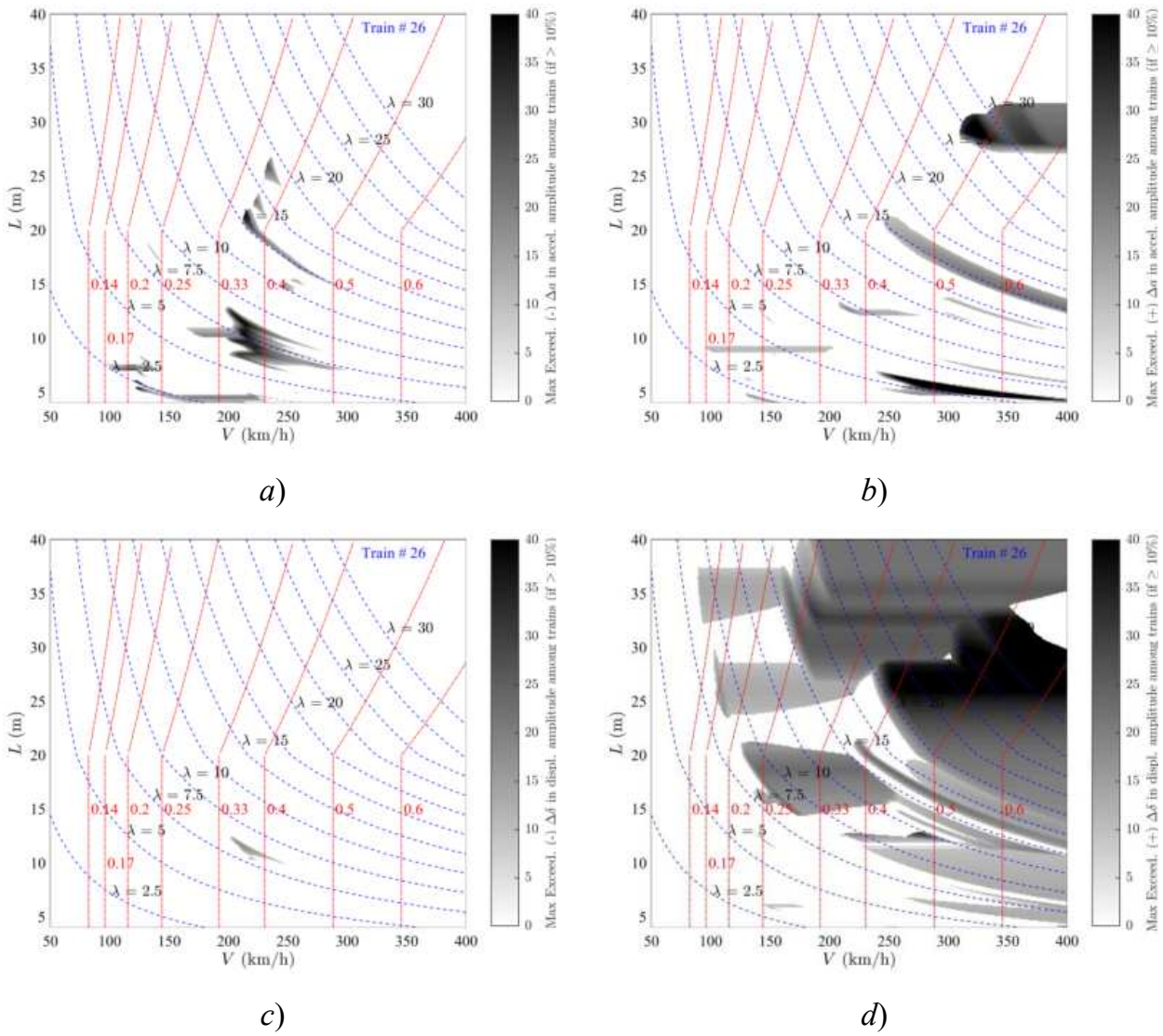

Figure 52. Exceedance Maps Train PT60-26 DER vs Duhamel: a) Δa(−); b) Δa(+); c) Δδ(−); d) Δδ(+). PSC bridges.

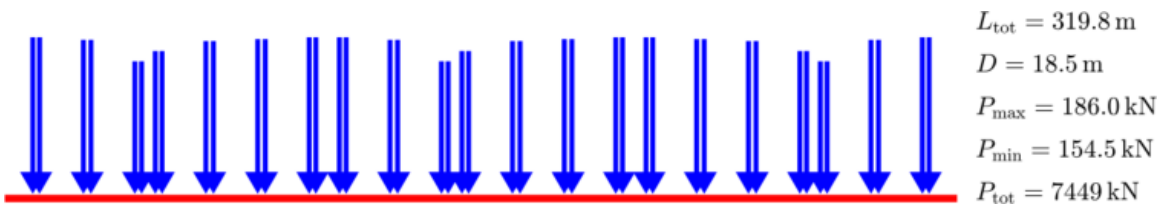

Figure Train PT60-27 [INB4EU-AB-027]

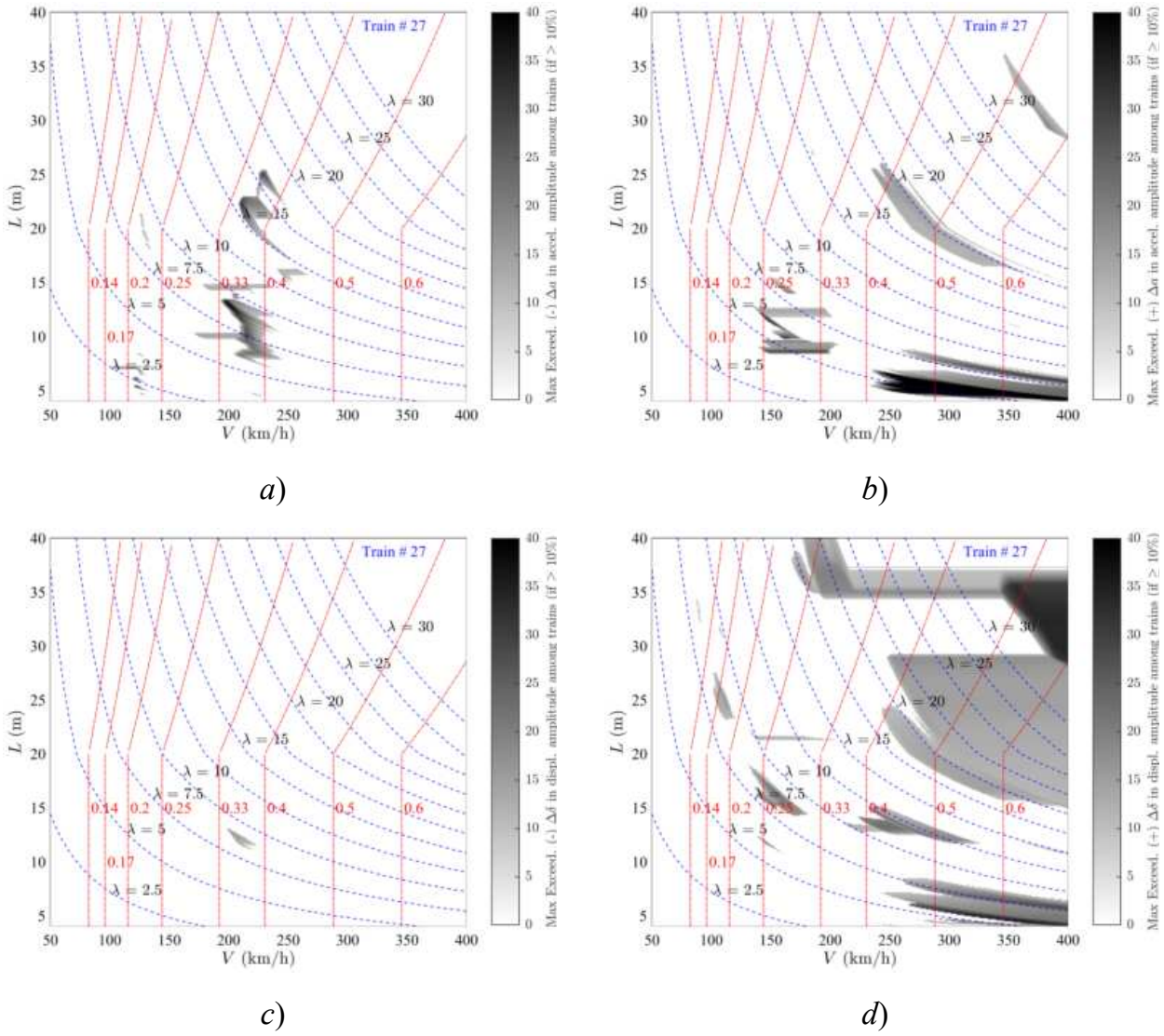

Figure 53. Exceedance Maps Train PT60-27 LIR vs Duhamel: a) Δa(–); b) Δa(+); c) Δδ(–); d) Δδ(+). PSC bridges.

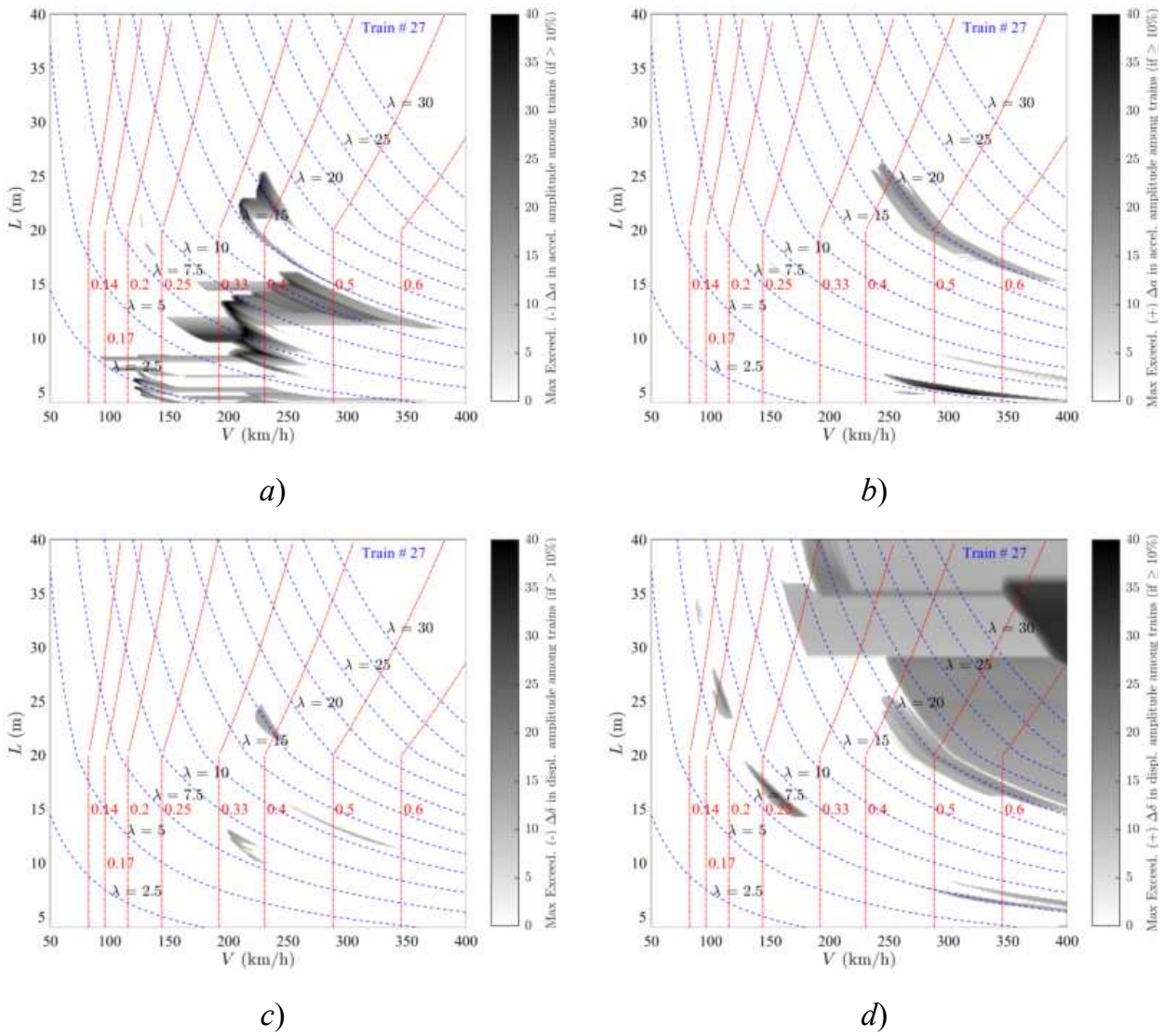

Figure 54. Exceedance Maps Train PT60-27 DER vs Duhamel: a) Δa(–); b) Δa(+); c) Δδ(–); d) Δδ(+). PSC bridges.

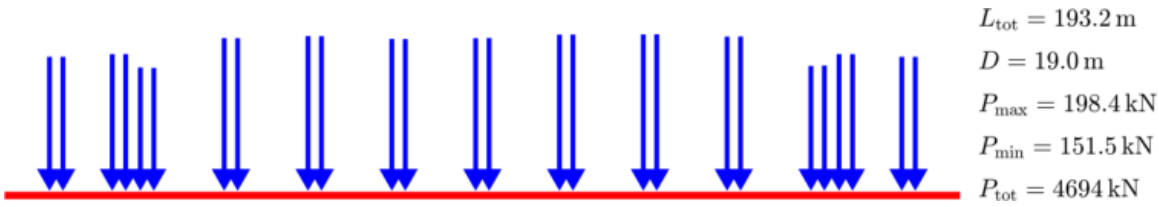

Figure Train PT60-28 [INB4EU-AB-004]

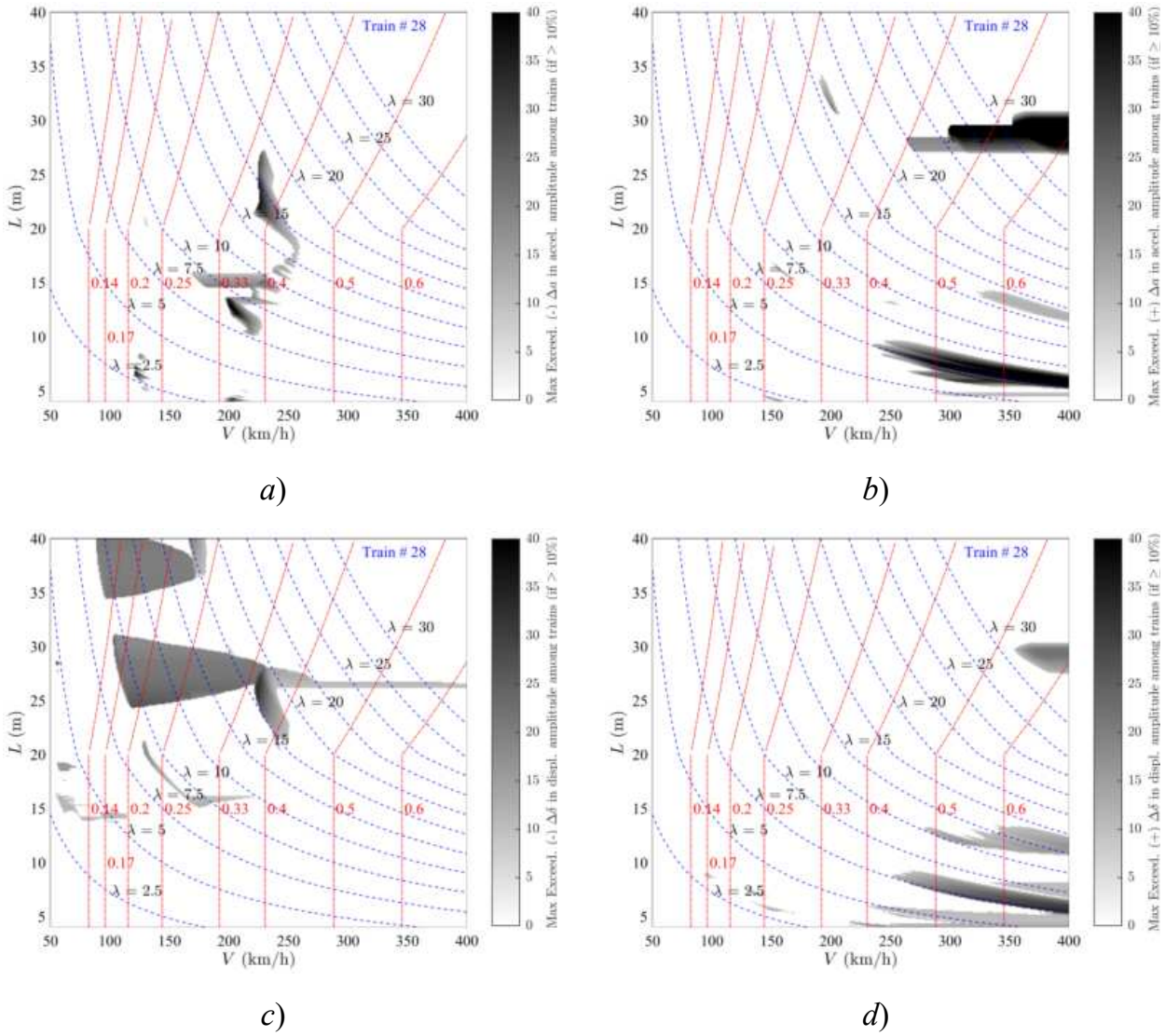

Figure 55. Exceedance Maps Train PT60-28 LIR vs Duhamel: a) Δa(–); b) Δa(+); c) Δδ(–); d) Δδ(+). PSC bridges.

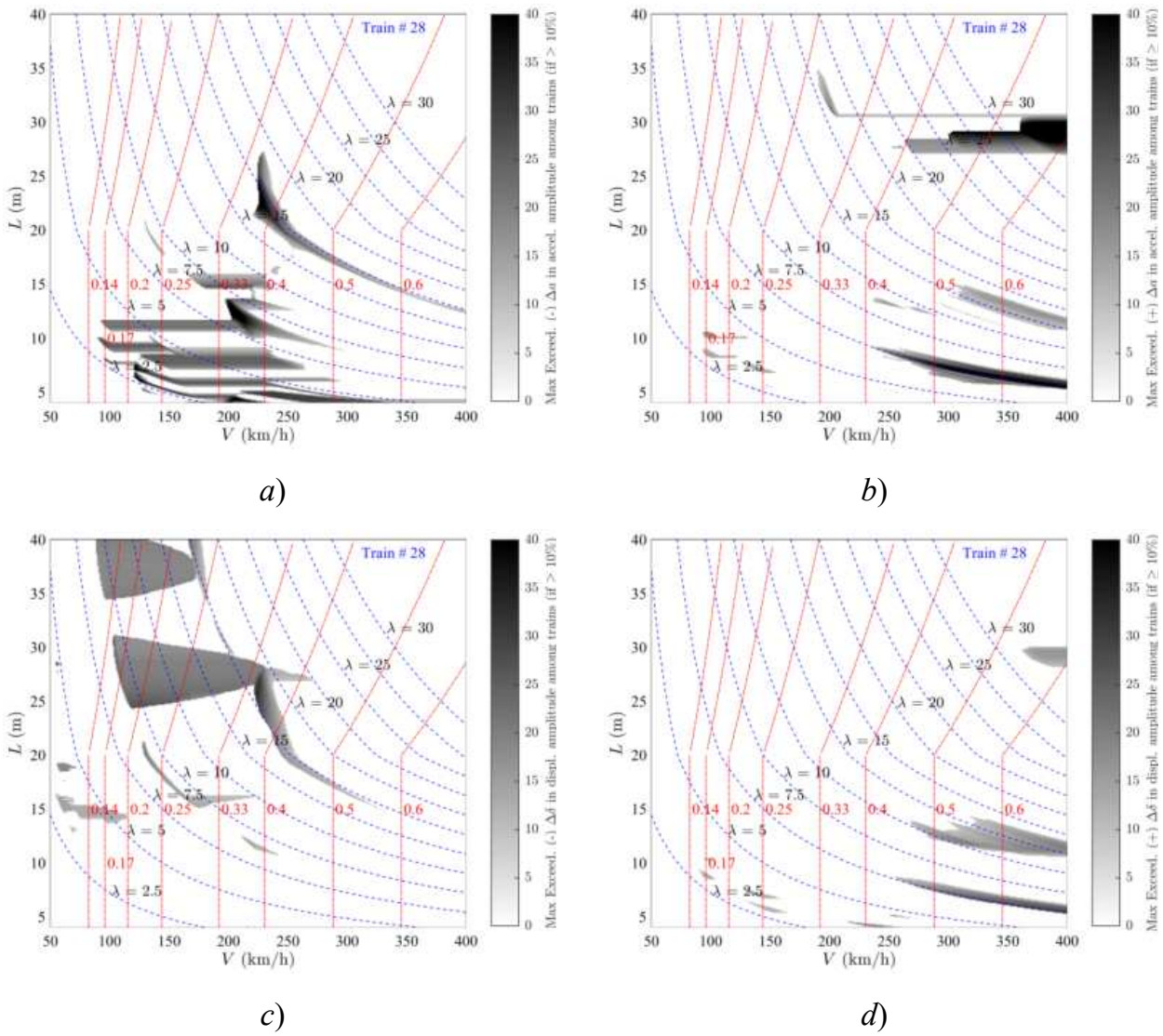

Figure 56. Exceedance Maps Train PT60-28 DER vs Duhamel: a) Δa(−); b) Δa(+); c) Δδ(−); d) Δδ(+). PSC bridges.

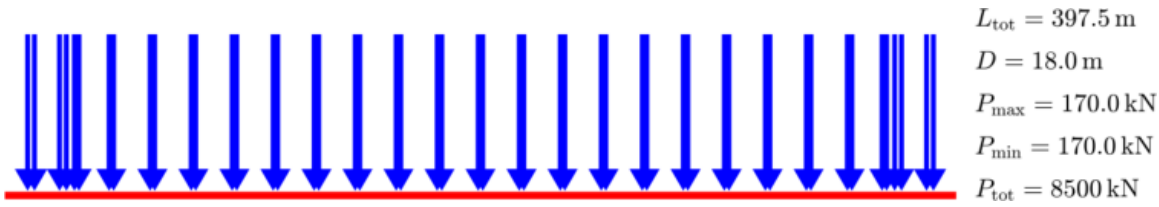

Figure Train PT60-29 [HSLM-A1]

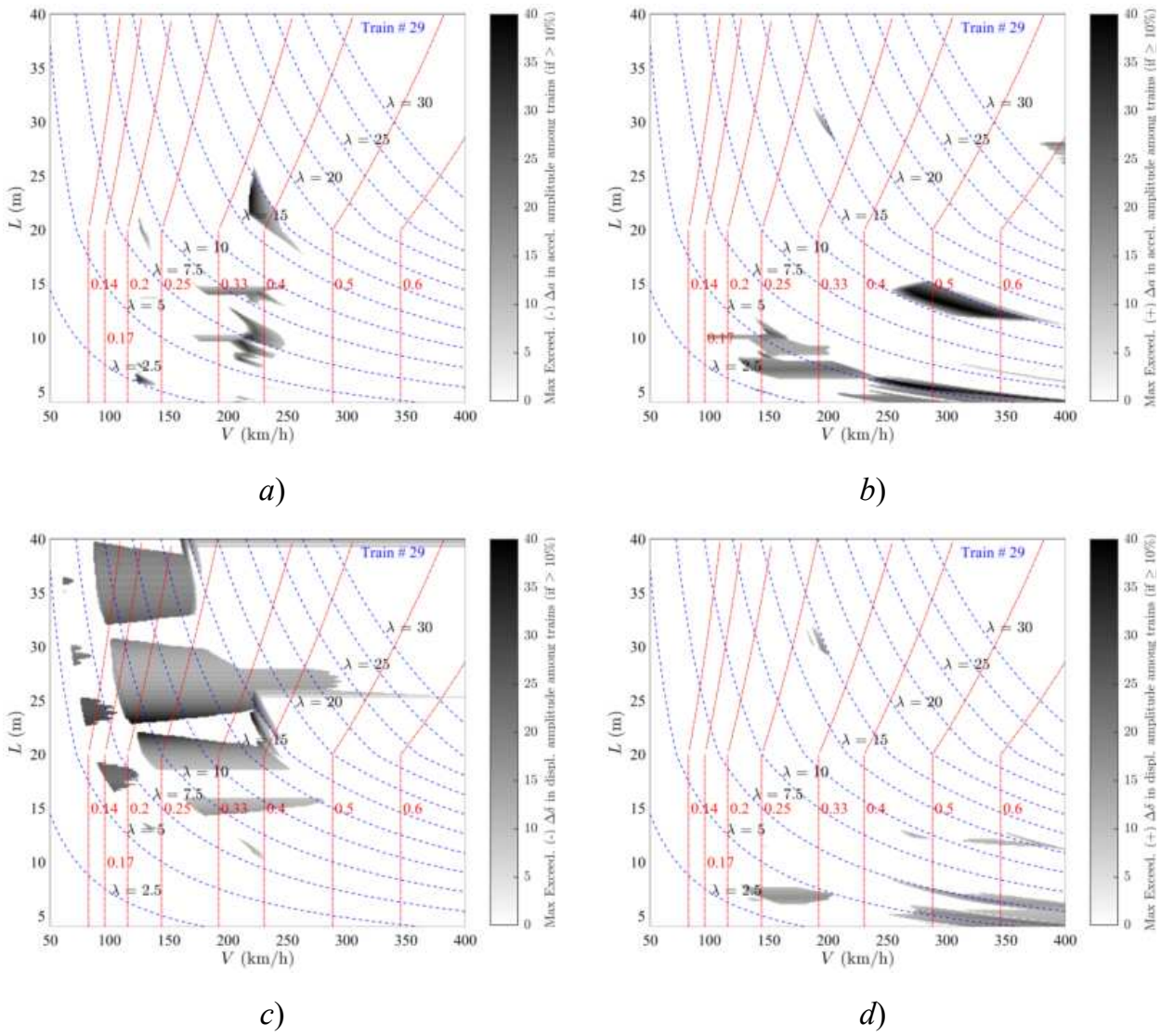

Figure 57. Exceedance Maps Train PT60-29 LIR vs Duhamel: a) Δa(–); b) Δa(+); c) Δδ(–); d) Δδ(+). PSC bridges.

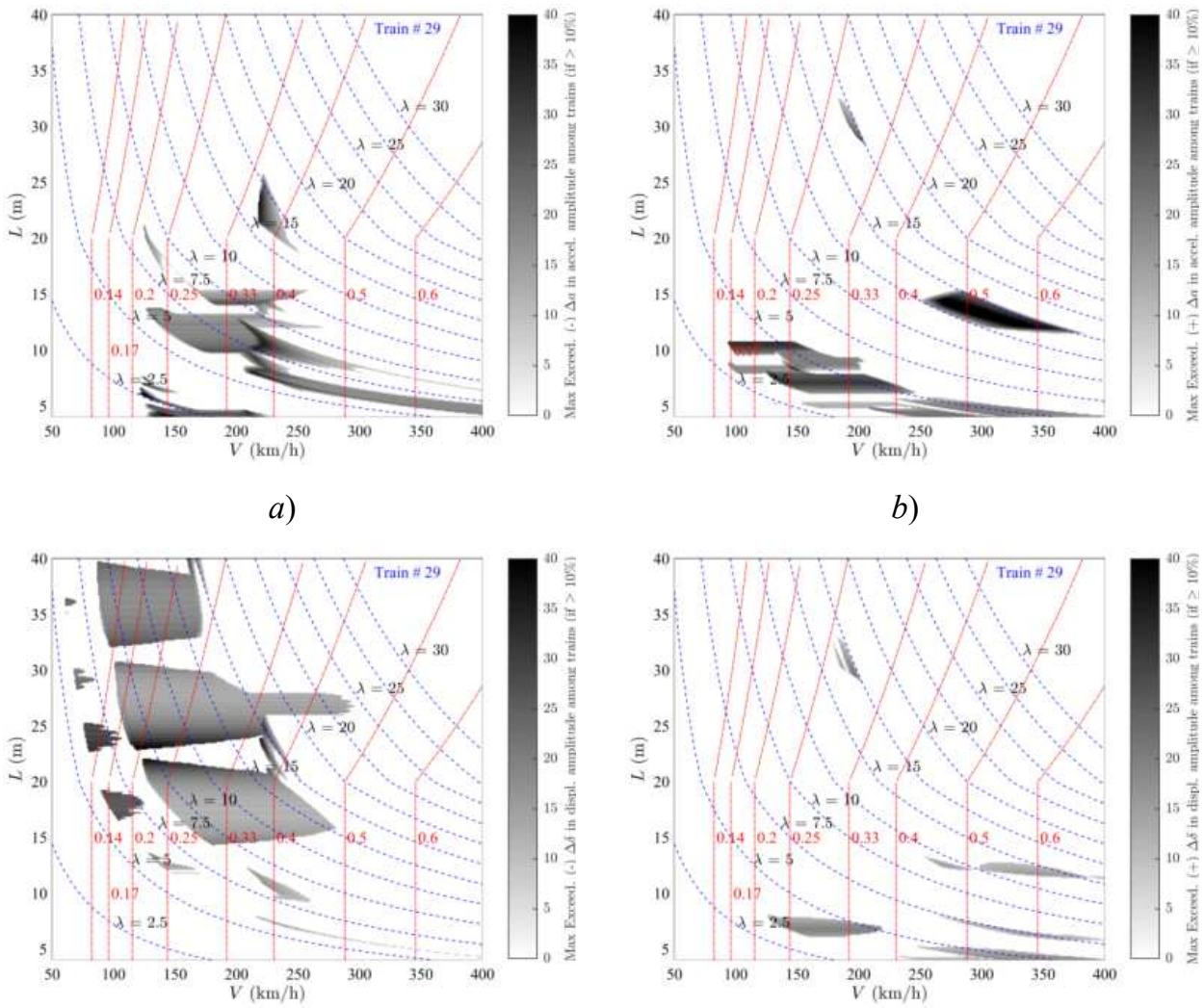

Figure 58. Exceedance Maps Train PT60-29 DER vs Duhamel: a) Δa(−); b) Δa(+); c) Δδ(−); d) Δδ(+). PSC bridges.

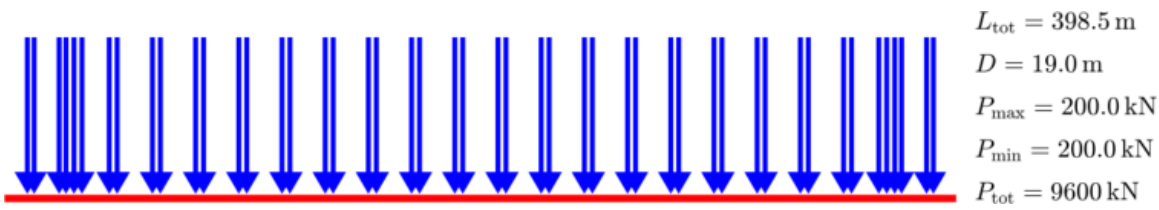

Figure Train PT60-30 [HSLM-A2]

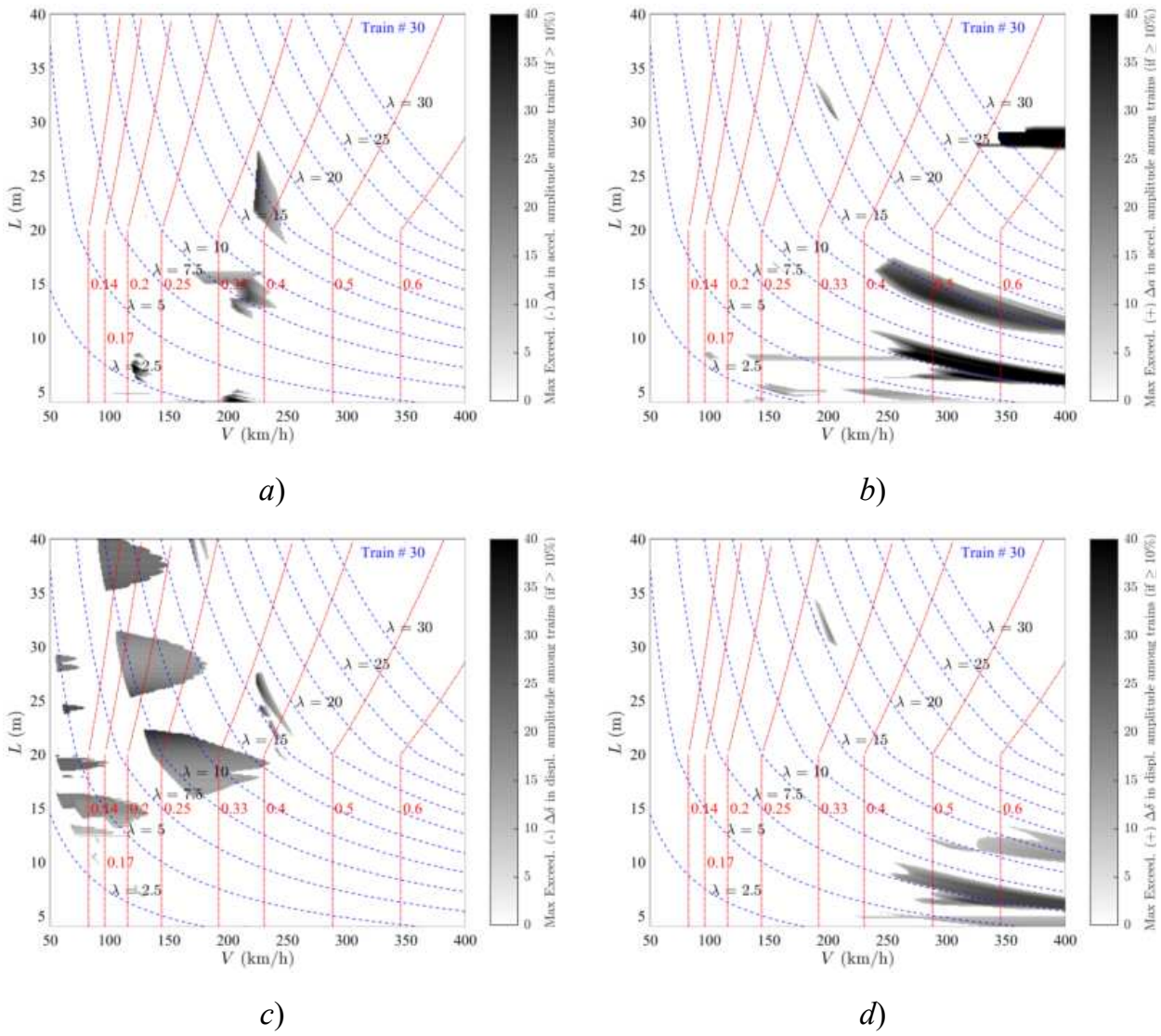

Figure 59. Exceedance Maps Train PT60-30 LIR vs Duhamel: a) Δa(–); b) Δa(+); c) Δδ(–); d) Δδ(+). PSC bridges.

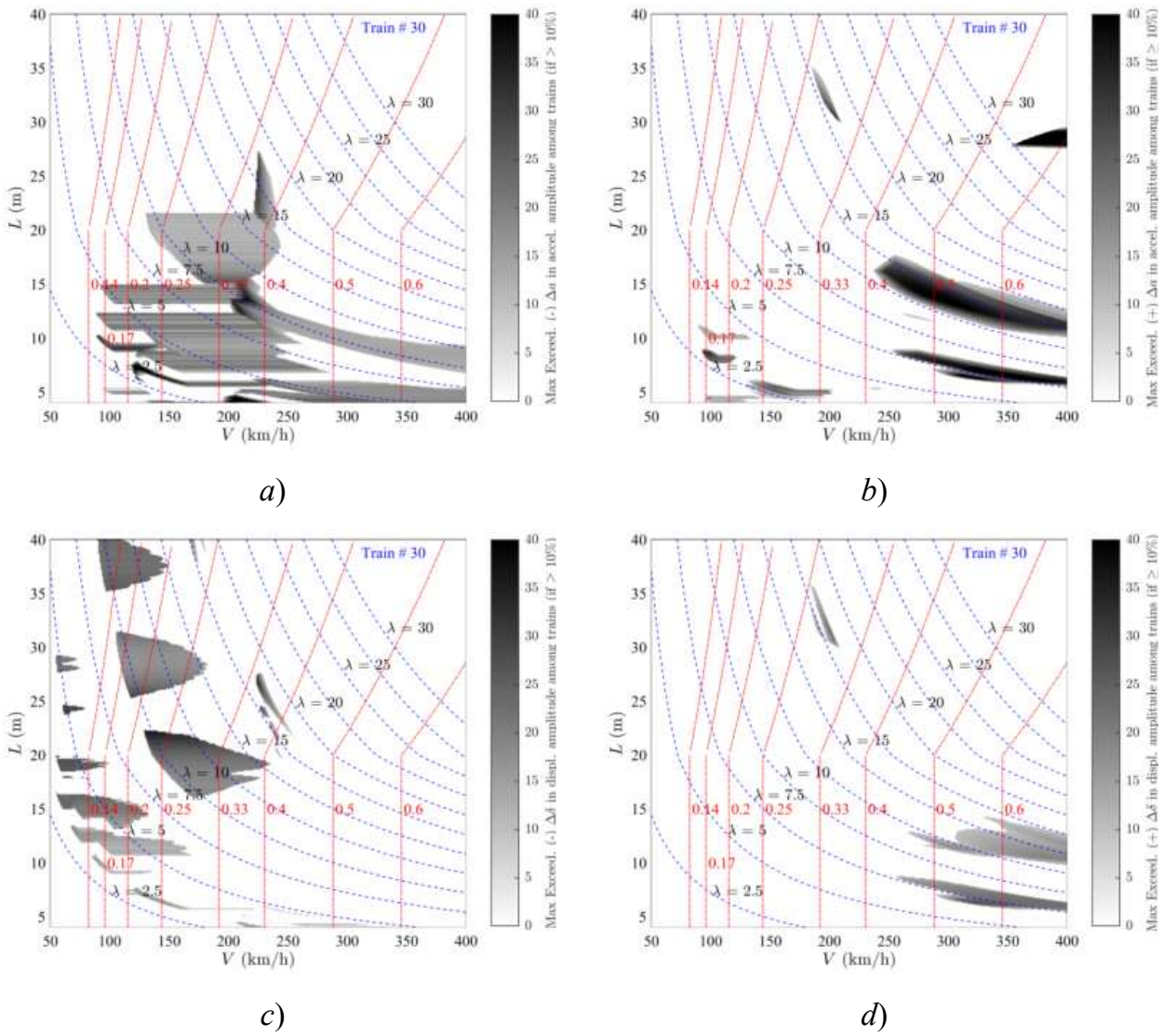

Figure 60. Exceedance Maps Train PT60-30 DER vs Duhamel: a) Δa(−); b) Δa(+); c) Δδ(−); d) Δδ(+). PSC bridges.

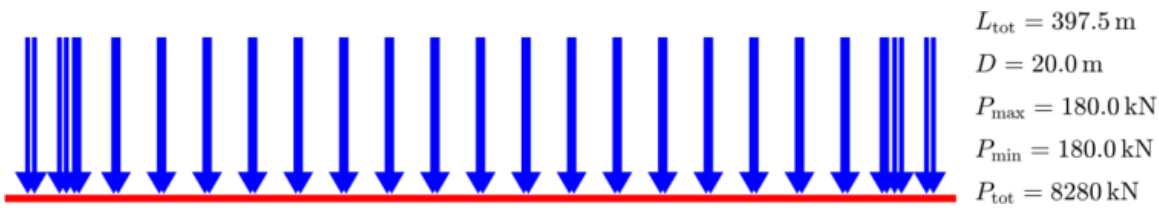

Figure Train PT60-31 [HSLM-A3]

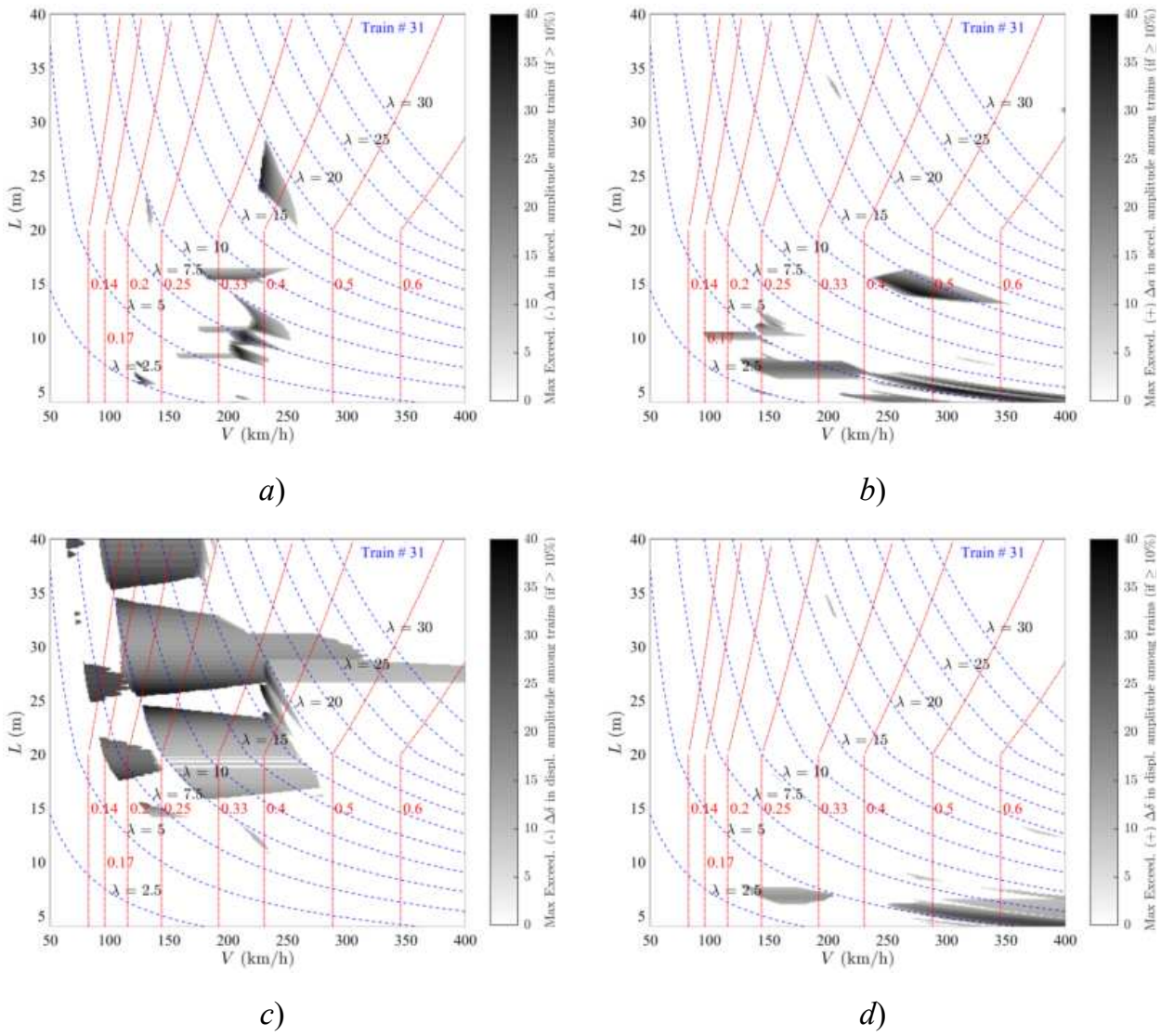

Figure 61. Exceedance Maps Train PT60-31 LIR vs Duhamel: a) Δa(–); b) Δa(+); c) Δδ(–); d) Δδ(+). PSC bridges.

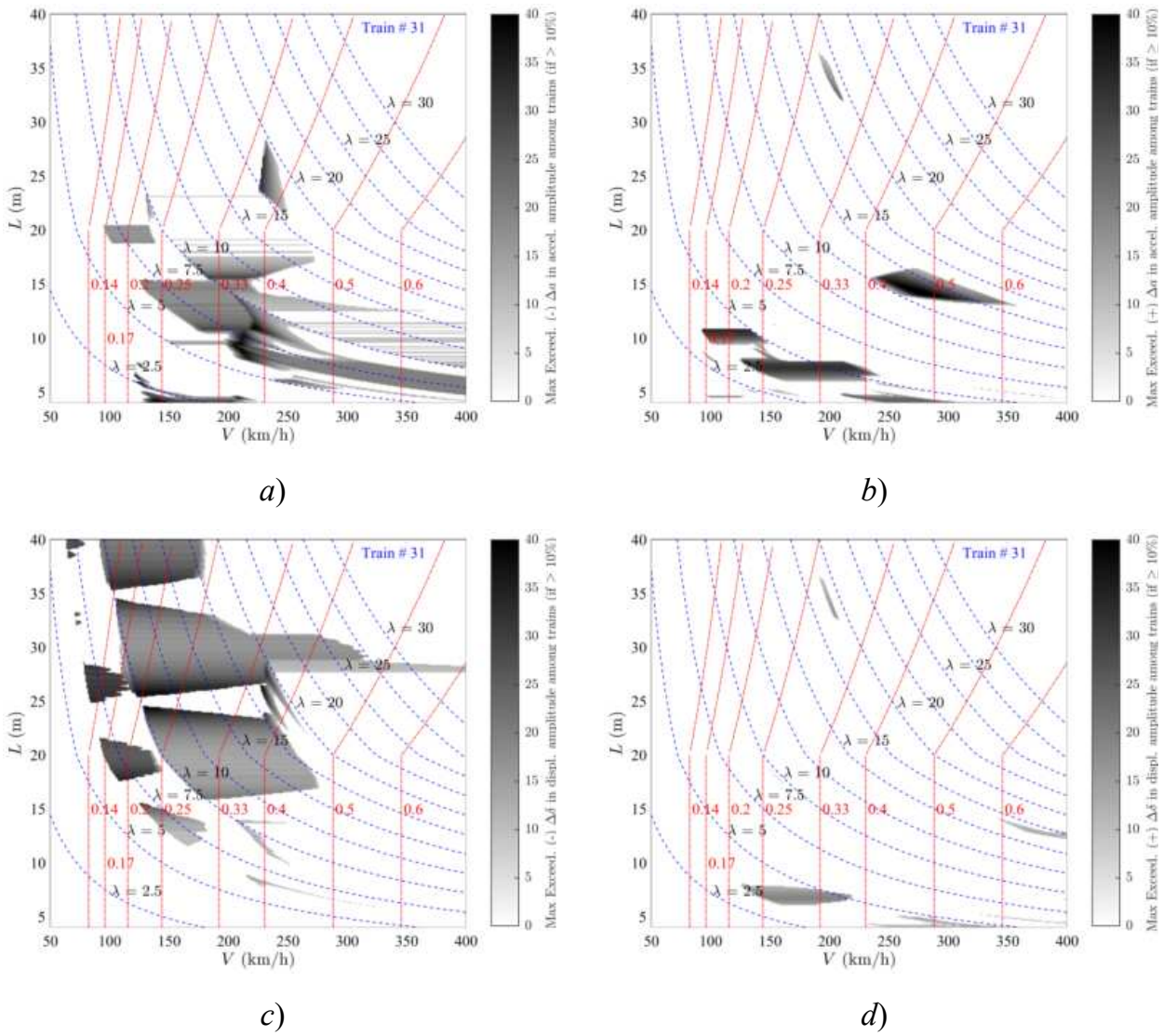

Figure 62. Exceedance Maps Train PT60-31 DER vs Duhamel: a) Δa(−); b) Δa(+); c) Δδ(−); d) Δδ(+). PSC bridges.

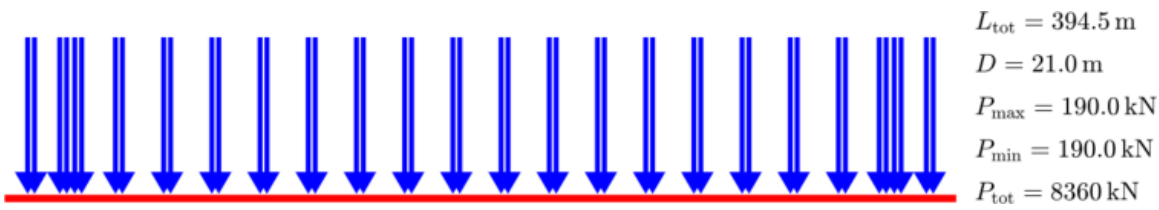

Figure Train PT60-32 [HSLM-A4]

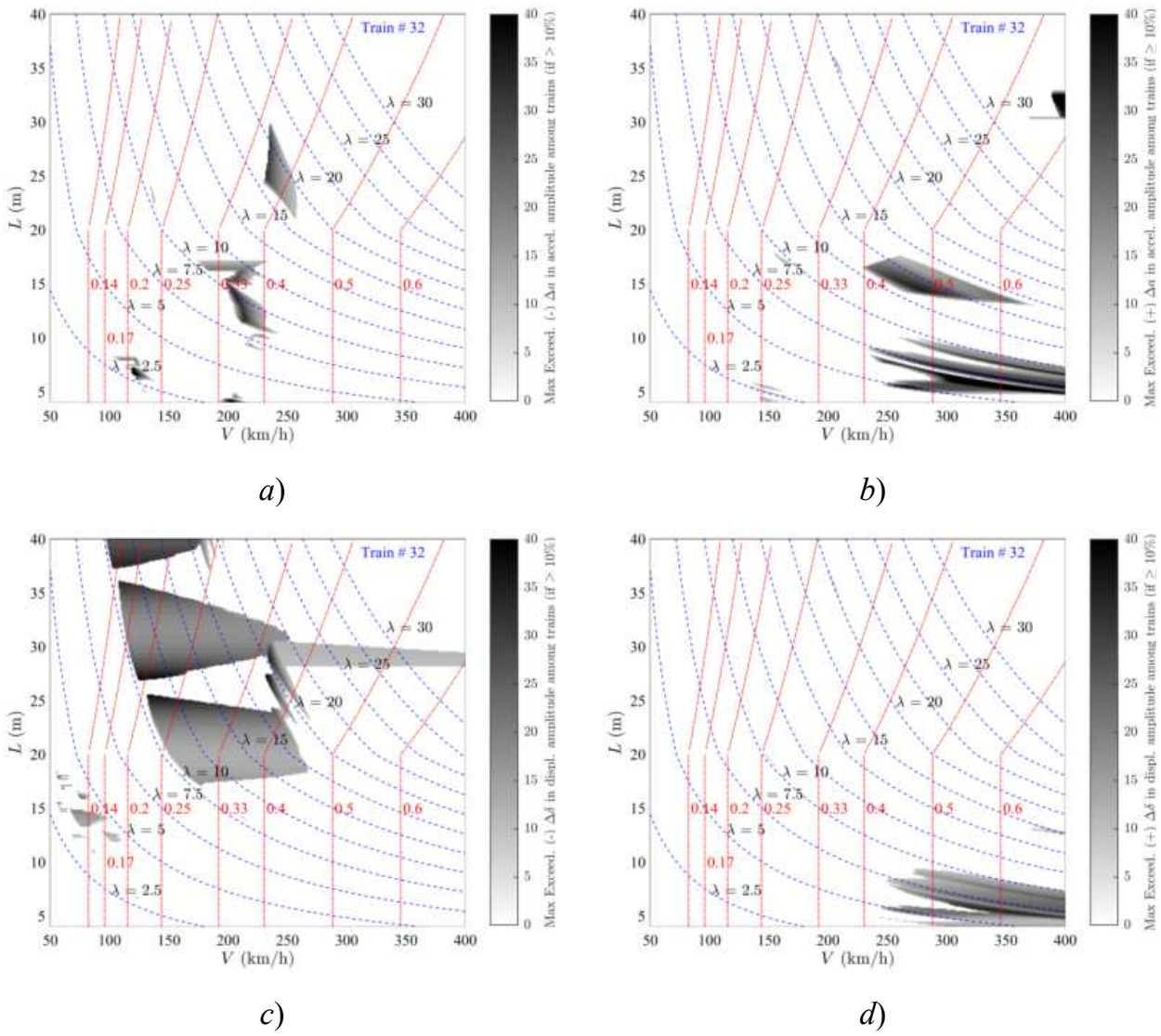

Figure 63. Exceedance Maps Train PT60-32 LIR vs Duhamel: a) Δa(–); b) Δa(+); c) Δδ(–); d) Δδ(+). PSC bridges.

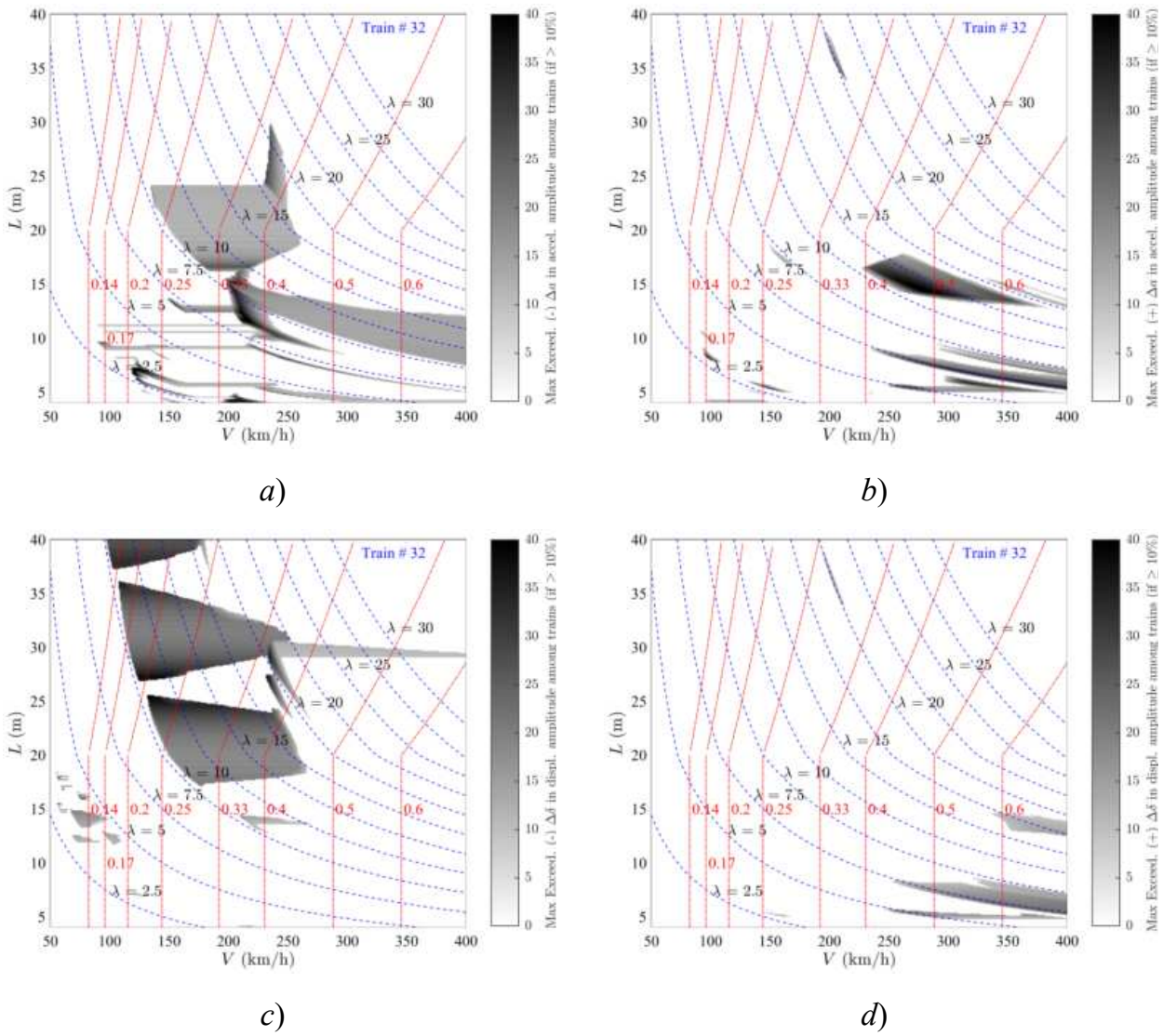

Figure 64. Exceedance Maps Train PT60-32 DER vs Duhamel: a) Δa(–); b) Δa(+); c) Δδ(–); d) Δδ(+). PSC bridges.

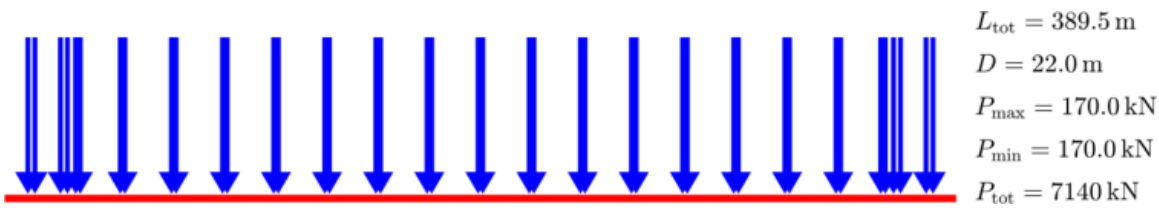

Figure Train PT60-33 [HSLM-A5]

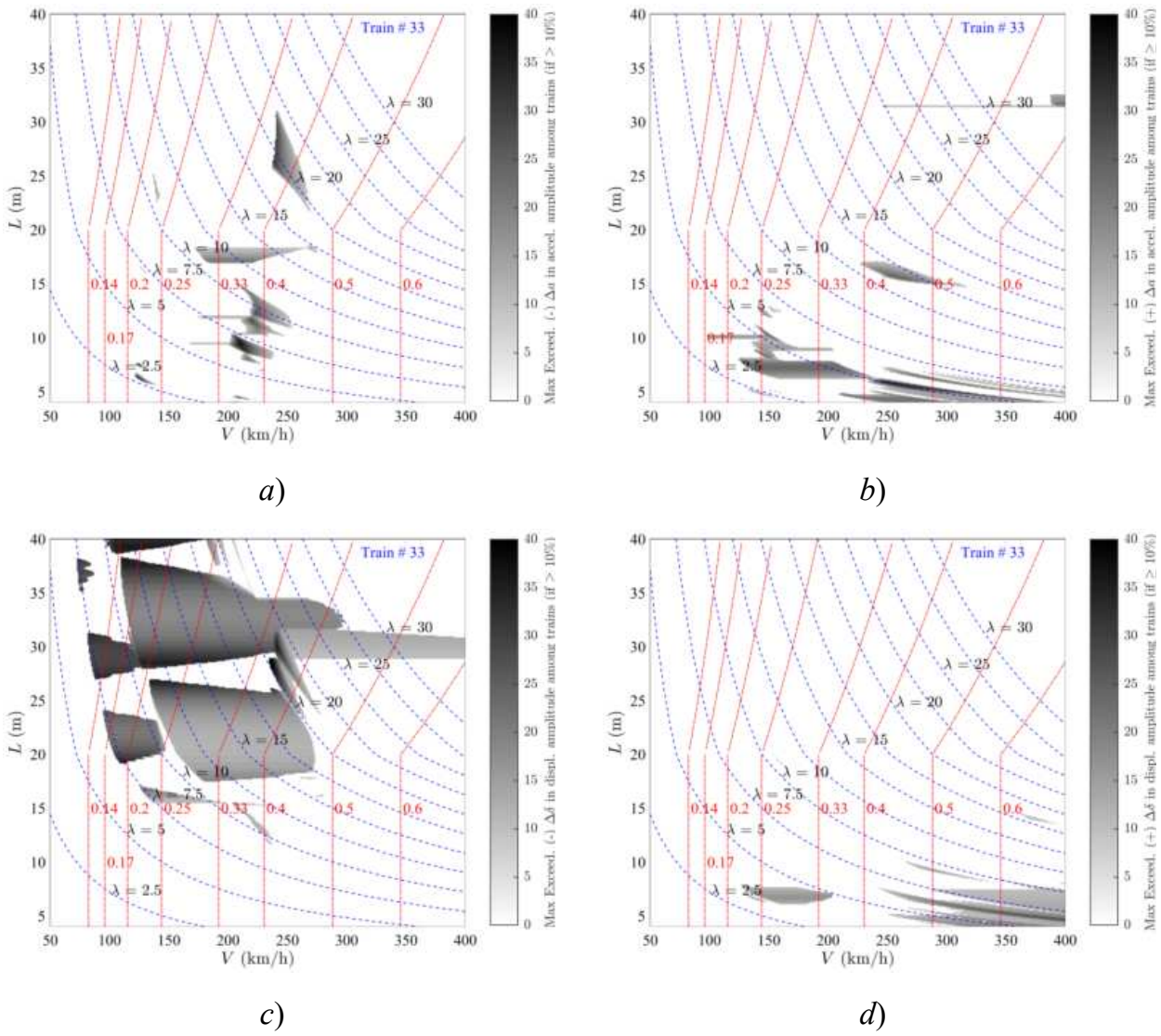

Figure 65. Exceedance Maps Train PT60-33 LIR vs Duhamel: a) Δa(–); b) Δa(+); c) Δδ(–); d) Δδ(+). PSC bridges.

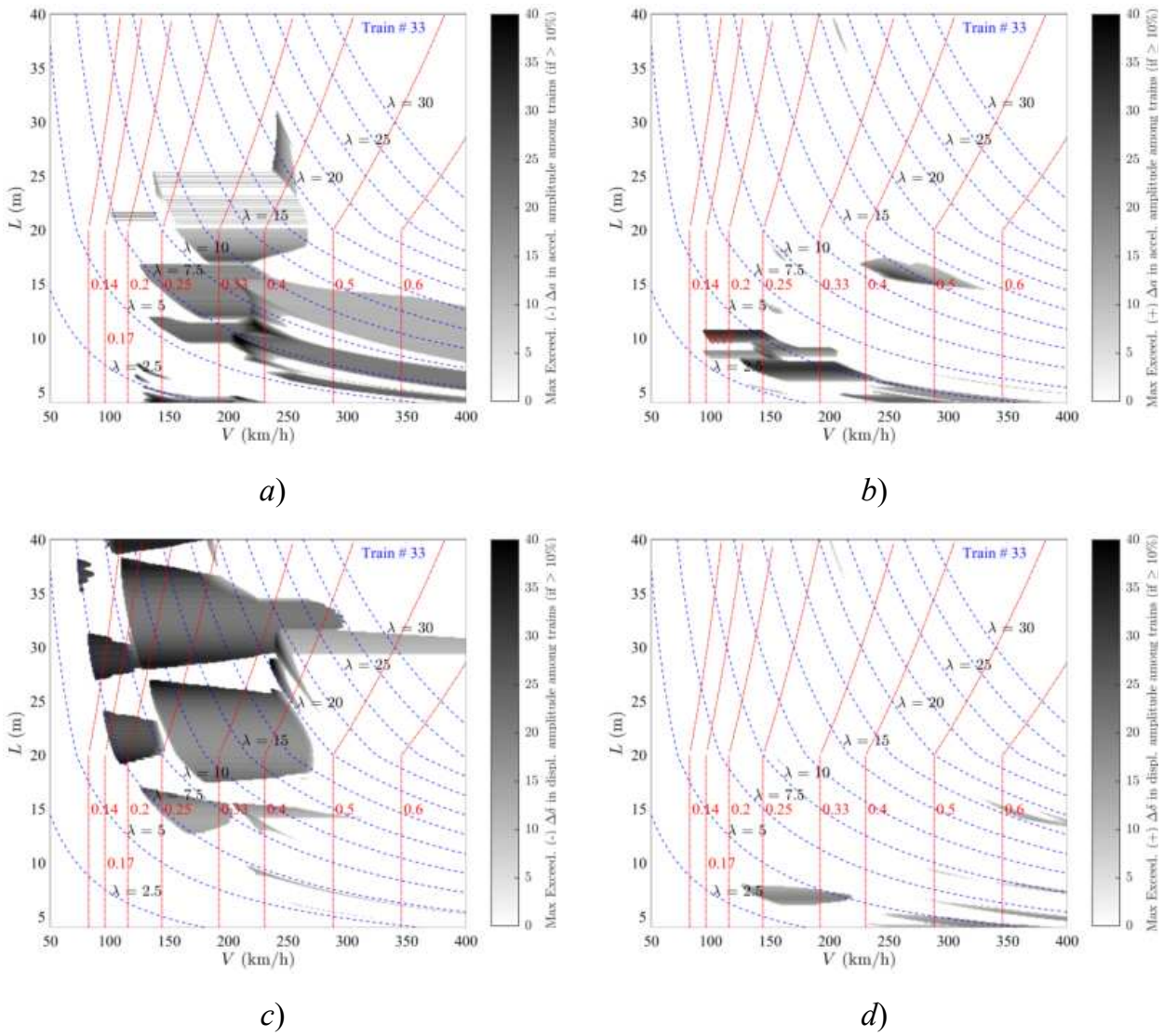

Figure 66. Exceedance Maps Train PT60-33 DER vs Duhamel: a) Δa(−); b) Δa(+); c) Δδ(−); d) Δδ(+). PSC bridges.

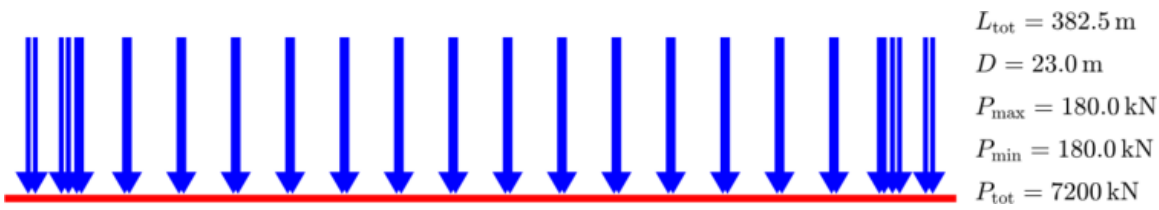

Figure Train PT60-34 [HSLM-A6]

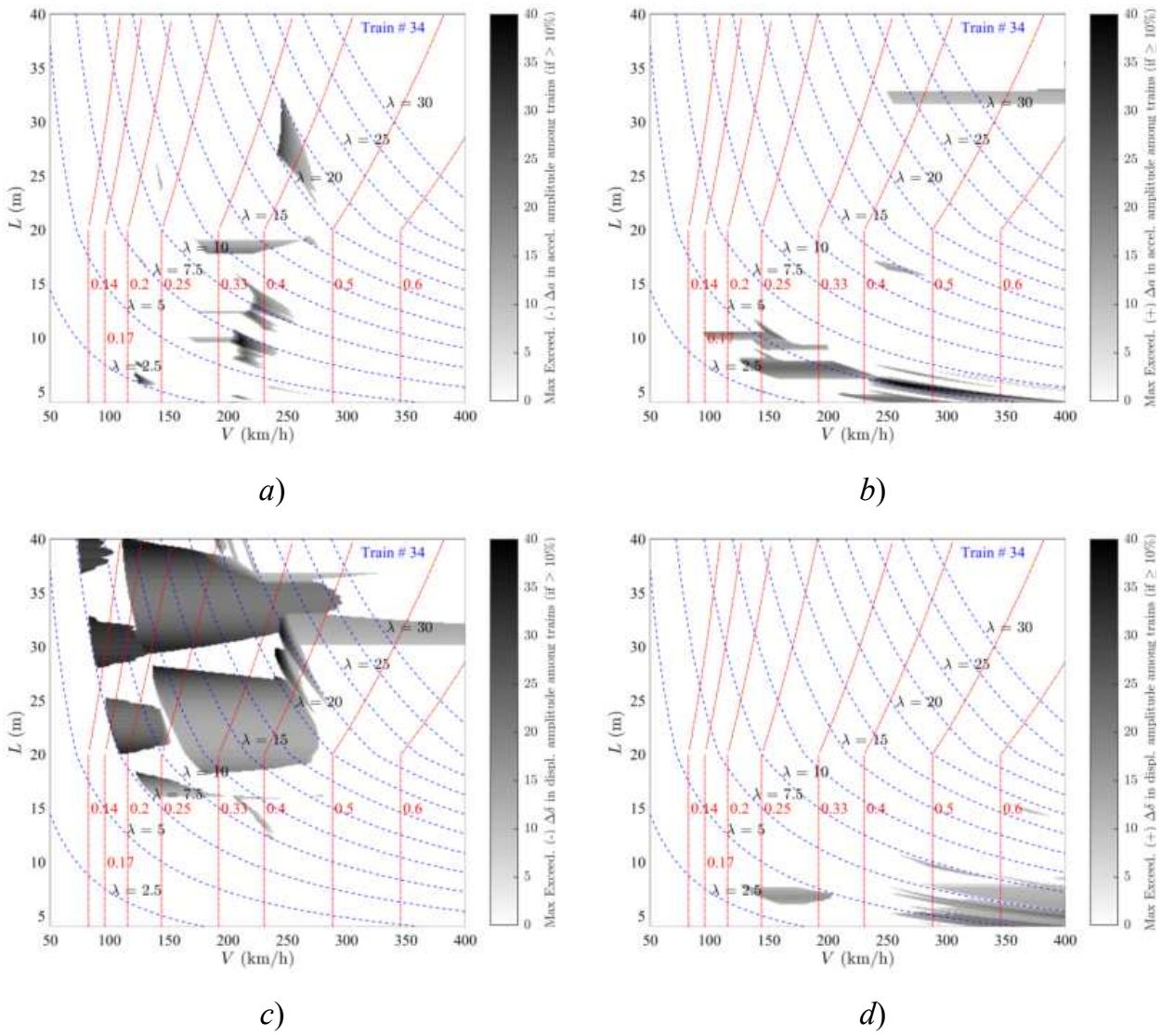

Figure 67. Exceedance Maps Train PT60-34 LIR vs Duhamel: a) Δa(–); b) Δa(+); c) Δδ(–); d) Δδ(+). PSC bridges.

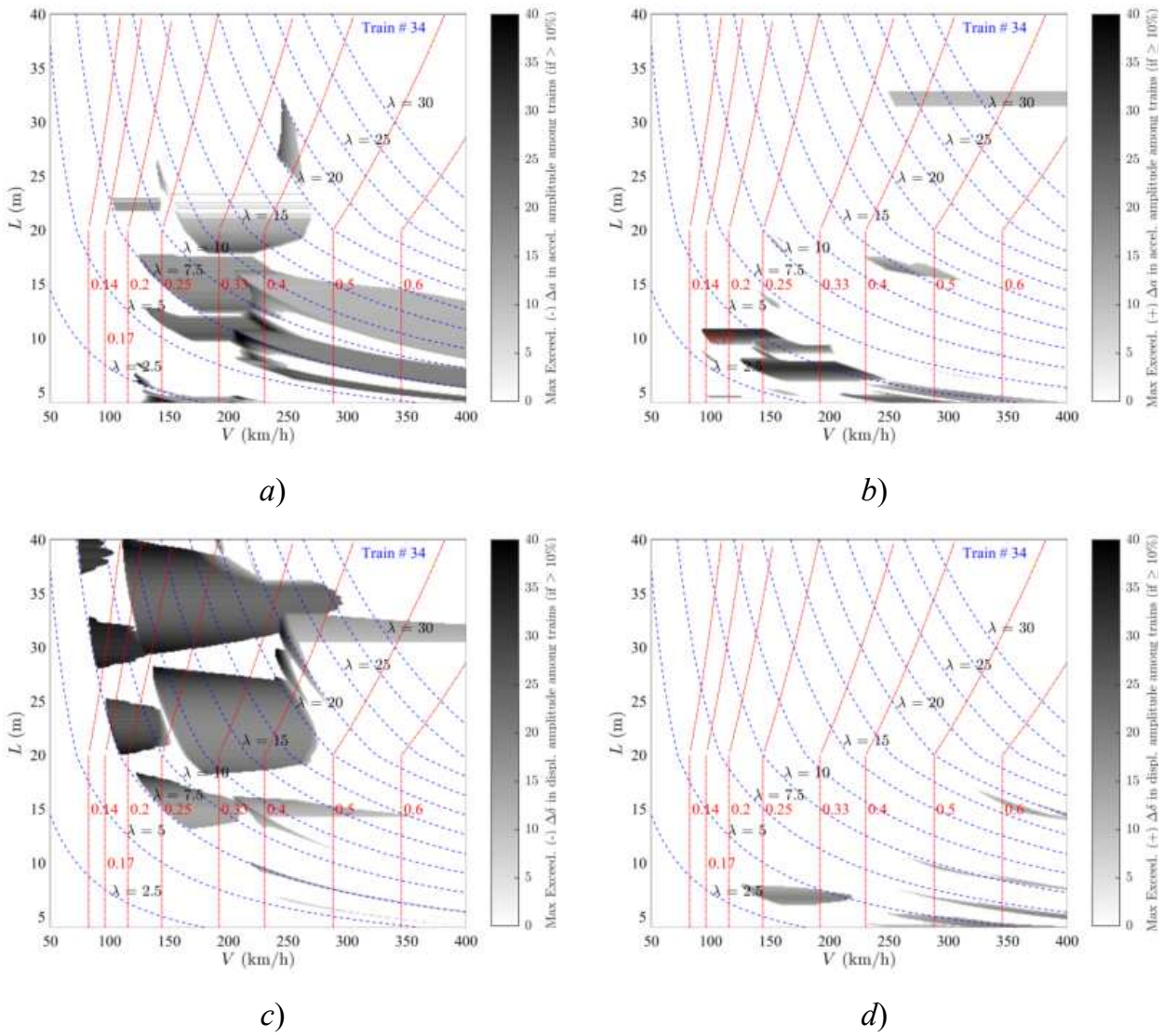

Figure 68. Exceedance Maps Train PT60-34 DER vs Duhamel: a) Δa(–); b) Δa(+); c) Δδ(–); d) Δδ(+). PSC bridges.

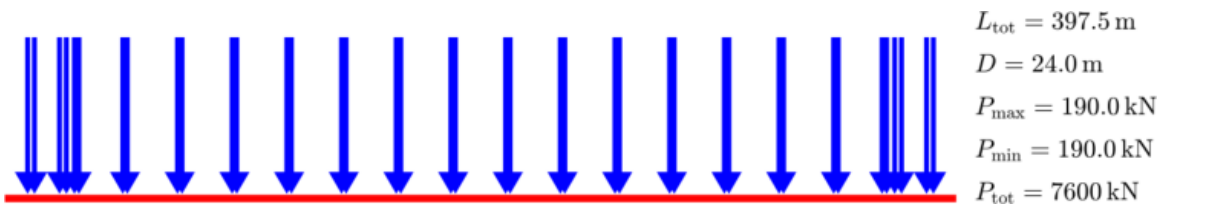

Figure Train PT60-35 [HSLM-A7]

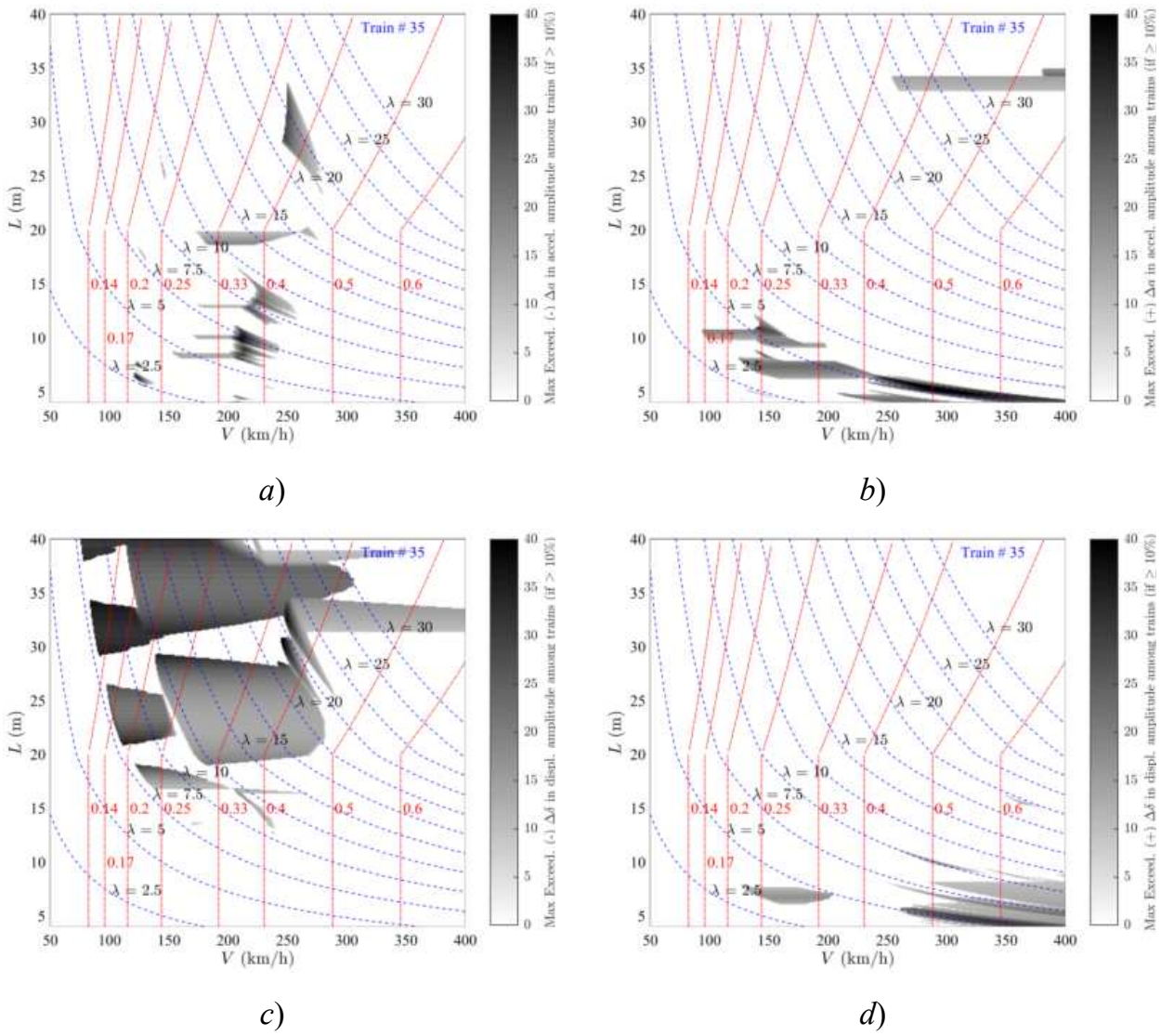

Figure 69. Exceedance Maps Train PT60-35 LIR vs Duhamel: a) Δa(–); b) Δa(+); c) Δδ(–); d) Δδ(+). PSC bridges.

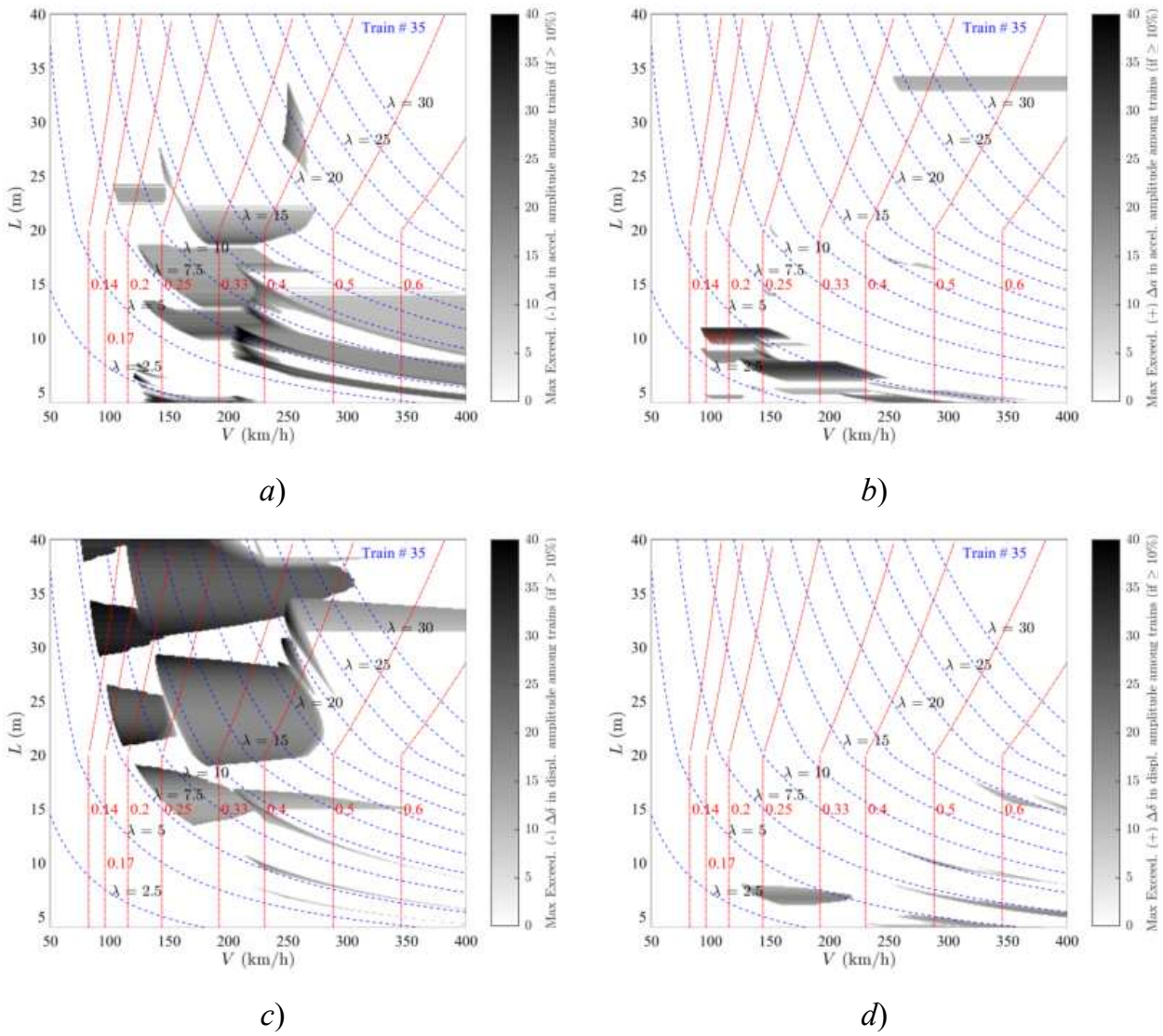

Figure 70. Exceedance Maps Train PT60-35 DER vs Duhamel: a) Δa(−); b) Δa(+); c) Δδ(−); d) Δδ(+). PSC bridges.

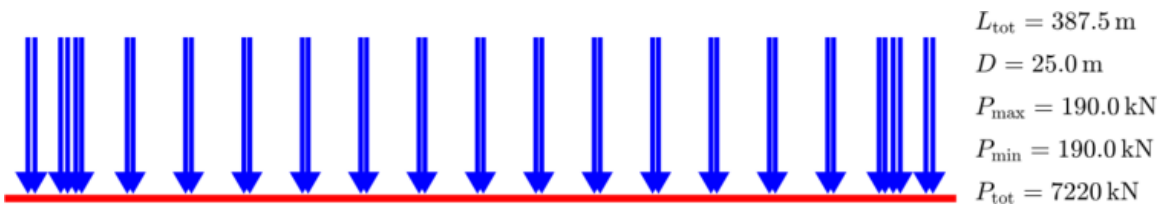

Figure Train PT60-36 [HSLM-A8]

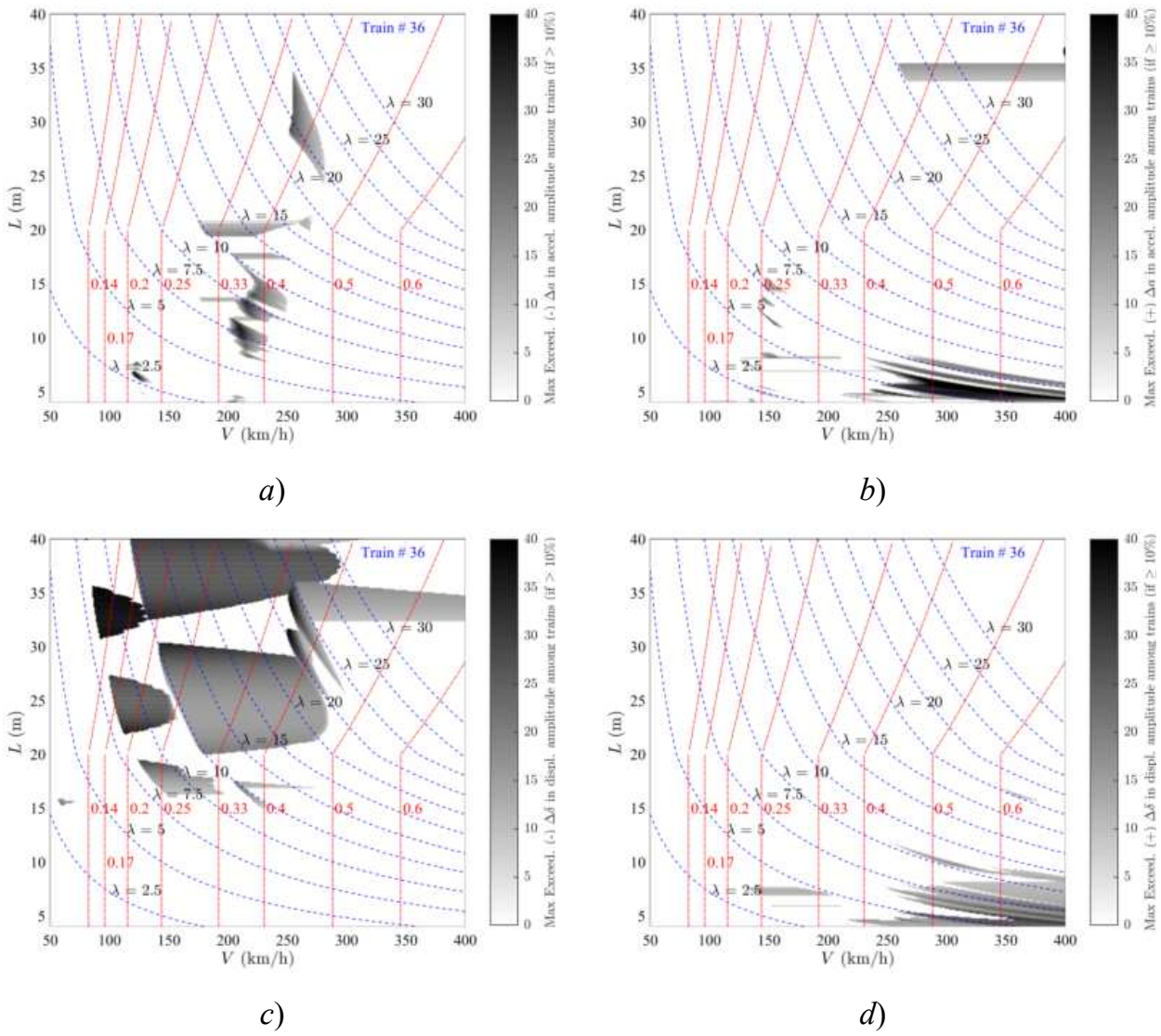

Figure 71. Exceedance Maps Train PT60-36 LIR vs Duhamel: a) Δa(–); b) Δa(+); c) Δδ(–); d) Δδ(+). PSC bridges.

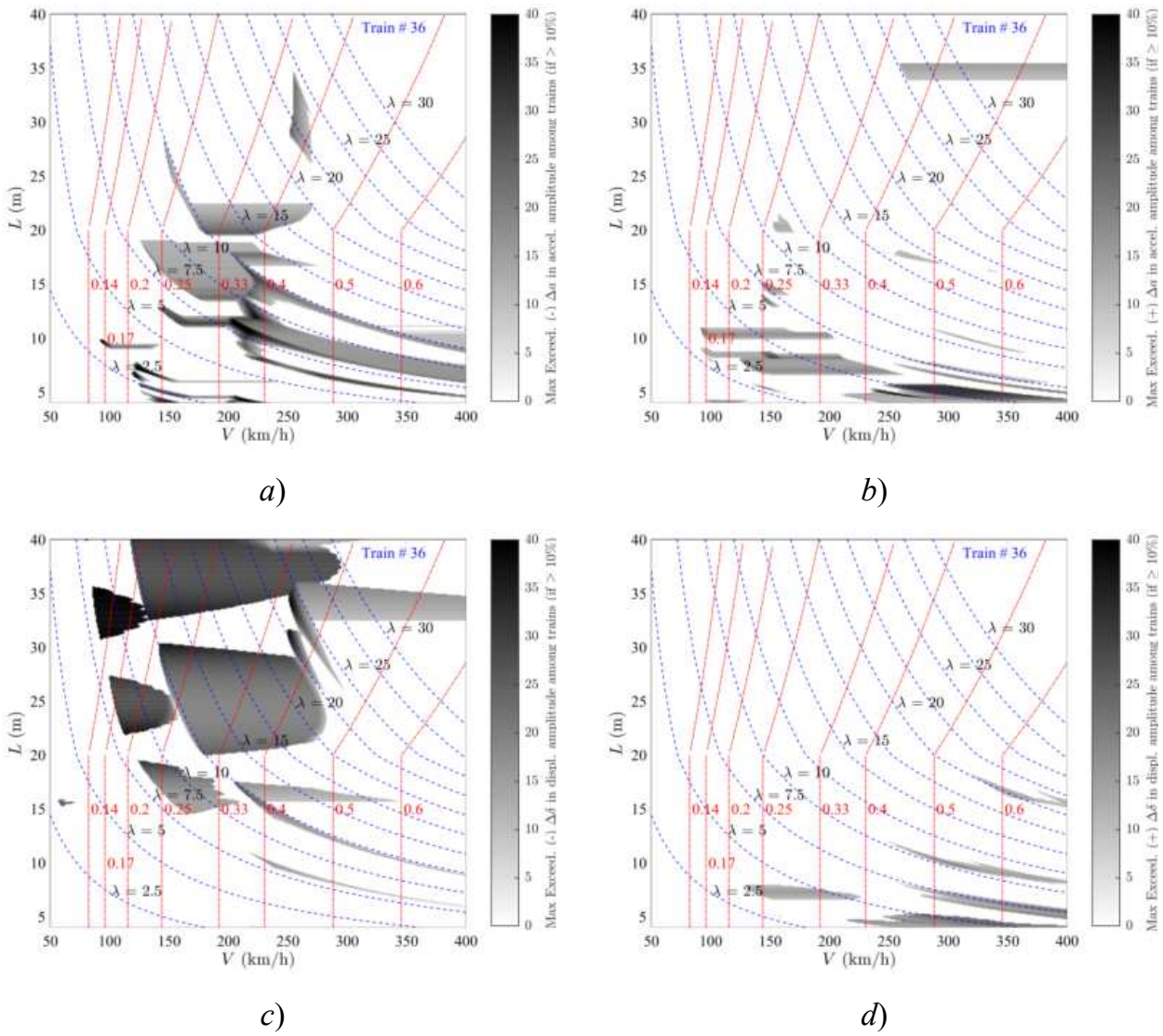

Figure 72. Exceedance Maps Train PT60-36 DER vs Duhamel: a) Δa(–); b) Δa(+); c) Δδ(–); d) Δδ(+). PSC bridges.

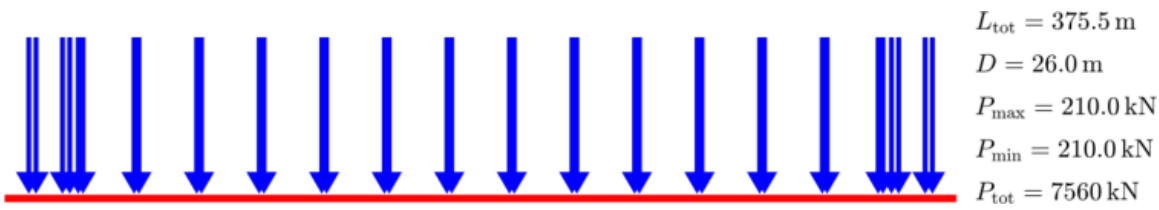

Figure Train PT60-37 [HSLM-A9]

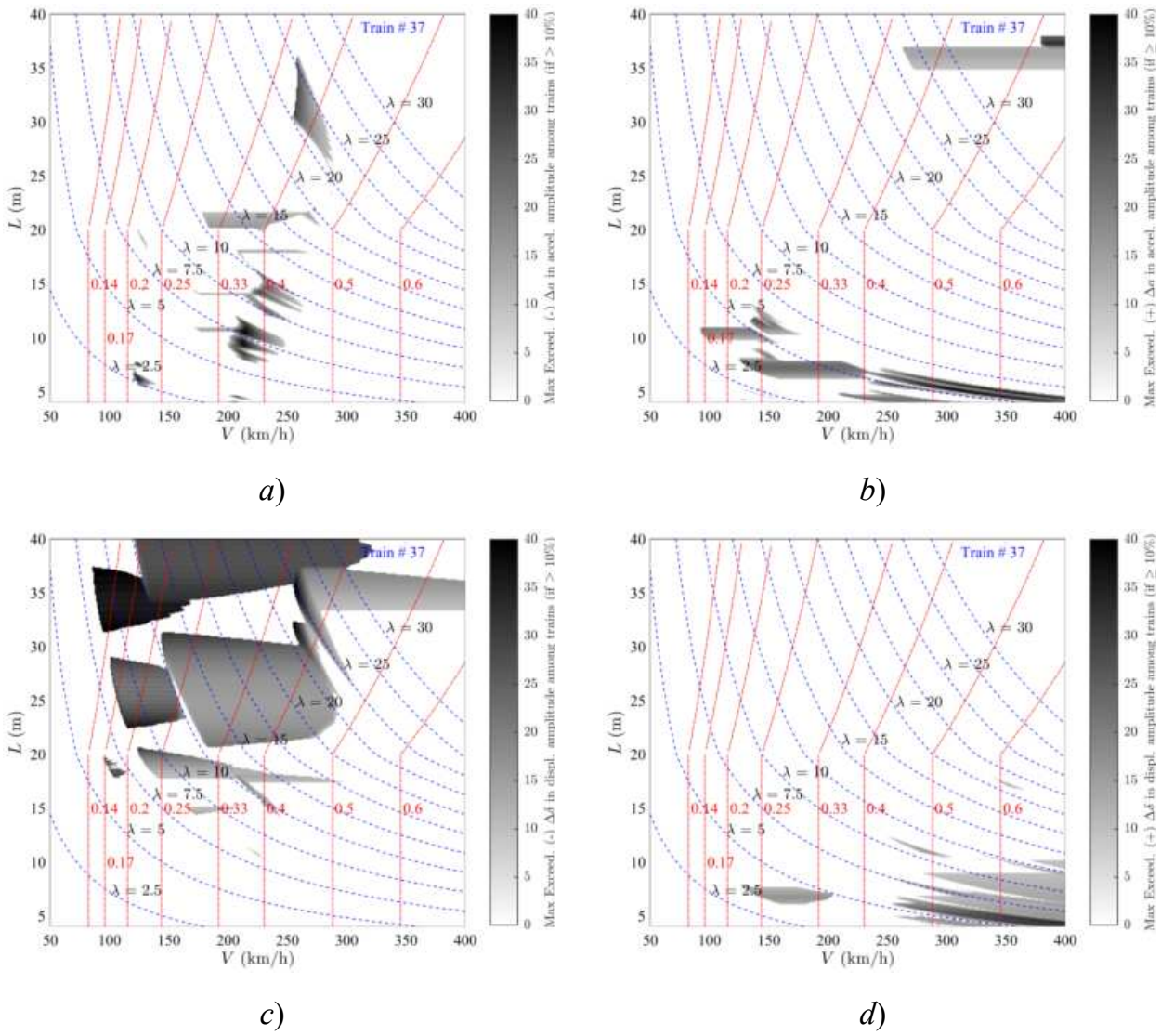

Figure 73. Exceedance Maps Train PT60-37 LIR vs Duhamel: a) Δa(–); b) Δa(+); c) Δδ(–); d) Δδ(+). PSC bridges.

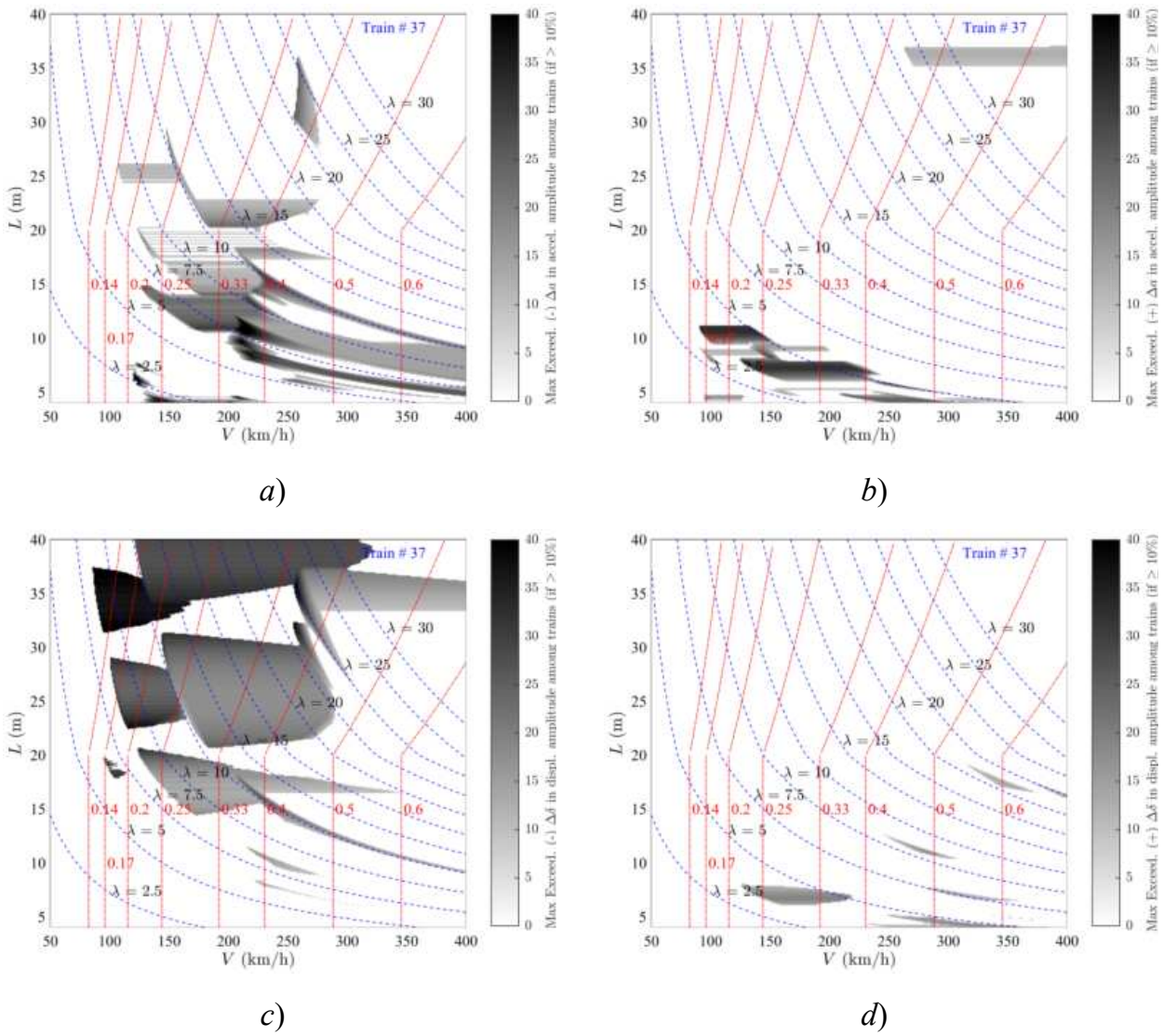

Figure 74. Exceedance Maps Train PT60-37 DER vs Duhamel: a) Δa(–); b) Δa(+); c) Δδ(–); d) Δδ(+). PSC bridges.

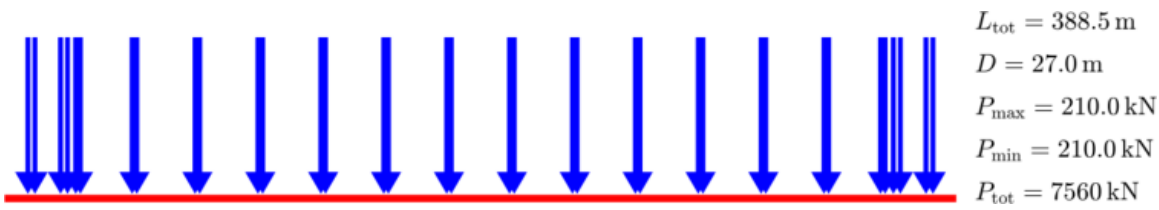

Figure Train PT60-38 [HSLM-A10]

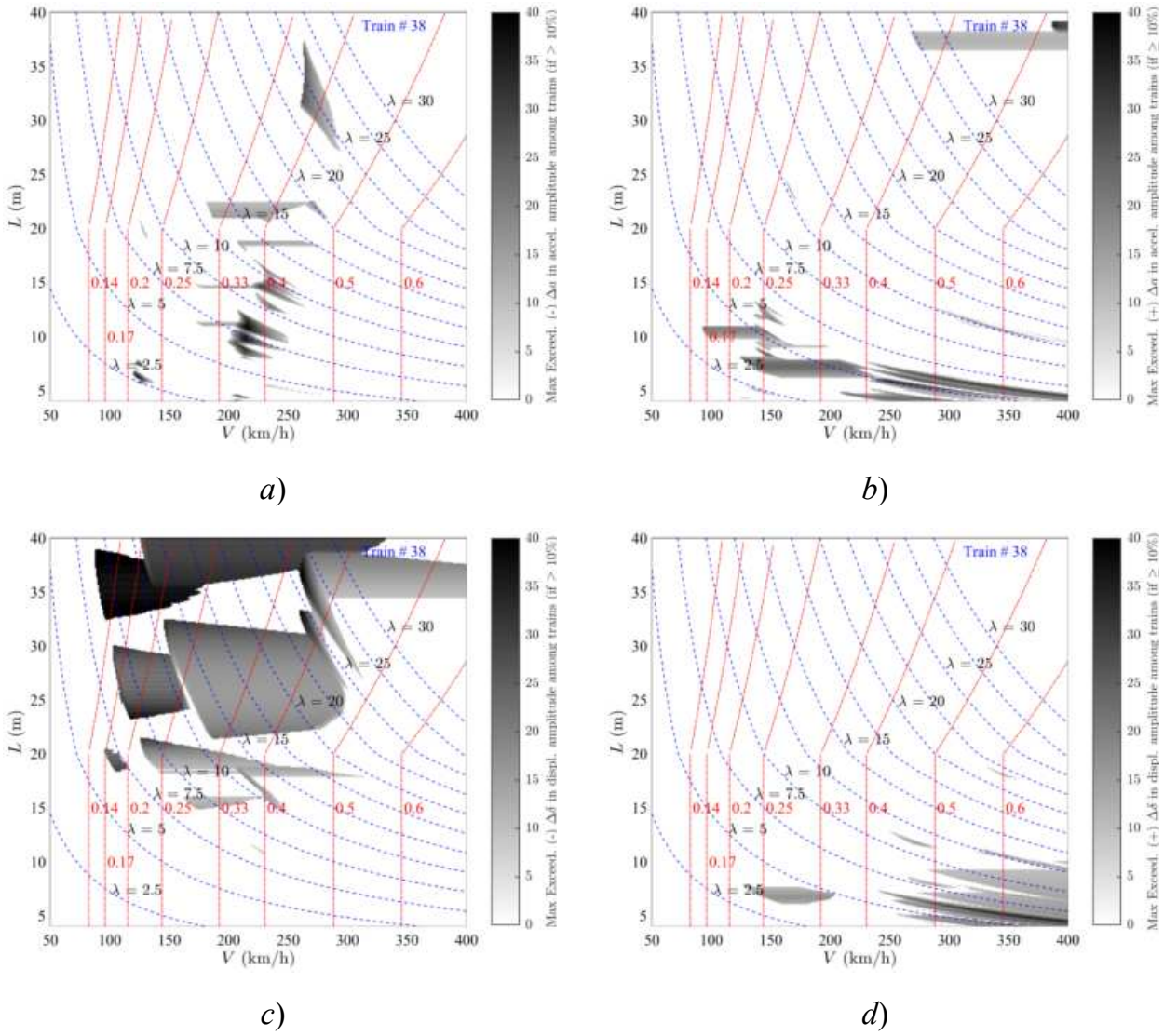

Figure 75. Exceedance Maps Train PT60-38 LIR vs Duhamel: a) Δa(–); b) Δa(+); c) Δδ(–); d) Δδ(+). PSC bridges.

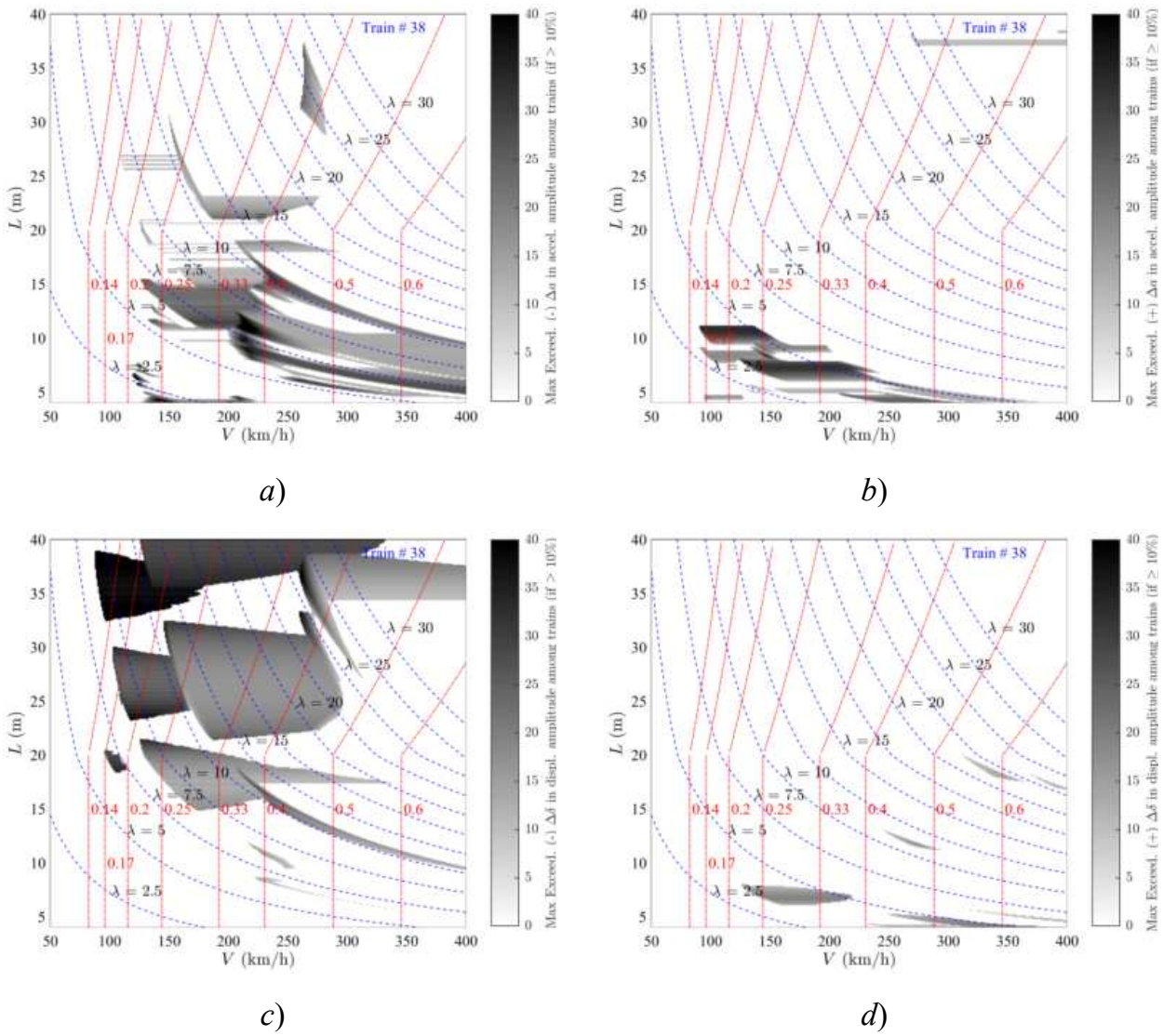

Figure 76. Exceedance Maps Train PT60-38 DER vs Duhamel: a) Δa(–); b) Δa(+); c) Δδ(–); d) Δδ(+). PSC bridges.

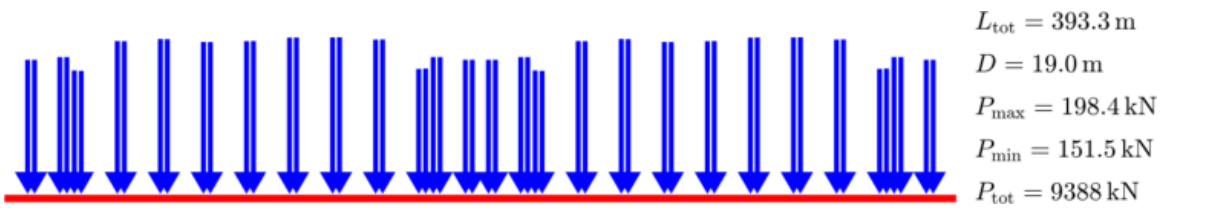

Figure Train PT60-39 [INB4EU-AB-039]

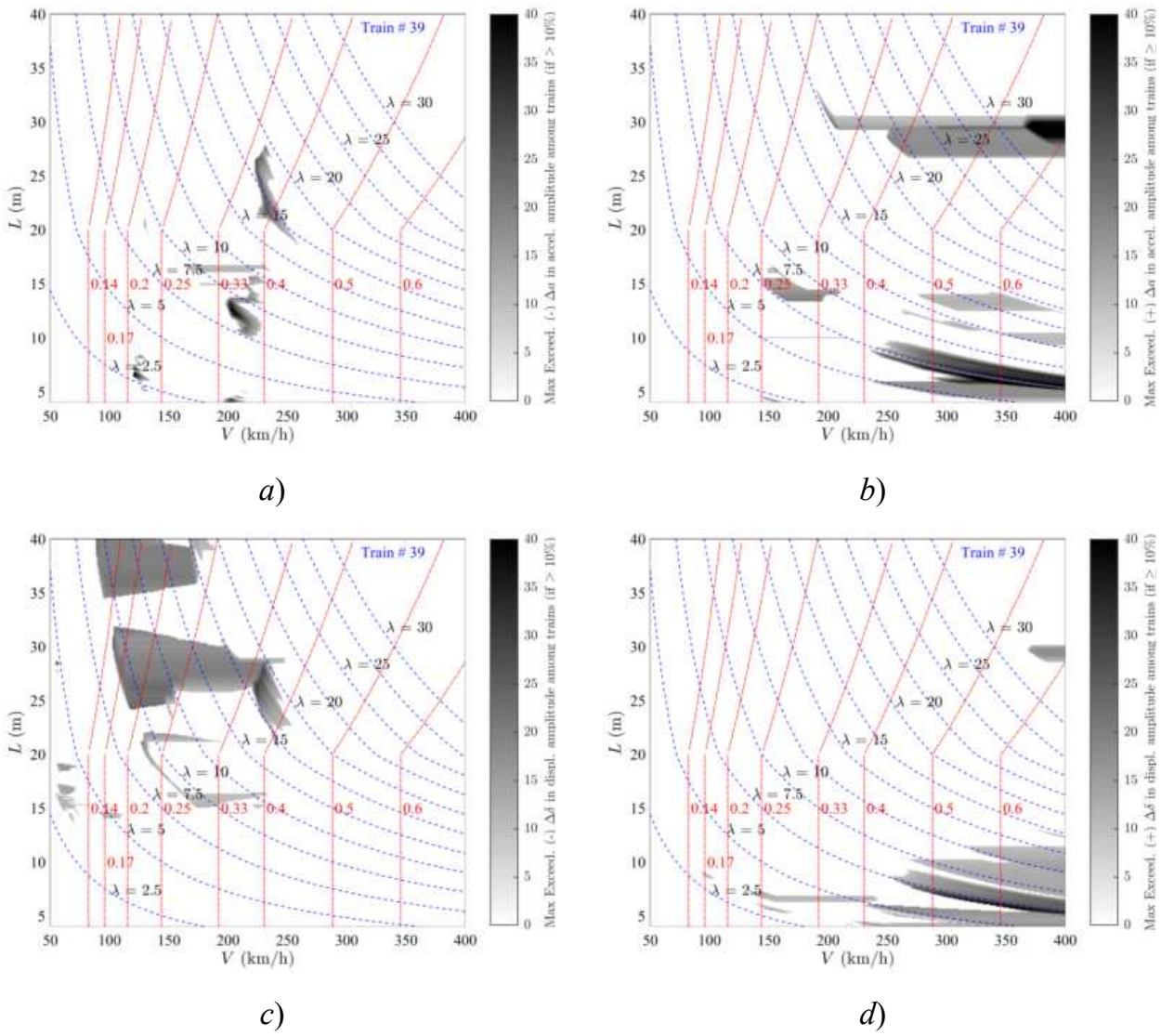

Figure 77. Exceedance Maps Train PT60-39 LIR vs Duhamel: a) Δa(–); b) Δa(+); c) Δδ(–); d) Δδ(+). PSC bridges.

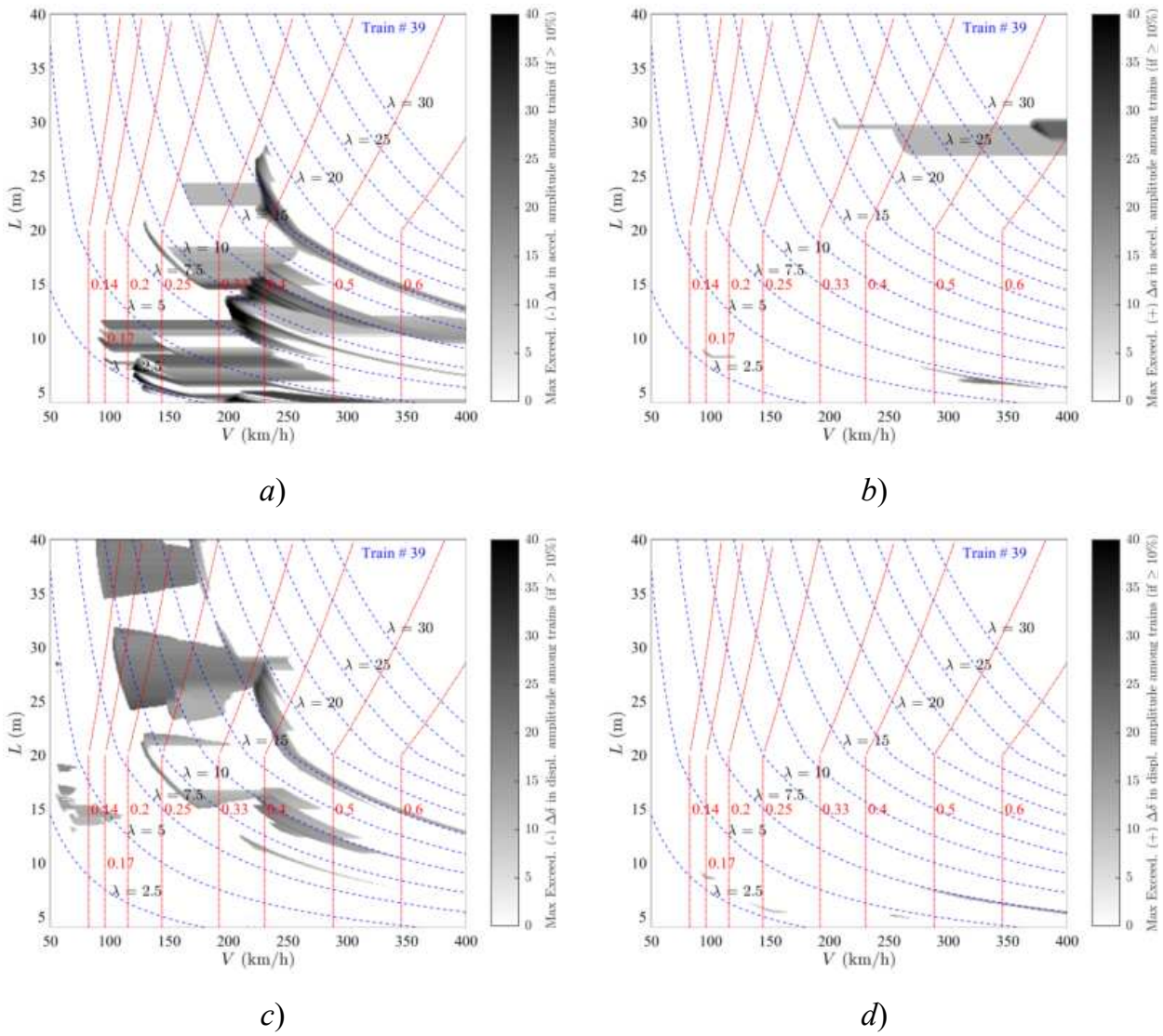

Figure 78. Exceedance Maps Train PT60-39 DER vs Duhamel: a) Δa(−); b) Δa(+); c) Δδ(−); d) Δδ(+). PSC bridges.

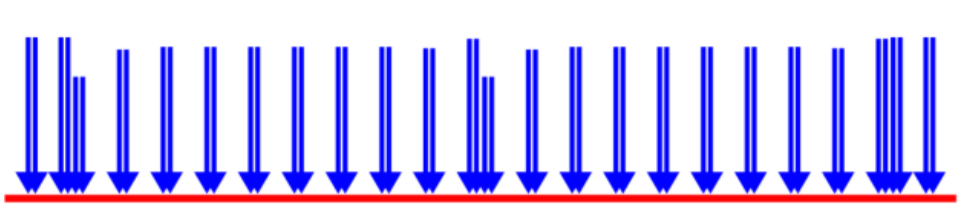

Figure Train PT60-40 [INB4EU-AB-016]

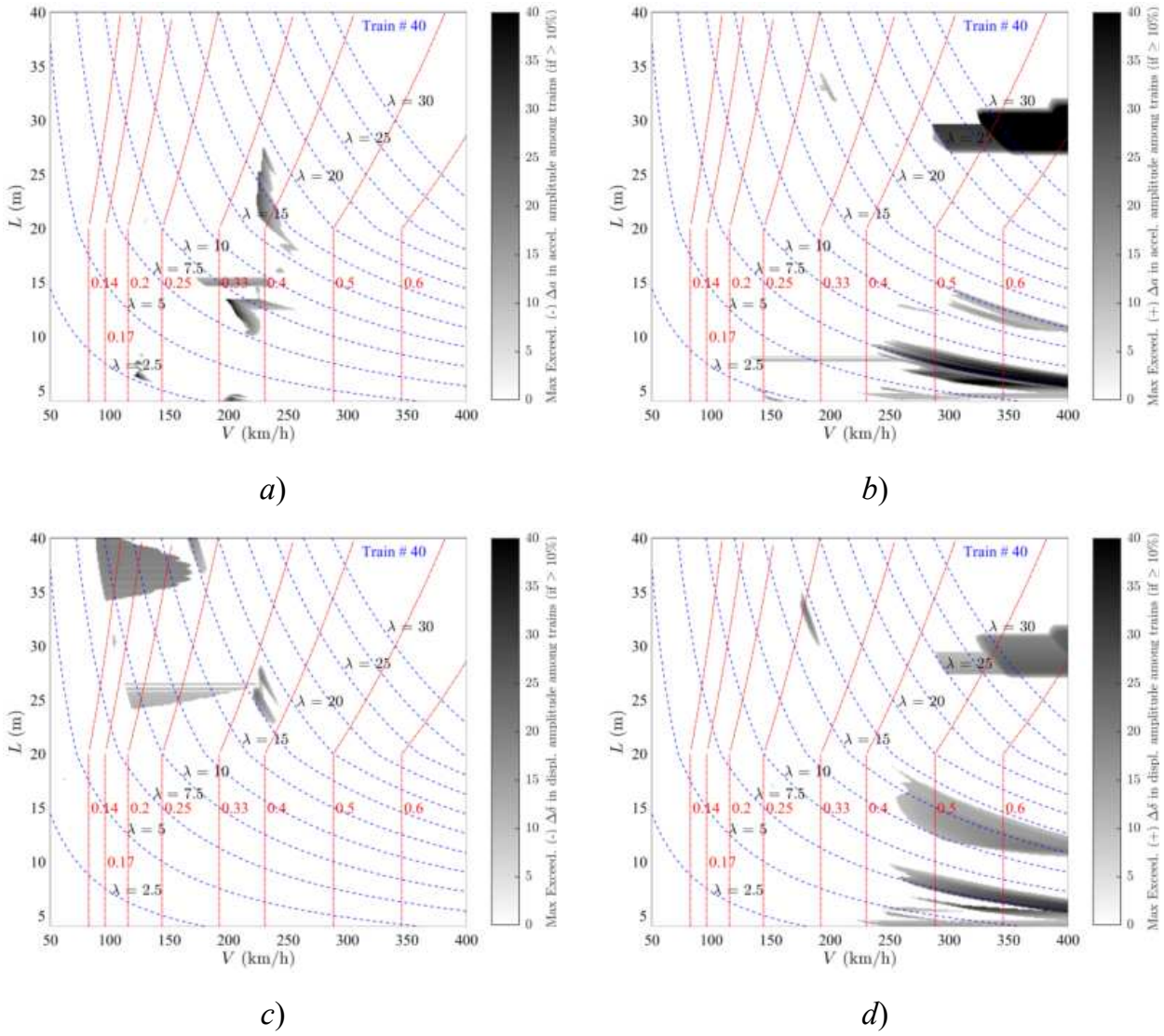

Figure 79. Exceedance Maps Train PT60-40 LIR vs Duhamel: a) Δa(–); b) Δa(+); c) Δδ(–); d) Δδ(+). PSC bridges.

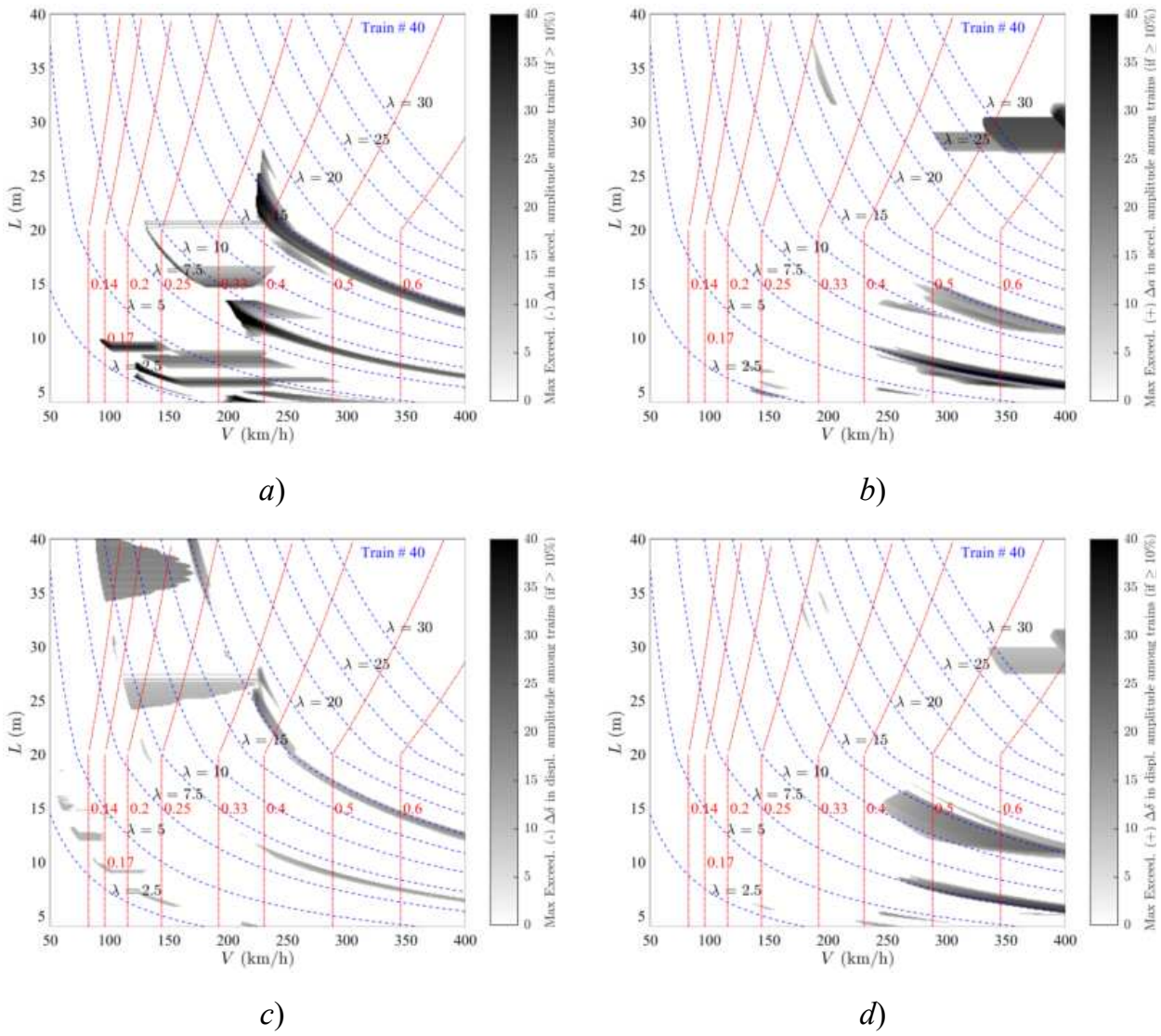

Figure 80. Exceedance Maps Train PT60-40 DER vs Duhamel: a) Δa(−); b) Δa(+); c) Δδ(−); d) Δδ(+). PSC bridges.

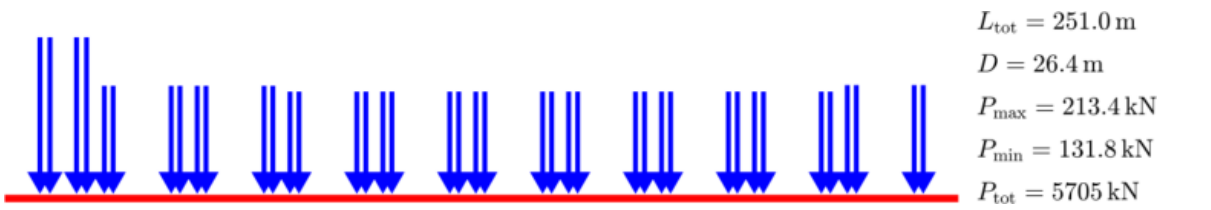

Figure Train PT60-41 [INB4EU-CB-003]

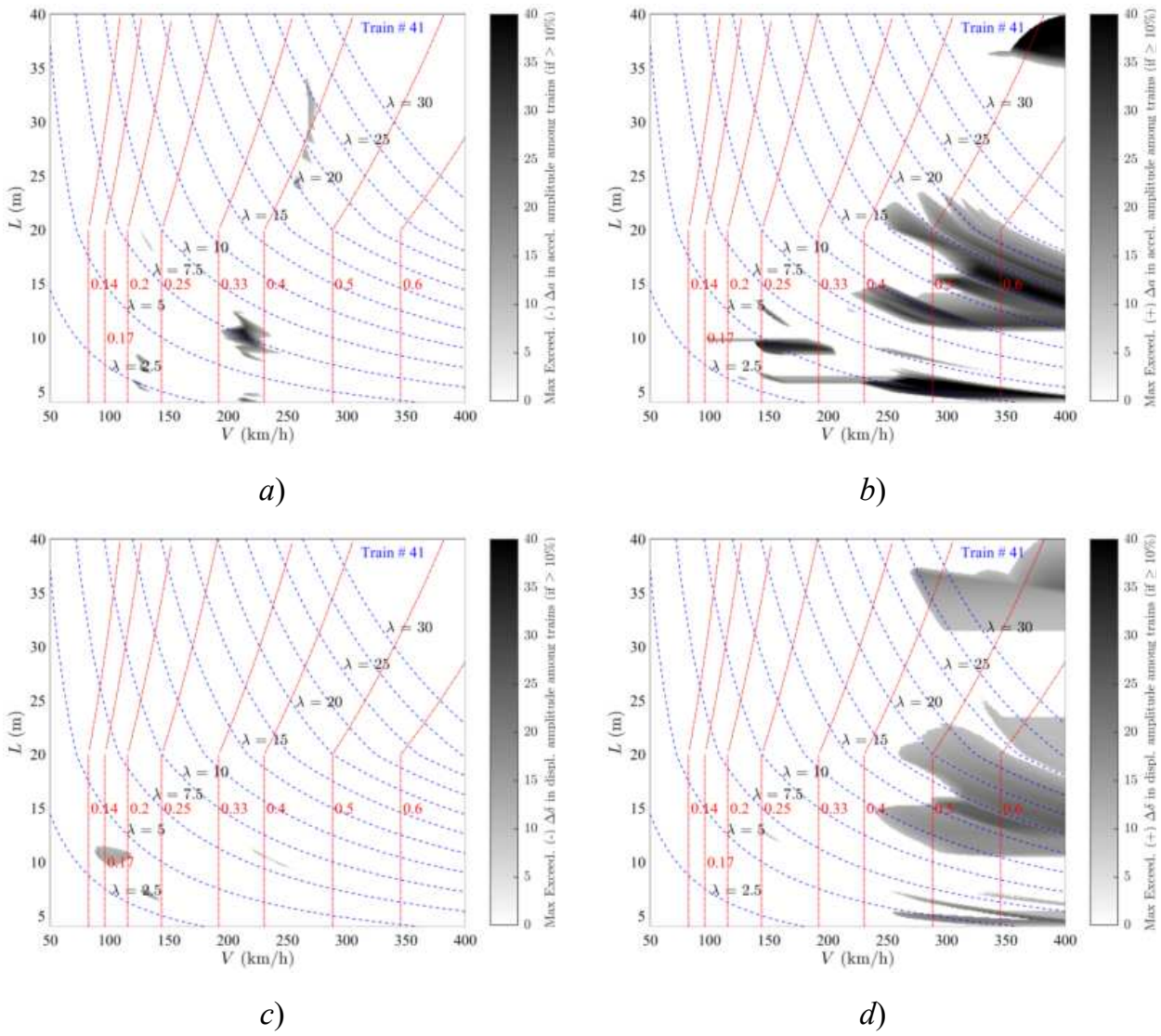

Figure 81. Exceedance Maps Train PT60-41 LIR vs Duhamel: a) Δa(–); b) Δa(+); c) Δδ(–); d) Δδ(+). PSC bridges.

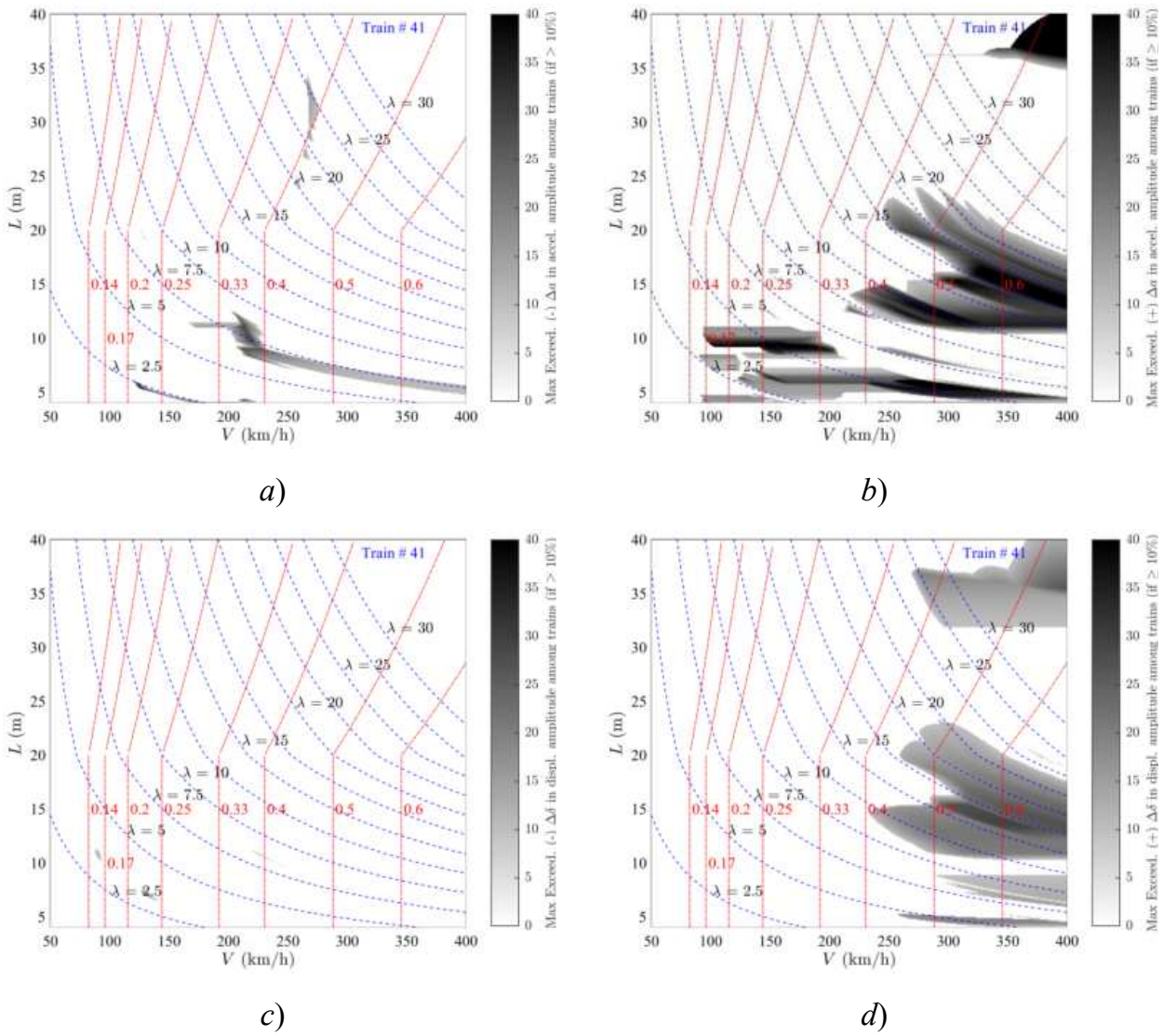

Figure 82. Exceedance Maps Train PT60-41 DER vs Duhamel: a) Δa(−); b) Δa(+); c) Δδ(−); d) Δδ(+). PSC bridges.

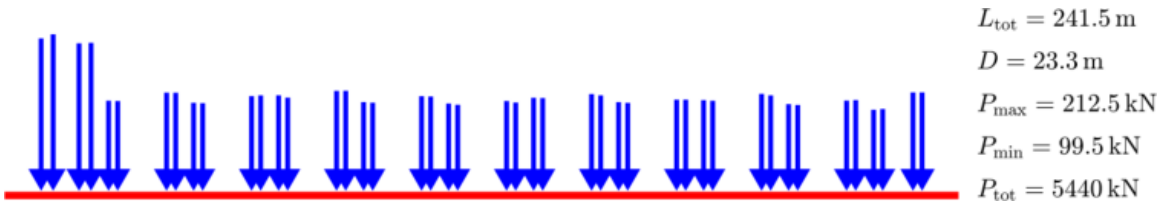

Figure Train PT60-42 [INB4EU-CB-075]

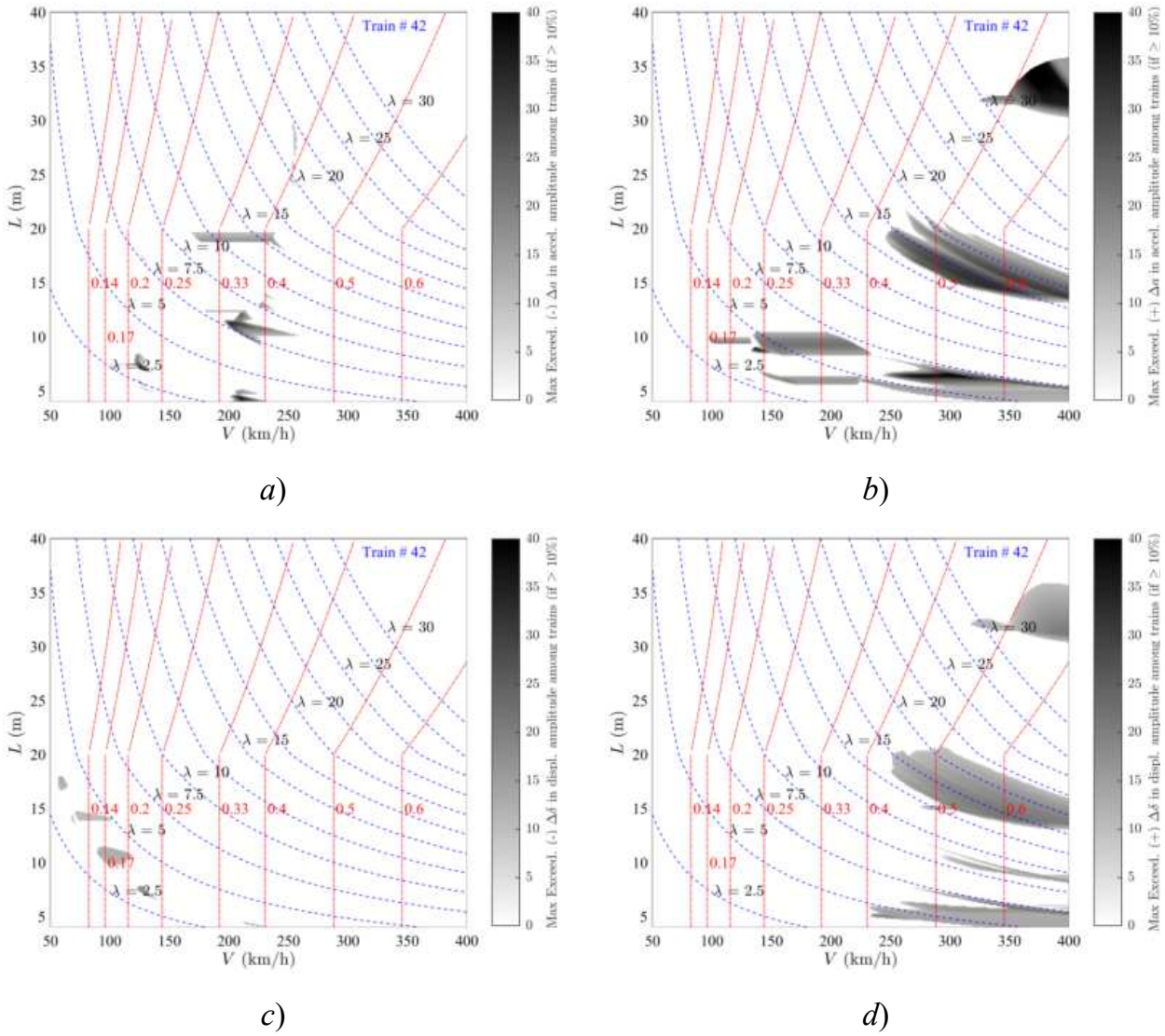

Figure 83. Exceedance Maps Train PT60-42 LIR vs Duhamel: a) Δa(–); b) Δa(+); c) Δδ(–); d) Δδ(+). PSC bridges.

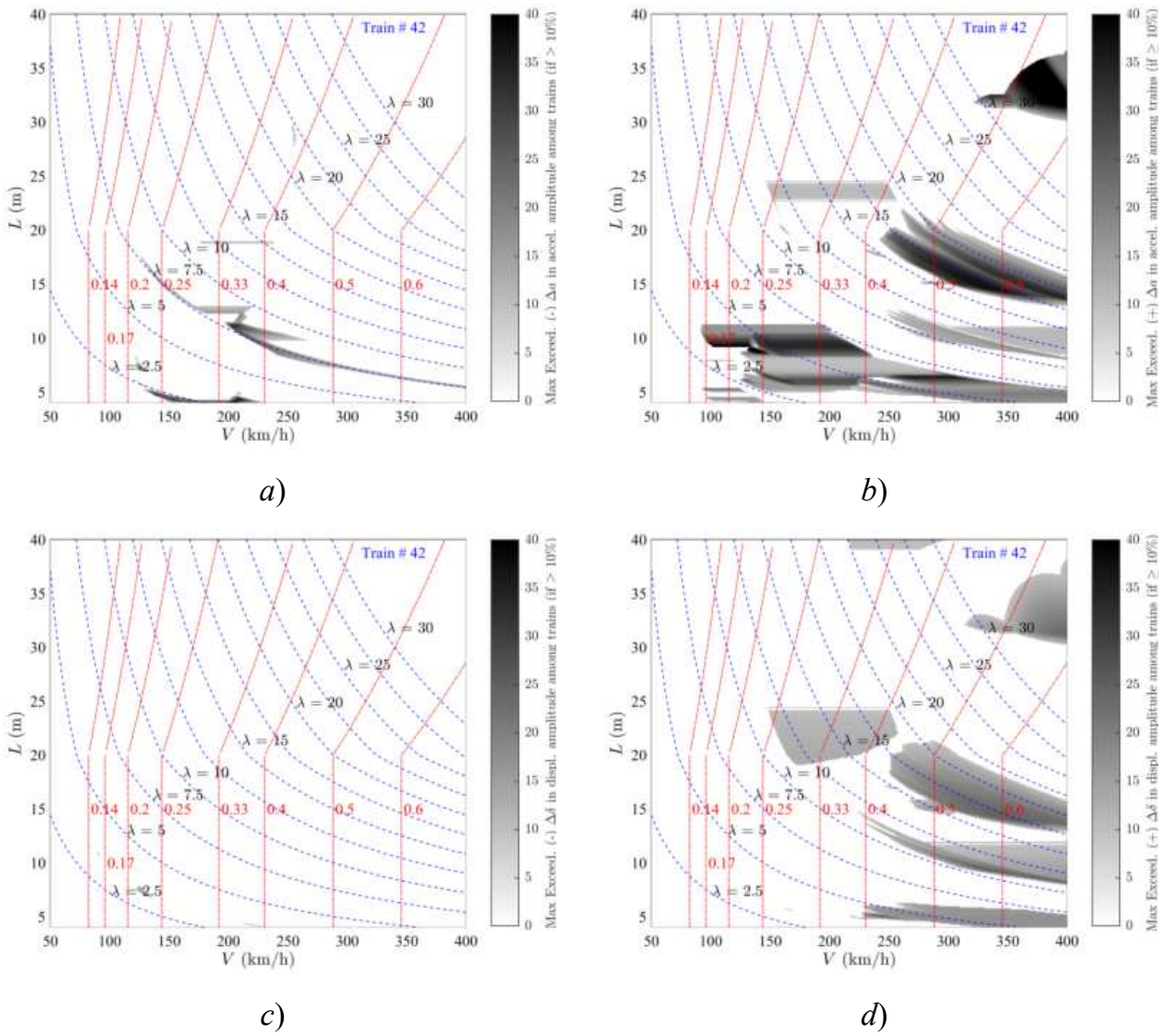

Figure 84. Exceedance Maps Train PT60-42 DER vs Duhamel: a) Δa(−); b) Δa(+); c) Δδ(−); d) Δδ(+). PSC bridges.

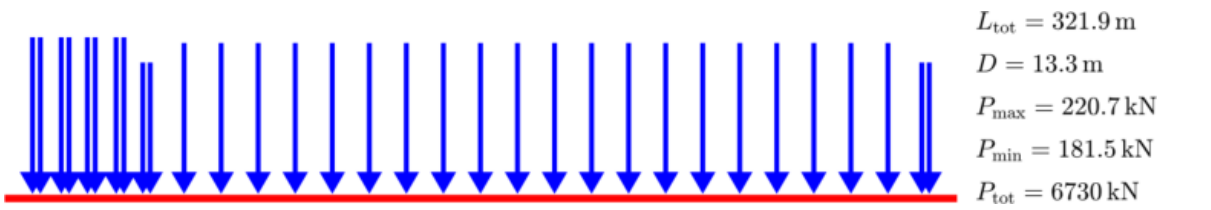

Figure Train PT60-43 [INB4EU-SA-021]

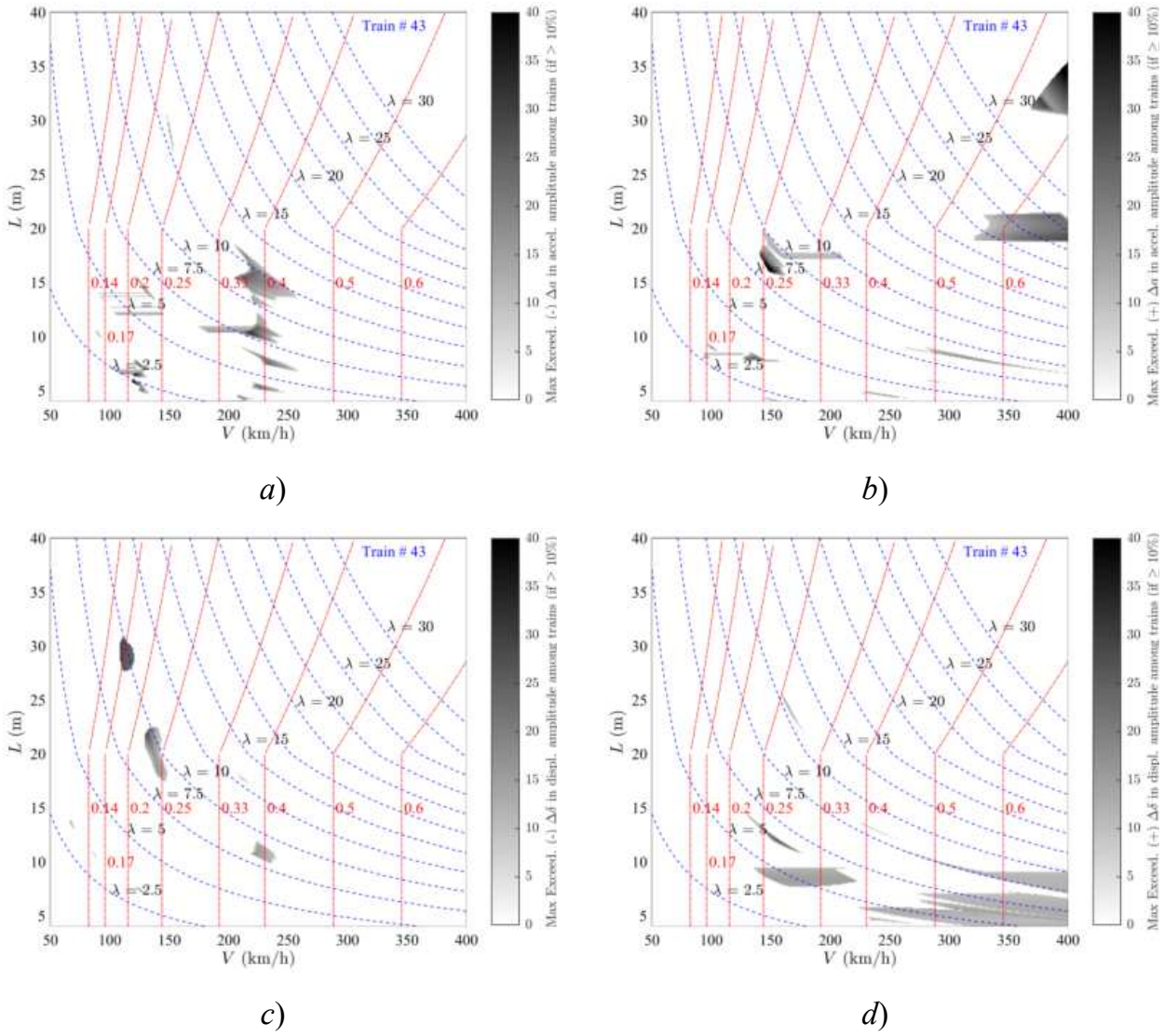

Figure 85. Exceedance Maps Train PT60-43 LIR vs Duhamel: a) Δa(–); b) Δa(+); c) Δδ(–); d) Δδ(+). PSC bridges.

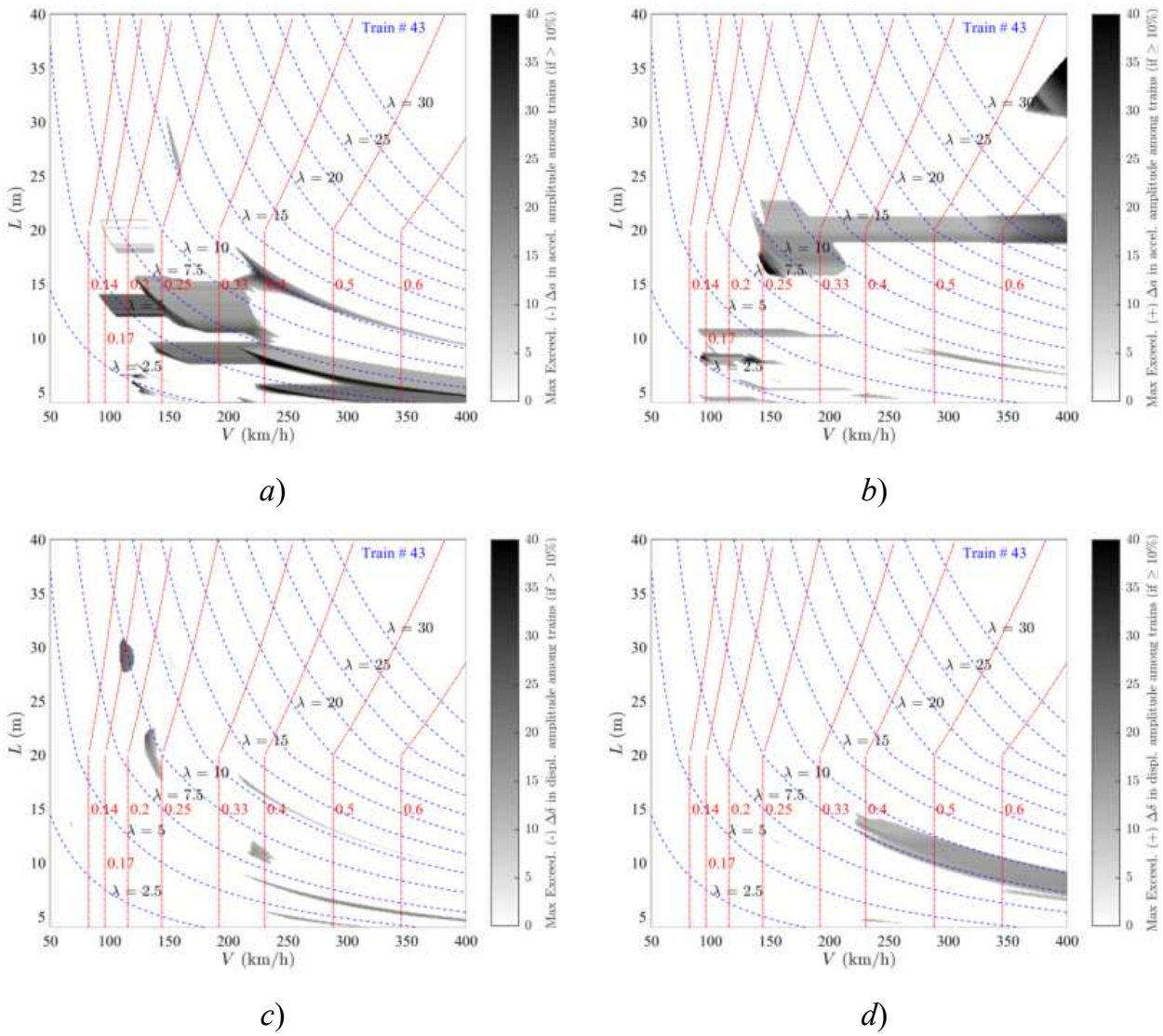

Figure 86. Exceedance Maps Train PT60-43 DER vs Duhamel: a) Δa(−); b) Δa(+); c) Δδ(−); d) Δδ(+). PSC bridges.

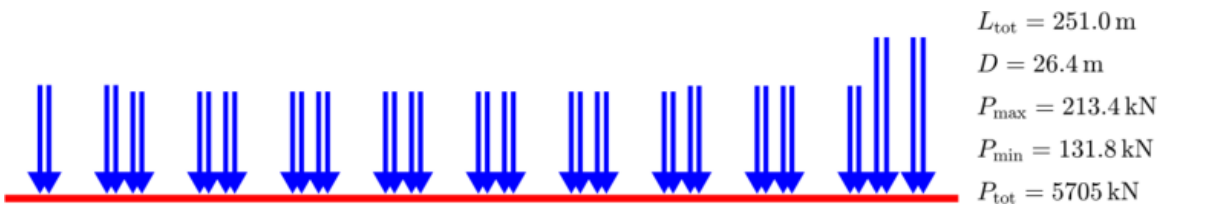

Figure Train PT60-44 [INB4EU-CB-081]

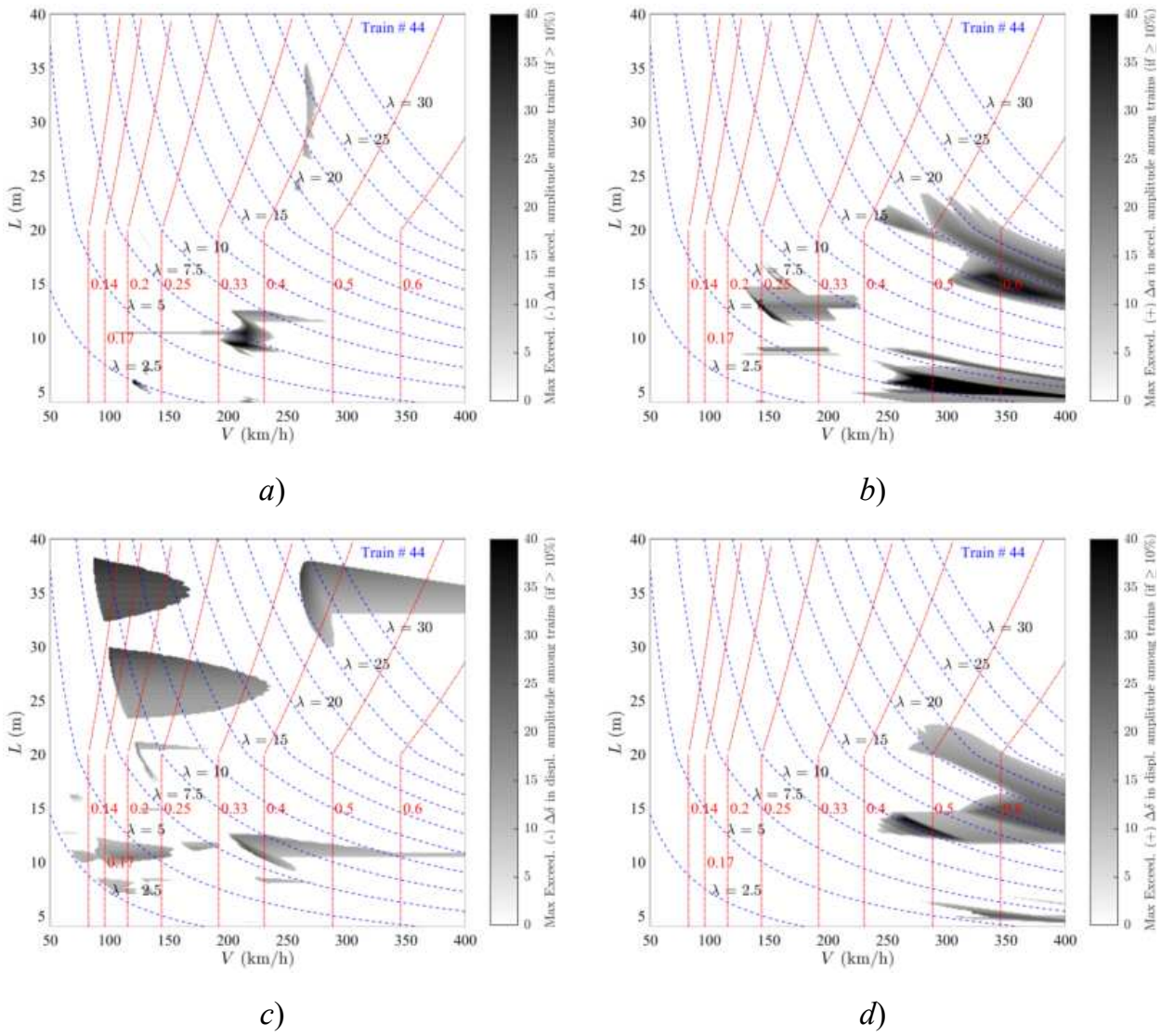

Figure 87. Exceedance Maps Train PT60-44 LIR vs Duhamel: a) Δa(–); b) Δa(+); c) Δδ(–); d) Δδ(+). PSC bridges.

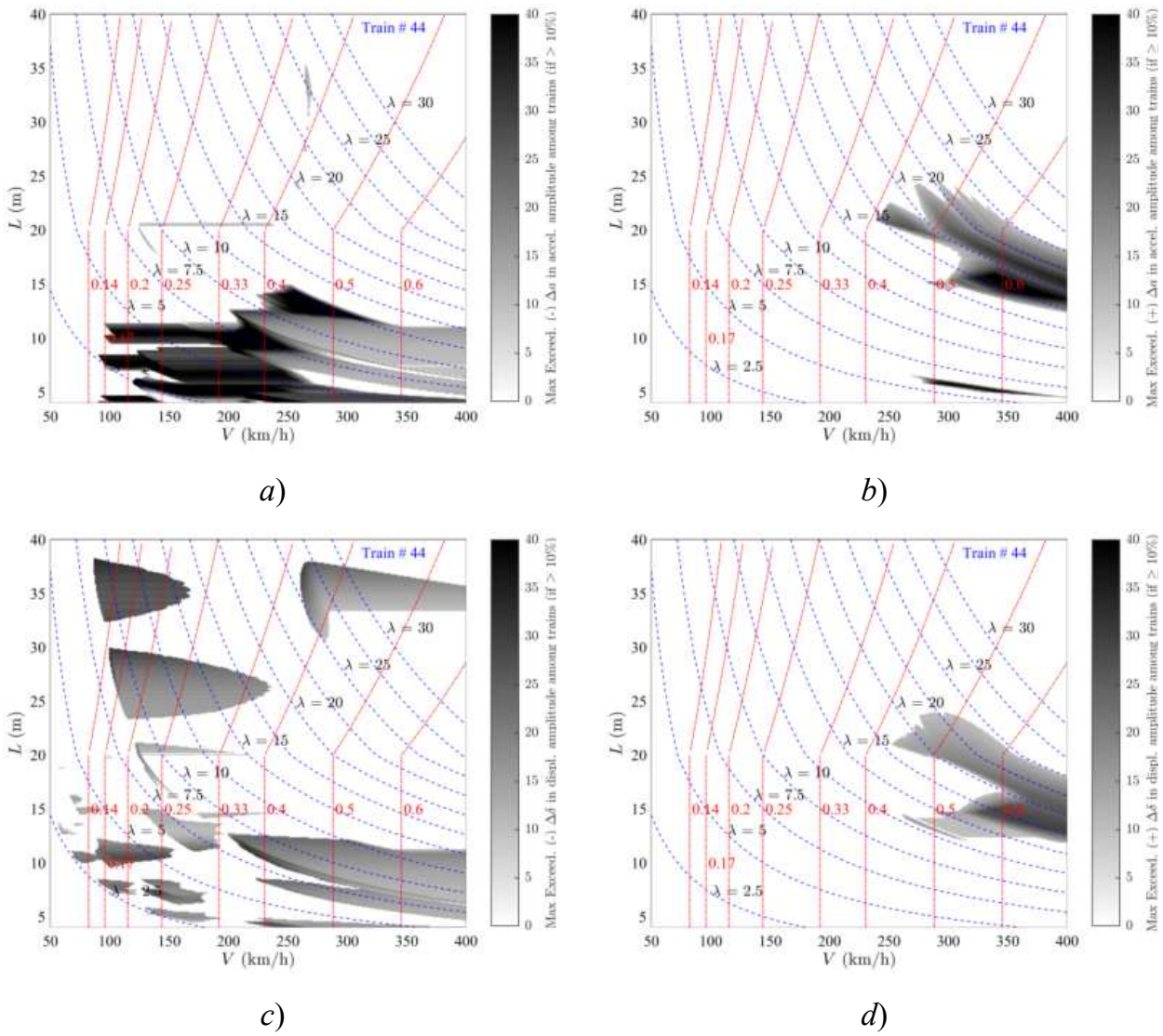

Figure 88. Exceedance Maps Train PT60-44 DER vs Duhamel: a) Δa(–); b) Δa(+); c) Δδ(–); d) Δδ(+). PSC bridges.

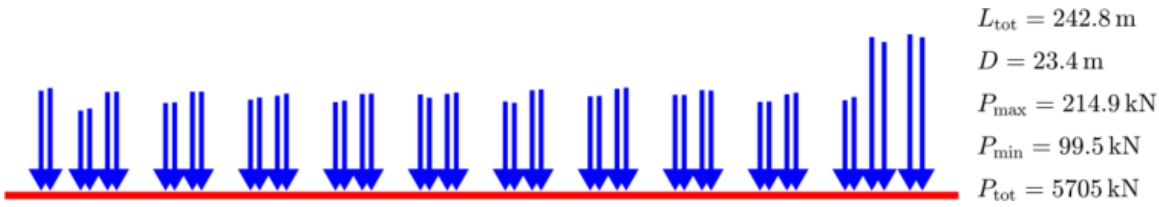

Figure Train PT60-45 [INB4EU-CB-124]

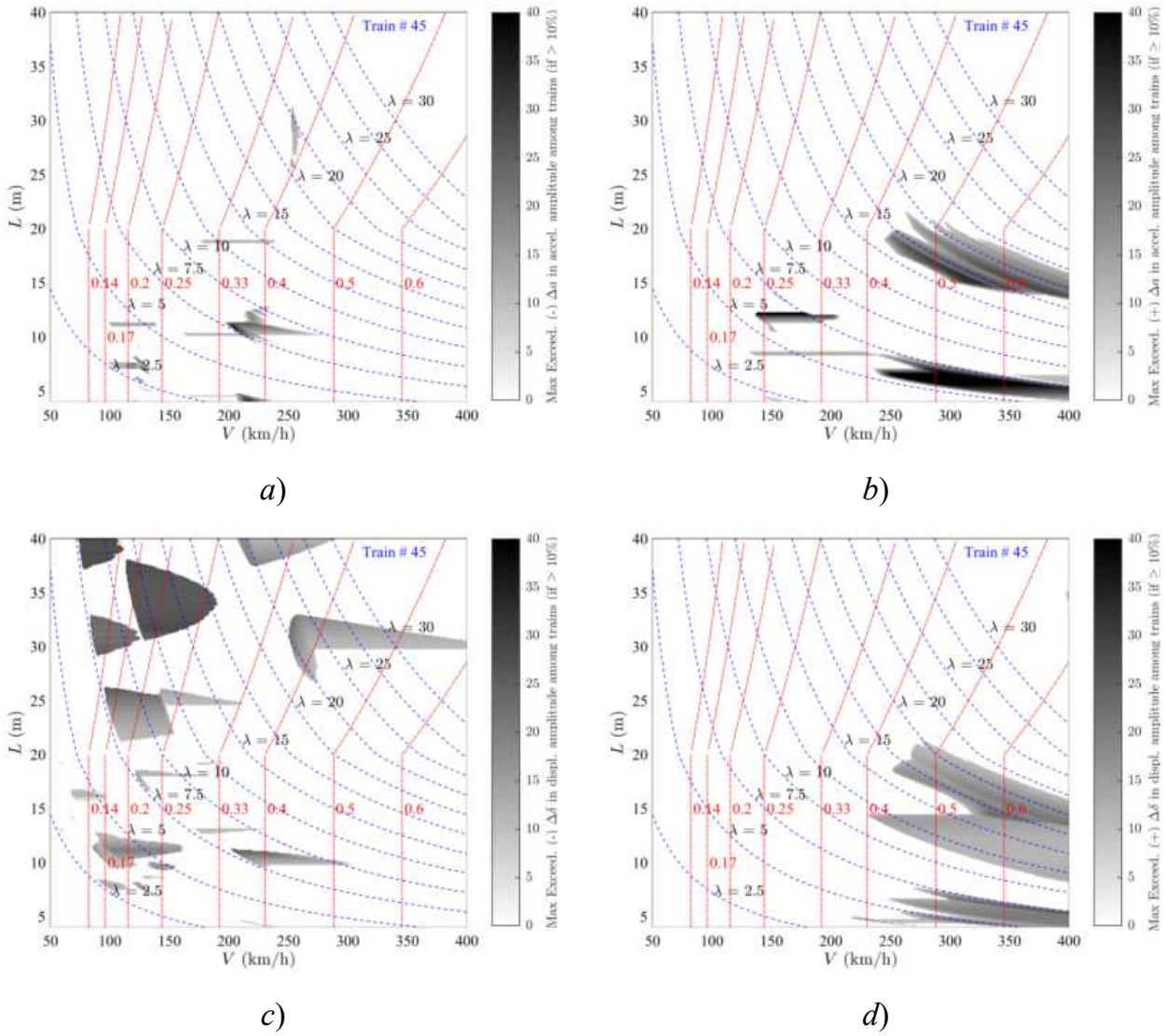

Figure 89. Exceedance Maps Train PT60-45 LIR vs Duhamel: a) Δa(–); b) Δa(+); c) Δδ(–); d) Δδ(+). PSC bridges.

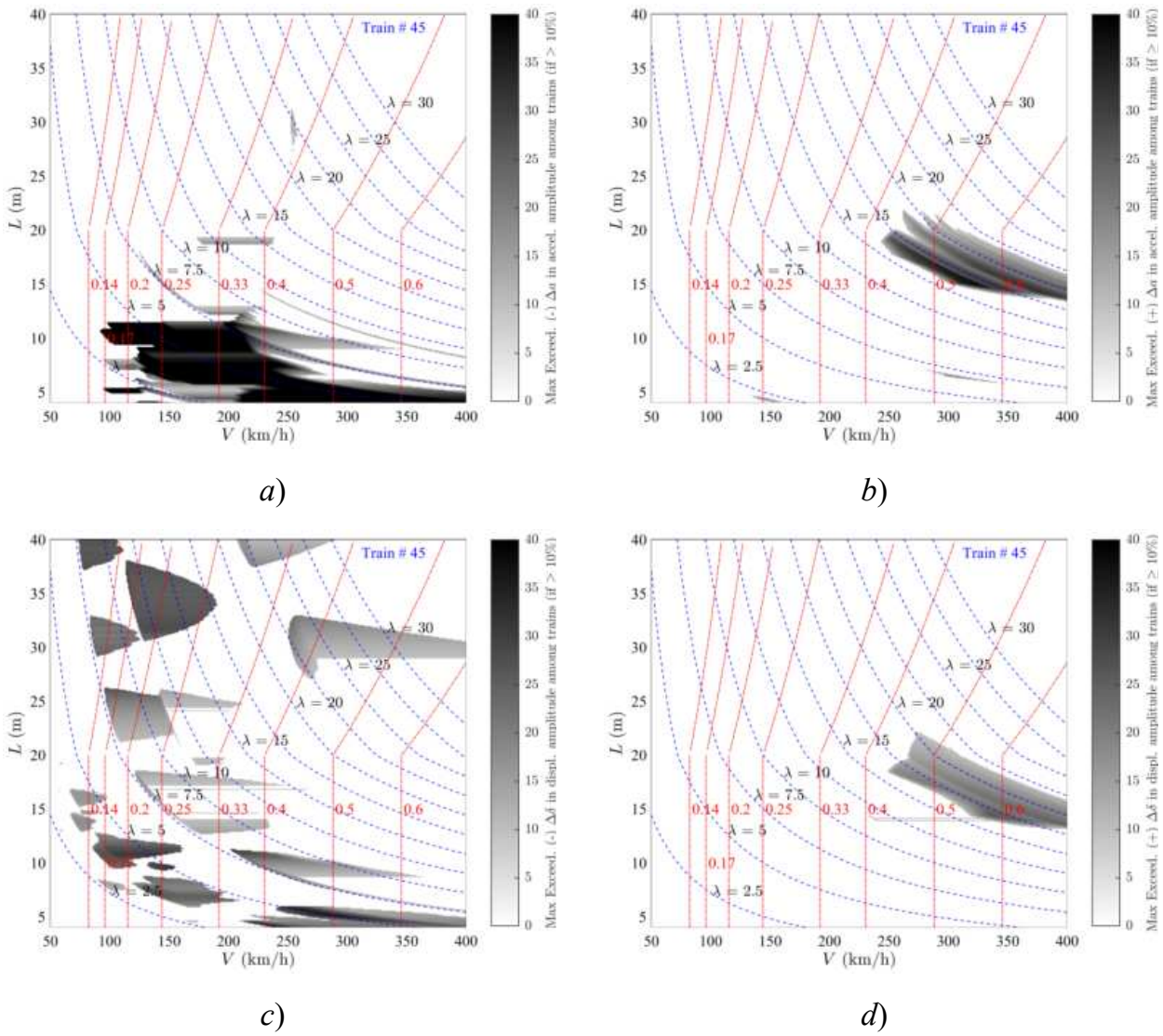

Figure 90. Exceedance Maps Train PT60-45 DER vs Duhamel: a) Δa(−); b) Δa(+); c) Δδ(−); d) Δδ(+). PSC bridges.

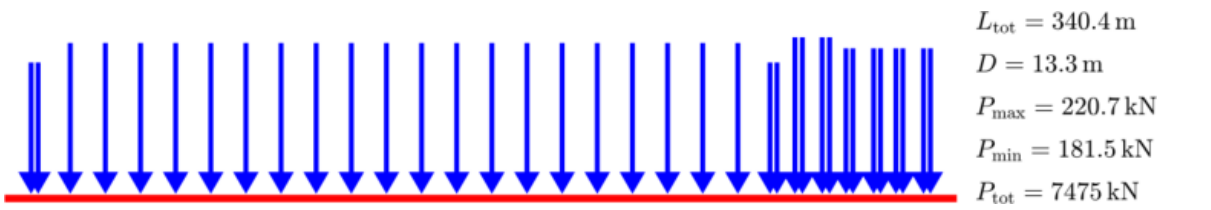

Figure Train PT60-46 [INB4EU-SA-035]

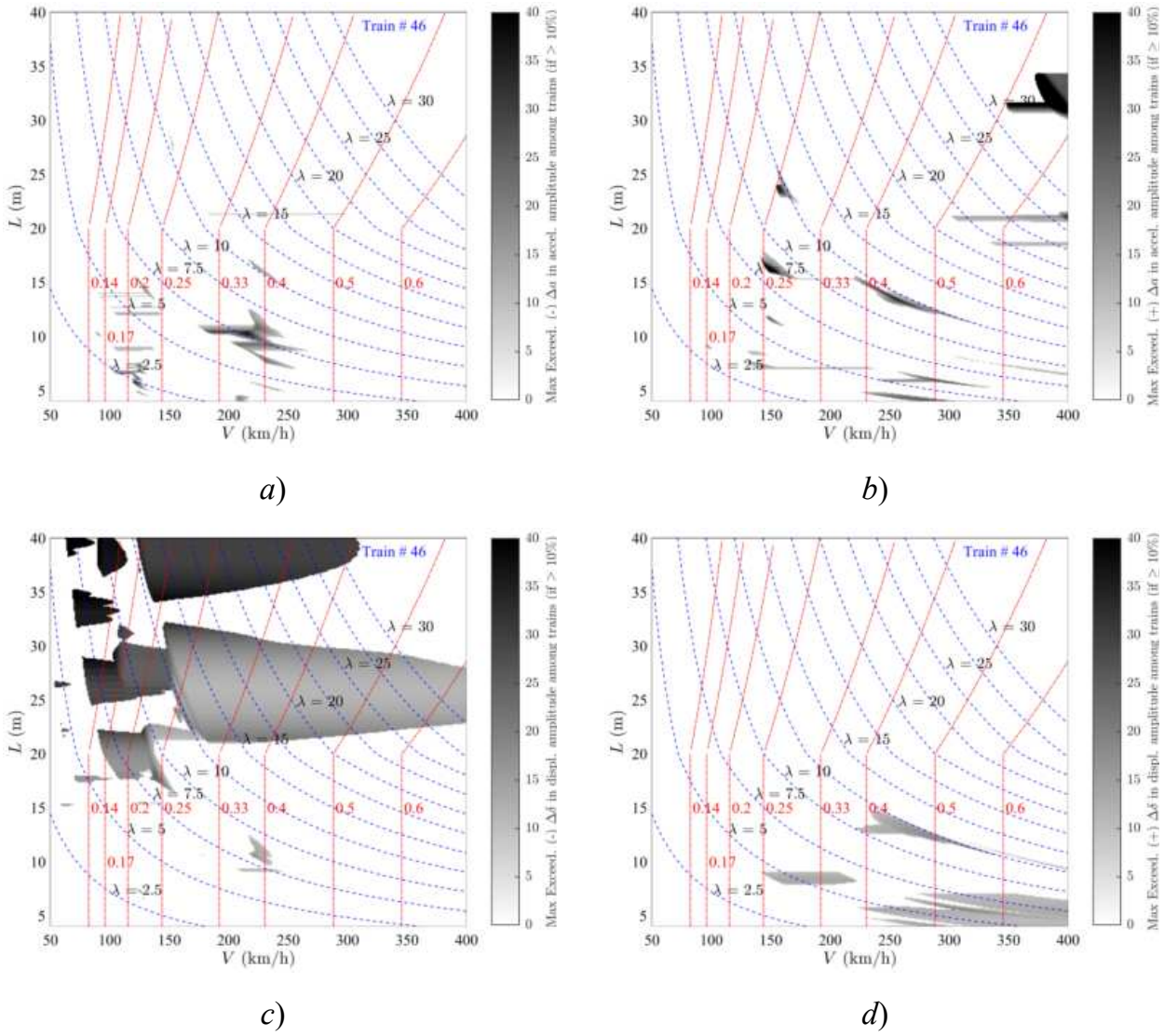

Figure 91. Exceedance Maps Train PT60-46 LIR vs Duhamel: a) Δa(–); b) Δa(+); c) Δδ(–); d) Δδ(+). PSC bridges.

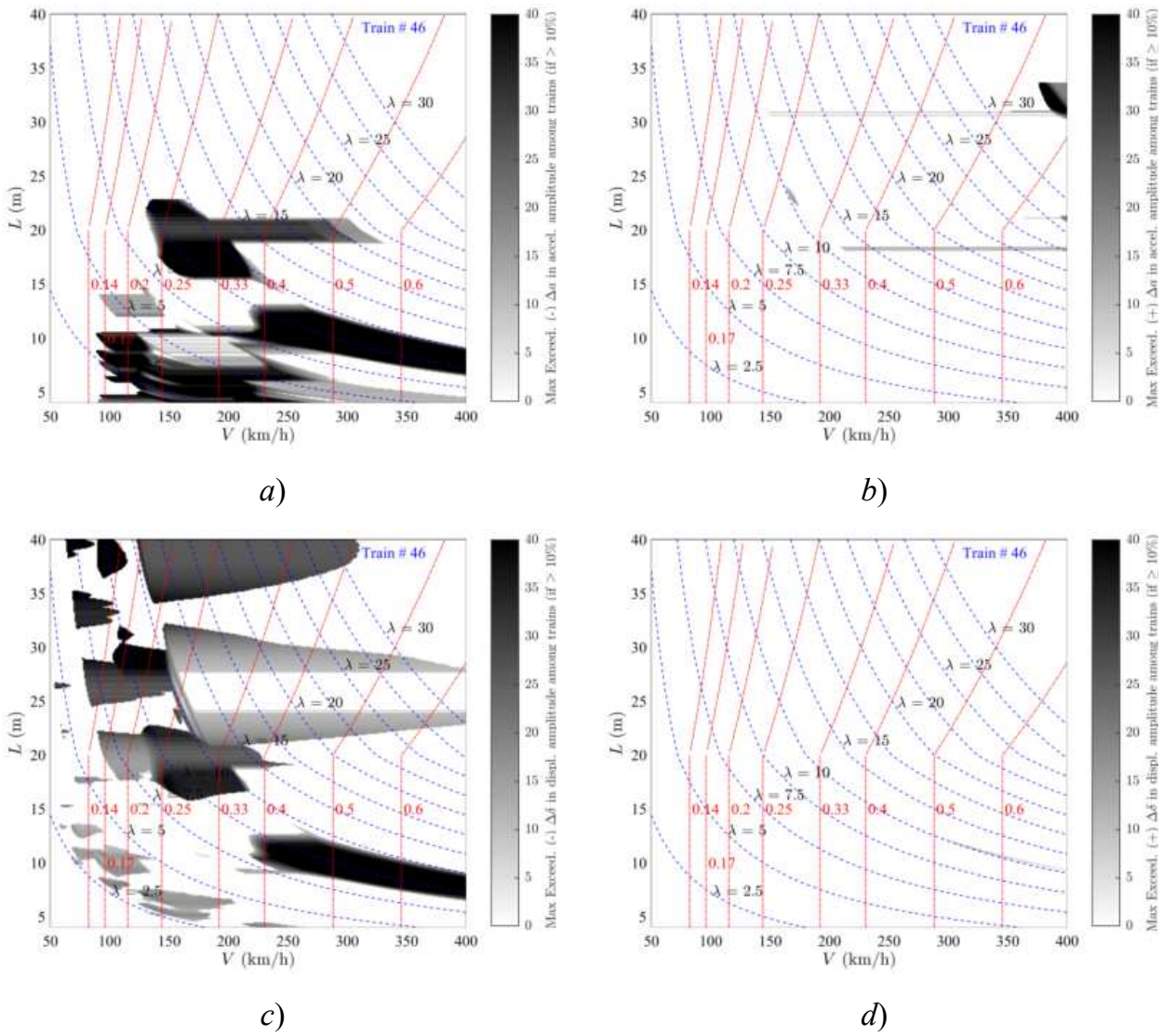

Figure 92. Exceedance Maps Train PT60-46 DER vs Duhamel: a) Δa(−); b) Δa(+); c) Δδ(−); d) Δδ(+). PSC bridges.

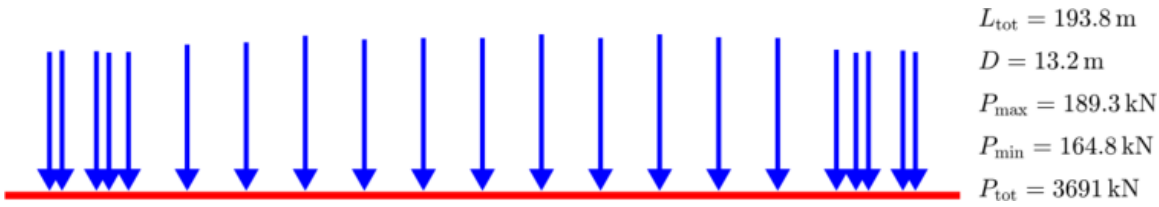

Figure Train PT60-47 [INB4EU-SA-001]

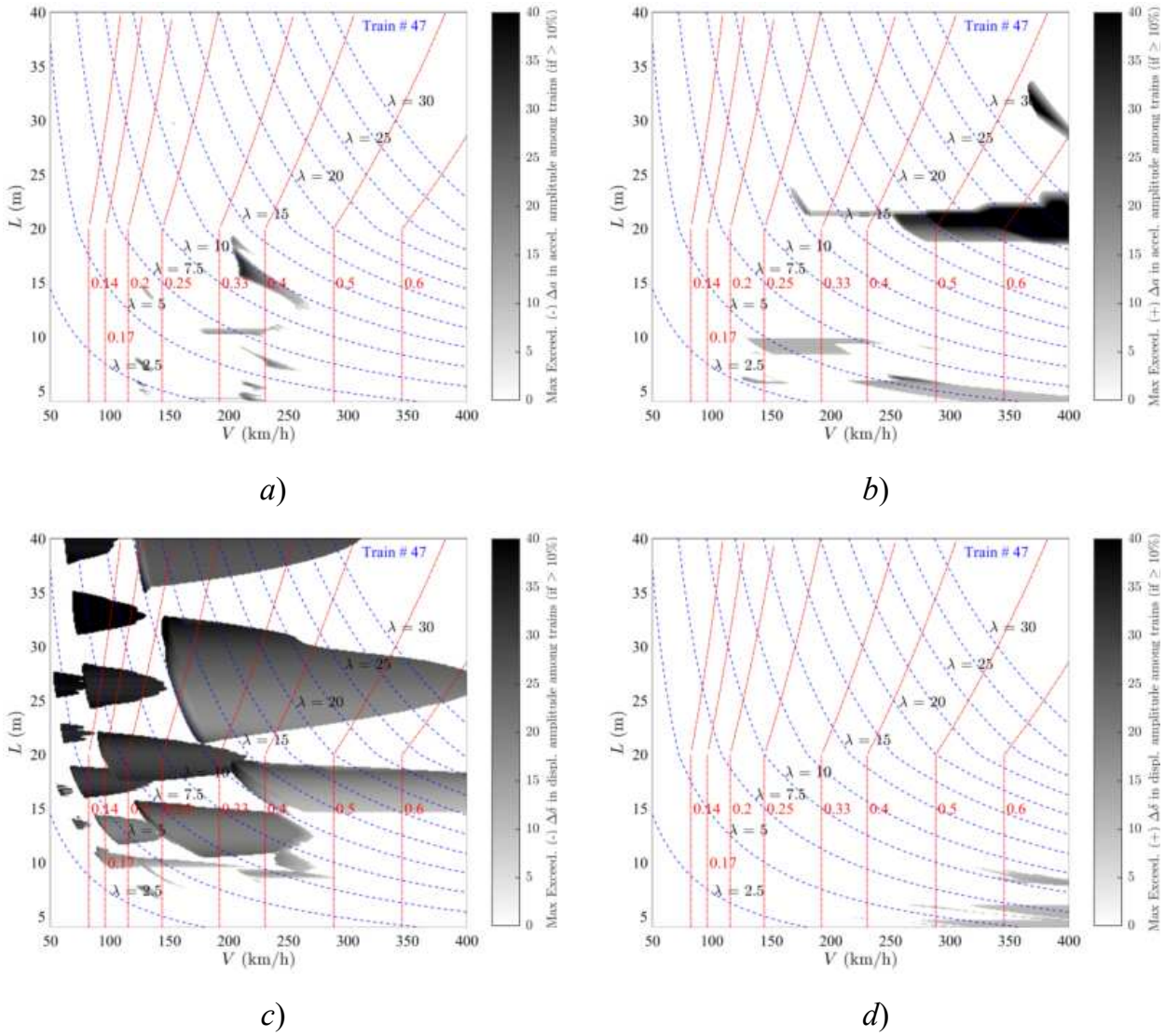

Figure 93. Exceedance Maps Train PT60-47 LIR vs Duhamel: a) Δa(–); b) Δa(+); c) Δδ(–); d) Δδ(+). PSC bridges.

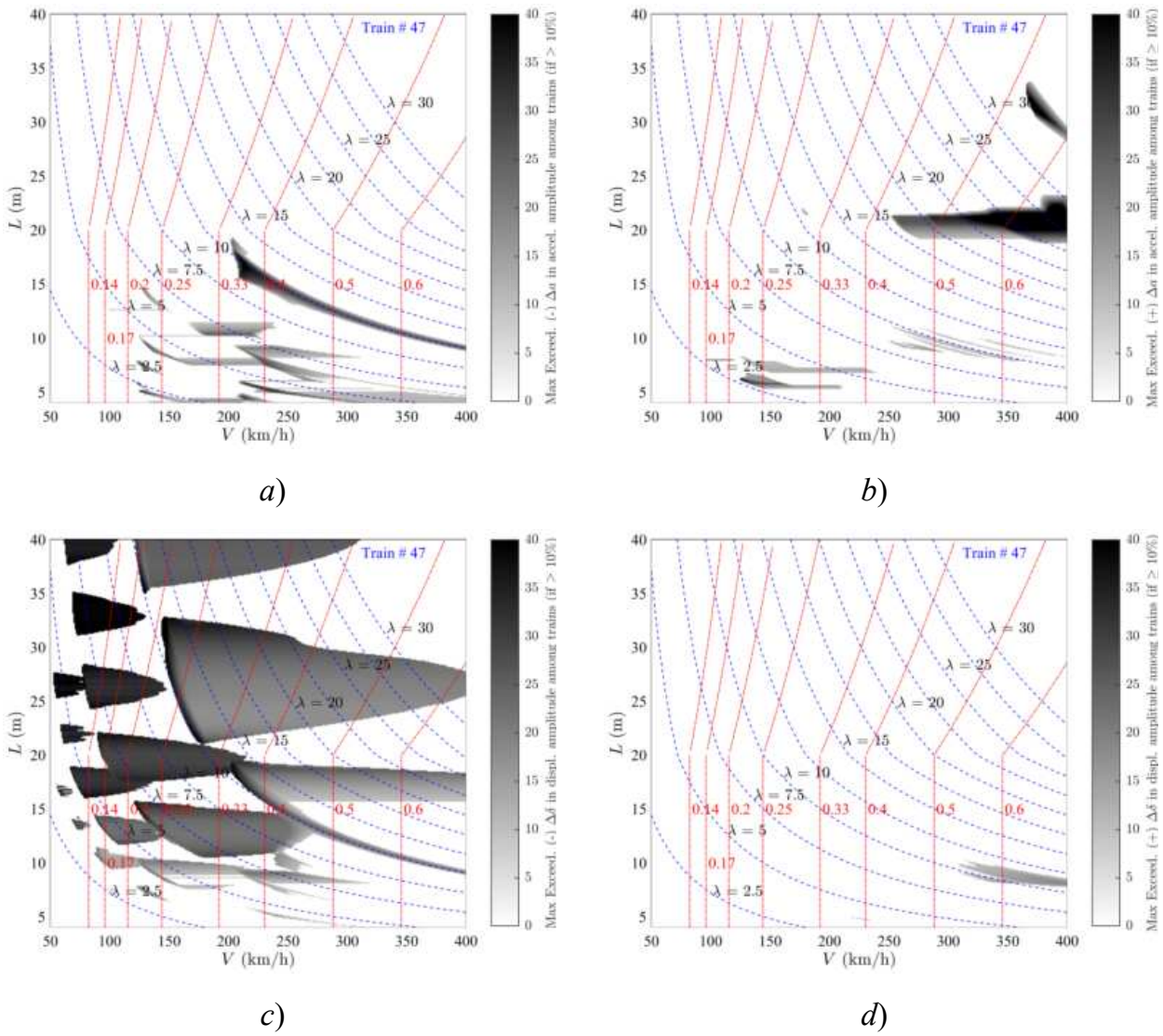

Figure 94. Exceedance Maps Train PT60-47 DER vs Duhamel: a) Δa(−); b) Δa(+); c) Δδ(−); d) Δδ(+). PSC bridges.

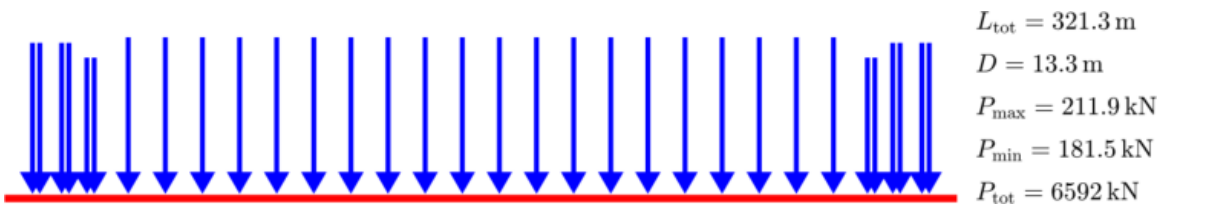

Figure Train PT60-48 [INB4EU-SA-022]

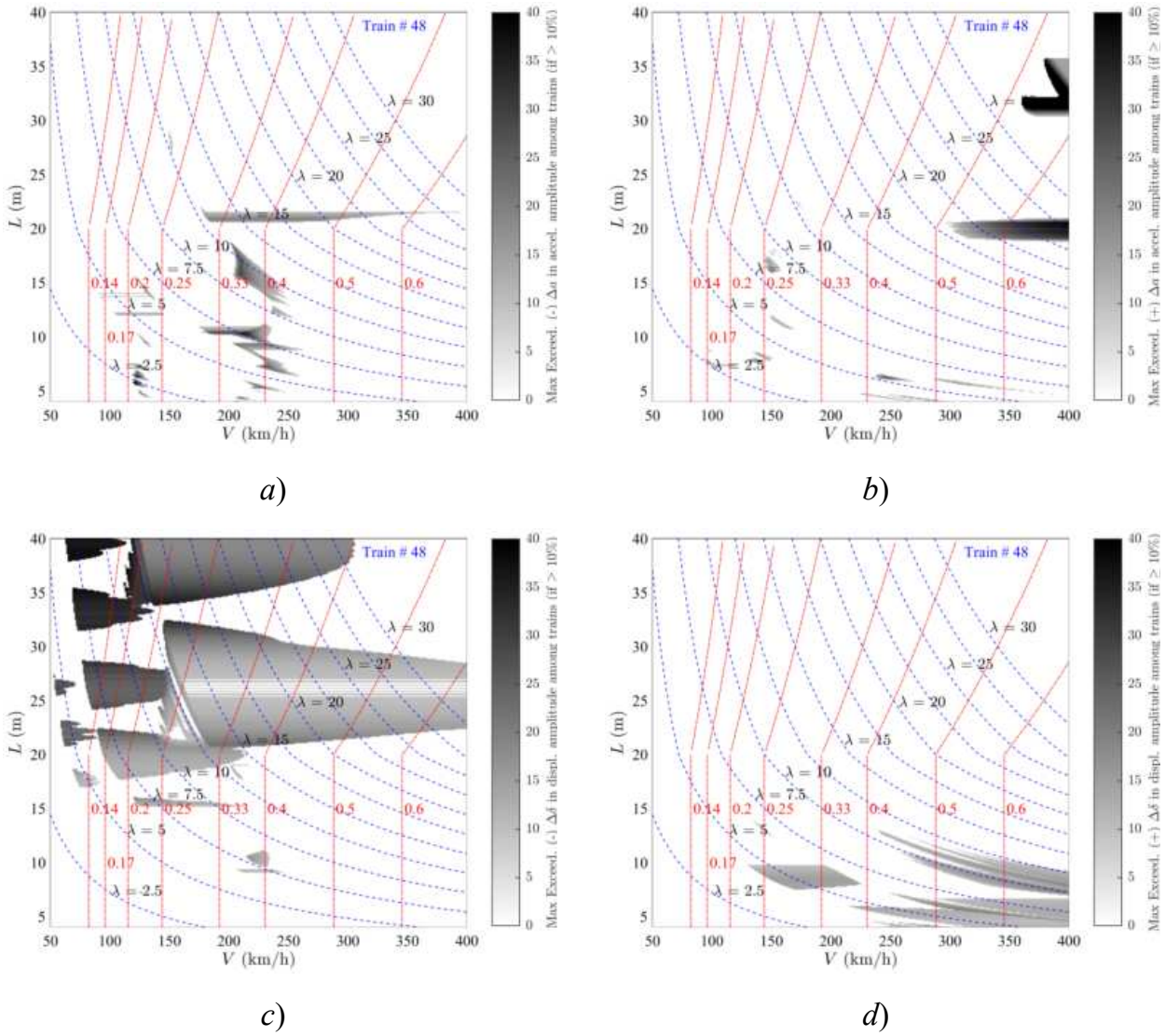

Figure 95. Exceedance Maps Train PT60-48 LIR vs Duhamel: a) Δa(–); b) Δa(+); c) Δδ(–); d) Δδ(+). PSC bridges.

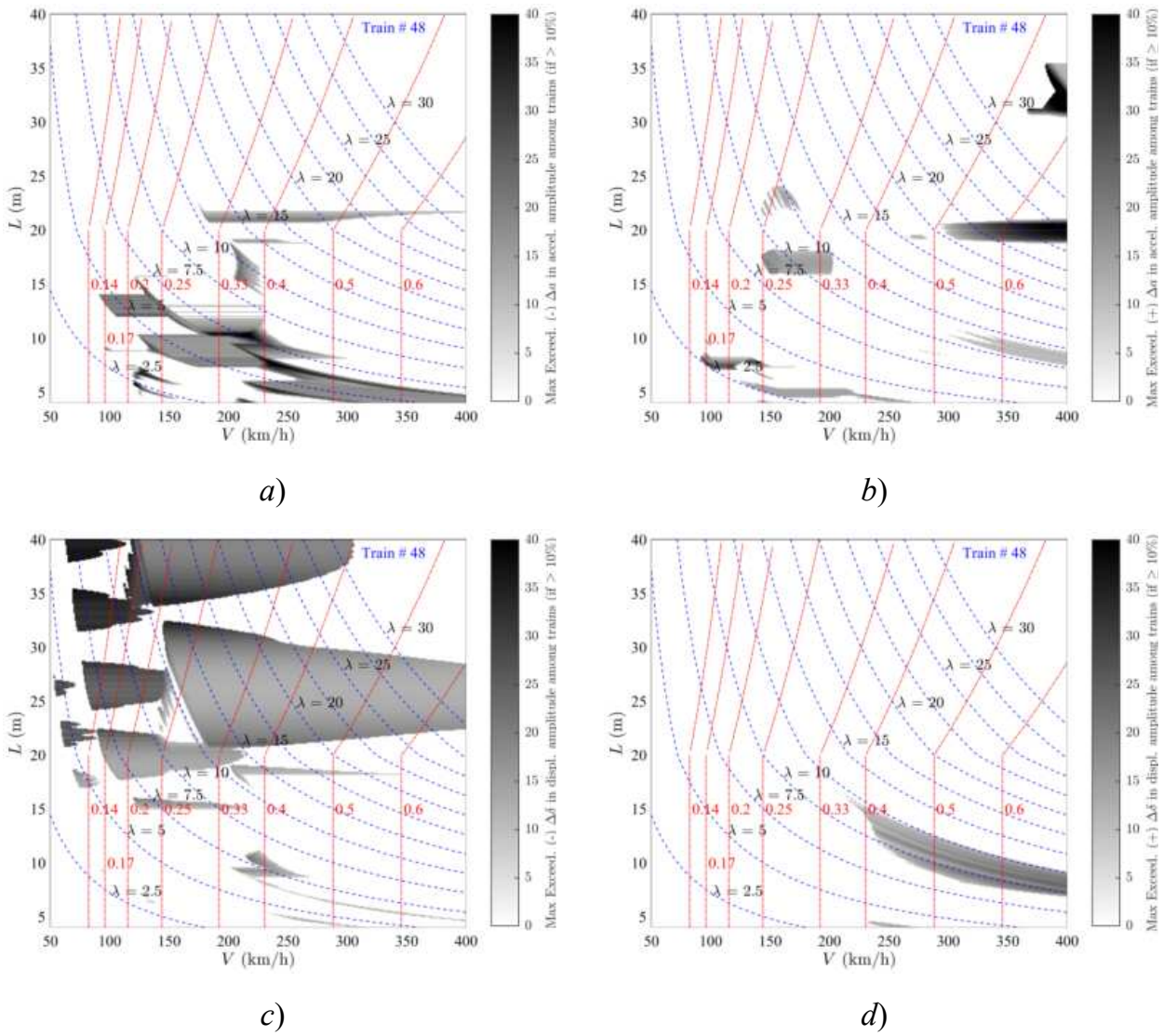

Figure 96. Exceedance Maps Train PT60-48 DER vs Duhamel: a) Δa(−); b) Δa(+); c) Δδ(−); d) Δδ(+). PSC bridges.

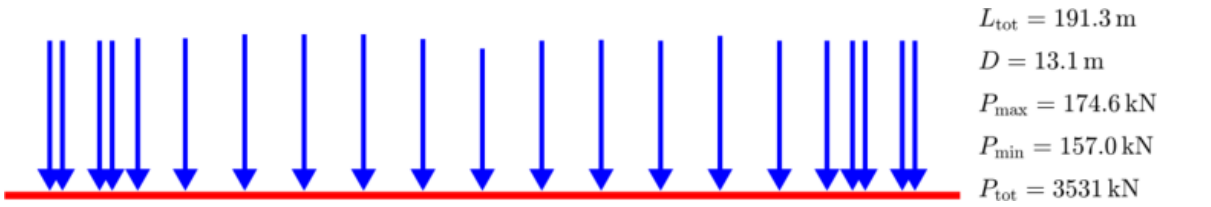

Figure Train PT60-49 [INB4EU-SA-004]

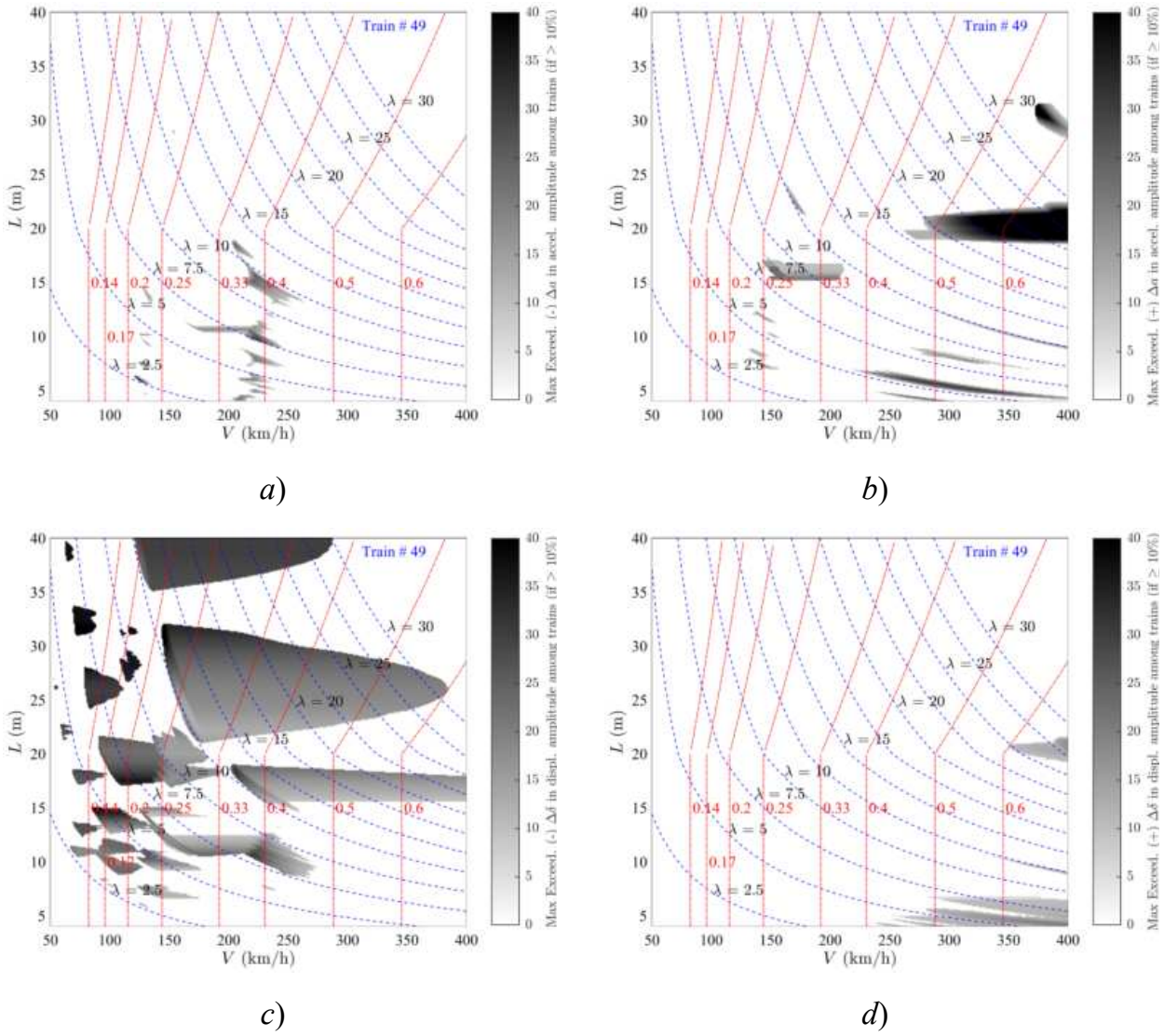

Figure 97. Exceedance Maps Train PT60-49 LIR vs Duhamel: a) Δa(–); b) Δa(+); c) Δδ(–); d) Δδ(+). PSC bridges.

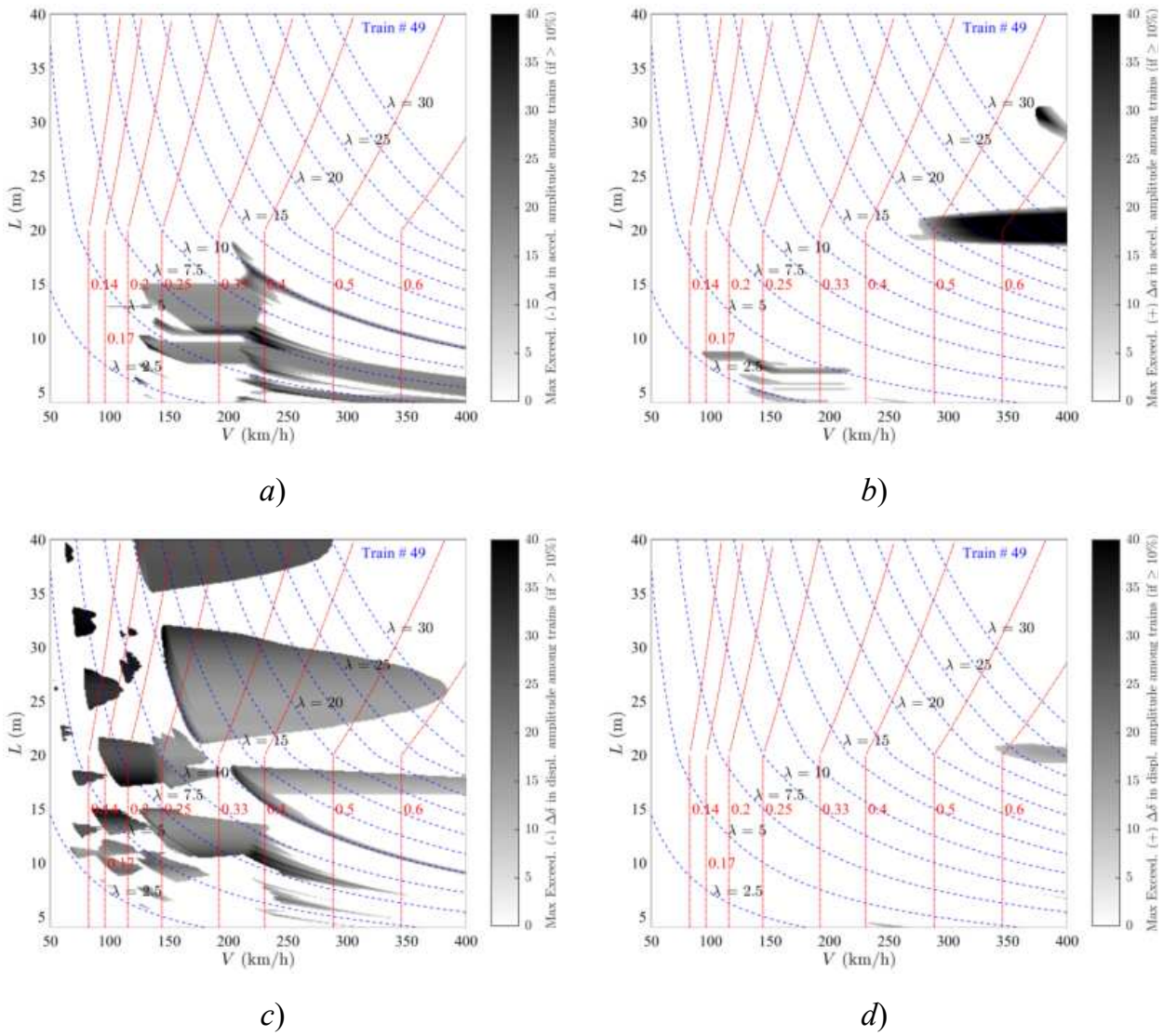

Figure 98. Exceedance Maps Train PT60-49 DER vs Duhamel: a) Δa(−); b) Δa(+); c) Δδ(−); d) Δδ(+). PSC bridges.

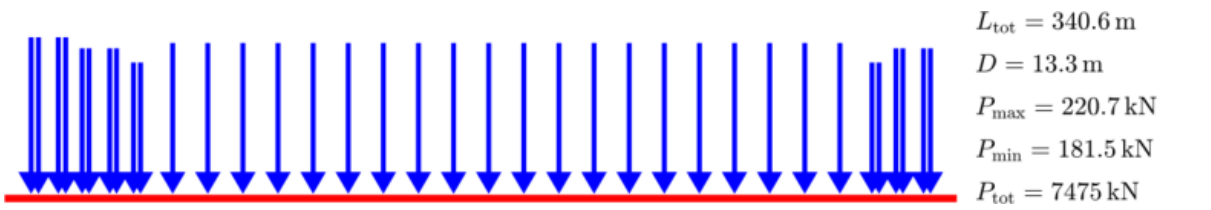

Figure Train PT60-50 [INB4EU-SA-029]

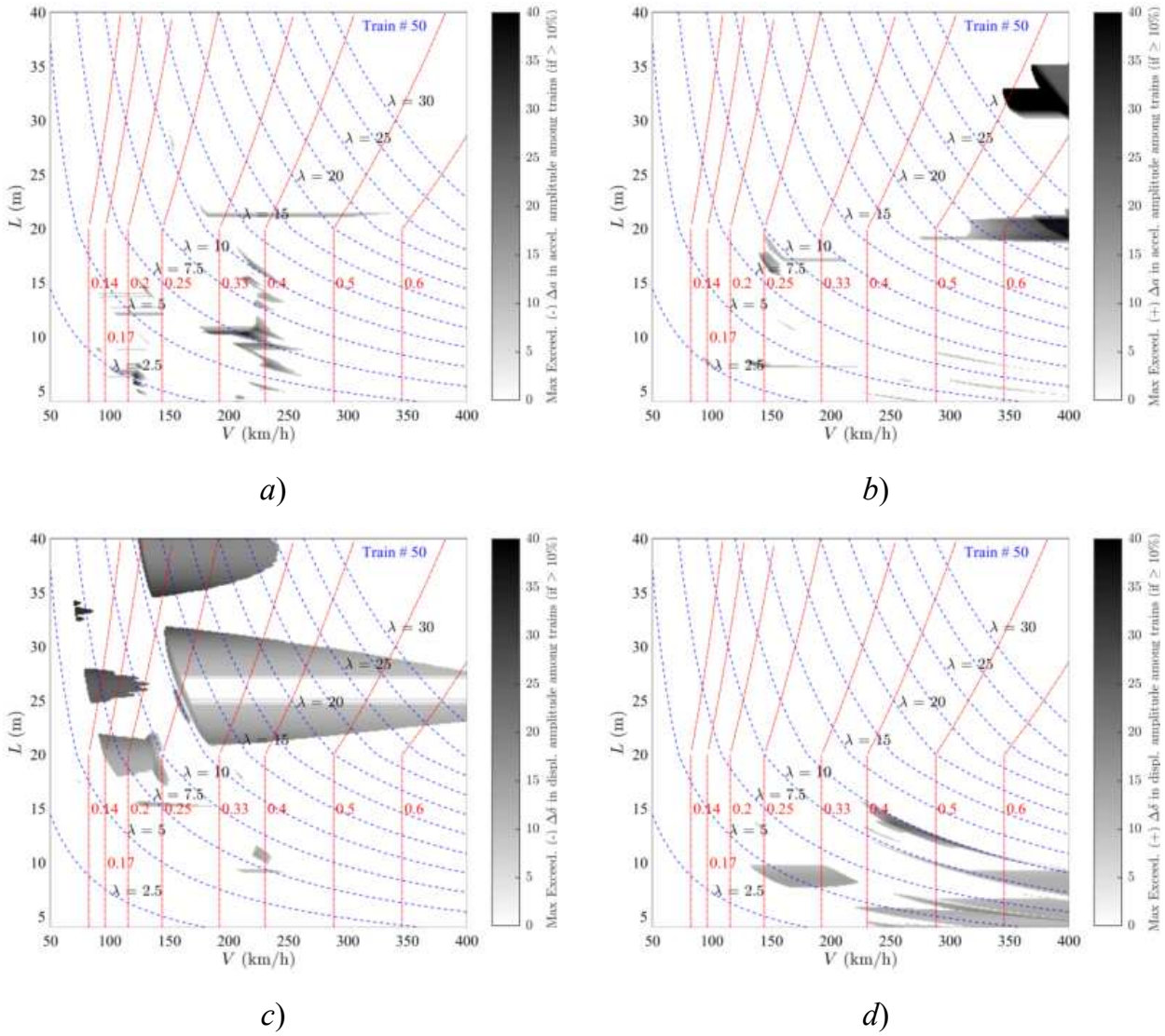

Figure 99. Exceedance Maps Train PT60-50 LIR vs Duhamel: a) Δa(–); b) Δa(+); c) Δδ(–); d) Δδ(+). PSC bridges.

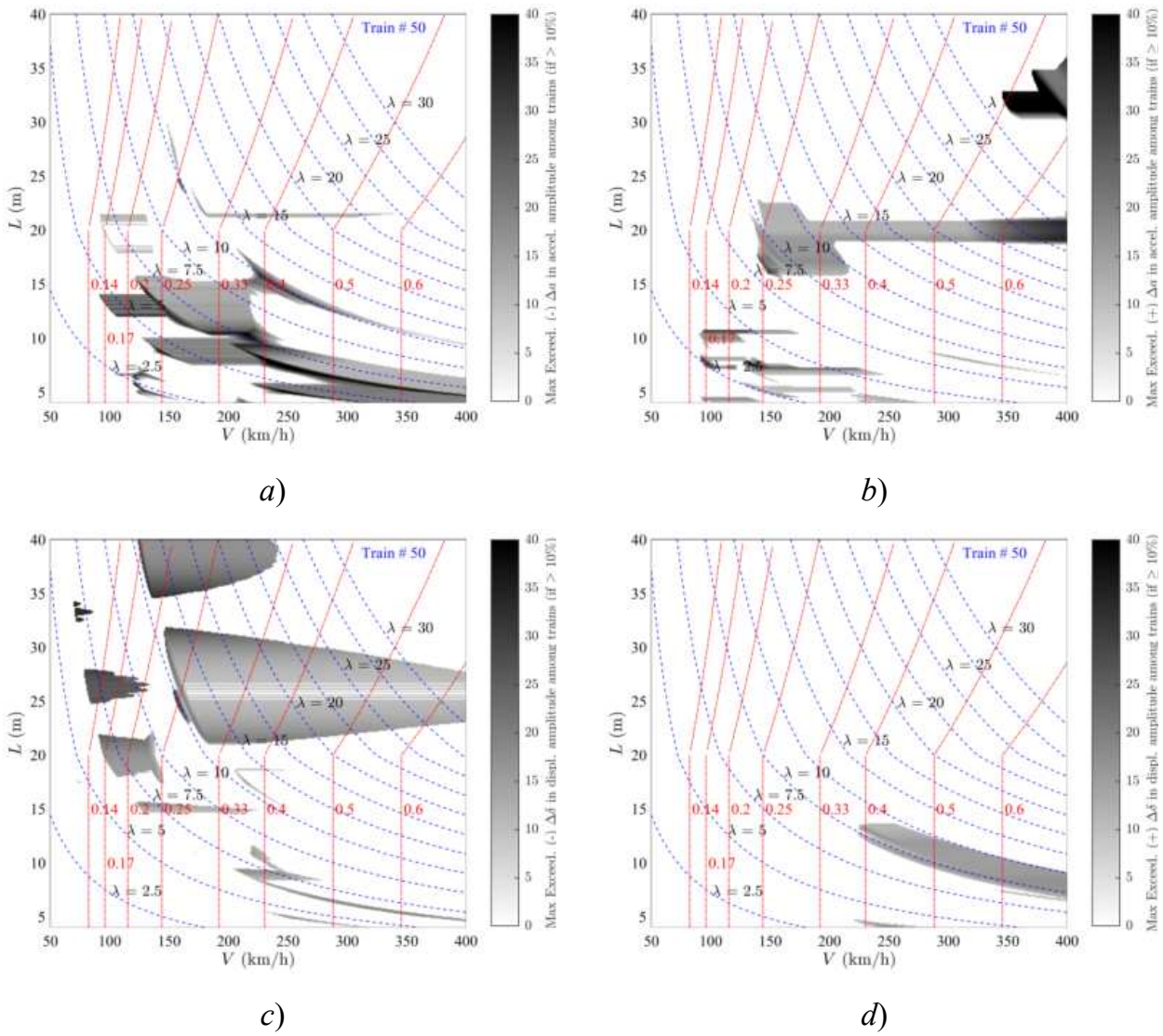

Figure 100. Exceedance Maps Train PT60-50 DER vs Duhamel: a) Δa(−); b) Δa(+); c) Δδ(−); d) Δδ(+). PSC bridges.

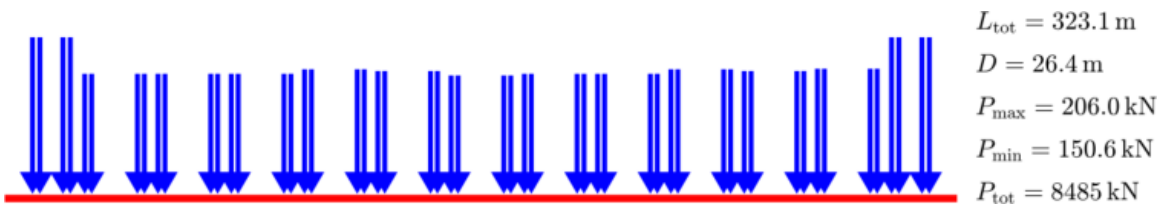

Figure Train PT60-51 [INB4EU-CB-021]

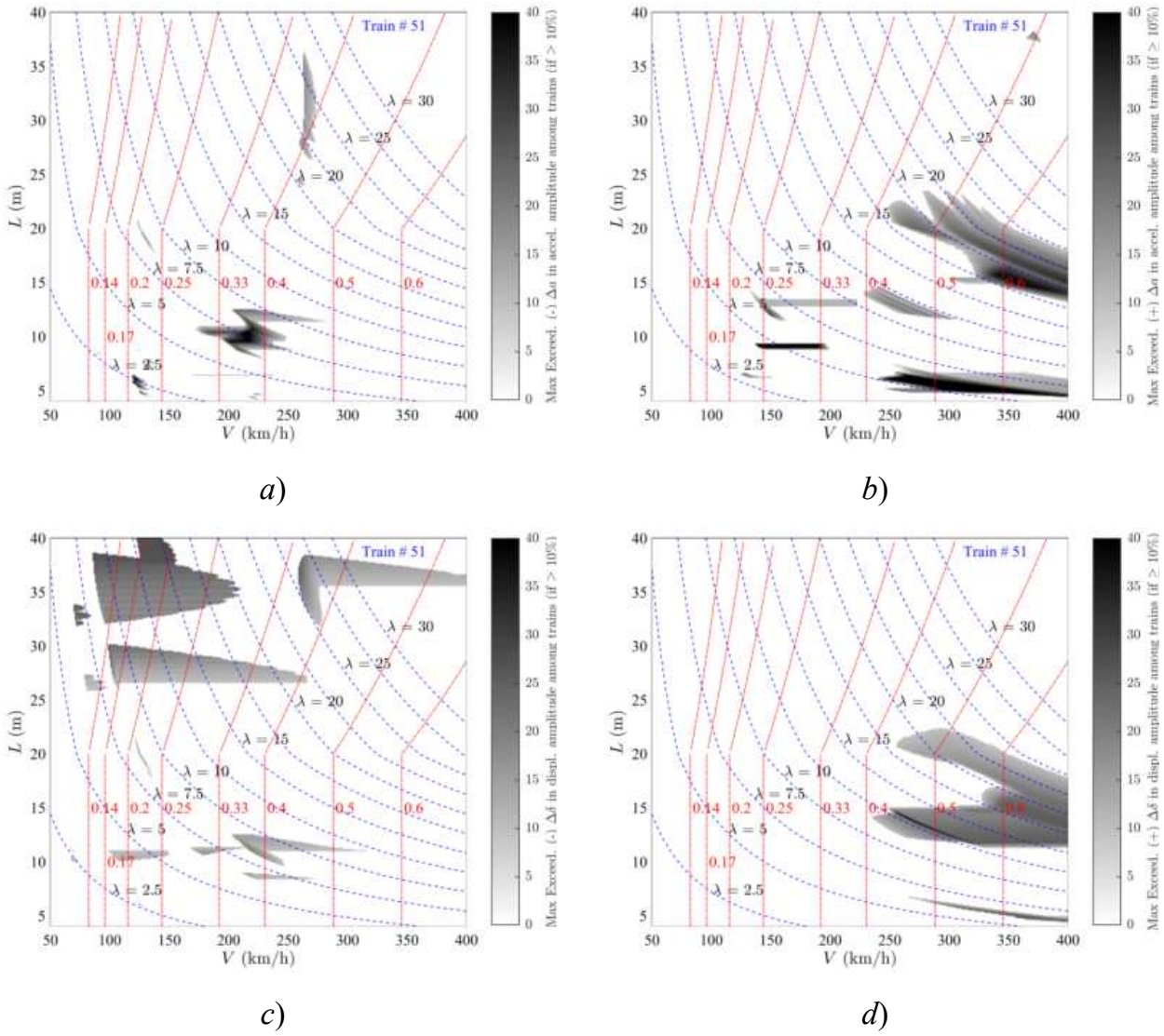

Figure 101. Exceedance Maps Train PT60-51 LIR vs Duhamel: a) Δa(−); b) Δa(+); c) Δδ(−); d) Δδ(+). PSC bridges.

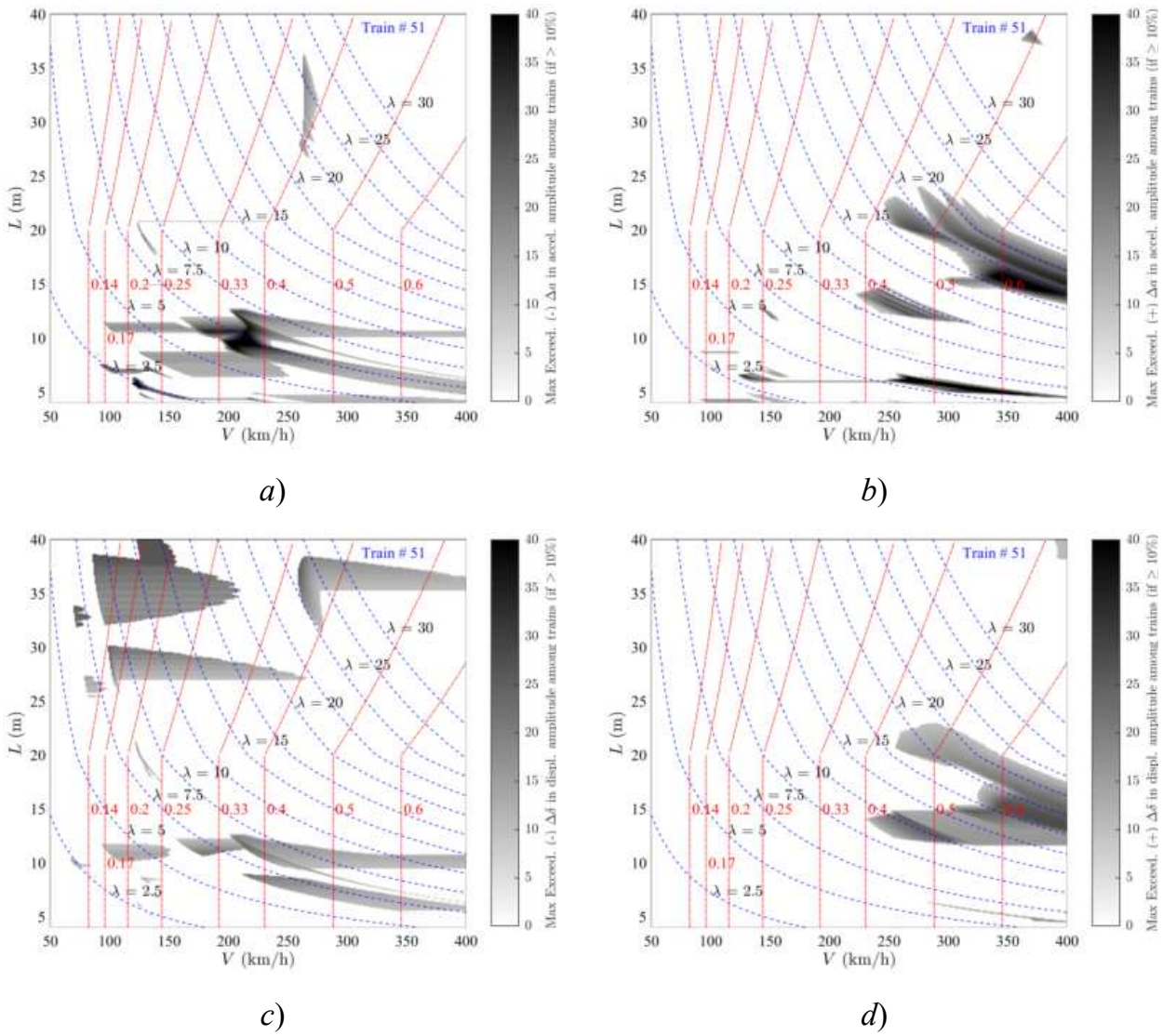

Figure 102. Exceedance Maps Train PT60-51 DER vs Duhamel: a) Δa(−); b) Δa(+); c) Δδ(−); d) Δδ(+). PSC bridges.

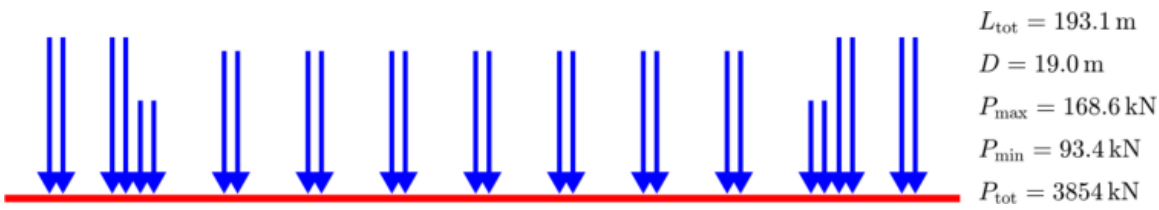

Figure Train PT60-52 [INB4EU-AB-008]

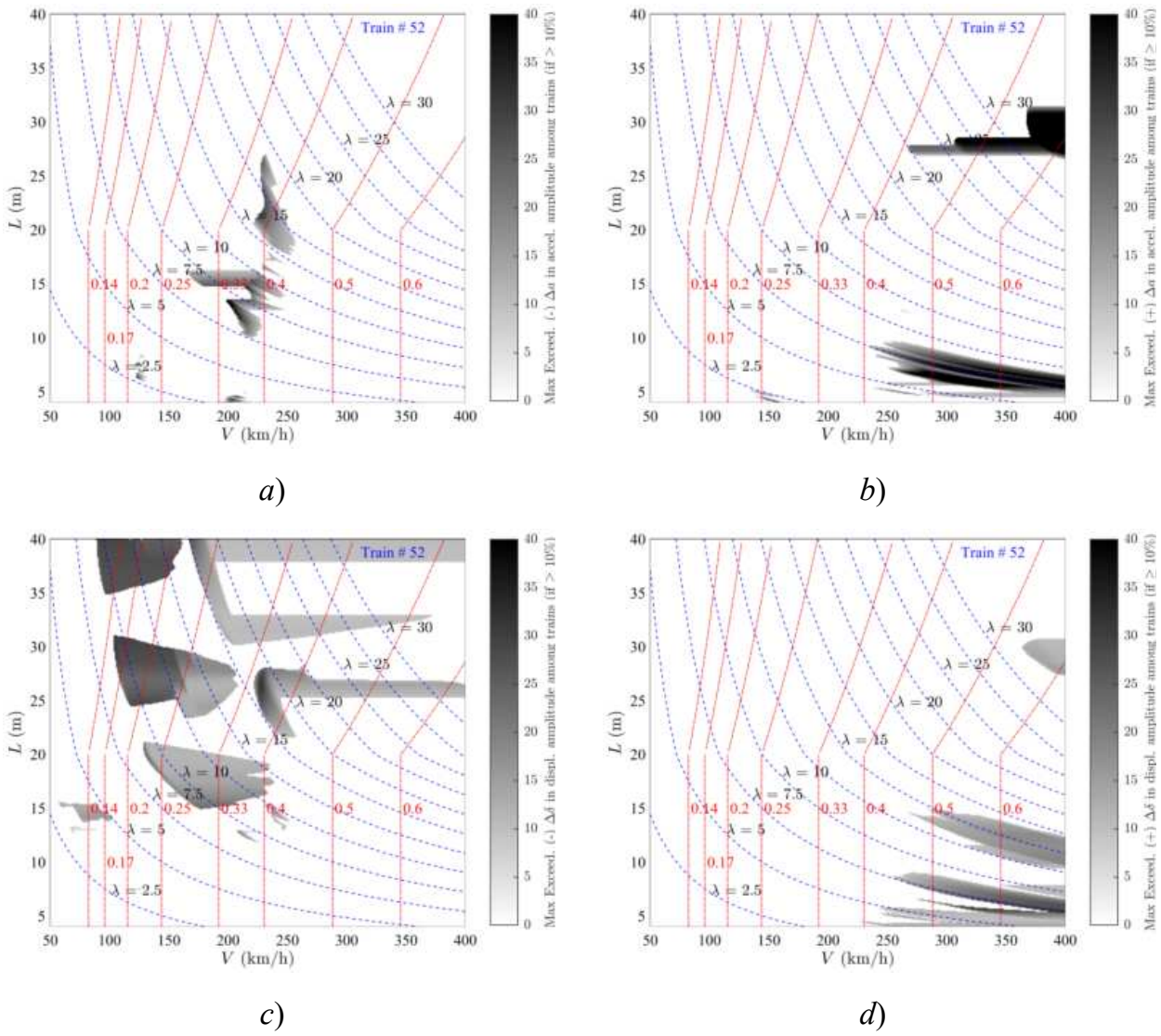

Figure 103. Exceedance Maps Train PT60-52 LIR vs Duhamel: a) Δa(−); b) Δa(+); c) Δδ(−); d) Δδ(+). PSC bridges.

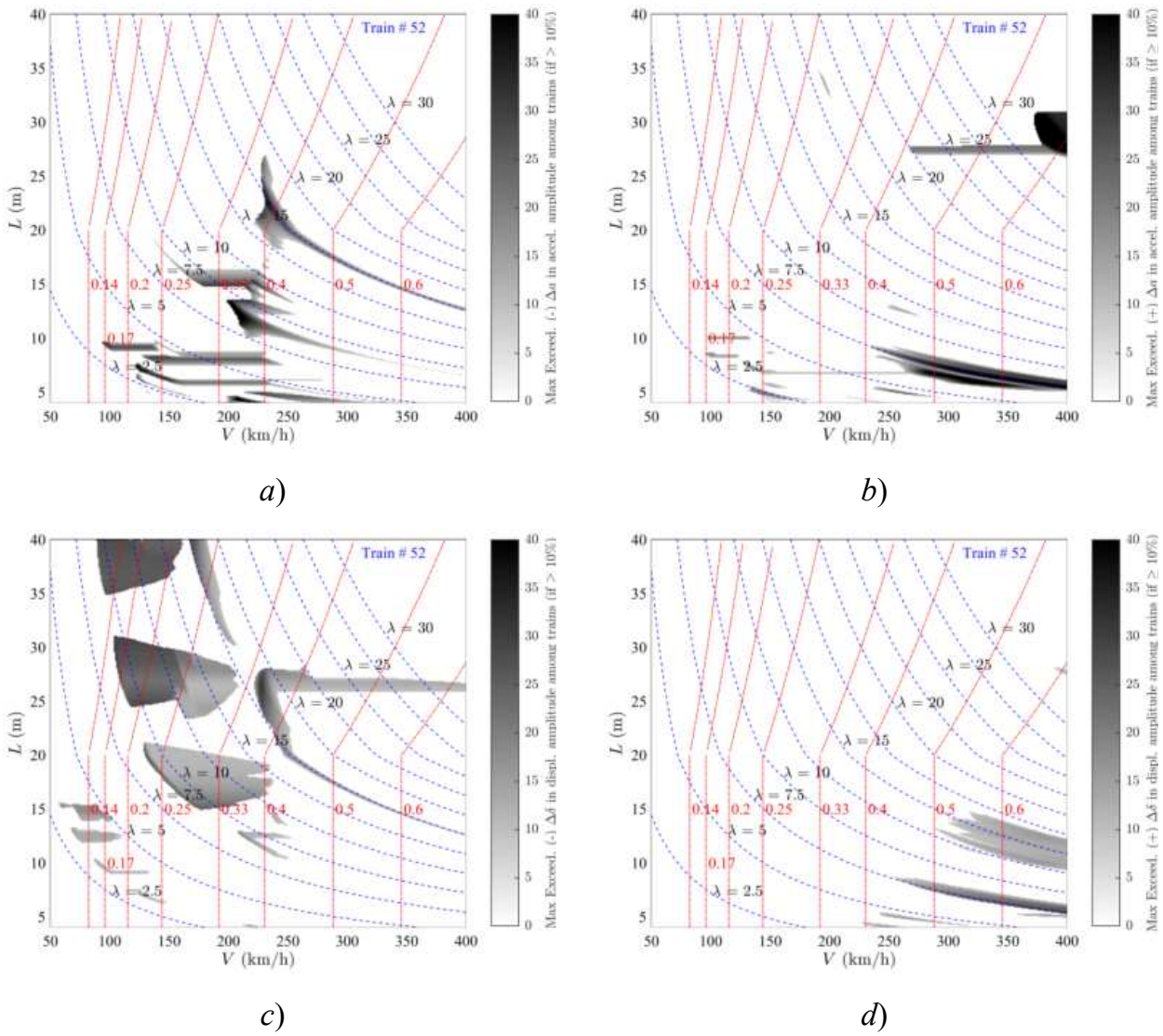

Figure 104. Exceedance Maps Train PT60-52 DER vs Duhamel: a) Δa(−); b) Δa(+); c) Δδ(−); d) Δδ(+). PSC bridges.

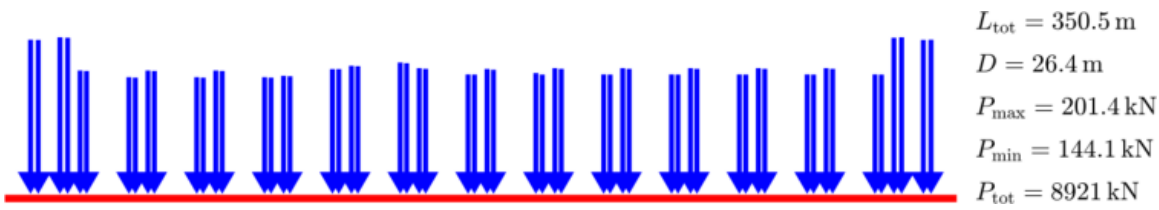

Figure Train PT60-53 [INB4EU-CB-013]

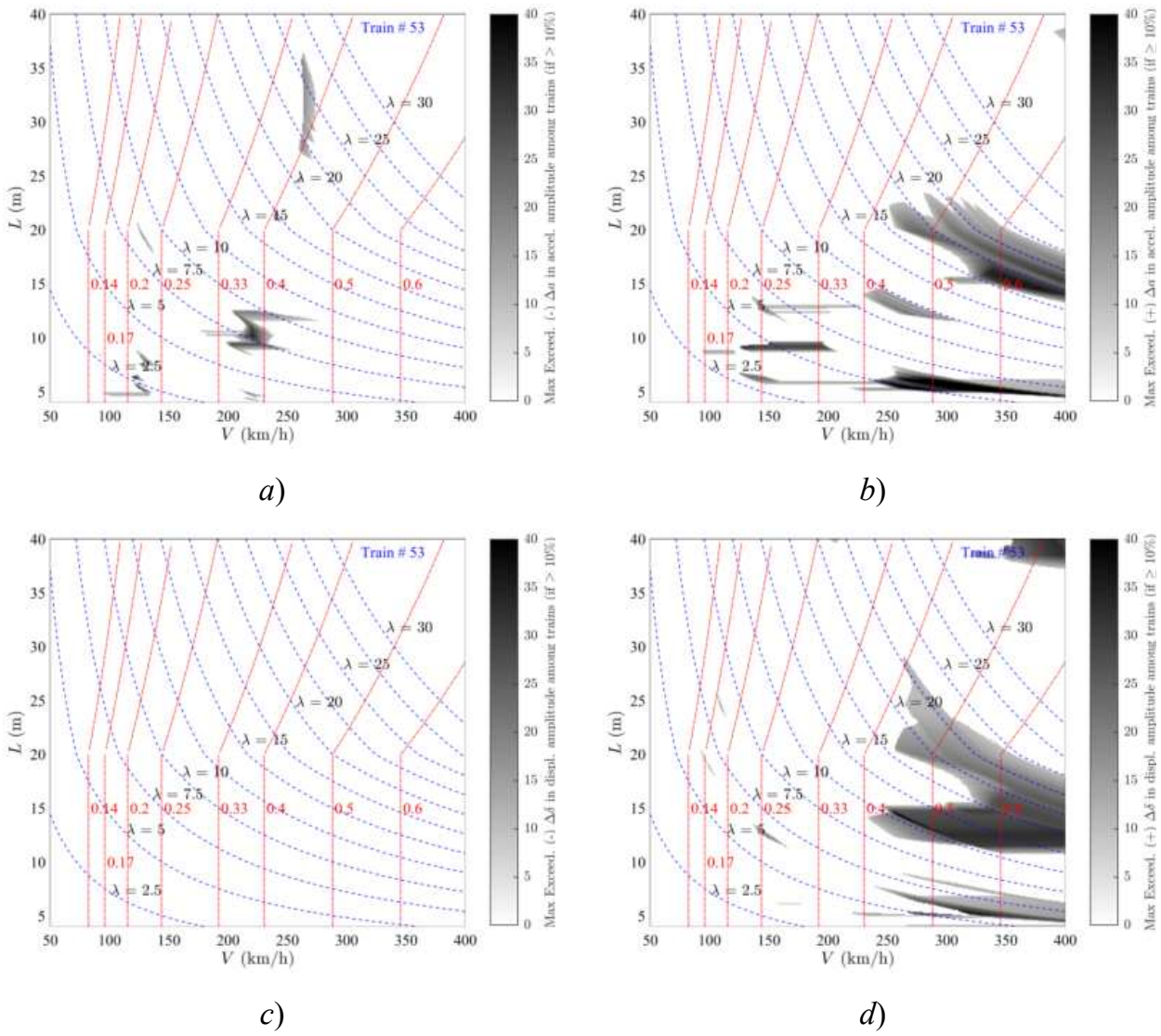

Figure 105. Exceedance Maps Train PT60-53 LIR vs Duhamel: a) Δa(−); b) Δa(+); c) Δδ(−); d) Δδ(+). PSC bridges.

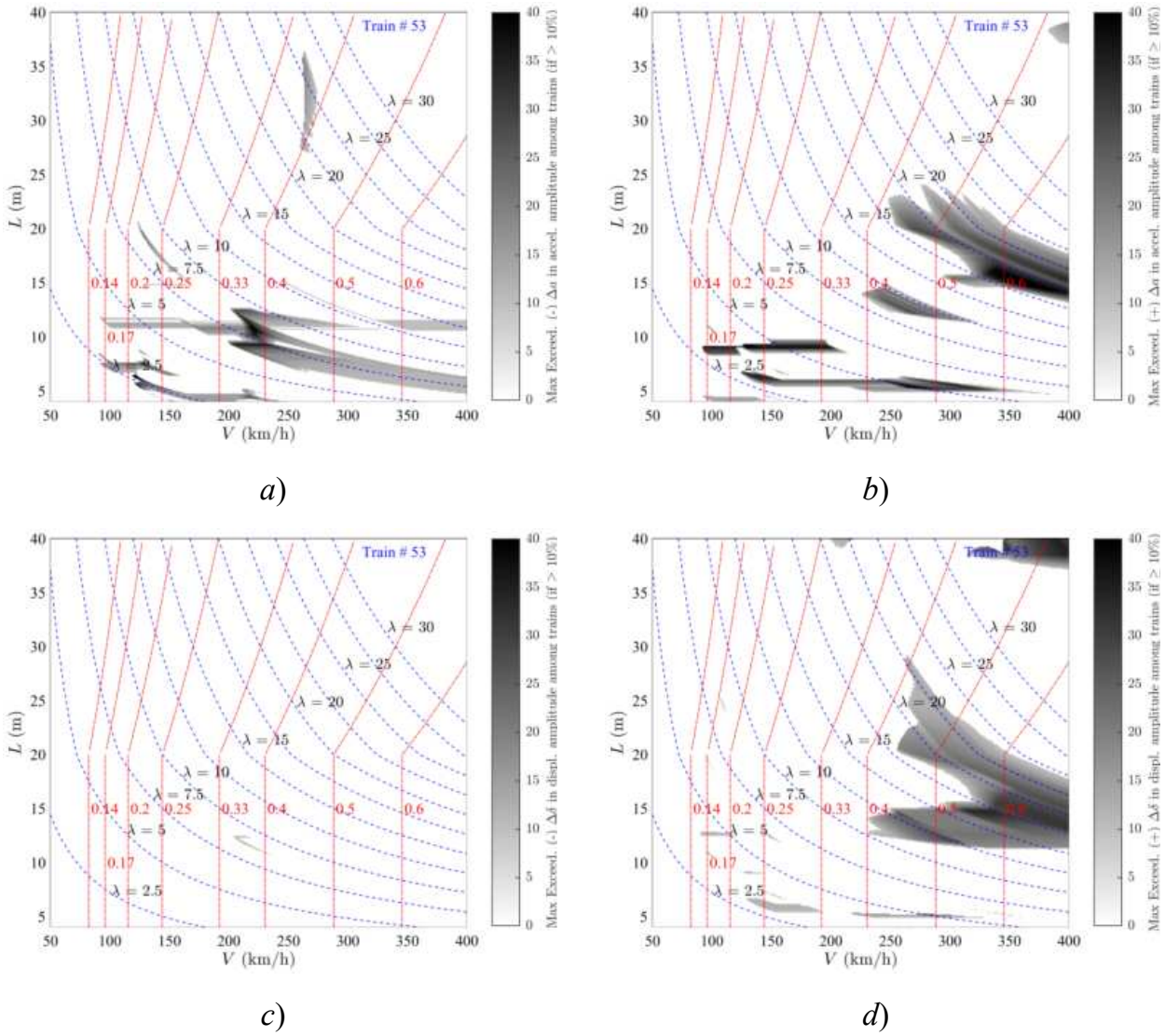

Figure 106. Exceedance Maps Train PT60-53 DER vs Duhamel: a) Δa(−); b) Δa(+); c) Δδ(−); d) Δδ(+). PSC bridges.

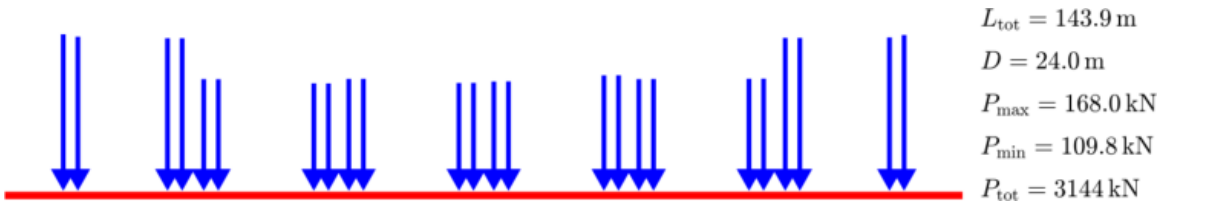

Figure Train PT60-54 [INB4EU-CB-030]

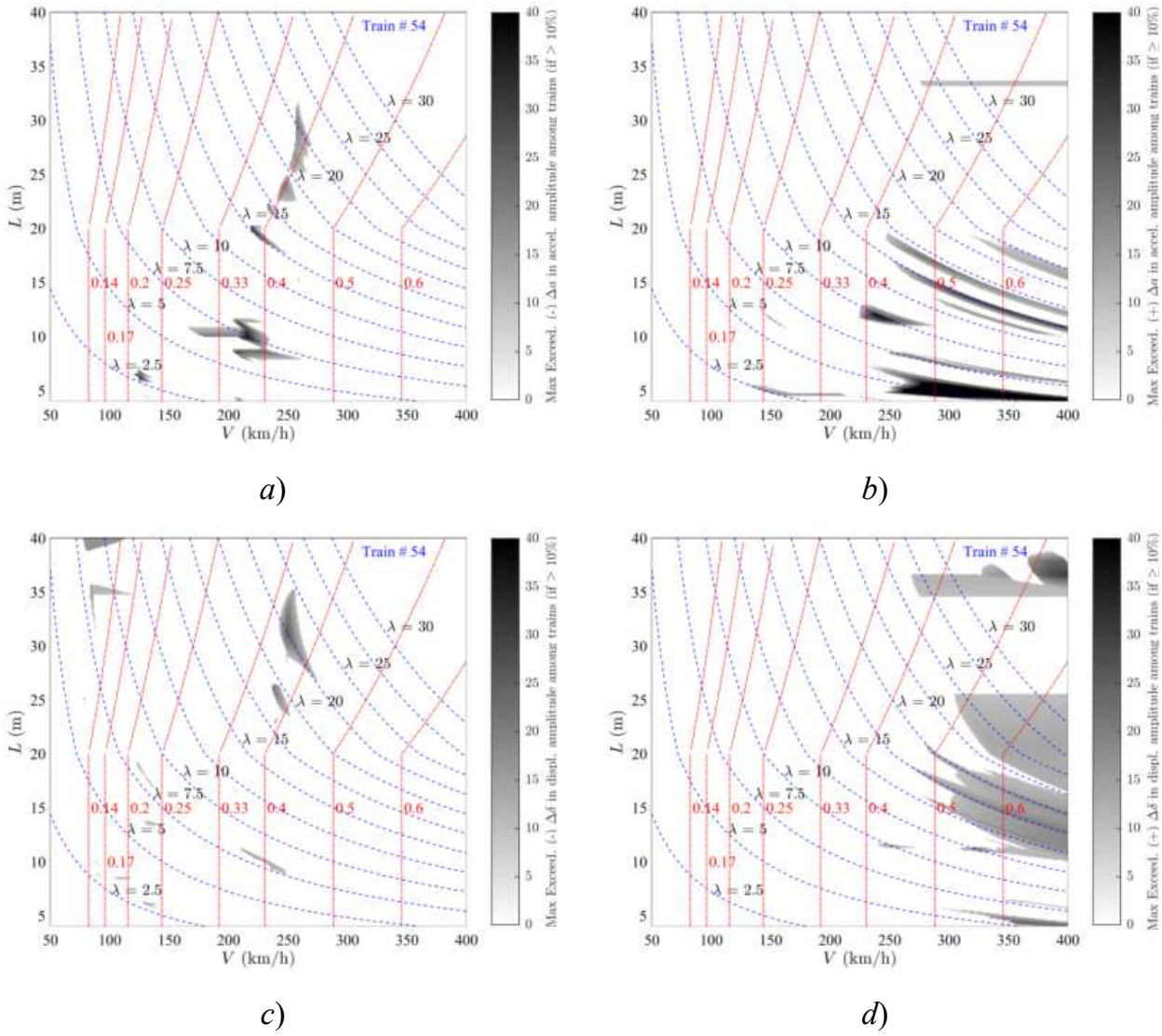

Figure 107. Exceedance Maps Train PT60-54 LIR vs Duhamel: a) Δa(−); b) Δa(+); c) Δδ(−); d) Δδ(+). PSC bridges.

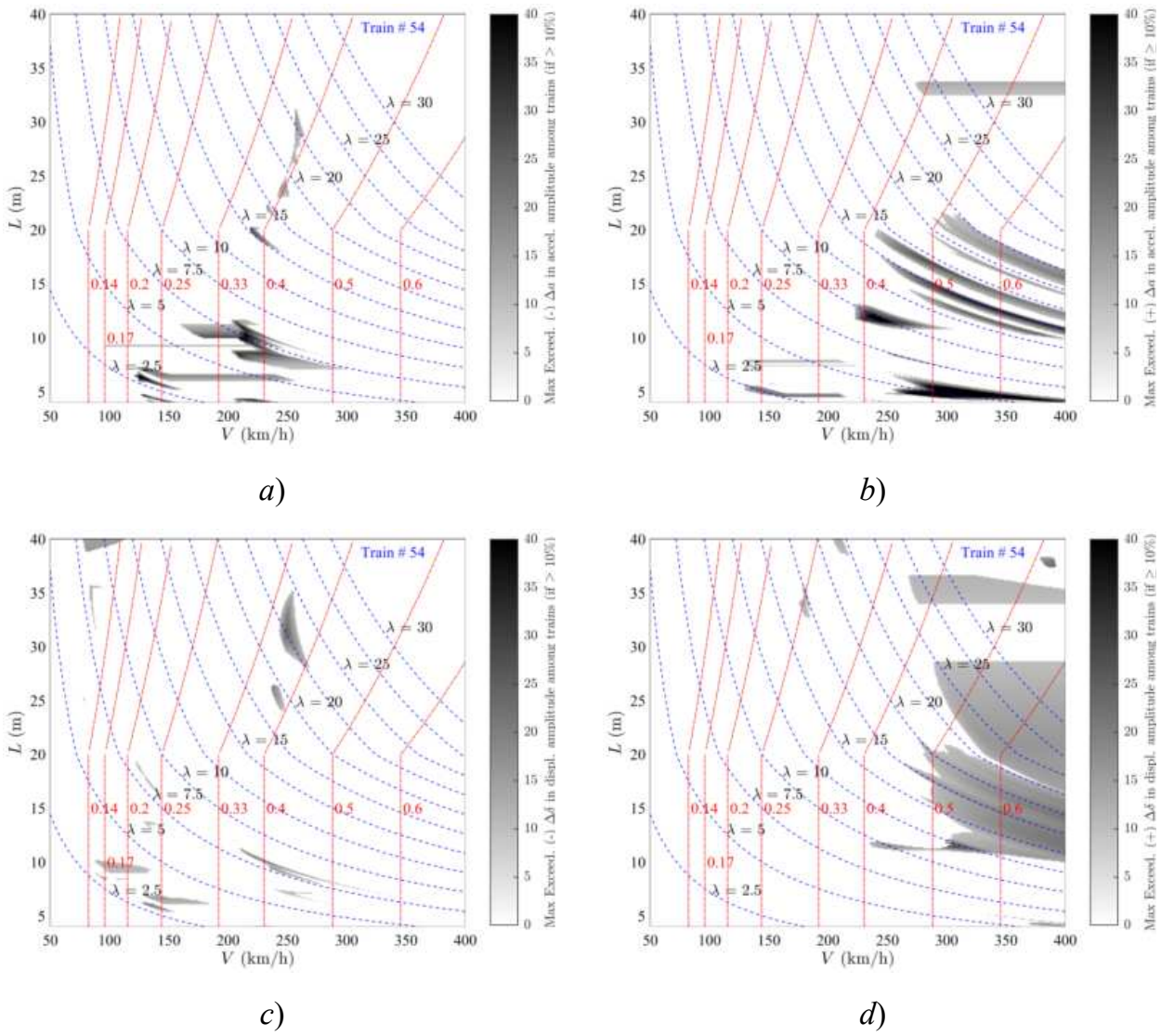

Figure 108. Exceedance Maps Train PT60-54 DER vs Duhamel: a) Δa(−); b) Δa(+); c) Δδ(−); d) Δδ(+). PSC bridges.

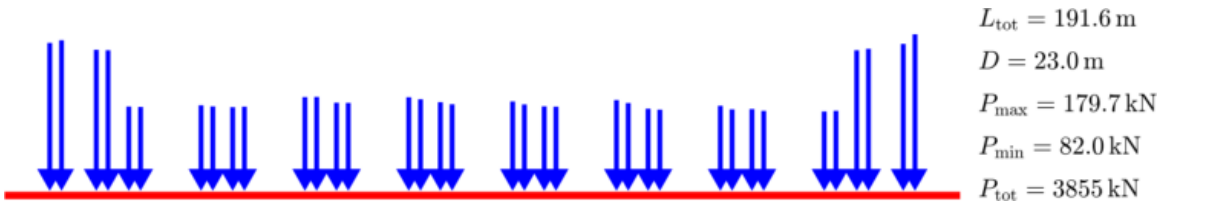

Figure Train PT60-55 [INB4EU-CB-077]

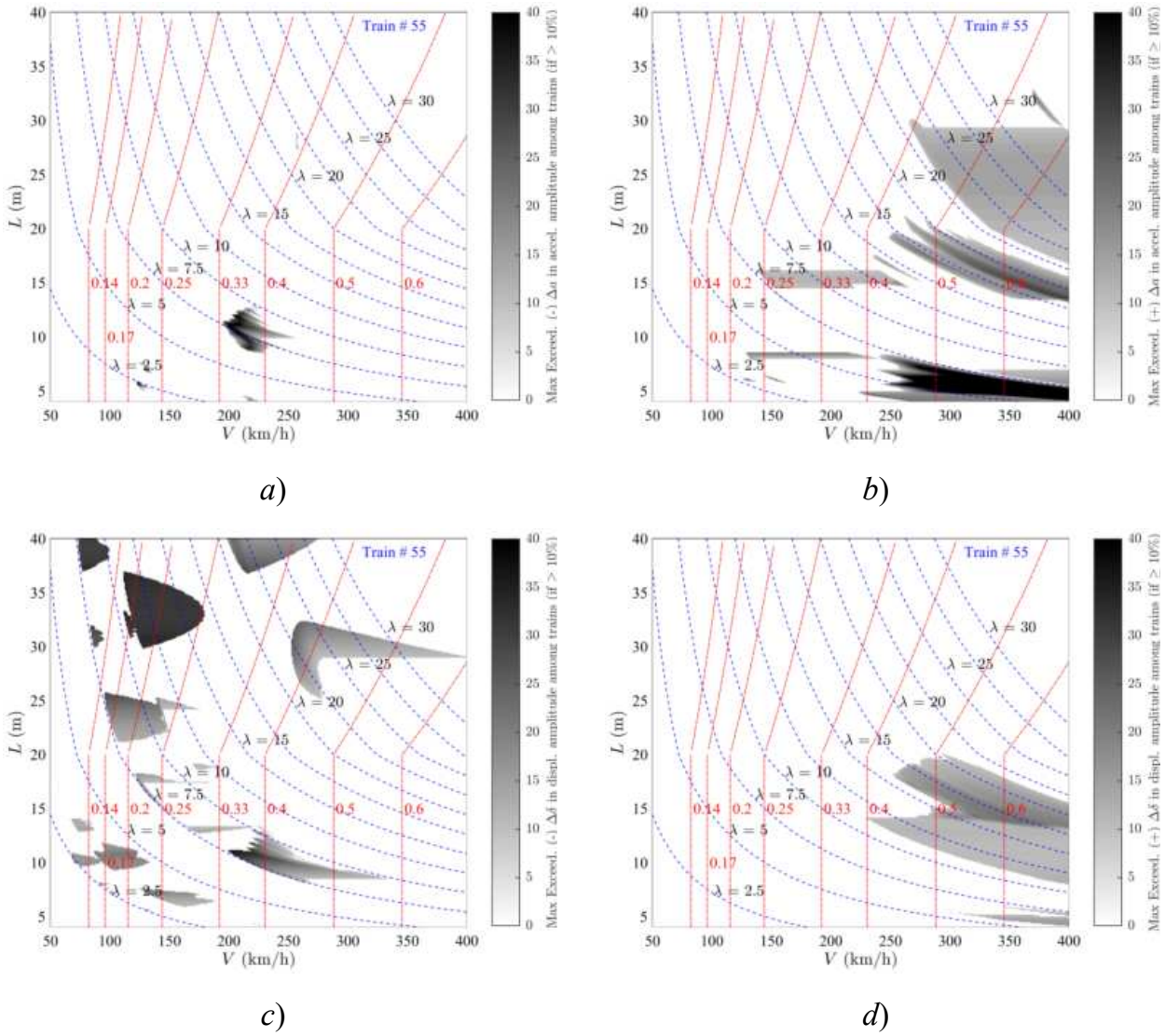

Figure 109. Exceedance Maps Train PT60-55 LIR vs Duhamel: a) Δa(−); b) Δa(+); c) Δδ(−); d) Δδ(+). PSC bridges.

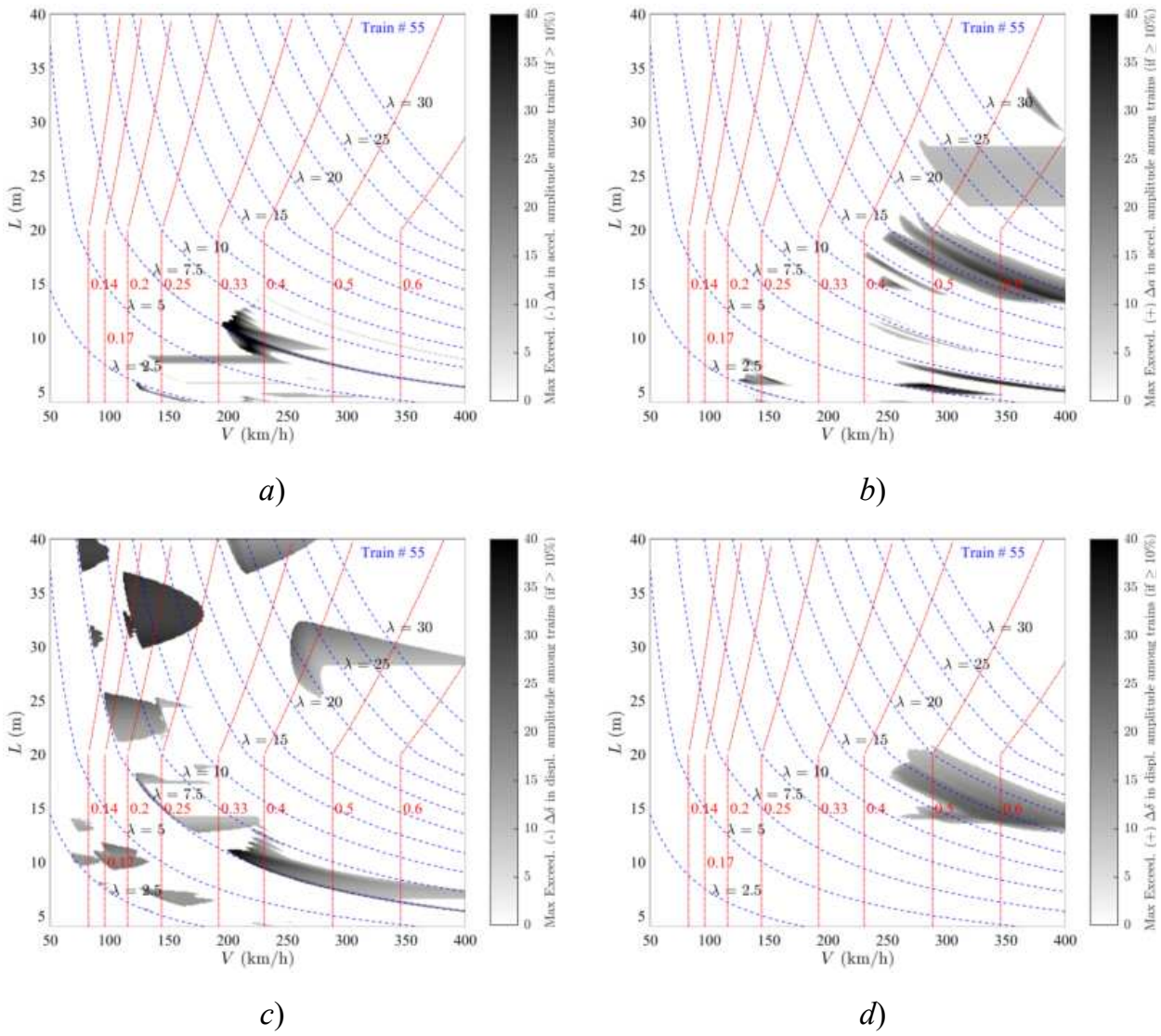

Figure 110. Exceedance Maps Train PT60-55 DER vs Duhamel: a) Δa(−); b) Δa(+); c) Δδ(−); d) Δδ(+). PSC bridges.

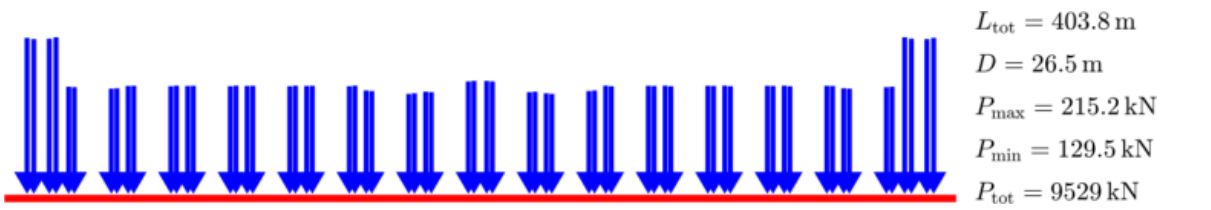

Figure Train PT60-56 [INB4EU-CB-138]

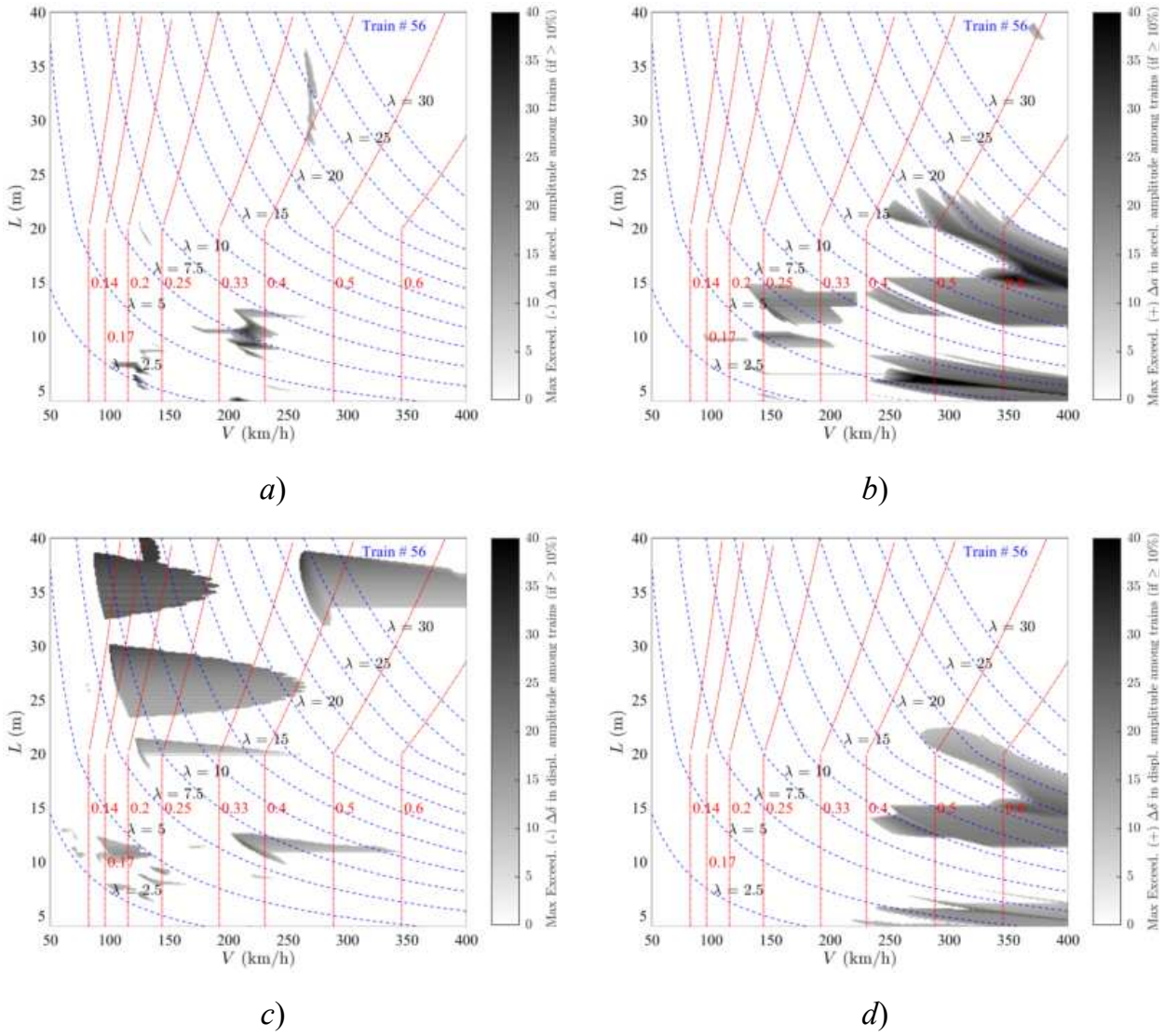

Figure 111. Exceedance Maps Train PT60-56 LIR vs Duhamel: a) Δa(−); b) Δa(+); c) Δδ(−); d) Δδ(+). PSC bridges.

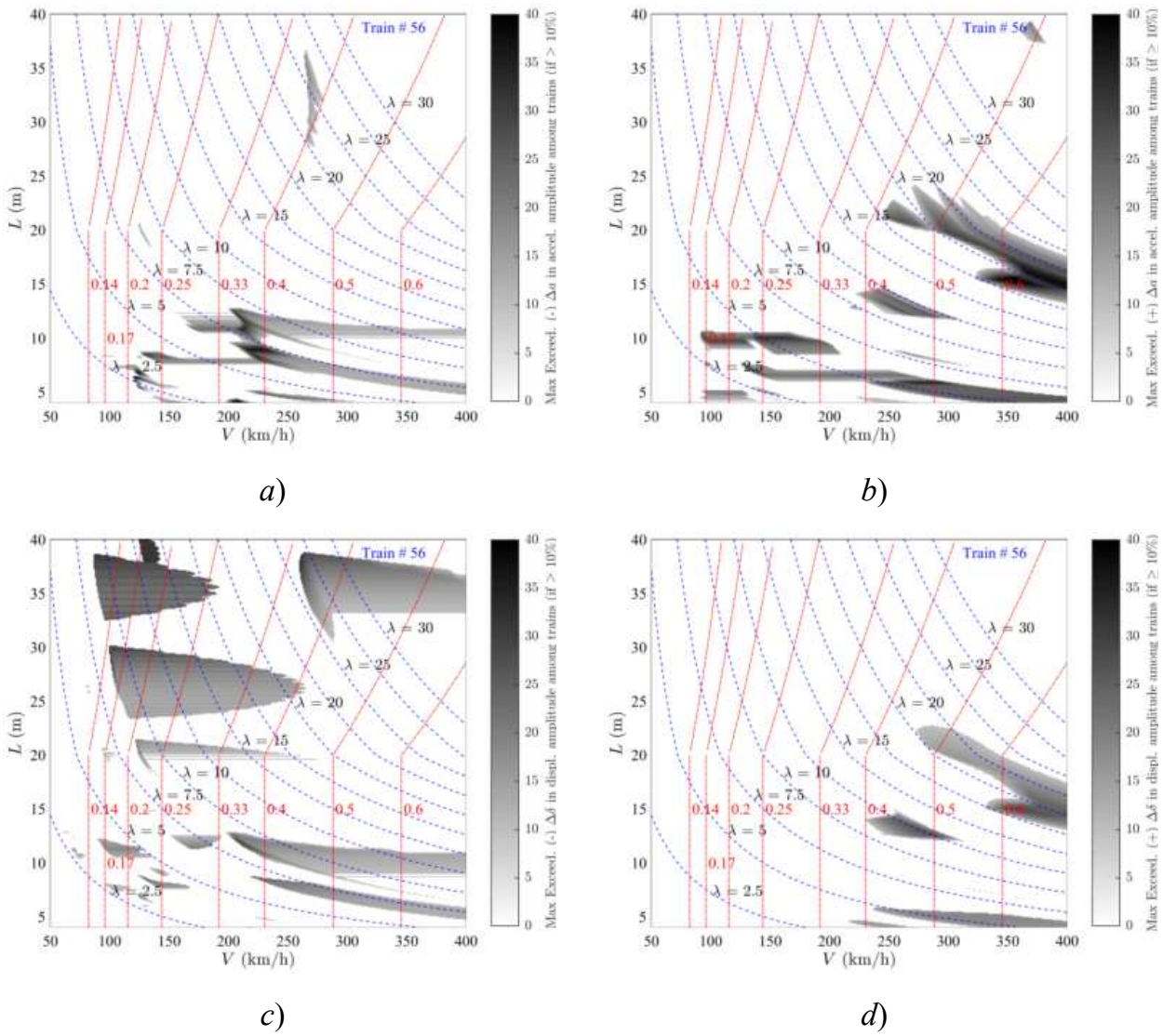

Figure 112. Exceedance Maps Train PT60-56 DER vs Duhamel: a) Δa(−); b) Δa(+); c) Δδ(−); d) Δδ(+). PSC bridges.

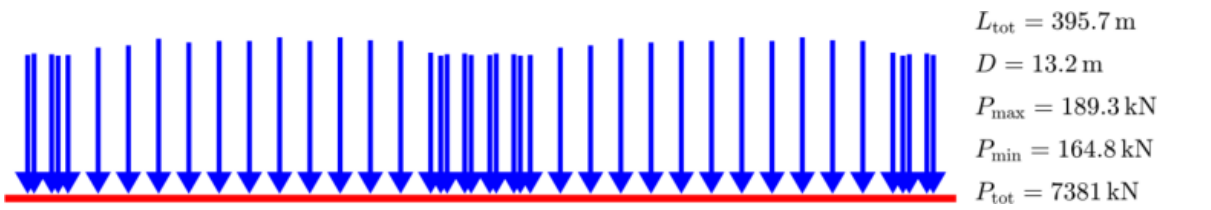

Figure Train PT60-57 [INB4EU-SA-040]

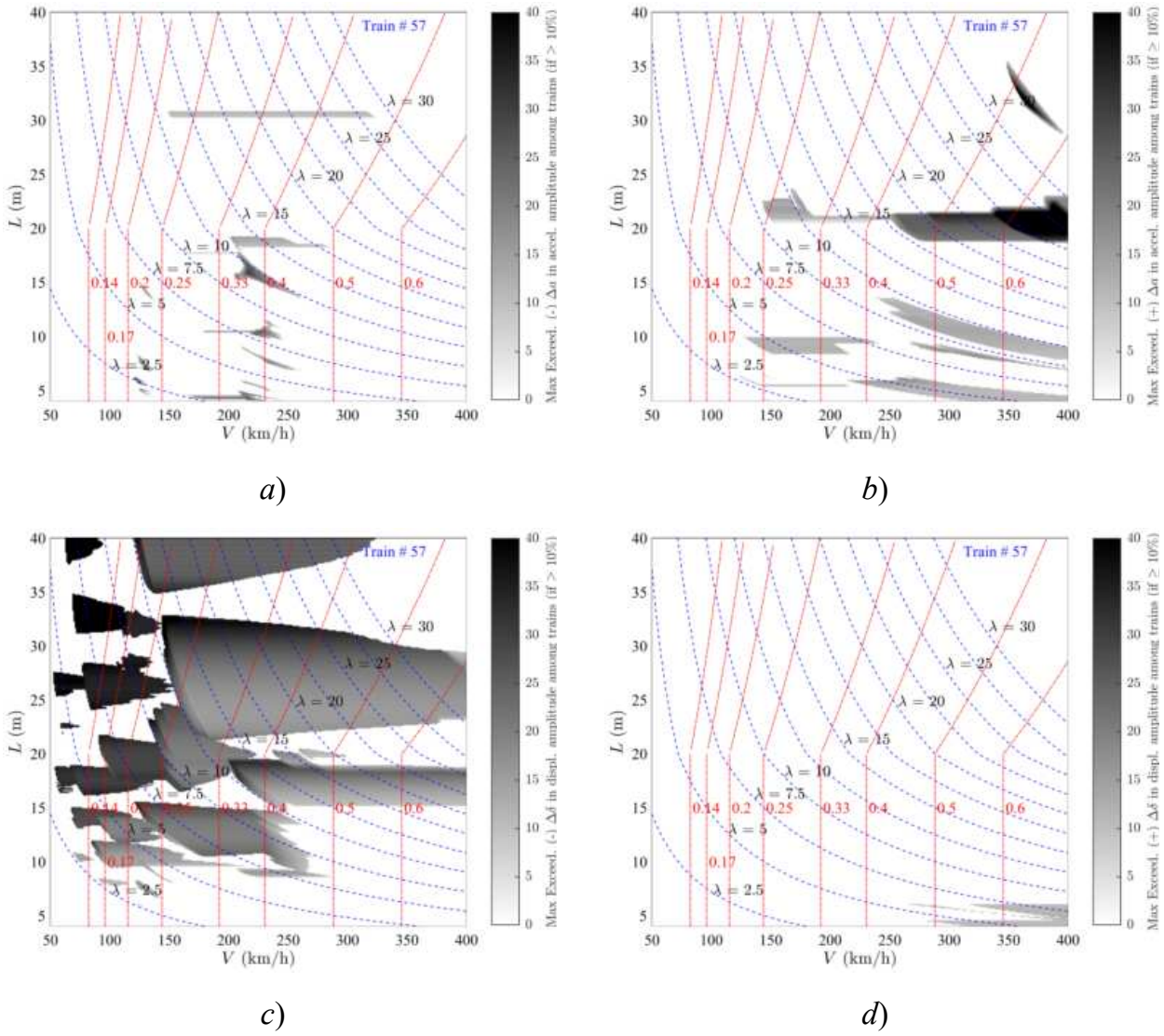

Figure 113. Exceedance Maps Train PT60-57 LIR vs Duhamel: a) Δa(−); b) Δa(+); c) Δδ(−); d) Δδ(+). PSC bridges.

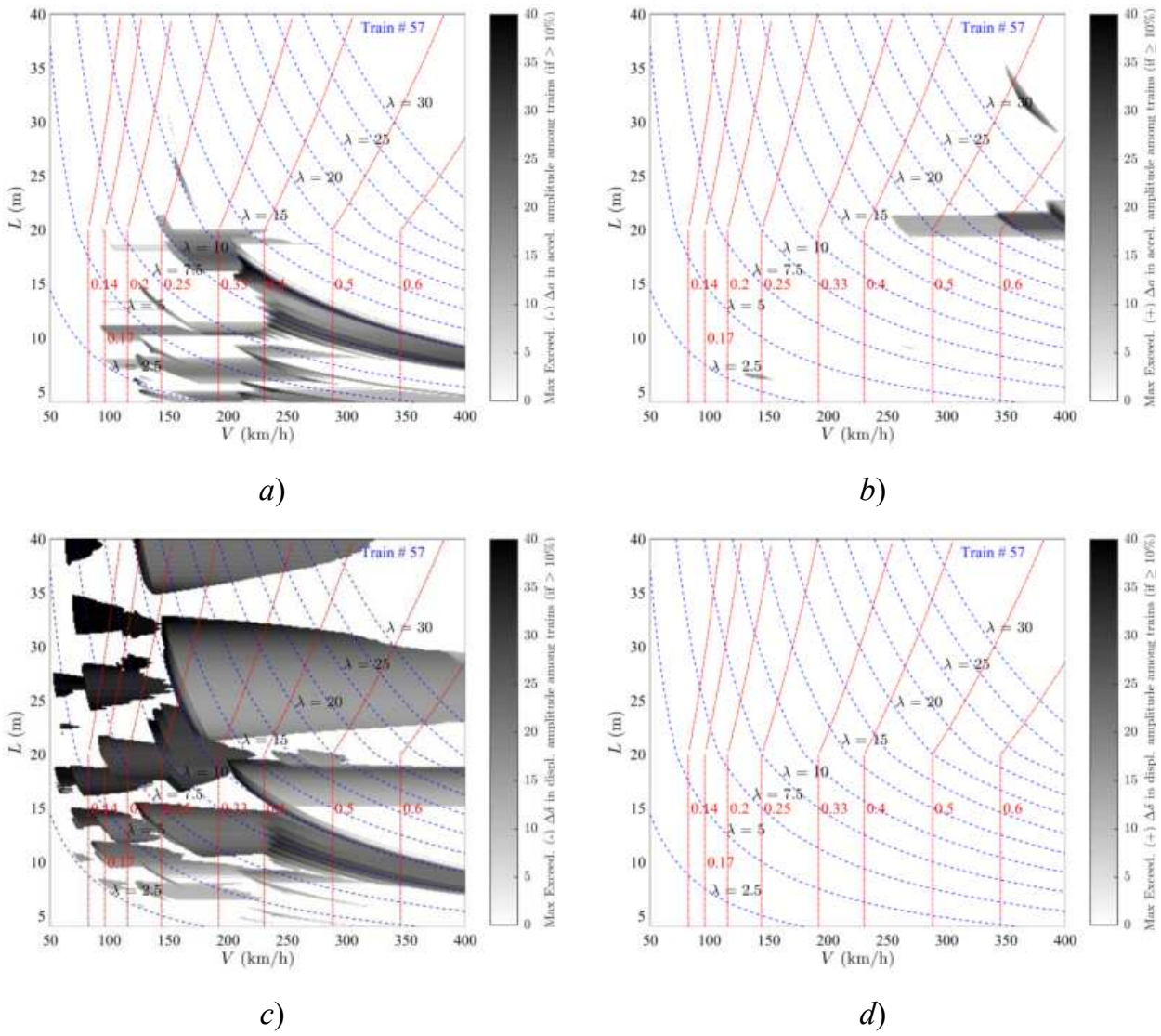

Figure 114. Exceedance Maps Train PT60-57 DER vs Duhamel: a) Δa(−); b) Δa(+); c) Δδ(−); d) Δδ(+). PSC bridges.

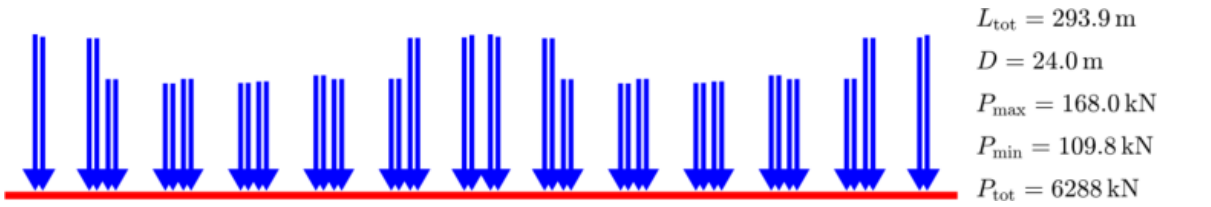

Figure Train PT60-58 [INB4EU-CB-142]

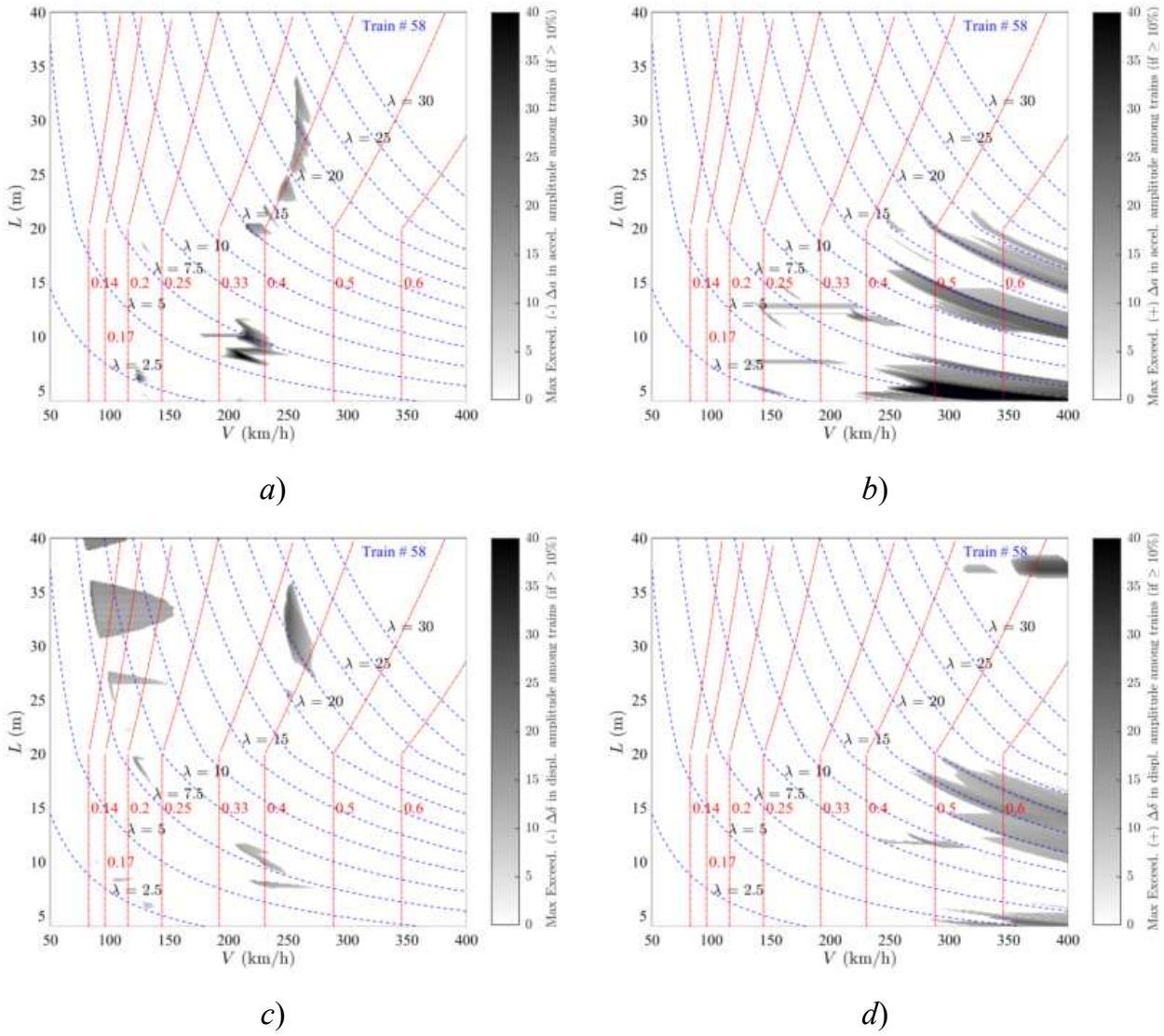

Figure 115. Exceedance Maps Train PT60-58 LIR vs Duhamel: a) Δa(−); b) Δa(+); c) Δδ(−); d) Δδ(+). PSC bridges.

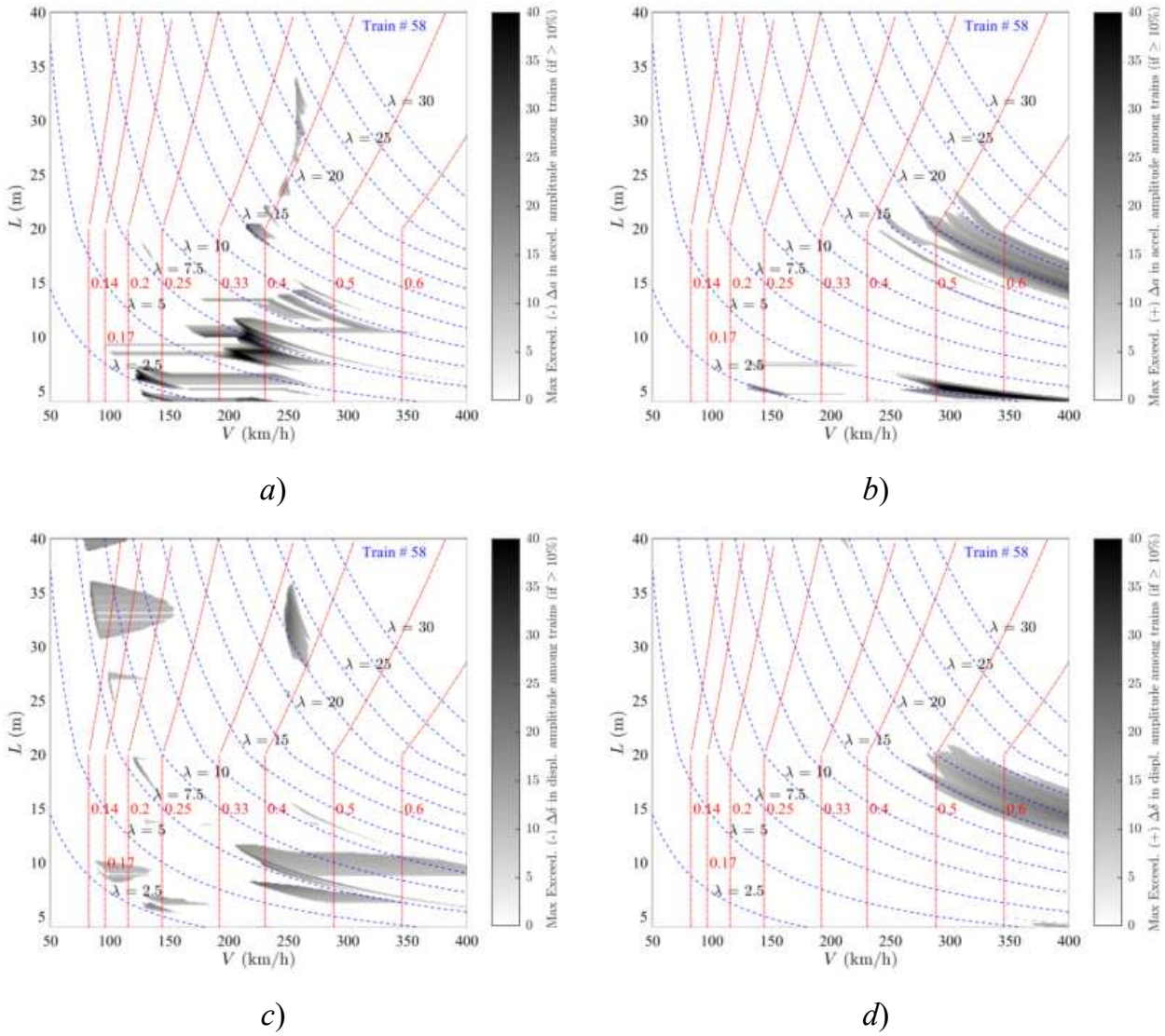

Figure 116. Exceedance Maps Train PT60-58 DER vs Duhamel: a) Δa(−); b) Δa(+); c) Δδ(−); d) Δδ(+). PSC bridges.

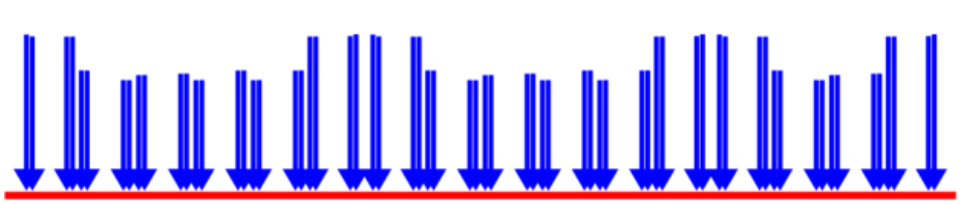

Figure Train PT60-59 [INB4EU-CB-146]

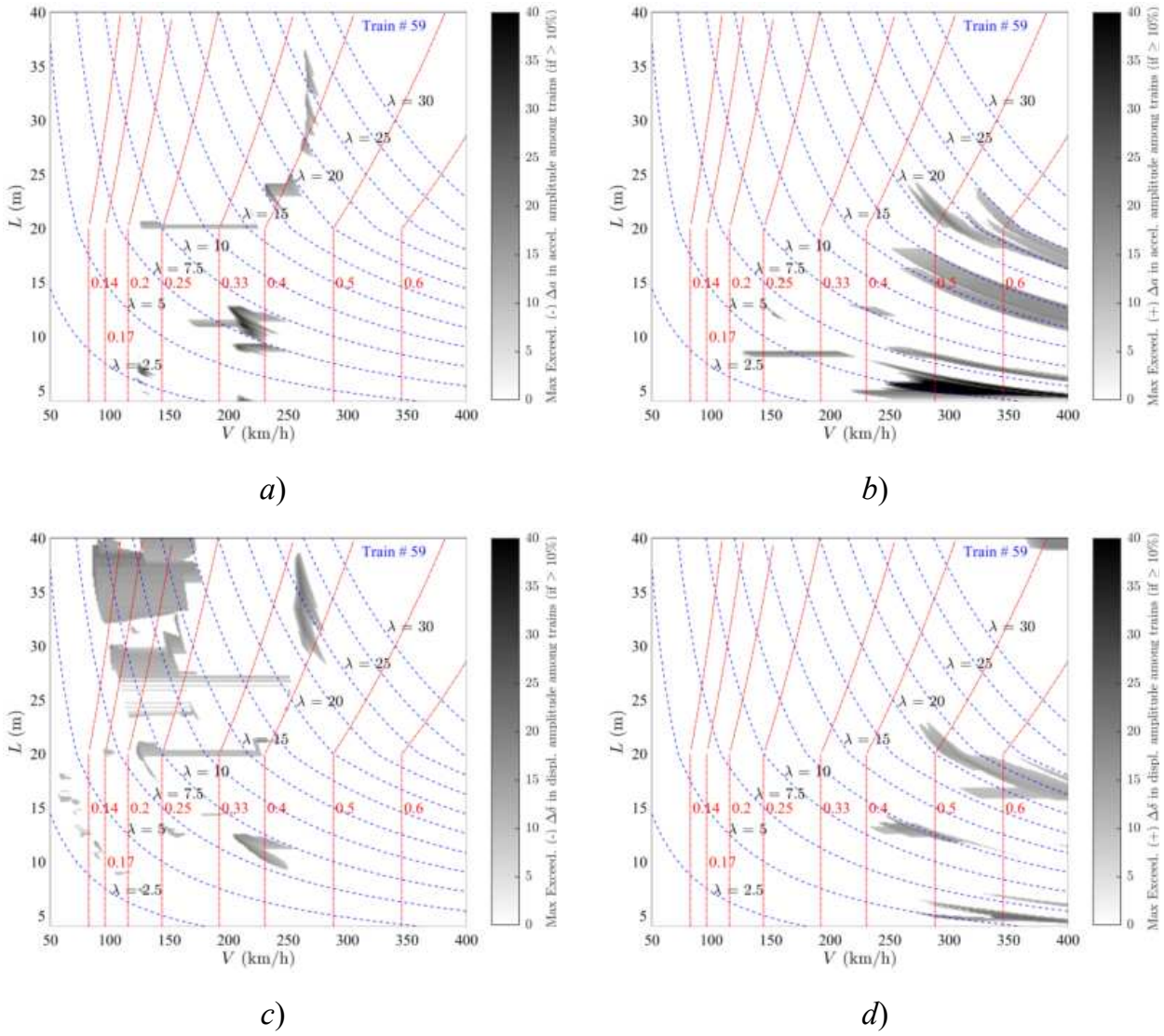

Figure 117. Exceedance Maps Train PT60-59 LIR vs Duhamel: a) Δa(−); b) Δa(+); c) Δδ(−); d) Δδ(+). PSC bridges.

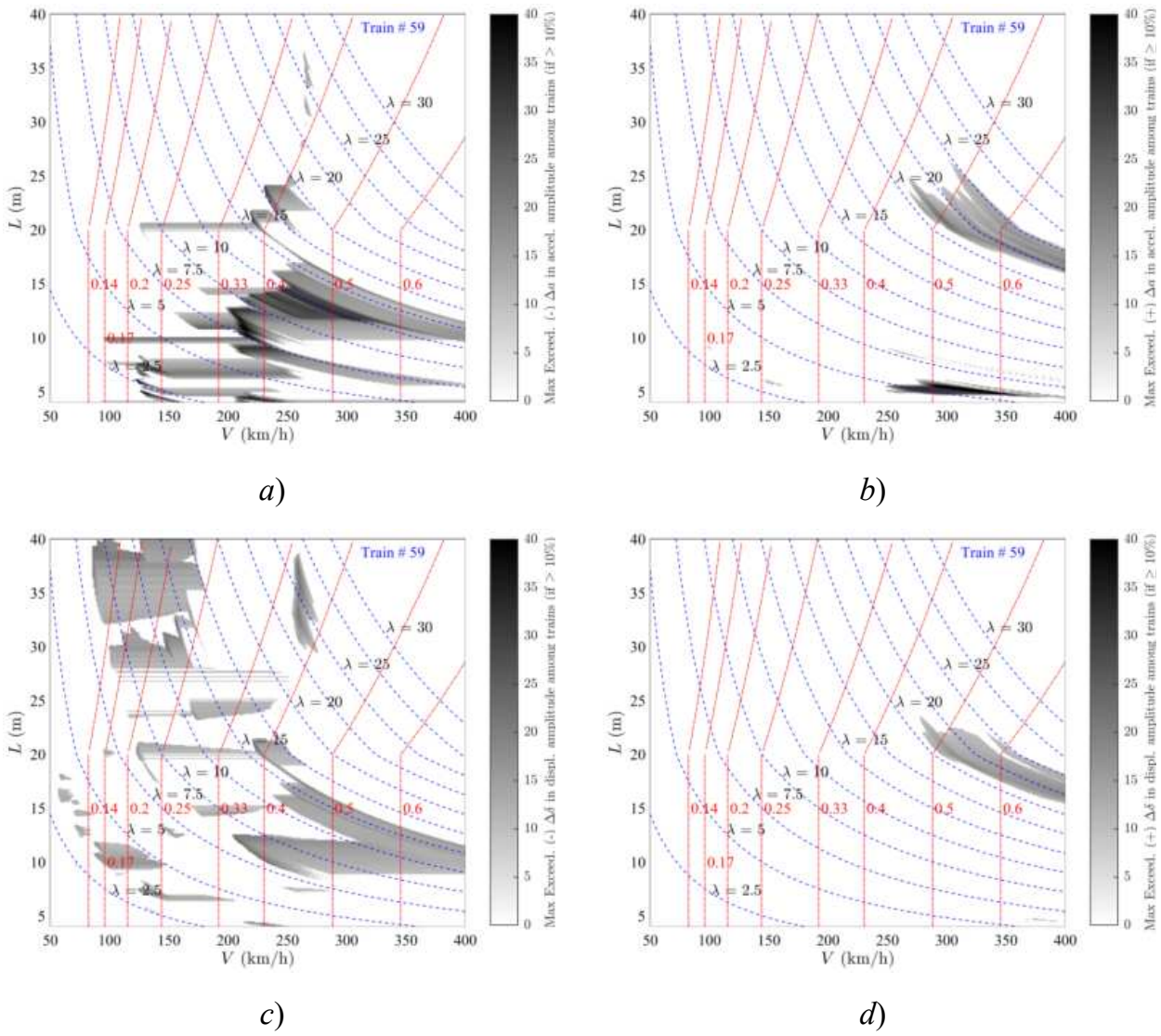

Figure 118. Exceedance Maps Train PT60-59 DER vs Duhamel: a) Δa(−); b) Δa(+); c) Δδ(−); d) Δδ(+). PSC bridges.

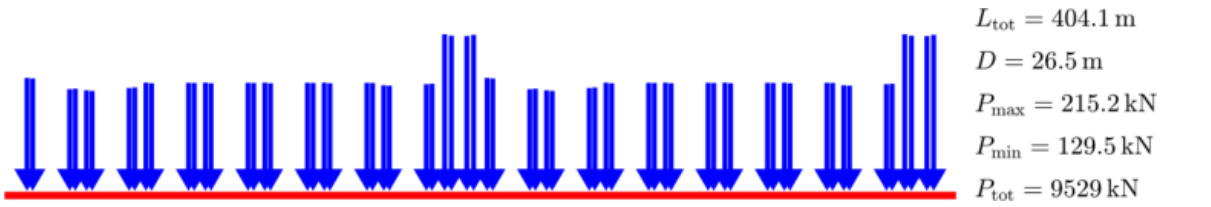

Figure Train PT60-60 [INB4EU-CB-140]

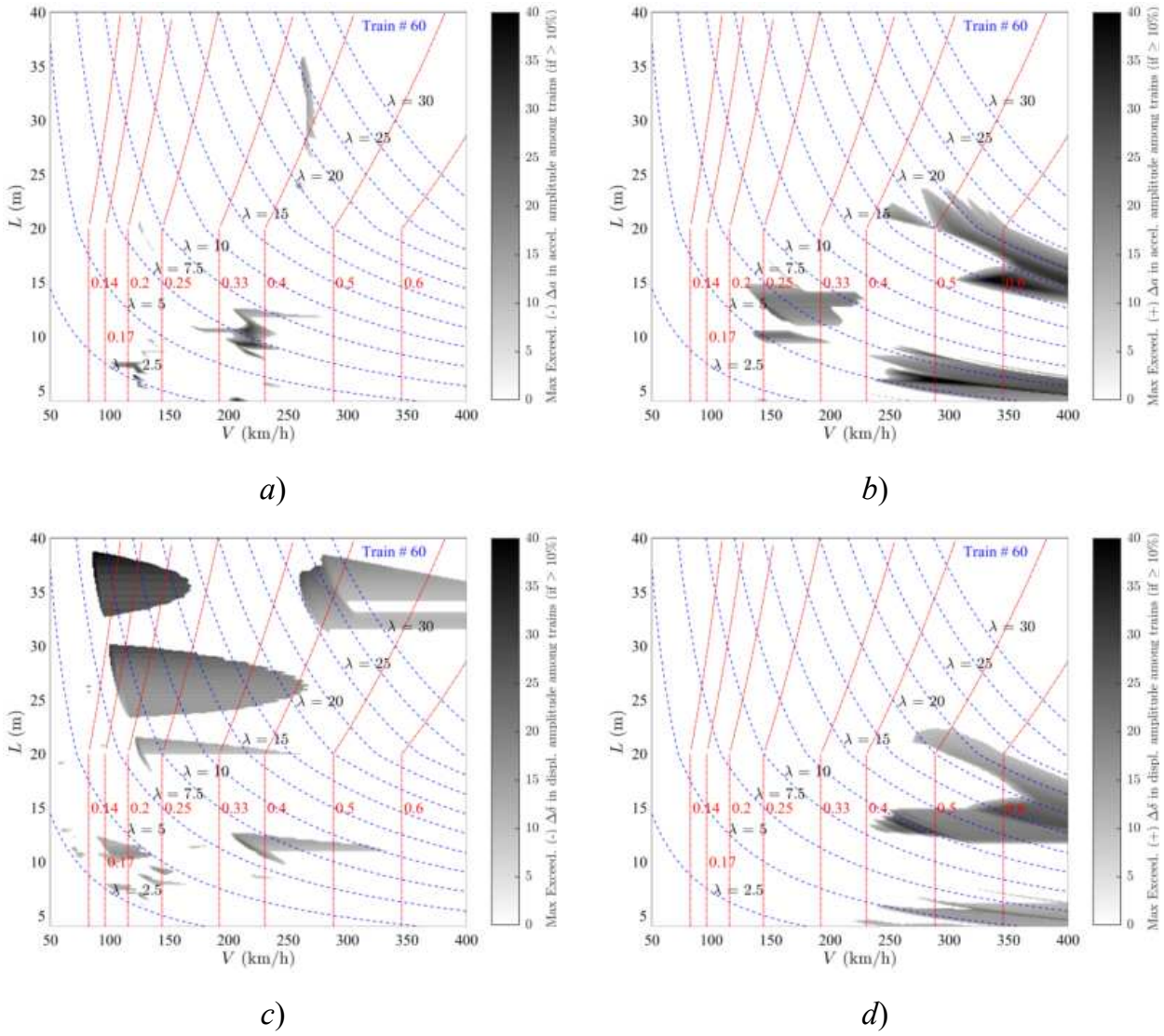

Figure 119. Exceedance Maps Train PT60-60 LIR vs Duhamel: a) Δa(−); b) Δa(+); c) Δδ(−); d) Δδ(+). PSC bridges.

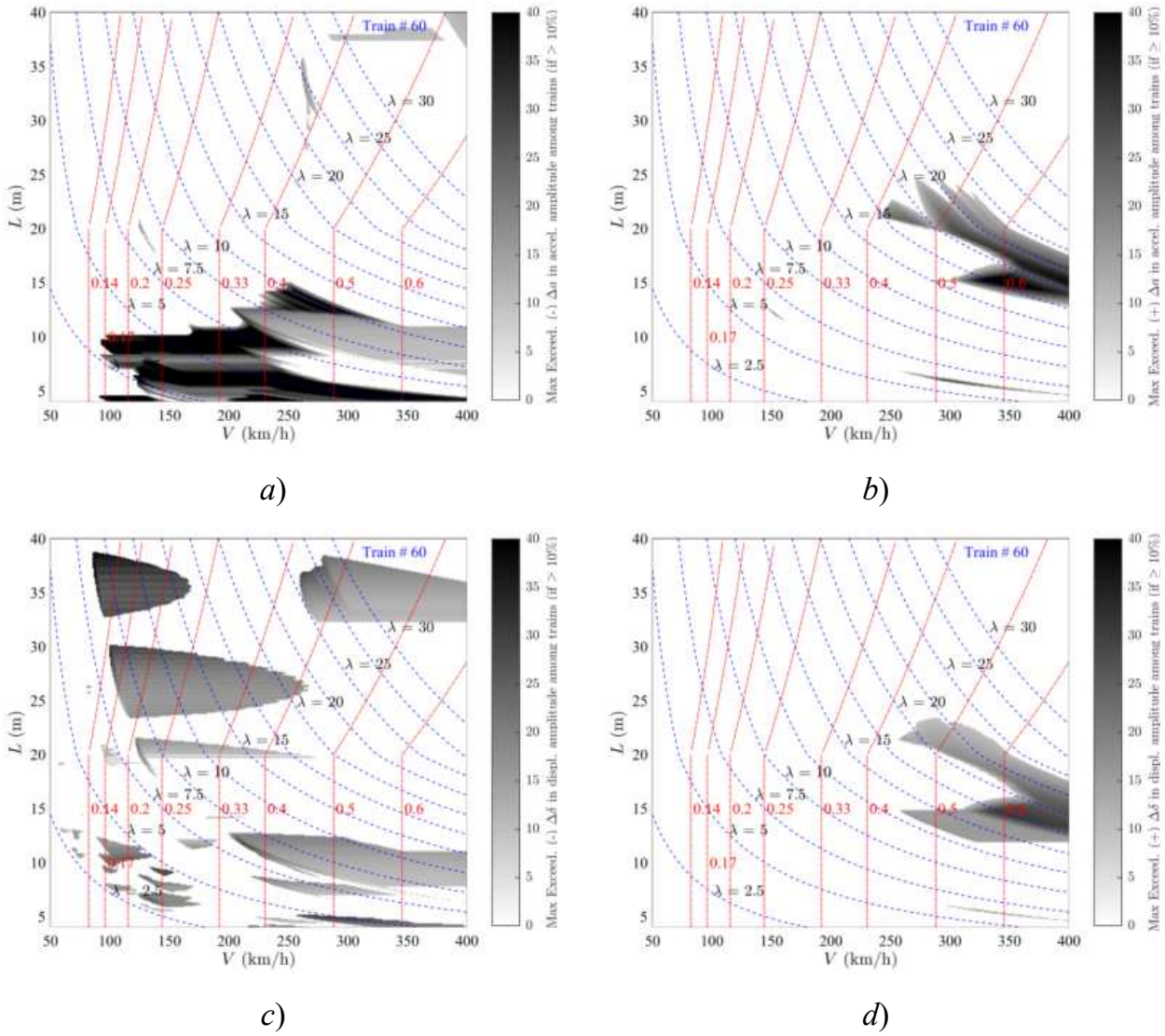

Figure 120. Exceedance Maps Train PT60-60 DER vs Duhamel: a) Δa(−); b) Δa(+); c) Δδ(−); d) Δδ(+). PSC bridges.